

To whom it concerns :

The results as incorporated in D46 'Final CLASH-report' were the results at the end of the CLASH-project (February 2005). Since then, more analysis towards the scale effects has been performed.

An updated version of the scaling procedure can be found in the paper by De Rouck et al. as presented at ICE2005, London, and as incorporated in this file. This updated scaling procedure was the result of intensive e-mailing between most of the authors.

Should the ongoing research show that more updates are necessary, these will be published in an upcoming special issue of Elsevier's Coastal Engineering.

Ghent University.  
November 2005.

# New Results on Scale Effects for Wave Overtopping at Coastal Structures

**J. De Rouck**, Ghent University, Department of Civil Engineering, Ghent, Belgium.

**J. Geeraerts**, Ghent University, Department of Civil Engineering, Ghent, Belgium.

**P. Troch**, Ghent University, Department of Civil Engineering, Ghent, Belgium.

**A. Kortenhaus**, Leichtweiß-Institut für Wasserbau, Braunschweig, Germany.

**T. Pullen**, HR Wallingford, Wallingford, UK.

**L. Franco**, Modimar Srl., Roma, Italy.

## Abstract

It is proven that wave run up on rough slopes is underestimated in small scale model tests due to scale / model effects. Given this fact, the same effects are suspected to be present for wave overtopping. A thorough comparison between prototype measurements of wave overtopping at three different coastal structures and scale model tests of these structures has been performed. The present paper gives the results from this comparison and presents a procedure to determine whether scale effects can be present in a certain situation. The procedure allows to calculate the magnitude of the scale and wind effect that can be expected. Since a lot of designs are based on physical model tests, this procedure has a broad range of applicability and its importance should be stressed.

## Introduction

Sea defences are very often designed for allowable wave overtopping conditions. Physical modelling or numerical modelling or a combination of both are used in the design. These models need to be calibrated and model results need to be verified against prototype conditions. One of the main outcomes of the EC OPTICREST project was that wave run-up height on a rubble mound breakwater is underestimated in small scale models compared to full scale by about 20% (De Rouck et al., 2001). As wave run-up is closely related to wave overtopping, small scale model tests might underestimate wave overtopping as well. The link between full scale and laboratory wave overtopping measurements has not been made in a systematic way yet.

Therefore, one of the main objectives of the research project CLASH, funded by the European Commission under contract n° EVK3-CT-2001-00058, is to solve the problem of suspected scale and / or model effects for wave overtopping. To accomplish this objective, field measurements on wave overtopping are carried out at three locations in Europe. The three prototype sites are modelled in at least two different laboratories and laboratory results are compared to prototype results to come to develop new guidance on possible scale and / or model effects.

## Previous Research

Scale effects cannot be assessed without evaluating the influence of measurement uncertainties and model effects, since distinction should be made between these various sources of differences between prototype and model (Kortenhaus et al., 2004a & 2004b).

Concerning the influence of different *measurement techniques* or measurement systems on overtopping, no model is yet available to (i) quantify the influence of measurement uncertainties on overtopping and (ii) to give recommendations on the preferred system to use for overtopping measurements.

The principal sources of dissimilarities in the hydraulic model (*model effects*) result from the unwanted generation of higher or lower harmonics in the wave trains (Oumeraci, 1999). Typical model effects in wave flumes (parasitic waves, wave generation, wave absorption etc.) are also described in Müller (1995). Limited research towards the influence and quantification of wind effects has been carried out. However, it is assumed that its influence, especially for very low overtopping rates, is relatively high. The quantification of these wind effects is also part of the CLASH-research (Gonzalez-Escrivá et al., 2004).

With respect to *scale effects* the influence of surface tension and kinematic viscosity on wave run-up and wave overtopping increases with decreasing flow velocity, so in the case of small overtopping rates (small layer thicknesses) the turbulent boundary layer no longer exists (Schüttrumpf, 2001). This means increasing hydraulic resistance on the slope and thus higher energy losses. This behaviour has been verified by test results in different model scales. Small-scale model investigations have shown lower wave run-up heights (Schulz, 1992) and lower overtopping rates (Kajima & Sakakiyama, 1994) as compared to large-scale model investigations. Theoretical investigations on scale effects for sea dikes have been performed by Schüttrumpf (2001). Formulae were developed to estimate the influence of scale effects on the most relevant processes related to sea dikes.

As already concluded from results of the OPTICREST project (De Rouck et al., 2001) this review showed that the influence of scale effects on the various physical processes in a rubble mound breakwater, on sea dikes and for vertical walls is not yet fully investigated.

## Field Measurements

Field measurements of overtopping have been made on three different types of coastal structures: a rubble mound breakwater armoured with flattened Antifer cubes at Zeebrugge, Belgium (De Rouck et al., 2003 and Troch et al., 2004), a rock armoured rubble mound breakwater in shallow water at Ostia, Italy (Franco et al., 2003) and a vertical seawall with rubble mound toe protection at Samphire Hoe, United Kingdom (Pullen et al., 2003).

### Field Sites

#### Zeebrugge Rubble Mound Breakwater

The Zeebrugge breakwater is a conventional rubble mound breakwater with a relatively low-crested superstructure. The armour layer consists of grooved (Antifer) concrete cubes (25 t). The breakwater core consists of quarry run (2-300 kg). The filter layer is composed of rock (1-3 t). Design conditions for the breakwater are: return period  $R = 500$  years, significant wave height  $H_s = 6.20$  m, period  $T = 9.0$  s and design water level  $DWL = Z + 6.75$  m ( $Z + 0.00$  m is chart datum).

An overall plan view of the location of wave and overtopping measurements is shown in Fig. 2. The cross section at the location of the overtopping measurements is shown in Fig. 1.

Wave characteristics are measured by 2 wave rider buoys, at respective distances of 150 m and 215 m from the breakwater. The water level just in front of the breakwater is determined by an infrared wave height meter placed on a measurement jetty (Troch et al. 1998). Waves overtopping the breakwater crest (see Fig. 3) are captured in a concrete overtopping tank (Fig. 1 and Fig. 4) with dimensions 7.4 m x 2.0 m x 2.0 m (length x width x height). The

volume of overtopping water is determined by continuous water level measurements by pressure transducers at the bottom of the tank. Outflow of the tank is controlled by a calibrated weir. The water level measurements and the weir's calibration formula allow the calculation of overtopping discharges. For more details on the measurements and calculations see [Troch et al. \(2004\)](#).

From 1999 to mid 2004, 11 storm events with wave overtopping have been measured at Zeebrugge. Wave heights  $H_{m0}$  vary between 2.6 m and 3.9 m, while wave periods  $T_p$  range between 7.3 and 10.3 s. Crest freeboards  $A_c$  vary between 4.9 and 6.0 m. Characteristics for the storm with the highest measured average overtopping rate,  $q = 0.86$  l/s/m, were  $H_{m0} = 3.9$  m,  $T_p = 8.6$  s and  $A_c = 7.4$  m. Full scale measurement data including detailed analysis of these data are found in [Geeraerts & Boone \(2004\)](#). Comparison of full scale data to literature prediction formulae are presented and discussed in detail in [Troch et al. \(2004\)](#).

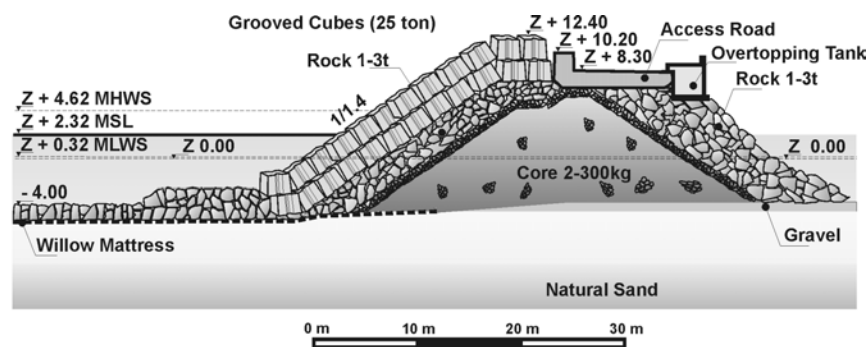


Fig. 1: Cross section of Zeebrugge rubble mound breakwater.



Fig. 2: Layout of Zeebrugge harbour.



Fig. 3: Wave overtopping over breakwater crest.



Fig. 4: Overtopping tank behind crest.

### Ostia Rubble Mound Breakwater

The Ostia yacht harbour is situated at the Italian Mediterranean Sea, near Rome. Full scale wave overtopping measurements are carried out since 2003 on the western breakwater protecting the harbour. Fig. 5 and 6 show the design cross section of the breakwater and the location of the overtopping measurements.



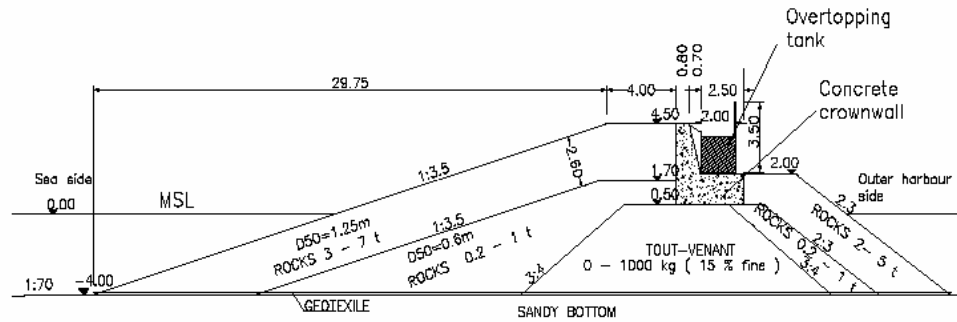


Fig. 5: Cross section of Ostia breakwater with overtopping tank.

Wave characteristics offshore are measured by 2 rider buoys at a water depth of 100 m and in front of the breakwater by a pressure transducer placed on the sea bottom at a distance of 200 m from the breakwater, at a water depth of 6.3 m. Waves overtopping the breakwater crest are captured in a steel overtopping tank (Fig. 7) with dimensions length x width x height = 4.0 m x 2.0 m x 2.0 m and overflowing weir similar to the one in Zeebrugge. Pressure measurements inside the tank and calculations of overtopping rates are carried out the same way as in Zeebrugge.

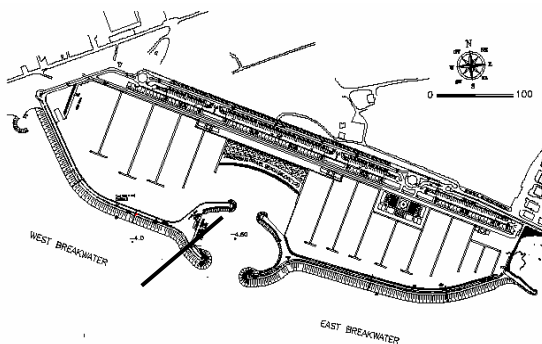


Fig. 6: Layout of Ostia harbour indicating cross-section of measurements.



Fig. 7: Wave overtopping in the tank at Ostia.

Between October 2003 and February 2004, 7 storms with moderate overtopping are registered in Ostia. During storms, waves are clearly depth-limited yielding wave heights slightly larger than  $H_{m0} = 2.0$  m at the toe of the breakwater combined with wave periods  $T_p$  about 9.0 s. Crest freeboard  $R_c = A_c$  is 4.5 m. First analysis of the Ostia data is presented in [Franco et al. \(2003\)](#).

### Samphire Hoe Vertical Wall

Samphire Hoe is located in the Southeast corner of England immediately to the west of Dover. It is an area of reclaimed land enclosed by a vertical seawall of which a cross section is shown in Fig. 8. The reclamation is subject to overtopping by green water or spray on approximately 30 days per year as a result of waves breaking over the rubble toe berm and impacting on the seawall face, as shown in Fig. 9. Waves are calculated from wind speeds at a nearby monitoring point using the UK Meteorological Office hindcast model, providing wave heights, periods, tide, surge levels and wind direction at hourly intervals. Waves overtopping the parapet wall are captured in three overtopping tanks (1.0 m x 0.30 m) distributed across the seawall promenade and shown in Fig. 8. These tanks are capable of recording the wave-

by-wave overtopping discharges by pressure measurements as well as providing information on the spatial distribution of the overtopping. During the winter of 2003/04 three storms were recorded using the field equipment at Samphire Hoe, with overtopping measurements ranging between threshold limits and violent peak volumes in excess of  $1\text{m}^3/\text{m}$  per wave. Further details describing the equipment and analysis of the results have been given by Pullen et al., 2003 & Pullen et al., 2004.

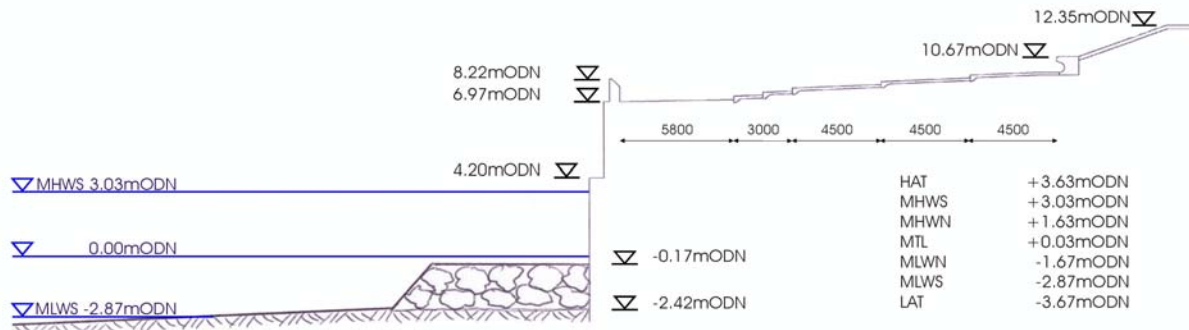


Fig. 8: Cross section of the Samphire Hoe Seawall.



Fig. 9: Violent wave overtopping at Samphire Hoe (Picture courtesy of Eurotunnel and the White Cliffs Countryside Project).



Fig. 10: Overtopping tanks at Samphire Hoe.

## Laboratory Modelling

Wave overtopping has been simulated at small scale for each of the three field sites, with tests in at least 2 laboratories for each site. Laboratory tests consisted of two main tasks: (i) reproduction of the measured prototype storms and (ii) parametric tests. Results from different scale models are compared to each other, to prototype results and to prediction formulae from literature.

## Rubble Mound Breakwater at Zeebrugge

Within CLASH the Zeebrugge rubble mound breakwater has been modelled in wave flumes at the University of Valencia (UPVLC), at Leichtweiß Institute (LWI) in Braunschweig (both scale 1:30) and at Ghent University (UGent) (scale 1:70). The cross section as shown in Fig. 1 has been modelled in the flumes where the following details have to be considered:

- the lower layer of Antifer cubes is placed in a regular pattern, but with the design porosity  $P = 45\%$ ;
- the upper layer of Antifer cubes was reproduced as accurately as possible using surveys and photos from the field;

- the foreshore bar (at a distance of about 500 m from the breakwater and at a level  $Z - 10$ ) was not modelled in the flume;
- the core material was assumed to be homogeneous in the field, distorted scaling of the core material was performed according to Burcharth et al. (1999) to assure that the Froude scale law holds for a characteristic pore velocity.

Analysis of *measurement uncertainties* has shown that wave heights and periods differ in the range of up to 5% when repeating tests or using different analysis (Kortenhaus et al., 2004). To determine the overtopping discharge, weighing was found to be the most accurate measuring system as compared to wave gauges or pressure transducers in the overtopping tank. When weighing the overtopping water, overtopping rates may differ up to 12% when repeating tests.

The influence of *model effects* has been studied at UPVLC (wind, pattern of Antifer cubes, foreshore bar, and repeatability of tests), LWI (repeatability pattern cubes, position and size of overtopping tray, number of waves) and UGent (pattern of cubes). Some details of these effects are given in Kortenhaus et al. (2004) and Garrido et al. (2004). Results show that the largest influence on wave overtopping results from on the one hand the pattern of the armour layer in combination with the width of the overtopping tray and on the other hand the magnitude of the overtopping discharge itself. Also, wind plays a major role for small overtopping discharges (Gonzalez-Escrivá et al., 2004). Quantification of these major effects is still ongoing, but preliminary results suggest factors up to one order of magnitude difference in overtopping discharge for the armour layer layout and also up to one order of magnitude for wind effects, if the wind velocity in prototype is comparable to a model wind velocity larger than 3 m/s in the model.

LWI has used the results of the aforementioned studies and rebuilt its model in the flume using a wider overtopping tray and the most accurate placement pattern of the Antifer cubes based on additional field surveys. Results of the model tests in comparison to the prototype are shown in Fig. 11 where the relative wave overtopping rate has been plotted over the relative crest freeboard  $A_c/H_{m0}$ . For comparison the van der Meer formula for smooth impermeable slopes using a roughness factor  $\gamma_f = 0.5$  has also been plotted in the graphs. All tests have been repeated twice in the model to verify accuracy of the results. Further tests with theoretical spectra rather than natural spectra, as used for the storms, have been plotted too (CLASH\_2).

The results show that reproduction of storms in the model at LWI worked reasonably well for some particular storms, obtaining differences between prototype and model in the range of less than one order of magnitude. However, some model storms still resulted in zero overtopping. The latter is confirmed by the tests performed at UPVLC where the three storms of 27 October 2002 ( $q$  up to 0.9 l/s/m) have been modelled and gave no overtopping without wind. Overtopping volumes in the model are less than 1 liter over 1500 waves only, so very small differences in the set-up of the model may lead to these differences.

Generally the results of both model and prototype are in relatively good agreement for the relatively larger overtopping discharges, especially when considering the uncertainties and model effects as given above. However, for small overtopping discharges, clear differences between model and prototype are observed.

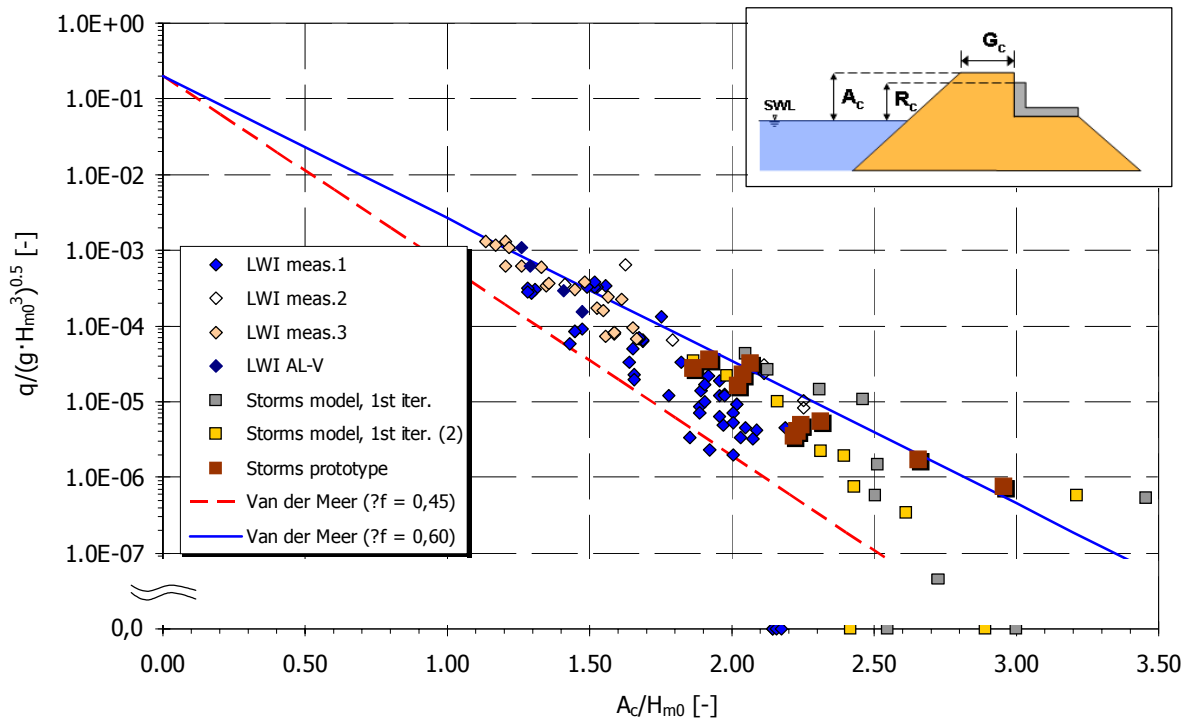


Fig. 11: Relative wave overtopping rate as a function of relative crest freeboard for the observed storms in prototype and LWI-model at Zeebrugge breakwater.

### Rubble Mound Breakwater at Ostia

The Ostia rubble mound breakwater has been modelled in a 2D wave flume in UGent (scale 1:20) and in a 3D wave basin in Flanders Hydraulics (FCFH) (scale 1:40). The cross-section as given in Fig. 5 has been modelled. However, the following modifications to the design drawing have to be taken into account (and have been modelled in the labs):

- field measurements and information from the contractor have shown the core and the filter to be one layer
- the seaward slope was 1:4 above still water level and 1:2 below still water level

Fig. 12 shows the results from both parametric tests and storm reproductions together with the prototype storm data. First of all it is clear that the prototype storms show considerably higher overtopping discharges than the model storm reproductions. 2D storm reproductions give zero overtopping. 3D reproductions give some overtopping, but end up at an overtopping discharge about 5 times smaller than in prototype. In the 2D model the water level must be increased by 0.7 m (prototype value) to obtain some overtopping, and by 1.3 m to obtain overtopping rates comparable to the prototype. Related to the wave height  $H_{m0} = 2.0$  m, the latter implies a decrease of the dimensionless crest freeboard from 1.8 to 1.3 to obtain overtopping.

2D parametric tests are in quite good agreement with the 3D parametric tests. However 2D tests generally produce smaller overtopping. 2D parametric tests in Fig. 12 only result from tests with higher water level, since tests with water level comparable to prototype and 3D tests result in zero overtopping. From the **parametric tests** a roughness coefficient for the Ostia breakwater was determined to be  $\gamma_f = 0.30$  which is a considerably smaller value than  $\gamma_f = 0.50$  which is often used for rock armoured slopes. This roughness coefficient was determined by comparison to test results on the same structure, but impermeable and smooth. Also the effect of the permeable crest berm was taken into account (see Geeraerts et al., 2004).

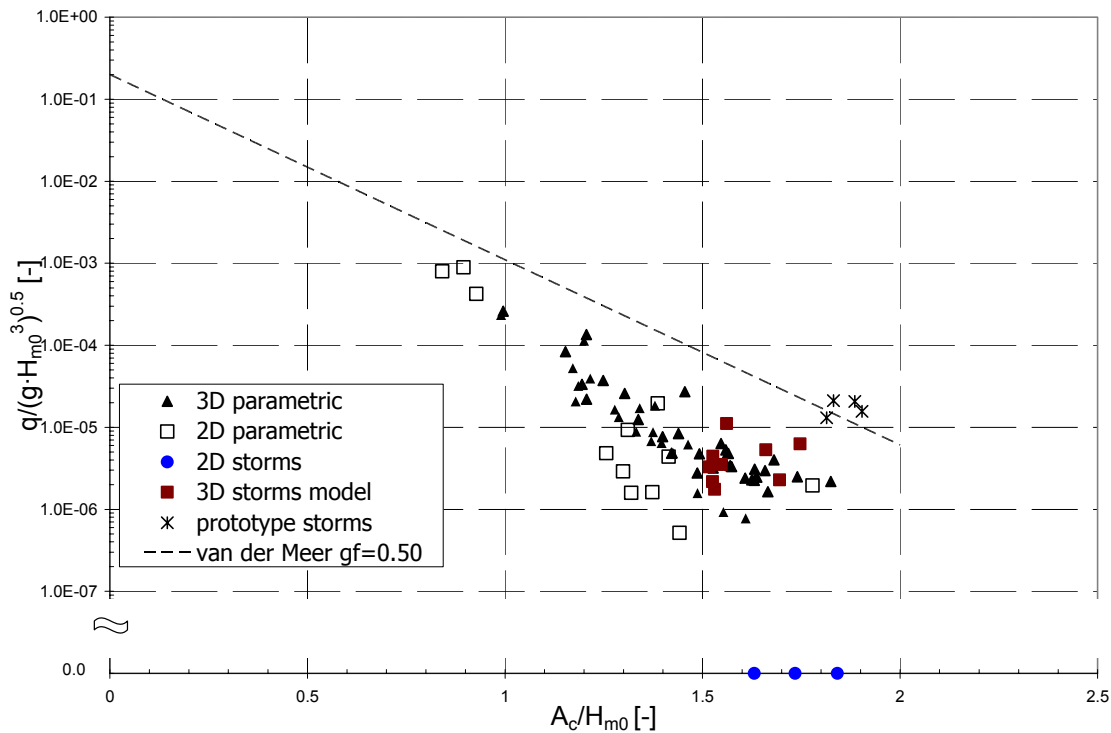


Fig. 12: Relative wave overtopping rate as a function of relative crest freeboard for storms in prototype and model and parametric tests at Ostia breakwater.

### Vertical Wall at Samphire Hoe

The composite vertical seawall at Samphire Hoe has been modelled in a 2D wave flume at the University of Edinburgh at a scale 1:40, and in 3D at a scale 1:20 at HR Wallingford. Each of the test structures was modelled according to the cross section shown in Fig. 8. Selected storm conditions have been simulated. In both laboratories individual wave-by-wave volumes and total discharges are measured. Fig. 13 shows the field data and the 2D & 3D laboratory results for Samphire Hoe against the empirical prediction method for a composite vertical seawall by Besley (1999). In the case of a composite wall the rubble toe causes the waves to impact on the structure or to reflect. The overtopping behaviour of both types of waves is significantly different and this is the reason that the representation according to Besley (Fig. 13), which takes this into account, has been used.

Generally, all the data show a good correlation with the prediction with very few points above the curve. The 2D results are very close to the prediction line with the scatter in the data well within the limits that might usually be expected for overtopping. The 1 May data from the field and for the 3D laboratory results deviate most from the prediction line for higher values of  $R_d$ . This may be due to the following effects. In the field the high velocity winds were distributing the overtopping discharges more widely and they were therefore not all captured in the overtopping tanks. In the 3D laboratory tests, with high relative freeboards, there is a tendency for discharges to be directed vertically without a horizontal component and fall back into the sea. Here a lack of wind prevents the potential discharge from travelling over the parapet and into the overtopping tanks.

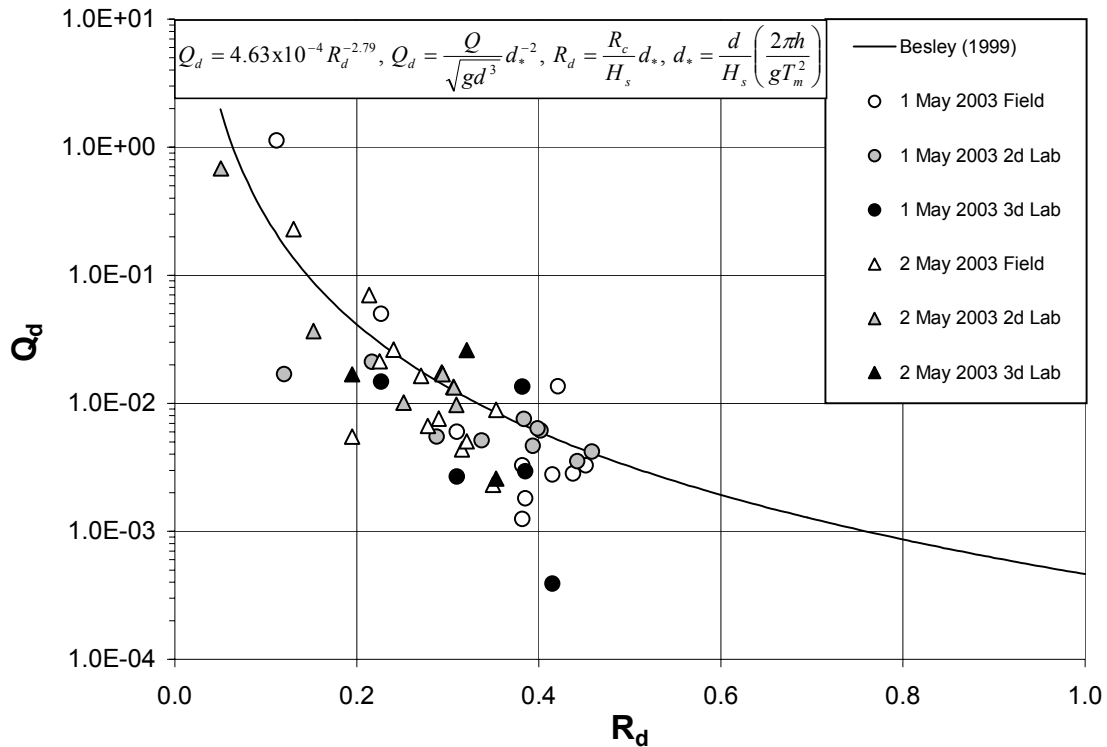


Fig. 13: Comparison of the recorded prototype data and the 2D and 3D model simulations two separate storms at Samphire Hoe shown with the empirical prediction formula of Besley (1999). ( $h$  = water depth in front of rubble toe,  $d$  = water depth above rubble toe).

## Scale Effects

A thorough comparison between field data and laboratory data for all three sites has been made. For the sloping rubble mound structures clear differences between model test and prototype results are identified: small overtopping discharges are clearly underestimated in small scale models. Part of the differences can be explained by laboratory effects (Kortenhaus et al. 2004a). However, from the present results and a literature review, it can be concluded that for these situations scale effects are present too. This section presents a procedure how to take into account scale / model and wind effects for wave overtopping starting from small scale model test results. Observations in the model and prototype, supported by literature show:

- scale effects have only been observed for sloping structures, not for vertical ones
- the scaling factor is larger for lower overtopping rates
- roughness of the slope must be included
- wind effects should be included
- structure's slope has an influence for rough structures

Fig. 14 shows data of both the Ostia and Zeebrugge sites. On the X-axis the overtopping rate from the model, upscaled to prototype scale by means of Froude scaling law is found. The Y-axis shows the ratio between the overtopping rate from on the one hand prototype and on the other hand the corresponding model reproduction, again upscaled. This ratio, when different from 1, represents a scaling factor to apply on small scale model overtopping results.

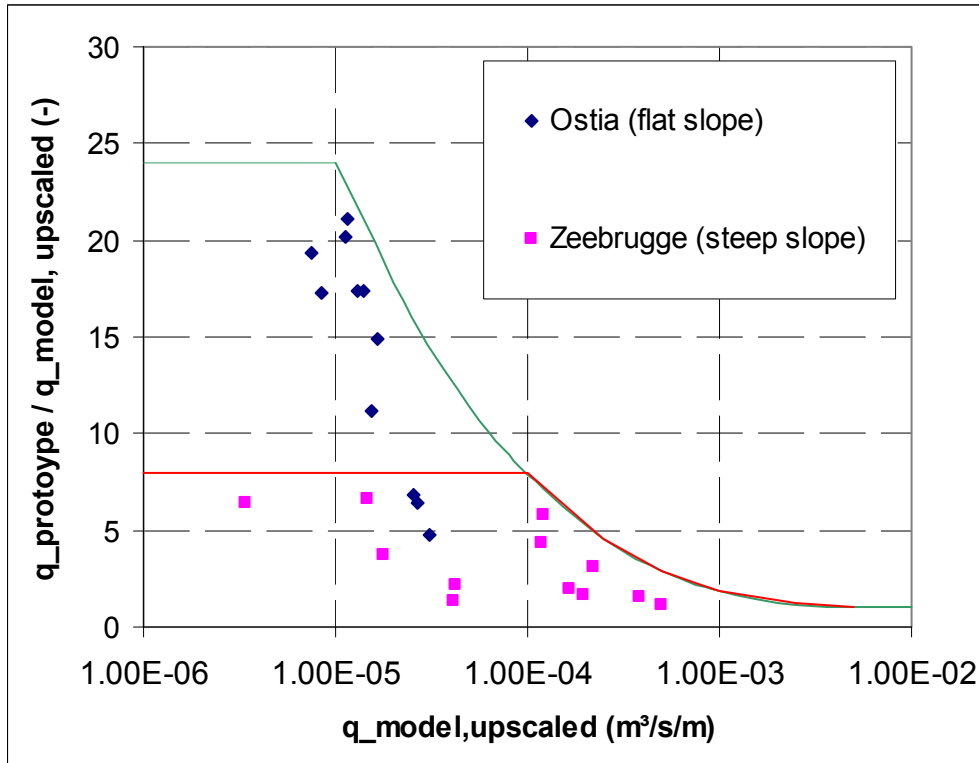


Fig. 14: Scaling factor to apply on small scale model overtopping results as a function of both structure slope and measured overtopping rate.

Fig. 14 indicates that the scaling factor (including model effects, like wind) decreases rather rapidly with increasing value of the overtopping rate. The graph also shows that the scaling factor is smaller for the Zeebrugge breakwater than for the Ostia breakwater. The different structure slope (1/1.4 for Zeebrugge; 1/3.5 for Ostia) is suspected to be the main reason for this difference. These findings have led to a distinction in the scaling procedure (see below) between flat and steep rubble mound breakwater slopes.

In an analogous way, overtopping data with and without wind have been compared (Kortenhaus et al. 2004b) to determine the effect of wind on the overtopping rate. The following formula for the factor  $f_{\text{wind}}$  has been determined:

$$f_{\text{wind}} = \begin{cases} 4.0 & \text{for } q_{\text{SS}} < 1 \cdot 10^{-5} \text{ m}^3 / \text{s} \cdot \text{m} \\ 1.0 + 3 \cdot \left( \frac{-\log q_{\text{SS}} - 2}{3} \right)^3 & \text{for } q_{\text{SS}} < 1 \cdot 10^{-2} \text{ m}^3 / \text{s} \cdot \text{m} \\ 1.0 & \text{for } q_{\text{SS}} \geq 1 \cdot 10^{-2} \text{ m}^3 / \text{s} \cdot \text{m} \end{cases} \quad (1)$$

In which  $q_{\text{SS}}$  is a small scale model overtopping result or a prediction by the CLASH Neural Network (van der Meer et al., 2005 or similar). It should be noted however, that  $q_{\text{SS}}$  is already scaled up to prototype scale by means of Froude scaling law.

In this instance the factor 4.0 is not a scaling factor as previously described, but it can be used to make an allowance for the effects of the wind, and also has the advantage of not using a separate technique. It is especially important to make this distinction, because no scaling effects for vertical and composite vertical structures have been observed. Eq. (1) gives the maximum influence of wind on the overtopping rate for vertical structures or smooth sloping structures.

## Scaling Procedure

The following procedure takes into account the above requirements and is described step by step. It starts from an overtopping rate  $q_{SS}$ , as defined above. To go through the procedure, following parameters are required:

- wave height  $H_{m0}$  at the toe of the structure,
- roughness coefficient  $\gamma_f$  for the seaward side of the structure,
- width of the seaward berm  $B$  of the structure,
- water depth over the horizontal berm  $d_h$ ,
- slope of the structure below the berm  $\cot\alpha_d$ ,
- slope of the structure above the berm  $\cot\alpha_u$

For a more detailed description of these parameters see Verhaeghe et al. (2004).

### Step 1: vertical structure?

Step 1 checks whether the structure is vertical or not. If the structure is vertical or almost vertical continue with ‘Step 4: Procedure wind effect’. If this is not the case go to ‘Step 2: rough structure’.

*Note:* To help distinguishing between vertical and non-vertical structures there are two configurations using the input parameters of the CLASH database which indicate a vertical structure. These are:

if  $\cot\alpha_u < 1$  and  $\cot\alpha_d < 1$  the structure is vertical or almost vertical.

if  $\cot\alpha_u < 1$  and  $B > 0$  and  $d_h > 0$  there is most probably a berm below swl and a vertical structure on top of the berm.

Please note that this parameter distinction cannot be used when parapets are used with the structure. Furthermore, for some complex structures the simple distinction proposed here may fail to give the correct answer.

### Step 2: rough structure?

Step 2 checks whether the structure is rough or smooth. If the structure is rough, continue with Step 3: rough sloping structure, if the structure is smooth continue with ‘Step 4: Procedure wind effect’.

*Note:* The roughness of a structure may be distinguished from the roughness coefficient  $\gamma_f$  of the CLASH database. If  $\gamma_f$  is smaller than 0.9 the structure is considered to be a rough sloping structure otherwise the structure is smooth.

### Step 3: rough sloping structure

Within this step the first decision to be made is whether to consider the influence of wind or not. If yes, the factor for scale and wind effects  $f_{scale\_wind\_max}$  can be calculated as follows (based on Fig. 14):

Flat sloping rubble mound breakwaters (based on slope 1:3.5):

$$f_{scale\_wind\_max} = \begin{cases} 24.0 & \text{for } q_{SS} < 1 \cdot 10^{-5} \text{ m}^3 / \text{s} \cdot \text{m} \\ 1.0 + 23 \cdot \left( \frac{-\log q_{SS} - 2}{3} \right)^3 & \text{for } q_{SS} < 1 \cdot 10^{-2} \text{ m}^3 / \text{s} \cdot \text{m} \\ 1.0 & \text{for } q_{SS} \geq 1 \cdot 10^{-2} \text{ m}^3 / \text{s} \cdot \text{m} \end{cases} \quad (2a)$$



Steep sloping rubble mound breakwaters (based on slope 1:1.4):

$$f_{\text{scale\_wind\_max}} = \begin{cases} 8.0 & \text{for } q_{\text{ss}} < 1 \cdot 10^{-4} \text{ m}^3 / \text{s} \cdot \text{m} \\ 1.0 + 7 \cdot \left( \frac{-\log q_{\text{ss}} - 2}{2} \right)^3 & \text{for } q_{\text{ss}} < 1 \cdot 10^{-2} \text{ m}^3 / \text{s} \cdot \text{m} \\ 1.0 & \text{for } q_{\text{ss}} \geq 1 \cdot 10^{-2} \text{ m}^3 / \text{s} \cdot \text{m} \end{cases} \quad (2b)$$

For slopes in between the given slopes

Eq. (2) delivers a scaling factor for really rough structures when  $\gamma_f \leq 0.7$ . When  $\gamma_f \geq 0.9$  the structure is smooth and the scaling factor will be  $f_{\text{scale}} = 1.0$ . In between both values a linear interpolation can be assumed so that the scaling factor for rough slopes  $f_{\text{scale\_wind}}$  can be determined by:

$$f_{\text{scale\_wind}} = \begin{cases} f_{\text{scale\_wind\_max}} & \text{for } \gamma_f \leq 0.7 \\ 5 \cdot (1 - f_{\text{scale\_wind\_max}}) \cdot \gamma_f + (f_{\text{scale\_wind\_max}} - 1) \cdot 4.5 + 1 & \text{for } 0.7 < \gamma_f < 0.9 \end{cases} \quad (3)$$

It should be noted that this factor, as calculated by eq. (2) or (3) includes both the influence of scale and wind effects, the latter being a model rather than a scale effect. Furthermore, for scale effects without any wind a maximum value of 16.0 is suggested (flat slopes). Assuming that factors for scale and wind effects should be multiplied to achieve an overall factor, a theoretical factor for wind of 1.5 would be obtained. This is lower than indicated in Eq. (1) for vertical walls, which is believed to be due to the effect of wind for vertical structures being larger than for rough sloping structures. Applying the factor of 1.5 for wind, leads to a maximum effect of 5.33 for scale effects without wind for steep sloping rubble mounds, which is changed to 6.0 for practical reasons. So, for scale effects without wind following equation is suggested:

$$f_{\text{scale\_nowind}} = \begin{cases} f_{\text{scale\_nw}} & \text{for } \gamma_f \leq 0.7 \\ 5 \cdot (1 - f_{\text{scale\_nw}}) \cdot \gamma_f + (f_{\text{scale\_nw}} - 1) \cdot 4.5 + 1 & \text{for } 0.7 < \gamma_f < 0.9 \end{cases} \quad (4a)$$

where

Flat sloping rubble mound breakwaters (based on slope 1:3.5):

$$f_{\text{scale\_nw}} = \begin{cases} 16.0 & \text{for } q_{\text{ss}} < 1 \cdot 10^{-5} \text{ m}^3 / \text{s} \cdot \text{m} \\ 1.0 + 15 \cdot \left( \frac{-\log q_{\text{ss}} - 2}{3} \right)^3 & \text{for } q_{\text{ss}} < 1 \cdot 10^{-2} \text{ m}^3 / \text{s} \cdot \text{m} \\ 1.0 & \text{for } q_{\text{ss}} \geq 1 \cdot 10^{-2} \text{ m}^3 / \text{s} \cdot \text{m} \end{cases} \quad (4b)$$

Steep sloping rubble mound breakwaters (based on slope 1:1.4):

$$f_{\text{scale\_nw}} = \begin{cases} 6.0 & \text{for } q_{\text{ss}} < 1 \cdot 10^{-4} \text{ m}^3 / \text{s} \cdot \text{m} \\ 1.0 + 5 \cdot \left( \frac{-\log q_{\text{ss}} - 2}{2} \right)^3 & \text{for } q_{\text{ss}} < 1 \cdot 10^{-2} \text{ m}^3 / \text{s} \cdot \text{m} \\ 1.0 & \text{for } q_{\text{ss}} \geq 1 \cdot 10^{-2} \text{ m}^3 / \text{s} \cdot \text{m} \end{cases} \quad (4c)$$

For slopes in between the tested slopes interpolation is possible (eq. 3 – 4).

Go to ‘Step 5: final calculation of mean overtopping rate’: to finalise the procedure.

#### Step 4: Procedure wind effect

For structures other than rough structures there might be a wind effect. First a decision has to be made whether wind effects are to be considered or not. If not, the factor for the wind-influence is set to  $f_{wind} = 1$ . If wind effects have to be considered, they can be calculated using Eq. (1).

Finally the factor for wind effects can be applied to the overtopping rate  $q_{SS}$ . This is performed in ‘Step 5: final calculation of mean overtopping rate’.

#### Step 5: Final calculation of mean overtopping rate

The final calculation of mean wave overtopping rates should include both a calculation for wind effects and smooth structures and a calculation for scale and wind effects and rough structures as follows:

$$q_{wind} = q_{SS} \cdot f_{wind} \quad (f_{wind} \text{ (eq. (1))}) \quad (5)$$

$$q_{scale\_wind} = q_{SS} \cdot f_{scale\_wind} \quad (f_{scale\_wind} \text{ (eq. 2 - 3)}) \quad (6)$$

$$q_{scale\_nw} = q_{SS} \cdot f_{scale\_nw} \quad (f_{scale\_nw} \text{ (eq. (4))}) \quad (7)$$

#### Step 6: Scaling map for coastal structures

The procedure described above is summarised in a simple scaling map for wave overtopping over coastal structures obtained from small-scale model tests (Fig.15). This map is only needed when wave heights  $H_{m0}$  for the structure are higher than 0.5 m; the user starts from model scale with wave heights  $H_{m0} < 0.5$  m. Furthermore, the distinction between vertical and sloped structures as given by the parameters as given in the ‘input’ to the overall procedure are only valid for structures which do not have parapets or overhanging elements..

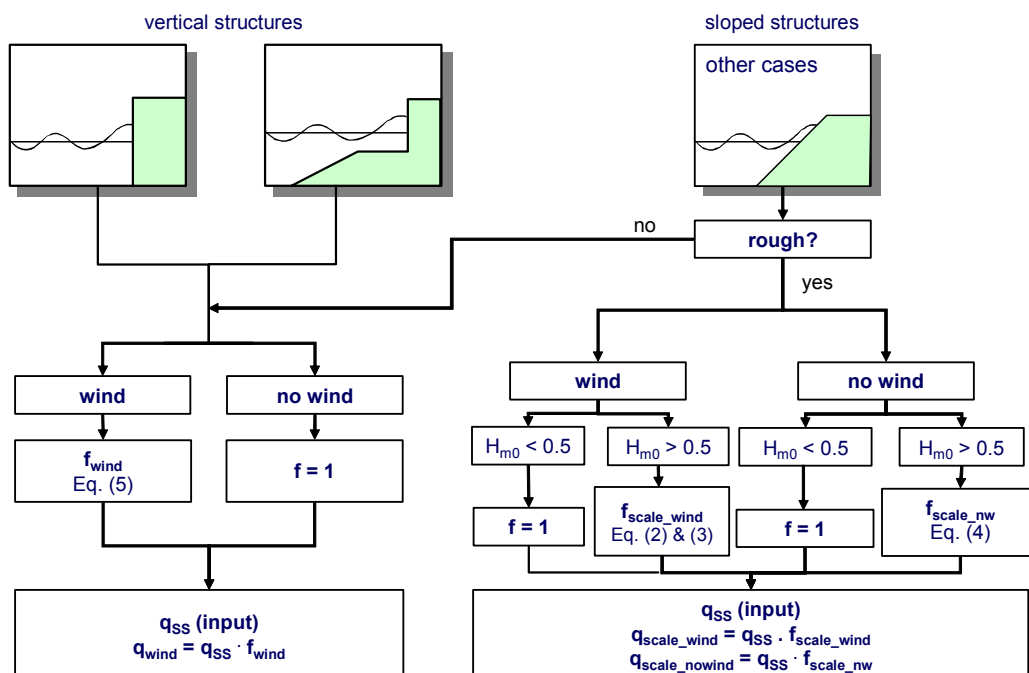


Fig. 15: Scaling map for wave overtopping results over coastal structures from small-scale model tests

## Conclusions

Comparison of overtopping discharges at prototype structures and scale models led to the following conclusions:

- Two different rubble mound structures were modelled and for both structures clear differences between prototype and model results were observed. Differences seem to occur mainly for small overtopping rates and increase for longer and flatter slopes. Wind is a very important factor for small overtopping rates. The observed differences are very important for small overtopping discharges where scale model tests predict zero overtopping for a prototype situation with overtopping.
- Vertical walls: general good agreement between prediction, prototype and laboratory reproduction were observed, existing differences can be explained by wind effects (model effects).

The present paper presents a procedure to take into account scale and wind effects starting from small scale model test results or NN predictions, which are on their turn based on small scale model test results.

## Acknowledgements

The research is carried out partly within the European Community funded project CLASH ('Crest Level Assessment of Coastal Structures by full scale monitoring, neural network prediction and Hazard analysis on permissible wave overtopping' – contract n°: EVK3-CT-2001-00058) within the Fifth Framework Programme (2002-2004). The financial support of the European Community is gratefully acknowledged. Additional support from national research projects is also acknowledged. The work carried out by HR Wallingford at Samphire Hoe was also supported by Defra / EA under project code FD2412.

## References

- Besley, P., 1999. Wave overtopping of Seawalls. Design and Assessment Manual. Hydraulics Research Wallingford. R&D Technical Report W178, ISBN 1 85705 069 X.
- Burcharth, H.F., Liu, Z., Troch, P. (1999): Scaling of core material in rubble mound breakwater model tests. Proc. Int. Conf. on Coastal and Port Engineering in Developing Countries (COPEDEC), no. 5, Cape Town, South Africa, pp. 1518-1528.
- De Rouck, J., Troch, P., Van de Walle, B., van Gent, M., Van Damme, L., De Ronde, J., Frigaard, P., Murphy, J., 2001. Wave run-up on sloping coastal structures: prototype versus scale model results. Proc. Int. Conf. on Coastlines, Structures and breakwaters 2001, 26-28 Sept. 2001, Institution of Civil Engineers, London, UK.
- De Rouck, J., Van de Walle, B., Geeraerts, J., Troch, P., Van Damme, L., Kortenhaus, A., Medina, J.R., 2003. Full scale wave overtopping measurements. Proc. of Conf. Coastal Structures '03, Portland, USA.
- Franco, L., Bellotti, G., Briganti, R., De Rouck, J., Geeraerts, J., 2003. Full Scale Measurements of wave overtopping at Ostia yacht harbour breakwater. Proc. of Conf. Coastal Structures '03, Portland, USA.
- Garrido, J.M., González-Escrivá, J.A., Medina, J.R., Kortenhaus, A., 2004: Spatial variability and foreshore influence on overtopping. Proc. 29th Int. Conf. Coastal Engineering, Lisbon, Portugal.
- Geeraerts, J., Boone, C. (2004). CLASH: Full Scale Measurements on the Zeebrugge breakwater- Second Winter Season, Ghent University, Belgium.
- Geeraerts, J., Troch, P., De Rouck, J., Willems, M., Franco, L., Bellotti, G., Briganti, R., 2004. Wave overtopping at Ostia yacht harbour breakwater – Comparison between prototype and model tests in 2D and 3D. Proc. 29th Int. Conf. Coastal Engineering, Lisbon, Portugal.

- Gonzalez-Escrivá, J.A.; Garrido, J.; Medina, J.R.; Geeraerts, J., 2004. Laboratory real storm reproduction using wind. Proc. 29th Int. Conf. Coastal Engineering, Lisbon, Portugal.
- Kajima, R., Sakakiyama, T., 1994. Review of works using CRIEPI flume and present work. Coastal Dynamics, Barcelona, Spain, pp. 614-627.
- Kortenhaus, A., Oumeraci, H., Geeraerts, J., De Rouck, J., Medina, J.R., Gonzalez-Escrivera, J.A., 2004a. Laboratory effects and other uncertainties in wave overtopping measurements. Proc. 29th Int. Conf. Coastal Engineering, Lisbon, Portugal.
- Kortenhaus, A., van der Meer, J.W., Burcharth, H., Geeraerts, J., van Gent, M., Pullen, T., 2004b. Final report on scale effects. CLASH WP7-report. LWI, Germany.
- Müller, D.R., 1995. Auflaufen und Überschwappen von Impulswellen an Talsperren. Mitteilungen der Versuchsanstalt für Wasserbau, Hydrologie und Glaziologie der ETH Zürich, Zürich, Switzerland, Band 137, S. 1-201. In German.
- Oumeraci, H., 1999. Strengths and limitations of physical modelling in coastal engineering – synergy effects with numerical modelling and field measurements. Proceedings Hydralab Workshop on Experimental Research and Synergy Effects with Mathematical Models, Evers, K.-U.; Grüne, J.; Van Os, A. (eds.), Hannover, Germany, pp. 7-38.
- Pullen, T., Allsop, N.W.H, Bruce, T., Geeraerts, J., 2003. Violent wave overtopping: Clash Field Measurements at Samphire Hoe. Proc. of Conf. Coastal Structures '03, Portland, USA.
- Pullen, T., Allsop, N.W.H, Bruce, T., Pearson, J. & Geeraerts, J., 2004. Violent wave overtopping at Samphire Hoe: Field and Laboratory Measurements. Proc. 29th Int. Conf. Coastal Engineering, Lisbon, Portugal.
- Schulz, K.-P., 1992. Maßstabeffekte beim Wellenaufwurf auf glatten und rauhen Böschungen. Mitteilungen Leichtweiß-Institut für Wasserbau der Technischen Universität Braunschweig, Heft 120, Braunschweig, Germany. In German.
- Schüttrumpf, H., 2001. Wellenüberlaufströmung bei Seedeichen – experimentelle und theoretische Untersuchungen. Fachbereich Bauingenieurwesen, Technische Universität Braunschweig. Mitteilungen Leichtweiß-Institut für Wasserbau der Technischen Universität, LWI, Braunschweig, Germany, Heft 149, S. 1-124. In German.
- TAW, 2002. [Dutch Technical Advisory Committee on Water Defence] Technisch Rapport Golfoploop en Golfoverslag bij Dijken [Technical Report on Wave Run-up and Wave overtopping at dikes]. In Dutch. 44pp, Delft, The Netherlands.
- Troch, P., Geeraerts, J., Van de Walle, B., De Rouck, J., Van Damme, L., Franco, L., Allsop, W., 2004. Full scale wave overtopping measurements on the Zeebrugge rubble mound breakwater. Coastal Engineering, Elsevier. Vol. 51 / 7 pp. 609-628.
- van der Meer, J.W., van Gent, M., Pozueta, B., Verhaeghe, H., Steendam, G.J., Medina, J.R., 2005. Applications of a neural network to predict wave overtopping at coastal structures. Proc. Int. Conf. on Coastlines, Structures and breakwaters 2005, Institution of Civil Engineers, London, UK.
- Verhaeghe, H., van der Meer, J.W., Steendam, G.J., 2004. Report: database on wave overtopping at coastal structures. CLASH - Crest Level Assessment of Coastal Structures, Workpackage 2.



COMMISSION  
OF THE EUROPEAN  
COMMUNITIES



FP5- EESD

CREST LEVEL ASSESSMENT OF  
COASTAL STRUCTURES BY  
FULL-SCALE MONITORING,  
NEURAL NETWORK PREDICTION  
AND HAZARD ANALYSIS  
ON PERMISSIBLE WAVE OVERTOPPING

# CLASH

EVK3-CT-2001-00058

R  
E  
P  
O  
R  
T

## D46 : Final report

### Full scientific and technical report

February 2005

Prof. Dr. Ir. J. De Rouck  
Ir. J. Geeraerts

Universiteit Gent



## Table of contents

List of tables

List of figures

List of symbols

0	Introduction .....	13
1	WP1 : General methodology .....	19
1.1	Objectives.....	19
1.2	Description of work performed .....	19
1.3	Conclusions / achievements .....	19
2	WP2 : Overtopping database.....	20
2.1	Objectives.....	20
2.2	Description of work performed .....	20
2.3	Conclusions / achievements .....	64
3	WP3 : Full scale measurements .....	65
3.1	Objectives.....	65
3.2	Description of work performed .....	65
3.2.1	Site 1 : Zeebrugge (Belgium).....	65
3.2.2	Site 2 : Ostia (Italy) .....	85
3.2.3	Site 3 : Samphire Hoe (UK).....	100
3.2.4	Site 4 : Petten (The Netherlands) .....	109
	Groyne section measurements.....	113
	ASMIV sea bed staff.....	113
	Wave run-up measurements .....	116
	Low-frequency waves .....	116
	Conclusions .....	117
3.3	General conclusion for WP3 .....	118
4	WP 4 : Laboratory investigation .....	119
4.1	Objectives.....	119
4.2	Description of work performed .....	119
4.2.1	Site 1 : Zeebrugge .....	119
4.2.2	Site 2 : Ostia .....	123
4.2.3	Site 3 : Samphire Hoe.....	128
4.2.4	Additional tests.....	132
4.3	General conclusion for WP4 .....	140
5	WP5 : Numerical modelling.....	141
5.1	Objectives.....	141
5.2	Description of work performed .....	141
5.2.1	Free surface capturing .....	143
5.2.2	Volume of Fluid methods.....	146
5.2.3	Long waves .....	151
5.2.4	Scale Effects.....	154
5.2.5	Shallow water models .....	160

Conclusions .....	162
6 WP 6 : Hazard analysis including socio-economic impacts .....	164
6.1 Objectives.....	164
6.2 Description of work performed .....	164
7.2.1 Background to development on hazard assessment guidance.....	164
7.2.2 Existing Guidance .....	166
7.2.3 New evidence on personnel hazards .....	167
7.2.5 Changing public perceptions.....	170
7.2.6 Awareness of coastal processes.....	171
7.2.7 Post overtopping velocities and loads .....	171
Overtopping velocities .....	171
Post overtopping wave loads on structures .....	173
7.2.9 Valuing overtopping hazards .....	175
Summary of hazard assessment and valuation procedures .....	178
Conclusions .....	179
7 WP 7 : Conclusions on scale effects and new data .....	180
7.1 Objectives.....	180
7.2 Description of work performed .....	180
8.2.1 Samphire Hoe vertical wall.....	180
8.2.2 Zeebrugge rubble mound breakwater.....	181
8.2.3 Ostia rock breakwater.....	182
8.2.4 Method to account for scale effects.....	184
Conclusions .....	194
8 WP 8 : Prediction method .....	195
8.1 Objectives.....	195
8.2 Description of work performed .....	195
Conclusions .....	204
9 WP 9 : Synthesis and formulation of guidelines .....	206
9.1 Objectives.....	206
9.2 Description of work performed .....	206
9.3 Conclusions / achievements .....	206
10 WP 10 : Exploitation and dissemination of the results .....	208
10.1 Objectives.....	208
10.2 Description of work performed .....	208
Conclusions .....	209
11 Acknowledgements .....	210
12 References .....	211

## List of tables

Table 1:	New derived values for $\gamma_f$ (see Pearson et al., 2004b).....	48
Table 2:	Estimated values for $\gamma_f$ based on included overtopping tests .....	49
Table 3:	Values of the complexity factor CF .....	56
Table 4:	Values of the reliability factor RF .....	57
Table 5:	Determination of the reliability factor RF .....	58
Table 6:	Information in the database .....	63
Table 7:	Measurement devices installed at the Zeebrugge rubble mound breakwater.....	68
Table 8:	Storms measured in Zeebrugge .....	74
Table 9:	Wave characteristics, surf similarity parameter and water level for the storms. .	75
Table 10:	Average overtopping rates for all storms, calculated using the 3 methods based on the continuity equation, the individual overtopping volumes and the water depth jumps, respectively with $N_{ov}$ the number of overtopping events. ....	75
Table 11:	Wave characteristics on Oct. 7th, 2003, Dec. 22th, 2003 and Febr. 8th, 2004. ...	81
Table 12:	Total and individual impacts measured by load cells (LC) on dummy2 during resp. storms.....	82
Table 13:	Total and individual impacts measured by load cells (LC) on dummy3 during resp. storms.....	82
Table 14:	Total and individual impacts measured by load cells (LC) on the vertical wall during resp. storms .....	83
Table 15:	Total and individual impacts measured by load cells (LC) on the pipeline during resp. storms .....	83
Table 16:	Dates and duration of the recorded overtopping events at Ostia breakwater.....	91
Table 17:	Ranges of variability of main wave parameters at toe (Ostia-P1) and offshore (Civitavecchia RON buoy) during the overtopping storms.....	93
Table 18:	Maxima values of measured average hourly overtopping rates during each of the 7 storms with corresponding relevant parameters.....	95
Table 19:	Measuring points and equipment at Petten field site.....	112
Table 20:	Roughness factors for breakwaters with slope 1:1.5, with crest berm width of 3Dn with a permeable core / underlayer. Values valid for breakwaters only (not for revetments). ....	137
Table 21:	Material characteristics for the 1/20 Ostia scale model .....	158
Table 22:	Initial Guidance on Tolerable Mean Overtopping Discharges (l/s.m).....	166
Table 23:	Suggested limits for overtopping mean discharges or peak volumes .....	175



## List of figures

Figure 1:	Interconnection diagram.....	18
Figure 2:	Main structure parts of rubble mound structure.....	31
Figure 3:	Typical position of berm, crest and toe.....	33
Figure 4:	Structure type with large toe.....	33
Figure 5:	Structure type with low situated berm.....	33
Figure 6:	Structure type with low situated crest.....	34
Figure 7:	Determination of $h_{\text{deep}}$ [m] and $m$ [-].....	35
Figure 8:	Determination of $h$ [m], $h_t$ [m] and $B_t$ [m].....	36
Figure 9:	Determination of $h$ [m], $h_t$ [m] and $B_t$ [m] in case of no toe.....	37
Figure 10:	Determination of $B$ [m], $B_h$ [m], $\tan\alpha_B$ [-], $h_b$ [m].....	38
Figure 11:	Determination of the transition depth $h_b$ [m] in case of a composite slope.....	39
Figure 12:	Determination of $R_c$ [m], $A_c$ [m] and $G_c$ [m].....	41
Figure 13:	Determination of $G_c$ [m].....	42
Figure 14:	Determination of the structures slope parameters.....	44
Figure 15:	Determination of the structures slope parameters, extra examples.....	45
Figure 16:	Structure type for which at least two slope parameters are requested.....	46
Figure 17:	Schematisation of a composite slope composed of 2 subsequent slopes.....	46
Figure 18:	Schematisation of a composite slope composed of 2 subsequent slopes.....	47
Figure 19:	Distinction between a large (a) and a small (b) recurve wave wall.....	51
Figure 20:	Schematisation of a large recurve wave wall.....	52
Figure 21:	Reduction factor for rough structures, graph (a) and smooth structures, graph (b).....	54
Figure 22:	Influence of a small recurve wave wall on $\gamma_f$ .....	55
Figure 23:	Location of Zeebrugge harbour at the Belgian North Sea Coast.....	66
Figure 24:	Location of the field site at Zeebrugge harbour.....	66
Figure 25:	Plan view with indication of both instrumented cross-sections.....	66
Figure 26:	Bathymetry for two instrumented cross-sections.....	67
Figure 27:	Cross-section of the Zeebrugge rubble mound breakwater at the location of the wave overtopping tank.....	69
Figure 28:	View at the overtopping tank on site.....	70
Figure 29:	Detail of one wavedetector.....	70
Figure 30:	Global view showing four different wave detectors.....	70
Figure 31:	Global view showing three installed instrumented dummies on site.....	71
Figure 32:	Global view showing the instrumented pipeline on site.....	72
Figure 33:	Cross-section showing the section with the measurement jetty. The position of the measurements on the vertical wall is indicated.....	72
Figure 34:	Detail of force transducer for force measurements on vertical wall.....	73
Figure 35:	Velocity meter in front of dummy.....	73
Figure 36:	Velocity meter in front of pipeline.....	73
Figure 37:	Definition figure of three different crest levels taken into account.....	76
Figure 38:	Comparison between measured and predicted average overtopping rates, using van der Meer et al. (1998, left column), Owen (1980, middle column) and Besley (1999, right column) prediction formulae; for crest freeboards $R_{c1}$ (a), $R_{c2}$ (b) and $R_{c3}$ (c).....	77

- Figure 39: Measured and predicted (top (a): van der Meer et al., 1998; bottom (b): Besley (1999)) non-dimensional average overtopping rates and 95 % confidence limits as a function of the non-dimensional crest freeboard for the crest freeboard  $R_{c3}$ , using surface roughness reduction factor  $\gamma_f = 0.51$ . Also indicated are predicted overtopping rates for  $\gamma_f = 0.50$  and  $\gamma_f = 0.55$  ..... 80
- Figure 40: Velocities measured in front of the pipeline on Febr. 8<sup>th</sup> 2004..... 84
- Figure 41: Location map and layout of Rome yacht harbour at Ostia..... 86
- Figure 42: Design cross section of the west breakwater at the overtopping wave tank. ... 87
- Figure 43: Foreshore grid bathymetry at Ostia (Tiber delta) (left panel) and local wave climate from directional wave records in the period 1990-1992 at a depth of -12 m MSL (buoy location in P0). P1, P2 and P3 indicate the points at which SWAN model results were extracted..... 87
- Figure 44: Left panel: Layout of the overtopping measurement station in Rome yacht harbour. The convention for wind and wave angles is also indicated. A local frame of reference has been defined:  $\zeta$  is the normal direction to the tank,  $\eta$  is the tangent direction.  $\Delta\phi_w = \phi_w - \beta_t$  is the relative wind direction being  $\beta_t$  the normal to the tank ( $^\circ$ N) and  $\phi_w$  is the wind direction ( $^\circ$ N),  $\Delta\beta_w = \beta_0 - \beta_t$  is the relative wave direction being  $\beta_w$  the wave direction ( $^\circ$ N). Right panel: aerial photo of the overtopping measurement station (nov 2003)..... 89
- Figure 45: Cross section and photo of the wave overtopping tank operational at Ostia breakwater. .... 90
- Figure 46: Scatter plots of the most important parameters recorded during the 86 overtopping events. Here  $Q^* = \frac{q_{\Delta h}}{\sqrt{gH_{m0}^3}}$ ,  $\xi_0 = \frac{\tan \alpha}{\sqrt{\frac{2\pi H_{m0}}{gT_{m-1,0}^2}}}$ ,  $w$  is the local wind speed,  $\Delta\beta_w$  is local wave direction relative to the normal to breakwater axis.  $H_{m0}$  is the significant wave height at the toe of the structure. .... 94
- Figure 47: Correlation between the mean hourly overtopping rate  $q_{\square h}$  and the maximum overtopping volume  $V_{\max}$  measured in the corresponding hour..... 96
- Figure 48: Comparison between the measured adimensional mean overtopping discharges and those predicted using Van der Meer et al. (1998) for breaking waves using  $\gamma_f = 0.5$  (solid line thick line) together with the 95% confidence.
- $$Q^* = \frac{q_{ov}}{\sqrt{gH_{m0}^3}} \sqrt{\frac{s_0}{\tan \alpha}} \quad \text{and} \quad R^* = \frac{R_c}{H_{m0}} \frac{\sqrt{s_0}}{\tan \alpha} \frac{1}{\gamma_b \gamma_\beta \gamma_v}$$
- Error bars indicate the maximum and the minimum value of mean unit overtopping discharge obtained using the two illustrated methods. .... 97
- Figure 49: Comparison between the measured adimensional mean overtopping discharges and those predicted using Van der Meer et al. (1998) for breaking waves using  $\gamma_f = 0.5$  (solid line thick line) together with the 95% confidence limits (solid thin lines).  $Q^* = \frac{q_{ov}}{\sqrt{gH_{m0}^3}}$  and  $R^* = \frac{R_c}{H_{m0}} \frac{1}{\gamma_\beta}$ . Error bars indicate the maximum and the minimum value of mean unit overtopping discharge obtained using the two illustrated methods..... 98
- Figure 50: Comparison between the measured mean unit overtopping discharges and those predicted using Owen (1980) formula (solid line) and with crest berm correction as proposed by Besley (1999) (dashed line) during six of the seven

measured storms with overtopping  $Q^* = \frac{q_{ov}}{gH_{m0}T_{om}}$  and  $R^* = \frac{R_c}{H_{m0}} \left( \frac{s_{om}}{2\pi} \right)^{0.5}$ . Error

bars indicate the maximum and the minimum value of mean unit overtopping discharge obtained using the two illustrated methods.  $\gamma_f = 0.5$ ..... 99

Figure 51:	Aerial view of Samphire Hoe with the study area in the foreground.....	101
Figure 52:	Section of the Samphire Hoe Seawall.....	102
Figure 53:	Violent wave overtopping at Samphire Hoe (Photograph courtesy of Eurotunnel and the White Cliffs Countryside Project).....	102
Figure 54:	The three tanks in position at Samphire Hoe.....	103
Figure 55:	The predicted overtopping discharges shown varying with the water level ..	105
Figure 56:	Trapezoidal distribution of overtopping discharges.....	107
Figure 57:	Measurements and predictions of overtopping during Storm 02.....	108
Figure 58:	Measurements and predictions of overtopping during Storm 03.....	108
Figure 59:	Location of Petten field site.....	109
Figure 60:	Measuring points at Petten field site (distance and height in metres).....	110
Figure 61:	Groyne section measurements Jarkus section 20,830.....	113
Figure 62:	ASMIV results near MP 6.....	114
Figure 63:	Water level at MP3 during the December 2003 storm.....	114
Figure 64:	Wave height and wave period during the December 2003 storm.....	115
Figure 65:	Spectra (including low frequency energy) calculated for instruments 031, 171 and 066.....	117
Figure 66:	Cross section of the model set-up of the Zeebrugge breakwater in the LWI wave flume.....	120
Figure 67:	Longitudinal cross section of the UPVLC wind and wave test facilities.....	120
Figure 68:	Cross section of the Zeebrugge scale model at UPVLC.....	120
Figure 69:	Zeebrugge model test results (no wind).....	121
Figure 70:	Zeebrugge model test results (influence of wind).....	121
Figure 71:	Cross-section of the complete 2D model set-up in the wave flume (values in cm model).....	125
Figure 72:	Cross-section of the 2D breakwater in the wave flume (values in mm model; elevations in m prototype).....	125
Figure 73:	Position and orientation of the Ostia breakwater in the wave basin for the 3D tests.....	126
Figure 74:	Cross-section with the overtopping tank in the wave basin (values in m model).....	126
Figure 75:	Ostia model test results.....	127
Figure 76:	Test set-up for 2D tests.....	129
Figure 77:	Plan view of the 3D model.....	130
Figure 78:	Samphire Hoe model test results.....	131
Figure 79:	Tested cross-section (dimensions in mm).....	132
Figure 80:	Layout in basin for testing 0° and 10°.....	133
Figure 81:	Layout in basin for testing 25°.....	133
Figure 82:	Layout in basin for testing 45° and 60°.....	134
Figure 83:	Evaluation of proposed direction factor against data from AAU.....	135
Figure 84:	Standard cross section. $H_0$ is the design wave height.....	136
Figure 85:	Tested cross-sections.....	138
Figure 86:	Porous media test: Velocity vectors for the whole domain, showing fully developed flow at the outlet.....	145
Figure 87:	Samphire Hoe: Overview of the test section.....	145

Figure 88:	Samphire Hoe: Computed water surface profiles at 0.5s intervals between $t = 2.0s$ and $t = 4.0s$ .....	146
Figure 89:	Computational domain on a non-uniform Cartesian cut-cell mesh for sea dike problems. WG0 to WG5 indicate the locations of five wave gauges. $l_1=1.0$ m, $l_1 + l_2 + l_3=6.3$ m and $d=0.7$ m. ....	148
Figure 90:	Velocity fields induced by the regular (left) and irregular (right) waves over a sea dike from $t = 32.2$ to $33.4$ s. ....	150
Figure 91:	Wave reflection as function of wave frequency for a selected condition; measured at MP17 on the Petten foreshore. ....	152
Figure 92:	Comparison between measured and computed contribution of low frequency energy. ....	153
Figure 93:	Increase of mean wave overtopping discharge as function of the ratio of low-frequency energy and total energy.....	154
Figure 94:	Computational domain with step porous structure.....	156
Figure 95:	The Darcy-Weisbach friction factor $\lambda$ against Reynolds numbers. ....	157
Figure 96:	Instantaneous dimensionless jet velocities (solid breakwater).....	157
Figure 97:	Free surface configuration of the Ostia breakwater model (scale 1/20), modelled using the VOFbreak <sup>2</sup> code, and showing wave breaking in front of and wave overtopping over the porous breakwater. ....	159
Figure 98:	Simulation results calculated at time 20 s for the 1/20 scale model. ....	159
Figure 99:	Dimensionless discharge ( $Qh$ ) plotted against dimensionless freeboard ( $Rh$ ) for the physical model and the numerical model. ....	161
Figure 100:	Categorisation of overtopping hazards at Samphire Hoe, low, moderate and high .....	168
Figure 101:	Public watching / dodging overtopping at Oostende .....	168
Figure 102:	Beach, seawall and promenade at San Sebastian, Spain .....	169
Figure 103:	Artificial beach, breakwaters and resort at Lanzarote.....	169
Figure 104:	Yacht harbour of Salivoli (Tuscany) during storm in November 2001 .....	169
Figure 105:	West Harbour, Hartlepool, under 1:50 year storm, physical model.....	169
Figure 106:	Extracts from video of overtopping incident at Giant's Causeway, 16 August 2002 .....	170
Figure 107:	Suggested velocity / depth limits from Ramsbottom <i>et al.</i> (2004).....	172
Figure 108:	Wave loads on person dummies (from tests at LWI, see Appendix J) .....	173
Figure 109:	Wave loads on person dummies (from tests at LWI, see Appendix J) .....	174
Figure 110:	Decision tree for choosing valuation techniques.....	177
Figure 111:	Prototype results, 2D and 3D test results with comparison to Besley formula.....	181
Figure 112:	Relative mean overtopping rates from LWI tests plotted against the relative freeboard with comparison to Van der Meer formula and prototype results..	182
Figure 113:	Relative mean overtopping discharges from FCFH (3D) and UGent (2D) tests plotted against the relative freeboard with comparison to Van der Meer formula and prototype results.....	183
Figure 114:	Reduction of wave overtopping due to reduction of wave run-up on the seaward slope for the Zeebrugge storm data .....	186
Figure 115:	Discharge rates and the effect of the transport factor $W_s$ .....	188
Figure 116:	Scaling map for wave overtopping results over coastal structures from small-scale model tests .....	192
Figure 117:	Results of the application of the parameter map for scaling to the test case of Zeebrugge .....	193

Figure 118:	Results of the application of the parameter map for scaling to the test case of Ostia.....	193
Figure 119:	Observations versus NN predictions .....	204

## List of symbols

$A_c$	= height of armour in front of crest element in relation to S.W.L.	[m]
$B$	= berm width, measured horizontally	[m]
$c_i$	= inshore wave celerity	[m/s]
$C_r$	= average reflection coefficient ( $= \sqrt{m_{0,r}} / \sqrt{m_{0,i}}$ )	[%]
CF	= complexity-factor of structure section = 1, 2, 3 or 4	[-]
$h$	= water depth just before the structure (before the structure toe)	[m]
$h_{\text{deep}}$	= water depth in deep water	[m]
$h_t$	= water depth on the toe of the structure	[m]
$h_b$	= berm depth in relation to S.W.L. (negative means berm is above S.W.L.)	[m]
$D_{n50}$	= nominal diameter of rock	[m]
$D_n$	= nominal diameter of concrete armour unit	[m]
$D(f,\theta)$	= directional spreading function, defined as:	[°]
	$S(f, \theta) = S(f) \cdot D(f,\theta) \text{ met } \int_0^{2\pi} D(f,\theta)d\theta = 0$	
$f$	= frequency	[Hz]
$f_p$	= spectral peak frequency i.e. frequency at which $S_n(f)$ is a maximum	[Hz]
$f_b$	= width of a roughness element (perpendicular to dike axis)	[m]
$f_h$	= height of a roughness element	[m]
$f_L$	= centre-to-centre distance between roughness elements	[m]
$g$	= acceleration due to gravity (= 9,81)	[m/s <sup>2</sup> ]
$G_c$	= width of armour in front of crest element	[m]
$H$	= wave height	[m]
$H_{1/x}$	= average of the highest 1/x th of the wave heights derived from time series	[m]
$H_{x\%}$	= wave height exceeded by x% of all wave heights	[m]
$H_s$	= $H_{1/3}$ = significant wave height	[m]
$H_{m0}$	= estimate of significant wave height based on spectrum = $4\sqrt{m_0}$	[m]
$H_{m0,\text{deep}}$	= estimate of significant wave height at deep water	[m]
$H_{m0,\text{toe}}$	= estimate of significant wave height at the toe of the structure	[m]
$k$	= angular wave number (= $2\pi/L$ )	[rad/m]

$L_{\text{berm}}$	= horizontal length between two points on slope, $1.0 H_{m0}$ above and $1.0 H_{m0}$ below middle of the berm	[m]
$L_{\text{slope}}$	= horizontal length between two points on the slope, $Ru_{2\%}$ above and $1.5 H_{m0}$ below S.W.L.	[m]
$L$	= wave length measured in the direction of wave propagation	[m]
$L_{0p}$	= peak wave length in deep water = $gT_p^2/2\pi$	[m]
$L_{0m}$	= mean wave length in deep water = $gT_m^2/2\pi$	[m]
$L_0$	= deep water wave length based on $T_{m-1,0} = gT_{m-1,0}^2/2\pi$	[m]
$m_n$	= $\int_{f_1}^{f_2} f^n S(f) df = n^{\text{th}}$ moment of spectral density	[m <sup>2</sup> /s <sup>n</sup> ]
	lower integration limit = $f_1 = \min(1/3.f_p, 0.05 \text{ full scale})$	
	upper integration limit = $f_2 = 3.f_p$	
$m_{n,x}$	= $n^{\text{th}}$ moment of x spectral density	[m <sup>2</sup> /s <sup>n</sup> ]
	x may be: i for incident spectrum r for reflected spectrum	
$N_{ow}$	= number of overtopping waves	[-]
$N_w$	= number of incident waves	[-]
$P(x)$	= probability distribution function	
$p(x)$	= probability density function	
$P_V$	= $P(\underline{V} \geq V) =$ probability of the overtopping volume $\underline{V}$ being larger or equal to $V$	[-]
$P_{ow}$	= probability of overtopping per wave = $N_{ow}/N_w$	[-]
$q$	= mean overtopping discharge per meter structure width	[m <sup>3</sup> /m/s]
$R_c$	= crest freeboard in relation to S.W.L.	[m]
RF	= reliability-factor of test = 1, 2, 3 or 4	[-]
$Ru$	= run-up level, vertical measured with respect to the S.W.L.	[m]
$Ru_{2\%}$	= run-up level exceeded by 2% of the incident waves	[m]
$s$	= wave steepness = $H/L$	[-]
$s_{0p}$	= wave steepness with $L_0$ , based on $T_p = H_{m0}/L_{0p} = 2\pi H_{m0}/(gT_p^2)$	[-]
$s_{0m}$	= wave steepness with $L_0$ , based on $T_m = H_{m0}/L_{0m} = 2\pi H_{m0}/(gT_m^2)$	[-]
$s_0$	= wave steepness with $L_0$ , based on $T_{m-1,0} = H_{m0}/L_0 = 2\pi H_{m0}/(gT_{m-1,0}^2)$	[-]
$S_{\eta,i}(f)$	= incident spectral density	[m <sup>2</sup> /Hz]
$S_{\eta,r}(f)$	= reflected spectral density	[m <sup>2</sup> /Hz]
$S(f, \theta)$	= directional spectral density	[(m <sup>2</sup> /Hz)/°]

$t$	= variable of time	[s]
$T$	= wave period = $1/f$	[s]
$T_m$	= average wave period (time-domain)	[s]
$T_p$	= spectral peak wave period = $1/f_p$	[s]
$T_{H1/x}$	= average of the periods of the highest $1/x$ th of wave heights	[s]
$T_s$	= $T_{H1/3}$ = significant wave period	[s]
$T_{mi,j}$	= average period calculated from spectral moments, e.g.:	[s]
$T_{m0,1}$	= average period defined by $m_0/m_1$	[s]
$T_{m0,2}$	= average period defined by $\sqrt{m_0/m_2}$	[s]
$T_{m-1,0}$	= average period defined by $m_{-1}/m_0$	[s]
$T_R$	= record length	[s]
$v_z, v_x$	= particle velocities in direction $z$ , and $x$	[m/s]
$V$	= volume of overtopping wave per unit crest width	[m <sup>3</sup> /m]
$\alpha$	= slope angle	[°]
$\alpha_{wall}$	= angle that steep wall makes with horizontal	[°]
$\alpha_{berm}$	= angle that sloping berm makes with horizontal	[°]
$\beta$	= angle of wave attack with respect to the structure alignment (0° is perpendicular to the structure axis)	[°]
$\eta(t)$	= surface elevation with respect to S.W.L.	[m]
$\gamma_b$	= correction factor for a berm	[-]
$\gamma_f$	= correction factor for the roughness of or on the slope	[-]
$\gamma_\beta$	= correction factor for oblique wave attack	[-]
$\gamma_v$	= correction factor for a vertical wall on the slope	[-]
$\xi_0$	= breaker parameter (= $\tan\alpha/s_0^{1/2}$ )	[-]
$\mu_{(x)}$	= mean of measured parameter $x$ with normal distribution	[..]
$\sigma$	= directional spreading	[°]
$\sigma_{(x)}$	= standard deviation of measured parameter $x$ with normal distribution	[..]
$\theta$	= direction of wave propagation	[°]
$\omega$	= angular frequency = $2\pi f$	[rad/s]



## 0 Introduction

The present text is the Full Scientific and technical report of the FP 5 project CLASH: Crest Level Assessment of coastal Structures by full scale monitoring, neural network prediction and Hazard analysis on permissible wave overtopping (EVK3-CT-2001-00058). This report is the final deliverable (D46) of the project and gives an account of the detailed scientific and technical outcome of the project referring to the whole project period (January, 1<sup>st</sup>, 2002 – December, 31<sup>st</sup>, 2004). For each Workpackage (WP), this report describes the work carried out and summarises the most important results and conclusions.

More detailed information on the scientific results and a description of the methodologies on how they are achieved are provided in the WP-related deliverables to which reference is made.

The project consortium was composed as follows:

<b>Partner</b>	<b>Abbreviation</b>	<b>Country</b>
<b>Universiteit Gent</b>	<b>Ugent</b>	<b>BE</b>
<b>Flanders Community Coastal Division</b>	<b>FCCD</b>	<b>BE</b>
<b>Flanders Community Flanders Hydraulics</b>	<b>FCFH</b>	<b>BE</b>
<b>Leichtweiss Institut für Wasserbau</b>	<b>LWI</b>	<b>D</b>
<b>Aalborg University</b>	<b>AAU</b>	<b>DK</b>
<b>Universidad Politécnica de Valencia</b>	<b>UPVLC</b>	<b>E</b>
<b>Modimar</b>	<b>MOD</b>	<b>IT</b>
<b>Delft Hydraulics</b>	<b>DH</b>	<b>NL</b>
<b>Infram</b>	<b>INF</b>	<b>NL</b>
<b>Rijkswaterstaat</b>	<b>RIKZ</b>	<b>NL</b>
<b>Manchester Metropolitan University</b>	<b>MMU</b>	<b>UK</b>
<b>University of Edinburgh</b>	<b>UEDIN</b>	<b>UK</b>
<b>Hydraulic Research Wallingford</b>	<b>HRW</b>	<b>UK</b>

Prof. J. De Rouck (Universiteit Gent) was the CLASH-coordinator.

For more information :

**Prof. dr. ir. J. De Rouck**

**Department of Civil Engineering – Ghent University**

**Technologiepark 904 ; 9052 Zwijnaarde ; Belgium**

**[Julien.Derouck@Ugent.be](mailto:Julien.Derouck@Ugent.be) ; [Nathalie.Rousseau@Ugent.be](mailto:Nathalie.Rousseau@Ugent.be)**

## 0.1 Overall objectives of the project :

The project origins from **two observations** :

- The proven fact that small scale model testing under predicts wave run-up on rough slopes;
- the lacking of generally applicable prediction methods for crest height design or assessment with respect to wave overtopping.

Therefore, the first overall objective of CLASH is to validate the present design methods by full scale monitoring of wave overtopping, small scale laboratory modelling and numerical modelling, and to solve the matter of scale/model effects and possible under predictions.

In order to tackle the problem of suspected scale/model effects, CLASH will pay large attention to full scale monitoring of wave overtopping at four different full scale sites with different structures and subjected to a variety of conditions representative for European coasts (Atlantic Ocean, Mediterranean Sea and North Sea). Two sites (a rubble mound breakwater (Zeebrugge (Belgium)) and a seadike in very shallow water (Petten (the Netherlands))) are already extremely well instrumented for measuring wave characteristics and wave run-up. Extra instrumentation is needed to focus on wave overtopping. Measurements at the Petten field site were focussed on long waves on the shallow foreshore as such long waves can not be reproduced in small scale research. The site located in the United Kingdom, Samphire Hoe (a vertically walled reclamation in moderate water depth) has been equipped with a simple hazard monitoring system. Instrumentation is required to measure more quantitative results of wave heights, wave overtopping volumes and spray. The fourth location, Ostia (Italy), a rubble mound breakwater, will be overtopped every winter and is an ideal location to validate this kind of structure. Instrumentation for wave characteristics and wave overtopping measurements had to be installed.

The full scale measurements of wave overtopping are to be simulated rigorously in various laboratories on a smaller scale in order to investigate scale effects and, if possible, by numerical simulation as such simulations can be done on full scale without scale effects. Each site is modelled in two different laboratories; in order to eliminate effects of different construction, measuring and analysis systems at each laboratory. Most of these tests are done

in wave flumes (2D). However, for both Ostia and Samphire Hoe site 3D modelling in a wave tank are performed too. Parametric tests are carried out in one laboratory per site. Finally, both two and three dimensional additional ‘white spot’ tests are carried out.

Numerical modelling is a helpful tool to solve the problem of scale effects. Actual models were capable of simulating wave breaking, vertical acceleration, the formation of spray, and of calculating detailed fluid behaviour (e.g. throw velocities, volume of water in an overtopping plume, maximum height of the plume and impact pressure on the structure) at prototype scale (without scale effects). Thus, numerical flume codes can be used to help assess scaling effects present in laboratory experiments. There were, however, a number of modelling difficulties that needed to be addressed. Firstly, while most codes included a porosity model, which can be applied to rubble mound breakwaters, these models are isotropic and thus not suited to modelling the air / armour layer. Secondly, as air is entrained by the breaking wave the fluid starts to become compressible – and energy is dissipated. Finally careful calibration of the bed and wall friction coefficients was required for optimised simulation of the wave-structures interaction.

The second overall objective is to make use of the many existing (sometimes site specific) data sets on overtopping and to develop a generally applicable design method. This method is developed to recognise patterns in large data sets, a large number of parameters when there is a lack of physical understanding, or lack of description of the physics of the phenomenon : the method of a neural network. The sophisticated technique of neural network modelling, which is a technique capable of recognizing patterns in large data sets, has proven to be very effective. A general algorithm of a neural network has already been developed. Through the calibration and validation of neural networks a prediction method can be obtained where the relevant parameters are input and the wave overtopping discharge is output.

Many, site specific, investigations have provided an enormous amount of data sets with respect to (mean) wave overtopping discharges (some published as complete reports, others in possession of the partners of CLASH). More than 10000 tests in different databases and for different structures are available. The first action is to gather all this existing data on wave overtopping and to screen the data on consistency in order to get a homogeneous total data set. This comprehensive work is required as it will form the basis of the prediction method. Also “white spots” in the data set are detected and extra tests are performed to fill this gap in

knowledge. The algorithm is trained on the screened data set and will form a first prediction method. After reaching conclusions on scale effects the neural network is corrected and also the full scale measurements and small scale and numerical simulations are added. This will give the final prediction method.

The knowledge on safety limits for overtopping hazards or guidance on acceptable levels of wave overtopping, including spray, has hardly been improved during the last two decades and is very poor. Permissible levels of wave overtopping discharge  $q$  [ $\text{m}^3/\text{s}$  per meter structure]. This may be sufficient for simple flooding studies, but gives insufficient information for the estimation of safety limits for people or for structures and other socio-economic impacts of wave overtopping. At low wave overtopping discharges, the contribution of spray is increasingly important, but there are no methods available to predict spray volumes or travel distances. More guidance is required and is delivered by this project.

The work necessary to meet the overall goals of CLASH is grouped into the following specific objectives :

1. to measure / monitor wave overtopping events at three different locations and for various structure types at full scale and to measure long waves at a fourth site to study their effect on wave overtopping;
2. to gather and screen the enormous amount of data on wave overtopping which is available. The screening of the database will a.o. result in a list of “white spots”;
3. to simulate measured storms and overtopping in small scale facilities and by numerical models in order to investigate and solve the problem of suspected scale effects. Extra tests are foreseen to fill in the “white spots” of the database;
4. to train the algorithm of a neural network to this data set, and later on, include the conclusions on scale effects and the new measurements;
5. to derive / refine limits for safety of pedestrians, car users, ... and limits of overtopping for hazard to buildings and related items, also taking into account the impacts on social and economic life in densely populated areas near the coast;
6. to develop a practical guideline on crest level assessment of coastal structures;
7. to establish communication among partners, with end-users and with the coastal engineering community.

The major innovations provided by CLASH can be summarised as follows :

CLASH intends to solve the problem of suspected scale effects in small scale modelling of overtopping by :

- full scale monitoring and measuring at different sites, including different geometries and circumstances (wave conditions and water depth);
- simulation by small scale and numerical modelling, including required improvements on numerical modelling.

CLASH will develop a generic prediction method for overtopping by :

- use of the enormous amount of existing data on overtopping;
- use of full scale measurements, extra measurements (small scale and numerical);
- incorporating the conclusions on and consequences of possible scale effects in small scale model tests;
- use of a new, but proven, technique of the neural network modelling.

CLASH will perform a hazard analysis, including socio-economic impacts in order to improve guidance on permissible overtopping.

CLASH will produce a guideline on wave overtopping / crest level design by means of a generic prediction tool and guidance on consequences of overtopping and permissible levels of overtopping.

To tackle these objectives, a detailed structure and overall methodology was established. The work to be done was structured in 10 distinct but clearly interrelated workpackages. Fig. 1 shows the interconnection diagram of the project's Workpackages. Each WP is described hereafter, giving for each of them the objectives, a description of the work performed and the conclusions / achievements.

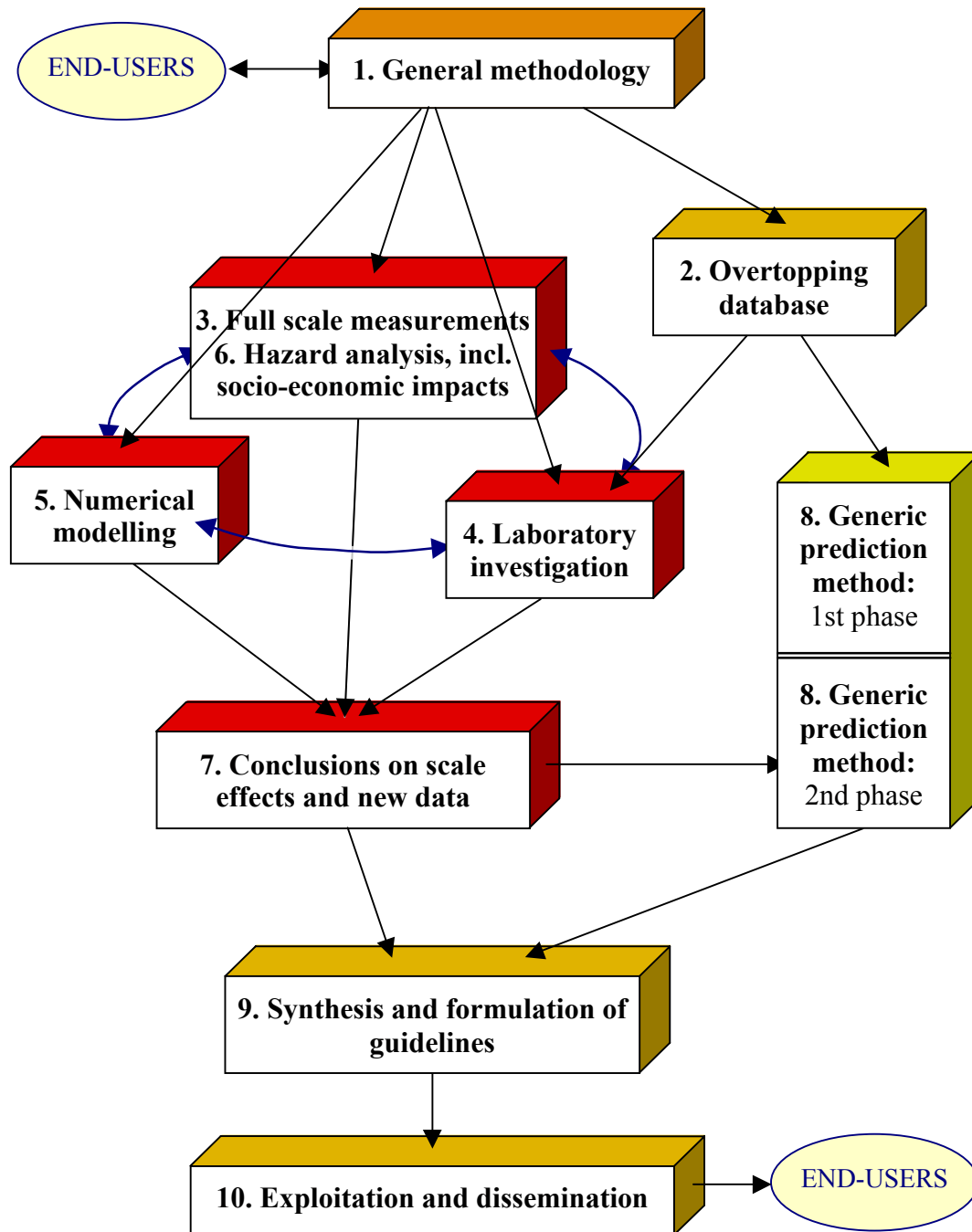


Figure 1: Interconnection diagram.

## **1 WP1 : General methodology**

### **1.1 Objectives**

The principal objectives of WP1 are to outline the overall methodology of the project and to detail the various connected tasks as follows :

- the collection of full scale data is crucial and the installation, measurements and analysis has to be established in detail for each site;
- the inventory of available overtopping data sets and detailed description of what will be required;
- detailing of similarity in the physical model tests and the numerical work.

### **1.2 Description of work performed**

All partners have contributed in setting up a general methodology, which is structured WP by WP and which details the agreements and the work to be carried out within a specific WP. Early in the project a draft report on this general methodology was written and spread amongst partners (Geeraerts & De Rouck, 2002). After one year the optimized version of this methodology report was spread (Boone et al., 2003).

### **1.3 Conclusions / achievements**

The main conclusion of this WP is the General Methodology Report, which provided guidelines to be followed during the whole project.

This workpackage delivered the following reports :

- the general methodology, draft version (D2)
- the report on general methodology (D5)

Additionally one milestone was achieved :

the general methodology for the whole project (M1).

## 2 WP2 : Overtopping database

**Important Note:** Given the very important character of this WP and the importance of the parameters defined in this WP, for good understanding of the further project, this WP is described into more detail within this final CLASH report.

### 2.1 Objectives

The final objective of this task is to create a screened homogeneous data base on wave overtopping tests at coastal structures, based on existing data bases at the possession of partners and elsewhere in Europe and worldwide. This data base is the input for the generic prediction method described in WP 8.

The final intention of the extended database on wave overtopping is dual:

- The objective of the overtopping database on its own is to give an inventory as complete as possible of reliable overtopping tests. It is estimated that more than half of the (reliable) data on overtopping existing in the world, is included in the database. Each overtopping test is included in the database by means of 31 parameters, what should give for each test a brief but complete overall view of the entire test situation with corresponding measured overtopping discharge.
- The more fundamental objective of the creation of an overtopping database is to use it for the development of a neural network method to predict mean overtopping discharges. The creation of a generic prediction method for wave overtopping, applicable for all kind of coastal structures, was a second task of the European CLASH-project (see WP 8).

### 2.2 Description of work performed

#### 2.2.1 *Origin of overtopping data*

During the last 30 years quite a lot of research has been done to overtopping at coastal structures, resulting in a lot of overtopping information available at different universities and



research institutes all over the world. The first phase of composing a database consisted therefore in collecting as much of these present data as possible. As the data were gathered within the CLASH project, a lot of data are originating from CLASH partners, but also data from non-CLASH institutes within Europe as well as from outside Europe contribute to the database. The percentage of data which was received from CLASH partners in the final database is about 80%.

Distinction could be made between publicly available data, often related to basic research and already described in literature, and confidential reports, in most cases related to overtopping tests performed for specific sites and practical situations. The publicly available data take about 75% of the data in the database, the remaining 25% concern confidential data.

During the first phase of the set-up of the database, about 6500 tests were gathered. During the second and last phase, not only about 4000 new overtopping tests were added, but also improvements were made on some parameters of the already existing database, resulting in an extended and improved final database. The 4000 extra overtopping tests added to the preliminary database contain prototype measurements gathered within CLASH (see WP 3), model tests performed within CLASH (see WP 4) and additional tests gathered from outside CLASH.

The improvements made in the final database concern mainly the values of the roughness/permeability factor  $\gamma_f$  (see section 2.2.5.3). As in the first stage of the CLASH project, little was known about the combined effect of roughness and permeability of structure slopes composed of concrete armour blocks, this effect was included in the preliminary database by means of estimated values for  $\gamma_f$ , see Verhaeghe et. al., 2003a. The white spot tests performed in this context, resulted in more precise roughness/permeability factors  $\gamma_f$  for a lot of armour types (see WP 4), replacing the estimated values of  $\gamma_f$  included in the first preliminary database.

Other improvements made on the preliminary database concern slightly adapted ideas on how to schematise special shaped structures, and new, better definitions for some parameters.

### 2.2.2 Methodology for gathering overtopping information

To obtain a complete and reliable overtopping database, detailed information on all overtopping measurements was needed. The reliability of the database was all the more important regarding its fundamental objective: to function as starting point for the development of a neural network prediction method.

From this point of view as much information as possible was gathered for all test series. Not only information about wave characteristics, test structure and corresponding discharge was gathered, but also information concerning the test facility used to perform the tests, the processing of the measurements and the precision of the work performed was looked upon.

For each overtopping test it was tried to answer following questions:

- considering the **wave characteristics**:
  - which were the wave characteristics of the measured or generated storm?
    - regular or irregular waves?
    - long-crested or short-crested waves?
    - characteristic wave heights, characteristic wave periods?
    - incident wave angle?
  
- considering the **test structure**:
  - what kind of structure was tested? (E.g. vertical wall? sloping structure?...)
  - which were the geometrical parameters of the structure?
  - which materials were used to construct the test section?
  - what was the exact foreshore?
  
- considering the measured **overtopping**:
  - what exactly was measured?
    - overtopping volume and/or percentage of waves overtopping?
  - how was overtopping volume measured?
    - by measuring increase of water level or weight of overtopping water?
  
- considering the **test facility** in which the tests were performed (not applicable for prototype tests):

- which test facility was used?
  - a wave basin or a wave flume? (3D or 2D tests?)
  - possibilities/restrictions of wave generation system?
- was reflection compensation performed during testing?
  - active or passive wave absorption?
- which model scale was used?
- considering the **processing** of the measurements:
  - did the researcher perform time domain analysis and/or spectral domain analysis?
  - did the researcher perform reflection analysis?
    - separation of incident and reflected waves or only determination of total waves?
  - how did the researchers measure incident waves?
    - calibration of the test facility (before construction of the structure) at the location of the structure, measurement of waves at the toe of the structure during testing or only measurement of waves at deep water?

Depending on the answers to these questions, each test could be assessed on reliability and complexity. This was taken into account in the database by defining for each test a Reliability Factor RF and a Complexity Factor CF, being a measure for reliability of the performed test and the complexity of the overtopping structure respectively. More detailed information on these two factors is given in section 2.2.6.

### 2.2.3 *Parameters in the database*

In view of using the overtopping database for the development of a neural network prediction method, each test had to be characterised by a fixed number of parameters. These parameters had to be chosen in such a way that an overall view as complete as possible of the overtopping test is achieved by these parameters. This implies inclusion of attacking wave characteristics, test structure properties, the measured overtopping result, but also the reliability of the measurements and the complexity of the structure should be represented.

At the same time it was tried to limit the number of parameters. Preference for simplicity over needless complexity can be mentioned here, given the fact that a neural network only can act well if the number of input parameters is restricted. This restriction does not depend only on

the number of tests which are available for the development of the neural network, but also the distribution of the tests within the available parameter ranges is important.

However at the moment of the set-up of the database, the precise parameters influencing the overtopping phenomenon were not known. During the development process of the neural network, the network revealed which of the parameters included in the database were significant in characterising the overtopping phenomenon. This implies that not all parameters in the overtopping database are equally relevant for the neural network prediction method.

Ultimately three groups of parameters were defined: general parameters, structural parameters and hydraulic parameters. The general parameters are related to general information about the overtopping test, the structural parameters serve to describe the test structure and the hydraulic parameters are describing the wave characteristics and the measured overtopping.

Two possible approaches can be distinguished regarding the wave characteristics describing the overtopping phenomenon. In a first approach the measured overtopping is linked to the waves measured at the toe of the structure, just before they attack the structure. The second approach considers only the deep water wave characteristics to link to the overtopping discharge. In this last case, the slope of the foreshore is an additional influencing parameter.

Both approaches appear in literature, although the most recent overtopping formulae recommend to use the wave characteristics at the toe of the structure. As one of the goals of the overtopping database is to provide detailed information on existing overtopping measurements, and to leave open the possibility to use either the wave characteristics at deep water or at the toe of the structure, the wave characteristics at both locations are included in the database. Additionally a parameter describing the slope of the foreshore is introduced.

The ultimate number of parameters included in the final database is 31. The parameters are enumerated below by group, together with a brief description. More detailed information follows in sections 2.2.4 (hydraulic parameters), 2.2.5 (structural parameters) and 2.2.6 (general parameters).

- 3 general parameters:

“Name”, “RF” and “CF”

1	Name	This parameter assigns a unique name to each test.
2	RF [-]	The ‘Reliability Factor’ gives an indication of the reliability of the test. It can adopt the values 1, 2, 3 or 4.
3	CF [-]	This parameter, called the ‘Complexity Factor’ gives an indication of the complexity of the test structure. It can adopt the values 1, 2, 3 or 4.

- 11 hydraulic parameters:

“ $H_{m0 \text{ deep}}$ ”, “ $T_p \text{ deep}$ ”, “ $T_m \text{ deep}$ ”, “ $T_{m-1,0 \text{ deep}}$ ”, “ $\beta$ ”, “ $H_{m0 \text{ toe}}$ ”, “ $T_p \text{ toe}$ ”, “ $T_m \text{ toe}$ ”, “ $T_{m-1,0 \text{ toe}}$ ”, “ $q$ ” and “ $P_{ow}$ ”

1	$H_{m0 \text{ deep}}$ [m]	Significant wave height from spectral analysis = $4\sqrt{m_0}$ , determined at deep water
2	$T_p \text{ deep}$ [s]	Peak period from spectral analysis at deep water
3	$T_m \text{ deep}$ [s]	Mean period either from spectral analysis = $m_2/m_0$ or from time domain analysis (zero-downcrossing) at deep water
4	$T_{m-1,0 \text{ deep}}$ [s]	Mean period from spectral analysis at deep water = $m_{-1}/m_0$
5	$\beta$ [°]	Angle of wave attack relative to the normal on the structure
6	$H_{m0 \text{ toe}}$ [m]	Significant wave height from spectral analysis = $4\sqrt{m_0}$ at the toe of the structure
7	$T_p \text{ toe}$ [s]	Peak period from spectral analysis at the toe of the structure
8	$T_m \text{ toe}$ [s]	Mean period either from spectral analysis = $m_2/m_0$ or from time domain analysis (zero-downcrossing) at the toe of the structure

9	$T_{m-1,0 \text{ toe}}$ [s]	Mean period from spectral analysis at the toe of the structure = $m_1/m_0$
10	$q$ [ $m^3/s.m$ ]	Overtopping discharge (volume per second) per meter width
11	$P_{ow}$ [-]	Percentage of the waves resulting in overtopping

- 17 structural parameters:

“ $h_{\text{deep}}$ “, “ $m$ “, “ $h$ “, “ $h_t$ “, “ $B_t$ “, “ $\gamma_f$ “, “ $\cot\alpha_d$ “, “ $\cot\alpha_u$ “, “ $\cot\alpha_{\text{excl}}$ “, “ $\cot\alpha_{\text{incl}}$ “, “ $R_c$ “, “ $B$ “, “ $h_b$ “, “ $\tan\alpha_B$ “, “ $B_h$ “, “ $A_c$ “ and “ $G_c$ “

1	$h_{\text{deep}}$ [m]	Water depth at deep water
2	$m$ [-]	Slope of the foreshore
3	$h$ [m]	Water depth just seaward of the toe of the structure
4	$h_t$ [m]	Water depth on the toe of the structure
5	$B_t$ [m]	Width of the toe of the structure
6	$\gamma_f$ [-]	Roughness/permeability factor for the structure
7	$\cot\alpha_d$ [-]	Cotangent of the structure slope downward of the berm
8	$\cot\alpha_u$ [-]	Cotangent of the structure slope upward of the berm
9	$\cot\alpha_{\text{excl}}$ [-]	Mean cotangent of the structure slope, without contribution of the berm
10	$\cot\alpha_{\text{incl}}$ [-]	Mean cotangent of the structure slope, with contribution of the berm
11	$R_c$ [m]	Crest freeboard of the structure
12	$B$ [m]	Width of the berm
13	$h_b$ [m]	Water depth on the berm
14	$\tan\alpha_B$ [-]	Tangent of the slope of the berm
15	$B_h$ [m]	Width of the horizontally schematised berm
16	$A_c$ [m]	Armour crest freeboard of the structure
17	$G_c$ [m]	Width of the structure crest

### 2.2.4 Determination of the hydraulic parameters

The wave characteristics and the measured overtopping are described by means of 11 hydraulic parameters, which are mentioned in the previous section.

Often several of these parameters were not available in the corresponding report of the test, simply because they were not measured or at least not written down during performing the test. In this context the following cases could be distinguished:

- only deep water wave characteristics were available, wave characteristics at the toe of the structure were missing
- only wave characteristics at the toe of the structure were available, deep water wave characteristics were missing
- only time domain analysis was performed to determine the wave characteristics
- only one or two of the three spectral wave periods at deep or shallow water were available
- the percentage of waves resulting in overtopping  $P_{ow}$  [-] was not measured

With the aim of obtaining an as complete database as possible, it was tried to find an acceptable value for these missing parameters where possible. Well-founded assumptions based on previous research and extra calculations were used to do this. Following sections describe these in detail. However, in some cases it was simply not possible to estimate missing hydraulic parameters accurately. Preference was given to leave the value of the missing parameter blank in the database in these cases. An example here concerns the value of  $P_{ow}$  [-], i.e. the percentage of waves overtopping. In most cases the percentage of waves overtopping was not measured during testing. As this parameter represents an overtopping result, additional to the mean overtopping discharge, it can not be estimated if not measured, leading to a blank value in the database if not available. Other cases leading to blank values in the database are treated in section 2.2.4.2.

The described calculations and estimations in sections 2.2.4.1 to 2.2.4.3 all led to approximate values for some of the wave characteristics. As this consequently had an influence on the reliability of the values, this fact was incorporated in the database by adapting the value of the reliability factor RF. If any calculations or estimations were needed, a minimum value of 2 was assigned to the factor RF. What exactly the value of RF stands for and how exactly the

influence of calculations and estimations was included, is explained in section 2.2.6.3 in detail.

To distinguish calculated/estimated parameters from measured parameters in the database, estimated/calculated values are marked with specific colours in the database, depending on the type of calculation/estimation. More information on this is given in section 2.2.7.

#### **2.2.4.1 Calculation of incident wave characteristics from given deep water wave characteristics and foreshore**

For a part of the gathered overtopping tests, wave characteristics were only available at deep water, wave characteristics at the toe of the structure were missing.

In these cases numerical simulations with the SWAN model were made: starting from the deep water wave characteristics and the present foreshore, the wave characteristics at the toe of the structure were calculated.

The version of SWAN which was used in this study is SWAN Cycle III version 40.11 (last revision October 19, 2000). The one-dimensional version of SWAN is used.

#### **2.2.4.2 Estimation of characteristic wave parameters in relatively deep water**

If characteristic wave parameters were missing, commonly used fixed relationships between wave parameters are used to approximate them.

As for double peaked or bi-model spectra, the value of the peak period  $T_p$  is irrelevant, corresponding overtopping tests have no value for  $T_p$ . In these cases the value of  $T_p$  is left blank in the database.

During part of the overtopping tests the wave characteristics were only measured at the toe of the structure and not in deep water. In case of relatively deep water at the toe of the structure, it was assumed that wave characteristics in deep water were the same as at the toe. When the water depth at the toe was rather shallow on the contrary, wave breaking was likely to appear, implicating that the spectral shape of the wave characteristics probably changed drastically compared to at deep water. In these cases the deep water wave characteristics ( $H_{m0 \text{ deep}}$ ,  $T_{p \text{ deep}}$ ,  $T_{m \text{ deep}}$  and  $T_{m-1,0 \text{ deep}}$ ) were also left blank in the database.



### 2.2.4.3 Determination of $H_{m0\ toe}$ from $H_{s\ toe}$ in shallow water depths

As wave height distributions in shallow water deviate from those in deep water due to the effects of the restricted depth-to-height ratio, the Rayleigh distribution is no longer valid and the known relationships between deep water wave heights can no longer be used.

In case of overtopping tests with rather shallow water depth at the toe of the structure the method of Battjes and Groenendijk (2000) can be used to determine the value of  $H_{m0\ toe}$  starting from  $H_{s\ toe}$ .

The input parameters for the point model are the given value  $H_{1/3\ toe}$ , the slope of the foreshore 1:m and the water depth  $h$  at the toe of the structure, leading to the corresponding value of  $H_{m0\ toe}$ .

This method allows us to determine a good approximation of the significant wave height at the toe of the structure in case of shallow water depths, on condition that the foreshore slope can be approximated by a uniform slope 1:m.

Table 3.7 (section 2.2.6.3) describes in detail how the value of the reliability factor RF was determined if calculations according to Battjes and Groenendijk (2000) were made.

### 2.2.5 *Determination of the structural parameters*

The starting-point for the determination of the structural parameters was the fact that as much overtopping structures as possible had to be schematised by these and only these parameters. Studying a lot of different overtopping sections, this finally led to the 17 structural parameters as described in section 2.2.3.

In this section, a detailed description is given of the methodology which was followed for determining these 17 parameters for all included overtopping tests in the database. As some values of parameters are approximations of the real situation, it is very important for the user of database to know exactly what value of which parameter stands for what structure part.

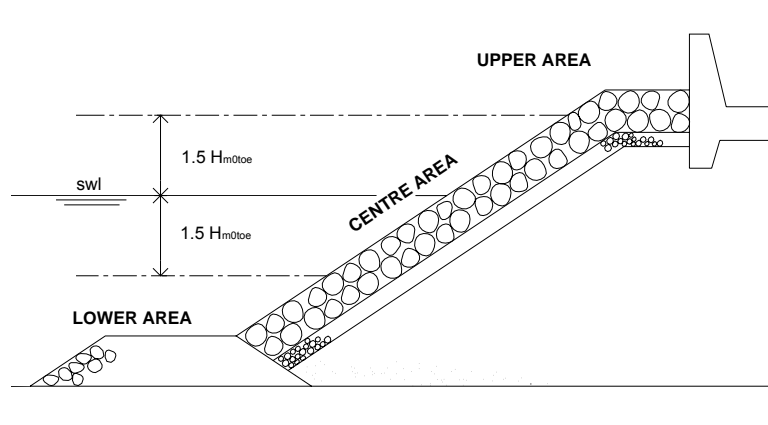
### 2.2.5.1 General schematisation of the structure in three areas

The first schematisation step of each overtopping structure consists of splitting up the structure into three main parts. The starting point here are the waves which attack the structure, as it is important to schematise the structures in the way the attacking waves ‘feel’ the structure. This implies that a geometrically identical structure can have a different schematisation depending on the water level and the attacking waves.

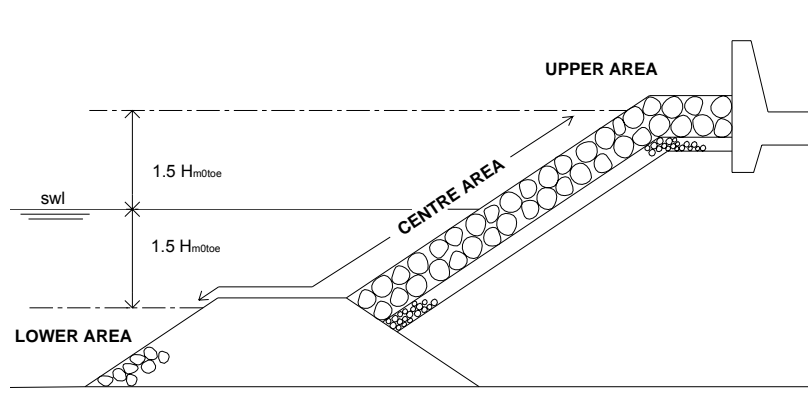
It is logical that the structure part around the swl is very important for the waves. According to the size of the waves, this area will be larger or smaller. Referring to Van der Meer et. al. (1998), the governing part of the structure where the wave action is concentrated on, is defined as the part between  $1.5H_{m0toe}$  above and  $1.5H_{m0toe}$  below the water line.

The area marked off by the value of  $1.5H_{m0toe}$  above and  $1.5H_{m0toe}$  below swl will be called the ‘**centre area**’ of the structure. The area below the centre area is called then the ‘**lower area**’ of the structure and the area above the centre area is called the ‘**upper area**’ of the structure. Depending on the wave height and the water level, the upper or lower area may be lacking.

Fig. 2 gives an example of the structure parts of a rubble mound structure. As can be seen in the example in Fig. 2, depending on the wave height and the water depth near the structure, the centre area can extend the structure slope only (a), but it can e.g. also enclose part of the toe structure (b). Logically lots of other possibilities can occur.



(a)



(b)

**Figure 2: Main structure parts of rubble mound structure**

### 2.2.5.2 Berm, toe and crest of a structure

Looking at structure sections of coastal structures in general (although in the context of this overtopping study), one can often distinguish:

- a structure body (consisting of a vertical wall, a sloping part or a combination of both), possibly containing a structure berm,
- a structure toe (meant to structurally protect the lower part of the structure), and
- a structure crest (often with a strengthening function for the upper part of the structure).

For the schematisation of a structure section, it was needed to clearly distinguish these three structure parts. In a lot of cases this distinction was quite straight forward. However in some

cases confusion could arise. This section examines in detail how the distinction between a berm, a toe and a crest was performed in the context of the set-up of the overtopping database. Fig. 3 to 6 are illustrations of this. The figures are discussed further in the text one for one.

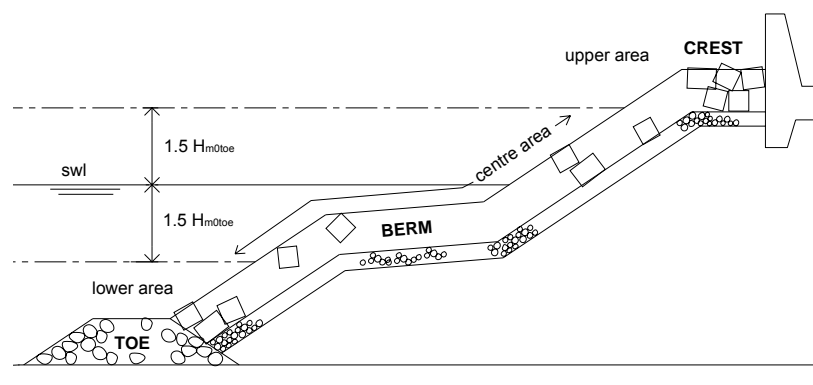
It was defined that a structure berm is most likely situated in the centre area of the structure (= area between  $1.5H_{m0\ toe}$  above and  $1.5H_{m0\ toe}$  below swl, see previous section). If the ‘berm’ (‘berm’ refers here to the name assigned to it in the corresponding report) is situated lower, it is more likely to be felt by the waves as a toe. If the ‘berm’ is situated higher, it is more likely to be felt as a crest. In connection with the position of the berm, a toe is defined as most likely to appear in the lower area of the structure (= lower than  $1.5H_{m0\ toe}$  below swl) and a crest in the upper area of the structure (= higher than  $1.5H_{m0\ toe}$  above swl).

Consequently it may happen that what is called a ‘berm’ in the original report, is called a ‘toe’ or ‘crest’ for the database, although the above described levels of toe, berm and crest are not totally binding, i.e.:

- tests with very small values of  $H_{m0\ toe}$ , leading to a very restricted centre area, are often schematised with a berm which is not situated in the centre area of the structure
- structure types with quite large toes, situated in relatively shallow water, can be schematised with a toe situated in the centre area of the structure
- low crested structures of which the upper point of the structure has a level within  $1.5H_{m0\ toe}$  above swl, are schematised with a crest situated in the centre area of the structure.

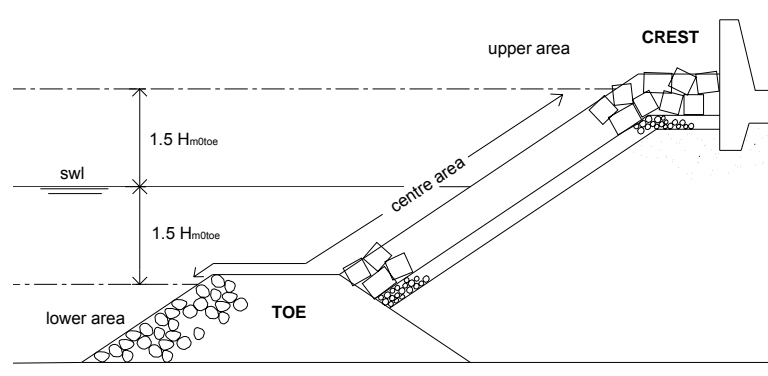
Above mentioned examples can be referred to as structures which do not fulfil the most likely position of a berm.

In Fig. 3 a typical rubble mound structure is shown. The centre area, defined by the value of the wave height  $H_{m0\ toe}$ , contains a slightly sloping berm. The crest is situated in the upper area, the toe is situated in the lower area. This example corresponds with the most common position of the mentioned three structure parts.



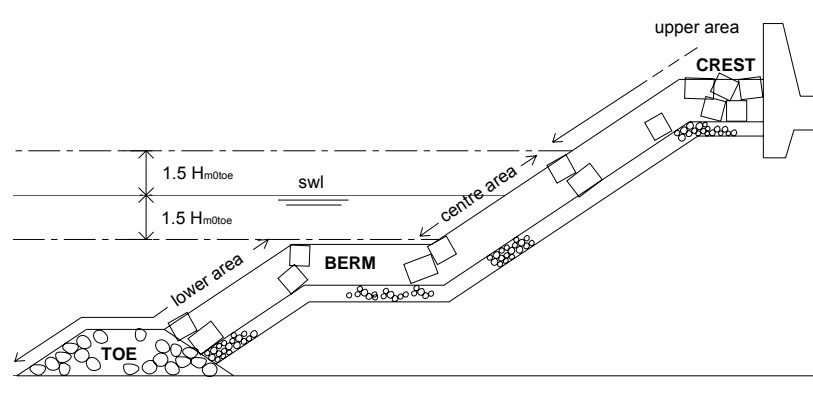
**Figure 3: Typical position of berm, crest and toe**

Fig. 4 gives an example of a structure with a high situated toe. The different structure materials contribute to the preference of schematising the lower part of the structure here as a large toe and not a berm.



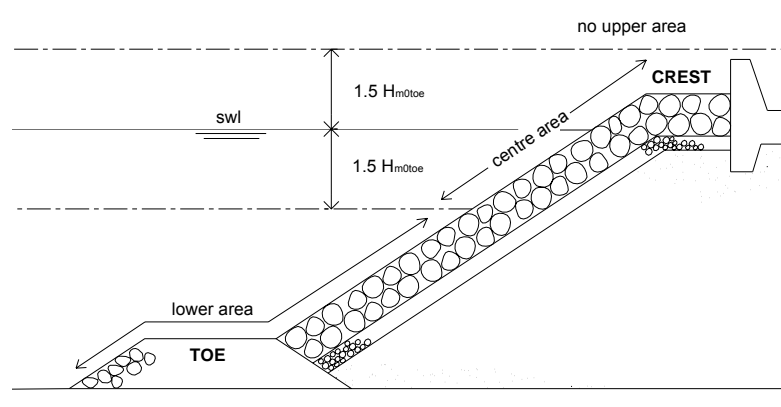
**Figure 4: Structure type with large toe**

Fig. 5 shows a structure for which the small value of  $H_{m0\text{ toe}}$ , leads to a situation in which the berm is situated in the lower part of the structure. It is quite logic in this case that it concerns a berm here and not a toe.



**Figure 5: Structure type with low situated berm**

In Fig. 6 at last an example is given of a structure with a low situated crest. Because of the high water level, the entire structure is situated lower than the  $1.5H_{m0\text{ toe}}$ -line above swl.



**Figure 6: Structure type with low situated crest**

It may be clear that it is not always straight-forward how to schematise a horizontal or slightly sloping part of a structure. In some cases more than one schematisation possibility exists.

Additional to the levels of the berm, crest and toe of a structure, some restrictions regarding the slope and the length of a berm are made in the schematisation for the database.

### 2.2.5.3 Determination of structural parameters

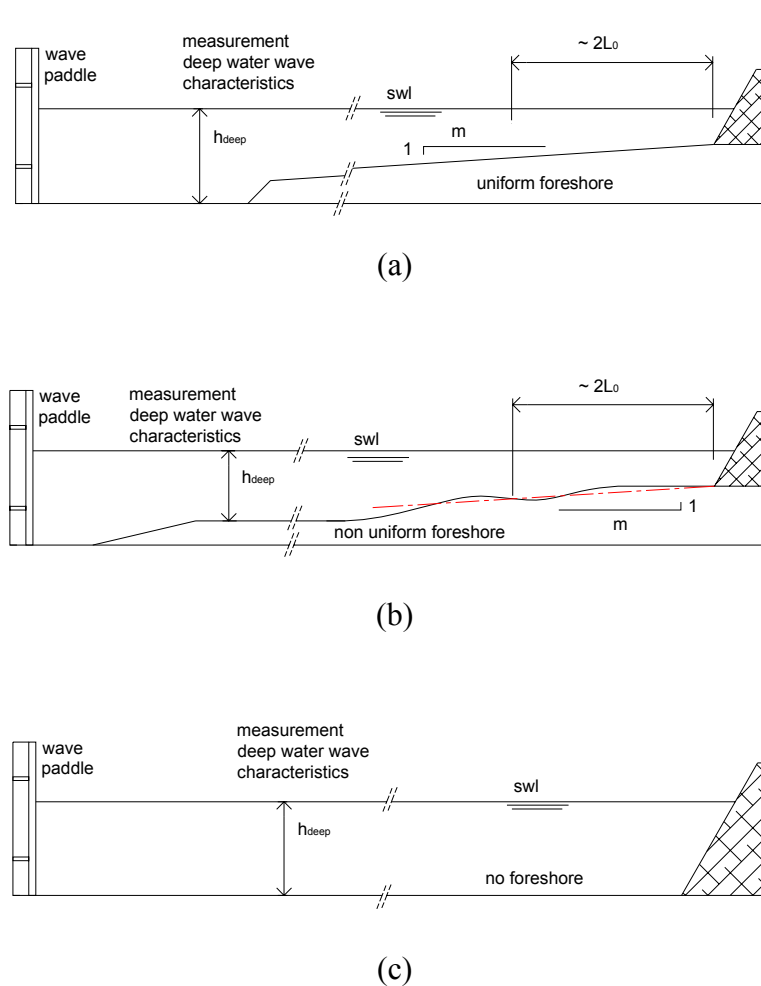
This section explains how to determine the schematisation parameters for a rather easy-to-schematise overtopping structure. In section 3.6.5 the schematisation of more complex sections is treated.

The 17 schematisation parameters are subsequently enumerated below with a detailed explanation how to determine them.

#### 2.2.5.3.1 Water depth at deep(er) water: $h_{\text{deep}}$ [m]

This is the water depth at deep(er) water. At this water depth the deep wave characteristics  $H_{m0\text{ deep}}$ ,  $T_{p\text{ deep}}$ ,  $T_{m\text{ deep}}$  and  $T_{m-1,0\text{ deep}}$  are present. This definition indicates that for laboratory tests,  $h_{\text{deep}}$  is not necessarily the deepest water depth which appears in the flume or basin. Depending on the location of the wave gauges, the value of  $h_{\text{deep}}$  is situated between the water depth at the toe of the structure and the deepest water depth in the flume. In Fig. 7 some

possibilities of measurement locations of  $h_{\text{deep}}$  are given. In the first graph (a), the deep water depth corresponds to the water depth in front of the wave paddle of the flume. In graph (b) an intermediate water depth is taken as the value for  $h_{\text{deep}}$  and finally graph (c) considers the special case in which no foreshore is present, resulting in a water depth  $h_{\text{deep}}$  equal to the water depth just in front of the structure.



**Figure 7: Determination of  $h_{\text{deep}}$  [m] and  $m$  [-]**

#### 2.2.5.3.2 Slope of the foreshore: $m$ [-]

The slope of the foreshore is described by the parameter  $m$  [-] by means of 1 (unit measured vertically) :  $m$  (units measured horizontally). If no uniform sloping foreshore exists, one has to approximate the value of  $m$ . A relevant approximation consists of the mean value of  $m$  over a horizontal distance of about 2 wave lengths  $L_{0p}$  in front of the structure. The restriction of the approximation to the foreshore just in front of the structure can be justified as this part is qualifying for the incident wave characteristics.

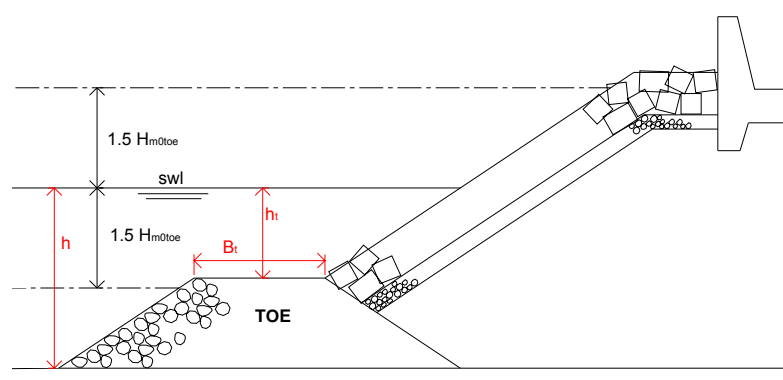
In Fig. 7 the values of  $m$  are indicated. Graph (c) is a special case with a flat bottom of the flume. Theoretically the value of  $m$  should be equal to infinite in such cases, but as a real, finite value is more workable, a value of 1000 was given to  $m$  in the database in these cases.

#### 2.2.5.3.3 Waterdepth in front of the toe: $h$ [m]

The value of  $h$  [m] refers to the water depth just seaward of the toe of the structure (Fig. 8). It is often referred to as the water depth ‘at the toe of the structure’. In case of a flat flume bottom, the value of  $h$  is equal to the value of  $h_{\text{deep}}$ .

#### 2.2.5.3.4 Toe paramers: $h_t$ [m], $B_t$ [m]

These are the water depth on the toe respectively the width of the toe. The value of  $h_t$  [m] is measured in the middle of the toe. The value of  $B_t$  [m] is measured on top of the toe. This is illustrated in Fig. 8.

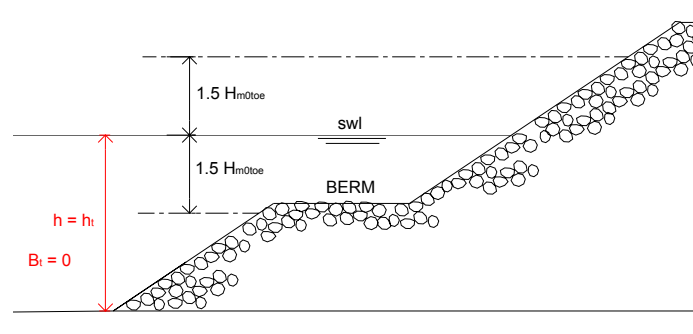


**Figure 8: Determination of  $h$  [m] ,  $h_t$  [m] and  $B_t$  [m]**

It has to be mentioned that the front slope of the toe is not included in the database, because it seems a less important parameter in view of the overall low position of the toe regarding to the water level. Moreover the front slope of a structure toe is in most cases  $\approx 1:2$ . An extra restriction for the definition of a toe could therefore be that the slope should be  $\approx 1:2$ .

If the structure has no toe, the value of the water depth on the toe  $h_t$  equals the value of the water depth at the toe of the structure  $h$ . In this case the width of the toe  $B_t$  is equal to zero, e.g. Fig. 9.





**Figure 9: Determination of  $h$  [m] ,  $h_t$  [m] and  $B_t$  [m] in case of no toe**

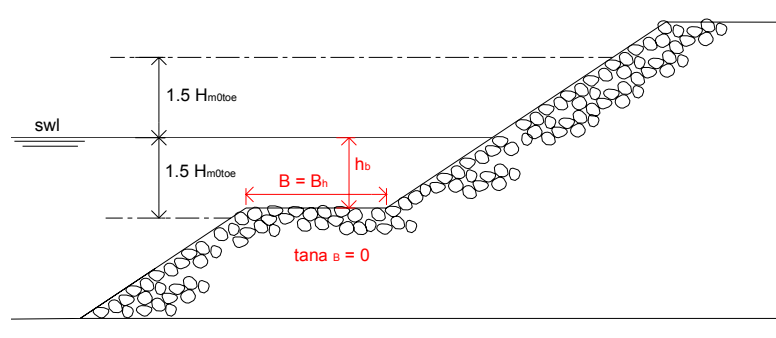
#### 2.2.5.3.5 Berm parameters $B$ [m], $h_b$ [m], $\tan\alpha_B$ [-], $B_h$ [m]

These four parameters describe the berm of an overtopping structure (Fig.10). The value of  $B$  [m] represents the berm width and is measured horizontally.  $h_b$  [m] is the water depth on the berm, measured in the middle of the berm. If the berm is situated above swl, the value of  $h_b$  is negative.

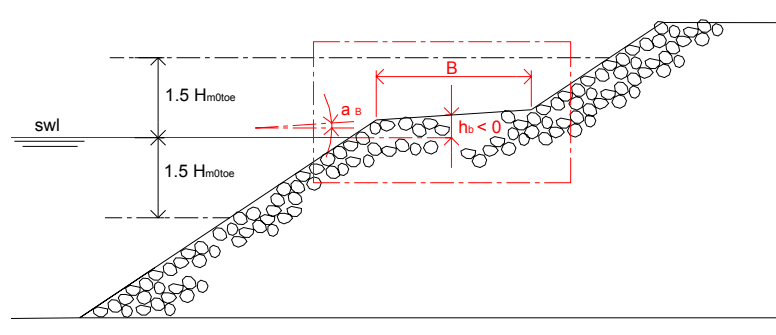
$\tan\alpha_B$  [-] is the tangent of the slope of the berm. If the berm is horizontal,  $\tan\alpha_B = 0$ .

The value of  $B_h$  [m] refers to the width of the horizontally schematised berm. In case of a horizontal berm (i.e.  $\tan\alpha_B = 0$ ) the value of  $B_h = B$ , but for a sloping berm,  $B_h < B$ . The value of  $B_h$  can be obtained by extending the upper and lower slope of the structure up to the level of the middle point of the berm. By connecting these two points, the horizontal schematisation of the berm is obtained.

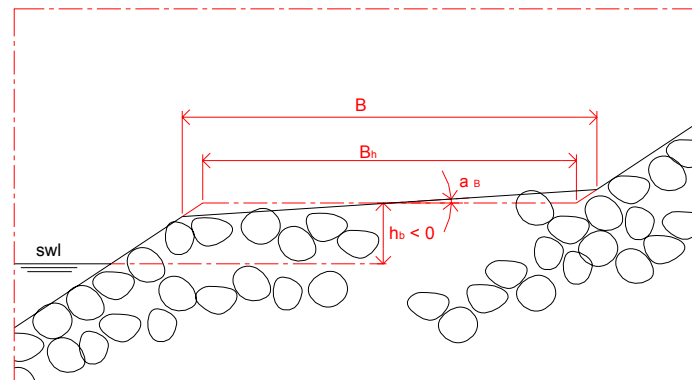
Fig. 10 (c) consists of the enlarged box of Fig. 10 (b), explaining the difference between  $B_h$  and  $B$ .



(a)



(b)



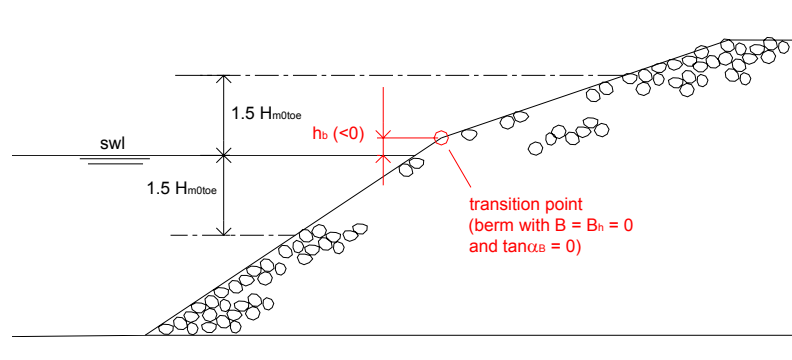
(c)

**Figure 10: Determination of  $B$  [m],  $B_h$  [m],  $\tan \alpha_B$  [-],  $h_b$  [m]**

If the structure has no berm, the values of  $B$ ,  $B_h$ ,  $\tan \alpha_B$ ,  $h_b$  are all equal to zero, except in case of a composite slope.

In case of a composite slope,  $h_b$  is defined as the transition depth between two successive slopes. Although no berm is present in this case, the value of  $h_b$  is different from zero. Defining  $h_b$  as the transition depth between two successive slopes, amounts to defining a berm

at this location with a berm width and slope equal to zero (Fig. 11). How the slopes of the composite slope are schematised is described in section 2.6.3.7.



**Figure 11: Determination of the transition depth  $h_b$  [m] in case of a composite slope**

#### 2.2.5.3.6 Crest parameters: $R_c$ [m], $A_c$ [m], $G_c$ [m]

These parameters describe the upper part of an overtopping structure (Fig. 12).

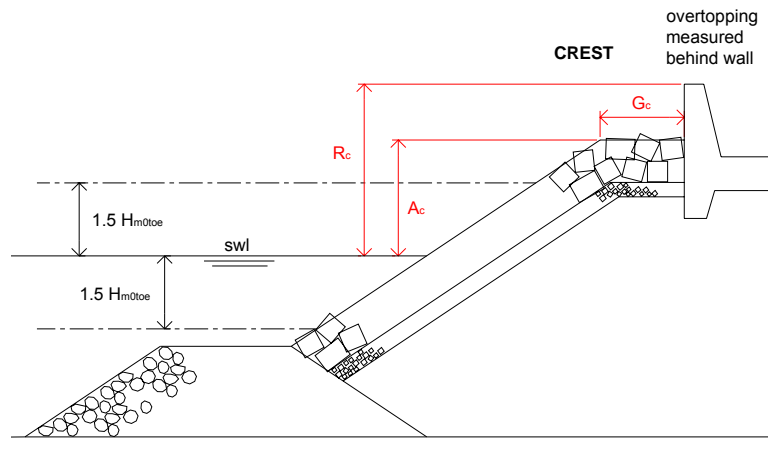
$R_c$  [m] is the crest freeboard of the structure. It is the distance, measured vertically, from swl to the point of the structure where overtopping is measured. This is not always the highest point of the structure, e.g. Fig. 12 (c).

$A_c$  [m] is called the armour crest freeboard of the structure. In case of armoured structures it is the distance, measured vertically from swl to the upper limit of the armour layer. In case of structures without armour, e.g. vertical structures or smooth slopes,  $A_c$  may be used together with  $R_c$  and  $G_c$ , to describe the crest of the structure more detailed, e.g. Fig. 12 (e).

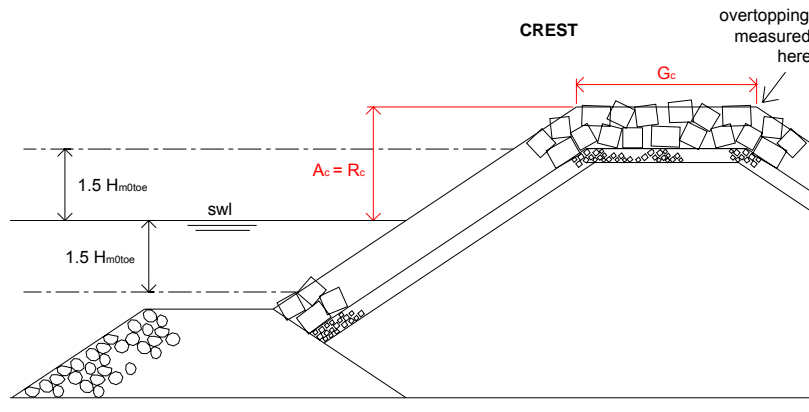
In a lot of cases,  $A_c = R_c$ .

$G_c$  [m] represents the crest width.

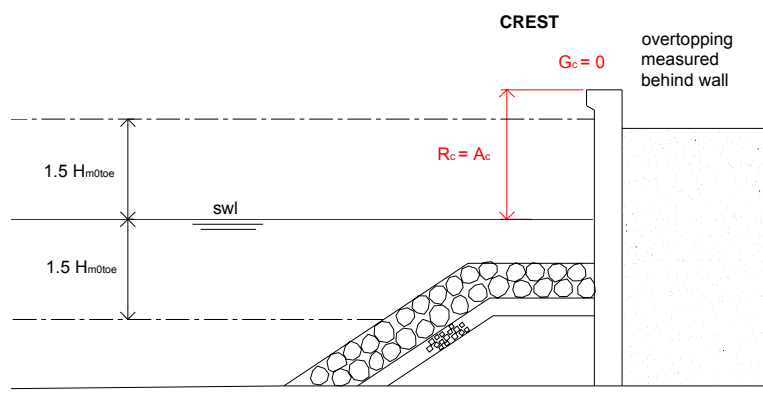
Fig. 12 gives several examples of crest structures with an indication of the corresponding parameters. As can be seen on the different figures,  $R_c$  can adopt a value larger, smaller or equal to  $A_c$ .



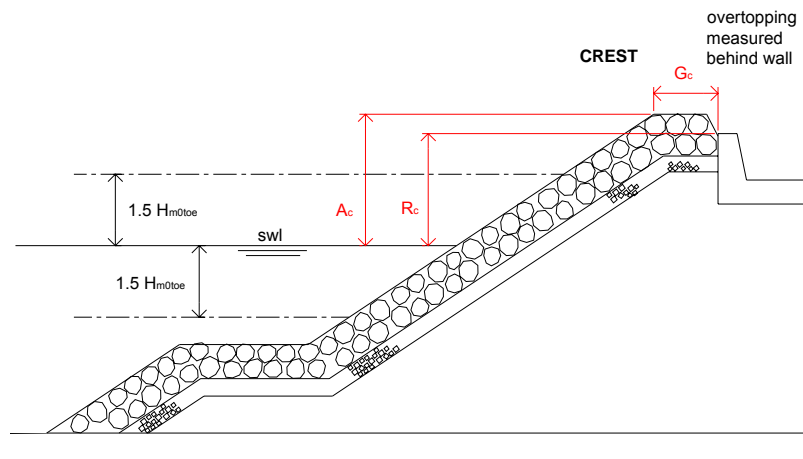
(a)



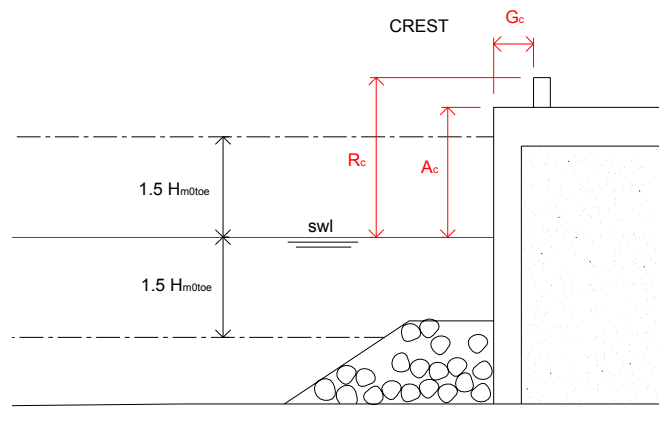
(b)



(c)



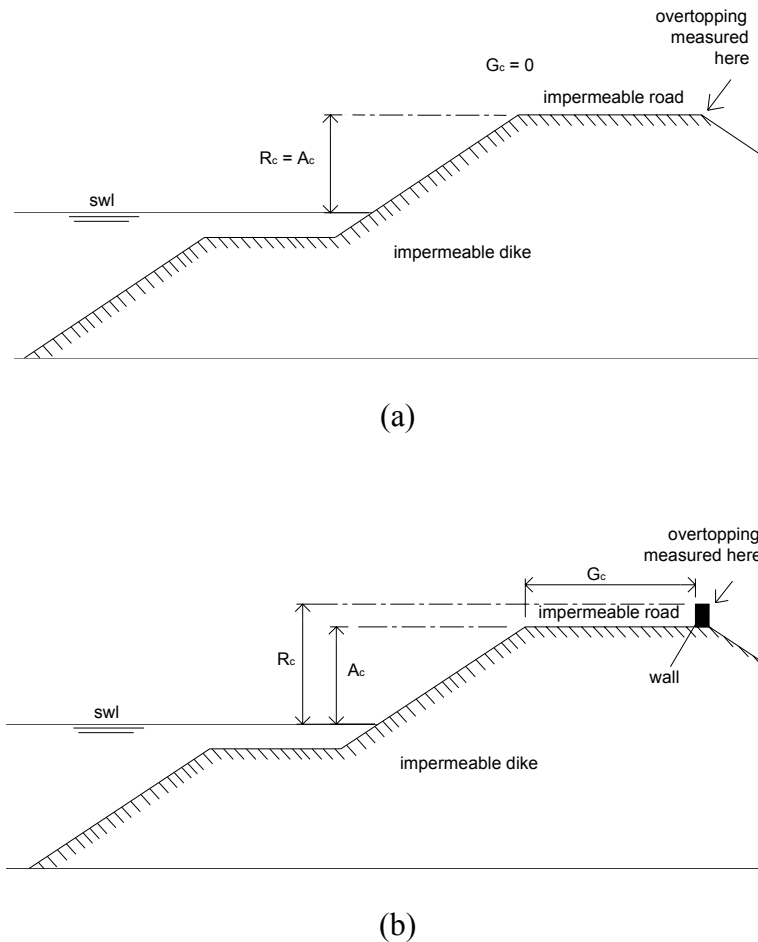
(d)



(e)

**Figure 12: Determination of  $R_c$  [m],  $A_c$  [m] and  $G_c$  [m]**

It has to be mentioned that the parameter  $G_c$  only includes the *permeable* horizontal part of the crest, as it is assumed that overtopping water just passes an impermeable surface if it reaches it. An example is given in Fig. 13 (a): as the crest consists of a horizontal impermeable surface, the value of  $G_c$  [m] is equal to zero. Logically, if the crest consists of an impermeable horizontal road, and the overtopping is measured behind a wall located at the landside of the road, the crest width  $G_c$  will be equal to the width of the road, as only the water which passes the wall itself will be measured. An example is given in Fig. 13 (b).



**Figure 13: Determination of  $G_c$  [m]**

#### 2.2.5.3.7 Slope parameters: $\cot\alpha_d$ [-], $\cot\alpha_u$ [-], $\cot\alpha_{\text{excl}}$ [-], $\cot\alpha_{\text{incl}}$ [-]

These parameters describe the slope(s) of the overtopping structure (figure 3.16 to 3.20). It has to be stressed that the toe and the crest of the structure are not included in these four slope parameters, as these are already described by separate parameters.

The four parameters provide three ways to describe the overtopping structure:

- with  $\cot\alpha_d$  and  $\cot\alpha_u$  or
- with  $\cot\alpha_{\text{excl}}$  or
- with  $\cot\alpha_{\text{incl}}$

The advantage of using two parameters to describe the structure slope is that in case of several sloping parts a more detailed schematisation of the structure can be made.

$\text{Cot}\alpha_d$  [-] and  $\text{cot}\alpha_u$  [-] are the cotangents of the mean slopes in the centre area of the structure below ( $\text{cot}\alpha_{\text{down}}$ ) and above ( $\text{cot}\alpha_{\text{up}}$ ) the berm respectively.

$\text{Cot}\alpha_{\text{excl}}$  [-] and  $\text{cot}\alpha_{\text{incl}}$  [-] are calculated ‘average’ slopes.  $\text{Cot}\alpha_{\text{incl}}$  is the average slope where the berm (if it is located in the centre area of the structure) is included in this average value ( $\text{cot}\alpha_{\text{inclusive berm}}$ ).  $\text{Cot}\alpha_{\text{excl}}$  is the average slope where the present berm is not taken into account ( $\text{cot}\alpha_{\text{exclusive berm}}$ ). If a structure has no berm,  $\text{cot}\alpha_{\text{incl}} = \text{cot}\alpha_{\text{excl}}$ .

It can be mentioned that the slope angles are presented here by means of their cotangent instead of their tangent (which was used for the slope of the berm). The reason for that is that the structure slopes can adopt values up to and even larger than  $90^\circ$  (see section 2.2.5.4 for this last case). A value of  $90^\circ$  results in a zero value of the cotangent of the slope (instead of an infinite value for the tangent of the slope), a value larger than  $90^\circ$  results in a negative value of the cotangent of the slope (instead of a positive value of the tangent of the slope, indistinguishable from the tangent of a slope of  $90^\circ - \alpha$ ). The other way round, the cotangent of a horizontal berm results in an infinite value, explaining the use of the tangent for the berm.

How the four slope parameters exactly are determined, is explained below (Fig. 14 and 15).

The upper slope of the structure  $\alpha_u$  is the slope upward the berm. It is determined by taking the point of the structure at a level of  $1.5H_{m0 \text{ toe}}$  above swl and connecting it with the leeside endpoint of the berm. If the crest of the structure is situated in the centre area of the structure (this implies that the crest is situated less than  $1.5H_{m0 \text{ toe}}$  above swl), then the starting point of the crest has to be used instead of the point at level  $1.5H_{m0 \text{ toe}}$  above swl to determine  $\alpha_u$ .

The lower slope of the structure  $\alpha_d$  is the slope downward the berm. It is determined by taking the point of the structure at a level of  $1.5H_{m0 \text{ toe}}$  below swl and connecting it with the seaside endpoint of the berm. If the toe of the structure is situated in the centre area of the structure (this implies that the toe is situated less than  $1.5H_{m0 \text{ toe}}$  below swl), then the starting point of the toe has to be used instead of the point at level  $1.5H_{m0 \text{ toe}}$  below swl to determine  $\alpha_d$ .

The average slope  $\alpha_{\text{incl}}$  is determined by taking the point on the upper slope at a level of  $1.5H_{m0 \text{ toe}}$  above swl and connecting it with the point on the lower slope at a level of  $1.5H_{m0 \text{ toe}}$  below swl. The subscript ‘incl’ refers to the fact that if there is a berm, it is included into the value of  $\text{cot}\alpha_{\text{incl}}$ . Also here applies that, if the toe and/or the crest of the structure are situated into the centre area, the lowest and/or the highest point which determine  $\text{cot}\alpha_{\text{incl}}$  are

determined by the nearest point of the toe (instead of by  $swl - 1.5 \cdot H_{m0\ toe}$ ) and/or the nearest point of the crest (instead of by  $swl + 1.5 \cdot H_{m0\ toe}$ ).

The average slope  $\alpha_{excl}$  is determined by subtracting the horizontal width of the berm  $B_h$  from the horizontal distance between the two points which determine  $\alpha_{incl}$  and dividing this value by the vertical distance between the two points which determine  $\alpha_{incl}$ .

In Fig. 14 the four slope angles are indicated, in graph (a) for a simple rubble mound structure without berm, in graph (b) for a rubble mound structure with a horizontal berm and in graph (c) for a rubble mound structure with a sloping berm.

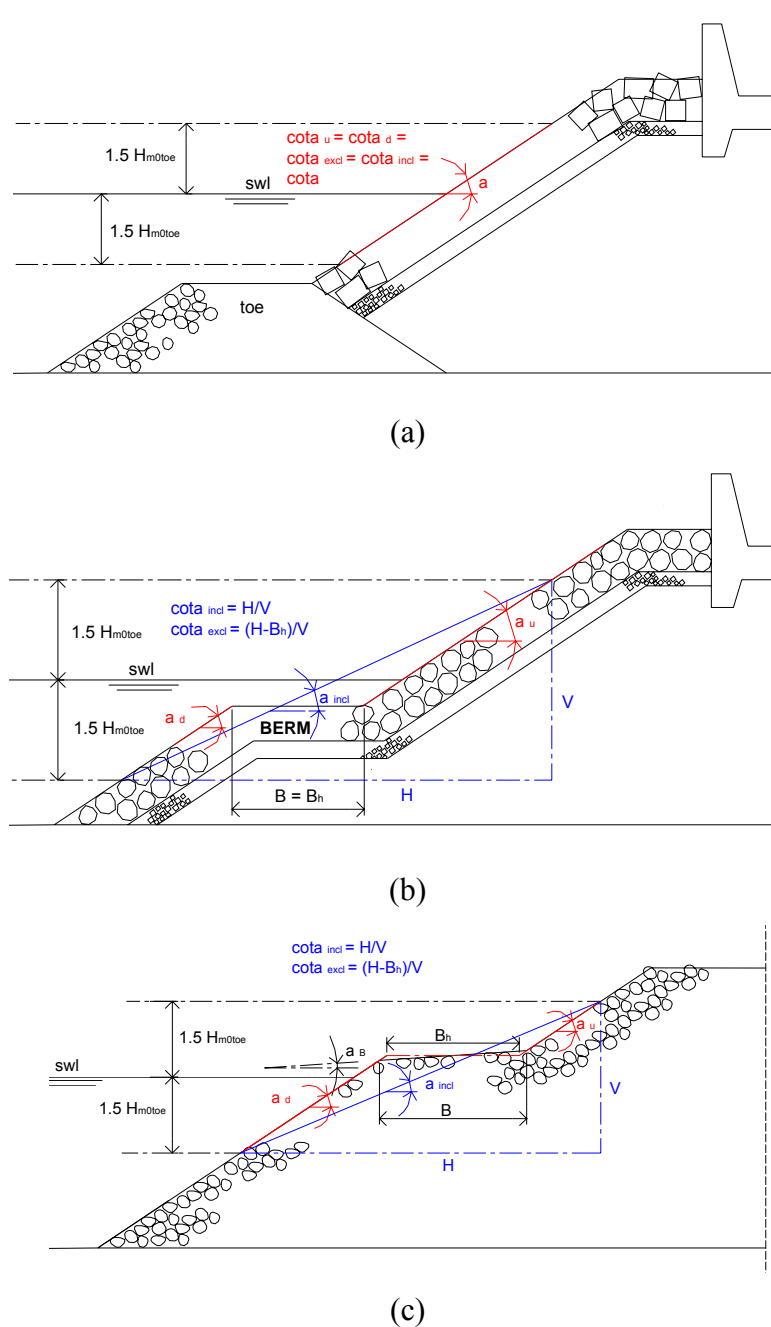
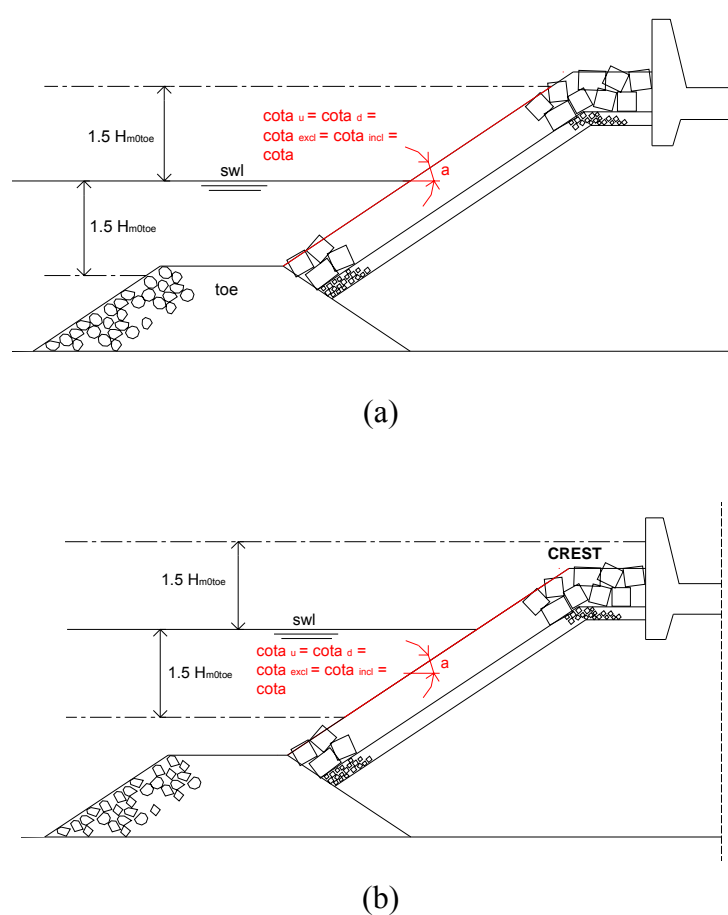


Figure 14: Determination of the structures slope parameters

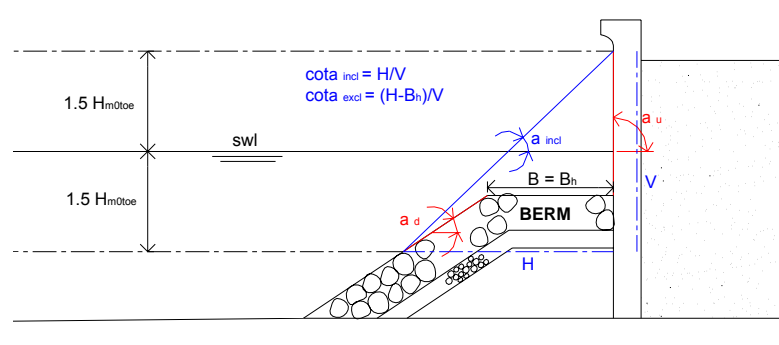


In Fig. 15 two extra examples regarding the determination of the structure slope parameters are given. In graph (a) the toe is situated in the centre area of the structure. As can be seen on the figure the starting point of the toe is used to determine  $\alpha_d$  instead of the point at level  $1.5H_{m0\text{ toe}}$  below swl. In graph (b) the crest is situated in the centre area of the structure. Analogous the starting point of the crest is used to determine  $\alpha_u$  here instead of the point at level  $1.5H_{m0\text{ toe}}$  above swl.



**Figure 15: Determination of the structures slope parameters, extra examples**

As mentioned already, the use of the two parameters  $\cot\alpha_u$  and  $\cot\alpha_d$  allows a better schematisation than the use of only one of the average slope  $\cot\alpha_{excl}$  or  $\cot\alpha_{incl}$ . An example of a structure type for which the use of an average slope leads to a bad schematisation is given in Fig. 16.

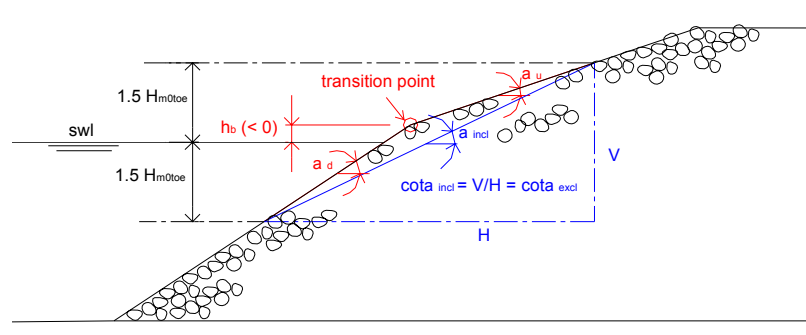


**Figure 16: Structure type for which at least two slope parameters are requested**

The use of the two slope parameters  $\cot\alpha_u$  and  $\cot\alpha_d$  also allows to schematise composite slopes (structures consisting of subsequent different slopes without a horizontal part in between) very well. As mentioned in section 2.2.5.3.5 the position of the transition point is indicated by  $h_b$ . The slope upward respectively downward the transition point is defined now by  $\cot\alpha_u$  and  $\cot\alpha_d$ .

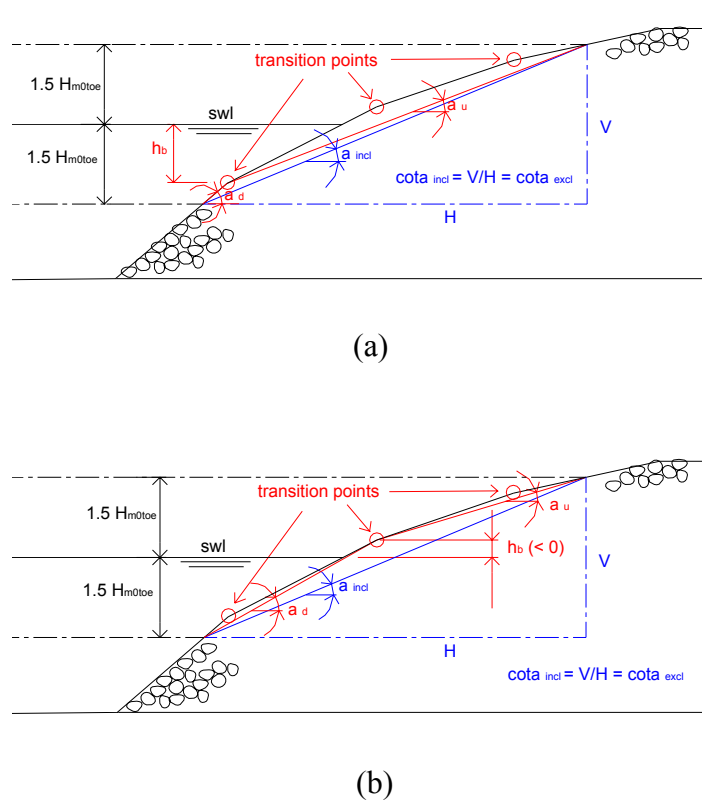
For composite slopes composed of more than two subsequent different structure slopes (and consequently more than one transition point), a rougher schematisation is needed, even with two parameters  $\cot\alpha_d$  and  $\cot\alpha_u$ .

Fig. 17 shows a composite slope with only one transition point. By using  $\cot\alpha_d$  and  $\cot\alpha_u$ , the structure is schematised very well.



**Figure 17: Schematisation of a composite slope composed of 2 subsequent slopes**

Fig. 18 shows a composite slope consisting of more than 2 subsequent slopes. Graph (a) and (b) give two possible schematisations, determined by the choice of the transition depth  $h_b$ . As can be seen on the figures, the schematisation in graph (b) fits the structure best.



**Figure 18: Schematisation of a composite slope composed of more than 2 subsequent slopes**

#### 2.2.5.3.8 Roughness factor: $\gamma_f$ [-]

The parameter  $\gamma_f$  [-] gives an indication of the roughness and the permeability of the structure. The rougher and more permeable a structure, the lower the overtopping will be as more energy is dissipated. Values for  $\gamma_f$  for several revetment types are presented by TAW (2002), resulting from new research with irregular waves, also on large scale, from 1974 up to 2002. TAW (2002) prescribes a value of 1 for  $\gamma_f$  in case of an impermeable smooth structure, and a value of 0.7 respectively 0.55 in case of a rubble mound structure with 1 respectively 2 layers of rock.

As already mentioned, extensive research was performed within the CLASH project to the roughness and permeability of different armour layers of rubble mound structures, especially with the aim of providing new information on the  $\gamma_f$  - value of these armour types for the set-up of the overtopping database (see Pearson et al., 2004b). Within this study, 426 new tests were performed on 10 types of armour layers, for each armour block starting from an identical hydrodynamic stability. Mean overtopping discharges on these structures were studied, together with the results of overtopping tests performed in 1999 (see Franco et al., 1999).

This study resulted in slightly adapted  $\gamma_f$ -values for rock slopes, and additionally, in new  $\gamma_f$ -values for several concrete armour units. Table 1 gives a summary of the obtained  $\gamma_f$ -values for the tested armour layers (see Pearson et al., 2004b).

**Table 1: New derived values for  $\gamma_f$   
(see Pearson et al., 2004b)**

<b>Type of armour layer</b>	<b><math>\gamma_f</math></b>
Smooth impermeable surface	1.00
Rock (1 layer, impermeable core)	0.60
Rock (1 layer, permeable core)	0.45
Rock (2 layers, impermeable core)	0.55
Rock (2 layers, permeable core)	0.40
Cubes (1 layer, smooth positioning, 30% porosity)	0.50
Cubes (2 layers, random positioning)	0.47
Antifers	0.47
HARO's	0.47
Accropods	0.46
X-blocks	0.45
Core-locs	0.44
Tetrapods	0.38

It can be remarked that this research resulted in a remarkably lower value of  $\gamma_f$  for a 2 layered rock slope (with permeable core): 0.40 instead of 0.55. An armour layer consisting of 2 layers of cubes or antifers performs somewhat worse than a 2 layered rock slope:  $\gamma_f = 0.47$  instead of 0.40. Tetrapods, with a  $\gamma_f$ -value of 0.38, seem to be the best armour blocks regarding roughness and permeability.

Additionally to table 1, values of  $\gamma_f$  for other types of armour layers were estimated, based on included data in the database. Table 2 gives an overall view of estimated values of  $\gamma_f$ . This

table is not supported by extensive research and has to be considered therefore as a provisional table.

**Table 2: Estimated values for  $\gamma_f$  based on included overtopping tests**

Type of armour layer	$\gamma_f$
SHEDS	0.55
Seabeas	0.50
Berm breakwater (reshaping)	0.40
Dolosse	0.43
Icelandic berm breakwater (not reshaping)	0.35

More types of armour units are present in the database than mentioned above. Some armour layers consist of very specific armour blocks which are not mentioned here, others consist of impermeable coverings with an energy-dissipating layout, e.g. stepped slopes. For these types of armour layers, a well-considered estimation of the roughness/permeability factor  $\gamma_f$  was made.

For composite structures such as vertical walls with a rubble mound protection, often kind of ‘average’ had to be determined for  $\gamma_f$ .

As the influence of the roughness/permeability of the part of the structure, which is situated below SWL, is found to be low (see TAW, 2002), the value of  $\gamma_f$  was determined only by the structure part situated above swl. This implies that in case of a vertical wall with a rubble mound protection situated entirely below SWL, a value of  $\gamma_f = 1$  was assigned to the structure. In case two different roughnesses/permeabilities appeared above SWL, a weighed average (considering the vertical distance) was taken for the  $\gamma_f$ -value over the height of  $1.5H_{m0\ toe}$  above SWL, taking into account the width of the eventually present berm (i.e. horizontal distance).

To distinguish estimated values of  $\gamma_f$  from the derived values of  $\gamma_f$  from model tests (table 1), all estimated values of  $\gamma_f$  are marked in the database in red colour, see section 2.2.7.

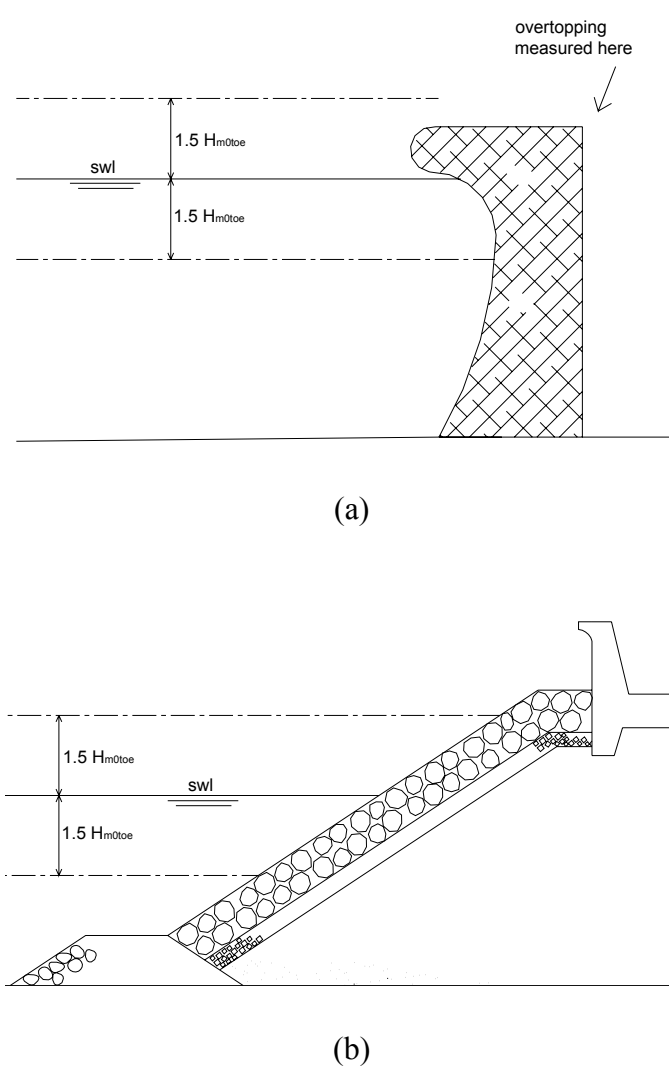
It has to be remarked here that the recent values for  $\gamma_f$  as mentioned in table 1 and 2 were only determined in the latest stage of the CLASH project. The developed neural network within CLASH (see Pozueta et al., 2004a), makes use of older values of  $\gamma_f$ , which are slightly different from the ones in table 3.4 and 3.5. The values which are used for the neural network prediction method of Pozueta et al. can be found in the corresponding report and user manual of the neural network prediction method (Pozueta et al., 2004b).

#### **2.2.5.4 Influence of a recurve wave wall**

Quite a lot of coastal structures are equipped with a (small or large) recurve wave wall with the aim of reducing the phenomenon of wave overtopping. A recurve wave wall ‘turns’ the waves at the top of the structure back seawards resulting in a lower overtopping quantity to some extent, depending on the relative height and the dimensions of the recurved part of the wave wall. At the moment of writing this study (end of 2004 - beginning of 2005), studies on the influence of a recurve wave wall are ongoing (see Pearson et al., 2004a), but the exact influence of the presence of it on the overtopping quantity is not known yet. In expectation of more detailed knowledge on this subject, the influence of a recurve wave wall was assessed as described in this section.

Within the set-up of the database, distinction was made between large and small recurve wave walls, leading to a different way of schematising the corresponding tests (Fig. 19).

A large recurve wave wall is defined within this study as a recurve wave wall having a dominant effect on the structure layout. A small recurve wave wall on the other hand is defined as a minor construction part, such as an extra curve which is given to a small wall on top of a rubble mound structure.

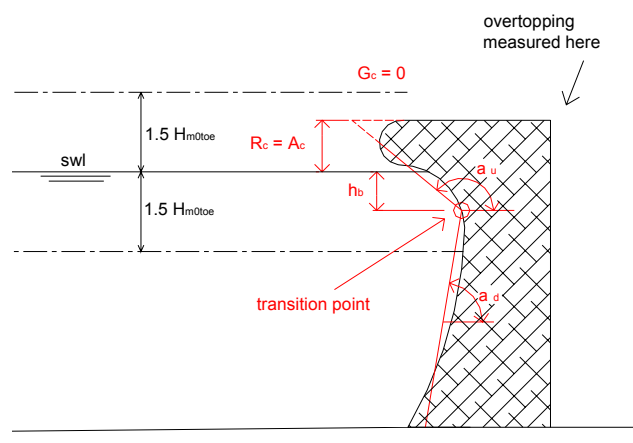


**Figure 19: Distinction between a large (a) and a small (b) recurve wave wall**

How each of these is incorporated in the schematisation of the structure for the database is explained below.

#### 2.2.5.4.1 Case (a): large recurve wave wall

As a large recurve wave wall influences the entire structure shape, it seems most adequate to include it in the main parameters describing the outlook of the structure (Fig. 19 (a)). In this way, the recurve wave wall can be considered as a composite slope consisting of two different slopes separated by a transition point at depth  $h_b$ . The upper slope leans back seaward introducing a negative value for the cotangent of it. In Fig. 20 the same recurve wave wall as in Fig. 19(a) is represented, together with a possible schematisation of it. The schematisation parameters describing the recurve wave wall are given in the figure.



**Figure 20: Schematisation of a large recurve wave wall**

The transition point is chosen rather arbitrary, providing upper and down slope with a good fitting to the structure.

#### 2.2.5.4.2 Case (b): small recurve wave wall

Compared to previous case, a small recurve wave wall is much less dominant regarding to the overall structure layout (Fig. 19(b)). It is clear that in case of a small recurve wave wall a description of it by means of the structure slope is not adequate.

The methodology for a small recurve wave wall which is used here, is based on the method proposed in TAW (2003) for vertical walls, in which the effect of a recurve wave wall is accounted for as a higher roughness of the structure felt by the waves, resulting in a lower value of  $\gamma_f$ .

Determining the final value of  $\gamma_f$  for the database is performed therefore in two steps. In a first step, the  $\gamma_f$ -value for a structure is determined according to section 2.2.5.3.8, resulting in a  $\gamma_f$ -value accounting for the roughness/permeability of the present armour layer. In a second step an eventually extra reduction for a recurve wave wall is carried out. How exactly this extra reduction is determined, based on TAW (2003), and extended for rough structure types, is described below.

Equations (1) and (2) describe the applied reduction for a small recurve wave wall. ' $\gamma_{f \text{ armour}}$ ' refers to the value of the roughness/permeability factor obtained solely due to the effect of roughness and permeability of the armour layer. This corresponds to the value of  $\gamma_f$  which is obtained by applying the methodology described in section 2.2.5.3.8 The mentioned ' $\gamma_f$ ' in



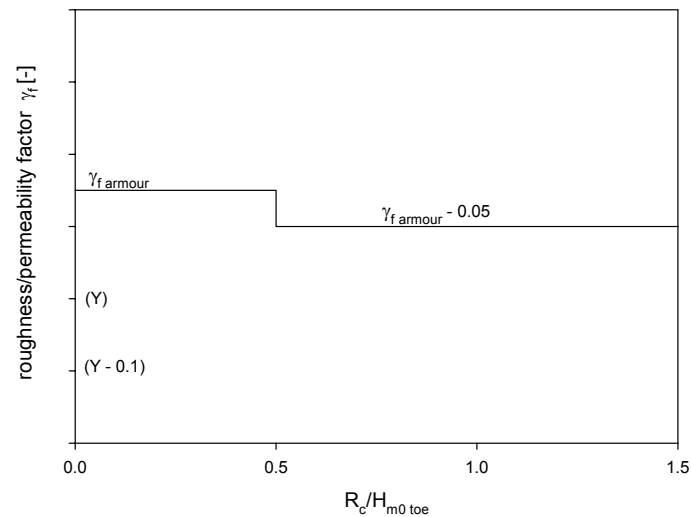
equations (1) and (2) refers to the final value of the roughness and permeability factor, including -beside the roughness/permeability of the armour layer- the effect of a small recurve wave wall. When further in this study the roughness/permeability factor ' $\gamma_f$ ' is mentioned, the effect of a small recurve wave wall is included.

In case of a <b>rough</b> structure, i.e. $\gamma_{f \text{ armour}} < 0.9$ :		(1)
for $R_c / H_{m0 \text{ toe}} \geq 0.5$	: $\gamma_f = \gamma_{f \text{ armour}} - 0.05$	
for $R_c / H_{m0 \text{ toe}} < 0.5$	: $\gamma_f = \gamma_{f \text{ armour}}$	

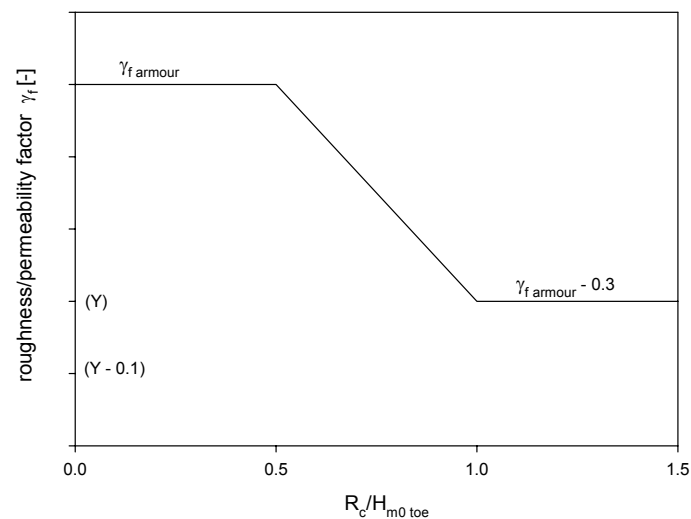
In case of a <b>smooth</b> structure, i.e. $\gamma_{f \text{ armour}} \geq 0.9$ :		(2)
for $R_c / H_{m0 \text{ toe}} > 1$	: $\gamma_f = \gamma_{f \text{ armour}} - 0.3$	
for $R_c / H_{m0 \text{ toe}} \leq 0.5$	: $\gamma_f = \gamma_{f \text{ armour}}$	
for $0.5 < R_c / H_{m0 \text{ toe}} \leq 1$	: interpolation	

As the effect of a recurve wave wall on the overtopping phenomenon is only significant for relatively high crests (for low crests the waves just pass the structure without 'feeling' the recurve wave wall), the reduction depends on the value of  $R_c / H_{m0 \text{ toe}}$ . As can be derived from equations (1) and (2), the reduction due to the presence of a small recurve wave wall is limited for rough structures. This is done to exclude unrealistic low values of  $\gamma_f$ .

In Fig. 21, equations (1) for rough structures and (2) for smooth structures are graphical represented in respectively graph (a) and graph (b).



(a)



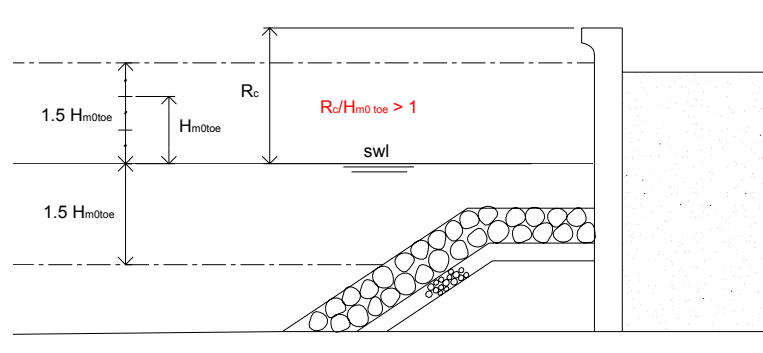
(b)

**Figure 21: Reduction factor for rough structures, graph (a) and smooth structures, graph (b)**

Although the discontinuity in the reduction factor for rough structure types at the value of  $R_c / H_{m0 toe} = 0.5$  (see graph (a) of Fig. 21), cannot appear in reality, it was utilised as approximation for practical use.

Fig. 22 shows an example of a structure with a small recurve wave wall. The value of  $\gamma_{f armour}$  is equal to 1, as the rubble mound structure is situated below the swl. Regarding the level of

the recurve wave wall ( $R_c / H_{m0\ toe} > 1$ ), equation (2) and Fig. 21, graph (b) leads to a value of  $\gamma_f$  equal to  $1 - 0.3 = 0.7$ .



**Figure 22: Influence of a small recurve wave wall on  $\gamma_f$**

As the reduction of  $\gamma_f$  to account for the presence of a small recurve wave wall concerns an estimation of  $\gamma_f$ , these reduced values are also marked in red in the database (see section 2.2.7).

## 2.2.6 Determination of the general parameters

The database contains for each overtopping test three general parameters: “Name”, “RF” and “CF”. This section explains how exactly these parameters are assigned a value.

### 2.2.6.1 Name of the test

The first parameter “Name” assigns a unique name to each test. It consists of a basic ‘test series’ number, which is the same for all the tests within the same test series, followed by a unique number for each test. The parameter “Name” always is composed of 6 characters. E.g. test 36 from test series 178 has the unique code: 178-036.

This parameter is just meant to recognise each test but has no further meaning.

### 2.2.6.2 The complexity factor CF

The complexity factor CF gives an indication of the complexity of the overtopping structure. As already mentioned in section 2.2.5.5, it is impossible to represent each structure type of the database exactly by means of the 17 structural parameters. Depending on the degree of

approximation which is obtained with the 17 structural parameters, the value of the complexity factor CF is determined.

Table 3 gives an overall view of the values the complexity factor CF can adopt. For each value a short explanation is given.

**Table 3: Values of the complexity factor CF**

<b>CF</b>	<b>Meaning</b>
1	simple section: the parameters describe the section exactly or as good as exactly
2	quite simple section: the parameters describe the section very well, although not exactly
3	quite complicated section: the parameters describe the section appropriate, but some difficulties and uncertainties appear
4	very complicated section: the section is too complicated to describe with the chosen parameters, the representation of the section by them is unreliable

The value of the complexity factor CF is only influenced by the schematisation of the test by means of the 17 structural parameters.

### 2.2.6.3 The reliability factor RF

The reliability factor RF gives an indication of the reliability of the considered overtopping test.

Table 4 gives an overall view of the values the reliability factor RF can adopt. For each value a short explanation is given.

**Table 4: Values of the reliability factor RF**

<b>RF</b>	<b>Meaning</b>
1	very reliable test: all needed information is available, measurements and analysis were performed in a reliable way
2	reliable test: some estimations/calculations had to be made and/or some uncertainties about measurements/analysis exist, but the overall test can be classified as 'reliable'
3	less reliable test: some estimations/calculations had to be made and/or some uncertainties about measurements/analysis exist, leading to a classification of the test as 'less reliable'
4	unreliable test: no acceptable estimations could be made, calculations and/or measurements/analysis include faults, leading to an unreliable test

The reliability factor RF is determined by several factors:

- the precision of the measurements/analysis of the researchers performing the overtopping tests
- the possibilities of the test facility used to perform the tests
- the estimations/calculations that had to be made because of missing values

Table 5 gives a detailed overall view of the qualifying factors of RF, and the corresponding value assigned to it, as determined for all overtopping tests included in the overtopping database.

**Table 5: Determination of the reliability factor RF**


---

- absorption system of the test facility:
 

---

  - active wave absorption is available: RF = 1
  - only passive wave absorption was available: RF = 2
  - no wave absorption system is available:
    - if low reflective structure: RF = 2
    - if high reflective structure: RF = 3

---
- wave generation system of the test facility:
 

---

  - regular waves are generated: RF = 4
  - irregular waves are generated:
    - if short-crested: RF = 1
    - if long-crested:
      - RF depending on angle of wave attack:
        - if  $\beta = 0^\circ$ : RF = 1
        - if  $0 < \beta \leq 30^\circ$ : RF = 2
        - if  $30 < \beta \leq 45^\circ$ : RF = 3
        - if  $\beta > 45^\circ$ : RF = 4

---
- wave measurements:
 

---

  - reflection analysis is performed (separation of incident from reflected waves):
    - RF = 1
  - no reflection analysis is performed (only total waves): RF = 3

---
- water depth at the toe of the structure:
 

---

  - if  $h \text{ [m]} \leq 0$  (implicating that no wave characteristics at the toe are known or possible to calculate): RF = 4
  - if  $h \text{ [m]}$  very small and no wave characteristics at the toe are available (no accurate calculations with SWAN are possible):
    - RF = 4

---

**Table 5 : Determination of the reliability factor RF (continue)**


---

- reliability of estimated wave periods at the toe of the structure if no calculations with SWAN (reliability dependent on degree of wave breaking):

---

→ if wave heights are known at deep water and at the toe of the structure:

- if  $H_{m0toe}/H_{m0deep} > 0.6$ : RF = 1  
(little breaking waves; spectral shape at the toe of the structure  $\approx$  spectral shape at deep water; reliable estimation)
- if  $H_{m0toe}/H_{m0deep} < 0.4$ : RF = 3  
(breaking waves; spectral shape at the toe of the structure  $\neq$  spectral shape at deep water; breaking = more energy for the low frequent component; no reliable estimation)
- if  $0.4 < H_{m0toe}/H_{m0deep} < 0.6$ : RF = 2  
(partially breaking waves; less reliable estimation)

→ if wave heights are only known at the toe of the structure:

- if  $H_{m0toe}/h < 0.73$ : RF = 1  
(little breaking waves)
- if  $H_{m0toe}/h > 1$ : RF = 3  
(breaking waves)
- if  $1 > H_{m0toe}/h > 0.73$ : RF = 2  
(partially breaking waves)

---

- Calculations with Battjes and Groenendijk (2000)

---

RF = 2

---

**Table 5 : Determination of the reliability factor RF (continue)**


---

- Calculations with SWAN:

---

→ Reliability dependent on dimension of situation:

- if two-dimensional situation (model test in wave flume): RF = 2
- if three-dimensional situation (model test in wave basin or prototype measurement): RF=3

→ Reliability dependent on degree of wave breaking ( $T_{m-1,0}$  always estimated):

➤ if  $H_{m0toe}/H_{m0deep} > 0.6$ : RF = 2  
(little breaking waves)

➤ if  $H_{m0toe}/H_{m0deep} < 0.4$ : RF = 4  
(breaking waves)

➤ if  $0.4 < H_{m0toe}/H_{m0deep} < 0.6$ : RF = 3  
(partially breaking waves)

➤ if  $H_{m0toe}/h < 0.73$ : RF = 2  
(little breaking waves)

➤ if  $H_{m0toe}/h > 1$ : RF = 4  
(breaking waves)

➤ if  $1 > H_{m0toe}/h > 0.73$ :  
RF = 3  
(partially breaking waves)

→ Reliability dependent on foreshore steepness:

- if foreshore slope 1/30 or less steep: RF = 2
  - if foreshore slope steeper than 1:30: RF = 3
- 

It has to be stressed that the indicated RF -values in table 5 are minimum values. This means that if more than one of the mentioned influence factors appears within one test, at least the highest value of RF (lowest reliability) should be restricted and eventually even a higher value of RF should be assigned to the corresponding test.



### 2.2.6 *Layout of the overtopping database*

The final database consists of more than 10500 overtopping tests which are represented by an equal number of rows in one datasheet.

All tests were put into the database in model values. As often in corresponding reports everything is given in prototype values, it was important to take note of the model scale of the tests to recalculate the values to the original model values. The prototype tests on the contrary were included by means of their real measured values (=prototype values).

It could be important for researchers who use the overtopping database for further research to know which parameter values in the database concern real measured values, which ones concern calculated values and which ones concern estimated values. This can not be checked by the value of the reliability factor RF as this factor only gives an overall indication of the reliability of the test.

To distinguish these cases from each other it was therefore decided to use colours in the datasheet to mark the calculated and estimated values, to make distinction from the real measured values possible.

Following colours were used:

- if wave characteristics at the toe of the structure were calculated with SWAN: values marked in blue
- if wave heights at the toe of the structure were calculated from  $H_{1/3}$  from time series with the method Battjes and Groenendijk (2000): values marked in green
- if wave period parameters were estimated from other period parameters: values marked in red
- if values of the roughness/permeability factor  $\gamma_f$  are estimated, which is the case for all armour layers which are not present in table 3.4, and also if an extra reduction for a small recurve wave wall according to equations (1) and (2) was included in it: values marked in red

Additionally to the already mentioned 31 columns in the database (resulting from 3 general parameters, 11 hydraulic parameters and 17 structural parameters), 2 more columns are part of the datasheet.

The first added column (column 32) is called “Remark” and contains a remark additional to the test. This is done mainly thinking of the neural network application of the database. One of the reasons are the model and scale effects which affect small scale overtopping measurements in specific cases.

Column 32 marks the three mentioned types of tests, and advises against using for the neural network development. Additionally for the laboratory tests with wind generation the generated wind velocity is mentioned.

The total number of prototype tests is 132. A number of 223 laboratory tests is performed with wind generation. Finally 154 tests concern synthetic laboratory test sections.

By excluding these series of tests from the neural network development, a network which is able to predict overtopping in laboratory, including the model effect of wind, and including scale effects, is obtained. A correction factor accounting for scale effects and the effect of wind in accordance with the scaling map of Kortenhaus et al. (2005), leads to a prediction of the mean overtopping discharge to be expected in prototype.

A second added column to the database (column 33) concerns the state of each overtopping test, regarding the confidentiality. For public tests, column 33 contains a reference to a report or paper describing the tests. This allows interested researchers to find more information on specific tests. As mentioned in section 2.2, about 75% of all data is publicly available.

Table 6 gives an overall view of the information summarised in the overtopping database.

**Table 6: Information in the database**

<b>Column number</b>	<b>Contents</b>	<b>Nature of parameter</b>
1	Name	general
2	$H_{m0 \text{ deep}}$ [m]	hydraulic
3	$T_p \text{ deep}$ [s]	hydraulic
4	$T_m \text{ deep}$ [s]	hydraulic
5	$T_{m-1,0 \text{ deep}}$ [s]	hydraulic
6	$h_{\text{deep}}$ [m]	structural
7	$m$ [-]	structural
8	$\beta$ [°]	hydraulic
9	$h$ [m]	structural
10	$H_{m0 \text{ toe}}$ [m]	hydraulic
11	$T_p \text{ toe}$ [s]	hydraulic
12	$T_m \text{ toe}$ [s]	hydraulic
13	$T_{m-1,0 \text{ toe}}$ [s]	hydraulic
14	$h_t$ [m]	structural
15	$B_t$ [m]	structural
16	$\gamma_f$ [-]	structural
17	$\text{cota}_d$ [-]	structural
18	$\text{cota}_u$ [-]	structural
19	$\text{cota}_{\text{excl}}$ [-]	structural
20	$\text{cota}_{\text{incl}}$ [-]	structural
21	$R_c$ [m]	structural
22	$B$ [m]	structural
23	$h_b$ [m]	structural
24	$\tan\alpha_B$ [-]	structural
25	$B_h$ [m]	structural
26	$A_c$ [m]	structural
27	$G_c$ [m]	structural
28	RF	general
29	CF	general
30	$q$ [m <sup>3</sup> /s/m]	hydraulic
31	$P_{\text{ow}}$ [-]	hydraulic
32	Remark	extra information
33	Reference	extra information

### 2.3 Conclusions / achievements

A database containing 10532 tests on wave overtopping has been set-up. Each test in the database has been described by 31 carefully selected parameters including wave characteristics, geometrical characteristics of the structure, overtopping related parameters and general information.

All of these parameters and how to define their value, have been described carefully and into detail.

The screened and homogeneous database has been used to develop a neural network to predict wave overtopping at coastal structures (see WP8).

This workpackage delivered the following reports :

- the report on the overtopping database (D6)

Additionally one milestone was achieved :

The wave overtopping database which is a collection of existing data on wave overtopping (M2).

### 3 WP3 : Full scale measurements

#### 3.1 Objectives

The main objective is to collect and analyse reliable full scale data on, or related to, wave overtopping at four different prototype sites.

Other task objectives are :

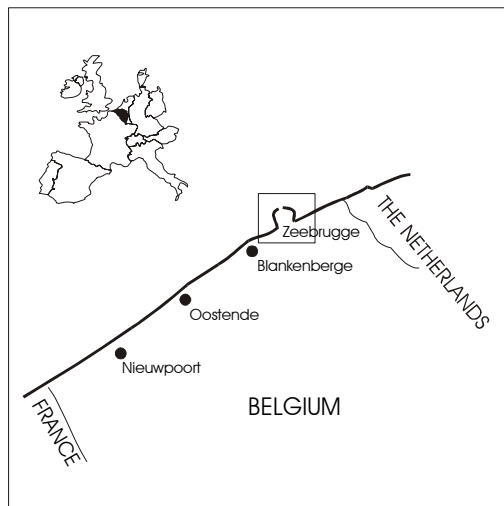
- to (supplementary) instrument the sites in such a way that the incident wave field is measured correctly;
- to (supplementary) instrument the sites, so that overtopping is measured correctly;
- to (supplementary) instrument and measure the long wave phenomenon on very shallow water and breaking waves at one site.

#### 3.2 Description of work performed

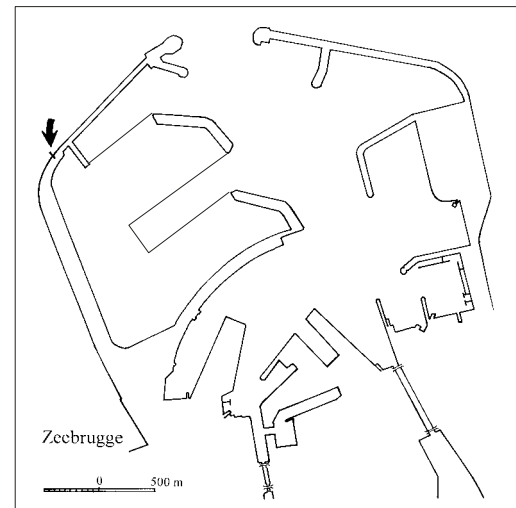
##### 3.2.1 Site 1 : Zeebrugge (Belgium)

The Zeebrugge field site is situated on the eastern part of the Belgian Coast (Fig. 23) at the outer Zeebrugge harbour (Fig.24). The outer harbour is protected by two rubble mound breakwaters. The slope of the breakwater is ca. 1:1.5 (1:1.4 where the measurements take place) and is protected by 25 tons grooved cubes which are somewhat flattened (Height/Width = 0.85). The core consists of quarry run (2-300 kg) and 1-3 ton rocks form a filter layer (Fig. 25). On the landward side, a filter construction is placed between the core and the sandfill.

The tidal range varies 4.30 m between  $Z+0.32$  and  $Z+4.62$  (mean spring tide) and  $Z+0.90$  and  $Z+3.88$  (mean neap tide) ( $Z + 0.00 = MLLWS + 0.08$ ). The design conditions are: significant wave height  $H_s = 6.20$  m, maximum peak period  $T_p = 10$  s, water level  $Z + 6.76$ . The average sea bottom level is about  $Z - 7.00$ , so the breakwater is about 20 m high, with the crest level at  $Z + 12.40$  (theoretical design level).

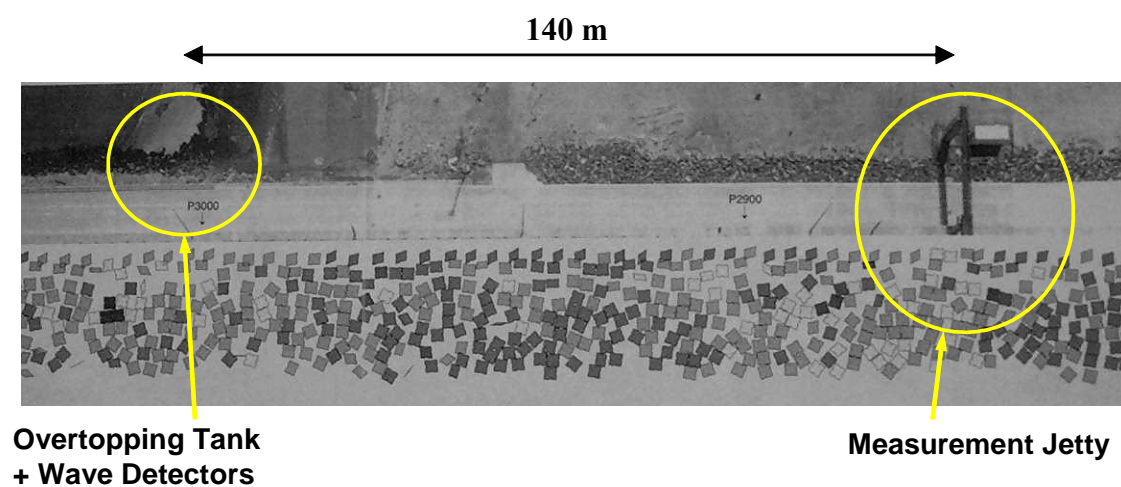


**Figure 23: Location of Zeebrugge harbour at the Belgian North Sea Coast**

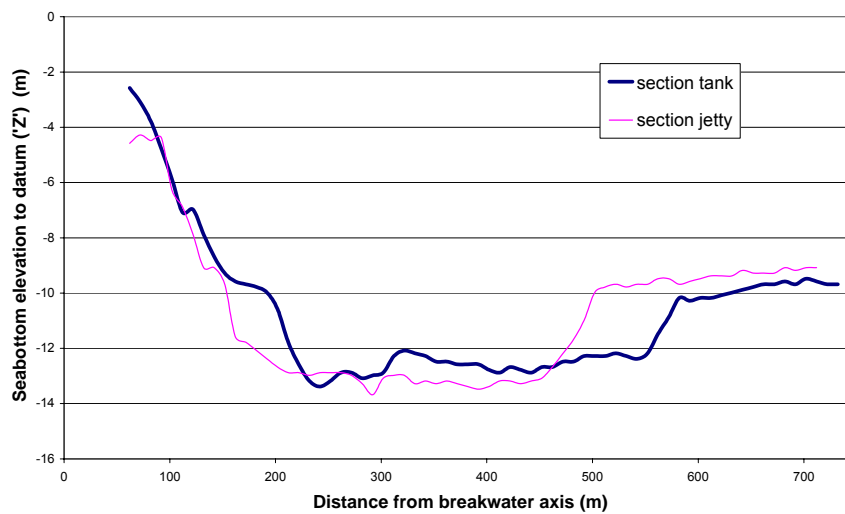


**Figure 24: Location of the field site at Zeebrugge harbour**

Full scale measurements are carried out on the northern part of the western breakwater of the outer harbour (Troch et al. (1998)). Two cross-sections (P2860 and P3000) of the breakwater, with an interspace of approximately 140 m, are instrumented. Fig. 25 shows a plan view with both instrumented cross-sections indicated. Bathymetric surveys in front of both instrumented cross-sections have been carried out in 1999. Results were confirmed during the surveys of 2002. Fig. 26 gives bathymetry for both cross-sections. Bottom elevation is referred to “Z”-level as defined above. The foreshore is characterized by an erosion pit in front of the breakwater and a flat slope more seaward.



**Figure 25: Plan view with indication of both instrumented cross-sections**



**Figure 26: Bathymetry for two instrumented cross-sections**

In the first cross-section (P2860) a measurement jetty of 60 m length is constructed on top of the breakwater. It is supported by a steel tube pile ( $\varnothing = 1.80$  m) at the breakwater toe and by concrete columns on top of the breakwater. Instruments placed in this cross-section are a directional wave rider buoy and a non-directional wave rider buoy to measure wave characteristics in front of the structure, a radar and an infrared meter to measure the water level and wave height in front of the structure and an anemometer. These are the instruments directly used within CLASH. Besides them, also run-up measurements along the breakwater's slope and pressure measurements inside the breakwater are carried out. Table 7 provides all available instruments and their position.

**Table 7: Measurement devices installed at the Zeebrugge rubble mound breakwater.**

Channel N°	Sensor	Z [m]	X [m]	Variables measured
1	Pressure sensor 3498	3.1	-6.88	hydrodynamic pressure
2	Pressure sensor 3499	0.83	-12.66	hydrodynamic pressure
3	Pressure sensor 3502	3.06	-7.26	hydrodynamic pressure
4	Pressure sensor 3504	0.74	-2.48	hydrodynamic pressure
5	Pressure sensor 3505	0.74	-8.96	hydrodynamic pressure
6	Pressure sensor 3507	0.77	-6.88	hydrodynamic pressure
7	Pressure sensor 3511	3	-2.48	hydrodynamic pressure
8	Pressure sensor 381	2.44	-2.48	hydrodynamic pressure
9	Pressure sensor 382	2.51	-6.88	hydrodynamic pressure
10	Pressure sensor 383	-0.35	-37.6	hydrodynamic pressure
11	Pressure sensor 384	2.32	8.97	hydrodynamic pressure
12	Pressure sensor 385	2.43	-10.06	hydrodynamic pressure
13	Pressure sensor 386	2.36	-7.78	hydrodynamic pressure
14	Pressure sensor 388	2.43	3.97	hydrodynamic pressure
15	Pressure sensor 137	1.09	-37.6	hydrodynamic pressure
16	Pressure sensor 138	2.9	-18.46	hydrodynamic pressure
17	Run-up gauge 1	11.96	-15.31	wave run-up
18	Run-up gauge 2	11.26	-13.51	wave run-up
19	Run-up gauge 3	10.64	-11	wave run-up
20	Run-up gauge 4	9.58	-9.12	wave run-up
21	Run-up gauge 5	7.45	-6.93	wave run-up
22	IR-Laser Waveheight meter	17.11	-30	surface elevation
23	Radar	17.11	-30	surface elevation
24	Waverider I buoy (close)	0	-150	surface elevation
25	Waverider II buoy (far)	0	-215	surface elevation
26	Stepgauge Spiderweb 1	2.75	-18.45	wave run-up & surface elevation
27	Stepgauge Spiderweb 2	4.03	-17.84	wave run-up & surface elevation
28	Stepgauge Spiderweb 3	6.39	-14.82	wave run-up & surface elevation
29	Stepgauge Spiderweb 4	7.3	-13.34	wave run-up & surface elevation
30	Stepgauge Spiderweb 5	9.5	-11.4	wave run-up & surface elevation
31	Stepgauge Spiderweb 6	10.14	-9.44	wave run-up & surface elevation
32	Stepgauge Spiderweb 7	11.12	-7.26	wave run-up & surface elevation
33	Pressure sensor 1123960	overtopping		hydrodynamic pressure
34	Pressure sensor 1123962	overtopping		hydrodynamic pressure
35	Digital wavedetector 1	overtopping		presence of seawater
36	Digital wavedetector 2	overtopping		presence of seawater
37	Digital wavedetector 3	overtopping		presence of seawater
37b	Digital wavedetector 4	overtopping		presence of seawater
37c	Digital wavedetector 5	overtopping		presence of seawater
38	Digital wavedetector 6	overtopping	-32	presence of seawater
39	Wind speed	17.5	-32	wind speed
40	Wind direction	17.5	-30	wind direction
	Videocamera	14		video images of the run-up







**Figure 28: View at the overtopping tank on site.**



**Figure 29: Detail of one wavedetector.**



**Figure 30: Global view showing four different wave detectors.**

On and near the crest armour units six wave detectors have been installed (Fig. 29 and Fig. 30). They measure the number of overtopping waves. By considering these measurements together one gets an idea about the extent of an overtopping event.

A wave detector consists of two electrodes which get short-circuited electrically when an overtopping wave hits the electrodes.

### **Measurements to identify hazards from wave overtopping**

Several instruments to identify and measure hazards resulting from wave overtopping have been installed at the Zeebrugge field site during CLASH. Within this framework wave forces on instrumented dummies, an instrumented pipeline and a vertical wall are measured. These impact measurements are supported by velocity measurements of overtopping water. Moreover, an investigation for the breaking of window glass is carried out. A detailed description of all measurement devices and the design is given in Geeraerts et al. (2003) and in Geeraerts & Boone (2004).

Three dummies have been installed and instrumented. Two of them are placed on the crest wall directly behind the armour units. The third (smaller) one is placed at the landward side of the access road on top of the breakwater's crest. The dummies are a rough schematization of human beings. They are instrumented to get information about the magnitude of forces exerted by overtopping waves on people walking or standing on top of a breakwater. Fig. 31 shows a general view at the three dummies as installed on site. Dimensions of the dummies' bodies are (1.70 m \* 0.50 m) for the large dummies and 1.40 m \* 0.40 m for the 'child' dummy. Forces on the dummies are measured by means of so-called S-shaped load cells (Tedeo-Huntleigh).



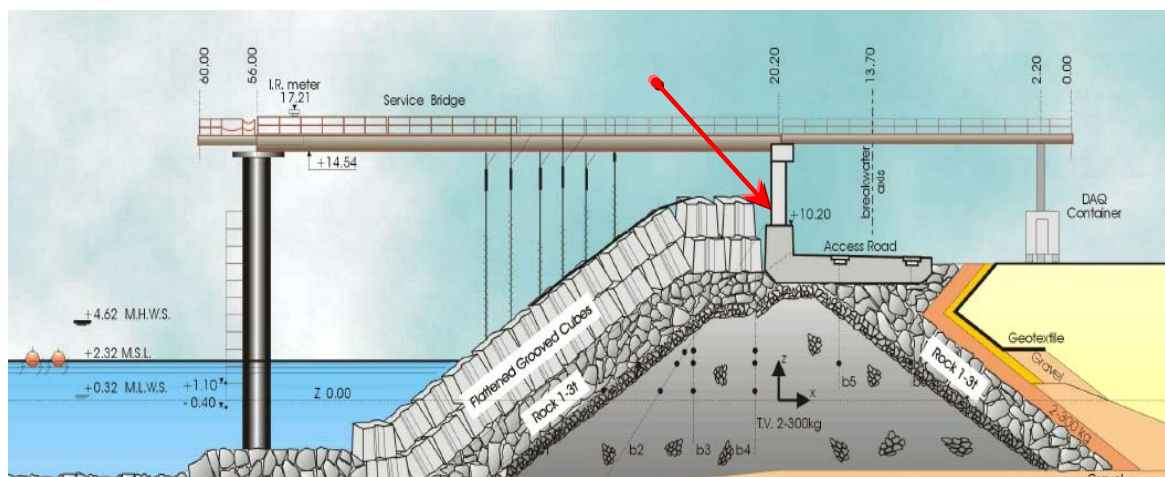
**Figure 31: Global view showing three installed instrumented dummies on site.**

In many harbours pipelines to transport oil or gas are installed on top of a breakwater. To gain information about overtopping wave forces on such pipelines, an instrumented "pipeline" (Fig. 31 and 32) has been installed. In fact it concerns a steel dredging hose with length = 6.00 m, diameter  $D = 0.65$  m and a wall thickness  $t = 0.01$  m. Horizontal and vertical force components on the pipeline are measured. Fig. 32 shows a general view of the pipeline as installed on site.



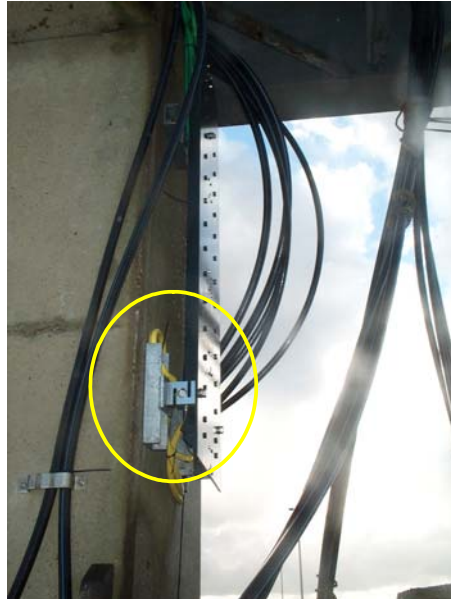
**Figure 32: Global view showing the instrumented pipeline on site.**

Force and pressure measurements on a vertical wall are carried out by measuring the force on an aluminium plate, with the same dimensions as the body plate of the dummies (1.70 m \* 0.50 m), mounted to the concrete column supporting the measurement jetty (see Fig. 33). This column serves as vertical wall. Forces are measured by three S-shaped load cells, with the same positioning and capacity as for the dummies. Fig. 34 shows a detail of the mounted body plate with indication of a mounted load cell. Moreover, pressures are measured by five flush-mounted pressure sensors positioned along a vertical line in the centre of the aluminium plate.



**Figure 33: Cross-section showing the section with the measurement jetty. The position of the measurements on the vertical wall is indicated.**





**Figure 34: Detail of force transducer for force measurements on vertical wall.**

Two velocity meters are installed at two locations between the armour units near the crest wall. One is located near the pipeline (Fig. 36); the other is situated in front of the large dummy nearest to the measurement jetty (Fig. 35). Each velocity meter consists of 2 (near pipeline) or 3 (near dummy) units that are horizontally installed on a metal frame. The one near the dummy consists of 3 units as the dummy is much higher than the pipeline. Each unit contains 3 pairs of electrodes which detect the presence of water at this location.



**Figure 35: Velocity meter in front of dummy.**



**Figure 36: Velocity meter in front of pipeline.**

## Measurement Results

Wave overtopping has been measured at the Zeebrugge breakwater during nine storms. An overview is given in Table 8.

**Table 8: Storms measured in Zeebrugge**

Storm No.	Date	Time	Duration (s)
1	6 November 1999	11h30 – 13h30	7200
2	6-7 November 1999	23h45 – 01h45	7200
3	8 November 2001	16h15 – 18h15	7200
4	26 February 2002	12h30 – 14h30	7200
5a	27 October 2002	17h00 – 18h00	3600
5b	27 October 2002	18h00 – 19h00	3600
5c	27 October 2002	19h00 – 20h15	4500
6	29 January 2003	10h00 – 12h00	7200
7	7 October 2003	12h00 – 14h00	7200
8	22 December 2003	00h00 – 02h00	7200
9	8 February 2004	14h45 – 16h45	7200

The time spans indicated are the time spans during which the *SWL* is almost constant (around the moment in time of high water  $t_{HW}$ ) and during which wave overtopping occurred.

Table 9 summarizes the wave characteristics for the different storms.

The wave overtopping data analysis results have been summarised in Table 10. The mean overtopping discharge per m structure width  $q$ , calculated according to three different methods as described in Troch et al. (2004) and Geeraerts & Boone (2004), is given there, together with the number of overtopping events.

**Table 9: Wave characteristics, surf similarity parameter and water level for the storms.**

Storm No.	$H_{m0}$ (m)	$H_s$ (m)	$T_{m-1,0}$ (s)	$T_p$ (s)	$T_m$ (s)	$\xi_0$ (-)	SWL (m Z)
1	3.04	2.89	6.88	7.34	5.70	3.52	5.28
2	2.60	2.44	6.93	9.3	5.36	3.88	5.11
3	3.47	3.31	8.41	10.28	6.35	4.05	5.01
4	2.63	2.52	6.49	7.91	5.32	3.68	4.21
5a	3.74	3.61	7.50	8.57	6.21	3.46	4.40
5b	3.86	3.71	7.64	8.57	6.35	3.47	4.60
5c	3.71	3.55	7.98	8.57	6.45	3.70	4.35
6	3.16	3.03	7.28	7.91	5.94	3.66	4.71
7	3.23	3.08	7.00	7.91	5.84	3.47	4.77
8	3.03	2.88	7.33	8.57	5.85	3.76	5.26
9	3.59	3.41	7.37	8.57	6.14	3.47	5.32

**Table 10: Average overtopping rates for all storms, calculated using the 3 methods based on the continuity equation, the individual overtopping volumes and the water depth jumps, respectively with  $N_{ov}$  the number of overtopping events.**

Storm No.	$q_{ceq}$ (l/sm)	$q_{vi}$ (l/sm)	$q_{\Delta h}$ (l/sm)	$N_{ov}$ (-)	$N_{ov}/\text{hour}$ (-)
1	3.161E-02	5.709E-02	4.677E-02	10	5
2	2.299E-02	2.211E-02	1.842E-02	3	1.5
3	2.825E-01	3.310E-01	3.588E-01	29	14.5
4	3.919E-03	1.010E-02	9.031E-03	1	0.5
5a	4.037E-01	5.158E-01	4.404E-01	19	19
5b	5.919E-01	8.585E-01	5.963E-01	30	30
5c	6.296E-01	7.036E-01	6.780E-01	31	24.8
6	8.479E-02	9.620E-02	8.646E-02	9	4.5
7	6.410E-02	8.920E-02	7.280E-02	9	4.5
8	2.900E-02	6.680E-02	5.590E-02	2	1
9	2.200E-01	5.910E-01	5.630E-01	16	8

Storms 1, 2, 4, 6, 7 and 8 have  $q$ -values lower than 0.1 l/sm, showing that there has been very little wave overtopping during these storms. Storms 3, 5a, 5b, 5c and 9 have  $q$ -values ranging between 0.3 (for storm 3) and 0.9 l/sm (for storm 5b), indicating more severe wave overtopping. The storms with small overtopping rates have a smaller number of overtopping events  $N_{ov}$ , whereas the storms with larger overtopping rates have a larger  $N_{ov}$ .

A comparison between the field data and three widely used prediction formulae has been made. The three prediction formulae used are the one according to Owen (1982); the update of the latter by Besley (1999) and the formula by van der Meer et al. (1998). In the formula by Besley (1999) the influence of a permeable crest berm is incorporated. All three formula need a value for the crest freeboard, i.e. the vertical distance between the still water level and the crest level, as input. Since this crest level is a very important parameter in the prediction, but is not clearly defined at the Zeebrugge site, three different values have been considered (Fig. 37). As minimum crest level the value corresponding to  $R_c$  as defined in WP2 was taken (i.e.  $Z+10.20$  m). As maximum crest level the value corresponding to  $A_c$  as defined in WP2 was taken. However, as can be seen in Fig. 37,  $A_c$  is not clearly defined for the Zeebrugge breakwater. For this reason the geometrical average of the bold line indicating the upper part of the armour in Fig. 37 was taken, i.e.  $Z+12.02$  m. Since water can pass in between the crest units of the armour, it was considered wise to consider also a third value for the crest level, i.e. the average value of the maximum and minimum crest level, i.e.  $Z+11.11$  m.

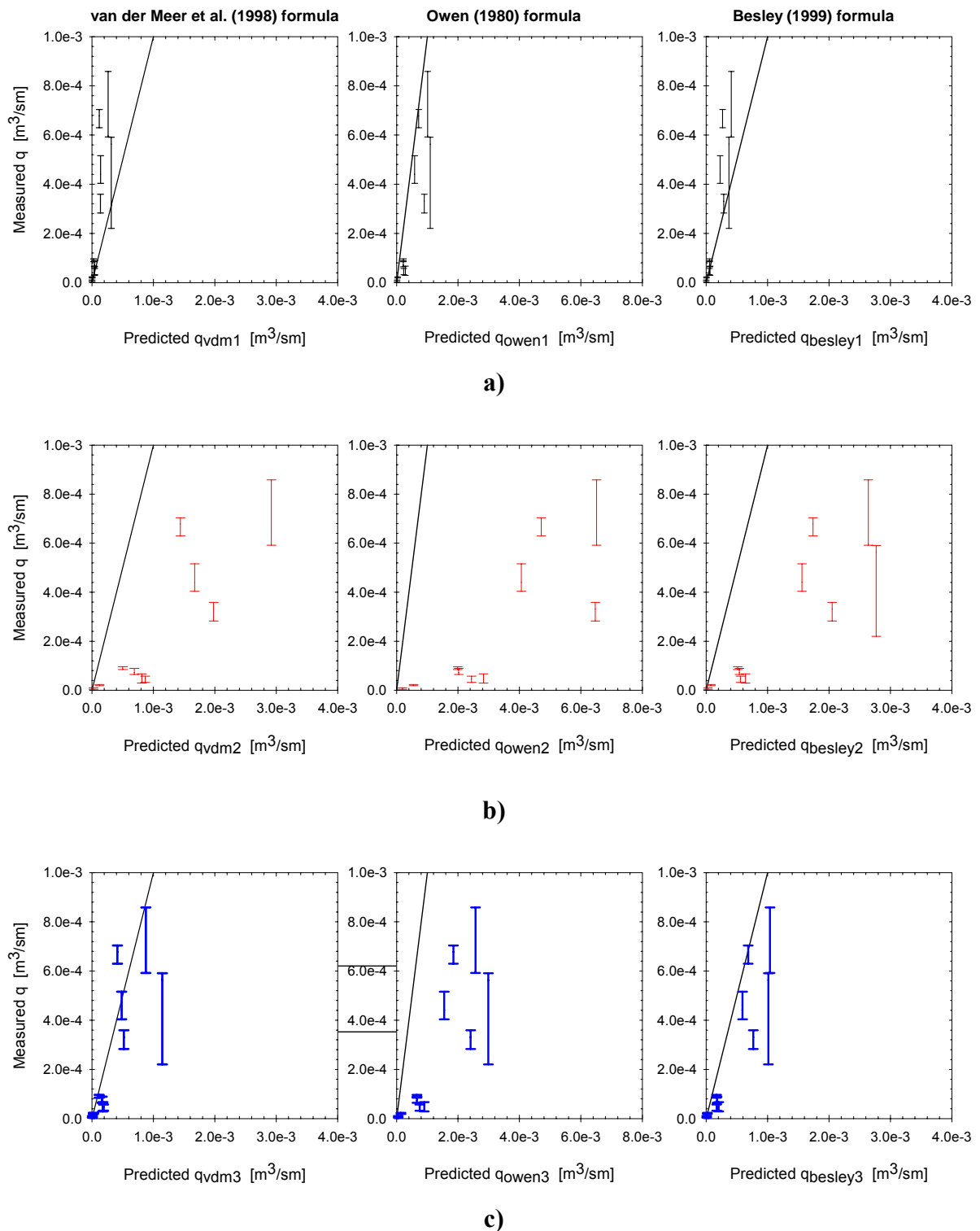


**Figure 37: Definition figure of three different crest levels taken into account.**

The measured average overtopping rates have been compared to the predicted average overtopping rates from van der Meer et al., Owen and Besley, in Fig. 38, for the three crest levels and associated crest freeboards. The range of the measured  $q$ -values obtained using the



three methods is indicated in Fig. 38 using a vertical bar. Linear scales have been used in the graphs.



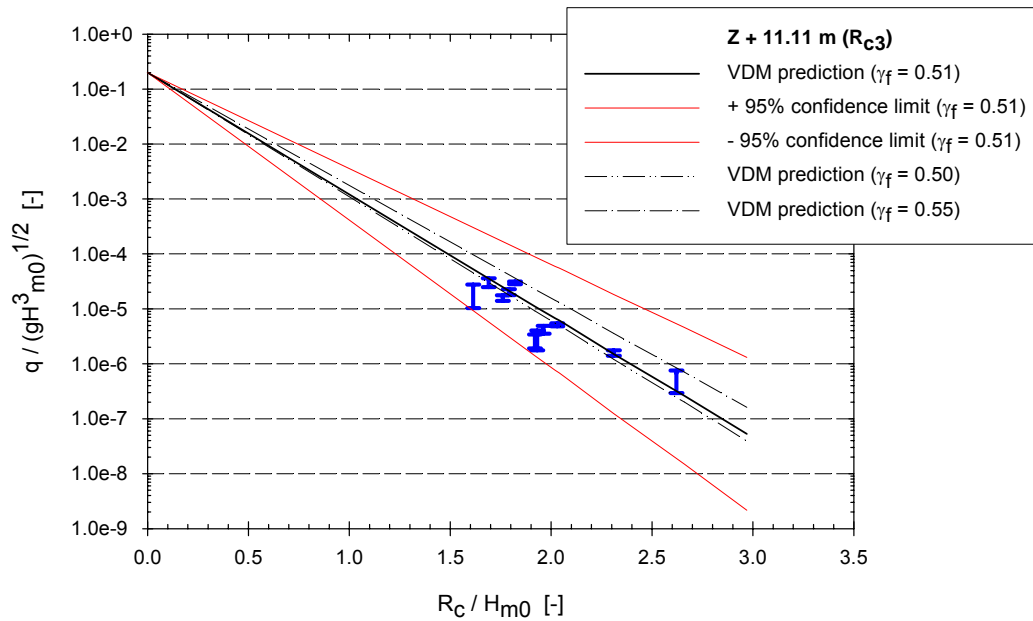
**Figure 38: Comparison between measured and predicted average overtopping rates, using van der Meer et al. (1998, left column), Owen (1980, middle column) and Besley (1999, right column) prediction formulae; for crest freeboards  $R_{c1}$  (a),  $R_{c2}$  (b) and  $R_{c3}$  (c).**

For the maximum crest level at  $Z + 12.02$  m (using  $R_{c1}$ , cf. Fig. 38(a)), the van der Meer et al. prediction underestimates the measured average overtopping rates by a factor up to about 6 (e.g. storm 5c), especially for higher  $q$ -values. Owen's prediction however slightly overestimates the measured overtopping rates, and the reduction of Besley shows good agreement for smaller  $q$ -values and underestimates larger  $q$ -values.

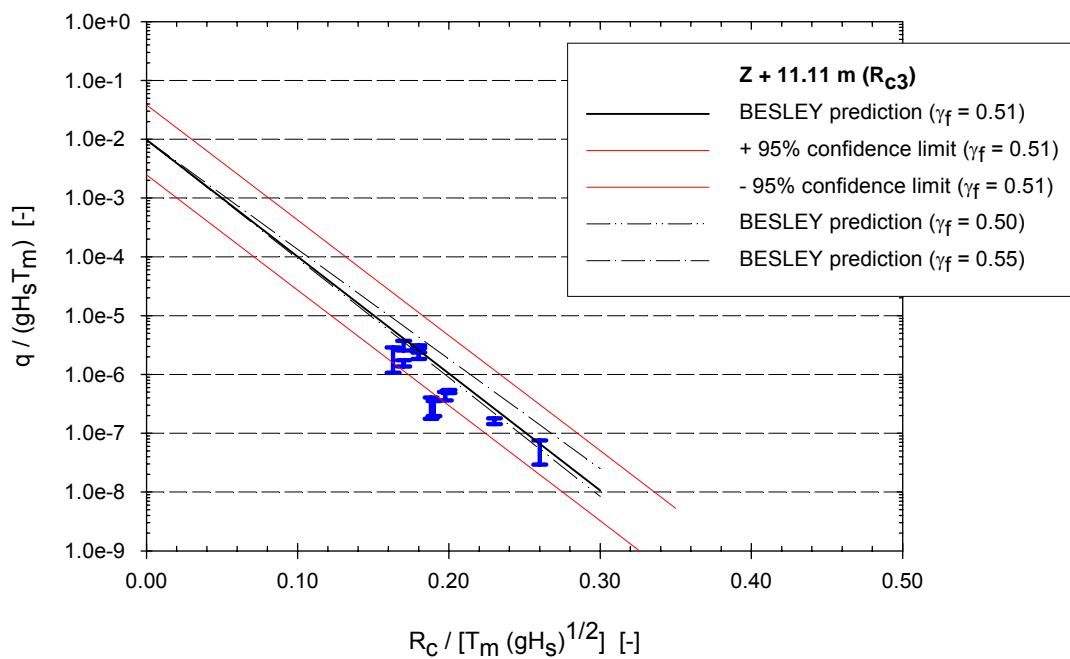
Using the minimum crest level at  $Z + 10.20$  m (using  $R_{c2}$ , cf. Fig. 38(b)), the predicted average overtopping rates from all formulae considerably overestimate the measured  $q$ -values. The van der Meer et al. and Besley predictions have the same magnitude, and the Owen prediction is about three times as large for the large overtopping rates. Finally, using the actual average crest level at  $Z + 11.11$  m (using  $R_{c3}$ , cf. Fig. 38(c)), the predicted  $q$ -values by van der Meer et al. and Besley are in relatively good agreement with the measured  $q$ -values, and the Owen prediction overestimates the measured average overtopping rates by a factor up to about 7 (for storm 3). In general best agreement between measured and predicted overtopping rates is observed using van der Meer et al.'s and Besley's prediction formulae for the actual average crest level  $Z + 11.11$  m and  $R_{c3}$ . Moreover Besley's prediction using  $R_{c3}$  is always on the safe (conservative) side.

A more traditional presentation of the prediction formulae is given in Fig. 39, where a dimensionless overtopping discharge (using a logarithmic scale) is plotted versus a dimensionless crest freeboard. The thick solid line is the prediction formula itself, the thin solid lines are the 95 % confidence intervals of the formula (based on variation coefficients provided by the author of the formula). For the prediction formula a roughness coefficient  $\gamma_f = 0.51$  was used. This factor originates from field measurements on run-up on the Zeebrugge breakwater (see Troch et al., 2004). The measured field data have been plotted in the same graph using vertical bars to indicate the scatter from using the three calculation methods. Fig. 39(a) and 39(b) show the resulting graphs for van der Meer et al. and Besley, respectively, for  $R_{c3}$  ( $Z + 11.11$  m).

The measured overtopping rates are within the 95 % confidence intervals of both prediction formulae (except one storm, for Besley's prediction, in Fig. 39(b)), and therefore good agreement is found between measured and predicted values. Also indicated in Fig. 70 are the prediction formulae using the recommended values for the surface roughness reduction factor  $\gamma_f = 0.50$  and  $\gamma_f = 0.55$  (applicable for designing a structure). For the case of the Zeebrugge breakwater, the value  $\gamma_f = 0.50$  shows best agreement with the measured overtopping rates.



a)



b)

**Figure 39: Measured and predicted (top (a): van der Meer et al., 1998; bottom (b): Besley (1999)) non-dimensional average overtopping rates and 95 % confidence limits as a function of the non-dimensional crest freeboard for the crest freeboard  $R_{c3}$ , using surface roughness reduction factor  $\gamma_f = 0.51$ . Also indicated are predicted overtopping rates for  $\gamma_f = 0.50$  and  $\gamma_f = 0.55$ .**

For average overtopping rates up to 1 l/sm very good agreement between the prototype average overtopping rates and the prediction formulae of van der Meer and Besley is achieved, taking into account the precise choice of surface roughness and crest freeboard parameters.

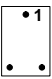
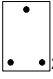
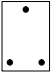
Wave impacts and overtopping velocities have been measured at the Zeebrugge breakwater since January 16<sup>th</sup>, 2003. From that moment on 3 storms have occurred: Oct. 7<sup>th</sup>, 2003, Dec. 22<sup>th</sup>, 2003 and Febr. 8<sup>th</sup>, 2004. The wave characteristics for these storms are repeated in Table 11.

**Table 11: Wave characteristics on Oct. 7<sup>th</sup>, 2003, Dec. 22<sup>th</sup>, 2003 and Febr. 8<sup>th</sup>, 2004.**

Storm No.	Date	Time	MWL (Z+ ...m)	H <sub>m0</sub> (m)	T <sub>p</sub> (s)
7	Oct. 7 <sup>th</sup> , 2003	12.00 - 14.00	4.77	3.23	7.91
8	Dec. 22 <sup>th</sup> , 2003	00.00 – 02.00	5.26	3.03	8.57
9	Febr. 8 <sup>th</sup> , 2004	14.45 – 16.45	5.32	3.59	8.57

No impacts were measured on the child dummy (dummy 1). Tables 12 and 13 present for each of these three storms the measured loads for the two most severe wave impact for the two respective dummies on the crest wall. From these tables it can be concluded that the highest impacts on the dummies - ca. 8100 N for dummy2 and ca. 8800 N for dummy3 - are measured during the storm of Febr. 8<sup>th</sup>, 2004

**Table 12: Total and individual impacts measured by load cells (LC) on dummy2 during resp. storms**

Date	LC1  (N)	LC2  (N)	LC3  (N)	Total impact (N)
Oct. 7 <sup>th</sup> , 2003	2520	120	655	3295
	610	800	590	2000
Dec. 22 <sup>th</sup> , 2003	375	405	390	1170
	315	430	155	900
Febr. 8 <sup>th</sup> , 2004	5590	1335	1185	<b><u>8110</u></b>
	2405	1790	1235	<b>5430</b>

**Table 13: Total and individual impacts measured by load cells (LC) on dummy3 during resp. storms**

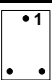

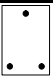
Date	LC1  (N)	LC2  (N)	LC3  (N)	Total impact (N)
Oct. 7 <sup>th</sup> , 2003	1245	1005	1375	3625
	665	995	1050	2710
Dec. 22 <sup>th</sup> , 2003	970	250	490	1710
	270	385	740	1395
Febr. 8 <sup>th</sup> , 2004	4970	1640	2225	<b><u>8835</u></b>
	1950	1015	1340	<b>4305</b>

Table 12 and 13 give measured loads for all load cells for respectively the plate on the vertical wall and the pipeline, together with the total load on both instruments during the two most heavy wave impacts.

**Table 14: Total and individual impacts measured by load cells (LC) on the vertical wall during resp. storms**

Date	LC1 (N)	LC2 (N)	LC3 (N)	Total impact (N)
Oct. 7 <sup>th</sup> , 2003	45	305	275	625
	135	55	105	295
Dec. 22 <sup>th</sup> , 2003	10	115	135	260
	205	50	-10	245
Febr. 8 <sup>th</sup> , 2004	411	630	386	<b><u>1427</u></b>
	505	115	110	<b>730</b>

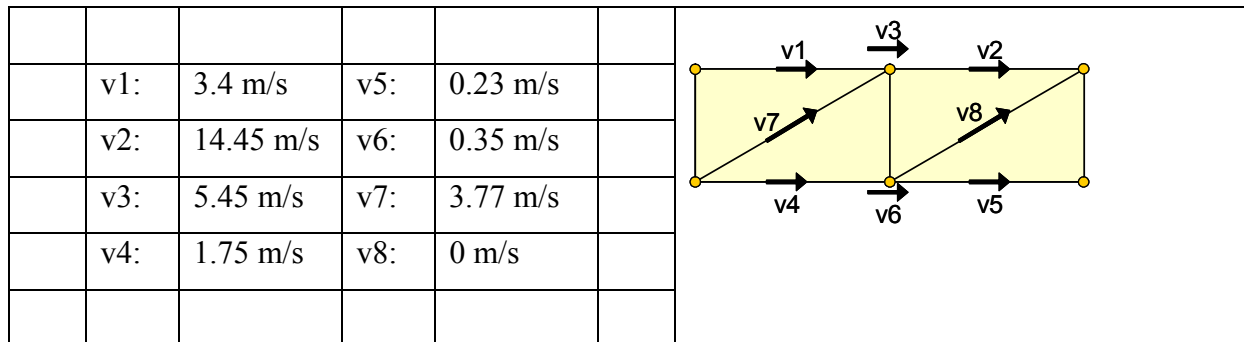
The maximum load (1425 N) on the vertical wall is measured on Febr. 8<sup>th</sup>, 2004.

**Table 15: Total and individual impacts measured by load cells (LC) on the pipeline during resp. storms**

Date	LC1 (N)	LC2 (N)	LC3 (N)	LC4 (N)	Total impact (N)	$\alpha$ (°)
Oct. 7 <sup>th</sup> , 2003	-450	-450	410	600	1350	-41.6
	465	525	285	215	1110	63.3
Dec. 22 <sup>th</sup> , 2003	805	815	645	565	2020	53.3
	725	890	645	1310	2535	39.5
Febr. 8 <sup>th</sup> , 2004	-2820	-2755	2460	2790	<b>7660</b>	-46.7

Comparable to the measurements of the dummies and the vertical wall, the highest total impact appears at Febr. 8<sup>th</sup> 2004. Impacts up to 5585 N and 7660 N are calculated over the whole length of the pipeline. These values correspond to line loads of resp. 930 N/m and 1300 N/m.

Maximum overtopping velocities have been measured during the Febr. 8<sup>th</sup> storm. At the moment of maximum impact at the pipeline (7660 N) velocities are measured in front of the pipeline. Fig. 40 gives an overview of the measured velocities at this specific moment. A maximum velocity of more than 14 m/s was measured.



**Figure 40: Velocities measured in front of the pipeline on Febr. 8<sup>th</sup> 2004.**

## Conclusions

The measurement set-up, using a waverider buoy to measure incident waves and an overtopping tank to catch the volumes of overtopping water, and equipped with an outflow weir on a short side and water depth measurements, has been used successfully to obtain reliable field data.

Eleven storm records have been used in the analysis of the field data, with duration between 1 and 2 hours, with significant wave heights ranging between 2.6 m and 3.9 m and peak periods ranging between 7 and 10 s. Although the measured storm conditions are considerably lower than the design storm conditions (with  $H_s = 6.20$  m and  $T_p = 9.0$  s), average overtopping rates close to 1 l/s.m (and  $\frac{q}{\sqrt{gH_s^3}} = O(10^{-5})$ ) have occurred.

Three methods for deriving the average overtopping rate inside the overtopping tank have been used, based on measurements of outflow discharge over the weir and instantaneous water depth inside the overtopping tank. These methods yield results that are in good agreement.

Average overtopping rates from the field data have been compared with predicted values from the widely used prediction formulae from van der Meer et al. (1998), Owen (1980) and



Besley (1999). For application of these formulae to the case of a rubble mound breakwater, the value of the reduction factor for the surface roughness of the armour layer used is 0.51.

The actual value for the crest freeboard parameter  $R_c$  for the case of the Zeebrugge breakwater is not obvious, and therefore a sensitivity analysis has been carried out, varying the crest freeboard between a maximum value  $R_{c1}$  (with crest level at  $Z + 12.02$  m), and a minimum value  $R_{c2}$  (with crest level at  $Z + 10.20$  m), and the average value  $R_{c3}$  (with crest level  $Z + 11.11$  m) between maximum and minimum values. Best agreement between measured and predicted values is observed using the average crest level (with  $R_{c3}$ ) and van der Meer et al's and Besley's prediction formulae.

For average overtopping rates up to 1 l/s.m very good agreement between the prototype average overtopping rates and the prediction formulae of van der Meer and Besley is achieved, taking into account the precise choice of surface roughness and crest freeboard parameters.

The measurement system to identify hazards is operational since January 2003. Since then, three storms with overtopping have been measured at the Zeebrugge breakwater: Oct. 7th, 2003, Dec. 22th, 2003 and Febr. 8th, 2004.

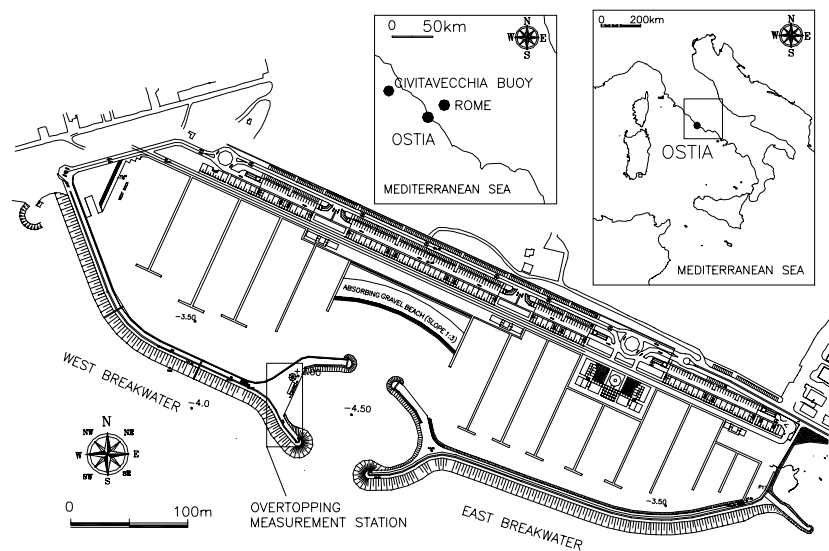
The highest impacts on the devices are measured during the storm of Febr. 8<sup>th</sup>, 2004: up to 8834 N/dummy and 7660 N/pipeline were measured. It has to be noted that these impacts were measured during a storm with only "moderate" mean wave overtopping  $q = 0.6$  l/s/m.

### 3.2.2 Site 2 : Ostia (Italy)

The measurement station is located in the new private yacht harbour of Rome, along the eroding sandy shores of Ostia, about 25 km from Rome, just South-West of the main mouth of the river Tiber, facing the Tyrrhenian Sea in central Italy (see Fig. 41). The harbour is protected by two rubble mound breakwaters (the west breakwater extending for some 600 m, the east one for 700 m), which converge to a central straight entrance to form an elliptic-shaped outer harbour with variable depths up to -5 m MSL. A gravel absorbing beach (slope 1:3) was created inside the harbour just facing the entrance in order to absorb waves penetrating into the basin.

The design cross-section of the final part of the west breakwater, which was chosen for the installation of the overtopping tank, is shown in Fig. 42. The crest level of the crown wall is set at +4.5 m MSL, also to reduce the visual impact. The rock armour seaward design slope is 1:3.5. The design armour stone gradation is 3-7 t.

The local tidal range is quite small (0.4 m), the water level at the structure toe is about -4.0 m MSL; waves at the toe of structure are depth-limited. The local wave climate can be obtained from the analysis of directional wave records available from a buoy installed at a depth of 12 m (see P0 in Fig. 43) during the period 1990-1992. As shown in Fig. 3 the highest and most frequent waves mainly come from the sector 240-250°N while there is a secondary sector between 190°N and 210°N.



**Figure 41: Location map and layout of Rome yacht harbour at Ostia.**

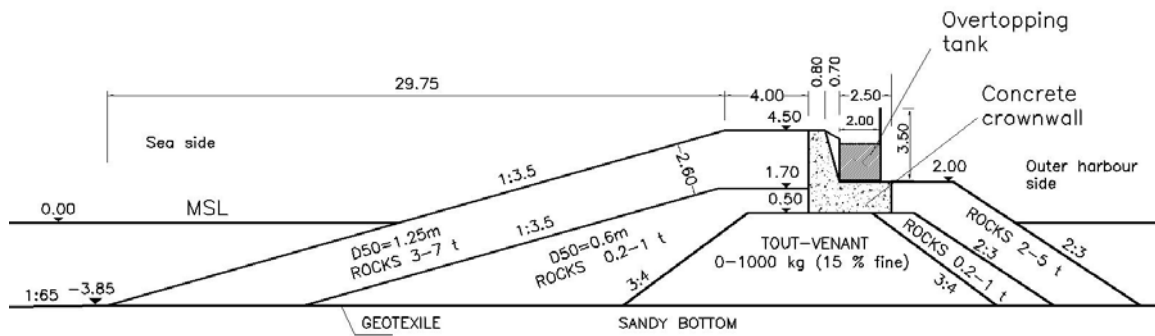


Figure 42: Design cross section of the west breakwater at the overtopping wave tank.

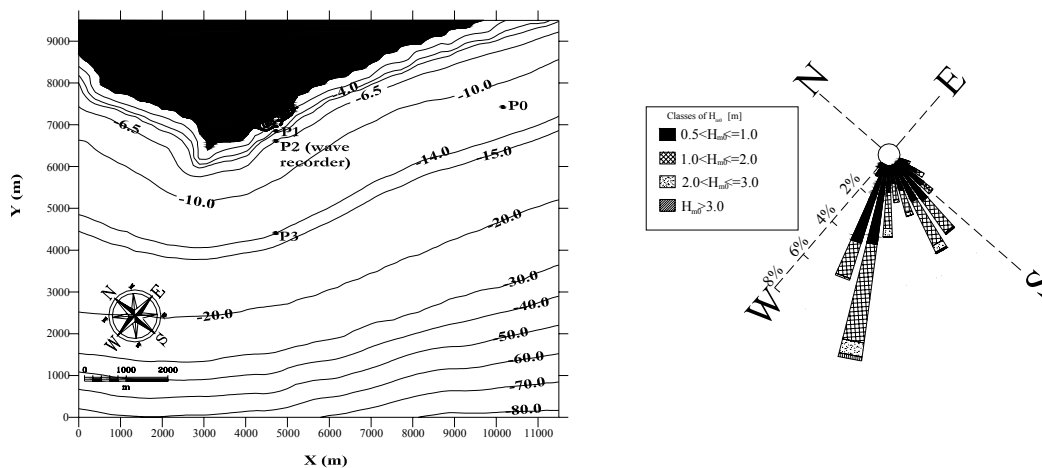


Figure 43: Foreshore grid bathymetry at Ostia (Tiber delta) (left panel) and local wave climate from directional wave records in the period 1990-1992 at a depth of -12 m MSL (buoy location in P0). P1, P2 and P3 indicate the points at which SWAN model results were extracted

The overtopping station is aimed at measuring individual volumes of waves overtopping the breakwater and the main meteorological and oceanographic conditions (waves, water levels, rain, wind, atmospheric pressure). The layout of the station with the location of all the instruments is shown in Fig. 44 together with the convention used in assessing the normal and tangential components of the wave attack and wind. The individual wave overtopping measurement technique also used with success in the companion field site of Zeebrugge

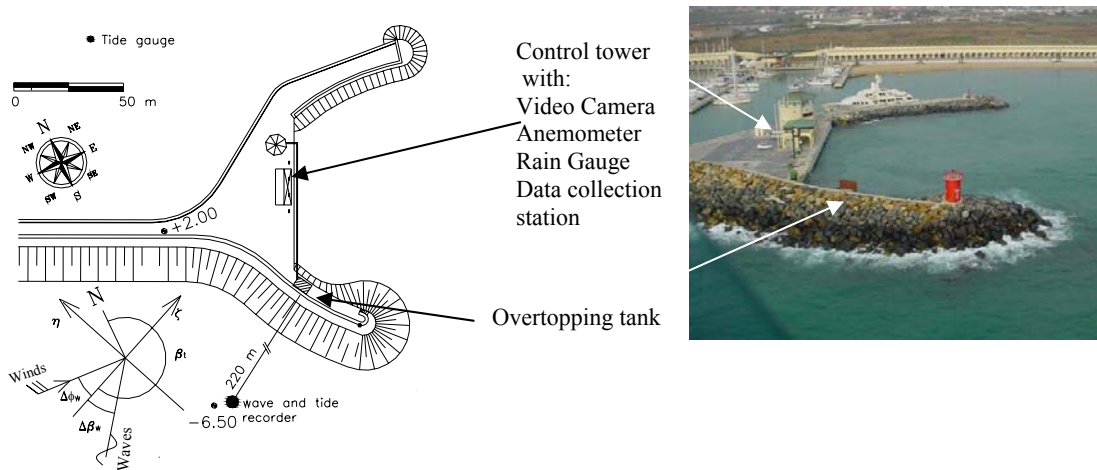
(Troch *et al.*, 2004). The method makes use of a tank collecting the overtopping waves; being the horizontal area of the tank known, the volume of each overtopping wave can be obtained by measuring the water level jumps.

The station was installed on the crown slab near the head of the west breakwater because of experienced localized occurrence of overtopping, vicinity to port control tower (daily control activity by the harbour personnel) and lack of interference with harbour activities and vehicular traffic. A simple steel tank (4 m x 2 m x 2 m height) was built and installed behind the parapet wall in October 2002 (see Fig. 45). A 1.5 m high screen was mounted on the inner side of the tank to ensure the collection of the highest overtopping waves, whose efficiency was actually confirmed by video records.

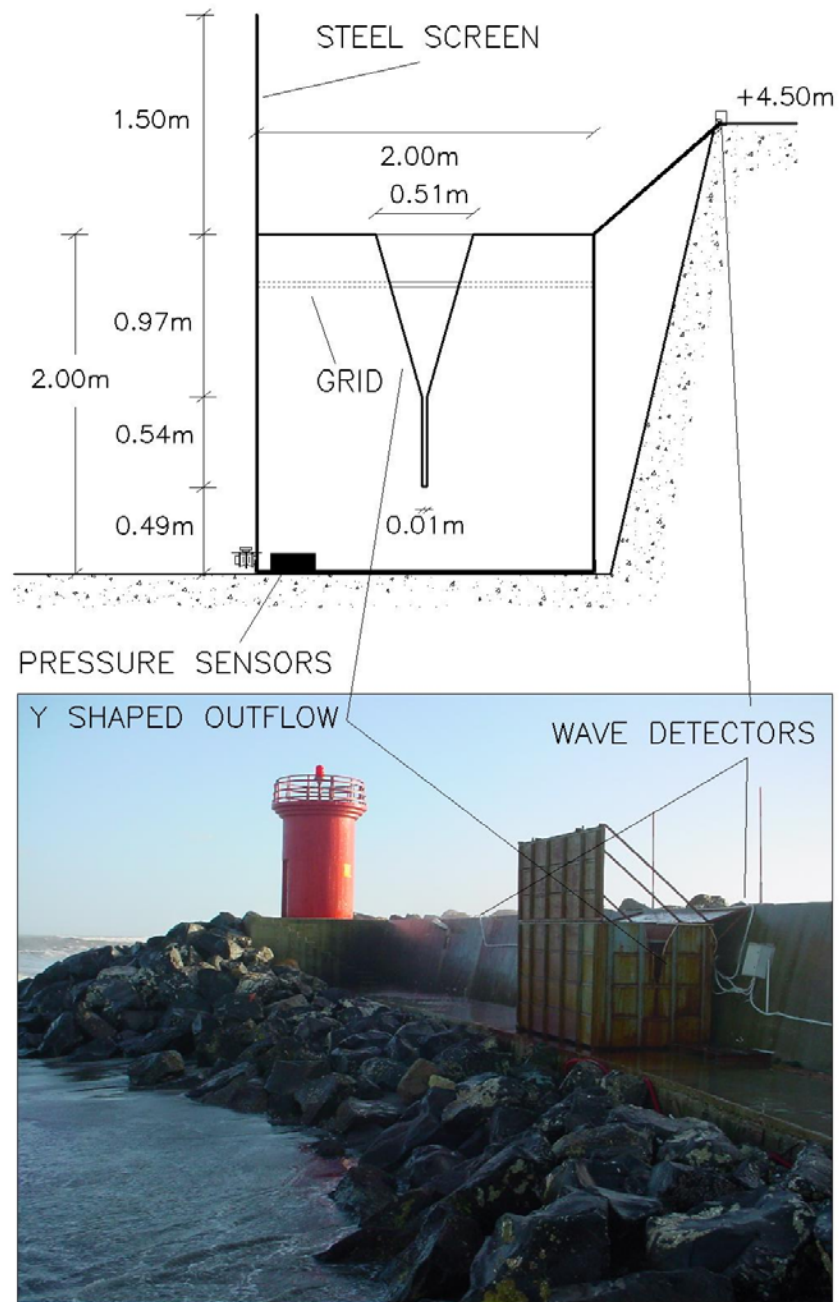
An outflow weir prevents the tank to be completely filled up during the overtopping storms. The outflow weir is designed in order to ensure a minimum outflowing discharge when collecting small overtopping waves, that are expected to induce small water level jumps of the water level inside the tank (order of magnitude of 1 cm) and larger outflow discharge when the level increases more quickly (10-20 cm) as a consequence of larger overtopping waves. The selected shape of the weir is therefore made up of two parts. The lower part begins 0.475 m from the tank base (see Fig. 45) and is a narrow rectangular vertical opening (width of 0.01 m, height of 0.54 m). The upper part is a V-shaped weir of height 0.97 m and upper width of 0.51 m.

The instantaneous water level inside the tank is measured by two pressure transducers (Druck 1830 PTX) working in the range 0-3 m which are installed in a box fixed on the bottom of the tank and hydraulically connected to the four corners of the tank to reduce the sloshing effects on the measurements. In late 2002 only one pressure transducer was installed; the second transducer was installed one year later in order to have redundancy of the measurements. The transducers signals, sampled at 10 Hz, are transmitted in real time by cable to a personal computer located in the nearby control tower and stored for later analysis. The water depth multiplied by the horizontal area of the tank (8 m<sup>2</sup>) gives the instantaneous volume of water inside the tank.

The normal to the long side of the wave tank (parallel to the wall), is aligned with the offshore direction of 229° N.



**Figure 44: Left panel: Layout of the overtopping measurement station in Rome yacht harbour. The convention for wind and wave angles is also indicated. A local frame of reference has been defined:  $\zeta$  is the normal direction to the tank,  $\eta$  is the tangent direction.  $\Delta\phi_w = \phi_w - \beta_t$  is the relative wind direction being  $\beta_t$  the normal to the tank ( $^\circ\text{N}$ ) and  $\phi_w$  is the wind direction ( $^\circ\text{N}$ ),  $\Delta\beta_w = \beta_w - \beta_t$  is the relative wave direction being  $\beta_w$  the wave direction ( $^\circ\text{N}$ ). Right panel: aerial photo of the overtopping measurement station (nov 2003).**



**Figure 45: Cross section and photo of the wave overtopping tank operational at Ostia breakwater.**

## Measured overtopping events

During fall-winter 2003-2004 seven severe storms with overtopping were recorded for a total of 86 hours of data. Table 16 indicates the dates and the durations of the recorded overtopping events.

During the first two recorded storms some connection problems occurred due to an unexpected oxidation of the electric contacts; hence the measurements stopped after about 9 hours of overtopping for both the storms. Storms 5 and 7 may be regarded as double peaked storms: hence, though the overtopping events didn't occur for a few hours within each storm, they are classified as single storms. Also during storms 6 and 7, the cable connection between the control tower and the tank experienced some problems and some measurements are missing. It is finally worth mentioning that the starting time of the records may be different from the actual starting time of the overtopping events as the instruments were not measuring continuously and the acquisition process had to be started each time by the research team.

Wave, sea level and wind conditions showed very moderate variation over typical duration of one hour; all the data have been therefore analysed on an hourly basis.

**Table 16: Dates and duration of the recorded overtopping events at Ostia breakwater.**

Storm No.	Date Dd/mm/yyyy	Start - end time of overtopping measurement (GMT+1)	Valid inshore (P2) wave and sea level records duration [hrs]	Valid offshore wave records duration at Civitavecchia [hrs]	Valid sea level records duration in the harbour [hrs]	Valid overtopping records duration [hrs]
1	05/10/2003	10:00 – 19:00	9	9	9	9
2	08/10/2003	00:00 – 09:00	9	9	9	9
3	23/10/2003	21:00 – 00:00	-	3	3	3
4	30/10/2003	09:00 – 20:00	-	2	11	11
5	27-28/11/2003	17:00 – 19:00	-	26	26	26
6	14-15/01/2004	18:00 – 15:00	-	21	21	13
7	23-24/01/2004	09:00 – 15:00	-	15	15	15
					total	86

Deep water wave characteristics have been retrieved from a directional wave buoy located offshore Civitavecchia (50 km north of Ostia), moored on a 100m depth (see Fig. 41 for the buoy location).

The non-directional wave recorder installed within the CLASH project provided information on wave characteristics in shallow water, since it was moored on a 6.5 m depth. Unfortunately, this instrument worked properly only during the first two storms: between storms 2 and 3 fishing activities (unauthorized in that area) caused serious damages to the wave recorder that required a long repairing time. In order to overcome the lack of information on shallow water wave conditions, consistently with the procedures used within the CLASH project (Steendam *et al.*, 2004), the state-of-the art spectral model SWAN (Ris *et al.*, 1999) was applied to study wave propagation from offshore to the harbour breakwater using, as offshore boundary conditions, the wave parameters provided by the Civitavecchia buoy. The bathymetry used in the calculations is shown in Fig. 43. Table 17 summarizes the ranges in which wave parameters in Ostia at P1 and Civitavecchia as well as relative freeboards ( $R_c/H_{m0}$ ) at P1 varied during overtopping measurements for all recorded storms.



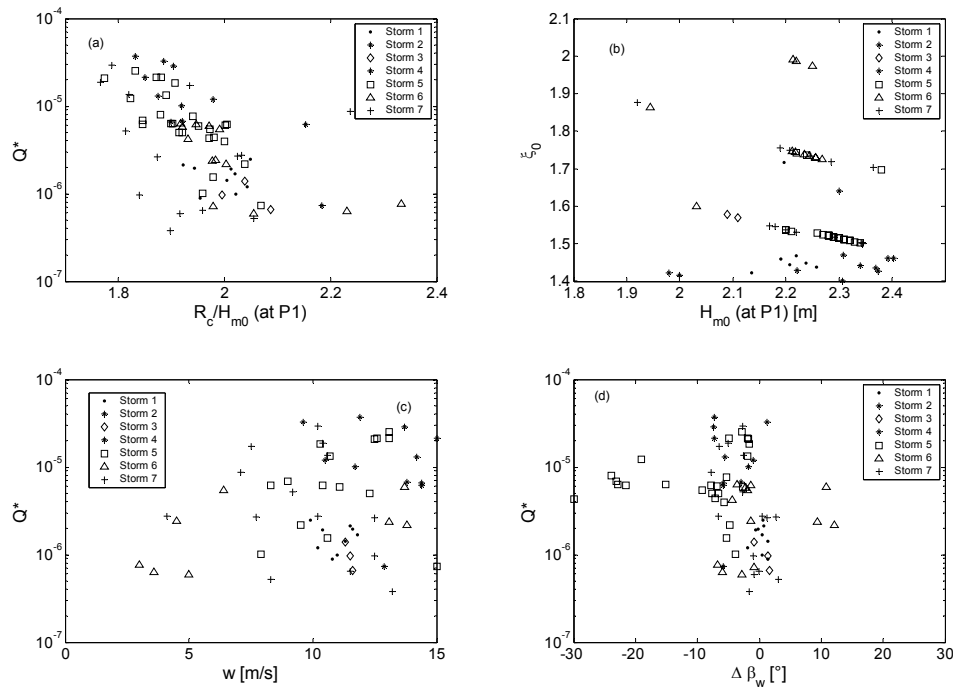
**Table 17: Ranges of variability of main wave parameters at toe (Ostia-P1) and offshore (Civitavecchia RON buoy) during the overtopping storms.**

Storm No.	Ostia at P1 (SWAN hindcasting); (in italic: measured data) (-4.0 m MSL)					Civitavecchia (-100 m MSL)		
		$H_{m0SWAN}$ [m]	$T_{pSWAN}$ [s]	Dir [°N]	$R_c/H_{m0}$	$H_{m0}$ [m]	$T_p$ [s]	Dir [°N]
1	Min	<i>2.14</i>	<i>8.39</i>	<i>230</i>	<i>2.05</i>	3.06	8.00	246
	Max	<i>2.26</i>	<i>9.56</i>	<i>229</i>	<i>1.92</i>	3.17	8.30	244
2	Min	<i>2.22</i>	<i>8.39</i>	<i>228</i>	<i>1.98</i>	3.01	8.00	242
	Max	<i>2.40</i>	<i>10.90</i>	<i>222</i>	<i>1.83</i>	3.47	10.00	234
3	Min	<i>2.09</i>	<i>8.39</i>	<i>228</i>	<i>2.09</i>	2.43	7.70	243
	Max	<i>2.11</i>	<i>8.39</i>	<i>230</i>	<i>2.00</i>	2.56	7.70	246
4	Min	<i>1.98</i>	<i>7.37</i>	<i>223</i>	<i>2.18</i>	2.34	6.90	232
	Max	<i>2.00</i>	<i>7.37</i>	<i>223</i>	<i>2.15</i>	2.27	6.90	234
5	Min	<i>2.15</i>	<i>7.37</i>	<i>199</i>	<i>2.07</i>	3.33	7.70	192
	Max	<i>2.38</i>	<i>10.89</i>	<i>227</i>	<i>1.77</i>	4.17	9.50	243
6	Min	<i>1.94</i>	<i>9.56</i>	<i>222</i>	<i>2.33</i>	1.95	8.30	236
	Max	<i>2.28</i>	<i>12.41</i>	<i>239</i>	<i>1.92</i>	4.16	9.50	292
7	Min	<i>1.74</i>	<i>9.56</i>	<i>222</i>	<i>2.57</i>	1.64	5.60	237
	Max	<i>2.37</i>	<i>10.90</i>	<i>224</i>	<i>1.77</i>	3.07	6.50	238

Wave overtopping rates have been calculated using two of the methods described in Troch et al. (2004) as explained in detail in Briganti *et al.* (2005, in review). Hence, according to the two different methods used, the overtopping rates computed using the numerical integration of the continuity equation will be referred as  $q_{ce}$ , while the value obtained applying the graphical method based on the level jumps in the overtopping signal (whose number is  $N_{jumps}$ ) will be referred as  $q_{\Delta h}$ .

In the following the number of overtopping events ( $N_{ov}$ ) will be considered equal to  $N_{jumps}$ .

In order to correlate the measured overtopping discharges with the most important related parameters, it is useful to analyse the scatter plots shown in Fig. 46.



**Figure 46: Scatter plots of the most important parameters recorded during the 86**

**overtopping events. Here  $Q^* = \frac{q_{\Delta h}}{\sqrt{gH_{m0}^3}}$ ,  $\xi_0 = \frac{\tan \alpha}{\sqrt{\frac{2\pi H_{m0}}{gT_{m-1,0}^2}}}$ ,  $w$  is the local wind speed,  $\Delta\beta_w$  is**

**local wave direction relative to the normal to breakwater axis.  $H_{m0}$  is the significant wave height at the toe of the structure.**

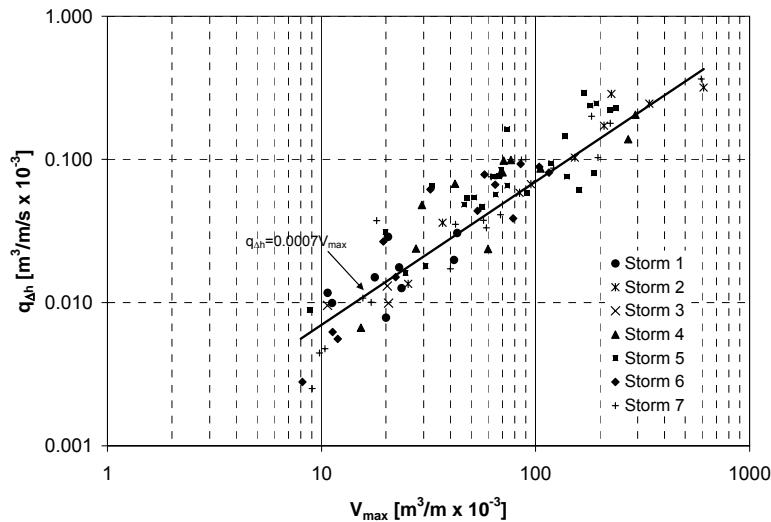
The non-dimensional wave overtopping rate  $Q^* = q_{\Delta h} / \sqrt{gH_{m0}^3}$  has been plotted against the wind speed module ( $w$ ), the relative freeboard ( $R_c/H_{m0}$ ) and the wave angle at the toe of the structure ( $\Delta\beta_w$ ). Also the surf similarity parameter ( $\xi_0$ ) has been plotted against the  $H_{m0}$  at the toe. A good inverse correlation is observed between  $Q^*$  and  $R_c/H_{m0}$ . Larger values of the dimensionless overtopping discharge ( $Q^*$ ) generally occurred with larger values of  $w$ .

Table 3 illustrates some parameters related to the peak mean unit overtopping discharges measured in all the recorded storms. It is evident that the  $H_{m0}$  at the toe of the structure spans within a very limited range, as it is depth-limited, while wave overtopping peak rates show a large variability among the storms.

**Table 18: Maxima values of measured average hourly overtopping rates during each of the 7 storms with corresponding relevant parameters.**

Storm No.	Time	$q_{\Delta h}$ [m <sup>3</sup> /m/s] x 10 <sup>-6</sup>	$q_{ce}$ [m <sup>3</sup> /m/s] x 10 <sup>-6</sup>	$H_{m0}$ [m]	$T_p$ [s]	$\Delta\beta$ [°]	$\xi$	$V_{max}$ [m <sup>3</sup> /m]	$N_{ov}$	$R_c/H_{m0}$
1	18:00	30.61	12.50	2.22	8.39	1	1.33	0.038	6	1.92
2	07:00	245.06	569.35	2.39	10.9	-7	1.46	0.340	4	1.83
3	22:00	13.07	20.44	2.09	8.39	-1	1.58	0.020	3	2.04
4	14:00	205.09	142.10					0.293	14	
5	13:00	293.06	256.95	2.34	9.56	-3	1.50	0.169	19	1.83
6	13:00	92.90	35.75	2.22	10.9	11	1.99	0.085	8	1.97
7	09:00	364.64	292.55	2.34	9.56	-3	1.50	0.595	13	1.79

Since the hazard related to wave overtopping is strictly related to the individual overtopping volumes (see Franco et al., 1995) it is also interesting to look for the correlation between the maximum individual volume per unit length recorded during each hour ( $V_{max}$ ) and the mean overtopping discharge (here  $q_{\Delta h}$  has been used as it is directly computed starting from the knowledge of individual overtopping volumes). This correlation is shown on a logarithmic scale in Fig. 47. No relevant differences appear in the correlation between these two parameters among the measured storms. Data have been plotted with a best-fitting line (regression coefficient  $R^2=0.74$ ) that reads:  $q_{\Delta h} = 0.0007V_{max}$ .



**Figure 47: Correlation between the mean hourly overtopping rate  $q_{\Delta h}$  and the maximum overtopping volume  $V_{\max}$  measured in the corresponding hour.**

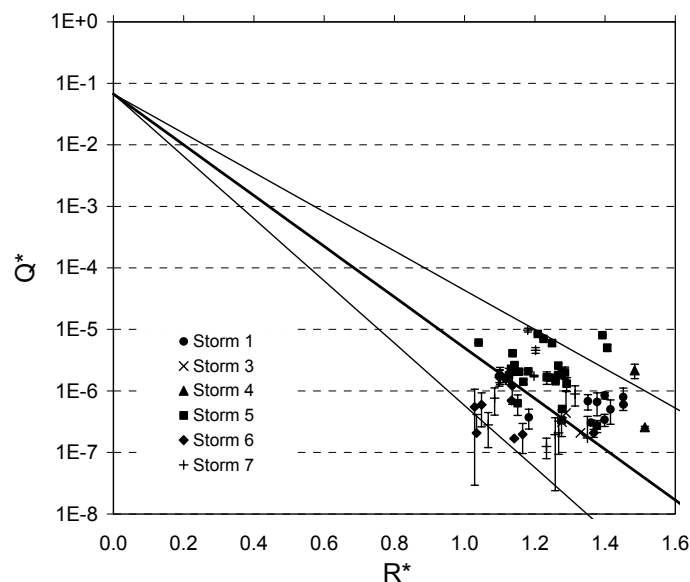
### Comparison between measured overtopping rates and prediction formulae

The overtopping events presented in this study are associated to oblique wave attacks and depth limited wave heights. Among the existing formulae, based on model studies, two of the most commonly used have been selected for predicting  $q_{ov}$  for the Ostia rock breakwater under investigation. The elder one is the one proposed by Owen (1980), originally developed for a straight and bermed impermeable slope subject to head-on irregular wave attacks. The use of a roughness factor extends the range of applicability of the formula to rough porous rubble mound structures. The alternative formula here considered for comparison is the van der Meer *et al.* (1998) formula, which included the effect of oblique wave attack, the formula here adopted makes use of the recommendations by TAW (2004). This latter formula, being the most widely used one for predicting overtopping rates at rubble mound breakwaters, will be presented first.

The comparison with the overtopping discharges predicted by the van der Meer *et al.* (1998) formula using the friction coefficient  $\gamma_f=0.5$  (Fig. 48 and Fig. 49) shows that almost all the prototype values fall within the confidence limits of the formula; only a few values for storm 5 and storm 7 fall out of the 95% confidence band of the parameter  $b_v$  used in the cited formula for defining the slope of the line in the  $Q^*$ - $R^*$  plane. As far as the storm 5 is concerned, the values show relatively large overtopping rates with high values of  $R_c/H_{m0}$ , as a possible consequence of an overestimation by SWAN of wave height reduction at P1 induced

by breaking. However it is worth pointing out that there is only a moderate tendency of the central value of the formula to underestimate the overtopping discharges. Furthermore it is to be considered that the used formula does not take into account the presence of the crest berm which has the effect of reducing the overtopping.

It can be concluded that prototype measurements are reasonably well predicted by the van der Meer *et al.* (1998) formula when using the suggested values of the reduction factors. However, when the effect of the crest berm (as it is present in reality) would be taken into account in this formula, the formula would underestimate the prototype results. Moreover, the roughness factor to be used for predictions is considerably smaller in this case (see also WP4), which results in an additional underprediction.

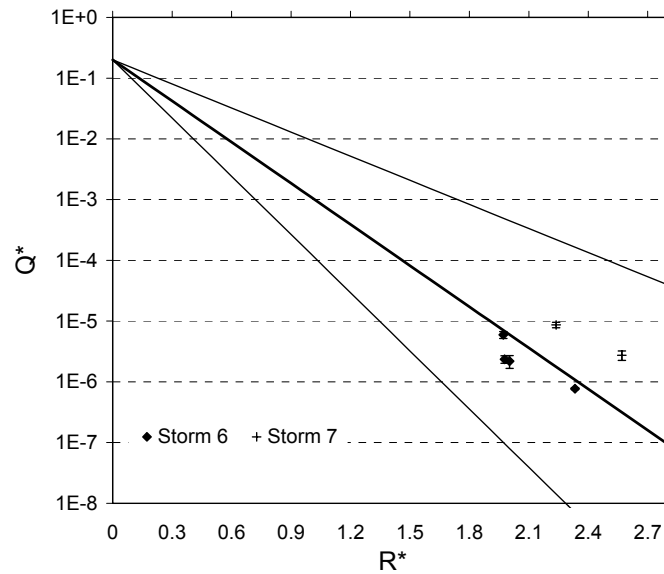


**Figure 48: Comparison between the measured adimensional mean overtopping discharges and those predicted using van der Meer *et al.* (1998) for breaking waves using  $\gamma_f = 0.5$**

(solid line thick line) together with the 95% confidence.  $Q^* = \frac{q_{ov}}{\sqrt{gH_{m0}^3}} \sqrt{\frac{s_0}{\tan \alpha}}$  and

$$R^* = \frac{R_c}{H_{m0}} \frac{\sqrt{s_0}}{\tan \alpha} \frac{1}{\gamma_b \gamma_\beta \gamma_v}. \text{ Error bars indicate the maximum and the minimum value of mean}$$

unit overtopping discharge obtained using the two illustrated methods.

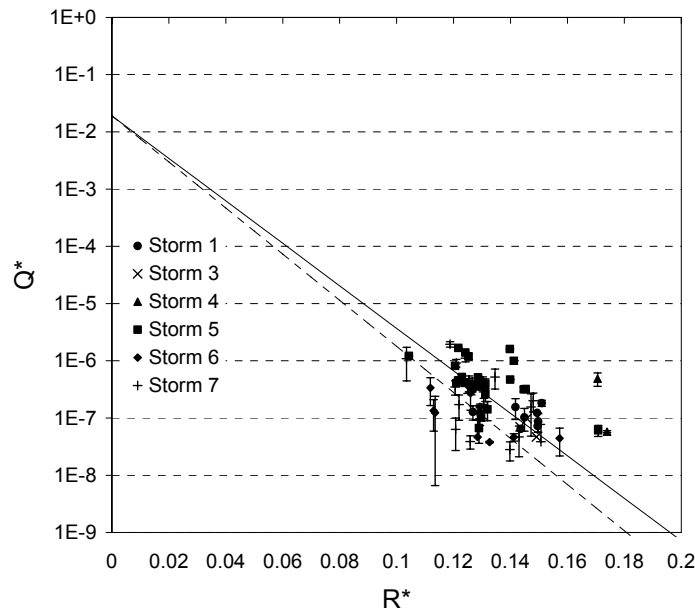


**Figure 49: Comparison between the measured adimensional mean overtopping discharges and those predicted using van der Meer et al. (1998) for breaking waves using  $\gamma_f = 0.5$  (solid line thick line) together with the 95% confidence limits (solid thin lines).**

$$Q^* = \frac{q_{ov}}{\sqrt{gH_{m0}^3}} \quad \text{and} \quad R^* = \frac{R_c}{H_{m0}} \frac{1}{\gamma_\beta}. \quad \text{Error bars indicate the maximum and the minimum}$$

**value of mean unit overtopping discharge obtained using the two illustrated methods.**

Fig. 50 illustrates the results of the comparison, being the Owen (1980) formula results represented by a solid line and Besley (1999) corection for accounting the presence of a crown berm by a dashed line. The prediction formulae, especially with the correction for the berm, has a tendency to underestimate the values of the overtopping rate.



**Figure 50: Comparison between the measured mean unit overtopping discharges and those predicted using Owen (1980) formula (solid line) and with crest berm correction as proposed by Besley (1999) (dashed line) during six of the seven measured storms with**

**overtopping  $Q^* = \frac{q_{ov}}{gH_{m0}T_{om}}$  and  $R^* = \frac{R_c}{H_{m0}} \left( \frac{s_{om}}{2\pi} \right)^{0.5}$ . Error bars indicate the maximum and the minimum value of mean unit overtopping discharge obtained using the two illustrated methods.  $\gamma_f = 0.5$ .**

## Conclusions

During the CLASH project an extensive (86 hours) and valuable field measurements of wave overtopping have been recorded at Rome-Ostia yacht harbour and analysed by MODIMAR. The setup of the prototype station is similar to the one presented in Troch *et al.* (2004) for Zeebrugge and developed during CLASH project as well. The reliability of the overtopping measurement procedure thereby introduced is then confirmed by the analyses here reported. Some relevant differences between the two sites may be highlighted. The Ostia site is characterised by a wide shallow foreshore which induces wave breaking before the structure hence, during overtopping storms, waves are always depth limited at the toe of the structure. Both wave measurements and wave model results (SWAN), validated on the recorded data of two storms, have been used to describe wave conditions across the foreshore and at the toe of the structure during overtopping storms. Furthermore, the Ostia rock breakwater has a slope

of 1:4, that is more gentle than the one of the Zeebrugge instrumented breakwater armoured with Antifer cubes (slope 1:1.4). Moreover oblique wave attacks causing overtopping have been also recorded and presented. It may be concluded that the most relevant difference between the two sites relies in the dissipation processes sustained by the waves in the propagation on the foreshore and on the structure itself.

A comparison of the measurements with two existing prediction formulae (i.e. the one proposed by van der Meer et al., 1998 and the one by Owen, 1980 with corrections by Besley, 1999) have been carried out. Both selected formulae show reasonably good estimates of the actual overtopping rates. It has to be noted that in this case prototype oblique waves and spectral characteristics which diverge from JONSWAP spectra have been taken into account for the first time.

The comparison carried out in the framework of CLASH seems however to confirm the suspected scale effects for wave overtopping at sloping rubble mound structures. The Owen (1980) formula as corrected by Besley (1999) to take into account the effect of a permeable crest berm, tends to underestimate the prototype results. The van der Meer et al. (1998) formula corresponds quite well to the prototype results. However, if the crest berm would be taken into account in the latter formula, it would also underestimate the results.

### 3.2.3 Site 3 : *Samphire Hoe (UK)*

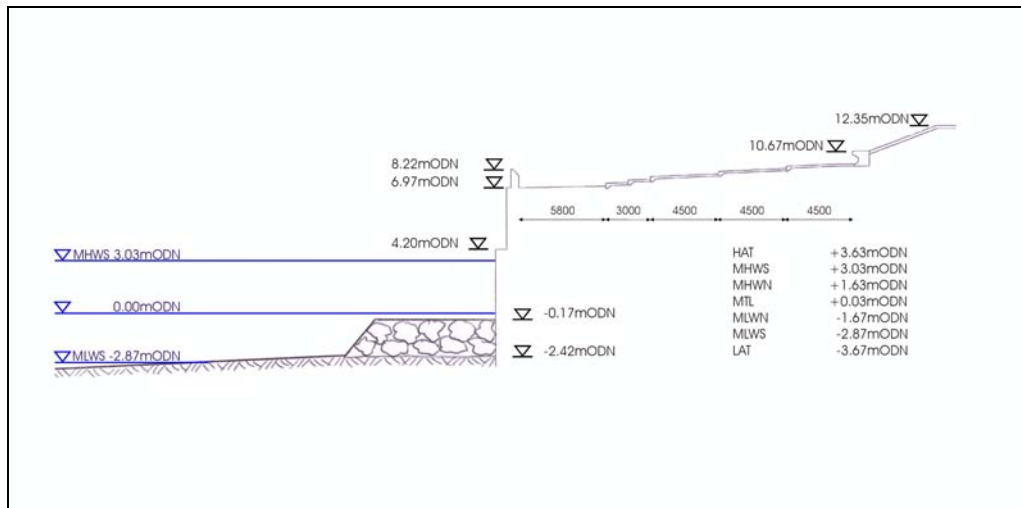
Samphire Hoe, shown in Fig. 50 where the study area has been boxed, is located in the Southeast corner of England immediately to the west of Dover, and is an area of reclaimed land comprising  $4.9\text{Mm}^3$  of chalk marl excavated from the Channel Tunnel. The area of approximately  $300000\text{m}^2$  is enclosed by a vertical seawall with a crest level at  $+8.22(\text{mODN})$  and a toe level at  $-2.42(\text{mODN})$ . To the top of the seawall is a 1.25m parapet wall fronting a 25m stepped promenade where the field monitoring equipment is deployed (see Fig. 51). Samphire Hoe, which is owned by Eurotunnel, has been landscaped and is operated by the White Cliffs Countryside Project as a public recreational area. The reclamation is exposed to waves from the southwest and southeast, and is subject to overtopping by spray (often termed white water overtopping) on approximately 30 days per year as a result of waves breaking over the rubble toe berm and impacting on the seawall face (see Fig. 52). Whole wave overtopping (usually termed “green water overtopping”) is also observed regularly.





**Figure 51: Aerial view of Samphire Hoe with the study area in the foreground**

HRW has designed and implemented over six years an overtopping hazard warning system using tailored input data from the UK Met Office, see Gouldby *et al.* (1999). These systems use forecasts of wind speed and direction with predicted tide and surge levels, to predict potential occurrences of hazards from wave overtopping. This system does not use direct calculations of overtopping discharges, but has been steadily refined over 5 years of operation, using hourly observations of hazard from overtopping, categorised as low, medium or severe, and recorded by on-site personnel who are responsible for the safety of the public. The site is, therefore, an ideal location to set up a programme of field measurements. In particular, the existing hazard warning system facilitated the identification of potential storms prior to the deployment of the field monitoring equipment.



**Figure 52: Section of the Samphire Hoe Seawall**

The principal objective in the design of the field monitoring equipment, was to be able to capture sufficient overtopping discharges across the promenade to determine with sufficient accuracy both the total volume and the spatial distribution. As can be seen from Figure 52, the overtopping discharge is distributed over a wide area and it would clearly have been impracticable to attempt to capture all of this discharge. Moreover, certain constraints were imposed on HRW by the site owner that prevented the placement of tanks in certain areas. Also, the equipment had to be transported to the site and installed on each visit, and so it had to be handled easily, constructed quickly and be easily transportable.



**Figure 53: Violent wave overtopping at Samphire Hoe (Photograph courtesy of Eurotunnel and the White Cliffs Countryside Project)**

The main pieces of equipment for measuring the overtopping, were three volumetric tanks placed across the promenade of the seawall. The first tank was placed directly behind the

parapet wall, and the others were placed inline with the first on the first and second steps of the promenade. This arrangement, along with the control box attached to the rear of the parapet wall, can be seen in Fig. 54. Each of the three tanks are divided into two compartments, each with a nominal capacity of 240 litres, and equipped with 350mbar Druck PTX1830 pressure transducers.



**Figure 54: The three tanks in position at Samphire Hoe**

The overtopping discharges captured in the tank compartments were allowed to drain freely, and so it was necessary only to capture the instantaneous head in each compartment following each individual overtopping event. This was necessary because the compartments would fill in a very short period during extreme conditions, but more particularly, it enabled the individual wave-by-wave discharges to be determined.

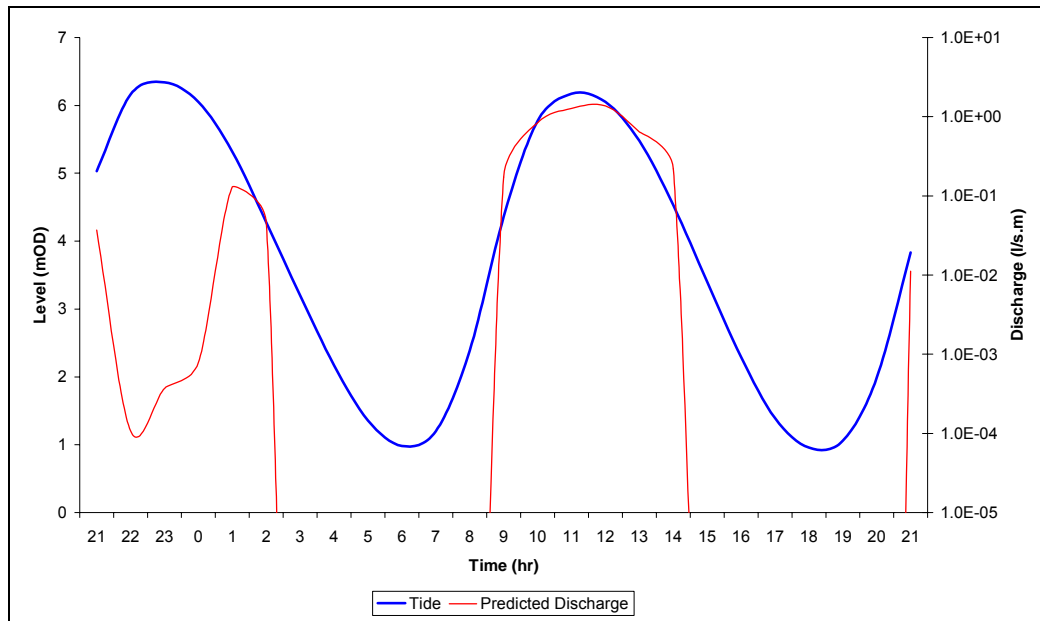
Design of the tanks was based on wave overtopping predictions and spatial distribution of the overtopping as suggested by Jensen & Sorensen (1979).

## Measurement Results

During the winter and spring of 2003 there were few storms that caused overtopping at Samphire Hoe, but weather forecasts suggested two occasions when it was useful to deploy the monitoring equipment at Samphire Hoe. The first visit was during March '03 where one storm was monitored on the 10<sup>th</sup>, and the second visit was during May '03 when storms were monitored on the 1<sup>st</sup> & 2<sup>nd</sup>. A range of conditions were encountered during these visits, and overtopping varied from light spray to high discharges from waves impacting violently on the seawall. For simplicity the three monitored storms will be referred to simply as Storm 01 (10 March), Storm 02 (1 May) & Storm 03 (2 May).

During Storm 01 overtopping water was seen to appear regularly over the top of the parapet wall, but this was in general sporadic and was spread along the length of the western splay wall. Those discharges that did pass over the top of the parapet wall were blown widely across the promenade as spray by high wind velocities, but no measurable quantities of overtopping discharge entered into the tanks. A conservative estimate of the mean overtopping discharge rate for this storm would be of the order of say 0.05 l/s.m.

Storm 02 was characterized by waves with  $H_s$  ranging from 1.5 to 2.2 m, while  $T_m$  was about 5.5 s. During the early stages of Storm 02 the wind speeds were at force 7, resulting in similar plumes of spray witnessed during the earlier storm. Predicted overtopping discharges are shown in Fig. 54 against the water level for this storm. From Fig. 54 it can be seen that a maximum overtopping discharge of approximately 1.4l/s.m was predicted at 12:00, but a peak discharge of 0.28l/s.m was recorded during the storm. This discrepancy is partially explained by the presence of the high winds, as most of the overtopping discharges were being blown across the seawall promenade and not falling into the overtopping tanks.



**Figure 55: The predicted overtopping discharges shown varying with the water level**

Storm 03 was characterized by wave heights  $H_s$  ranging between 1.3 and 2.6 m,  $T_m$  was about 6 s. For this storm there were very high winds during the early stages of the storm, and observations were made in this area when plumes of overtopping water were being blown over distances in excess of 100 m. Considerable quantities of this discharges were falling directly behind the parapet wall, where individual discharge volumes of between approximately 300 l/m and 500 l/m were estimated. If it is assumed that this represents about half the water in each overtopping event, then the remaining half was being blown across areas of the order of 3000 m<sup>2</sup>. Clearly the conditions were hazardous, and it was possible to determine a qualitative description of the hazards.

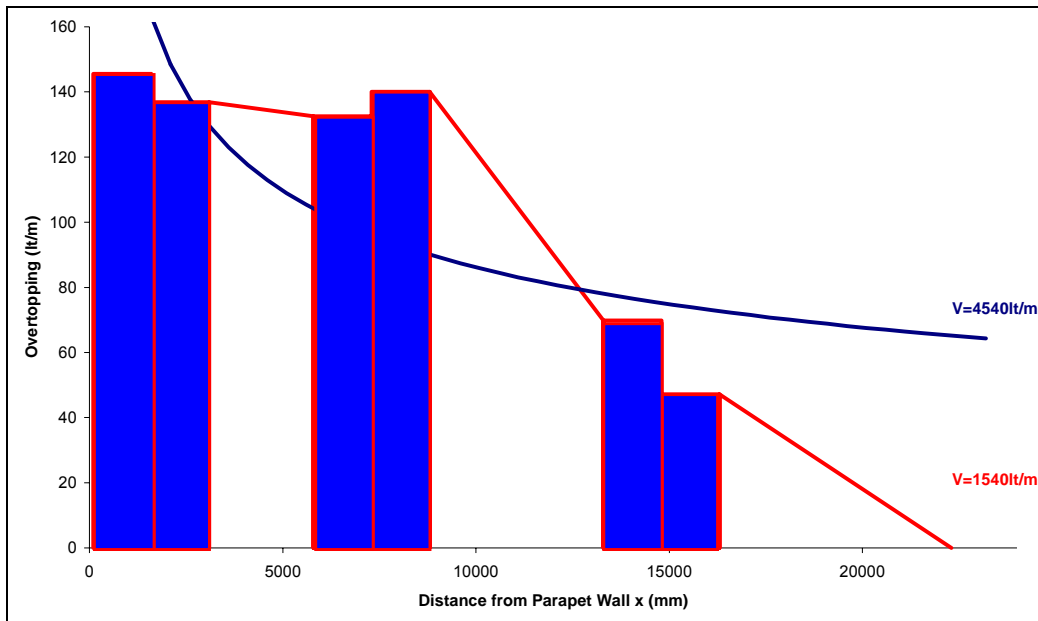
The volumes of water landing across the promenade became less severe on each tier, with the least landing on the top tier. It was decided that the only way to gain an improved scientific understanding of the potential hazards involved, was to stand directly in the path of the overtopping plume. It was agreed that standing on the top tier was equivalent to standing in a very heavy rain shower. Towards the lower tier, where it was still considered to be reasonably safe, the experience was similar to that which might be expected during a heavy hailstorm accompanied by a firm push on the back. Under these conditions, any unprepared people would be at high probability of being knocked over. Conditions directly behind the parapet wall were too hazardous to be approached closely. Later, when the water level had risen far enough to bring the overtopping to the measurement site, the wind speeds had become

insignificant. Without the winds the overtopping discharges were being directed vertically upwards and coming down in the area directly behind the parapet wall.

Each of the storms, specifically Storms 01 & 02, lasted several hours, and the water levels and wave conditions changed throughout this time. To allow for this, the measurements have been divided up into  $\frac{1}{2}$  hour periods. Each  $\frac{1}{2}$  hour period was assessed separately, and the recorded mean discharges were compared with Besley's (1999) predictions for mean overtopping discharges for a composite vertical wall. Strictly speaking, this technique is not wholly correct, as the Samphire Hoe seawall is actually slightly battered, stepping back as it does in three distinct sections. Nonetheless, they do provide an adequate means of comparing the results to known methods for these types of structures. Increased factors of 1.3 & 1.4 for walls battered to 10:1 & 5:1, respectively, are given by Bruce *et al.* (2001), and it is probable that these could be applied to composite structures, too.

Having established the individual overtopping discharges in each of the tank compartments, it was first necessary to approximate the discharges that had fallen outside of the tanks. Only then could a realistic comparison be made. The anticipated spatial distribution of the discharges might be similar to that described by Jensen & Sorensen (1979). Whilst this serves as a useful description, more often the actual behaviour was very different. For example, from the account of Storm 03 given above, it is noted that the overtopping discharges were often directed vertically upwards and came down directly behind the parapet wall, with the result that discharges were only captured in the front two tank compartments. For other events there was little difference among the volumes collected in the front four compartments.

For the analysis of the data a trapezoidal distribution of the individual volumes was assumed between the recorded data points and the back of the promenade 23.2 m from the seawall crest. The trapezoidal distribution of a large discharge is shown in Fig. 55, which shows overtopping distributed across all 6 tank compartments. Different distributions were assumed depending on how many tanks received a discharge, but each assumed this basic approach. In effect, the missing water was calculated between compartments 2 & 3, 4 & 5 and from the end of 6 to the point at 23.2 m in front of the recurve as appropriate. When the last discharge was in compartments 1, 3 or 5 then the distribution would stop at that point. The total discharge is therefore the sum of the discharges in the tanks and the interpolated discharges between the tanks. A comparison of the difference between a trapezoidal (1540 l/m) and a logarithmic discharge (4540 l/m) is also shown in Fig. 55 for the same captured volumes, and it is clear from this example that the trapezoidal distribution is a more realistic approximation.



**Figure 56: Trapezoidal distribution of overtopping discharges**

The analysed results of Storm 02 are shown in Fig. 56, and those for Storm 03 are shown in Fig. 58. These figures compare the field measurements with Besley's (1999) empirical overtopping prediction method for a composite vertical seawall. It is clear that they show that the general behaviour over the valid range is in agreement with the predictions. The most significant observation that can be made is that the data are slightly below the prediction line in Fig. 57 but more or less on the prediction line in Fig. 58. This should be expected as much of the overtopping water was being blown across the promenade during Storm 02, and so therefore the captured overtopping will be below that predicted. However, for Storm 03 the wind had little or no affect on the overtopping plumes, and so we see a good agreement with the prediction. For a more detailed discussion on these field measurements refer to Pullen *et al.* (2004a). No storms were measured at Samphire Hoe during the wintern 2003– 2004.

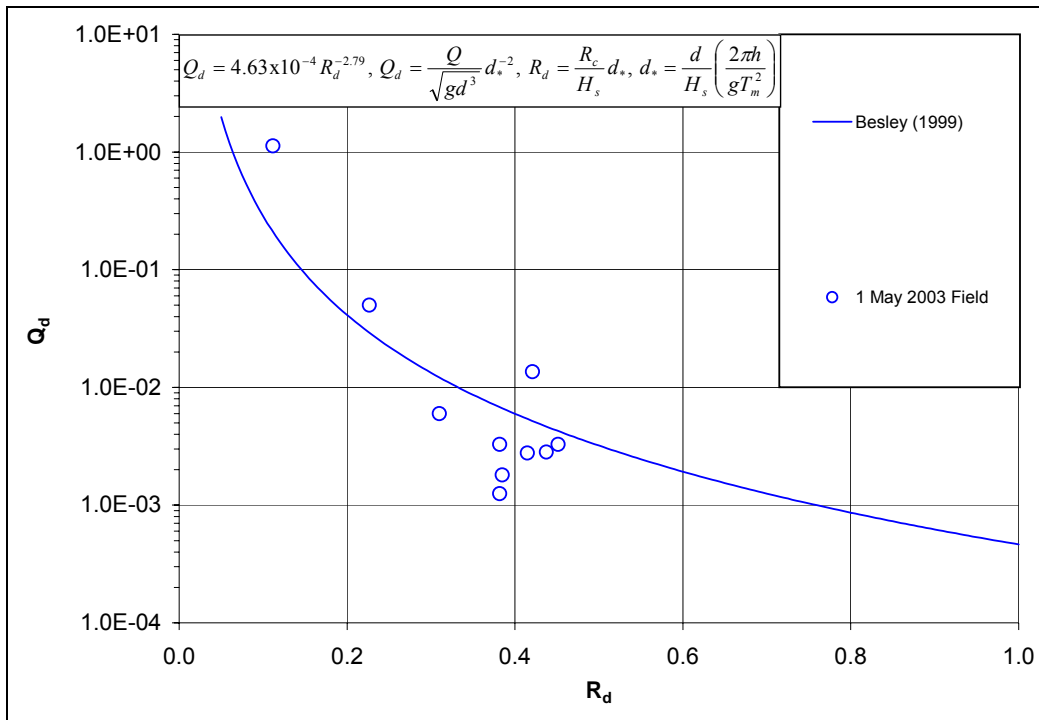


Figure 57: Measurements and predictions of overtopping during Storm 02

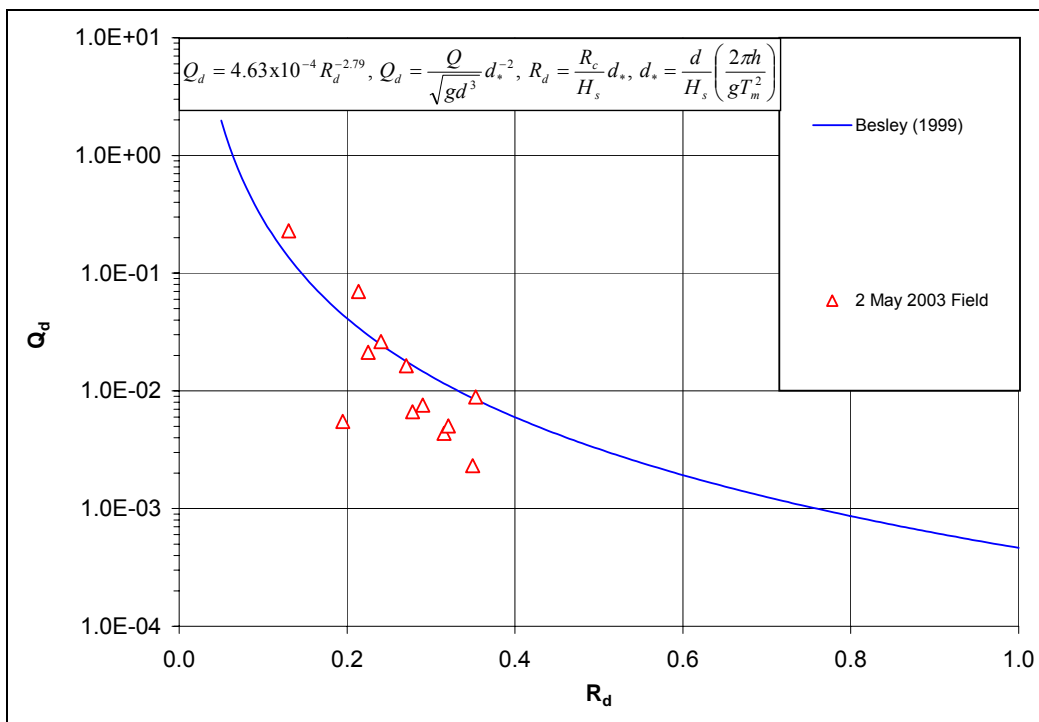


Figure 58: Measurements and predictions of overtopping during Storm 03

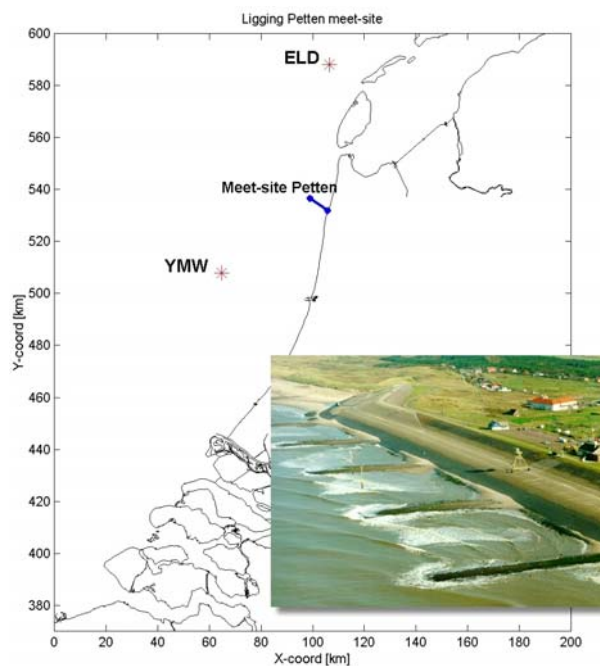


## Conclusions

Wave overtopping has been measured successfully at the Samphire Hoe field measurement site. The results are in agreement with the empirical prediction method for a composite vertical wall by Besley (1999). The spatial distribution of the overtopping has been established.

### 3.2.4 Site 4 : Petten (The Netherlands)

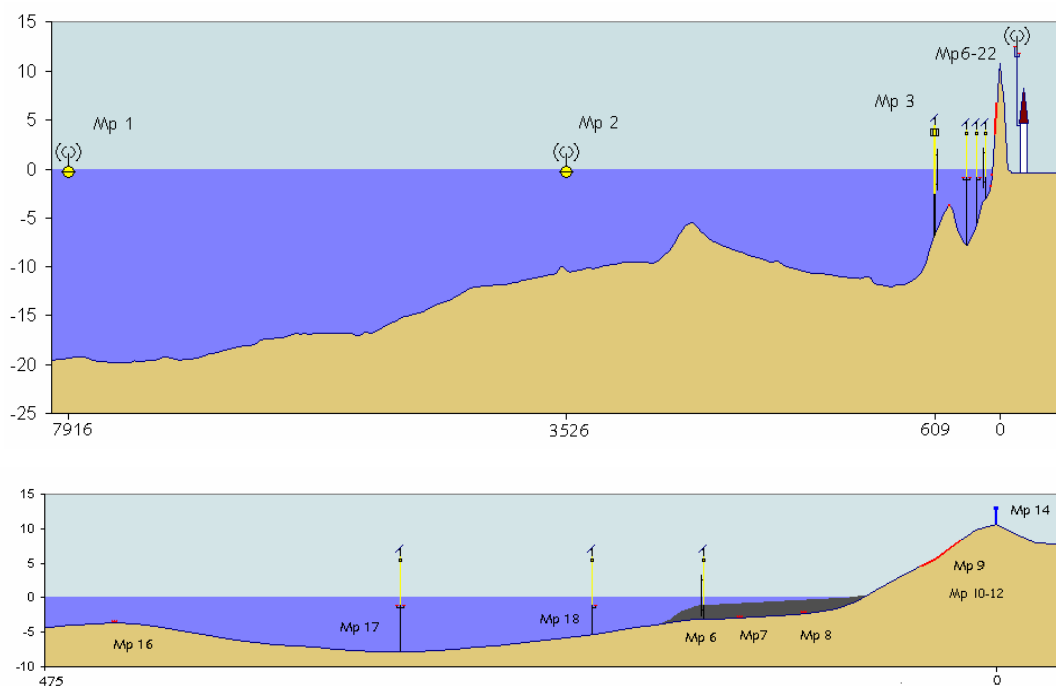
The field site is located off the coast of the province of North Holland near the town of Petten, where the Petten Sea Defence (Fig. 59) gives local shelter to the coastline. Determination of the height of the sea dike is based on a safety level with a chance of exceedence of 1/10000 per annum, and measures 12.75 metres above Dutch vertical reference level NAP. Over the years the adjacent dune areas have retreated, so that in comparison with the coastline the Petten Sea Defence extends slightly out into sea.



**Figure 59: Location of Petten field site**

To gain an understanding of wave propagation from deep water to the coastline, on-site measurements are taken at various distances from the dike at measuring points within or near section 20,830 of the Rijkswaterstaat annual coastal sounding programme. Wave run-up measurements are furthermore taken along the dike slope for use by the Road & Hydraulic Engineering Division. Fig. 59 shows the locations of all measuring points in a cross-shore profile corresponding with the measuring section. To avoid confusion, an enlarged graph of the relevant area shows the positions immediately offshore.

Some of the factors in selecting the measuring equipment are the location, the variables to be measured and the instruments available. The measuring points (MPs), the types of instrument and the locations are listed in table 19.



**Figure 60: Measuring points at Petten field site (distance and height in metres)**

### Morphological measurements

Especially during the last season some extra morphological measurements have been done to investigate the variability of the bottom profile in front of the dike.

Currents and waves cause sediment transport which in turn leads to constant changing of the cross-shore profile at the Petten Sea Defence. As the cross-shore profile has a direct effect on wave height, it is essential to monitor not only the waves but also the bottom topography changes. During storm season 2003–2004, the seabed was mapped several times by means of

soundings and groin section measurements. These random registrations do give information on the general seabed behaviour during the storm season, but not on the erosion depth during storms. To map the maximum erosion depth, which defines the maximum wave height, during storm season 2003–2004 the seabed level near MP 6 was also measured non-stop with an ASMIV seabed staff.

**Table 19: Measuring points and equipment at Petten field site**

Measuring point	Sensor/instrument	Dist. to ref. pt. <sup>1</sup> [m]	X coord RD [m]	Y coord RD [m]	Z [ <i>NAP</i> +/- m]	Location
MP 13	Anemometer (131), wind vane (132); Barometer (133)	-35	105798	531673	0.00	<i>Dijk te Kijk</i>
			105798	531673	0.00	
MP 22	Barometer (221)	-35	105798	531673	0.00	<i>Dijk te Kijk</i>
MP 14	Video camera 1 (141)	-0.2	105769	531693	17.3	Crest of dike
MP 19	Video cameras 2, 3 (191, 192)	1.1	105759	531677	16.6	Crest of dike
MP 12	Pressure sensor (121)	12.7	105749	531683	9.28	Dike's upper slope
MP 11	Pressure sensor (111)	18.2	105744	531685	7.23	Dike's upper slope
MP 9	Wave run-up staff (091)	19.4 (centre)	105743	531686	6.92 (centre)	Dike's upper slope
MP 10	Pressure sensor (101)	25.6	105738	531689	5.70	Dike's lower slope
MP 8	Pressure sensor (081)	55.7	105720	531719	0.55	Dike's lower slope
MP 7	Pressure sensor (071)	75.4	105703	531730	0.23	Groyne post
	Pressure sensor (072)	75.4	105703	531730	-0.29	Groyne post
MP 6	Capacitance wire (061)		105663	531752	-0.38	}
	Pressure sensor (062)	122.9	105663	531752	-0.92	}
	Radar level meter (063)	122.7	105663	531752	9.01	} Breaker
	Anemometer (064)	122	105663	531752	12.58	} bar post
	Wind vane (065)	122	105663	531752	12.58	}
	Water level staff (066)	122	105663	531752	-0.93	}
	ASM-IV (067)	122.7	105661	531715		}
MP 18	Pressure sensor (181)	170,5	105617	531771	-1.20	Sea bed
MP 17	Pressure sensors (171, 175)	276.7	105522	531817	-3.13	Sea bed
	Current meters (172, 173, 174)	276.7	105522	531817	-3.13	Sea bed
MP 16	Pressure sensors (161, 162)	436.6	105377	531886	-2.50	Sea bed
MP 3	Water level staff (031)	609	105234	531985	-3.00	Post
	Digital level meter (032)	609	105234	531985	0.00	Post
	Radar level meters (033/034)	609	105234	531985	11.32	Post
MP 2	Directional waverider (021)	3526	102896	533802		Petten <i>Polder</i>
MP 1	Directional waverider (011)	7916	99003	535832		<i>NAP</i> -20m

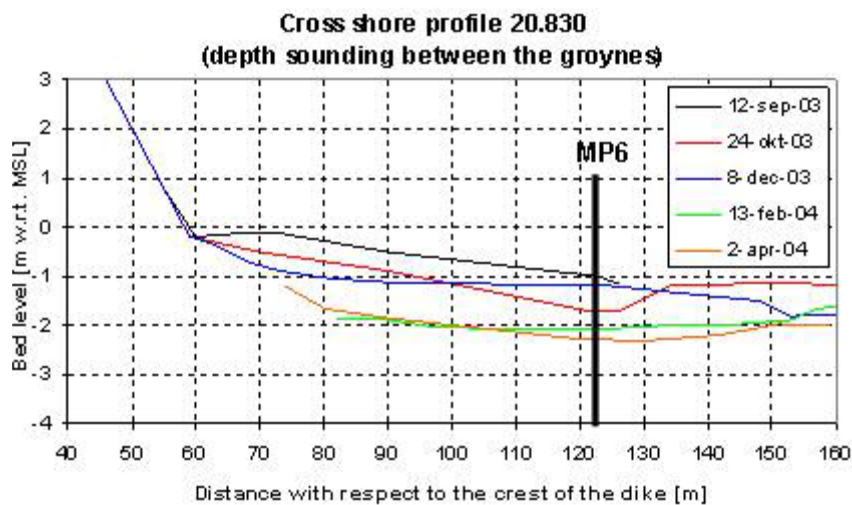
<sup>1</sup> The distance to the reference point is defined in relation to section 20,830 with zero coordinates

x = 105767, y = 531690 (corresponding with approx. the crest of the dike) and direction (nautical) 297,9 degrees

### *Groyne section measurements*

The groin section measurements were carried out for 7 parallel sections between the groins north and south of the measuring section. By using ‘WESP’, the seabed topography was registered to 100–150 metres seaward of the crest of the dike. The groin section measurements during storm season 2003-2004 were carried out on the following dates:

12 September 2003, 24 October 2003, 8 December 2003, 13 February 2004 and 2 April 2004



**Figure 61: Groyne section measurements Jarkus section 20,830**

Fig. 61 shows the results for the central section, i.e. section 20,830, corresponding with the measuring section. The registration on 12 September 2003 shows a typical summer profile with a large quantity of sand off the toe of the dike. It furthermore clearly shows that during the storm season there was considerable seabed erosion along the full section.

The data required for 3D processing are digitally available in ASCII format (X, Y, Z).

### *ASMIV sea bed staff*

Fig. 62 gives the levels near MP 6 as measured by the seabed staff from 17 October 2003 to 31 April 2004.

Fig. 62 shows that during the most recent storm season the bed level near MP 6 is subject to major changes. To determine the effect of erosion on the waves just off the dike, however, it does not suffice to make measurements at one single location. A more detailed analysis, where the ASMIV data are linked to spatial information, i.e. soundings and groin section measurements, is therefore strongly recommended.

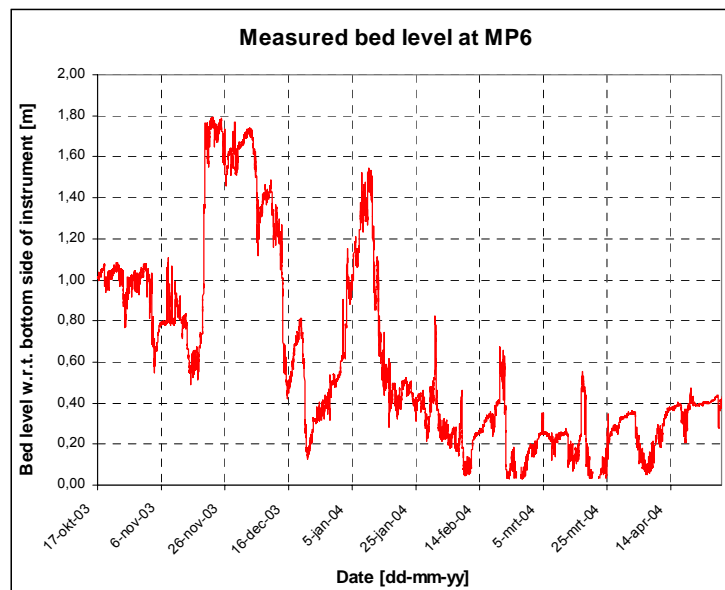


Figure 62: ASMIV results near MP 6

### Wave measurements

During the two storm seasons three interesting storm periods occurred : 25-28 October 2002, 20-22 December 2003 and 7-9 February 2004. Here the most interesting one will be described, storm period 20-22 December 2003. Figure 63 and 64 show the water levels and wave heights during this storm period.

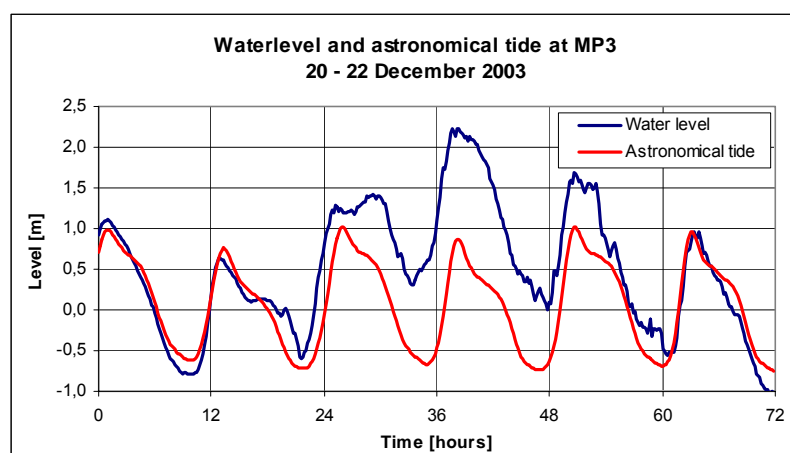
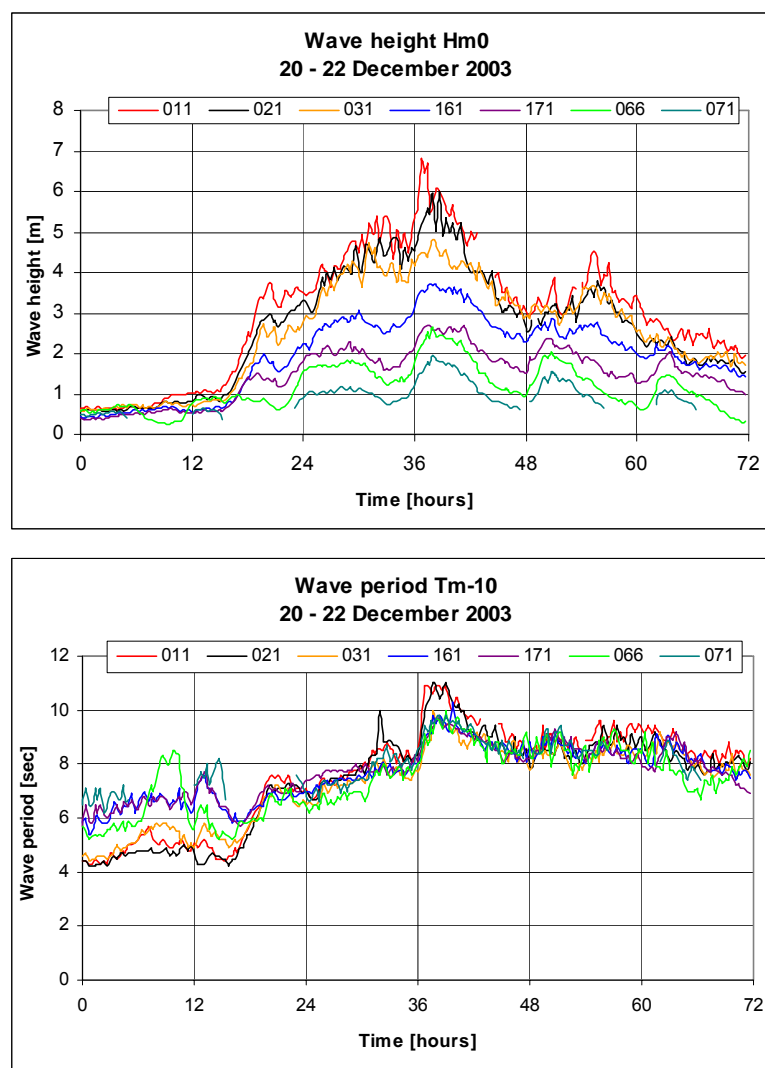


Figure 63: Water level at MP3 during the December 2003 storm.

Figure 64 clearly shows that on the first day and over a short period of time, wave height near MP 1 increases strongly to nearly 4 metres. The highest waves were measured at high tide in the early afternoon of 21 December, when wave height  $H_{m0}$  varied between 2 metres off the dike and nearly 7 metres near MP 1.

The wave period  $T_{m-1,0}$ , which is susceptible of low frequency energy, i.e. long waves, increases to a maximum of approx. 11 seconds at MP 1. Another clear illustration is that after the peak of the storm  $T_{m-1,0}$  decreases only very gradually, which can be explained by the fact that there is still an extensive amount of low frequency energy present in the area after the storm.



**Figure 64: Wave height and wave period during the December 2003 storm.**

### ***Wave run-up measurements***

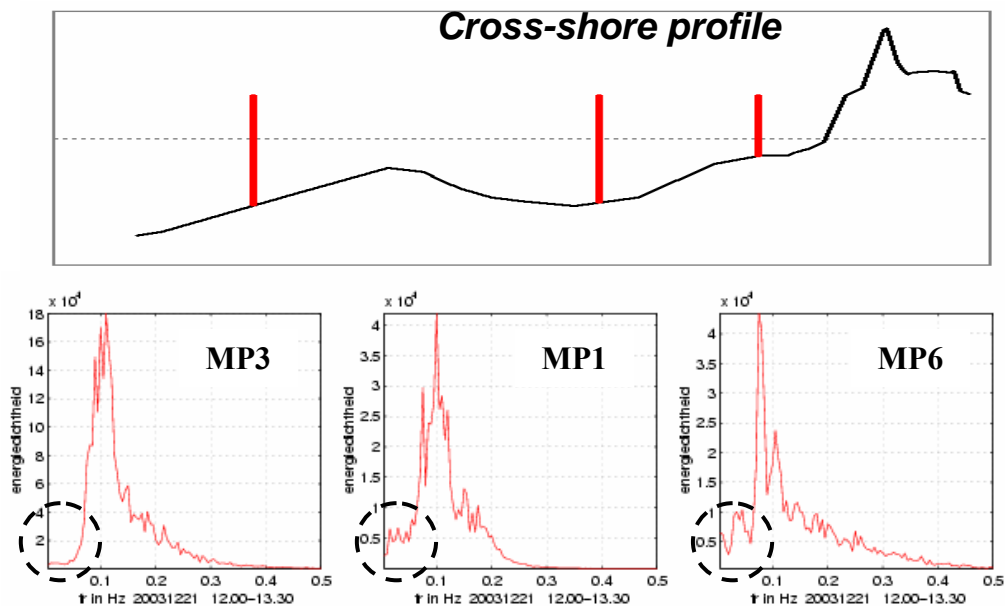
Run-up against the upper slope of the dike is measured by, among other instruments, a run-up staff placed in the dike revetment. The bottom end of this staff, which is 12 metres long, lies at NAP +5.70 metres. On 21 December 2003 run-up was measured between 12:45 hours and 18:00 hours, where it exceeded the levels NAP +6 metres, NAP +7 metres and NAP +8 metres during 527 seconds, 51 seconds and 12 seconds respectively. The highest run-up was NAP +8.91m.

### ***Low-frequency waves***

On the Petten field site, low frequency waves are most often measured during storm, where a distinction can be made between two types of long waves: low frequency waves originating from an earlier storm field elsewhere, also referred to as swell, and low frequency waves generated locally. This local generating is caused by the interaction between shorter waves and wave breaking in shallow water. The low frequency waves generated locally, with  $T_{m-1,0}$  exceeding 75 seconds, do not run up against the dike but cause a temporary water surface elevation, which enables shorter waves to run up higher against the dike.

To get an impression of the quantity of low frequency energy generated locally during the storm of 20–22 December, wave spectra are calculated for the peak of the storm (Fig. 65). It shows that there was some, although minimal, increase in low frequency energy between MPs 3 and 17 and between MPs 17 and 6.





**Figure 65: Spectra (including low frequency energy) calculated for instruments 031, 171 and 066.**

To gain an understanding of the relative share of the energy of low frequency waves (LFE) in the energy of the total spectrum, an analysis was made of both a storm period (27-28 October 2002) and a very calm day with (seaward) eastern wind (13 October 2002). On 13 October the  $H_{m0\_LFE}$  is no more than 0.04 metres but this is a relative share of 10% to 20% in wave height, and of 1% to 4% in the wave energy. It turns out that under storm conditions the low frequency wave height  $H_{m0\_LFE}$  increases considerably (on 27 October to approx. 0.60 metre). Local generating of long waves causes this increase. On 27 October the relative share of long waves compared to the total spectrum is approx. 10% ( $(H_{m0\_LFE}/H_{m0\_TOT})^2 = 0.30 * 0.30$ ).

## Conclusions

At the Petten field site, long waves are measured under both calm and stormy conditions. On 13 October 2002, a calm day with a seaward wind and short waves at a height of approx. 0.40 metres at MP 3, the relative share of long waves in the total spectrum's energy amounts 1% to 4%. The wave height for the filtered low frequency part of the spectrum is approx. 0.04 m.

Under storm conditions, the relative share of low frequency energy increases as a result of local generating of long waves. On 27 October, a storm day with waves up to approx. 5.5

metres at MP 3, values are measured up to approx. 0.60 metres for wave height  $H_{m0\_LFE}$ . With their long periods ( $T_{m-1,0}$  is approx. 75 sec), these long waves do not run up against the dike, but result in a temporary water surface elevation of approx. 0.30 m. The relative share of long waves in the total spectrum's energy is approx. 10%.

### 3.3 General conclusion for WP3

This WP delivered the following reports / deliverables:

a) for the Zeebrugge site:

- the report on full scale measurements, 1<sup>st</sup> full winter season (D15)
- the report on full scale measurements, 2<sup>nd</sup> full winter season (D31)

b) for the Ostia site:

- the report on full scale measurements, 1<sup>st</sup> full winter season (D16)
- the report on full scale measurements, 2<sup>nd</sup> full winter season (D32)

c) for the Samphire Hoe site:

- the report on full scale measurements, 1<sup>st</sup> full winter season (D17)
- the report on full scale measurements, 2<sup>nd</sup> full winter season (D33)

d) for the Petten site:

- the report on full scale measurements, 1<sup>st</sup> full winter season (D19)
- the report on full scale measurements, 2<sup>nd</sup> full winter season (D37)

Two milestones were achieved within this WP:

After the first full winter season (month 18 for the Zeebrugge, Ostia and Samphire Hoe site and month 19 for the Petten site), full scale measurements of all four sites are analysed and reported (M3). After the second full winter season (month 30 for the Zeebrugge, Ostia and Samphire Hoe site and month 31 for the Petten site), measurements of all sites are analysed and reported.

## 4 WP 4 : Laboratory investigation

### 4.1 Objectives

The main objective was to carry out a focused and well-directed set of scale model tests in order to provide data on overtopping for the comparison with full scale results. This comparison is performed in WP7 in order to solve the problem of suspected scale effects.

Another objective was to generate more and also missing data on overtopping to complete the homogeneous database (results of WP2). In WP2 possible missing parameters ranges were detected. These missing parameter ranges were the base for the additional tests carried out under WP4.

### 4.2 Description of work performed

Three different prototype sites were modelled in two different laboratories each. Additional tests to cover white spots in the database were carried out in three different laboratories. First the site specific tests are discussed and then the additional tests.

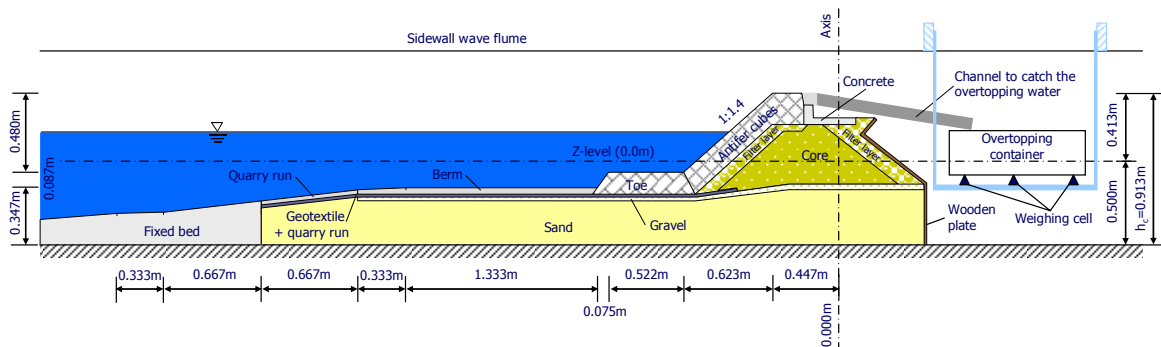
#### 4.2.1 Site 1 : Zeebrugge

CLASH focuses on investigations of wave overtopping for different structures in prototype and in laboratory. The Zeebrugge breakwater has been modelled in small-scale in the wave flume of Leichtweiß-Institute (LWI) at a scale of 1:30 and in the wind and wave test facility of the Universidad Politécnica de Valencia (UPVLC) at a 1:30 scale. The model investigations have concentrated on parametric tests on wave overtopping (LWI, UPVLC) and the analysis of measurement uncertainties and model effects (LWI, UPVLC) as well as the reproduction of storms (LWI, UPVLC), the influence of wind effects (UPVLC) and the positioning of armour elements (LWI, UPVLC).

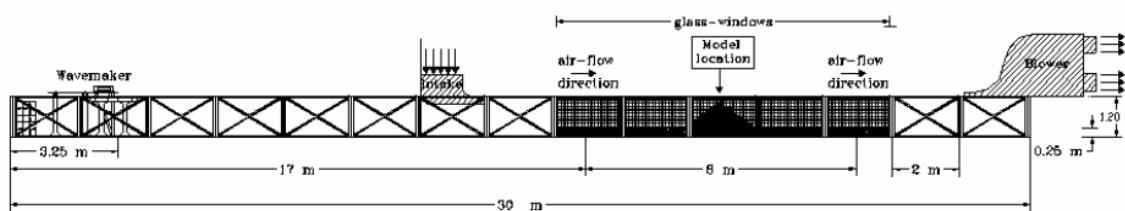
At LWI results regarding overtopping discharges for parametric tests, velocities of overtopping waves and forces on model dummies on top of the breakwaters crown wall were achieved. Altogether 226 tests have been performed; many of them were focussing on various uncertainty measurements such as repeatability, influence of position of the overtopping tray,

position of wave gauges, and various analysis methods. Furthermore, the influence of the armour layer was tested by exchanging the layer two times and performing the same tests. At UPVLC 53 parametric tests with and without wind, 17 repeatability and variability tests without wind, and 18 prototype tests with and without wind have been performed.

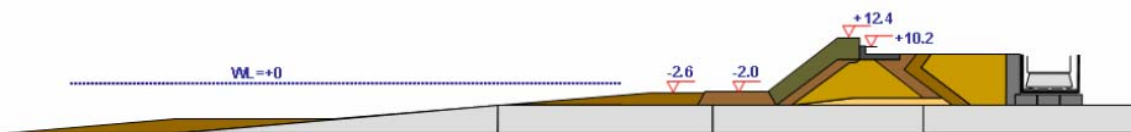
Fig. 66 gives a cross-section of the model set-up in the LWI flume. Fig. 67 and Fig. 68 give a cross-section of respectively the wind and wave facility and the Zeebrugge model at UPVLC.



**Figure 66:** Cross section of the model set-up of the Zeebrugge breakwater in the LWI wave flume.



**Figure 67:** Longitudinal cross section of the UPVLC wind and wave test facilities.



**Figure 68:** Cross section of the Zeebrugge scale model at UPVLC.

Fig. 69 and Fig. 70 show graphical representations of all model tests in a typical non-dimensional plot. Fig. 69 gives all parametric tests together with storm reproductions (all without wind), while Fig. 70 gives the influence of wind (three different wind speeds) on the measured overtopping.

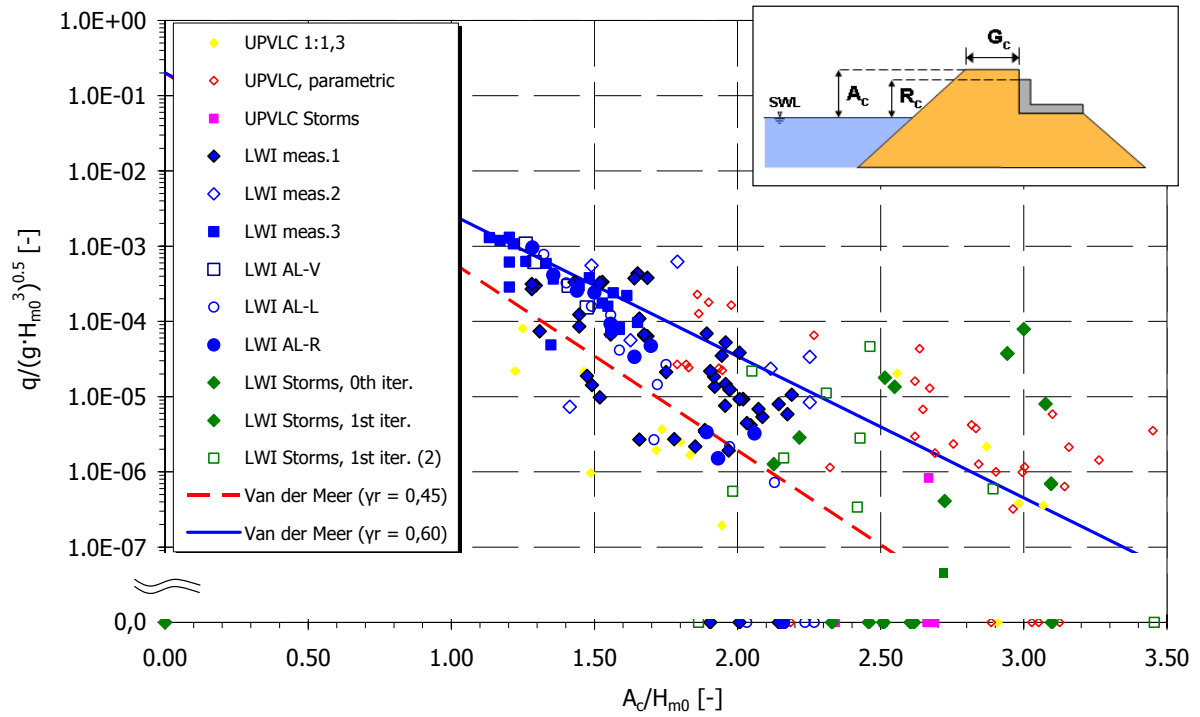


Figure 69: Zeebrugge model test results (no wind).

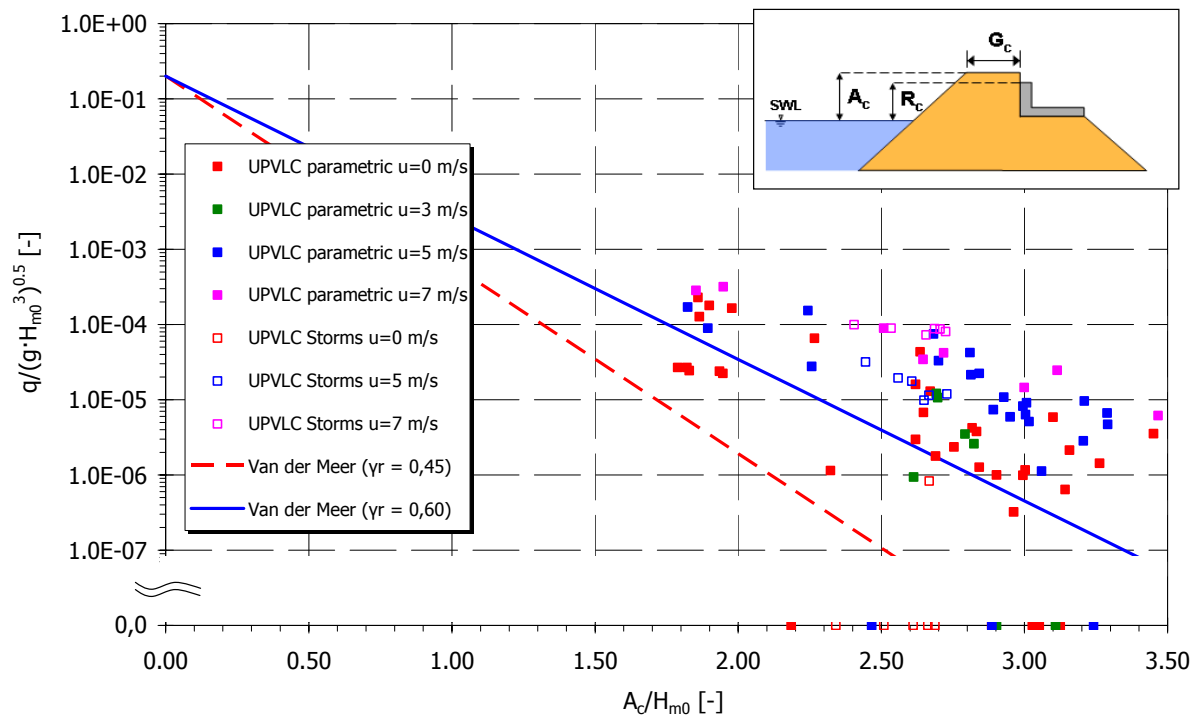


Figure 70: Zeebrugge model test results (influence of wind).

## Conclusions

The analysis of results of tests at both institutes provides the following conclusions with respect to overtopping:

### Uncertainty of measurements:

- Repeatability of tests with respect to wave parameters was found to be very good in both flumes. Regarding overtopping, mean differences were found to be slightly higher at LWI as compared to UPVLC. Both values increase when different wave generation files are used;
- Different wave analysis (different time windows) and wave generation methods (different time series from the same spectrum file) have no significant influence on the measured wave parameters;
- The number of waves generated in the flume has some effect on wave overtopping measurements, a comparison of 200 to 1000 waves has led to 20% differences in wave overtopping, although this is accompanied by using different wave generation files which has caused differences in results of the same order of magnitude;

### Model effects:

- Significant differences were found in overtopping measurements when the overtopping tray is moved as compared to prototype. This may either result from a different pattern of armour layer stones in front of the tray or the influence of the side wall of the flumes;
- Widening of the tray collecting the overtopping water has led to differences in overtopping in the same range of test repeatability. The widening was limited to a factor of 2.0 at LWI (first test phase) for which the former results (uncertainty of measurements) were obtained. For tests in the second test phase (reproduction of storms) the tray was widened up to 1.0 m in the model which seemed to have a larger influence than 10%;

- Repositioning of the armour units significantly affects the overtopping rates. Small changes in the positioning of armour elements may change the overtopping rate by a factor of 2.0 and more;
- Wind influences were investigated in detail by UPVLC and resulted in differences of up to one order of magnitude when wind speeds up to 7.0 m/s were compared with no wind in the model. It is however still unclear how wind can be scaled from prototype to the model;
- Further differences in overtopping measurements in Zeebrugge may result from the unknown placement pattern of the bottom armour layer (rectangular pattern in the models) and long waves in prototype, which have not been varied in the model.

#### **Scale effects:**

- The comparison between model and prototype results has shown some clear differences for low overtopping rates which could partly be explained by some model effects. For further conclusions on scale effects, reference is made to WP7.

More details on the model tests on the Zeebrugge breakwater are found in Kortenhaus et al. (2004).

#### **4.2.2 Site 2 : Ostia**

The Ostia breakwater has been modelled in small-scale in the wave flume of Ghent University (UGent) at a scale of 1:20 and in the wave basin at Flanders Hydraulics (FCFH) at a scale of 1:40. The model investigations have concentrated on parametric tests on wave overtopping (mainly at UGent, a limited number at FCFH) as well as the reproduction of storms (UGent, FCFH). In 2D further tests with regular waves are performed for the calibration of the numerical models (WP5). Altogether 180 2D tests have been performed at UGent on the Ostia breakwater. Many of them were focussing on various uncertainties with regard to the measurements and the model such as repeatability, influence of the spectral type, influence of the breakwater's slope, influence of a longer foreshore, influence of the packing density of the armour, influence of a permeable or impermeable core .... Also tests with a smooth structure

were performed to make an as accurate as possible comparison between a smooth and a rough structure.

AT FCFH 71 3D tests have been performed on the Ostia breakwater. These tests were mainly storm reproductions, but also some parametric tests were performed. For the storm reproductions, the influence of the angle of wave attack was investigated. Parametric tests were selected to have the same wave parameters as in 2D in order to achieve a situation as good as possible suited for direct comparison between 2D and 3D.

Fig. 71 gives a cross section of the wave flume with the Ostia model and foreshore, including the positions of the wave gauges. Fig. 72 gives a cross section of the 2D breakwater model itself. Fig. 73 and Fig. 74 show respectively a view on the position and orientation of the 3D model in the wave basin and a cross section with the overtopping tank of the model and the foreshore.

Fig. 75 gives results from both the 2D and the 3D model in a typical non-dimensional overtopping graph.



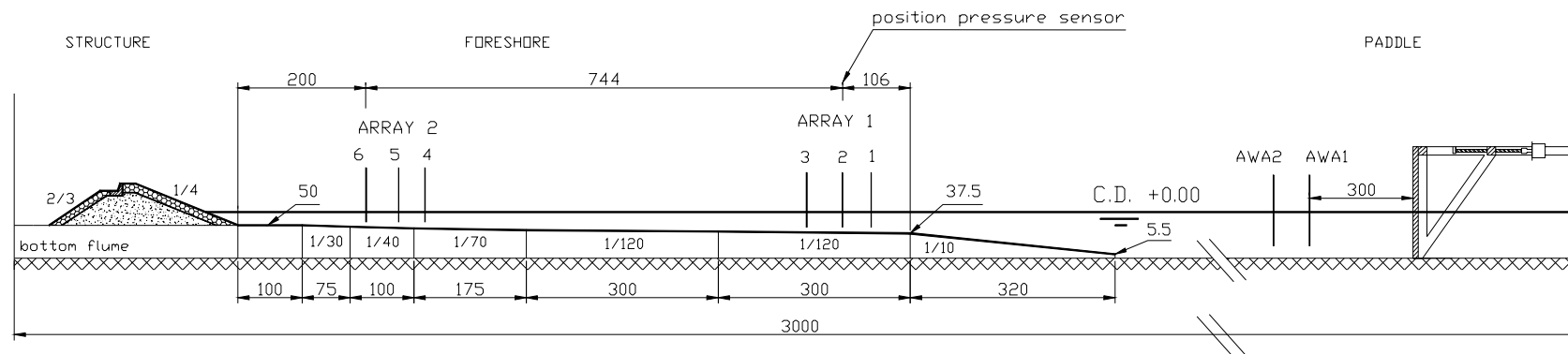


Figure 71: Cross-section of the complete 2D model set-up in the wave flume (values in cm model).

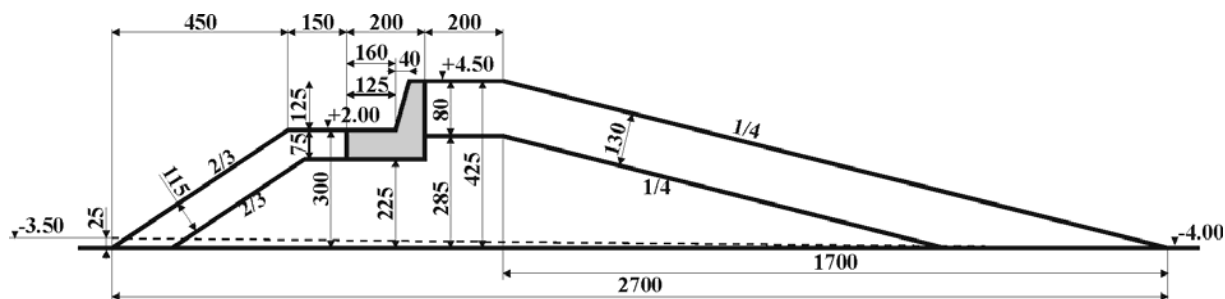


Figure 72: Cross-section of the 2D breakwater in the wave flume (values in mm model; elevations in m prototype).

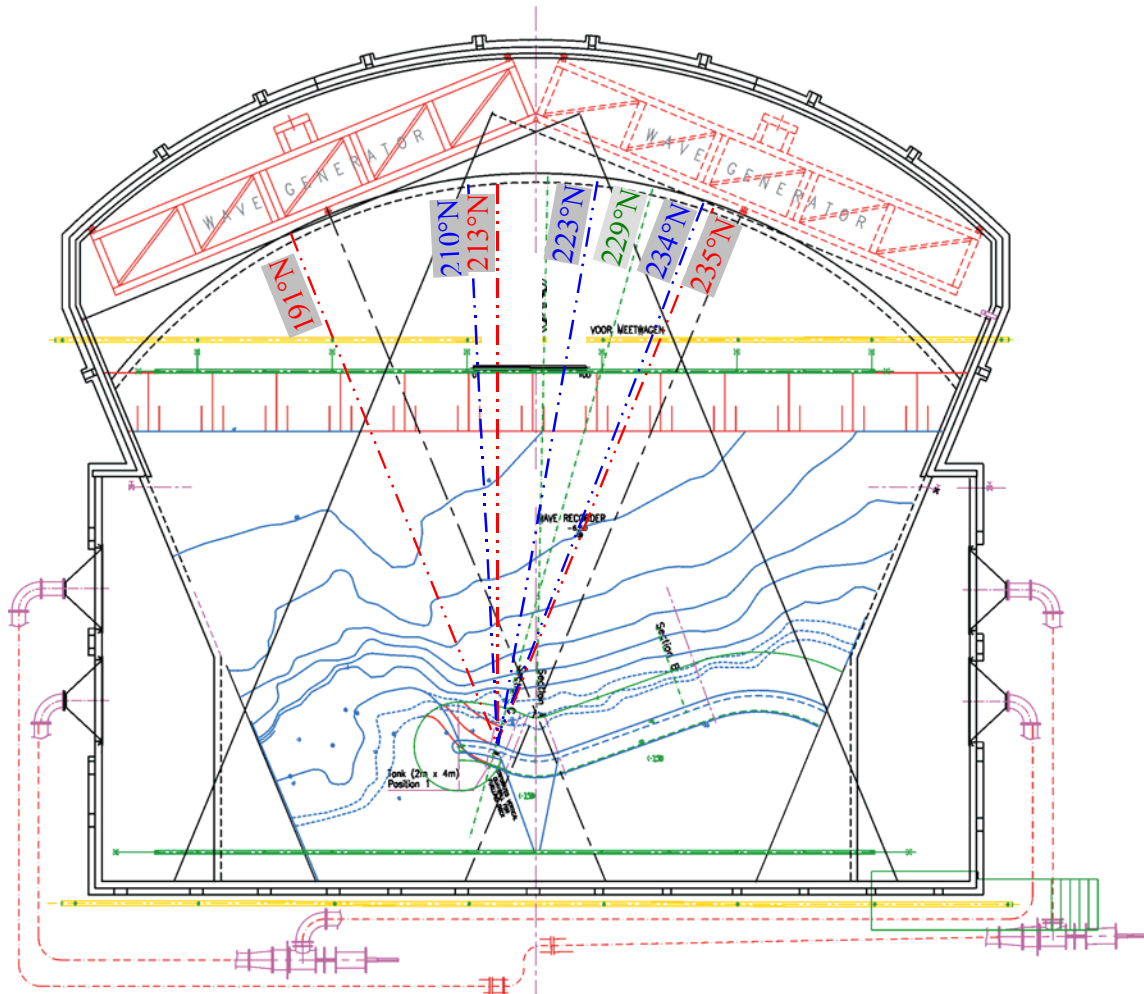


Figure 73: Position and orientation of the Ostia breakwater in the wave basin for the 3D tests.

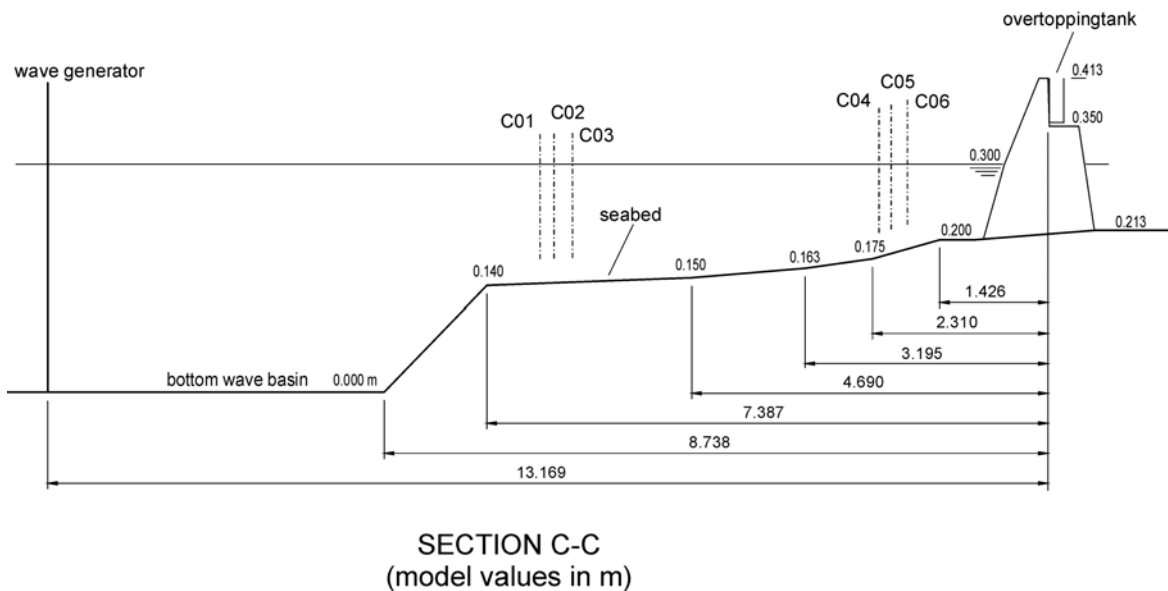


Figure 74: Cross-section with the overtopping tank in the wave basin (values in m model).

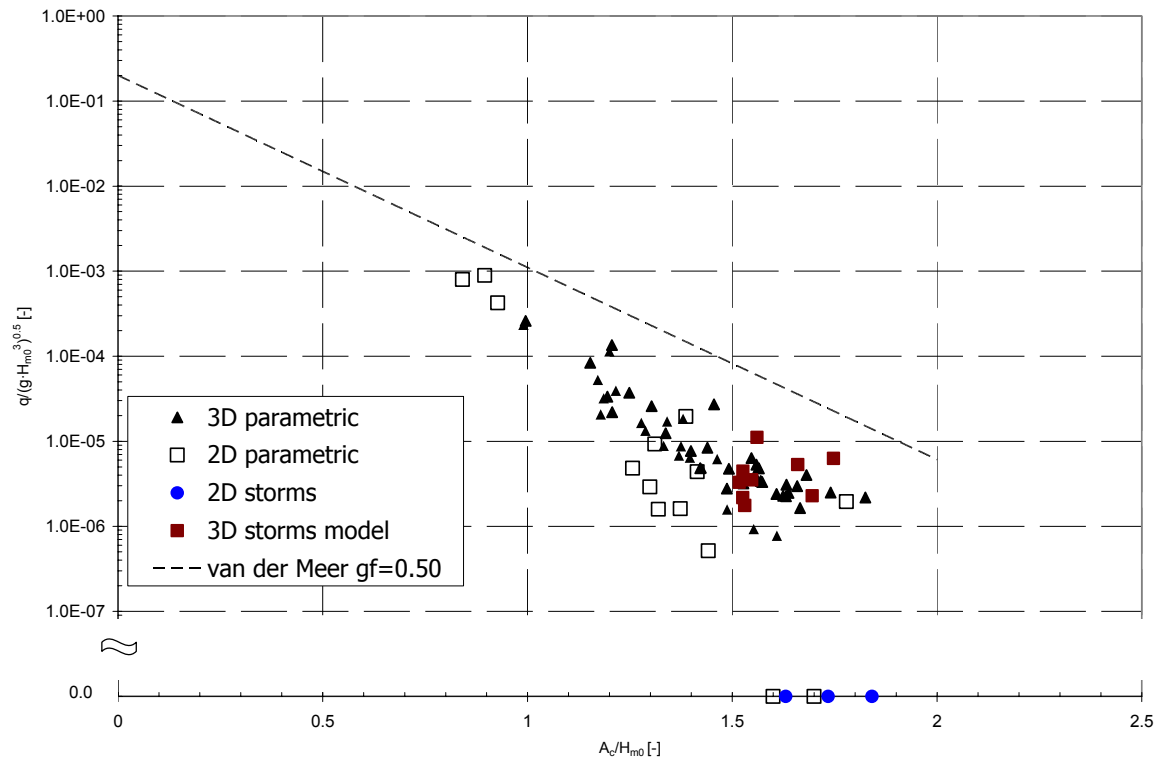


Figure 75: Ostia model test results.

## Conclusions

The analysis of results of tests at both institutes provides the following conclusions with respect to overtopping:

2D storm reproductions result in ZERO overtopping, even when applying an impermeable core and an armour with very low porosity. To obtain some overtopping in the 2D model the water level must be increased with 0.70 cm as compared to the prototype situation, which means an increase of the dimensionless crest freeboard from ca. 1.85 to 2.15. To obtain overtopping discharges comparable to the prototype, the water level increase must be 1.30 m. This means a very big change of the dimensionless crest freeboard, i.e. from 1.85 to 2.45.

3D storm reproductions do give some overtopping, but end up a factor 5 to 10 smaller than in prototype.

Comparison of 2D and 3D model results indicates the existence of a clear 3D effect, which also could be observed from prototype videos showing a very non-uniform distribution of overtopping along the breakwater.

Parametric tests in 2D only produce overtopping for water levels 0.70 m higher than in prototype. Apart from this, the 2D parametric test results are rather similar to the 3D parametric test results. However, 2D results are generally lower than 3D results.

From the parametric tests a roughness coefficient  $\gamma_r = 0.30$  has been determined for the Ostia Breakwater, based on a comparison with the smooth structure tests. To determine this coefficient, the presence of the permeable crest berm has been taken into account.

Further in WP4 additional tests to determine  $\gamma_r$  for different armour types are described. The values found there for rock are higher than what is found here for the Ostia case. However in this case the structure's slope is considerably flatter (1/4) than in case of the additional tests (1/1.5 – 1/2). It is clear that the roughness coefficient is not constant for all slopes.

More details on the tests on the Ostia breakwater are found in Geeraerts & Willems (2004). The main results are also presented in Geeraerts et al. (2004).

#### 4.2.3 Site 3 : *Samphire Hoe*

The Samphire Hoe seawall has been modelled in small-scale in the wave flume of Edinburgh University (UEDIN) at a scale of 1:40 and in the wave basin at Hydraulic Research Wallingford (HRW) at a scale of 1:20. The model investigations have concentrated on parametric tests on wave overtopping (HRW) as well as the reproduction of storms (HRW and UEDIN). Moreover, at both HRW and UEDIN the spatial distribution of the wave overtopping has been measured. At HRW the influence of wind on wave overtopping was studied too.

Fig. 76 gives the model set up together with a cross section of the model seawall for the 2D tests. Fig. 77 shows a plan view of the 3D model.

Fig. 78 gives the results of both 2D and 3D model tests compared to the prediction for these kind of structures by Besley (1999). Both 2D and 3D test results are generally in good agreement with the overtopping formula of Besley (1999) for composite vertical walls.

The spatial distribution of overtopping water behind the wall was measured both for the 2D and the 3D tests. The results confirm the exponential decay with the landward distance. From the test with wind it was observed that the wind will increase the landward distance of the splash down location of the overtopping water as expected. When the overtopping discharge is low it was observed that wind could increase the overtopping discharge by one magnitude.

For much higher discharge almost no influence of wind on the overtopping discharge was observed.

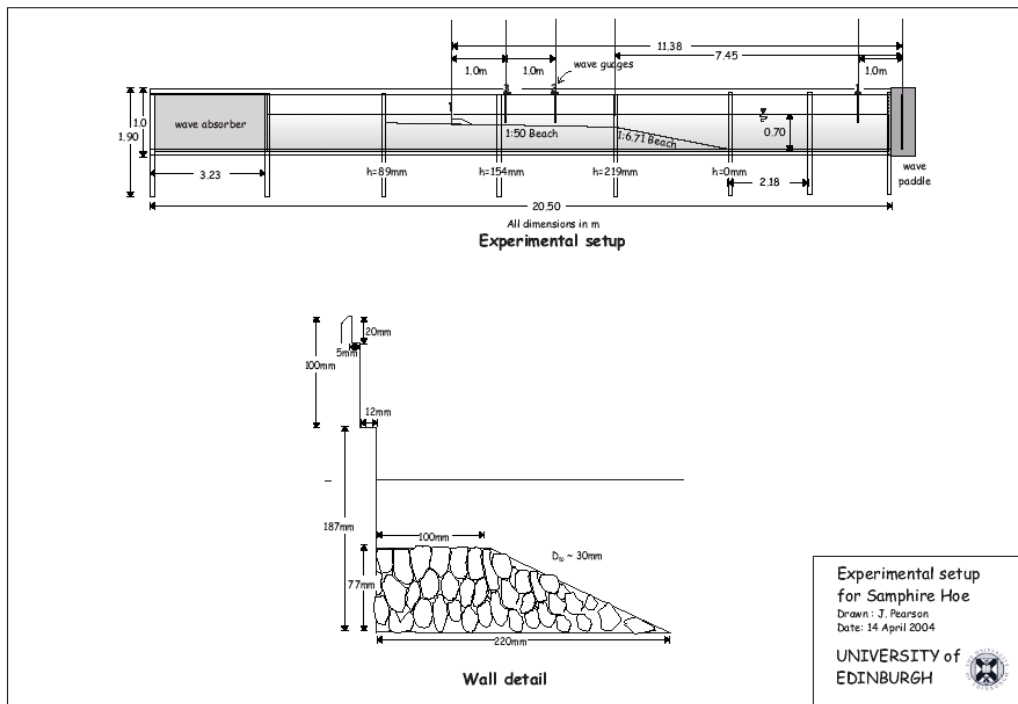


Figure 76: Test set-up for 2D tests.

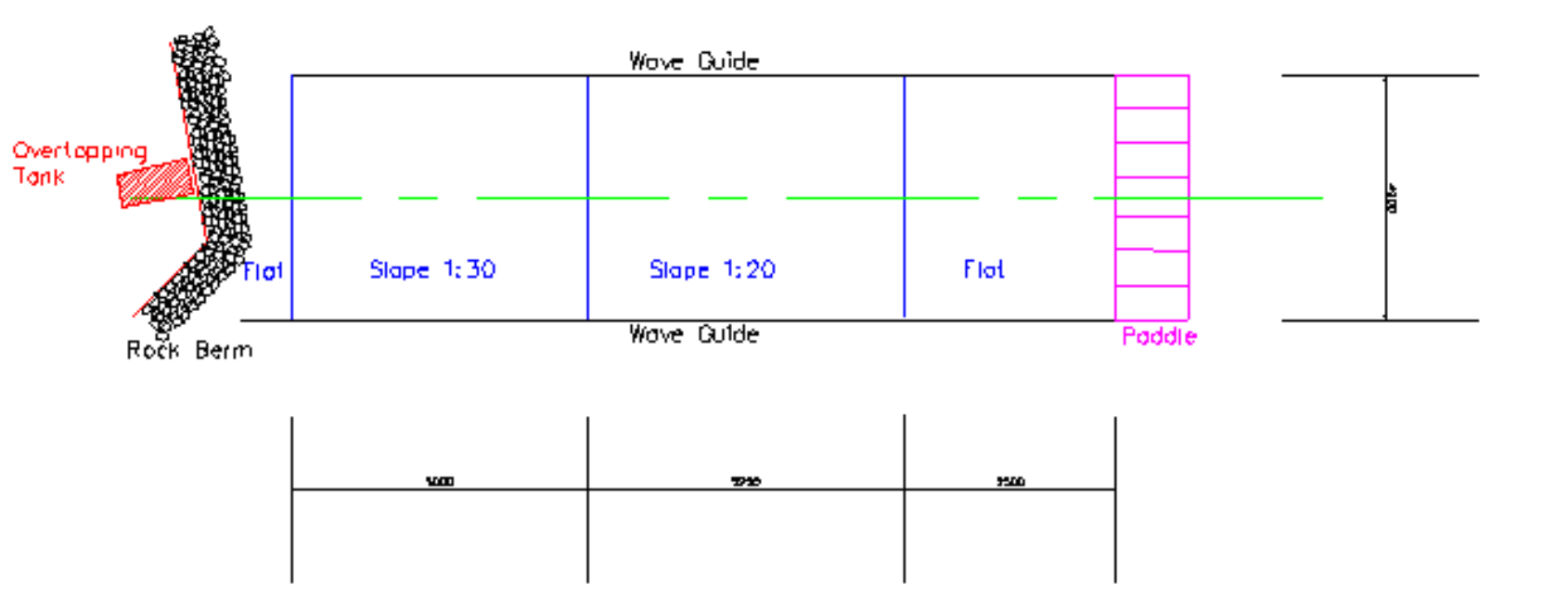


Figure 77: Plan view of the 3D model.

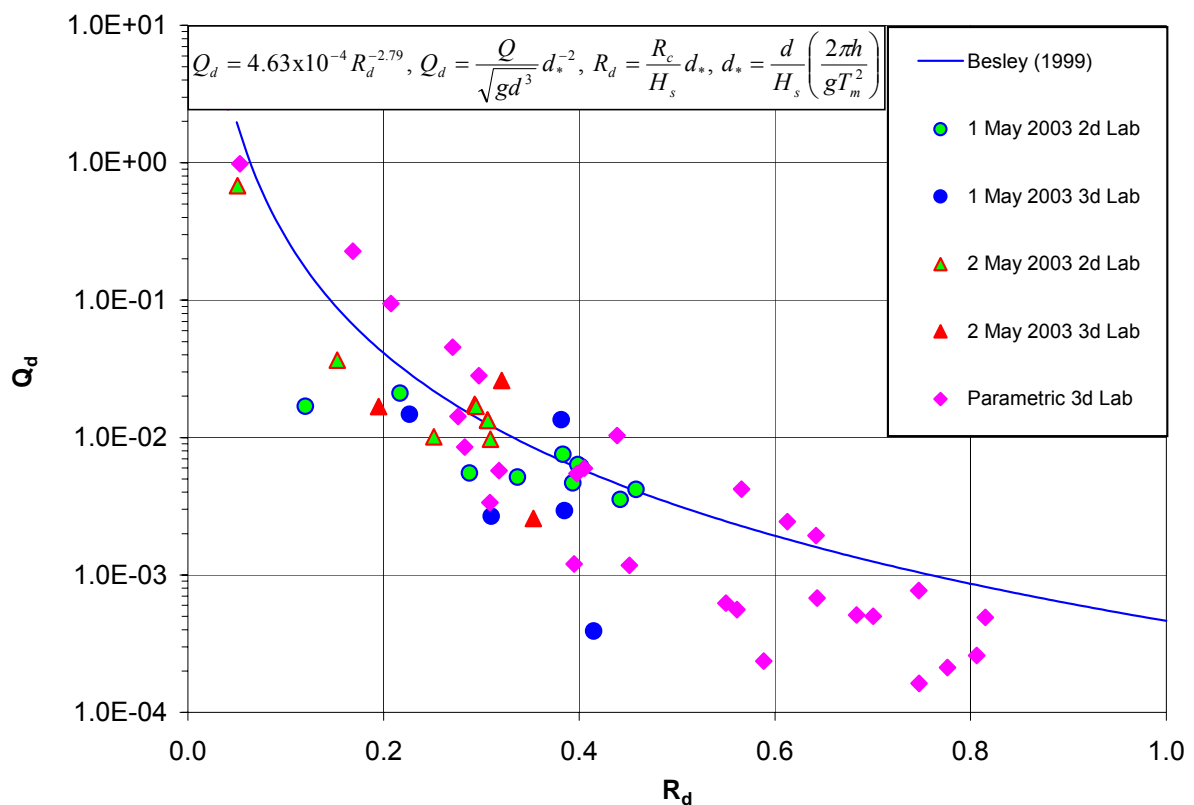


Figure 78: Samphire Hoe model test results.

## Conclusions

The results from field and 2d & 3d laboratory measurements of mean overtopping discharges have been compared. These results have also been compared with the empirical prediction method of Besley (1999) for a composite vertical wall. There are differences among the results, and these can generally be ascribed to modelling effects. These are due to differences between the overtopping tanks in the field and the laboratory, and the presence of wind. It has been shown that there are no scale effects when the field and laboratory measurements are compared, and that generally the results are in agreement with Besley (1999).

More details on the tests on Samphire Hoe seawall are found in Pullen (2004). The main results are also presented in Pullen et al. (2004).

#### 4.2.4 Additional tests

Four different white spots in the database were selected for additional tests:

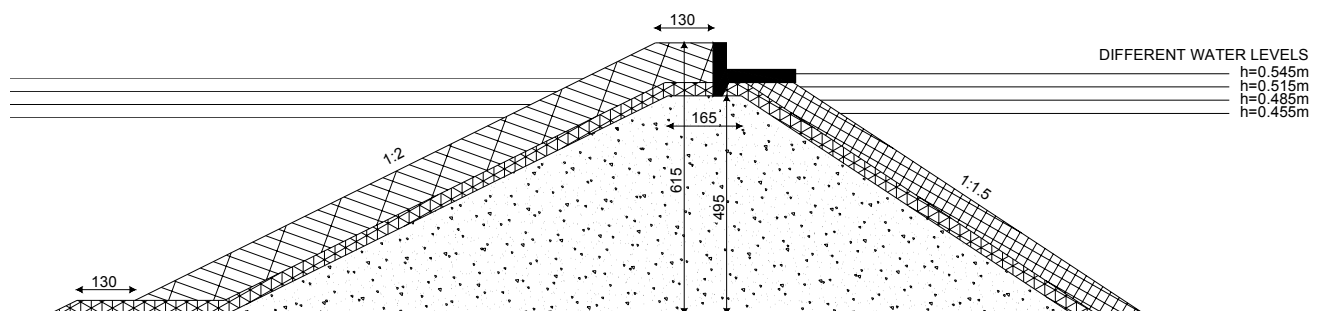
- a) Wave obliquity and spreading
- b) Structure roughness/permeability
- c) Low wave steepness ( $s_{0p} < 0.01$ )
- d) Berm breakwaters

##### *Part A : influence of wave obliquity*

Three different 3-dimensional models with different orientation were constructed and tested at Aalborg University in order to give information on the influence of wave obliqueness and wave spreading (directionality) on the overtopping of conventional rubble mound breakwaters. On each of the three models tests were performed with both rock and cubes as armour.

The number of tests performed was 736. All tests were performed with a minimum of 1500 irregular waves. Overtopping was measured in an array of trays in order to collect information on the spatial distribution. Furthermore the variation in time of the overtopping was measured.

Fig. 79 shows the cross-section which was tested. Fig. 80, 81 and 82 show the three different orientations with regard to the wavemaker of the model in the basin.



**Figure 79: Tested cross-section (dimensions in mm).**



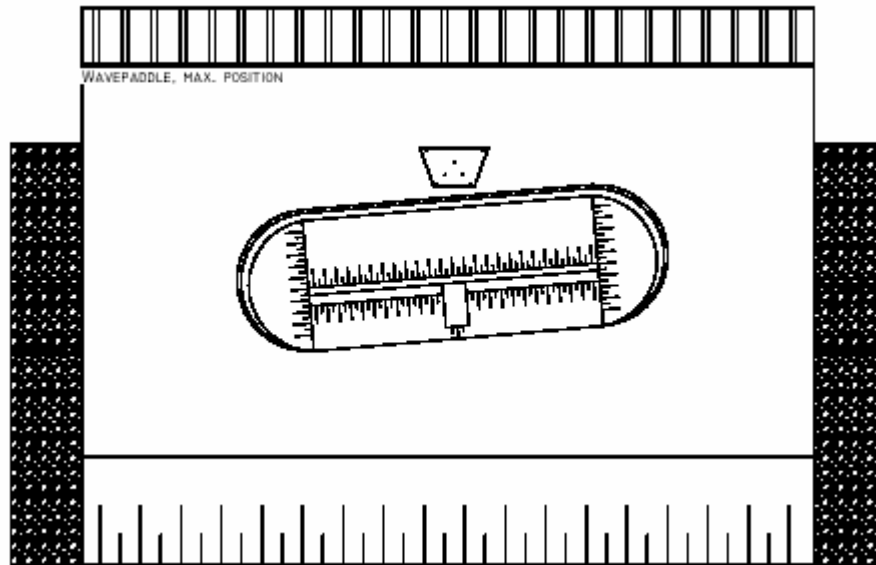


Figure 80: Layout in basin for testing 0° and 10°.

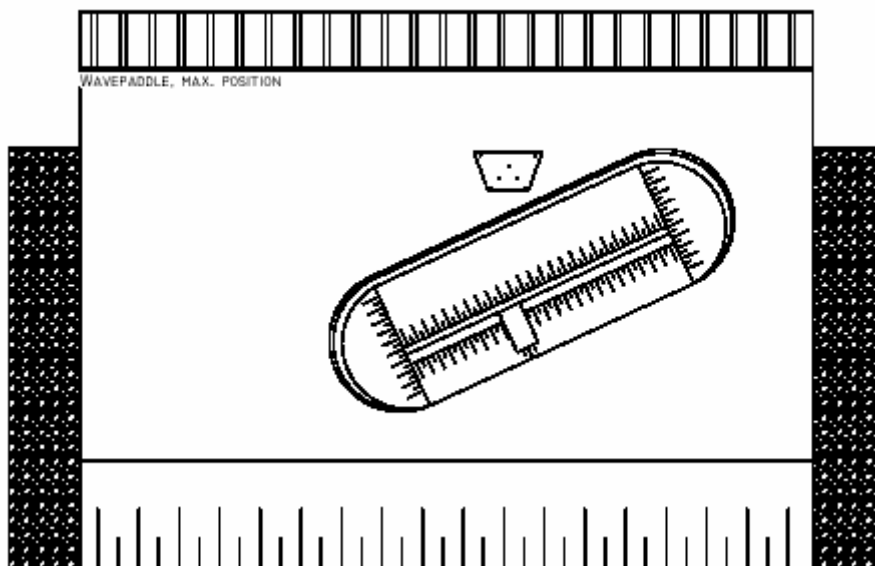


Figure 81: Layout in basin for testing 25°.

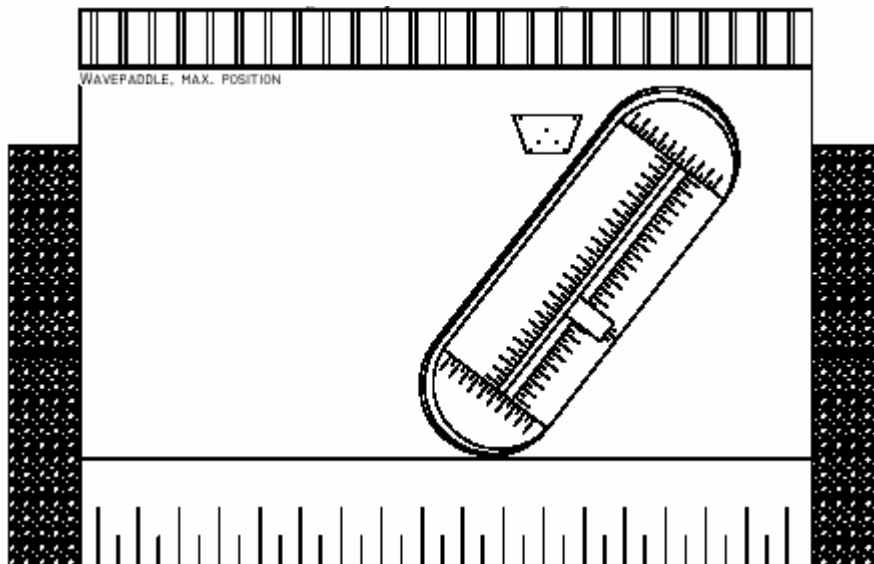
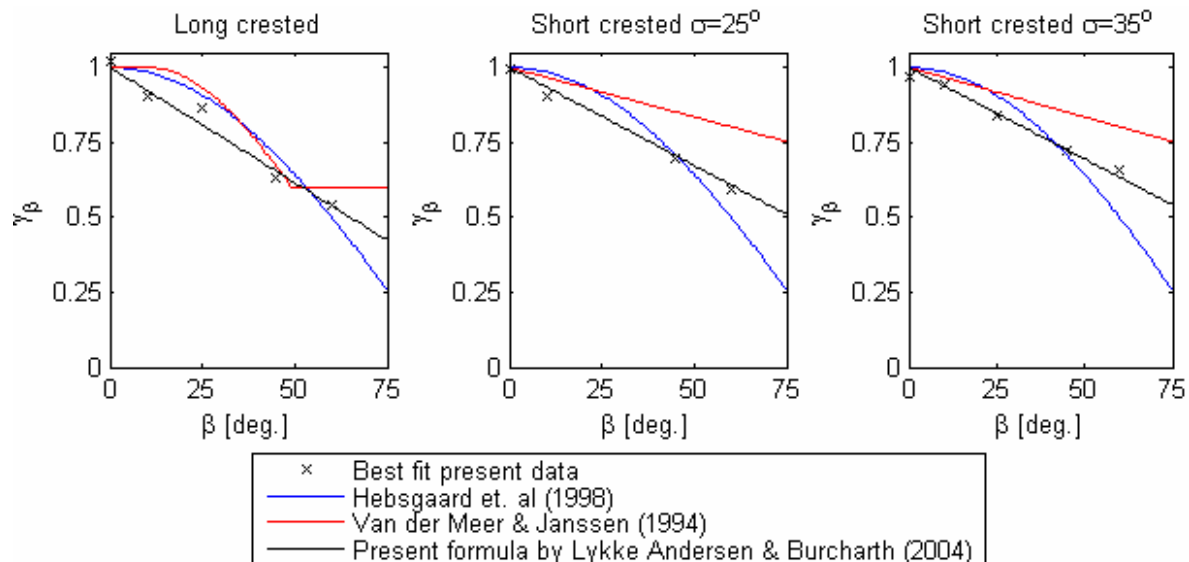


Figure 82: Layout in basin for testing 45° and 60°.

The method to predict overtopping comprised two steps. Depending on the waves (wave height, period, breaker type etc.) and type of structure (geometrical lay out, roughness, porosity etc.) a formula describing the overtopping for head-on long crested waves is first found. Effects of wave obliqueness and wave spreading are then introduced through a correction factor. The overall idea is that the correction factor can be used more or less generic improving the value of flume tests on new structures. The correction factor is given in Eq.3 and evaluated in Fig. 83 against new data from AAU model tests.  $\beta$  is the mean wave direction in degrees and  $\sigma$  is directional spreading in degrees.

$$\gamma_{\beta} = 1 - (0.0077 - 4.6 \cdot 10^{-5} \cdot \sigma) \cdot \beta \quad (3)$$



**Figure 83: Evaluation of proposed direction factor against data from AAU.**

The results obtained related to 3D white spot tests were:

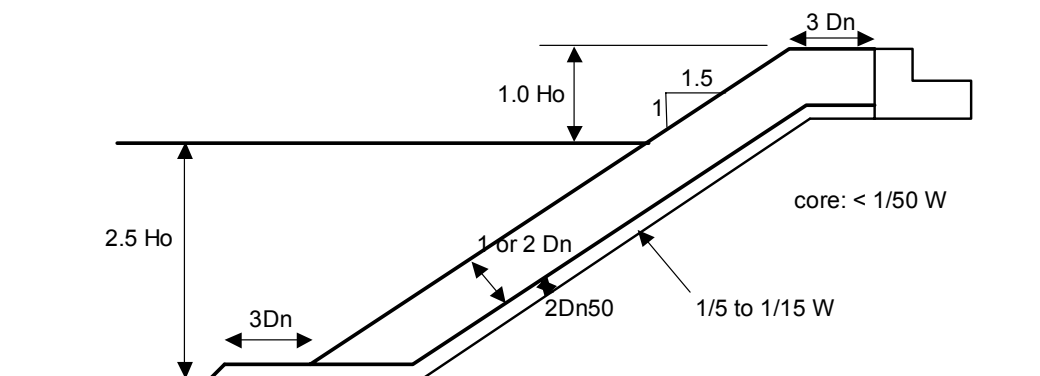
- 1) In relation to the formulae of Van der Meer & Janssen (1994), all tests performed correspond to non-breaking waves. The results from tests with head-on wave attack correspond to a roughness factor ( $\gamma_f$ ) between 0.3 and 0.45 which is a significantly lower value than suggested by Van der Meer & Janssen (1994).
- 2) Very good agreement exists between the data from the present tests and the formula of Hebsgaard et al. (1998) derived on the basis of long crested waves only. Consequently as expected the agreement to the present test results from short crested very oblique wave attack is not so good. Consequently a new/modified formula for the correction factor has been proposed by Lykke Andersen and Burcharth (2004a) to take into account the directional spreading and wave obliquity (eq. 3). The new correction factor makes it possible to predict overtopping for oblique wave attack up to 60 degrees.
- 3) The intensity of wave overtopping behind the breakwater decreased very rapidly with the horizontal distance from the breakwater crest. In Lykke Andersen and Burcharth (2004a) a diagram presenting the spatial distribution is given.

*Part B : determination of roughness factors*

14 different models with a standard cross-section, as shown in Fig. 84, were constructed at University of Edinburgh with different armour configurations. 307 tests have been performed in total covering the following armour configurations:

- 1) Smooth slope
- 2) Rock (2 different sizes)
- 3) Cubes (2 layers random placed)
- 4) Antifer cubes
- 5) Haro
- 6) Tetrapod
- 7) 1 layer of cubes
- 8) Accropod
- 9) CoreLoc®
- 10) Xbloc®

Smooth slopes and rock were tested as reference cases.



**Figure 84: Standard cross section.  $H_0$  is the design wave height.**

Dependent on the available model units (with their specific weight), the design wave height was tuned to represent a “similar stability behaviour” for all tested types of armour units.

Rock and cubes were tested both with 1:1.5 and 1:2 front slopes.

Results of the present study, together with results from previous studies (Aminti-Franco 1988, Franco-Cavani 1999) and parallel tests undertaken at AAU and UGent, were discussed amongst CLASH-partners. It was concluded that the roughness factor depends on the slope of

the structure. Finally, a deeper study of the results lead to the selection of roughness factors  $\gamma_f$  for a sloping structure with slope 1:1.5, a crest berm width of  $3D_n$ , and a permeable core / underlayer.

Table 20 presents the roughness factors which have been determined for the various tested armour layers.

**Table 20: Roughness factors for breakwaters with slope 1:1.5, with crest berm width of  $3D_n$  with a permeable core / underlayer. Values valid for breakwaters only (not for revetments).**

Type of armour	No Layers	Final $\gamma_f$
Smooth		1.00
Rock	2	0.40
Cube	2	0.47
One layer of cubes	1	0.50
Antifer	2	0.47
Haro	2	0.47
Tetrapod	2	0.38
<i>Dolosse (estimated)</i>	2	0.43
Accropode	1	0.46
Coreloc®	1	0.44
Xbloc®	1	0.45
<i>Berm Breakwater (estimated)</i>		0.40
<i>Icelandic Bermbreakwater (estimated)</i>		0.35
<i>Seabeas &amp; Sheds (estimated)</i>		0.50

### *Part C : influence of wave steepness*

Very limited data existed in the first database with wave steepness ( $s_{0p}$ ) less than 1%. Therefore white spot tests were carried out at University of Gent to study the influence of low wave steepness on three different smooth structures.

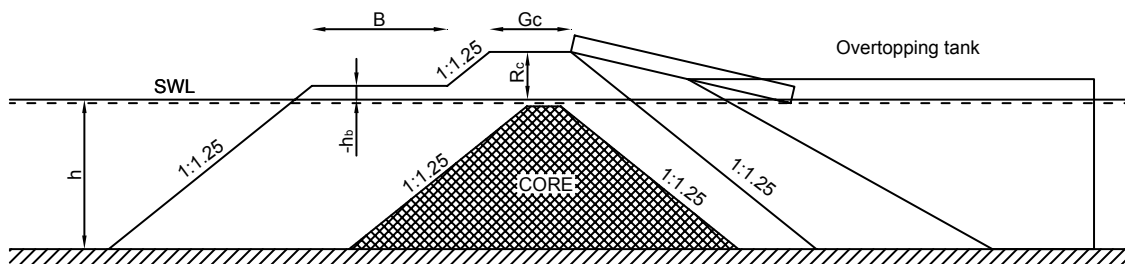
- 1) simple smooth dike
- 2) simple smooth dike with a small vertical part (same crest level as geometry 1)

- 3) simple smooth dike with a small vertical part and an impermeable sloping crest (crest level slightly higher than geometry 1 and 2)

From the test results it can be concluded that for same wave height in front of the structure waves with steepness  $s_{0p} < 0.017$  produce more overtopping on the simple smooth dike than waves with higher steepness. For the two geometries where a vertical part is present the distinction between higher steepness is not as clear as for the simple smooth dike. However, the waves with  $s_{0p} < 0.017$  generally produce more overtopping. The specific set-up of the tests allowed determination of the influence of the vertical part on top of the dike and the crest width.

*Part D : berm breakwaters*

Overtopping as well as front and rear slope stability were studied on reshaping berm breakwaters with a homogeneous berm. 82 tests have been performed at Aalborg University in order to describe the influence of sea state, crest freeboard and crest width. Fig. 85 gives the start profile of the tested geometries.



**Figure 85: Tested cross-sections.**

All of the 700 tests were performed with a minimum of 1500 irregular long crested waves, and repeated minimum once (Lykke Andersen and Burcharth (2004b)).

The conclusions fall into three categories:

- 1) A new and reliable overtopping formula was derived. In order to make design easier only non-reshaped geometrical parameters are included in the formula. The stability index  $H_0T_0$  is used as an indicative measure of the reshaping as the formula does not

contain geometrical parameters which describe the reshaping directly. For dynamically stable profiles the actual reshaping can be estimated by the method of Van der Meer (1992). Wave parameters are related to the incident waves at the toe of the structure.

$$Q_* = 4.56 \cdot 10^{-3} \cdot (H_0 T_0)^{1.31} \cdot s_{0p}^{-2.95} \cdot \exp[-13.9 \cdot R_*^{0.40} - 0.92 \cdot G_*^{1.24} - 0.76 \cdot h_{b*}^{1.32} \cdot B_*^{1.24}]$$

where

$$Q_* = \frac{q}{\sqrt{g \cdot H_{m0}^3}}$$

$$H_0 T_0 = \frac{H_{m0}}{\Delta \cdot D_{n50}} \cdot \sqrt{\frac{g}{D_{n,50}}} \cdot T_m$$

No reshaping takes place for  $H_0 T_0 < 30$ . For such cases use  $H_0 T_0 = 30$ .  $H_{m0}$  is the significant wave height at the toe of the structure (frequency domain parameter).

$$R_* = \frac{R_c}{H_{m0}} ; \quad G_* = \frac{G_c}{H_{m0}} ; \quad B_* = \frac{B}{H_{m0}}$$

$$h_{b*} = \frac{3 \cdot H_{m0} - h_b}{3 \cdot H_{m0} + R_c} \quad \text{when } h_b > 3 \cdot H_{m0} \text{ use } h_{b*} = 0$$

The new overtopping formula covers a white spot.

- 2) Front side slope stability was studied in order to describe the damage due to the waves. Good agreement between measured and calculated profiles by the method of Van der Meer (1992) was observed in all cases with dynamically stable profiles. For statically stable reshaping breakwaters the method overpredicts the amount of reshaping.
- 3) Rear side slope stability was studied in order to link the mean overtopping discharge and the rear slope erosion. Although only valid for small scale tests Lykke Andersen and Burcharth (2004b) presented diagrams relating the rear side damage to the overtopping.

### 4.3 General conclusion for WP4

This WP delivered the following reports / deliverables:

a) for the Zeebrugge model:

- the report on laboratory measurements (D18)
- the final report on laboratory measurements (D34)

b) for the Ostia model:

- the report on laboratory measurements (D20)
- the final report on laboratory measurements (D35)

c) for the Samphire Hoe model:

- the report on laboratory measurements (D21)
- the final report on laboratory measurements (D36)

d) for the additional tests:

- the report on additional tests (D24)

Two milestones were achieved within this WP:

After the first full winter season (month 18 for the Zeebrugge, Ostia and Samphire Hoe site and month 19 for the Petten site), full scale measurements of all four sites are analysed and reported (M3). After the second full winter season (month 30 for the Zeebrugge, Ostia and Samphire Hoe site and month 31 for the Petten site), measurements of all sites are analysed and reported



## 5 WP5 : Numerical modelling

### 5.1 Objectives

The main objective of this task is to use numerical simulation of wave overtopping in order to contribute to the solution of the problem of suspected scale effects.

A second objective of the workpackage is to improve existing codes in such a way that they are able to really simulate wave overtopping in a reliable way.

Another objective is to numerically model long waves on the shallow foreshore at site 4 in order to understand the phenomenon of long waves and the effect on wave overtopping.

### 5.2 Description of work performed

The main objective of this work package is to use numerical simulation software which solves an appropriate set governing equations in order to predict wave overtopping, and thus to address the problem of suspected scale effects. In order to achieve this objective it has been necessary to improve the capabilities of two existing models namely, the AMAZON-SC code developed by MMU and the VOFbreak<sup>2</sup> codes developed by UGent. Furthermore, to enable the simulation of 3D effects a numerical wave basin, called LVOF, has been developed by UGent. The MMU code, AMAZON-SC, is a numerical wave flume based on the free surface capturing approach, while the UGent codes are based on the volume of fluid approach. Both models have been made available to the commission as a confidential deliverable (D26) and the enhancements made have been described in two reports (Ingram et al; 2003 and Ingram et al; 2004).

Realistic simulations of wave overtopping require numerical methods which are able to simulate accurately the shoaling, breaking and possible overturning of waves prior to their impact on the coastal defence. It is a further requirement that the simulation continues after impact, modelling the formation of the overtopping jet and the reflection of the wave. Both the AMAZON-SC and LVOF codes solve the turbulent Navier-Stokes equations in order to provide such detailed simulations. The MMU code, AMAZON-SC, is a numerical wave flume based on the free surface capturing approach, while the UGent code, LVOF, is a numerical wave basin based on the volume of fluid approach. The codes have been applied to various

cases, discussed by Ingram et al (2004), including: a test problem involving wave overtopping of a smooth sea dike, wave overtopping at Samphire Hoe (one of the structures which has been examined both in the field as part of WP3 and experimentally as part of WP4 and an investigation of scale effects on rough impermeable structures and at Ostia breakwater. In order to perform these simulations the modelling capabilities of the codes have been improved. In the case of the MMU code the existing 2D code has been extended to include the effects of porosity and turbulence, while the team at UGent have developed a new 3D numerical model (Li et al., 2004b).

The remaining objective was to simulate long waves on the shallow foreshore at Petten in order to understand the phenomenon of long waves and their effect on overtopping. These simulations were conducted by Delft Hydraulics using ODIFLOCS and SURFBEAT and these simulations together are described by van Gent and Giarrusso (2003).

Additional modelling work has been conducted by HR Wallingford using their ANENOME-OTT to investigate the propagation of bore waves across the hinterland behind a sloping sea defence and to compare the predictions from the AMAZON-CC and ANENOME-OTT codes with experimental measurements for overtopping jet velocities (Richardson et al., 2003). MMU have also applied the AMAZON-CC code to study the applicability of shallow water models to impulsive overtopping by comparing predicted overtopping volumes with experimental results obtained under the VOWS project (Richardson et al., 2002; Shiach et al., 2004). This additional modelling has been conducted using models which are based on the shallow water equations (derived by considering the depth integrated form of the Navier-Stokes equations) which provide a computationally efficient but less sophisticated model of overtopping. Using shallow water methods typically allows 1000 waves to be simulated in less than one hour on a desktop PC, as opposed to the significant computational resources required to run the 2D and 3D numerical solvers based on full Navier-Stokes equations for only a few waves.

### 5.2.1 *Free surface capturing*

One approach which can be used to develop a 2DV numerical wave flume (or fully 3D numerical wave basin) is the free surface capturing approach (Kelecy and Pletcher, 1997). This approach forms, together with a novel Cartesian cut cell treatment (Causon et al. 2001) forms the basis of the AMAZON-SC code (Qian et al., 2003a). Specifically, in this case, the mathematical model of an immiscible two fluid system is formulated as a set of partial differential equations which govern the motion of an inviscid, incompressible, variable density fluid. These equations consist of a mass conservation (density) equation (which is mathematically equivalent to the volume fraction transport equation), momentum equation and an incompressibility constraint that are solved simultaneously using the finite volume method. The formulation is based on the artificial compressibility method (Chorin, 1967; Beddhu et al., 1994) in which the pressure, density and velocity fields are directly coupled to produce a hyperbolic system of equations. To achieve a time accurate solution for unsteady flow problems an implicit dual time iteration technique has been used (Soh and Doodrich, 1988; Rogers and Kwak, 1990) in which the solution at each real time step is obtained by solving a steady state problem in a pseudo time domain. To evaluate the inviscid fluxes, Roe's flux function is adopted locally at each cell interface assuming a 1D Riemann problem in the direction normal to the cell face. To achieve a second order accurate solution in space, a piecewise linear model for the stored cell centre variables is used in conjunction with a slope limiter to prevent overshoots or undershoots in the interpolated data at cell interfaces before the two Riemann states are computed. At the pseudotime iteration level, however, a first order upwind scheme is sufficient to calculate the inviscid fluxes and the resultant linear equations are solved using an approximate LU factorisation scheme (Pan and Lomax, 1988). At every real time step, once the flow variables including density, have been calculated, the position of the material interface can be defined as the contour with the average density value of the two fluids. A number of different boundary conditions including inlet, outlet (open boundary) and solid walls are implemented to facilitate the applications to real flow problems. Complex geometries (Causon et al., 2001) arising in real coastal engineering problems can be easily represented by cut cells which provide a fully boundary fitted mesh capability without any mesh generation in the conventional sense. A novel scheme has also been proposed for the accurate treatment of the pressure gradient term within the free surface capturing method for flows under the influence of gravity (Qian et al., 2003b). The vertical pressure gradient term

is split into hydrostatic and kinematic pressure gradient terms which are then calculated separately in order to exactly balance the gravity source term in each cell.

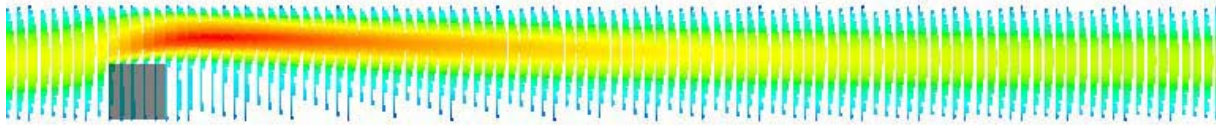
In order to extend the solver to deal with rubble mound structures, a porosity model must be included. In order to achieve this, the body force term of the Navier-Stokes equations is extended to include terms modelling the porosity, using the method proposed by Huang et al. (2003). In this model the frictional losses associated with the porous structure are parameterised using the three following quantities;  $K_p$  ( $m^2$ ) is the permeability coefficient of the structure,  $N_w$  is the, dimensionless, intrinsic porosity of the structure, and,  $C_f$  is a dimensionless turbulent resistance associated with the structure. In general  $N_w$  is a design parameter of the structure and is known along with a nominal diameter  $d_n$  of the rubble. The turbulent resistance may be determined using the correlation proposed by Arbabhiramar and Dinoy (1973). Whilst various correlations exist for computing  $K_p$  Huang et al. (2003) recommend using the correlation proposed by McDougall, i.e.,

$$K_p = 1.643 \times 10^{-7} \left( \frac{d_n}{d_0} \right)^{1.57} \frac{N_w^3}{(1 - N_w)^2}$$

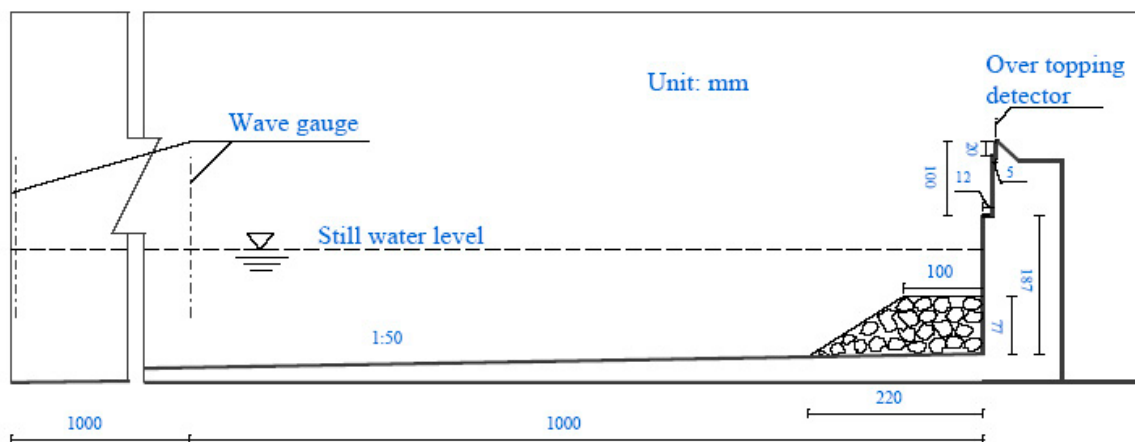
where  $d_0=10\text{mm}$ .

To complete the numerical solution the intrinsic permeability and porosity coefficients are stored for each grid cell in the computational domain. The additional terms in the body force vector are then computed for each porous grid cell. Rubble mound structures are thus represented by defining a region of grid cells with non-zero  $N_w$ .

In order to test the porosity model the updated solver has been applied to the steady state test case described by (Fu et al., 1996). A porous block is located in a two dimensional channel with height. The downstream part of the channel is long enough for the fully developed flow to be recovered behind the block. The inlet velocity profile is prescribed to as a parabolic distribution and the average velocity is chosen to ensure a Reynolds number of 500. Fig. 86 shows the computed velocity distribution, analysis of the velocity distributions along the edges of the block show good agreement with the results of Fu et al. (1996).



**Figure 86: Porous media test: Velocity vectors for the whole domain, showing fully developed flow at the outlet**

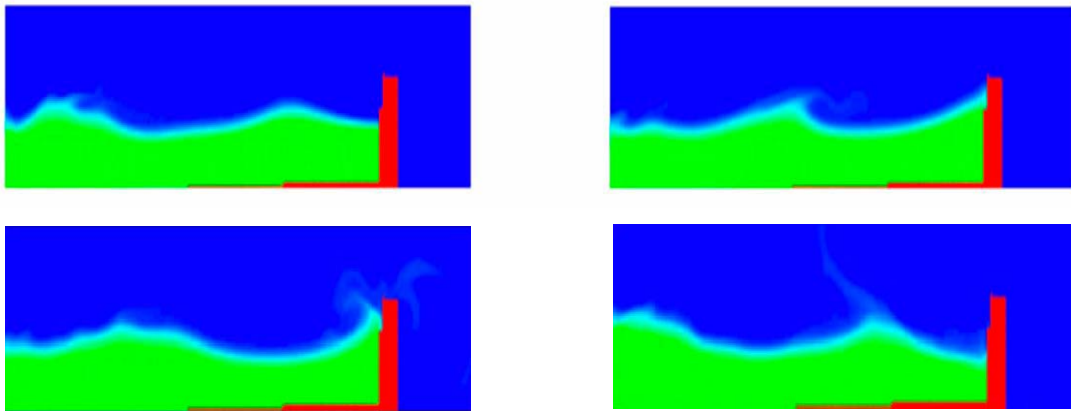


**Figure 87: Samphire Hoe: Overview of the test section**

### *Samphire Hoe*

The AMAZON-SC code has been applied to examine selected wave overtopping events at Samphire Hoe. The computational domain, geometry of the sea wall and the locations of the numerical wave gauges is shown in Fig. 87. This test section is identical to that modelled in the Edinburgh experiments (WP4). The armour at the toe of the structure consists of fairly angular, 4 ton, narrowly graded rock with a  $dn_{50}$  of around 1.5m. The porosity of the toe is estimated at approximately  $N_w = 35\%$  and that consequently, using the equation,  $K_p = 4.35 \times 10^{-5} m^2$ , while  $C_f = 0.06407$ . The simulated case uses a series of random waves at the seaward boundary generated using a JONSWAP spectrum with the same spectral parameters as those used in the laboratory experiment ( $T_p = 0.9416s$  and  $H_s = 0.1037m$ ), it should be noted that it is not possible to use the same time series as the information required for the seaward boundary condition cannot easily be reconstructed from the available wave gauge data. The resulting time series has been examined for significant event and the simulation was started at an appropriate time. Fig. 88 shows the interaction of two large waves with the

seawall over a five second period. The second wave results in an overtopping event, which occurs between 3.44 and 3.5 seconds after the start of the simulation. During this event  $0.033 \text{ m}^3$  overtops the wall, which at prototype scale equates of an instantaneous discharge of  $1.32 \text{ m}^3$ . This low overtopping discharge is composed almost entirely of spray and results from the wave breaking near the toe of the rubble mound. Repeating the simulations at a model scale of 1:20 (i.e. twice the laboratory scale) show almost identical behaviour indicating that for the tested flow conditions the turbulent effects of the rubble mound structure are negligible. This conclusion is in agreement with the results obtained by Pullen et al (2004).



**Figure 88: Samphire Hoe: Computed water surface profiles at 0.5s intervals between  $t = 2.0\text{s}$  and  $t = 4.0\text{s}$**

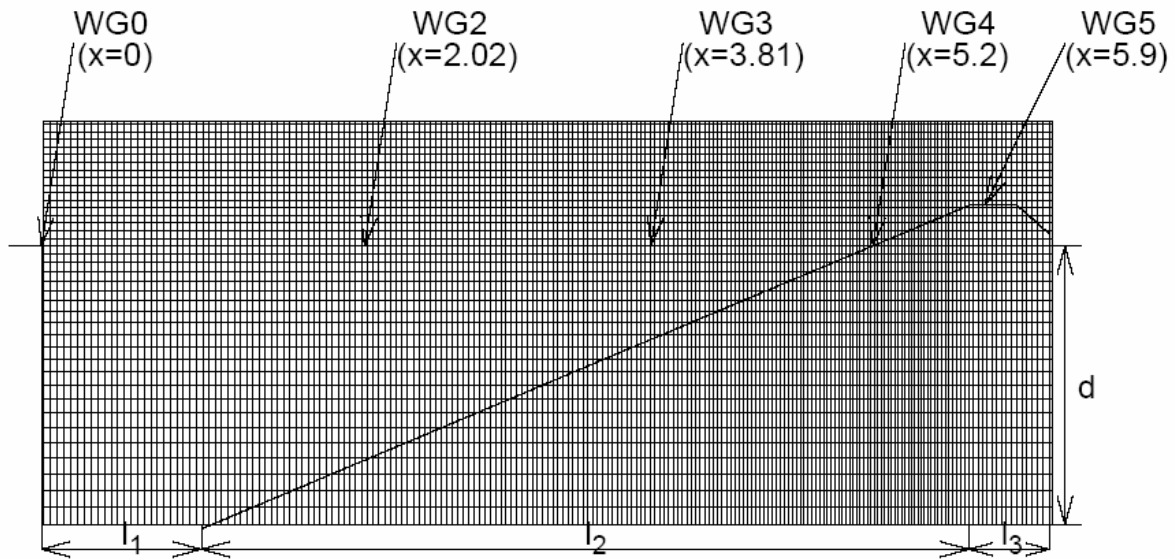
### 5.2.2 Volume of Fluid methods

The VoF method is one of the most popular schemes used for free surface flows and has an established track record (Youngs, 1982; Hirt and Nichols, 1981; Lafaurie et al., 1994; Ubbink and Issa, 1999; Troch et al., 2003). It should be noted that the method is intrinsically mass conservative. Additionally, no special procedures are required to model topological changes of the free surface. The location of the free surface is computed by tracking the evolution of the volume fractions (denoted  $\alpha$ ) in all the cells. A volume fraction of 0 or 1 indicates that a cell contains only one fluid whilst a volume fraction  $0 < \alpha < 1$  indicates the cell contains a mixture, by convention  $\alpha = 0.5$  is used to represent interfaces. The initial distribution of  $\alpha$  is specified by considering the shape and location of the initial interface. A solution procedure used to update  $\alpha$  involves a two stage process: firstly, an interface reconstruction algorithm; and, secondly, an advection algorithm for  $\alpha$ .

Under the CLASH project, UGent have developed a new solver (Li et al., 2004b) for modelling of wave run-up and wave overtopping events using a VoF method. The code is capable of simulating the breaking of the periodic wave trains on the seaward slope of a sea

dike. The solver is based on a split implicit time differencing scheme, which solves the spatially filtered Navier-Stokes equations on a Cartesian cut cell mesh using a cell staggered finite volume (FV) formulation, while incompressibility is enforced through an iterative Poisson solver for the pressure. The free surface is tracked using a VoF method that is simple enough to solve practical problems but still general enough to describe the physical behaviour of the free surface. The key to this development is the use of an implicit process. In this approach, the pressure and surface tension over mixed cells are treated implicitly. Thus allowing the application of the normal dynamic free surface boundary condition to be significantly simplified. In this way, the pressure at mixed cells is incorporated directly into the corresponding field equation, while the surface tension effects are modelled as part of the body force terms. Furthermore, no explicit expression for interface reconstruction is required during tracking, this is similar to the level set method widely applied to many fields. The resulting algorithm can be easily extended to three spatial dimensions (Li et al., 2004b). UGent's work in this area has been to develop an approach which preserves both the smoothness of the interface and its sharp definition over one cell; this requires that numerical diffusion associated with the upwind advection scheme must not be excessive. To achieve this a weighted upwind advection scheme is used together with an operator split second order explicit Adams Bashforth method. When applied to test cases involving complex flows caused by waves, the results demonstrate that the proposed approach is computationally efficient. The current solver, LVOF, comprises (Li et al., 2004a,b): a large eddy simulation model of turbulence, using the dynamic form of Smagorinsky's model; a fully implicit cell staggered FV approach with a cut cell Cartesian technique; a novel VoF advection scheme; a blend of second and fourth order artificial damping; and, an absorbing generating boundary condition for a wave generator. This solver has been applied to: study the wave overtopping over coastal structures; to study the effect of current on breaking wave structure interactions; to investigate the effects of viscosity on the wave boundary layer; to estimate wave impacts; and, 3D effects.





**Figure 89: Computational domain on a non-uniform Cartesian cut-cell mesh for sea dike problems. WG0 to WG5 indicate the locations of five wave gauges.  $l_1=1.0$  m,  $l_1 + l_2 + l_3=6.3$  m and  $d=0.7$  m.**

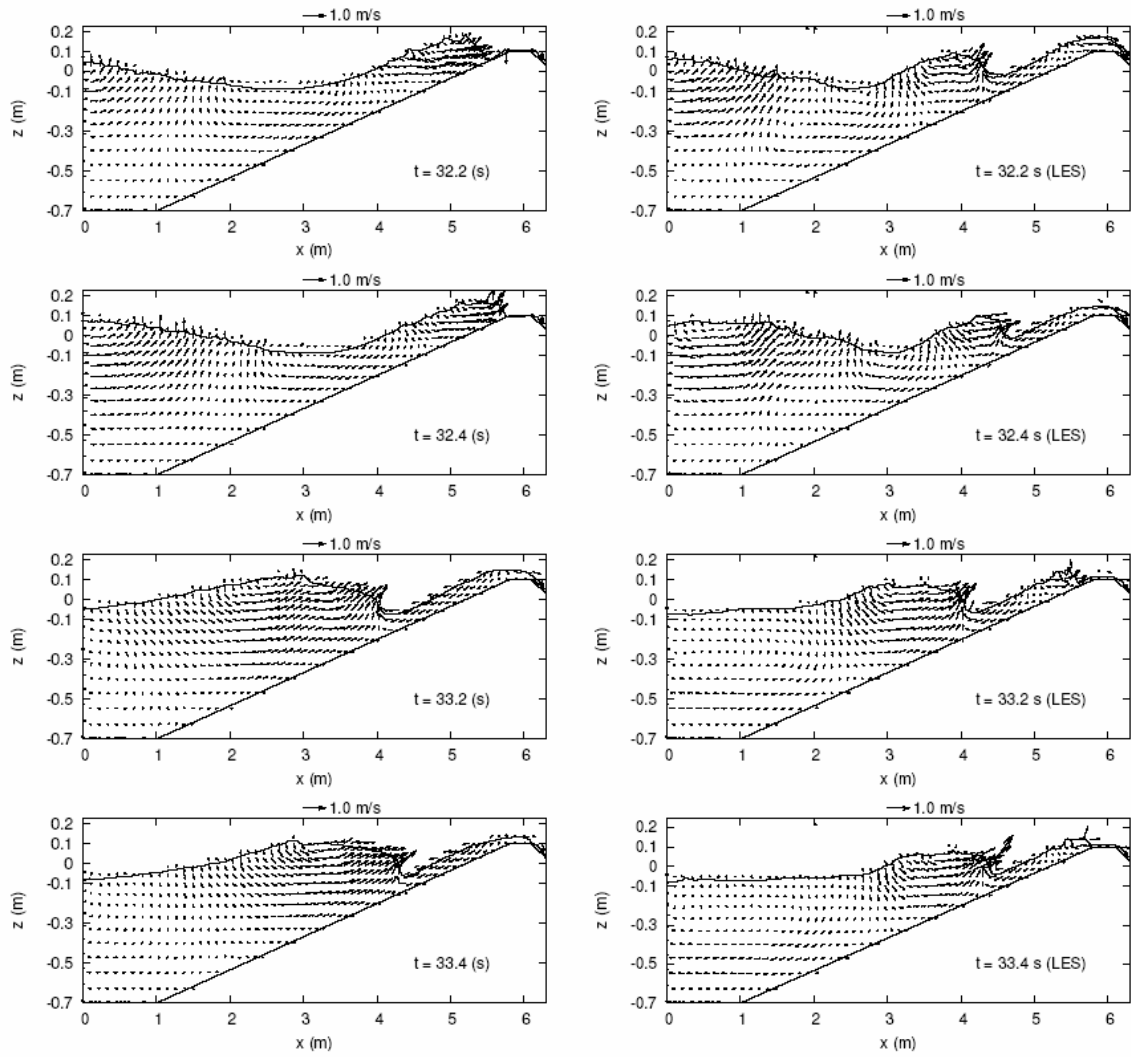
*Test Case: Wave overtopping on a smooth sea dike*

In order to validate the numerical modelling approach described previously, two well known test cases associated with overtopping of waves on a smooth sea dike have been selected. Both cases involve wave breaking on the seaward slope of the dike during overtopping. Flows are driven by a wave generator, located at the seaward boundary, for either regular or irregular waves. For the former case, monochromatic waves ( $H=0.16$  m,  $T=2$  s) are generated in 0.7 m deep water, while in the latter case the waves are created by superimposing series of regular waves drawn from an appropriate energy spectrum. Computations are conducted in the numerical flume, with the computational domain overlaying the dike has a total length of 6.3 m and a height of 1 m (see Fig. 89, the bathymetry of the foreshore and the dike embankment itself are generated by cutting the dike out of the background Cartesian mesh, using Cartesian cut cells. A number of tests have been performed on this problem to examine the convergence history, the effects of mesh refinement, dynamic and static LES models, the development of waves at the dike crest, pressure measurements on the dike slope, wave induced velocity fields, breaking wave current structure interactions and, the effect of viscosity on the wave generated boundary layer. Finally some three dimensional tests have been performed, using long crested waves and a uniform dike cross-section. Full details of these tests are detailed in



report D27 and in the literature (Li et al. 2004a,b). To illustrate the capabilities of the LVOF code, however, the development of the wave induced velocity field is considered.

Fig. 90 shows the velocity fields at times from  $t = 32.2\text{s}$  to  $33.4\text{s}$  for both regular and irregular waves. It illustrates the wave induced motions on the seaward slope of the dike during the wave attack, run-up, rundown, waves breaking to overtopping of one wave. As expected, motions caused by the irregular waves are more complex than those by the regular waves. Generally, as more waves pass over the dike crest, the flow becomes fully turbulent after an initial transient period so that the features of the flow pattern tend to be very complex, often subjected to the steepness of the free surface most likely associated with a cycle of splashing and the vortex formation created by the velocity. Waves continuously break, while the energy of waves is dissipated by turbulence and convected by vortices. At  $t = 32.2\text{ s}$ , the wave height increases as it shoals on the front face. By  $32.4\text{ s}$ , a violent overtopping jet will occur again. Additionally, the corresponding motions display the down wash at  $t = 33.2\text{ s}$ , while the next big wave is approaching the dike. Finally, the wave breaks on the upper reach of the dike at  $t = 33.4\text{ s}$ .



**Figure 90: Velocity fields induced by the regular (left) and irregular (right) waves over a sea dike from  $t = 32.2$  to  $33.4$  s.**

### 5.2.3 Long waves

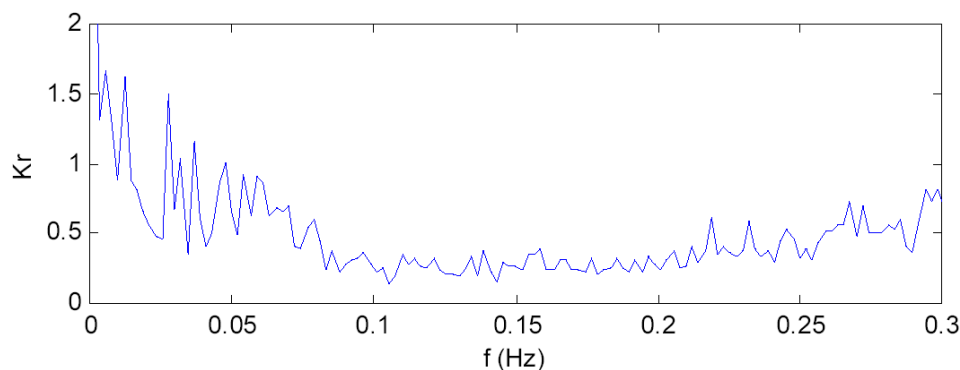
The crest elevation of dikes is determined on the basis of estimates of wave overtopping discharges. For instance, dikes along parts of the Dutch coast have a crest elevation such that a maximum mean overtopping discharge of 1 l/s/m can occur. These estimates of wave overtopping discharges are based on empirical formulae that require the wave conditions at the toe of the dike. The wave conditions at the toe of the dike are different from those at deep water. Numerical models are used to compute the wave propagation over the foreshore to provide the wave conditions at the toe of the dike. Especially for shallow foreshores this wave propagation is complex, for instance due to the effects of wave breaking. Wave breaking on shallow foreshores involves not only dissipation of energy but also a transfer of wave energy to other wave frequencies, for instance from short waves to low frequency waves (i.e., 'long waves'). Nowadays, procedures to assess the wave conditions at the toe of dikes do not take into account energy in low frequency waves. This means that part of the wave energy is neglected. Therefore, it is relevant to study the possible influence of low frequency waves on wave overtopping. The purpose of this part of WP5, is to provide insight into the possible influence of low frequency waves on mean wave overtopping discharges. For this purpose, field measurements on the foreshore of the Petten Sea defence (which has been studied under WP3) and numerical model results are used.

Rijkswaterstaat (RIKZ) have performed field measurements at the Petten Sea defence for some time. This site is characterised as a dike with a shallow foreshore and waves have been measured at several locations on the foreshore, and also wave run-up measurements have been performed during a number of storm events. A description of the field measurements is given in De Kruif (2000) and Hordijk (2003). All data signals from these field measurements have been provided by Rijkswaterstaat (RIKZ). Storms measured in January 1995 have been used for analysis in a number of previous studies. Analysis of these storms has included: an analysis of low frequency waves (e.g. De Haas et al. (1999)), comparisons with physical model tests (van Gent, 1999, 2001; van Gent et al., 2001), and comparisons with numerical models (van Gent and Doorn, 2001).

This part of WP5 is mainly focussed on the storm period October 25-28, 2002, although the storms of January 1995 have also been considered. During the 2002 storms more measurement equipment was operational than during 1995 events. It is important to note, however, that the sandy foreshore has not been stable over the years; fluctuations have been observed from year to year, from season to season, and also within storms. The Petten Sea defence is so high that the probability of occurrence of wave overtopping events is almost

negligible. Therefore, measured wave conditions in combination with a numerical model that can simulate wave overtopping (using an artificially lower crest level) for observed wave conditions have been considered.

The field measurements were analysed to obtain a number of test conditions with an approximately constant water level and significant wave height. These conditions were then analysed to obtain incident waves from the measured surface elevations. This analysis shows that the dike reflects low frequency waves up to 100% (on average 61%), while wave reflection coefficients based on the energy in the short waves are on average 23%. Fig. 90 shows the dependency of reflection coefficient on frequency for one of these conditions. It should be noted that the accuracy of the reflection analysis is reduced at higher frequencies.

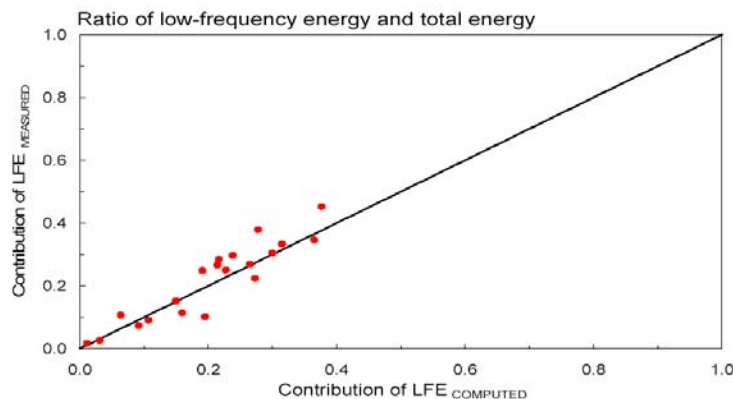


**Figure 91: Wave reflection as function of wave frequency for a selected condition; measured at MP17 on the Petten foreshore.**

Two different numerical models have been applied to examine the overtopping performance, one for wave propagation over the foreshore and one for the wave motion on the dike itself. The TRITON model was used for wave propagation over the foreshore, whilst the ODIFLOCS model has been used to simulate the wave motion and subsequent overtopping on the dike. TRITON has been used to examine whether the amount of low frequency energy can be computed accurately and it has then been applied to obtain wave conditions at the toe of the dike. Time signals from measurements and computations have been used as input for the ODIFLOCS model in order to simulate wave overtopping. Because the Petten Sea defence on site is so high that no wave overtopping occurs, in the computations the crest was artificially lowered.

The TRITON model solves the Boussinesq equations developed at Delft Hydraulics. This model is described by Borsboom et al. (2001a,b & c) and Groeneweg et al. (2003). Boussinesq type

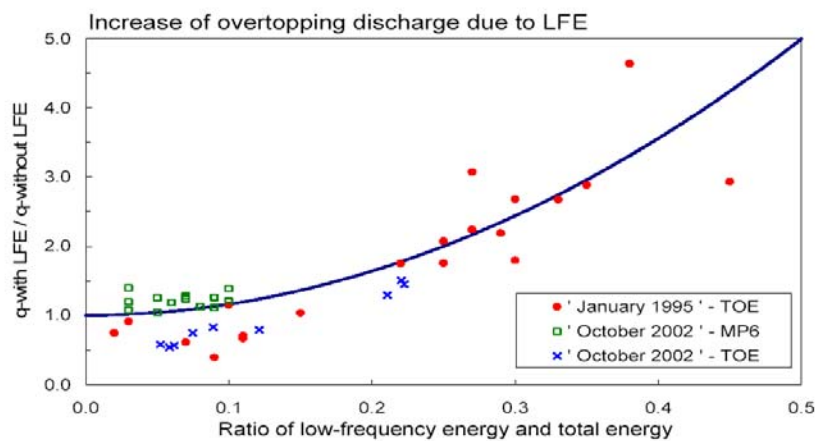
wave models are in principle suitable to model wave propagation in coastal regions and harbours. Especially for the wave propagation of short waves, where nonlinear effects, dispersion and shoaling play an important role, this type of model can be adequately applied and provide valuable information on the wave field (e.g., time series of surface elevations and velocities in shallow regions) which cannot accurately be obtained from many other types of models. In TRITON wave breaking is described using a new method by Borsboom et al. (2001c) where wave breaking is modelled as an eddy viscosity model in combination with a surface roller. Another important aspect of the model is the modelling of weakly reflecting boundaries, based on the concepts by Borsboom et al. (2001a,b & c). A validation of the model based on measured conditions on the foreshore of Petten is given in van Gent and Doorn (2001). From an analysis of the January 1995 storms it can be concluded that the model is capable of providing good estimates of the amount of low frequency waves for these 20 storm conditions. Fig. 92 illustrates the accuracy of the numerical model.



**Figure 92: Comparison between measured and computed contribution of low frequency energy.**

The ODIFLOCS numerical model is a time domain model which can simulate the wave motion on the slope of coastal structures (van Gent (1994); van Gent (1995)). The model allows for simulations of normally incident wave attack on various types of structures. Use is made of the nonlinear shallow water wave equations where steep wave fronts are represented by bores. The model is based on concepts by Hibberd and Peregrine (1979) who developed a numerical model with an explicit dissipative finite difference scheme (Lax Wendroff) for impermeable slopes without friction. Consequently, the model allows for simulations of the wave interaction with permeable coastal structures. The model is able to deal with either regular or irregular waves which attack various types of structures with arbitrary seaward slopes, smooth or rough, permeable or impermeable, overtopped or not. Since the nonlinear shallow water

wave equation overestimates the nonlinear effects, because these effects are not counteracted by frequency dispersion, inaccuracies will occur when wave the waves are propagated over long distances. Therefore, for many applications it is advisable to start the wave simulations at the toe of the structure. On the slope itself the distances are relatively small and nonlinear effects are more important than frequency dispersion. Many applications show that sufficiently accurate results can be obtained. Tests based on the conditions identified previously show that conditions with the highest percentage of low frequency energy result in the highest increase of the mean wave overtopping discharge (Fig. 93).



**Figure 93: Increase of mean wave overtopping discharge as function of the ratio of low-frequency energy and total energy.**

The results of this analysis indicate that for the studied storm conditions low frequency energy increases the mean overtopping discharge with a factor up to a maximum of 5. This increase depends on the percentage of low frequency energy. For the analysed storm period October 2002, a much lower factor was found (up to 1.4). Also for a condition considered as a super storm condition a factor of 1.4 was found. A factor of 1.4 would have a rather small effect on the required crest elevation due to the influence of low frequency energy.

#### 5.2.4 Scale Effects

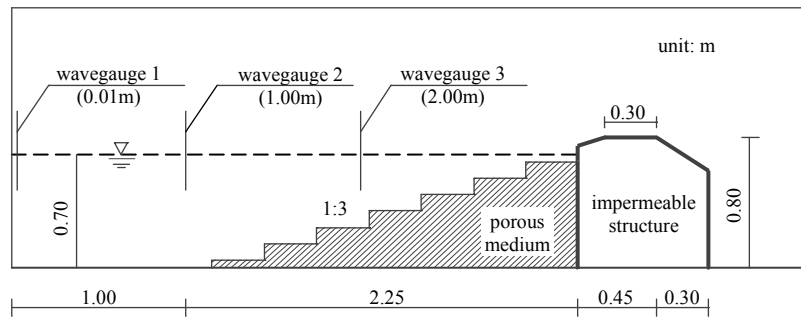
Results reported under WP4 have shown that the measured volumes in laboratory simulations of overtopping on the rough porous breakwaters at Zeebrugge and Ostia are lower than those observed in the prototype measurements. It is clear that scale or model effects are present. Experiments have been conducted at UPV to investigate the effects of wind (model effect) at

Zeebrugge, whilst the work in this part of workpackage 5 aims to support the research towards the effects of scale on overtopping.

When Froude scaling is applied to overtopping on a rough structure the relative roughness probably scales correctly as the thickness of the overtopping jet is expected to scale according to the Froude law, whilst the length scale of the armour layer is a characteristic length and will have been scaled accordingly. Unfortunately the viscosity of the fluid will not have been scaled so, even if, the characteristic velocity of the overtopping jet scales with the Froude law the Reynolds number will be different. Work on smooth and rough dikes (Schulz, 1992) has shown that provided the model and prototype structures are both in regimes with high enough Reynolds numbers the friction-factor can be considered to be constant. Schulz (1992) suggests that provided the Reynolds number is above  $10^5$  the friction factor can effectively be considered to be constant. This threshold of hydraulic independence is supported by work on an armoured sea wall by Sakakiyama & Kajima (1998); see WP7 (Chapter 8) for further details.

#### **6.2.4.1 Numerical simulation of 2D wave overtopping on a porous model structure.**

In order to provide an understanding of the physics, a simple structural configuration has been tested, under regular wave conditions, using AMAZON-SC. The model scale structure (Fig. 94), consists of a porous breakwater ( $K=0.56$ ,  $N_w=35\%$ ), 0.7m tall with 1:3 front face, consisting of ten, 10cm tall steps (to simulate an armour layer). Behind the porous face is a solid, impermeable region, 0.8m tall. The breakwater was subjected to 0.16m high regular waves with a period of 2.0s. and overtopping was measured across the crown of the structure. The numerical study allowed instantaneous measurements of both jet velocity and jet thickness to be obtained. In addition to the porous tests the structure has been tested with a completely impermeable configuration. To examine the effects of scale both configurations have been tested with Froude scalings of 1:2, 1:1, 2:1 and 4:1 and in addition the model scale test has been subjected to 2s waves of 0.08, 0.10, 0.12 and 0.16m; the complete test matrix thus comprises 14 tests.



**Figure 94: Computational domain with step porous structure**

For each case the instantaneous discharge and the overtopping jet thickness have been measured and used to compute the instantaneous jet Reynolds number, by analogy with steady state flow over rough surfaces the Darcy-Weisbach friction factor has then been computed and plotted on the Moody diagram. This analysis, following the approach taken by Schulz (1992) and which is based on a quasi-static assumption, is shown in Fig. 95. The results show that for hydraulic independence (i.e. approximately constant  $\lambda$ ) the Reynolds number,  $Re$ , should be above  $10^5$ , requiring tests to be undertaken at scales larger than 4:1 (i.e. in a 100m wave flume, with a 3.2m high wall in 2.8m of water). It should be noted however, that at smaller Reynolds numbers (e.g.  $Re \leq 10^4$ ) the difference in friction factor is fairly small and the associated dimensionless jet velocities (Fig 96) and overtopping volumes are similar. It is worth noting that the characteristic length scale associated with the tested structure is large and that the variation in  $l$  with  $Re$  is larger for smoother structures.



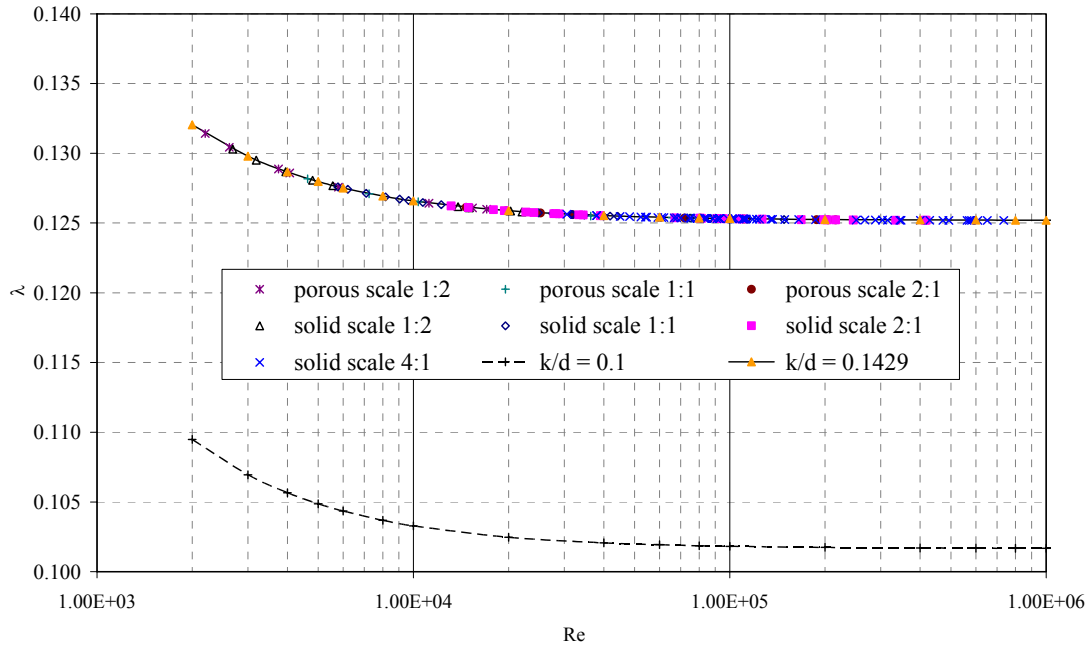


Figure 95: The Darcy-Weisbach friction factor  $\lambda$  against Reynolds numbers.

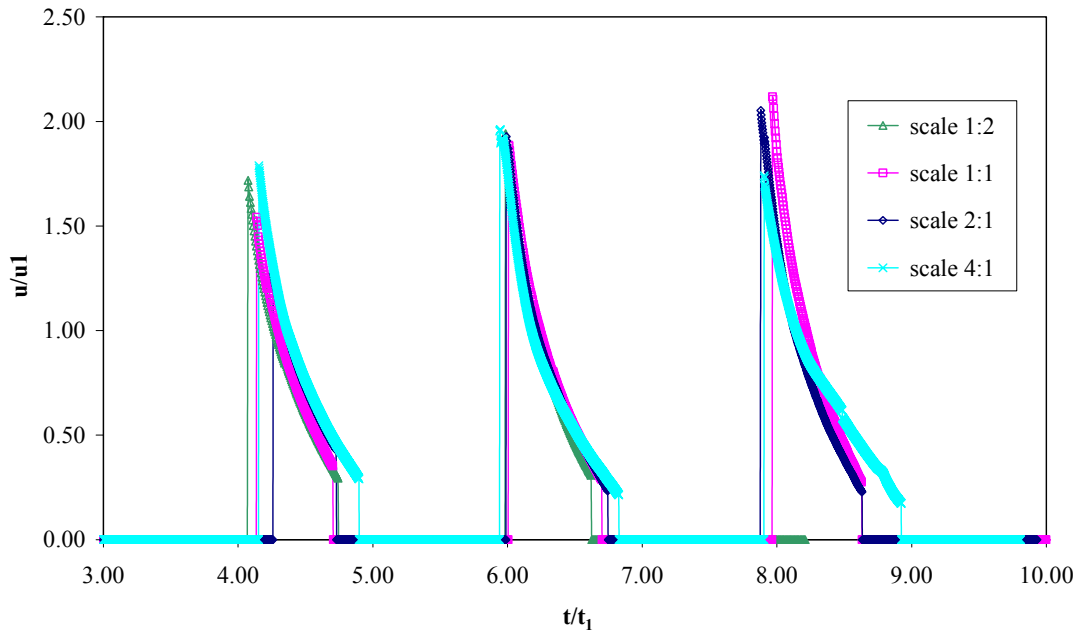


Figure 96: Instantaneous dimensionless jet velocities (solid breakwater)

### 6.2.4.2 Numerical simulation results of 2D wave overtopping at Ostia breakwater

#### Introduction

Numerical simulations of wave overtopping at the Ostia porous rubble mound breakwater have been carried out using the UGent VOFbreak<sup>2</sup> code. As a reference case, the 2D 1/20 physical scale model (tested in the UGent wave flume within WP 4) has been used. The physical scale model dimensions have been adopted in the numerical model. Regular wave conditions have been used, identical to the characteristics of the regular wave tests in the physical model. The 1/20 model is used as the reference case for simulating overtopping at the Ostia breakwater, and the numerical model has been used at scales 1/10 and 1/1 subsequently. The scaling is carried out using Froude scaling laws, keeping gravity and viscosity constant for the three different model sizes.

#### Model description

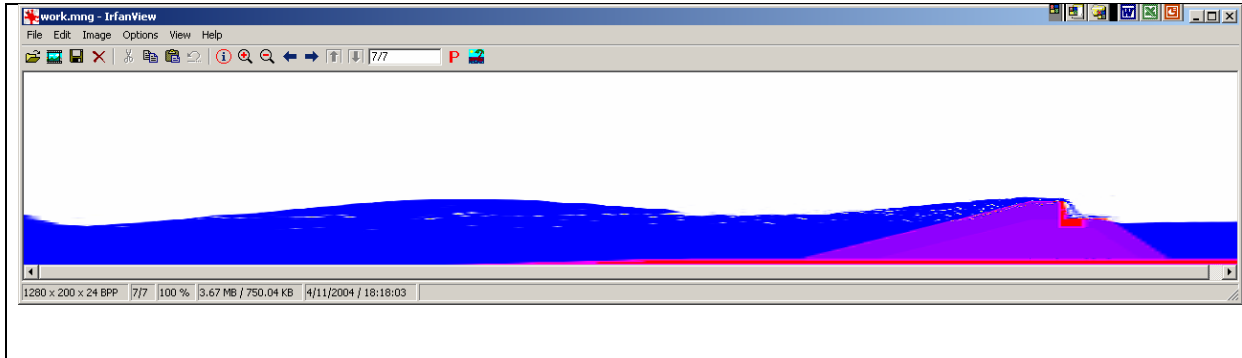
Incident wave conditions are: wave height  $H = 0.175$  m, wave period  $T = 2.24$  s in water depth (near the paddle)  $d = 0.80$  m (and 0.30 m at the toe). The porous breakwater is composed of a core and an armour layer, with material characteristics as given in Table 21.

**Table 21: Material characteristics for the 1/20 Ostia scale model**

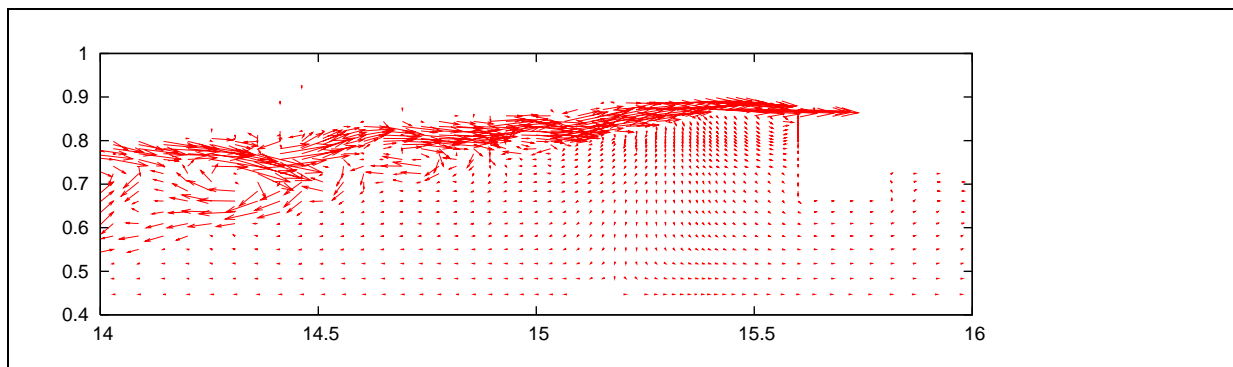
	Core	Armour layer
Porosity $n$ [-]	0.39	0.44
Stone diameter $d_{50}$ [m]	0.025	0.075
Shape factor $\alpha$ [-]	0	0
Shape factor $\beta$ [-]	2.9	2.7

## Simulation results

A typical result of the numerical simulation of the free surface configuration for the 1/20 scale model after 5 waves is shown in Fig.97. The velocity fields calculated at time 20.0 s for the 1/20 scale model is shown in Fig.98.



**Figure 97: Free surface configuration of the Ostia breakwater model (scale 1/20), modelled using the VOFbreak<sup>2</sup> code, and showing wave breaking in front of and wave overtopping over the porous breakwater.**



**Figure 98: Simulation results calculated at time 20 s for the 1/20 scale model.**

The results taken from the simulations are the averaged (during one wave period) layer thickness  $h$ , the averaged flux (or overtopping rate)  $q$  and the averaged Reynolds number  $Re$ , taken at two specific locations: on the breakwater slope (at the intersection with the SWL) and on the crest (seaward side). For scaling the 1/20 model to scales 1/10 and 1/1, two approaches have been used. In the first approach the permeability has been kept constant (stone diameter and  $\beta$  are not scaled, so  $b$  is constant), using the second approach, the permeability has been scaled (stone diameter has been scaled).

Reynolds numbers on the slope and on the crest are derived from the results: for the small scale model (1/20) we obtain  $Re = 7000$  on the slope and 1800 at the crest. For the prototype (1/1) we obtain  $Re \sim 1 \times 10^5$  at the crest and  $5 \times 10^5$  at the slope.

Since the core is completely saturated during wave overtopping, porous flow scale effects will be minimal. For flow in the lower part of the run-up wedge (i.e. on the slope), the 1/20 model yields a Reynolds number  $Re \approx 0.7 \times 10^4$  (close to the critical value  $Re_{crit} = 1 \times 10^5$  for wave overtopping), and higher  $Re$ -values for larger scales, so no scale effects are expected in this region. For flow in the upper part of the run-up wedge (i.e. on the crest), the 1/20 model yields a Reynolds number  $Re \approx 0.2 \times 10^4$  so scale effects are expected in this region.

### 5.2.5 *Shallow water models*

Violent overtopping events are difficult to model using current numerical methods. Ideally, the Navier-Stokes equations should be solved to provide a good model of the overtopping events, using some form of free surface resolving model. However, numerical solvers for these equations require extensive computational resources and, as such are impractical for design calculations by a practicing engineer on a desk top computer, thus an alternative method is required.

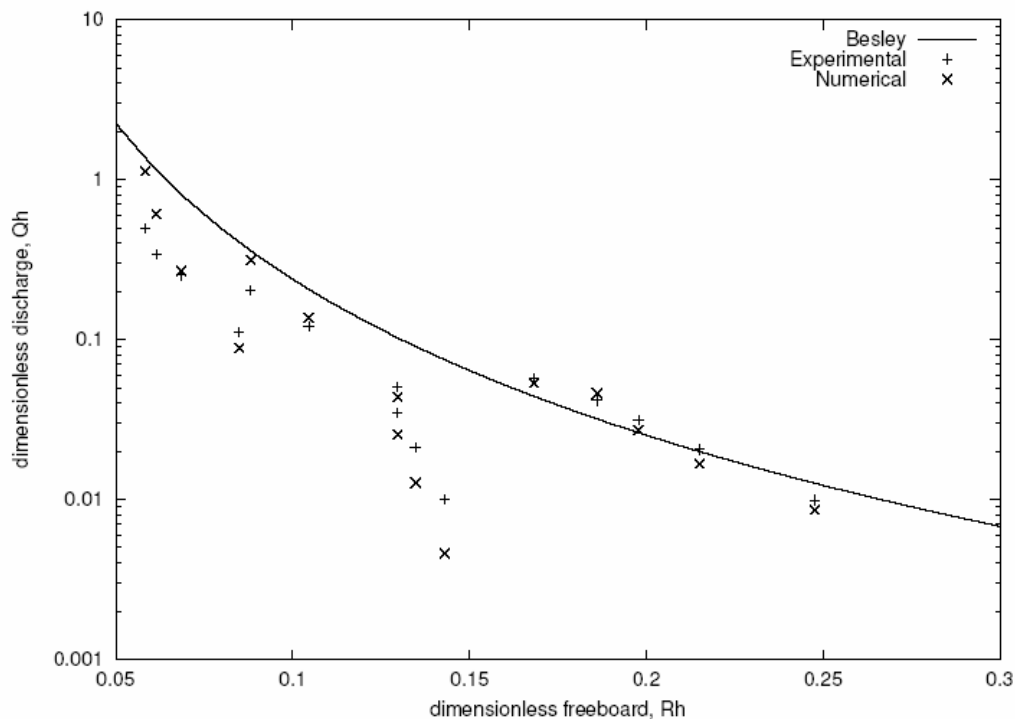
A depth averaged formulation of the Navier-Stokes equations exists in the shallow water equations (SWE). As the SWE are depth averaged, any vertical velocity is neglected. Thus, these equations, in theory, may not be suitable as a basis for a numerical model for violent wave overtopping where vertical velocities are a major feature. However, SWE models are easy to implement and computationally efficient. Therefore, before discarding them altogether, an analysis of the limitations of the SWE model is required.

Existing models that make use of the SWE to model wave run-up and overtopping include ODIFLOCS and ANEMONE. These models have been used to give predictions of wave run-up and overtopping of sea dikes where wave conditions are less impacting and violent overtopping is less likely to occur. Shiach et al. (2004) used the AMAZON-CC code to perform detailed comparisons between the VOWS wave overtopping experiments on a 10:1 battered wall (Allsop et al., (2004)). The numerical scheme used is based on the MUSCL Hancock scheme (van Leer, 1984) which is a high resolution Godunov type scheme that uses MUSCL reconstruction to prevent spurious oscillations and incorporates the surface gradient method

(Zhou et al., 2001, 2002) was implemented to model both the seawall and the approach bathymetry.

Comparisons between water surface elevations of the physical and numerical models show that although the waves occur at the same time, the numerical surface over predicts the heights of each wave. This can be attributed to the lack of dispersion within the shallow water equations that are being used in non-shallow water. Fig. 99 shows the dimensionless discharge ( $Q_h = (Q/(gh^3)^{0.5})/h^{*2}$ ) plotted against the dimensionless freeboard ( $R_h = (R_c/H_s)h^*$ ) for the physical model and the numerical model.

Shiach et al. (2004) concluded that the shallow water equations provide a useful alternative to more computationally expensive models for violent wave overtopping provided the  $h^*$  parameter does not fall below 0.075 and that the seaward boundary condition is sufficiently close to the structure. This model provides a useful engineering design tool with 1000 wave simulations taking less than two minutes to run on a moderately fast PC.



**Figure 99: Dimensionless discharge ( $Q_h$ ) plotted against dimensionless freeboard ( $R_h$ ) for the physical model and the numerical model.**

## Conclusions

The AMAZON-SC code developed by MMU, which provides a numerical wave flume in which the flow equations are solved both in the air and the water, has been extended under the CLASH project to include both the effects viscosity and a porous flow model. The resulting flow code has been applied to examine a selected overtopping event from the experimental study of Samphire Hoe before being applied to examine the effects of scale on the overtopping of both permeable and impermeable rough structure. The results on scaling are in broad agreement with those from previous experimental work, indicating that for hydraulic independence of the friction factor the Reynolds number, associated with the overtopping jet, should be greater than  $10^5$ . The results from these scale effect test have helped to enlighten the discussion on scaling effects undertaken in WP7.

At UGent, a new solver based on a Large Eddy Simulation (LES) turbulence model has been developed for the simulation of overtopping of water waves over sloping and vertical structures in a numerical wave tank. The new solver has been validated with two test cases for both regular and irregular waves, respectively. These results demonstrate that UGent's new solver can describe most of the significant features of breaking wave-induced flows. In particular, the wave form is well captured even during a lengthy computation that agrees with measurements available under grid refinements. As a result, this solver can yield detailed information of wave-induced motions on design in coastal engineering using CFD.

Long wave simulations of the Petten site have been computed and the effect of surf-beat at this site has been assessed.

Computations by MMU and HRW have shown that under certain circumstances shallow water models may be used to provide reasonable estimates of overtopping discharge for impulsive overtopping of near vertical sea walls and for overtopping jet velocities for mildly sloping structures.

This workpackage delivered the following reports :

- the draft report on numerical modelling (D9)
- the report on simulation of long waves (D25)

- the numerical model (D26)
- the final report on numerical modelling (D27)

Additionally one milestone was achieved :

New numerical modelling techniques have been implemented (M4)

## 6 WP 6 : Hazard analysis including socio-economic impacts

### 6.1 Objectives

The overall aim of this workpackage is the derivation / refinement of guidance on various levels of hazard imposed on people by overtopping at seawalls and related sea defence structures.

Specific objectives are

- To compare measured events and hindcast events with records of observed hazard in order to derive / refine limits for safety of pedestrians of different levels of mobility, car users, etc.
- To derive / refine limits of overtopping for hazard to buildings and related items
- To evaluate the risk of economic losses

### 6.2 Description of work performed

#### 6.2.1 *Background to development on hazard assessment guidance*

This section gives some definitions and key parameters in the hazard assessment.

Based on the degrees of overtopping related to coastal structures expected hazards can be identified. Hazards from wave overtopping may arise under three general categories:

- a) Direct hazard** of injury or death to people living, working or travelling in the area defended;
- b) Damage to property, operation and / or infrastructure** in the area defended, including loss of economic (environmental or other) resource, or disruption / delay to an economic activity / process;
- c) Damage to defence structure(s)**, either short-term or longer-term.

Hazards or consequences of overtopping are both site- and event-specific, see discussion in Bouma *et al.* (2004). The hazards are driven by overtopping processes usually categorised by the direct responses:

- mean overtopping discharge,  $q$ ;



- peak overtopping volumes,  $V_i$  and  $V_{max}$ ;
- overtopping velocities, horizontally and vertically,  $v_x$  and  $v_z$ ;

Less direct responses may also be needed in assessing the effects of these processes, perhaps categorised by:

- overtopping falling distance,  $x_c$ ;
- pulsating (quasi-static) or impulsive pressures,  $P_{qs}$  or  $P_{imp}$ ;
- post-overtopping flow depths,  $h$ , and horizontal velocities,  $v_x$ .

When considering the effects of wave action, it may be convenient to start by defining degrees of overtopping under three levels of severity and two types of load application:

**Light overtopping**, no impulsive effects or direct structural damage to lightly engineered structures, minor or very local flooding, damage chiefly by inundation only;

**Moderate overtopping**, no impulsive effects and little / no direct structural damage to engineered structures, local flooding causing some inundation damage;

**Heavy overtopping** requiring significant engineering to resist direct effects without damage, overtopping flows / volumes are unlikely to cause damage to a well engineered defence structure, but local and wider flooding is possible as is flood flow damage to lighter structures;

**Overtopping flows** with no significant “slam” effect, damage caused by velocity driven drag forces;

**Impulsive overtopping** with sudden and wave “slam” forces generally caused by the leading edge of an overtopping jet or bore, may lead to direct damage to property close behind and/or damage to the defence itself.

Depending on the expected levels of overtopping, the risks of economic losses can be identified. In making funding decisions, makers of policies to decide on acceptable levels of overtopping will be confronted with assessing both the costs and benefits of controlling

overtopping. Clearly, these assessments take place within a decision-making process context that is different for each of the EU member states. The research under WP 6 provides guidance to determine the perceptions and valuation of hazards.

### 6.2.2 Existing Guidance

Previous research, taking into account different overtopping processes lead to guidance on overtopping hazards already available at the start of the project. This guidance is summarized in table 22 which indicates limits for the average overtopping rate  $q$ . The mean discharge is expressed as flow rate per metre run of seawall, typically l/s.m.

**Table 22: Initial Guidance on Tolerable Mean Overtopping Discharges (l/s.m)**

<b>Embankment Seawalls :-</b>				
No damage		$q$	<	2
Damage if crest not protected	2	<	$q$	< 20
Damage if back slope not protected	20	<	$q$	< 50
Damage even if fully protected		$q$	>	50
<b>Promenade Seawalls :-</b>				
No damage		$q$	<	50
Damage if promenade not paved	50	<	$q$	< 200
Damage even if promenade is paved		$q$	>	0.2
<b>Buildings :-</b>				
No damage		$q$	<	0.001
Minor damage to fittings etc	0.001	<	$q$	< 0.030
Structural damage		$q$	>	$3 \times 10^{-5}$
<b>Vehicles :-</b>				
Safe at moderate / higher speeds		$q$	<	0.001
Unsafe at moderate / higher speeds	0.001	<	$q$	< 0.02
Dangerous		$q$	>	0.02
<b>Pedestrians :-</b>				
Wet, but not unsafe		$q$	<	0.003
Uncomfortable, but not unsafe	0.003	<	$q$	< 0.03
Dangerous		$q$	>	0.03

It has been argued (see e.g. Besley, 1999) that use of mean overtopping discharges only in assessment of safety levels is questionable. It was regarded as probable that the maximum individual volume was of much greater significance than the average discharge to hazards. Franco *et al.* (1994) and Besley (1999) have shown that, for a given level of mean discharge, the volume of the largest overtopping event can vary significantly with wave condition and structural type. There are however two difficulties in specifying safety levels with reference to peak volumes and not to mean discharges. Firstly, methods to predict peak volumes are significantly less well-validated than for mean discharge. Secondly, the data relating individual overtopping events to hazard levels have been rare.

Within CLASH, however, other important parameters, as defined in section 6.2.1 have been taken into account to refine the guidance on overtopping hazards.

### **6.2.3 New evidence on personnel hazards**

Every year, people drown after being swept from breakwaters, seawalls and rocky coasts. Example incidents for the UK gleaned from a single source for 1999-2002 are summarised in Appendix C to the report by Allsop (2004) (Deliverable D38) and for Italy between 1983 and 2002 in Appendix D to this report. To the individual, the waves responsible for such incidents may appear to be sudden and surprising, so it is probable that the people concerned had relatively little idea of the hazard to which they exposed themselves. It is however likely that many of these events could be predicted by informed analysts using some weather / wave forecasting and the results of recent research.

An early example of a custom-built overtopping warning system is described by Gouldby *et al.* (1999) for the low-lying reclamation at Samphire Hoe near Dover. This artificial reclamation was formed by chalk spoil from the excavations of the Channel Tunnel retained by a vertical sheet pile wall. The broad promenade is widely used as a leisure resource, but is subject to wave overtopping during storms. Careful management of access was therefore important to ensure visitor safety. A warning system was therefore developed in which overtopping above agreed thresholds were predicted by output from an appropriate numerical wave model. Wave conditions were correlated with incidents of known overtopping hazard, categorised as low, moderate or high, see Fig. 100. These warning levels were then communicated by the use of warning flags, and ultimately by closing access to the seawall.

Examples of the occurrence of perceived hazards are categorised, and mean overtopping discharges were calculated for each “hazard” event. These were used by Allsop *et al.* (2003) to support the continuing use of  $q \leq 0.03$  l/s.m as a safe limit for (unaware) pedestrians when subject to impulsive jets.



**Figure 100: Categorisation of overtopping hazards at Samphire Hoe, low, moderate and high**



**Figure 101: Public watching / dodging overtopping at Oostende**

The general approach to reducing risks is however only possible where an owner / operator has the means and resources to obtain advance forecasts of hazards, and then to operate such an exclusion system. Elsewhere it is generally only possible to issue warnings.

#### **6.2.4 Perceptions of overtopping**

It is appreciated by engineers and coastal managers that seawalls reduce wave overtopping, but it requires a sophisticated understanding to be aware that seawalls do not always stop, but simply reduce overtopping. Under storm action, waves still overtop seawalls, sometimes frequently and perhaps violently. These processes may excite considerable public interest, see the example in Fig. 101 at Oostende where tourists gather during storms (situation before June 2004).

The key problem identified during the PPA project is that most messages to tell the public about the seaside and coastal activities (particularly those marketing a vision) present only the “sunny” view of coastal processes. There is no motivation for the developer / architect / advertiser to show “stormy” or winter views where hazards might be more easily perceived. This imbalance is compounded by tools that communicate messages of hazard well to engineers and scientists, but do not carry the same message to members of the public.

Examples of this problem are illustrated in Fig. 102, 103, 104 and 105. The first of these show example of coastal structures as experienced by most members of the public. The sun is shining, the waves are small. There are no obvious hazards. Contrasting views of substantially greater hazard are shown in Fig. 104 and 105 showing severe waves at two small harbours. The first photo shows waves of  $H_s = 3-3.5\text{m}$  at the Italian harbour of Salivoli (Tuscany) in November 2001. The second shows waves equivalent to  $H_s = 4\text{m}$  at the harbour of Hartlepool, UK, as modelled at a scale of about 1:40. All coastal engineers will be able to perceive equivalent levels of hazard to either situation, experienced as she / he is in scaling the process to full scale. The problem identified by the non-engineer members of the PPA project is that members of the public cannot easily make the same mental jump. To them, there is no obvious hazard from waves of 50-100 mm height! It was clear, therefore, that any graphic or photograph seeking to explain wave / coastal / overtopping processes would have to take account of this perception “blind-spot”.



**Figure 102:** Beach, seawall and promenade at San Sebastian, Spain



**Figure 103:** Artificial beach, breakwaters and resort at Lanzarote



**Figure 104:** Yacht harbour of Salivoli (Tuscany) during storm in November 2001



**Figure 105:** West Harbour, Hartlepool, under 1:50 year storm, physical model



### 6.2.5 *Changing public perceptions*

Changes to public behaviour will partially be driven by changes to direct management practices at coastal sites, but will also require improvements in awareness of potential hazards, and some understanding of the key drivers. This will require changes on a number of fronts: increasing general awareness of sea / coastal processes; greater awareness of hazards posed by wave overtopping and related processes; and use of site specific warnings.

At the most general level, work is needed by coastal engineers in general to engage with the public media to explain coastal engineering processes in general. Most such work is most obviously focussed on teaching, where each learning increment builds on previous understanding. A major danger in producing simplifying explanations are the consequences of media tendencies to sensationalise the issue, submerging reality in hyperbole. Use of the term “freak waves” for any large wave (however predictable by modelling of wave statistics or processes of wave-wave interactions) is the prime example of such distortions. The use of such “tabloid” expressions debases the public view of the probability of encountering large waves. A particular area of weakness is the widespread lack of understanding of shoaling of swell waves, likely to give inshore waves many times greater than offshore where waves of low steepness (say  $s_{op} < 0.5\%$ ) shoal up over steep slopes. Given that this is exactly the process by which surfing waves are generated, it is perhaps surprising that so few professionals and public appreciate the process which was probably the prime cause of the incident at Giant’s Causeway shown in Fig. 106.



**Figure 106:** Extracts from video of overtopping incident at Giant's Causeway, 16 August 2002

In this incident on 16 August 2002 at Giant's Causeway, 8 children and a "responsible" adult were swept into the sea by a "freak" wave. All were rescued, but this incident highlights typical misperceptions of risk in such situations, and lack of serious attention to warnings.

With climate change bringing increased storminess, there will be more locations where these hazard will increase. The public are aware of climate change, but will not make the link to overtopping hazards unless better informed. This is aggravated by media references to "freak waves" that are in truth entirely predictable by an informed person, and media concentration on tsunamis and other "televisual" hazards of very low probability.

### **6.2.6 Awareness of coastal processes**

The most immediate action of any owner or responsible authority aware of a potential hazard is to ensure that the public are made aware of the hazard. The general issue of hazards on coastal structures has been discussed by Halcrow (1997) and Heald (2002) who show examples of poor signage.

Some tools that can be used to train coastal engineers, scientists, and perhaps managers, may not be so useful in informing the public. Example cartoons developed by HRW and the PPA project for the UK Environment Agency are shown in Appendix M to the mentioned deliverable to illustrate the development of overtopping and possible damage under extreme storms.

### **6.2.7 Post overtopping velocities and loads**

#### ***Overtopping velocities***

Until recently, few data have been available on overtopping velocities. Pearson *et al* (2002) have presented measurements at small and large scales of upward velocities ( $u_z$ ) from vertical / battered walls under impulsive and pulsating conditions. They related the measured upward velocity  $u_z$  to the inshore wave celerity given by  $c_i = (gh)^{1/2}$ . Relative velocities,  $u_z/c_i$ , were plotted against the wave breaking parameter,  $h^*$ . Non-dimensional velocities were roughly

constant at  $u_z/c_i \approx 2.5$  for pulsating and slightly impulsive conditions  $h^* > 0.2$ , but overtopping velocities increase significantly for impulsive conditions when  $h^* \leq 0.2$  reaching  $u_z/c_i \approx 3 - 7$ .

For simply sloping embankments, Richardson *et al* (2002) measured crest velocities of around  $u_z/c_i \approx 2$  behind a 1:2 slope under plunging conditions. Simulations for 1:1-1:5 slopes discussed in Appendix H to deliverable D38 showed overtopping bore velocities in the range  $u = 2-5$  m/s.

Further data on overtopping velocities have been presented by Romestaing in Appendix F to D38. Analysis of video of overtopping velocities in the Samphire Hoe 3D model gave peak velocities of  $u_z = 1-9$  m/s, corresponding to  $u_z/c_i \approx 0.2 - 1.2$ , much lower than found by the VOWS tests. Analysis of video recordings from the Carlyon 3D model, gave horizontal overtopping velocities behind the recurve seawall of  $u_x = 3.5$  to 5.5 m/s.

These levels of velocity may be put into context by findings from UK studies on flood risks to people, see Ramsbottom *et al.* (2004) who present hazard classification tables based on flow depths and velocities. The suggested limits are re-represented here as Fig. 107. As these velocity / depth limits were originally derived for relatively steady flows, it would be wise to take a precautionary view of these limits in the derivation of any suggested limits. The middle threshold in Fig. 107 suggests that flow velocities above  $u_z \geq 2.5$  m/s will be difficult to resist for depths greater than  $d > 0.5$  m, and  $u_z \geq 5$  m/s will be difficult to resist for depths greater than  $d > 0.25$  m.

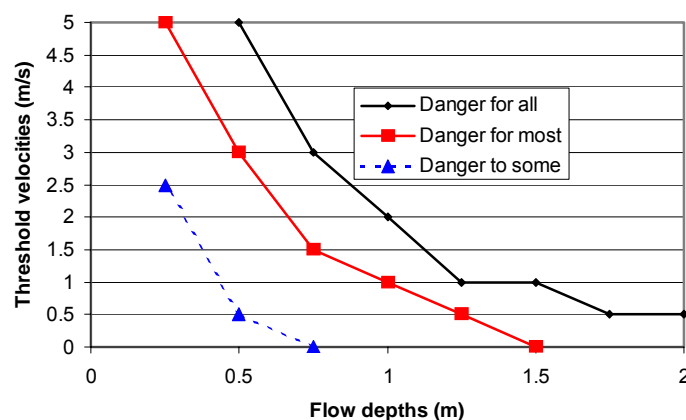


Figure 107: Suggested velocity / depth limits from Ramsbottom *et al.* (2004)



### ***Post overtopping wave loads on structures***

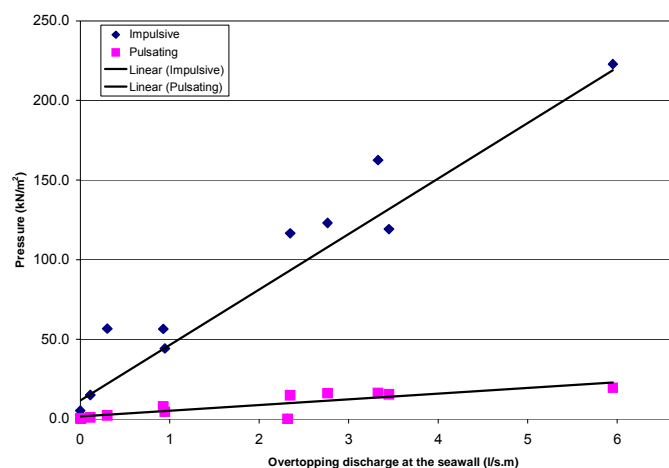
Wave loads have seldom been measured on defence structures, buildings behind sea defences, or on people. Under CLASH, post overtopping loads on person-sized dummies and a length of pipeline have been measured at full scale at Zeebrugge (Geeraerts & Boone, 2004), and at small scale at LWI (Kortenhaus et al., 2004) and HRW.

For test conditions described by Romestaing in Appendix F to D38, wave pressures measured on the 1m high secondary wall set 7m back from the primary (recurve) wall measured.

The impulsive pressures were approximately 11 x greater than the quasi-static loads. Extrapolating the trend lines in Figure 22 down to an overtopping condition of  $q = 0.03$  l/s.m suggest that the quasi-static pressures might reduce to  $p_{q-s} \approx 2$  kN/m<sup>2</sup>, but that impulsive pressures might not fall below  $p_{imp} \approx 20$  kN/m<sup>2</sup>. These may be put into context when noting that few buildings are designed for horizontal wind loads above  $p_{av} \approx 0.5$  kN/m<sup>2</sup>.

Measurements on the person dummies are also discussed in the above mentioned Appendix J, and a summary graph of results is shown here in Fig. 109.

These measurements suggest that wave loads on a person increase rapidly for increasing overtopping discharges. Advice quoted in Appendix J cites work by Endoh et al as giving force limits on individuals of up to  $F_h = 140$  kN. Given other data collected for this and related studies, this force limit appears much too high.



**Figure 108: Wave loads on person dummies (from tests at LWI, see Appendix J)**

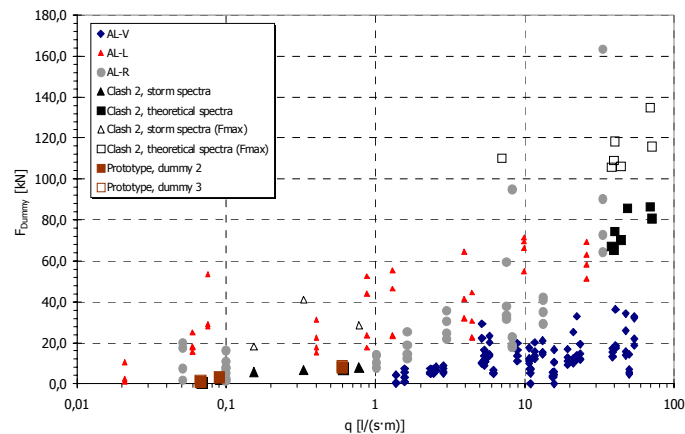


Figure 109: Wave loads on person dummies (from tests at LWI, see Appendix J)

### 6.2.8 Present Guidance

This section presents the present state of knowledge on tolerable wave overtopping. It includes guidance derived from the CLASH field and laboratory work, and builds on previous guidance, see Fukuda *et al.* (1975), Owen (1980), Besley (1999) and Allsop *et al.* (2003). A number of limits are suggested in Table 23 for mean overtopping discharge or peak overtopping volume. These limits derive from a generally precautionary principle informed by previous guidance and by the various observations and measurements made by the CLASH partners and research colleagues.

**Table 23: Suggested limits for overtopping mean discharges or peak volumes\***

<i>Hazard type / reason</i>	<i>Mean discharge, q</i>	<i>Peak volume, V<sub>max</sub></i>	<i>Comments or other limits</i>
<b><i>Pedestrians</i></b>			
Unaware pedestrian, no clear view of the sea, relatively easily upset or frightened, narrow walkway or close proximity to edge	0.03 l/s.m	2-5 l/m at high level or velocity	
Aware pedestrian, clear view of the sea, not easily upset or frightened, able to tolerate getting wet, wider walkway.	0.1 l/s.m	20-50 l/m at high level or velocity	
Trained staff, well shod and protected, expecting to get wet, overtopping flows at lower levels only, no falling jet, low danger of fall from walkway	1-10 l/s.m	500 l/m at low level,	$d \cdot u^2 < 1-5$ $m^3/s^2 \cdot m$ (see Fig. 107)
<b><i>Vehicles</i></b>			
Driving at moderate or high speed, impulsive overtopping giving falling or high velocity jets	0.01-0.05 l/s.m	5 l/m at high level or velocity	
Driving at low speed, overtopping by pulsating flows at low levels only, no falling jets	10-50 l/s.m	1 m <sup>3</sup> /m	
<b><i>Property</i></b>			
Sinking small boats set 5-10m from wall. Damage to larger yachts	q = 10 l/s.m	1 - 10 m <sup>3</sup> /m	Volumes depend on vessel position etc., form of overtopping flow and wave transmission
Significant damage or sinking of larger yachts	q = 50 l/s.m	5 - 50 m <sup>3</sup> /m	

\* Overtopping at "Low level" is overtopping flowing over or close to the promenade. Overtopping at "high level" is overtopping flying through the air.

High or low velocities depending on flow depth, see Fig. 107 for guidance.

### 6.2.9 Valuing overtopping hazards

The perception of direct hazards indicates that the risk of death is an ultimate level of hazard. If this is to be included into the economic assessment this is to be decided on by the decision makers themselves. If, the answer is yes, then Bouma et al. (2004) (Deliverable D39) provide valuation methods based on methods available in literature.

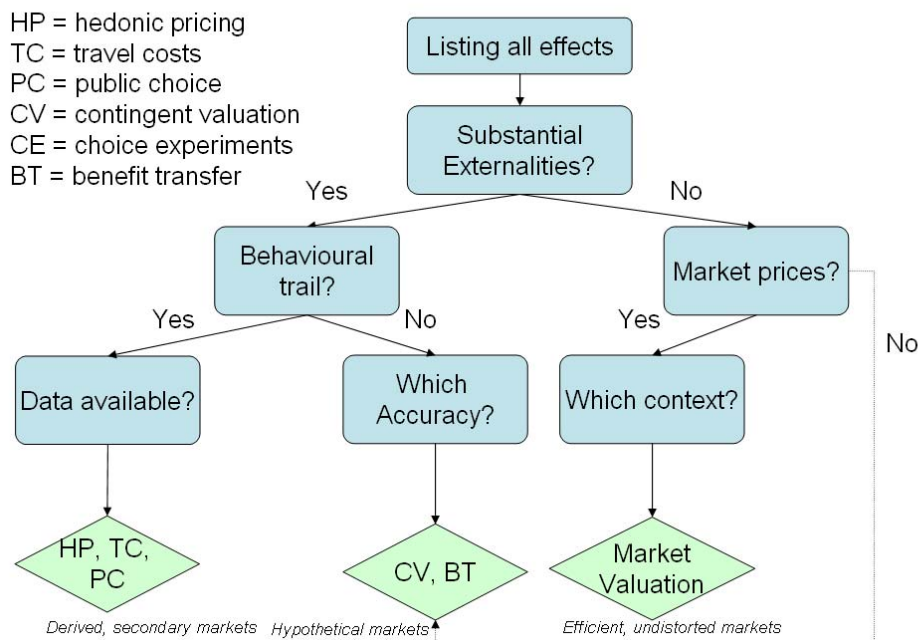
Deliverable D38 gives outline details of deaths from overtopping and related processes in Italy and UK. In many cases the context is such that this valuation will not take place in such an explicit way but will be dealt with implicitly by introducing safety norms. These norms may not necessarily define the acceptable level of overtopping (**defence standard**) but might also provide norms with respect to:

- **Acceptance of human activities** (thereby modifying the land use category and/or habitat status of the area affected by the overtopping (hazard zone))
- **Acceptance of occasional hazard** at acceptable probability (acceptable risk) by providing for temporary use and/or short-term evacuation with reliable warning and evacuation systems, and/or use of temporary / demountable defence systems;

With respect to the valuation of hazards these can be either be valued by using existing values or by applying valuation techniques. When the effects of overtopping are to be valued by using monetary provided by the valuation literature, examples are given in Bouma et al. (2004).

Hence, if policy makers want to assess effects (hazards) themselves in order to be site specific these values can be derived by applying valuation techniques. Selecting the appropriate valuation techniques is related of the type of effects that are to be valued. For example, damage to houses and furniture, can be defined by using market prices (market analysis). Whereas damage to ecosystems (defined as an externality) can be valued by using a Contingent Valuation Method (CVM). If no substantial externalities occur than the effects can be valued by using market prices related to the hazard. Fig. 110 provides a simple decision-rule to identify the appropriate valuation technique.

## Choice of Valuation Methods



**Figure 110: Decision tree for choosing valuation techniques**

Environmental economists tend to prefer pure survey based CV methods, but when market prices for direct and indirect damages can be obtained, mixed approaches can be more informative for decision making.

When evaluating flood alleviation schemes by means of Cost-Benefit Analysis, identifying and imputing a value on costs and benefits is an essential task. However, other crucial factors are the determination of the appropriate discount rate and the project life of the proposed flood alleviation scheme.

The outcome of the use of a valuation technique is often used to calculate present values in the context of Cost-Benefit Analyses. This implies that weights are attached to the effects of flooding in the future. Deliverable D39 provides details on selecting a discount rate and the use of discounting tables and annuities in Cost-Benefit Analysis. Two case studies, incorporated in the mentioned deliverable illustrate how the effects of overtopping can be valued. The first case of *De Haan* shows how the total damage of overtopping can be estimated by applying the technique of public pricing. By using this techniques the averting expenditures are determined. Since people would not normally spend more to prevent a problem than would be caused by the problem itself, averting expenditures can provide a

lower-bound estimate of the damage caused by pollution (Tietenberg, 2000). In the context of flooding, a vast amount of measures can be categorised as Averting Expenditures. Averting Expenditures on bringing back the natural retention capacity of a river can be mentioned e.g. creation, development and management of retention and flood control areas (Schuijt, 2001). Other examples are the construction of storage reservoirs, waterproofing of the lower floors of existing buildings, flood warning systems, levees or walls to prevent inundation from floods below some specific design flood flow, drainage and pumping facilities, diversion structures, channel modifications, construction of elevated boulevards (dikes), efforts to raise homes and the creation of individual dikes around properties.

The second case (Rapallo) illustrates the use of market prices to calculate the damage to property and the method Value of a Statistical Life to estimate the direct hazard.

### ***Summary of hazard assessment and valuation procedures***

When the optimum level of overtopping prevention is to be determined the procedure of a Cost Benefit Analysis is proposed. However, it must be stated that such a formal procedure will often not take place as the prevention of overtopping is often covered by meeting legal standards with respect to meeting the requirements on reducing the risks of flooding.

If a formal Cost Benefit Analysis is performed the following steps should be undertaken:

1. Define the project;
2. Determine the physical effects (including the prevention of hazards);
3. Choosing the discount rate;
4. Valuation of the physical effects and calculating the Net Present Value;
5. Performing a sensitivity analysis.

Clearly, before the costs and benefits of preventing overtopping can be assessed the project and its system boundaries need to be clearly defined. Questions need to be answered such as what is the project and the area for which the hazards and physical impacts are to be identified. While using a certain discount rate the present value of the costs and benefits can be calculated. The prevented hazards of overtopping are presented as benefits. The example of the Haan show that for the valuation of these damages estimates can be derived by looking

similar projects at other sites for which the costs spend by governments provide an indication (public pricing). However, each benefit item itself can also be valued separately for which an array of valuation techniques are available.

## **Conclusions**

Guidance on permissible wave overtopping has been refined based on new prototype measurements and laboratory modelling.

From the socio-economic point of view, methods to value hazards have been presented.

This workpackage delivered the following reports :

- the report on hazard analysis (D38)
- the report on socio-economic impacts (D39)

Additionally one milestone was achieved :

- the hazard analysis (including socio-economic impacts) workpackage is completed (M11).

## 7 WP 7 : Conclusions on scale effects and new data

### 7.1 Objectives

The main objective of WP 7 is to compare full and large scale measurements on overtopping with simulation by laboratory scale model tests and numerical modelling and to come to a conclusion on suspected scale effects. This conclusion is essential for WP8, where the database will be used to develop a generic prediction tool.

### 7.2 Description of work performed

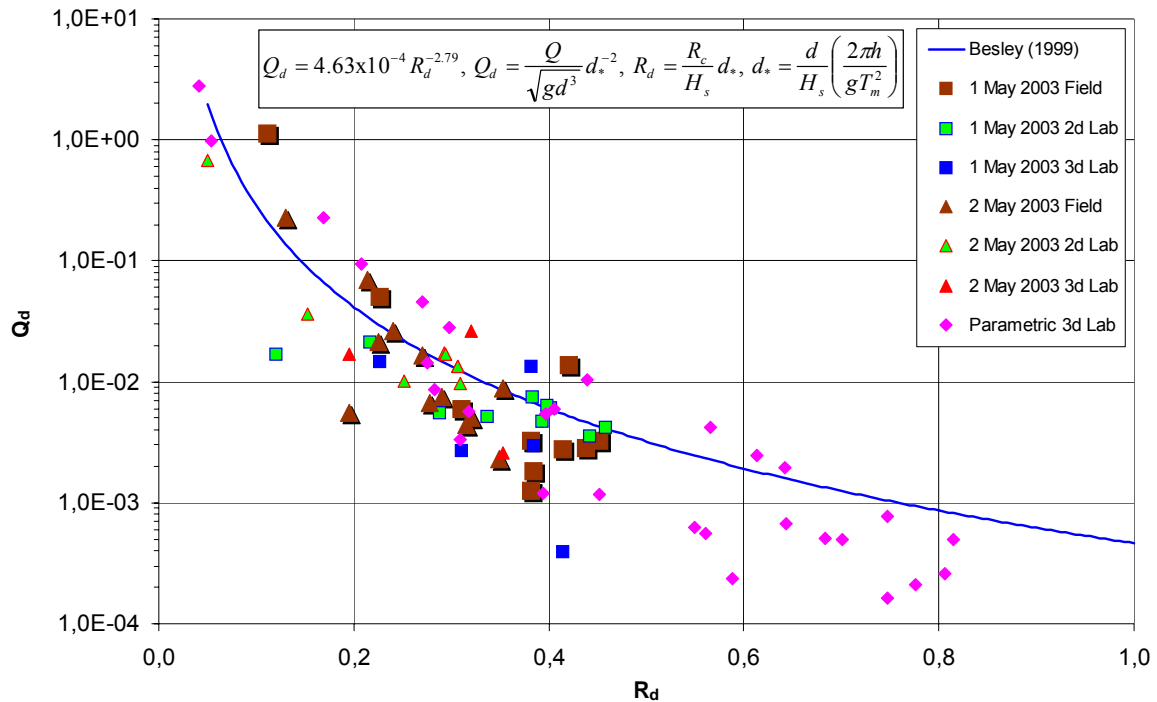
The work in WP 7 comprises a number of steps which has finally led to a conclusion on scale effects for the structures investigated within CLASH. The background research and the aforementioned procedure is described in this section.

#### 7.2.1 *Samphire Hoe vertical wall*

Videos have been recorded from the field and the model tests which show very similar behaviour in the water mass being thrown up at the vertical wall. The significant difference seems to be the wind blowing much of the spray beyond the overtopping container.

In Fig. 111 the overtopping results from the prototype as well as the model tests at UEDIN (2D) and HRW (3D) are plotted together with the overtopping rate against the freeboard  $R_d$ . The Besley formula (1999) is also plotted. It should be noted that the 1 May storm data with strong wind effects have been multiplied by a factor of 3.0 to account for the spray blown beyond the overtopping containers.





**Figure 111: Prototype results, 2D and 3D test results with comparison to Besley formula**

The results in Fig.111 show a relative good agreement between the Besley curve, most of the data points and the prototype storms. No major differences between field and model data can be observed suggesting that there are only few model (except wind effect) and scale effects.

### 7.2.2 Zeebrugge rubble mound breakwater

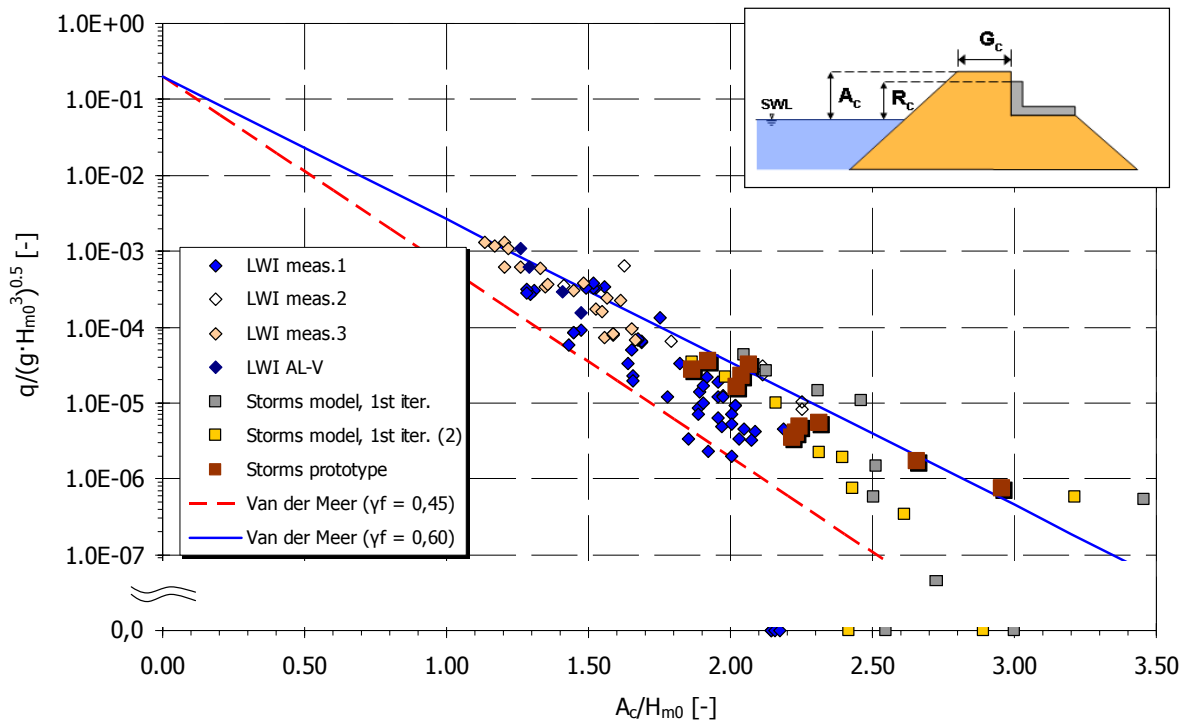
In Fig. 112 all overtopping results at LWI and the prototype results are plotted together as relative mean overtopping rate against the relative freeboard  $A_c/H_{m0}$ . The Van der Meer formula for non-breaking waves, Van der Meer (1998), for a roughness factor of  $\gamma_r = 0.60$  and  $\gamma_r = 0.45$  were also plotted.

The results in Fig. 112 show a relative good agreement between the curves, most of the data points and the prototype storms. However, there is some reasonable scatter in the data and three observations which are of particular importance:

- for higher relative crest freeboard  $A_c/H_{m0} > 1,7$  the parametric tests seem to be slightly lower than the prototype storms. This is supported by some of the data points which are even zero for  $A_c/H_{m0} > 2,0$
- storm reproductions at UPVLC have shown that only one of the three storm events could be reproduced without wind. The other two reproductions had zero overtopping.

- higher wind speeds in the flume gave considerably higher wave overtopping rates. This cannot be seen from Fig. 112 but has been reported by Kortenhaus et al. (2004b) and González-Escrivá et al. (2004)

Details of differences and reasons for the scatter of the data points are explained in Kortenhaus et al. (2004a)

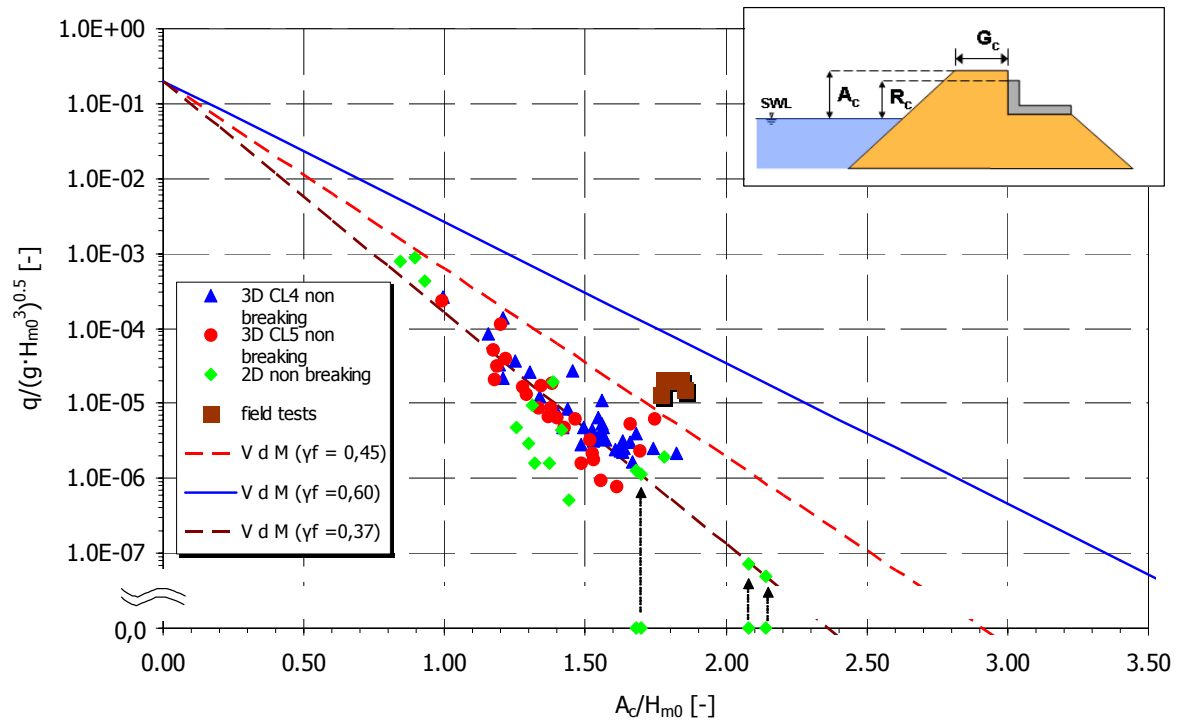


**Figure 112: Relative mean overtopping rates from LWI tests plotted against the relative freeboard with comparison to Van der Meer formula and prototype results**

### 7.2.3 Ostia rock breakwater

For the Ostia breakwater the comparison of videos from field and model is shows that more overtopping occurs in the field rather than in the model. It seems that similar waves cause different behaviour on the slope of the breakwater.

In Fig. 113 all overtopping results at FCFH (3D) and UGent (2D) as well as the prototype results are plotted together as relative mean overtopping rate against the relative freeboard  $A_c/H_{m0}$  (for the Ostia breakwater  $R_c = A_c$ ). The Van der Meer formula for non-breaking waves and a roughness factor of  $\gamma_f = 0.60$ ,  $\gamma_f = 0.45$  and  $\gamma_f = 0.37$  were also plotted.



**Figure 113: Relative mean overtopping discharges from FCFH (3D) and UGent (2D) tests plotted against the relative freeboard with comparison to Van der Meer formula and prototype results<sup>1</sup>**

All results in Fig.113 show a relative good agreement between most of the laboratory data points although some scatter can be observed due to variation of some model parameters and influence of wave period. The prototype storm results are higher than the model results (up to a factor of 10).

There are four data points in Fig.113 where the relative mean overtopping rate is zero. No overtopping occurred during the model tests for these data points. It can be assumed, that in the field overtopping could emerge for these ratios  $A_c/H_{m0}$  since the measurement accuracy in the flume is not high enough for these small overtopping volumes. In order to calculate prototype values from these data points and account for scale effects, a mean overtopping rate greater than zero has to be determined. Using the Van der Meer formula and a roughness factor of  $\gamma_f = 0.37$  (i.e. best fit through all data), all data points of the model tests can be represented as shown in Fig. 113. By means of this curve it is possible to achieve relative mean overtopping discharges for the data points with no overtopping. The arrows in Fig. 113 indicate this procedure.

<sup>1</sup> Note: almost all data points above a relative crest freeboard of  $A_c/H_{m0} > 1.6$  during the model tests were zero whereas prototype data still resulted in overtopping rates

#### 7.2.4 *Method to account for scale effects*

A number of possible reasons for differences between prototype and model scale has been listed in Kortenhaus et al. (2005) (Deliverable D40). It has been shown that all measurement uncertainties and model effects may have a considerable effect on wave overtopping so that most data points fall within the differences of one standard deviation of the result. Therefore, scale effects are very difficult to observe since differences in the resulting plots may be all due to model effects only.

##### a) Requirements for scale effects

The theoretical investigations and review of the available literature in Deliverable D40 has shown that differences in wave run-up heights for rough slopes (both permeable and impermeable) have been observed in many cases. Therefore, the wave run-up height should be included in any guidance on how to scale wave overtopping. The following requirements may be derived from the literature and observations in the model and prototype tests:

- scaling effects have only been observed for sloped structures but not for vertical ones;
- the scaling factor must be higher for lower overtopping rates; it even has to work for ‘no overtopping’ measurements in the flume, knowing that for the same conditions some overtopping is measured in prototype;
- roughness of the slope has to be included; critical Reynolds numbers can be defined;
- the core permeability needs to be included where lower permeability in the core creates more run-up on the slope and more overtopping
- wind effects should be included since wind increases wave overtopping rates considerably;

##### b) Factor resulting from scale effects on wave run-up

The second and third requirement may be fulfilled by a simple approach. Schulz (1992) and others have indicated that the increase of run-up heights from small-scale to large-scale models are in the range of 15%. If this is introduced as an additional ‘roughness’ factor (to be

treated in the same way as a traditional roughness factor) to a standard wave overtopping formula it gives:

$$\frac{q_{\text{red}}}{\sqrt{g \cdot H_{m0}^3}} = q_0 \cdot \exp\left(b \frac{R_c}{H_{m0}} \cdot \frac{1}{\gamma_f} \cdot \frac{1}{\gamma_s}\right) \quad (4)$$

where  $\gamma_s$  is the scaling reduction due to scale effects on the seaward slope ( $\gamma_s = 1,15$  here). Eq. (4) differs from the standard wave overtopping formula by a factor  $1/\gamma_s$  only so that  $q_{\text{red}}$  can be calculated as  $q_{\text{red}} = q(1/\gamma_s)$ . The relative scaling factor  $f_{s,q} = q_{\text{red}}/q$  can then be calculated as:

$$f_{s,q} = \frac{q_{\text{red}}}{q} = \frac{q^{1/\gamma_s}}{q} \quad (5)$$

where  $q_{\text{red}}$  is the theoretically reduced overtopping rate as given by Eq. (4). In Fig.114 the factor given by Eq. (5) is plotted against the wave overtopping discharge using the Zeebrugge parametric tests at LWI from the first test phase. The latter have been scaled up to prototype conditions using Froude law. Each data point is then achieved by performing the following steps:

- derive  $q$  for specified tests from measurements;
- scale  $q$  up to prototype using Froude law (if  $q$  is from model tests);
- calculate the reduced overtopping rate using Eq. (4);
- calculate  $f_{s,q}$  for each data point using Eq. (5)

Furthermore, an additional formula for a factor  $f_{\text{scale\_nowind}}$  has been plotted which shows a similar behaviour than Eq. (5) but is closer to the data. This curve can be described by the following equation:

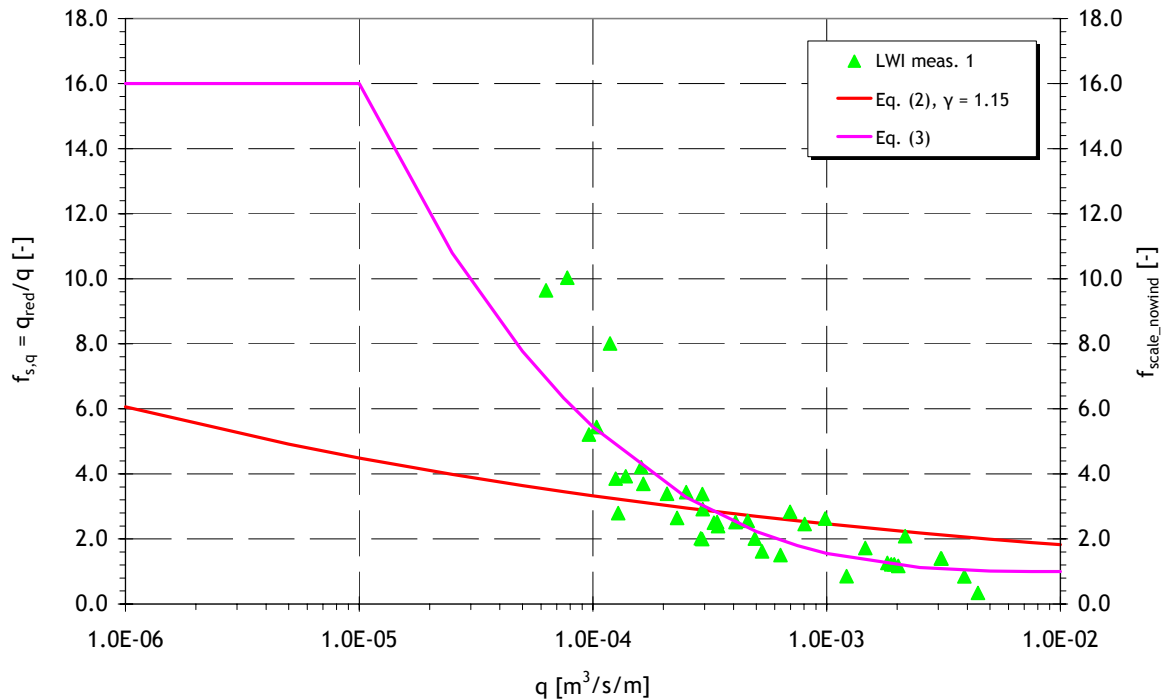
$$f_{\text{scale\_nowind}} = \begin{cases} f_{\text{scale\_nw}} & \text{for } \gamma_f \leq 0.7 \\ 5 \cdot (1 - f_{\text{scale\_nw}}) \cdot \gamma_f + (f_{\text{scale\_nw}} - 1) \cdot 4.5 + 1 & \text{for } 0.7 < \gamma_f < 0.9 \end{cases} \quad (6a)$$

where

$$f_{\text{scale\_nw}} = \begin{cases} 16.0 & \text{for } q_{\text{SS}} < 1 \cdot 10^{-5} \text{ m}^3 / \text{s} \cdot \text{m} \\ 1.0 + 15 \cdot \left( \frac{-\log q_{\text{SS}} - 2}{3} \right)^3 & \text{for } q_{\text{SS}} < 1 \cdot 10^{-2} \text{ m}^3 / \text{s} \cdot \text{m} \\ 1.0 & \text{for } q_{\text{SS}} \geq 1 \cdot 10^{-2} \text{ m}^3 / \text{s} \cdot \text{m} \end{cases} \quad (6b)$$

It should be noted that  $q_{SS}$  is a value based on small scale measurements, but already scaled up to prototype scale by means of Froude scaling law.

Eq. (6a) delivers a scaling factor for really rough structures when  $\gamma_f \leq 0.7$ . When  $\gamma_f \geq 0.9$  the structure is smooth and the scaling factor will be  $f_{scale\_nw} = 1.0$ . In between both values a linear interpolation can be assumed.



**Figure 114: Reduction of wave overtopping due to reduction of wave run-up on the seaward slope for the Zeebrugge storm data**

It can be seen from Fig.114 that factors may easily go up to one order of magnitude for lower overtopping rates whereas they are still in the same range as without run-up reduction for higher overtopping rates. Since data from comparison between small-scale and large-scale model do not support regions of overtopping ratios lower than  $1 \cdot 10^{-5} \text{ m}^3/\text{s}\cdot\text{m}$  the formula will not go up to higher values than a factor of 16.0.

Eq. (5) is determined for a scaling factor which is only valid for rough slopes and no wind effects. The latter can be assumed since comparisons between large-scale and small-scale tests are always referring to tests in either the GWK in Hannover or the Delta flume in De Voorst which both do not include any wind.

Therefore, a method needs to be found which summarises the various influences of scale and wind effects. This method will be discussed in the subsequent section. Since the magnitude of

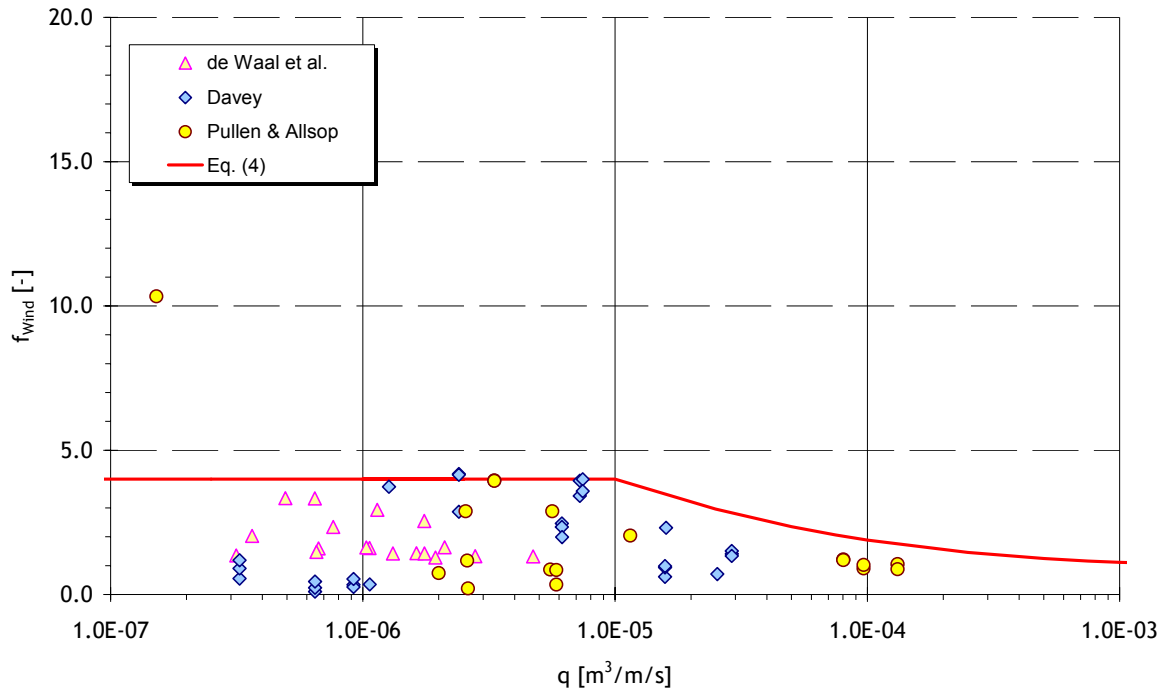
the influence of scaling the core material is not known up to date this influence will be ignored in the following.

c) Factor resulting from wind effect on vertical structures

It is possible to examine the results of de De Waal et al. (1996), Davey (2004) and Pullen & Allsop (2004) (D36), as described in D40. By examining the data it is possible to ascribe the following formula to the transport factor  $f_{\text{wind}}$  (Fig.115):

$$f_{\text{wind}} = \begin{cases} 4.0 & \text{for } q_{\text{SS}} < 1 \cdot 10^{-5} \text{ m}^3 / \text{s} \cdot \text{m} \\ 1.0 + 3 \cdot \left( \frac{-\log q_{\text{SS}} - 2}{3} \right)^3 & \text{for } q_{\text{SS}} < 1 \cdot 10^{-2} \text{ m}^3 / \text{s} \cdot \text{m} \\ 1.0 & \text{for } q_{\text{SS}} \geq 1 \cdot 10^{-2} \text{ m}^3 / \text{s} \cdot \text{m} \end{cases} \quad (7)$$

In this instance the factor 4.0 is not a scaling factor as previously described, but it can be used to make an allowance for the effects of the wind, and also has the advantage of not using a separate technique. It is especially important to make this distinction, because it has been demonstrated in D36, that there are no scaling effects for vertical and composite vertical structures. Fig.114 shows that a factor of 4.0 provides a conservative estimate of the effect of the overtopping discharge  $q$ .



**Figure 115: Discharge rates and the effect of the transport factor  $f_{wind}$ .**

d) Overall procedure

*Input*

The final CLASH-procedure to determine the overtopping discharge, taking into account scale effects starts with a mean overtopping rate predicted by small-scale model tests  $q_{SS}$

Besides the  $q_{SS}$  the following parameters are required:

- wave height  $H_{m0}$  at the toe of the structure (output scale<sup>2</sup>),
- roughness coefficient  $\gamma_f$  for the seaward side of the structure,
- width of the seaward berm  $B$  of the structure,
- water depth over the horizontal berm  $d_h$ ,
- slope of the structure below the berm  $\cot\alpha_d$ ,
- slope of the structure above the berm  $\cot\alpha_u$

For a more detailed description of these parameters see Verhaeghe et al. (2003). The wave height  $H_{m0}$  is needed to distinguish between model scale, full-scale or any other scale in between. The roughness coefficient  $\gamma_f$  is needed to distinguish between a smooth and a rough

<sup>2</sup> output scale' means that  $H_{m0}$  needs to be given in the scale where the final result with respect to wave overtopping rates are needed



structure whereas all other parameters are needed to select vertical structures or sloped structures.

### *Output*

There are three possible outputs of the procedure which are:

- mean overtopping rate with possible **wind effect**  $q_{wind}$ : wind may play a role for all vertical structures and all smooth (sloping) structures which are believed to have no scale effects
- mean overtopping rate with possible **scale and wind effects on rough structures**  $q_{scale\_wind}$ : this output will only be relevant for rough structures and includes both possible scale and wind effects.
- mean overtopping rate with **scale effects on rough structures without wind**  $q_{scale\_nowind}$ : this output will only be relevant for rough structures and includes only scale effects. The main interest of this third output is to predict wave overtopping rates for large-scale tests without wind.

The prediction method gives all these four mean overtopping discharges  $q_{SS}$ ,  $q_{wind}$ ,  $q_{scale\_wind}$  and  $q_{scale\_nowind}$ . Differences between these values may give the user a good idea what kind of effect could play a role in his given situation.

### *Step 1: vertical structure?*

Step 1 checks whether the structure is vertical or not (Fig. 116). If the structure is vertical or almost vertical continue with ‘Step 4: Procedure wind effect’. If this is not the case go to ‘Step 2: rough structure?’.

*Note:* To help distinguishing between vertical and non-vertical structures there are two configurations using the input parameters of the CLASH database which indicate a vertical structure. These are:

- if  $\cot \alpha_u < 1$  and  $\cot \alpha_d < 1$  the structure is vertical or almost vertical.
- if  $\cot \alpha_u < 1$  and  $B > 0$  and  $d_h > 0$  there is most probably a berm below swl and a vertical structure on top of the berm.

Please note that this parameter distinction cannot be used when parapets are used with the structure. Furthermore, for some complex structures the simple distinction proposed here may fail to give the correct answer.

### Step 2: rough structure?

Step 2 checks whether the structure is rough or smooth. If the structure is rough, continue with Step 3: rough sloping structure, if the structure is smooth continue with ‘Step 4: Procedure wind effect’.

*Note:* The roughness of a structure may be distinguished from the roughness coefficient  $\gamma_f$  of the CLASH database. If  $\gamma_f$  is smaller than 0.9 the structure is considered to be a rough sloping structure otherwise the structure is smooth.

### Step 3: rough sloping structure

Within this step the first decision to be made is whether to consider the influence of wind or not. If yes, the factor for scale and wind effects  $f_{\text{scale\_wind\_max}}$  can be calculated as follows:

$$f_{\text{scale\_wind\_max}} = \begin{cases} 24.0 & \text{for } q_{\text{SS}} < 1 \cdot 10^{-5} \text{ m}^3 / \text{s} \cdot \text{m} \\ 1.0 + 23 \cdot \left( \frac{-\log q_{\text{SS}} - 2}{3} \right)^3 & \text{for } q_{\text{SS}} < 1 \cdot 10^{-2} \text{ m}^3 / \text{s} \cdot \text{m} \\ 1.0 & \text{for } q_{\text{SS}} \geq 1 \cdot 10^{-2} \text{ m}^3 / \text{s} \cdot \text{m} \end{cases} \quad (8)$$

It should be noted that this factor includes both the influence of scale and wind effects, the latter being a model rather than a scale effect. Furthermore, Eq. (6) suggested a maximum factor of 16.0 for scale effects without any wind. Assuming that factors for scale and wind effects should be multiplied to achieve an overall factor, a theoretical factor for wind of 1.5 would be obtained. This is lower than indicated in Eq. (7) for vertical walls, which is believed to be due to the effect of wind for vertical structures being larger than for rough sloping structures.

Eq. (8) delivers a scaling factor for really rough structures when  $\gamma_f \leq 0.7$ . When  $\gamma_f \geq 0.9$  the structure is smooth and the scaling factor will be  $f_{\text{scale}} = 1.0$ . In between both values a linear interpolation can be assumed so that the scaling factor for rough slopes  $f_{\text{scale\_wind}}$  can be determined by:

$$f_{\text{scale\_wind}} = \begin{cases} f_{\text{scale\_wind\_max}} & \text{for } \gamma_f \leq 0.7 \\ 5 \cdot (1 - f_{\text{scale\_wind\_max}}) \cdot \gamma_f + (f_{\text{scale\_wind\_max}} - 1) \cdot 4.5 + 1 & \text{for } 0.7 < \gamma_f < 0.9 \end{cases} \quad (9)$$

If there is no wind it needs to be decided under which scale the procedure is applied. Therefore, a distinction will be made with respect to the wave height  $H_{m0}$ . For wave heights at output scale  $H_{m0} < 0.5$  m the factor for scaling is  $f_{\text{scale}} = 1.0$ . For all other cases the calculation of  $f_{\text{scale\_nowind}}$  can be performed using Eq. (6). Go to Step 5: Final calculation of mean wave overtopping rate to finalise the procedure.

#### *Step 4: Procedure wind effect*

For structures other than rough structures there might be a wind effect. First a decision has to be made whether wind effects are to be considered or not. If not, the factor for the wind-influence is set to  $f_{\text{wind}} = 1$ . If wind effects have to be considered, they can be calculated using Eq. (7).

Finally the factor for wind effects can be applied to the overtopping rate  $q_{\text{SS}}$  which is performed in “Step 5: Final calculation of mean wave overtopping rate”.

#### *Step 5: Final calculation of mean wave overtopping rate*

The final calculation of mean wave overtopping rates should include both a calculation for wind effects and smooth structures and a calculation for scale and wind effects and rough structures as follows:

$$q_{\text{wind}} = q_{\text{SS}} \cdot f_{\text{wind}} \quad (f_{\text{wind}} \text{ (eq. (7))}) \quad (10)$$

$$q_{\text{scale\_wind}} = q_{\text{SS}} \cdot f_{\text{scale\_wind}} \quad (f_{\text{scale\_wind}} \text{ (eq. 8-9)}) \quad (11)$$

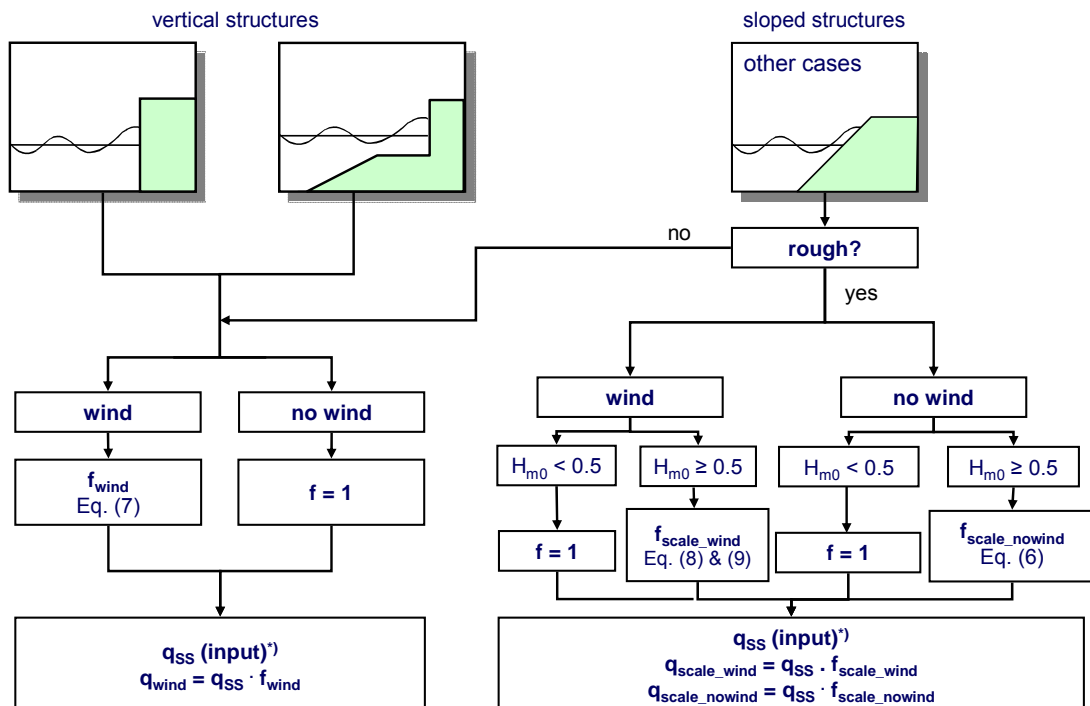
$$q_{\text{scale\_nowind}} = q_{\text{SS}} \cdot f_{\text{scale\_nowind}} \quad (f_{\text{scale\_nowind}} \text{ (eq. (6))}) \quad (12)$$

#### *Step 6: Scaling map for coastal structures*

The procedure described above is summarised in a simple scaling map for wave overtopping over coastal structures obtained from small-scale model tests (Fig.116). This map is only needed when

- wave heights  $H_{m0}$  for the structure the user is interested in are higher than 0.5 m;
- the user starts from model scale with wave heights  $H_{m0} < 0.5$  m

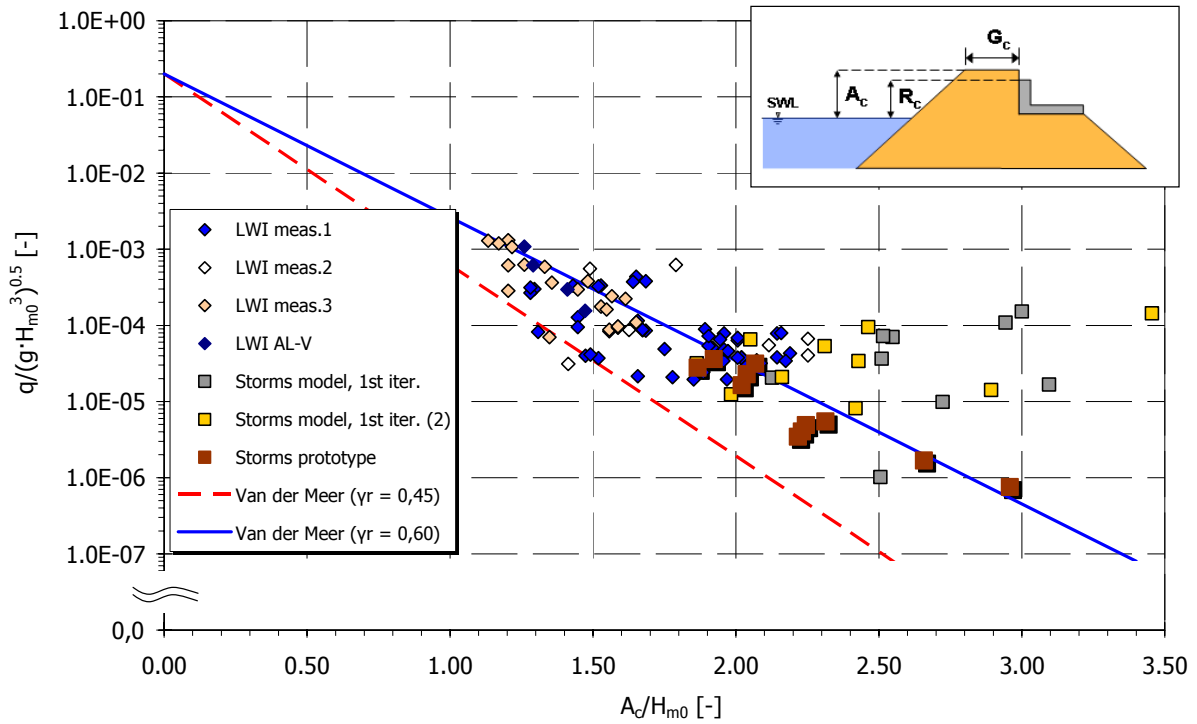
Furthermore, the distinction between vertical and sloped structures as given by the parameters as given in the ‘input’ to the overall procedure are only valid for structures which do not have parapets or overhanging elements.



**Figure 116: Scaling map for wave overtopping results over coastal structures from small-scale model tests**

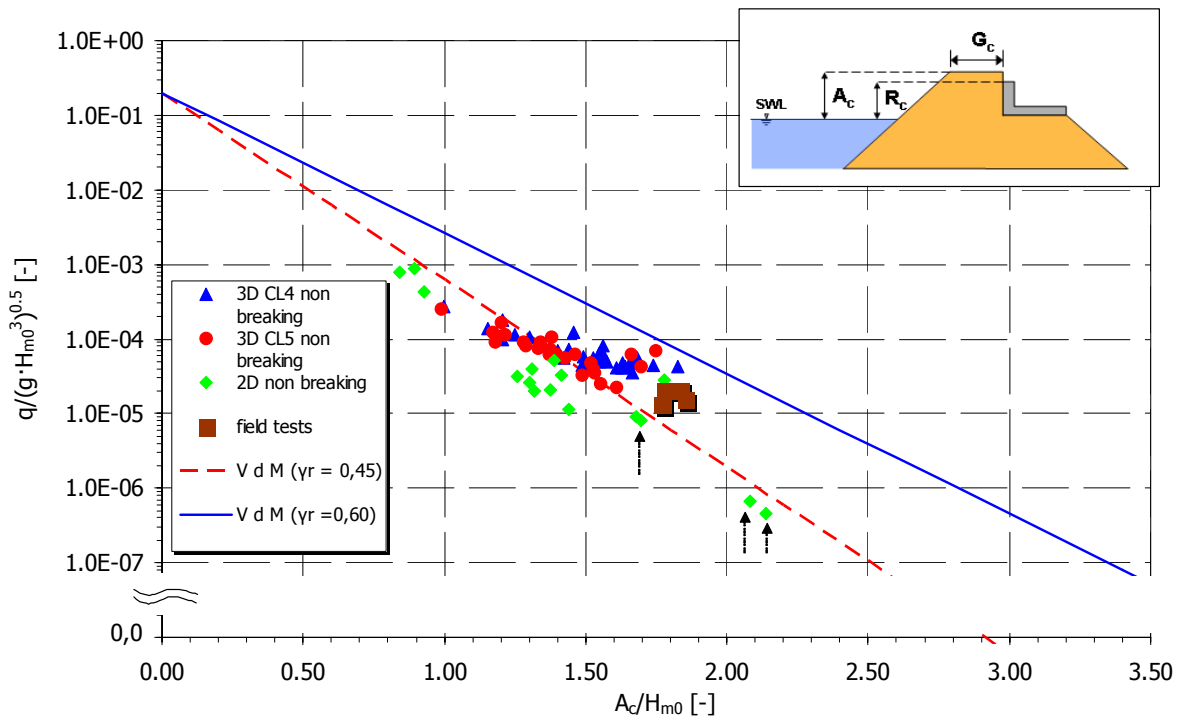
e) Application of procedure to data from Zeebrugge and Ostia

The aforementioned final procedure to account for scale effects (Fig. 116) has been applied to data from hydraulic model tests for the Zeebrugge and Ostia case. First, the Zeebrugge test case (Fig. 112) has been used. The results are shown in Fig. 117. It can be seen that compared to the results in Fig. 112 that the increase in wave overtopping rates for the parametric tests such as ‘LWI meas. 1’ and ‘LWI meas. 2’ lead to a better comparison of scale model and prototype data. In general, there is a significant increase of the mean overtopping rate mainly for relative crest freeboards  $A_c/H_{m0} \geq 1.7$  where the overtopping rates are up to 24 times higher. Especially the reproductions of storm data during the second phase of the LWI tests are now much higher than the prototype storm data. However, this second phase data have been produced with a different model construction and possibly with a different armour layer setup. This has been shown to have significant influence on the overtopping rates and it is therefore very difficult to compare the different phases of the Zeebrugge tests directly.



**Figure 117: Results of the application of the parameter map for scaling to the test case of Zeebrugge**

In a second step the method was also applied to the data of the Ostia case as shown in Fig. 113. The results of the modifications obtained are given in Fig. 118.



**Figure 118: Results of the application of the parameter map for scaling to the test case of Ostia**

The four data points indicated by the arrows in Fig. 118 correlate to the ones mentioned in before, where the zero value for the mean overtopping rates of four data points was substituted by mean overtopping rates using the Van der Meer formula. The model and prototype data show a much better agreement in Fig. 118 than in Fig. 113 before where especially for the lower overtopping rates a higher increase of all model tests was achieved. In Fig. 118, a roughness factor  $\gamma_r = 0.45$  fits well to the data, whereas before the application of the scaling procedure this was  $\gamma_r = 0.37$ . Comparing the application for Zeebrugge and Ostia it seems that the developed method gives acceptable results for the cases investigated here.

## Conclusions

Results for all field and model investigations have been plotted for the investigated sites using data from the field and two models of smaller scale. Results have shown that model tests performed for the vertical wall in Samphire Hoe do not deviate much from the prototype data points. However, for the steep Zeebrugge rubble mound breakwater and for the flatter slope in Ostia differences between prototype and model have been observed in the order of up to one order of magnitude.

A new parameter map for scaling was proposed for scaling wave overtopping rates obtained from small-scale model tests with wave heights smaller than 0.5 m. The map depends on whether or not the structure is ‘rough and sloping’ and eventually suggests a scaling predictor. The latter was then applied to the test cases of Zeebrugge and Ostia.

This workpackage delivered the following reports / deliverables:

- the completed dataset, including full scale measurements and full scale data (D28)
- a final report (D40), containing a conclusion on scale effects and how to deal with them

Additionally one milestone was achieved:

- the formulation of the conclusion on scale effects (M12)

---

## 8 WP 8 : Prediction method

### 8.1 Objectives

The objective of this workpackage is to develop a generic prediction method for overtopping discharges at major types of coastal structures. This prediction method is based on the final wave overtopping database. The prediction method that was developed and described is based on the technique of Neural Network modelling. Moreover, a method was developed to obtain the confidence intervals around these predictions. The latter is a new essential step since neural network modelling results in a tool that acts for users as a kind of black box. Therefore, predictions are extended with information regarding their reliability.

### 8.2 Description of work performed

For the design, safety assessment and rehabilitation of coastal structures reliable predictions of wave overtopping are required. Several design formulae exist for dikes, rubble mound breakwaters and vertical breakwaters. Nevertheless, often no suitable prediction methods are available for structures with non-standard shapes. The overtopping highly non linear dependency of many wave and structural characteristics makes the problem difficult to solve. Within CLASH, a method is developed to provide a conceptual-design tool to estimate wave overtopping discharges for a wide range of coastal structures. Only one schematisation is used for all types of coastal structures, where not only dikes, rubble mound breakwaters or vertical breakwaters are defined, but also other non-standard structures are included. Additionally, not only is the effect of the most common parameters (i.e. wave height, wave period and crest freeboard) analysed herein, but also the effect of many other wave/structural characteristics is considered. The prediction method described is based on the technique of Neural Network modelling. For this purpose use is made of a data set obtained from a large number of physical model tests. Most of these data were provided by the partners of the CLASH project. The present investigation focuses on the development of a neural network for estimating mean overtopping discharges. Also the confidence intervals around these predictions are determined. It is important that predictions are extended with information regarding their reliability. The main activities under this workpackage are described in Deliverable D41 (Pozueta et al, 2004). Hereafter information is combined into a summary of activities in the entire workpackage.

### *Description of database*

The database used for the set up of the present neural network (hereafter “NN”), is the database created within the framework of the European project CLASH. This database includes tests collected from several laboratories and new tests performed within the CLASH project to fill in “white spots” in the parameter domain. This database is described in detail in WP2 of this report.

About 10,000 tests are included in this database. Each of these tests is described by a number of parameters that represent hydraulic information (incident wave characteristics, measured overtopping discharge) and structural information (characteristics of the test section). Moreover, each of the tests includes some general information regarding the estimated reliability of the test and the complexity of the structure. The **reliability** of each test was estimated and defined in terms of a *Reliability Factor (RF)*. The values of the *RF* ranged from  $RF = 1$ , for a ‘very reliable’ test (i.e. test for which all needed information was available, no estimations needed, reliable measurements), to  $RF = 4$ , for a ‘not-reliable’ test (i.e. test for which the estimation of some parameters was not acceptable and for which the measurements included many uncertainties). In the same way, the **complexity** of each test was established on the basis of the complexity of the structure and was defined in terms of a *Complexity Factor (CF)*. The values of the *CF* ranged from  $CF = 1$ , for a test with a ‘very simple’ structure (i.e. test for which the parameters describe the cross-section exactly), to  $CF = 4$ , for a test with a ‘very complex’ structure (i.e. test for which the cross-section cannot accurately be described by the chosen parameters).

These *Reliability* and *Complexity Factors* played an important role in the configuration of the NN. With the purpose of giving more weight to tests with high reliability in the NN configuration, the *RF* and the *CF* were combined into a kind of *Weight Factor*. This *WF* was defined as a combination of the *RF* and *CF* according to  $WF = (4-RF) \cdot (4-CF)$ . This *Weight Factor* was defined for each of the tests and was taken into account in the *training (calibration)* of the NN.

Since the quality of the NN depends highly on the quality of the database (erroneous data can severely degrade the performance of the NN), the initial database of more than 10,000 tests



was reduced by removing the data that was qualified as ‘non-reliable’ tests (e.g. tests with a ‘reliability factor’  $RF = 4$ , as defined previously) or the data for which the cross-section was considered as ‘very complex’ (e.g. tests with a ‘complexity factor’  $CF = 4$ , as defined previously). All remaining tests related to registered overtopping events were considered (i.e. all tests such that  $q \neq 0 \text{ m}^3/\text{s}/\text{m}$ ). Some data corresponding to overtopping events such that  $q > 10^{-6} \text{ m}^3/\text{s}/\text{m}$  were rather randomly checked and clear inconsistencies within the database were eliminated. The resulting database consisted of 8,372 tests.

Since most of the tests in the database originate from small-scale tests, very low overtopping discharges are likely to be less accurate due to measurement techniques/errors in these small-scale tests. Relatedly, it should be noted that for the NN configuration, all the tests with observed overtopping discharges  $q < 10^{-6} \text{ m}^3/\text{s}/\text{m}$  (i.e. 1 ml/s/m), were considered as less accurate than larger overtopping discharges, and were given a weight factor  $WF = 1$  (i.e.  $RF = CF = 3$ ).

#### *Parameters involved*

Due to the large number of parameters involved in the process of wave overtopping, it is difficult to describe the influence of all of them. The technique of NN modelling allows for the analysis of wave overtopping with a larger amount of structure characteristics.

For the description of the wave field, the effects of 3 parameters were considered here: the spectral significant wave height at the toe of the structure ( $H_{m0}$ ), the mean spectral wave period at the toe of the structure ( $T_{m-1,0}$ ), and the direction of wave attack ( $\beta$ ). For the description of the geometrical shape of the structure, the effects of 12 parameters were considered: the water depth in front of the structure ( $h$ ), the water depth at the toe of the structure ( $h_t$ ), the width of the toe berm ( $B_t$ ), the roughness/permeability of the armour layer ( $\gamma_f$ ), the slope of the structure downward of the berm ( $\cot \alpha_d$ ), the slope of the structure upward of the berm ( $\cot \alpha_u$ ), the width of the berm ( $B$ ), the water depth on the berm ( $h_b$ ), the slope of the berm ( $\tan \alpha_b$ ), the crest freeboard of the structure ( $R_c$ ), the armour crest freeboard of the structure ( $A_c$ ) and the crest width of the structure ( $G_c$ ).

### *Neural network modelling*

Neural networks (NN) are data analyses or modelling techniques commonly used in artificial intelligence. NN are often used as generalised regression techniques for the modelling of cause-effect relations and have proven to be very effective in solving difficult optimization problems in a variety of technical and scientific fields. They are an alternative technique for processes in which the interrelationship of parameters is unclear while sufficient experimental data is available. This technique has been successfully used in the past. Examples of NN modelling on coastal structures are: Mase *et al.* (1995); Van Gent and Van den Boogaard (1998); Medina *et al.* (1999, 2002, 2003); and Panizzo *et al.* (2003). Here, NN are used for prediction of mean wave overtopping discharges and makes use of a much larger data set than in the other NN studies. Details regarding the NN constructed on the basis of the database are described in Pozueta *et al.* (2004).

NN are organised in the form of layers and within each layer there are one or more processing elements called 'neurons'. A standard multi-layer feed-forward NN consists of several units connected in one direction only. The first layer is called the input layer and consists of a number of neurons equal to the number of input parameters. The last layer is called the output layer and consists of a number of neurons equal to the number of output parameters to be predicted. The layers between the input and output layers are called hidden layers and consist of a number of neurons to be defined in the preparation of the NN. Each neuron in each layer receives information from the preceding layer through connectivities. A weight factor is assigned to each connectivity as a result of the training of the NN. The input of a neuron consists of a weighted sum of the outputs of the preceding layer; for the current investigation, the output of a neuron is generated using a non-linear activation function for the hidden layers and a linear activation function for the output layer (Haykin, 1994). This procedure is followed for each neuron. The output neuron generates the final prediction of the NN.

A number of NN techniques have been used during the past decade to solve a variety of hydraulic engineering problems. The most popular technique is the use of static feedforward NN models with one hidden layer and a backpropagation learning algorithm (Rumelhart & McClelland, 1986). In the present study a three-layered NN (one hidden layer) is applied as

well. The learning rule used herein is called the *standard error back-propagation rule* and it is the most common learning rule for this type of network.

Since it was the aim of the NN to be applicable both for small-scale and prototype conditions, all the input and output parameters in the database were scaled to  $H_{m0,toe} = 1$  m using Froude's similarity law. The advantage of using Froude's law, taking into account that the database was mainly based on small-scale tests, is that a better generalisation for large-scale applications can be obtained. Since physical knowledge was then incorporated in the NN, this procedure allowed for predictions at different scales. This approach required somehow a less complex configuration of the NN, since the number of input-patterns used reduced from 15 to 14 (once all input-patterns were scaled to  $H_{m0,toe} = 1$  m, this parameter,  $H_{m0}'$ , is constant and was not used anymore as a separate input pattern to the NN).

For user applications, when a prediction of the wave overtopping discharge is required for a certain input-pattern [ $H_{m0}$ ,  $T_{m-1,0}$ ,  $\beta$ ,  $h$ ,  $h_t$ ,  $B_t$ ,  $\gamma_f$ ,  $\cot \alpha_d$ ,  $\cot \alpha_u$ ,  $B$ ,  $h_b$ ,  $\tan \alpha_b$ ,  $R_c$ ,  $A_c$ ,  $G_c$ ] this input-pattern is scaled according to Froude's similarity law to an input-pattern with a wave height on which the NN was trained ( $H_{m0,toe} = 1$  m). The NN prediction ( $q'$ ) is then scaled back ( $q$ ) to the original wave height using again Froude's law.

In the NN-modelling Froude's scaling law was used to extrapolate the information from small-scale tests to prototype conditions. However, the small-scale tests may, to some extent, be affected by scale effects. However, there is no clear quantitative evidence on the magnitude of scale effects for each test condition (type of structure, wave conditions, etc). Nevertheless, in Workpackage 7 suggestions are given to estimate the (combined) magnitude of model, scale and wind effects. The NN predictions do not incorporate the influence of model, scale and wind effects but, as described later in this chapter, the NN output can be corrected by using estimates of model, scale and wind effects.

### *Training and testing of NN*

The preparation of the NN model was performed in two phases, the *training/learning* phase and the *testing/validation* phase.

The process of calibration or *training* phase of the NN involves the adjustment of its configuration (calibration of the NN's weights) based on the performance of standard operations that allows the NN to *learn* from the input-output relations for each of the parameters included in the tests selected as *training set*. The iterative adjustment of the NN's weights or *training* of the NN is performed by minimisation of some *cost function* (error function) that quantifies the differences between the predicted outputs and the desired measured/observed outputs, often called *targets*. A common form of the *cost function* is a superposition of the squared differences. For the minimisation of the *cost function*, gradient based methods turned out to be the most efficient. For the computation of the gradient of the cost function, the well known error-backpropagation rule was used. It should be noted that the training of the NN was performed considering the logarithm of the observed overtopping discharges scaled with Froude's law ( $\log q_{obs}$ ) as the targets. The root-mean-square (RMS) error used herein is defined as follows:

$$RMS_{train} = \sqrt{\frac{1}{N_{train}} \sum_{n=1}^{N_{train}} ((\log q_{obs})_n - (\log q_{NN})_n)^2} \quad (13)$$

where  $N_{train}$  is the number of tests considered in the NN training.

Once trained (or during training), the correct performance of the resulting model is evaluated with a *testing set*, i.e. a set of input-output combinations not used before for training. This step is called *validation* or *testing* phase of the NN.

It should be noted, that the actual partition of the data over the training and testing sets may significantly affect the outcome of the NN. Therefore, special attention must be given to this aspect. The present strategy was to train many NN's each time with different data in the training and testing phase. *Resampling Techniques* (Van den Boogaard *et al.*, 2000) were used for the construction of such training and testing sets.

#### *Optimum number of neurons in the hidden layer*

An important step in the configuration of the NN is to find the optimal number of neurons in the hidden layer. By increasing the number of neurons in the hidden layer, the differences between the NN output and the desired (observed) output of the data used for training will decrease because more hidden neurons lead to more degrees of freedom (more adjustable

parameters in the NN model). However, after a certain number of hidden neurons, the NN starts to model *noisy fluctuations* in the dataset which is unfavourable for the accuracy of the real predictions; the performance of the NN for the training set increases (RMS error decreases), while that of the testing set decreases (RMS error increases). At that moment the NN is said to be *overtrained*. To avoid *overtraining* of the NN, an *early stopping* (Heskes, 1997) criterion is used in the NN training process. With this technique, the training process of the NN is stopped when the performance of the NN in the testing set starts to decrease. The optimal number of hidden neurons can be found by training the NN several times for a range of number of neurons in the hidden layer, and comparing each time the performance of the NN (RMS error) on the training and testing sets. The optimum number of hidden neurons was chosen as 20, since the use of more hidden neurons did not increase the accuracy of the NN while it increased the complexity of its architecture.

### *Confidence intervals*

After obtaining the optimal NN configuration, predictions of mean overtopping discharges could be made; i.e. for a set of input parameters, a set of output parameters (overtopping discharge) could be obtained. Van Gent and Van den Boogaard (1998) developed a method to add information on the reliability of NN predictions. The method to add information on the *reliability* of the NN predictions has been developed further within this investigation, and makes use of how the available data are spread over the entire domain of applications. With the double purpose of solving the matter of choosing the data to be used in the training and testing phases, and assessing the uncertainty of the NN predictions, resampling techniques were used.

Resampling techniques are generic devices used for uncertainty analysis in statistics and model calibration. The use of these techniques involves the development of a set of NNs (*resamples*) based on the original database. This implies firstly that the training and testing processes are redone many times solving the problem of representativeness of the training and testing sets; and secondly, that the set of NNs developed results in a *set of predictions* (a so called *ensemble*) of overtopping discharge, allowing the estimation of the reliability of the predictions (i.e. standard deviation or 95 % confidence intervals). As a result, the NN does not only give a prediction of the wave overtopping discharge but also a measure for the uncertainty of the prediction.

The two most commonly applied forms of resampling are *jackknifing* and *bootstrapping* (Efron, 1982). In the current investigation, the technique of *bootstrap resampling* was used.

A *bootstrap* resample is a random selection of  $N$  data out of the  $N$  original data. The  $N$  individual draws within one such resample are independent but with replacement so that every time there is a probability of  $1/N$  that a particular sample (input-output combination) of the original set is selected. At the end some samples are then selected once or more than once while other samples are absent in a resample. The samples selected in each resampling correspond to the tests that are used for the training of the NN, while the ones not selected correspond to the tests that are used in the testing/validation of the NN. The probability that an original sample is not present in a resample is  $(1-1/N)^N$  which for large  $N$  is close to  $1/e$ . Therefore, within each resample, the probability that a test was selected (used for training) was 63%, while the probability that a test was not selected (used for testing) was 37%. In this way a set of  $L$  of such resamples is generated. This  $L$  should be sufficiently large and in practice it is typically of the order of a hundred or a few hundreds, somewhat depending on the statistics to be computed. For each resample of the data set (and the corresponding division into a training and testing set) the NN is trained.

A set of about 500 NNs or resamples was performed herein. As a result, the bootstrap yielded 500 estimates of the wave overtopping discharge ( $\log q_1', \dots, \log q_{500}'$ ). The estimate of the model (NN output) is given by the mean of all these predictions,

$$1/L \cdot \sum_{i=1}^L \log q_i', \text{ where } L = 500, \text{ in this case.} \quad (14)$$

In the bootstrap resampling the weights are included as follows. If a weight  $WF$  is assigned to a particular input-output pattern,  $i$ , and within a resampling this pattern is selected  $N$  times, the total weight of the pattern is set to  $WF_i \cdot N$ . The contribution of this pattern to the cost function is then,

$$WF_i \cdot N \cdot ((\log q_{obs}')_i - (\log q_{NN}')_i)^2 \quad (15)$$

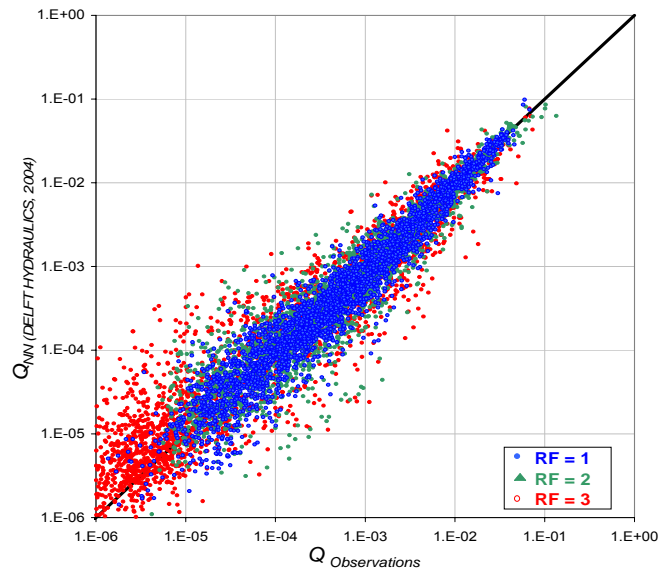
and the total cost function during training in a bootstrap resample is the superposition of such terms for all the input-output patterns that are actually selected.

The set of 500 NNs is further used to provide the uncertainty of the model with respect to the accuracy of its predictions. This uncertainty can be quantified by a standard deviation, or the variance, or a confidence interval. In this respect, the prediction method developed herein provides several statistics. Besides the mean of the predictions which is used as the model prediction ( $\mu = q_{NN}$ ), the output of the prediction method includes the standard deviation or spread,  $\sigma$ , and quantiles of several orders,  $q_{2.5\%}$ ,  $q_{5\%}$ ,  $q_{25\%}$ ,  $q_{50\%}$ ,  $q_{75\%}$ ,  $q_{95\%}$  and  $q_{97.5\%}$ . The 95% confidence interval is given by the quantiles  $q_{2.5\%}$  and  $q_{97.5\%}$ .

It should be noted that the uncertainty assessment is based on how data is spread over the entire domain of application; it still assumes that the database is correct. The uncertainty levels do not account for systematic error or inaccuracies in the database (for instance caused by model effects, scale effects or measurement equipment).

#### *Performance of Neural network*

Fig. 119 shows the observed wave overtopping discharge ( $q_{obs}$ ) versus the predicted wave overtopping discharge ( $q_{NN}$ ). As described in the previous section, the predicted overtopping discharge (model prediction) corresponds to the mean of the set of 500 NNs. It can be observed that the predictions of the NN are reasonably accurate, especially in the range of high overtopping discharges. In this respect, it should be noted that the repetition of a certain test in the laboratory often can give a factor 5 difference.



**Figure 119: Observations versus NN predictions**

The  $(Q_{obs}, Q_{NN})$  samples are plotted with the corresponding Reliability Factor ( $RF$ ) of the observed overtopping discharge. It can be observed that the majority of the relatively large differences between measured and predicted discharges corresponds to tests with low reliability ( $RF = 3$ ). These  $(Q_{obs}, Q_{NN})$  samples are non-dimensional overtopping discharges where  $Q = q / (g H_s^3)^{0.5}$ .

It should be noted that the predictions are mainly based on small-scale tests. In reality model effects, scale effects and wind may cause differences between results in small-scale tests and in reality. Scale and model effects for overtopping have been dealt within CLASH WP 7. The presented NN takes into account scale and model effects by applying an appropriate factor on the NN – output.

## Conclusions

A prediction method has been developed for the estimation of the mean wave overtopping discharge for many types of coastal structures, and the assessment of the uncertainties of these predictions.

The presented results show that Neural Networks can successfully be used to model the relationship between the input parameters involved in the process of wave overtopping and



the mean overtopping discharge at coastal structures. As for any NN, also the quality of the present NN is largely determined by the quantity and quality of the database.

Resampling techniques have been used for the estimation of the uncertainties of the NN predictions. In general, it has been shown that the agreement between the predicted overtopping discharge and the measured overtopping discharge is good; the predictions are rather accurate compared to the observed overtopping discharges.

The output of the Neural Network can be corrected to take into account influences of model effects, scale effects and wind, when predicting wave overtopping discharges for prototype conditions.

This workpackage delivered the following reports :

- a preliminary generic prediction method for wave overtopping based on a preliminary wave overtopping database (D10)
- the report on the preliminary generic prediction method (D11)
- the final generic prediction method (D41)
- the final report on generic prediction method (D42)

The following milestones were achieved :

- first version of the neural network is finished (M5)
- the generic prediction method is available (M13)

## 9 WP 9 : Synthesis and formulation of guidelines

### 9.1 Objectives

Objectives of this workpackage are :

- to synthesise all obtained results and to check to the objectives of the project and to draw final conclusion;
- to draw up a guideline on crest level design or assessment based on permissible overtopping the guideline will be short and focussed on practical application by end users.

### 9.2 Description of work performed

Based on the contributions of the different WP-leaders, a final full scientific report, which is the present report (D46), has been written. The main results and the overall conclusions of the project have been summarised. For detailed information this final report refers to the individual WP-reports and deliverables.

A guideline on crest level design and assessment has been written (D43). The generic prediction method together with the permissible overtopping as concluded from the hazard analysis in WP 6 forms the basis for this guideline. The background on how to deal with the scale / model effects is also incorporated in this guideline.

The generic CLASH overtopping prediction method is an applicable and validated procedure to design and assessment of the crest height of coastal structures with regard to overtopping hazards. The CLASH overtopping prediction methodology is published on the internet, including (1) the hazard analysis method (WP 6), (2) the scale and model effects analysis method (WP 7) and (3) the NN general prediction method (WP 8).

### 9.3 Conclusions / achievements

CLASH WP9 has produced a **guideline** on wave overtopping/crest level design by means of a generic prediction tool and guidance on consequences of overtopping and permissible levels of overtopping.

A final project report (D46) has been written at the end of the project. The guidelines (D43), including the generic prediction method (exe-file) are available through the internet as well.

This workpackage delivered the following reports / deliverables :

- the guidelines, including the generic prediction method (D43)
- the final project report (D46)

Additionally one milestone was achieved :

An overall synthesis is made and the guidelines have been formulated (M14).

---

## 10 WP 10 : Exploitation and dissemination of the results

### 10.1 Objectives

The only but very important objective of this workpackage is to exploit and to disseminate the final results of the project as wide as possible.

### 10.2 Description of work performed

Dissemination of project results has already started in an early phase of the project and was constantly updated during the course of the project. The following activities have taken place so far:

- a website has been created at the beginning of the project and is permanently updated under <http://www.clash-eu.org>;
- papers have been presented at conferences and have been submitted to international journals;
- expert seminars have been organised to disseminate the key results of CLASH obtained so far (e.g. Oceanology International in London on 18 March 2004);
- a flyer of CLASH has been designed and distributed during international conferences and amongst partners for disseminating the information to colleagues and clients;
- a Powerpoint presentation is available and can be downloaded from the web page. The presentation introduces the project and gives the key objectives together with some information on further contacts;
- a CLASH poster has been drafted and presented to an international audience at the Coastal Structures Conference 2003 in Portland/USA;
- News Letters have been set up to circulate key information inside the project to maintain a permanent high level of information at all participating institutes;

Exploitation of CLASH results will start immediately after the project is finished. However, the overall CLASH database is already available and has been used by CLASH partners to homogenise their databases of test results and to obtain comparison data sets for tests performed in their flumes. Results from hazard analyses due to overtopping have already led to proposals of design guidance on hazards in the UK.

## Conclusions

The dissemination of project results is on its way and is making good progress within and outside CLASH. All partners are contributing to these issues by submitting papers to conferences and journals, by holding national seminars or conferences and contributing to international ones. CLASH has been internationally presented at various conferences which are very relevant for the coastal engineering community such as the ICCE conference 2002 in Cardiff, UK, the Coastal Structures Conference in Portland/USA in 2003, and the ICCE 2004 conference in Lisbon/Portugal. CLASH is therefore already well known by the international coastal engineering community.

In terms of exploitation of the project the key CLASH results (e.g. database, hazard analysis, scale effects, generic prediction method) will be used by all project partners for their further research and consultancy projects. It is also expected that end-users will download these results from the website and use them within their own projects. It is therefore expected that CLASH will have a significant input to the coastal community worldwide working on the design of coastal structures related to wave overtopping.

This workpackage delivered the following reports :

- the technological implementation plan, draft version (D12)
- the technological implementation plan, final version (D44)
- the project website ([www.clash-eu.org](http://www.clash-eu.org)) (D47)

## 11 Acknowledgements

CLASH was a EU 5<sup>th</sup> framework research project, funded by EU under contract number EVK3-CT-2001-00058. The financial support of the EU is very much acknowledged. Furthermore our EC-scientific officers Mr. H. Barth and previously Mr. C. Fragakis are very much acknowledged for their understanding cooperation during the whole project duration. The authors also want to thank all CLASH-partners for the fruitful cooperation.

## 12 References

- Allsop, W. (2004). Report on hazard analysis. CLASH – WP 6 report ([www.clash-eu.org](http://www.clash-eu.org)), HR Wallingford, UK.
- Allsop, W., Bruce, T., Pearson, J., Alderson, J & Pullen, T.A. (2003). Violent overtopping at the coast, when are we safe? Int. Conf. on Coastal Management, Brighton, pp 54-69, ISBN 0 7277 3255 2, publ. Thomas Telford, London.
- Allsop, N., Bruce, T., Pearson, J., and Besley, P. (2004) “Wave overtopping at vertical and steep seawalls.” Water and Maritime Engineering Journal, page In Press.
- Aminti P., Franco L. (1988) Wave overtopping on rubble mound breakwaters, Proc. 21st International Conference on Coastal Engineering, Vol.1, ch.57, pp. 770-781, Malaga, 20-25 June 1988, Ed.Billy Edge, ASCE, NewYork, 1989.
- Arbhabhiramar, A. and Dinoy, A. (1973). Friction factor and Reynolds number in porous media flow. Journal of the Hydraulics Division, ASCE, 99(HY6):901–911.
- Battjes, J.A., Groenendijk, H.W. (2000). Wave height distributions on shallow foreshores, Coastal Engineering, 40, pp.161-182.
- Beddhu, M., Taylor, L., and Whitfield, D. (1994). A time accurate calculation procedure for flows with a free surface using a modified artificial compressibility formulation. Applied Mathematics and Computation, 65(1):33–48.
- Besley, P. (1999). Wave overtopping of seawalls: design and assessment manual. R&D Technical Report, HR Wallingford, no. W178, Wallingford, U.K., 37 pp., 5 tables (also from: <http://www.environment-agency.gov.uk/commondata/105385/w178.pdf>).
- Borsboom, M., Doorn, N., Groeneweg, J., and van Gent, M. (2001a). A boussinesq type wave model that conserves both mass and momentum. In Edge, B. (editor), “Coastal Engineering 2000,” pages 148–161. ASCE, Reston, Virginia.
- Borsboom, M., Groeneweg, J., Doorn, N., and van Gent, M. (2001b). Flexible boundary conditions for a boussinesq type wave model. In “Proceedings of Waves 2001, San Francisco,” pages 884–993. ASCE.
- Borsboom, M., Groeneweg, J., Doorn, N., and van Gent, M. (2001c). Near shore wave simulation with a boussinesq type wave model including wave breaking. In “Proceedings of Coastal Dynamics 2001”, Lund, Sweden pages 759–768. ASCE.
- Boone, C., Geeraerts, J., De Rouck, J. (2002). General Methodology Report (D5) CLASH –

- WP 1 report ([www.clash-eu.org](http://www.clash-eu.org)), Ghent University, Belgium, 127 pp.
- Bouma, J.J., Schram, A., François, D.(2004). Report on socio-economic impacts. (D39) CLASH- WP6 report ([www.clash-eu.org](http://www.clash-eu.org)), Ghent University, Belgium.
- Briganti, R., Bellotti, G., Franco, L., De Rouck, J., Geeraerts, J. (2005). Field measurements of wave overtopping at the rubble mound breakwater of Rome-Ostia yacht harbour. Manuscript submitted for publication – Coastal Engineering (Elsevier).
- Bruce, T, Allsop, N.W.H. & Pearson, J. (2001). Violent overtopping of seawalls – extended prediction methods Proc. Coastlines, Seawalls and Breakwaters 2001 ICE, publ Thomas Telford, London.
- Bruce, T. Pullen, T. Allsop, W. & Pearson, J. (2005). How far back is safe? Spatial distributions of wave overtopping. Proc. Coastlines, Seawalls and Breakwaters, ICE, Thomas Telford, London.
- Burcharth, H.F. and Lykke Andersen, T. (2003). Overtopping and rear slope stability of reshaping breakwaters. COPEDEC VI, Colombo, Sri Lanka.
- Causon, D., Ingram, D., Mingham, C., and Pearson, R. (2001). A Cartesian cut cell method for shallow water flows with moving boundaries. *Advances in Water Resources*, 24(2001):899–911.
- Chorin, A. (1967). The numerical solution of the Navier-Stokes equations for an incompressible fluid. Report NYO148082, New York University.
- Davey, T. (2004). Overtopping discharge - effect of wind. MEng project report, School of Engineering & Electronics, University of Edinburgh, Edinburgh, U.K.
- De Rouck, J., Van de Walle, B., Geeraerts, J., Troch, P., Van Damme, L., Kortenhaus, A., Medina, J, 2003. Full scale wave overtopping measurements. Proc. of Conf. Coastal Structures '03, Portland, USA, pp. 494-506.
- De Haas, P., Rijks, D., Ruessink, B., Roelvink, J., Reniers, A., and van Gent, M. (1999). Onderzoek naar lange golven bij Petten (in Dutch); Investigations on long waves at Petten. Report H3345, University Utrecht and Delft Hydraulics, Delft.
- De Waal, J.P.; Tonjes, P.; van de Meer, J.W. (1996). Wave overtopping of vertical structures including wind effects. *Proceedings 25th International Conference Coastal Engineering (ICCE)*, ASCE, Volume 2, Orlando, Florida, USA, pp. 2216-2229.
- De Kruif, A. (2000). Storm data of the Petten field site: 1995-2000. Report RIKZ/OS/2000/34X, Rijkswaterstaat (RIKZ), The Hague, The Netherlands.



- Dodd, N. (1998). A numerical model of wave run-up, overtopping and regeneration. Proc. ASCE Journal of Waterways, Port and Coastal Engineering, 124(2):73–81.
- Efron, B. (1982). The Jackknife, the Bootstrap and Other Resampling Plans, 92pp., SIAM, Philadelphia, PA.
- Endoh K & Takahashi S (1994). Numerically modelling personnel danger on promenade breakwater due to overtopping waves. Proc. 24th ICCE, Kobe, pp 1016-1029, publ. ASCE.
- Franco, L., de Gerloni, M. & van der Meer, J.W. (1994). Wave overtopping on vertical and composite breakwaters. Proc 24<sup>th</sup> Int Conf Coastal Eng., Kobe, ASCE.
- Franco, L., De Gerloni, M., Van Der Meer, J. (1995). Wave overtopping on vertical and composite breakwaters, Proc. 24<sup>th</sup> ICCE, Kobe, Japan, 23-28 October 1994. Ed. B. Edge, ASCE, NY.
- Franco L., Cavani A (1999). Overtopping Response Of Core-Locs, Tetrapods And Antifer Cubes, Coastal Structures '99, Proc. Int.Conf. CS'99- Santander (Spain) 7-10 June 1999, vol.1, pp.383-387, Edited by I.Losada, Balkema, Rotterdam 2000.
- Franco, L., Briganti, R., Bellotti, G. (2004). Report on full scale measurements, Ostia, 2<sup>nd</sup> full winter season (D32), CLASH - WP3 report ([www.clash-eu.org](http://www.clash-eu.org)) , Modimar, Rome, Italy.
- Fu, W., Huang, H., and Liou, W. (1996). Thermal enhancement in laminar channel flow with a porous block. International Journal of Heat and Mass Transfer, 39(10):2165–2175.
- Fukuda N., Uno T. & Irie I (1974). Field observations of wave overtopping of wave absorbing revetment" Coastal Engineering in Japan, Vol 17, pp 117-128, Japan Society of Civil Engineers, Tokyo.
- Geeraerts, J., De Rouck, J., (2002). General Methodology Draft Report (D2). CLASH – WP 1 report ([www.clash-eu.org](http://www.clash-eu.org)), Ghent University, Belgium, 99 pp.
- Geeraerts, J., Troch, P., De Rouck, J., Van Damme, L., Pullen, T. (2003). Hazards resulting from wave overtopping – Full scale measurements. Proc. Conf. Coastal Structures, Portland, Oregon, USA, pp. 481-493.
- Geeraerts, J., Boone, C. (2004). Report on full scale measurements Zeebrugge – Second Full Winter Season. CLASH – WP 3 report ([www.clash-eu.org](http://www.clash-eu.org)), Ghent University, Belgium, 71 pp.
- Geeraerts, J., Willems, M. (2004). Final report on laboratory measurements – Ostia (D31). CLASH - WP 4 report ([www.clash-eu.org](http://www.clash-eu.org)), Ghent University, Belgium, 79 pp.
- Geeraerts, J., Troch, P., De Rouck, J., Willems, M., Franco, L., Bellotti, G., Briganti, R. (2004). Wave overtopping at Ostia yacht harbour breakwater – Comparison between

prototype and model tests in 2D and 3D. 29<sup>th</sup> International Conference on Coastal Engineering, Lisbon, Portugal.

Goda, Y. (2000). Random seas and design of maritime structures. Advanced series on Ocean Engineering, Vol. 15, . World Scientific Publishing Co, ISBN 981-02-3256-X.

Gouldby B.P., Sayers P.B. & Johnson D. (1999). Real-time hazard forecasting: Review of implementation and two years operation at Samphire Hoe, Dover. Paper to MAFF Conference on River and Coastal Engineers, Keele.

González-Escrivá, J.A.; Garrido, J.; Medina, J.R.; Geeraerts, J. (2004). Laboratory real storm reproduction using wind. *Proceedings 29th International Conference Coastal Engineering (ICCE)*, ASCE, Lisbon, Portugal, 13 pp.

Groeneweg, J., Doorn, N., Borsboom, M., and van Gent, M. (2003). Boussinesq type modelling of measured wave breaking on a circular shoal. In McKee-Smith, J. (editor), “Coastal Engineering 2002,” volume 1, pages 495–507. ASCE, World Scientific, New Jersey.

Halcrow. (1997). Public safety of access to coastal structures, Report to Environment Agency, EA report 522.

Heald, G. (2002). Design on the Rocks?, Proc. Breakwaters, coastal structures & coastlines, pp 471-481, (ICE) ISBN 0 7277 3042 8, Thomas Telford, London.

Haykin, S. (1994). Neural networks: a comprehensive foundation. Macmillan College Publishing Company, Inc.

Hebsgaard, M., Sloth, P. and Juul, J. (1998). Wave overtopping of rubble mound breakwaters. ICCE 1998, Copenhagen. Paper no. 325.

Heskes, T. (1997). Practical confidence and prediction intervals. In Mozer, Jordan and Petsche (eds.), Advances in neural information processing systems 9, Cambridge, MIT Press.

Hibberd, S. and Peregrine, D. (1979) “Surf and run-up on a beach: a uniform bore.” *Journal of Fluid Mechanics*, 95(2):323–345.

Hirt, C. and Nichols, B. (1981) “Volume of Fluid (VoF) methods for dynamics of free boundaries.” *Journal of Computational Physics*, 39:201–225.

Hordijk, D. (2003). Report on field measurements (D19); Petten sea defence; storm season 2002/2003. CLASH - WP3 report ([www.clash-eu.org](http://www.clash-eu.org)). Technical Report RIKZ/OS/2003/135X, Rijkswaterstaat (RIKZ), The Hague, The Netherlands.

Huang, C., Chang, H., and Hwung, H. (2003). Structural permeability effects on the

interaction of a solitary wave and a submerged breakwater. *Coastal Engineering*, 49(2003):1–24.

Ingram, D., Causon, D., Gao, F., Mingham, C., Troch, P., Li, T. and De Rouck, J. (2003). Improvements Made to the Numerical Wave Flumes VOFbreak<sup>2</sup> and AMAZON-SC. CLASH - WP 5 Report, Manchester Metropolitan University, UK.

Jensen, O.J. & Sorensen, T., 1979. Overspilling / overtopping of rubble mound breakwaters. Results of studies, useful in design procedures. *Coastal Engineering* Vol. 3 1979 pp. 51-65.

Kelecy, F. and Pletcher, R. (1997). The development of a free surface capturing approach for multidimensional free surface flows in closed containers. *Journal of Computational Physics*, 138:939–980.

Kortenhaus, A.; Medina, J.R.; González-Escrivá, J.A.; Garrido, J. (2004a). Laboratory measurements on the Zeebrugge breakwater (D33). CLASH – WP 4 report ([www.clash-eu.org](http://www.clash-eu.org)), Braunschweig/Valencia, 74 pp.

Kortenhaus, A.; Oumeraci, H.; Geeraerts, J.; De Rouck, J.; Medina, J.R.; González-Escrivá, J.A. (2004b). Laboratory effects and other uncertainties in wave overtopping measurements. *Proceedings 29th International Conference Coastal Engineering (ICCE)*, ASCE, Lisbon, Portugal, 13 pp.

Kortenhaus, A.; Van der Meer, J.W.; Burcharth, H.F.; Geeraerts, J.; Pullen, T.; Ingram, D.; Troch, P. (2005). Quantification of measurement errors, model and scale effects related to wave overtopping (D40). CLASH – WP 7 report., Braunschweig, Germany, 60 pp.

Lafaurie, B., Nardone, C., Scardovelli, R., Zaleski, S., and Zanetti, G. (1994). Modelling merging and fragmentation in multiphase flows with SURFER. *Journal of Computational Physics*, 113:134–147.

Li, T., Troch, P., and De Rouck, J. (2004a). Large eddy simulation of wave overtopping on non-uniform Cartesian cut cell grids. In Chung, J., Izumiyama, K., Sayed, M., and Hong, S. (editors), “Proceedings of The Fourteenth (2004) International Offshore and Polar Engineering Conference, Toulon, France,” volume 3, pages 276–284. ISOPE, Cupertino, California, USA.

Li, T., Troch, P., and De Rouck, J. (2004b). Wave overtopping over a sea dike. *Journal of Computational Physics*, 198:686–726.

Lykke Andersen, T. and Burcharth, H. F. (2004a). Report on Additional Tests (D24);

- CLASH – WP 4 report ([www.clash-eu.org](http://www.clash-eu.org)), Aalborg University, Denmark.
- Lykke Andersen, T. and Burcharth, H.F. (2004b). Overtopping and rear slope stability of reshaping and non-reshaping berm breakwaters. ICCE 2004, Lisbon, paper 290.
- Mase, H., Sakamoto, M and Sakai, T. (1995). Neural network for stability analysis of rubble-mound breakwaters. *J. of Waterway, Port, Coastal and Ocean Engrg*, ASCE, nov/dec 1995, pp. 294-299.
- Medina, J.R. (1999). Neural network modelling of runup and overtopping. ASCE, Proc. Coastal Structures 1999, Santander, Vol. 1, pp 421-429.
- Medina, J.R, J.A. González-Escrivá, J. Garrido and J. De Rouck (2002). Overtopping analysis using neural networks. 28<sup>th</sup> International Conference on Coastal Engineering, Cardiff, UK.
- Medina, J.R, Garrido, J., Gómez-Martín, E. and C. Vidal (2003). Armour damage analysis using neural networks. ASCE, Proc. Coastal Structures 2003, Portland, USA.
- Owen, M.W. (1980). Design of sea walls allowing for wave overtopping, Rep. EX924, HR Wallingford.
- Owen M.W. (1982). The hydraulic design of sea-wall profiles. Proc. ICE Conf. on Shoreline Protection, September 1982, pp 185-192, publ. Thomas Telford, London, UK.
- Pan, D. and Lomax, H. (1988). A new approximate LU factorisation scheme for the Navier-Stokes equations. *AIAA Journal*, 26:163–171.
- Panizzo, A., R. Briganti, J.W. van der Meer and L. Franco (2003). Analysis of wave transmission behind low-crested structures using neural networks. ASCE, Proc. Coastal Structures 2003, Portland.
- Pearson J., Bruce T., Allsop W. & Gironella X (2002). Violent wave overtopping – measurements at large and small scale, 28th International Conference on Coastal Engineering, Cardiff, UK.
- Pearson, J., Bruce, T., Allsop, W., Kortenhuis, A., Van der Meer, J.W. (2004a). Effectiveness of recurve wave walls in reducing wave overtopping on seawalls and breakwaters, 29th International Conference on Coastal Engineering, Lisbon, Portugal, Book of Abstracts, Paper No 319.
- Pearson, J., Bruce, T., Franco, L., Van der Meer, J. (2004b). Report on additional tests, part B, CLASH WP4 report, University of Edinburgh, Edinburgh, United Kingdom.
- Pedersen, J. W. (1996). Wave Forces and Overtopping on Crown Walls of Rubble Mound Breakwaters – An Experimental Study. Series Paper 12, Hydraulics & Coastal Engineering

Laboratory, Department of Civil Engineering, Aalborg University.

Pozueta, B., Van Gent, M.R.A., Van den Boogaard, H.F.P. (2004a). Neural Network prediction method, CLASH – WP8 report ([www.clash-eu.org](http://www.clash-eu.org)), Delft Hydraulics, Delft, The Netherlands.

Pozueta, B., M.R.A. Van Gent, H.F.P. Van den Boogaard, and J.R. Medina (2004b), Prediction method; Neural network modelling of wave overtopping at coastal structures (November, 2004), Delft Hydraulics report H3969.

Pullen, T.A. & Allsop, N.W.H. (2004a). Samphire Hoe field measurements. CLASH - WP 3 report ([www.clash-eu.org](http://www.clash-eu.org)), Technical Report TR133, HR Wallingford, UK.

Pullen, T.; Allsop, N.W.H. (2004b). Clash workpackage 4 - Samphire Hoe physical model studies. CLASH – WP 4 report ([www.clash-eu.org](http://www.clash-eu.org)), no. TR 147, HR Wallingford, U.K.

Pullen, T., Allsop, W., Bruce, T., Pearson, J., Geeraerts, J. (2004). Violent wave overtopping at Samphire Hoe: Field and laboratory measurements. 29<sup>th</sup> International Conference on Coastal Engineering, Lisbon, Portugal.

Qian, L., Causon, D., Ingram, D., and Mingham, C. (2003a). A Cartesian cut cell two fluid solver for hydraulic flow problems. ASCE Journal of hydraulic Engineering, 129(9):688–696.

Qian, L., Causon, D., Ingram, D., and Mingham, C. (2003b). A pressure splitting scheme for free surface capturing methods for flows with gravity effects. Journal of Computational Physics, page submitted.

Ramsbottom D, Wade S, Bain V, Floyd P, Penning-Rowell E, Wilson T & Fernandez A (2004). Flood Risks to People, *Phase 2 Interim Report 1, R & D Report FD 2321/IR1*, DEFRA Flood Management section, London.

Richardson, S., Ingram, D., Mingham, C., and Causon, D. (2002). On the Validity of the Shallow Water Equations for Violent Wave Overtopping. In Edge, B. (editor), “Ocean Wave Measurement and Analysis,” pages 1112–1125. ASCE, Reston, Virginia.

Richardson, S., Pullen, T., and Clarke, S. (2003). Jet velocities of overtopping waves on sloping structures: Measurement and computation. In Smith, J. (editor), “Proceedings of the 29th International Congress on Coastal Engineering,” volume 2, pages 2239–2250. ASCE, Reston, Virginia, World Scientific, New Jersey.

Ris, R.C., Booij, N. and Holthuijsen, L.H. (1999). A third-generation wave model for coastal regions, Part II: Verification, J. Geoph. Research, 104, C4,7667-7682.

- Rogers, S. and Kwak, D. (1990). An upwind difference scheme for the time accurate incompressible Navier-Stokes equations. *AIAA Journal*, pages 113–134.
- Rumelhart, D.E. and J.L. McClelland (1986). *Parallel distributed processing: Explorations in the microstructure of cognition*, Vol. 1, Cambridge, MIT Press.
- Sakakiyama, T. and Kajima, R. (1998). Scale effects on wave overtopping of seawall covered with armour units. In “Proceedings 26th International Conference on Coastal Engineering (ICCE).”
- Shiach, J., Mingham, C., Ingram, D., and Bruce, T. (2004). The applicability of the shallow water equations for modelling violent wave overtopping. *Coastal Engineering*, 51(1):1–15.
- Schulz, K.-P. (1992). Maßstabeffekte beim Wellenaufwurf auf glatten und rauhen Böschungen. *Mitteilungen Leichtweiß-Institut für Wasserbau der Technischen Universität Braunschweig*, Heft 120, Braunschweig, Germany, S. 135-244.
- Soh, W. and Doodrich, J. (1988). Unsteady solution of incompressible Navier-Stokes equations. *Journal of Computational Physics*, 79:113–134.
- Steendam, G.J., J.W. van der Meer, H. Verhaeghe, P. Besley, L. Franco and M.R.A. van Gent (2004). The international database on wave overtopping. *Proc. ASCE, 29th ICCE*, Lisbon, Portugal.
- TAW (2002). Technical report wave run-up and wave overtopping at dikes, Technical Advisory Committee on Flood Defence, The Netherlands.
- TAW (2003). Leidraad Kunstwerken, B2 Kerende hoogte, mei 2003 (in Dutch). Technical Advisory Committee on Water Defences, The Netherlands.
- TAW (2004). Dutch Technical Advisory Committee on Flood Defence. Technical Report on Wave Run-up and Wave overtopping at dikes. Delft, The Netherlands.
- Troch P., De Rouck J., Van Damme L. (1998). Instrumentation and prototype measurements at the Zeebrugge rubble mound breakwater, *Coastal Engineering* 35, pp. 141 – 166.
- Troch, P., Li, T., De Rouck, J., and Ingram, D. (2003). Wave interaction with a sea dike using a VOF finite volume method. In Chung, J., Prevosto, M., Mizutani, N., Kim, G., and Grilli, S. (editors), “Proceedings of the 13th International Offshore and Polar Engineering Conference,” volume 3, pages 325–332. International Society of Offshore and Polar Engineering.
- Troch, P., Geeraerts, J., Van de Walle, B., De Rouck, J., Van Damme, L., Franco, L., Allsop, W. (2004) Full scale wave overtopping measurements on the Zeebrugge rubble mound

- breakwater. Coastal Engineering, Elsevier. Vol. 51 / 7 pp. 609-628.
- Ubbink, O. and Issa, R. (1999). A method for capturing sharp fluid interfaces on arbitrary meshes. Journal of Computational Physics, 153:26–50.
- Van den Boogaard, H., Mynett, A.E. and Heskes, T. (2000). Resampling techniques for the assessment of uncertainties in parameters and predictions of calibrated models. Proc. Hydroinformatics Conference, IOWA.
- van der Meer, J. W. (1992). Stability of the seaward slope of berm breakwaters. Coastal Engineering, Vol. 16, pp 205-234.
- van der Meer, J.W. and Janssen, J.P.F.M. (1994). Wave run-up and wave overtopping at dikes. Wave forces on inclined and vertical wall structures, ASCE.
- Van der Meer, J.W. (1998). Wave run-up and overtopping. In: *Pilarczyk, K.W. (ed.): Dikes and revetments*, Rotterdam/Brookfield: A.A. Balkema, pp. 145-160.
- van der Meer, J.W., Tönjes, P., de Waal, H. (1998). A code for dike height design and examination, Proceedings International Conference on Coastlines, Structures and Breakwaters, Institution of Civil Engineers, London, Thomas Telford, London, pp. 5 - 19.
- van Gent, M. (1994). The modelling of wave action on and in coastal structures.” Coastal Engineering, 22:311–339.
- van Gent, M. (1995). Wave interaction with permeable coastal structures. Ph.D. thesis, Delft University of Technology, Delft University Press, Delft, The Netherlands.
- van Gent, M.R.A and H.F.P. Van den Boogaard (1998). Neural network modelling of forces on vertical structures, ASCE, Proc. ICCE 1998, Vol. 2, pp. 2096-2109.
- van Gent, M. (1999). Physical model investigations on coastal structures with shallow foreshores; 2d model test on the Petten sea defence. Report H3129, Delft Hydraulics, Delft.
- van Gent, M., de Kruif, A., and Murphy, J. (2001). Field measurements and laboratory investigations on wave propagation and wave run-up. In “ASCE, Proc. Waves 2001,” pages 734–743.
- van Gent, M. and Doorn, N. (2001). Wave propagation and wave run-up on dikes with shallow foreshores. In “ASCE, Proc. Coastal Dynamics 2001, Lund, Sweden.”, pages 769–778.
- van Gent, M. and Giarrusso, C. (2003). Influence of low-frequency waves on wave overtopping: A study based on field measurements at the Petten Sea-defence, CLASH – WP



---

5 report (D25), ([www.clash-eu.org](http://www.clash-eu.org)), published as Report H4297, WL| Delft Hydraulics, The Netherlands.

van Leer, B. (1984). On the Relation Between the Upwind Differencing Schemes of Godunov, Engquist, Osher and Roe. *SIAM Journal on Scientific and Statistical Computing*, 5(1):1–20.

Verhaeghe, H., J.W. van der Meer, G.-J. Steendam, P. Besley, L. Franco and M.R.A. van Gent (2003). Wave overtopping database as the starting point for a neural network prediction method, ASCE, Proc. Coastal Structures 2003, Portland.

Verhaeghe, H.; Van der Meer, J.W.; Steendam, G.J. (2003). Database on wave overtopping at coastal structures. CLASH - WP 2 report ([www.clash-eu.org](http://www.clash-eu.org)), Infram, Marknesse, The Netherlands, 34 pp.

Youngs, D. (1982). Time dependent multi-material flow with large fluid distortion. In Morton, K. and Baines, M. (editors), “Numerical Methods for fluid dynamics,” pages 237–285. Academic Press, London.

Zhou, J., Causon, D., Ingram, D., and Mingham, C. (2002). Numerical solutions of the shallow water equations with discontinuous bed topography. *International Journal for Numerical Methods in Fluids*, 38:769–788.

Zhou, J., Causon, D., Mingham, C., and Ingram, D. (2001). The surface gradient method for the treatment of source terms in the shallow water equations. *Journal of Computational Physics*, 168:1–25.





COMMISSION  
OF THE EUROPEAN  
COMMUNITIES



FP5- EESD

CREST LEVEL ASSESSMENT OF  
COASTAL STRUCTURES BY  
FULL-SCALE MONITORING,  
NEURAL NETWORK PREDICTION  
AND HAZARD ANALYSIS  
ON PERMISSIBLE WAVE OVERTOPPING

# CLASH

EVK3-CT-2001-00058

R  
E  
P  
O  
R  
T

## D46 : Final report

### Full scientific and technical report

February 2005

Prof. Dr. Ir. J. De Rouck  
Ir. J. Geeraerts

Universiteit Gent



## Table of contents

List of tables

List of figures

List of symbols

0	Introduction .....	13
1	WP1 : General methodology .....	19
1.1	Objectives.....	19
1.2	Description of work performed .....	19
1.3	Conclusions / achievements .....	19
2	WP2 : Overtopping database.....	20
2.1	Objectives.....	20
2.2	Description of work performed .....	20
2.3	Conclusions / achievements .....	64
3	WP3 : Full scale measurements .....	65
3.1	Objectives.....	65
3.2	Description of work performed .....	65
3.2.1	Site 1 : Zeebrugge (Belgium).....	65
3.2.2	Site 2 : Ostia (Italy) .....	85
3.2.3	Site 3 : Samphire Hoe (UK).....	100
3.2.4	Site 4 : Petten (The Netherlands) .....	109
	Groyne section measurements.....	113
	ASMIV sea bed staff.....	113
	Wave run-up measurements .....	116
	Low-frequency waves .....	116
	Conclusions .....	117
3.3	General conclusion for WP3 .....	118
4	WP 4 : Laboratory investigation .....	119
4.1	Objectives.....	119
4.2	Description of work performed .....	119
4.2.1	Site 1 : Zeebrugge .....	119
4.2.2	Site 2 : Ostia .....	123
4.2.3	Site 3 : Samphire Hoe.....	128
4.2.4	Additional tests.....	132
4.3	General conclusion for WP4 .....	140
5	WP5 : Numerical modelling.....	141
5.1	Objectives.....	141
5.2	Description of work performed .....	141
5.2.1	Free surface capturing .....	143
5.2.2	Volume of Fluid methods.....	146
5.2.3	Long waves .....	151
5.2.4	Scale Effects.....	154
5.2.5	Shallow water models .....	160

Conclusions .....	162
6 WP 6 : Hazard analysis including socio-economic impacts .....	164
6.1 Objectives.....	164
6.2 Description of work performed .....	164
7.2.1 Background to development on hazard assessment guidance.....	164
7.2.2 Existing Guidance .....	166
7.2.3 New evidence on personnel hazards .....	167
7.2.5 Changing public perceptions.....	170
7.2.6 Awareness of coastal processes.....	171
7.2.7 Post overtopping velocities and loads .....	171
Overtopping velocities .....	171
Post overtopping wave loads on structures .....	173
7.2.9 Valuing overtopping hazards .....	175
Summary of hazard assessment and valuation procedures .....	178
Conclusions .....	179
7 WP 7 : Conclusions on scale effects and new data .....	180
7.1 Objectives.....	180
7.2 Description of work performed .....	180
8.2.1 Samphire Hoe vertical wall.....	180
8.2.2 Zeebrugge rubble mound breakwater.....	181
8.2.3 Ostia rock breakwater.....	182
8.2.4 Method to account for scale effects.....	184
Conclusions .....	194
8 WP 8 : Prediction method .....	195
8.1 Objectives.....	195
8.2 Description of work performed .....	195
Conclusions .....	204
9 WP 9 : Synthesis and formulation of guidelines .....	206
9.1 Objectives.....	206
9.2 Description of work performed .....	206
9.3 Conclusions / achievements .....	206
10 WP 10 : Exploitation and dissemination of the results .....	208
10.1 Objectives.....	208
10.2 Description of work performed .....	208
Conclusions .....	209
11 Acknowledgements .....	210
12 References .....	211

## List of tables

Table 1:	New derived values for $\gamma_f$ (see Pearson et al., 2004b).....	48
Table 2:	Estimated values for $\gamma_f$ based on included overtopping tests .....	49
Table 3:	Values of the complexity factor CF .....	56
Table 4:	Values of the reliability factor RF .....	57
Table 5:	Determination of the reliability factor RF .....	58
Table 6:	Information in the database .....	63
Table 7:	Measurement devices installed at the Zeebrugge rubble mound breakwater.....	68
Table 8:	Storms measured in Zeebrugge .....	74
Table 9:	Wave characteristics, surf similarity parameter and water level for the storms. .	75
Table 10:	Average overtopping rates for all storms, calculated using the 3 methods based on the continuity equation, the individual overtopping volumes and the water depth jumps, respectively with $N_{ov}$ the number of overtopping events. ....	75
Table 11:	Wave characteristics on Oct. 7th, 2003, Dec. 22th, 2003 and Febr. 8th, 2004. ....	81
Table 12:	Total and individual impacts measured by load cells (LC) on dummy2 during resp. storms.....	82
Table 13:	Total and individual impacts measured by load cells (LC) on dummy3 during resp. storms.....	82
Table 14:	Total and individual impacts measured by load cells (LC) on the vertical wall during resp. storms .....	83
Table 15:	Total and individual impacts measured by load cells (LC) on the pipeline during resp. storms .....	83
Table 16:	Dates and duration of the recorded overtopping events at Ostia breakwater.....	91
Table 17:	Ranges of variability of main wave parameters at toe (Ostia-P1) and offshore (Civitavecchia RON buoy) during the overtopping storms.....	93
Table 18:	Maxima values of measured average hourly overtopping rates during each of the 7 storms with corresponding relevant parameters.....	95
Table 19:	Measuring points and equipment at Petten field site.....	112
Table 20:	Roughness factors for breakwaters with slope 1:1.5, with crest berm width of 3Dn with a permeable core / underlayer. Values valid for breakwaters only (not for revetments). ....	137
Table 21:	Material characteristics for the 1/20 Ostia scale model .....	158
Table 22:	Initial Guidance on Tolerable Mean Overtopping Discharges (l/s.m).....	166
Table 23:	Suggested limits for overtopping mean discharges or peak volumes .....	175

## List of figures

Figure 1:	Interconnection diagram.....	18
Figure 2:	Main structure parts of rubble mound structure.....	31
Figure 3:	Typical position of berm, crest and toe.....	33
Figure 4:	Structure type with large toe.....	33
Figure 5:	Structure type with low situated berm.....	33
Figure 6:	Structure type with low situated crest.....	34
Figure 7:	Determination of $h_{\text{deep}}$ [m] and $m$ [-].....	35
Figure 8:	Determination of $h$ [m], $h_t$ [m] and $B_t$ [m].....	36
Figure 9:	Determination of $h$ [m], $h_t$ [m] and $B_t$ [m] in case of no toe.....	37
Figure 10:	Determination of $B$ [m], $B_h$ [m], $\tan\alpha_B$ [-], $h_b$ [m].....	38
Figure 11:	Determination of the transition depth $h_b$ [m] in case of a composite slope.....	39
Figure 12:	Determination of $R_c$ [m], $A_c$ [m] and $G_c$ [m].....	41
Figure 13:	Determination of $G_c$ [m].....	42
Figure 14:	Determination of the structures slope parameters.....	44
Figure 15:	Determination of the structures slope parameters, extra examples.....	45
Figure 16:	Structure type for which at least two slope parameters are requested.....	46
Figure 17:	Schematisation of a composite slope composed of 2 subsequent slopes.....	46
Figure 18:	Schematisation of a composite slope composed of 2 subsequent slopes.....	47
Figure 19:	Distinction between a large (a) and a small (b) recurve wave wall.....	51
Figure 20:	Schematisation of a large recurve wave wall.....	52
Figure 21:	Reduction factor for rough structures, graph (a) and smooth structures, graph (b).....	54
Figure 22:	Influence of a small recurve wave wall on $\gamma_f$ .....	55
Figure 23:	Location of Zeebrugge harbour at the Belgian North Sea Coast.....	66
Figure 24:	Location of the field site at Zeebrugge harbour.....	66
Figure 25:	Plan view with indication of both instrumented cross-sections.....	66
Figure 26:	Bathymetry for two instrumented cross-sections.....	67
Figure 27:	Cross-section of the Zeebrugge rubble mound breakwater at the location of the wave overtopping tank.....	69
Figure 28:	View at the overtopping tank on site.....	70
Figure 29:	Detail of one wavedetector.....	70
Figure 30:	Global view showing four different wave detectors.....	70
Figure 31:	Global view showing three installed instrumented dummies on site.....	71
Figure 32:	Global view showing the instrumented pipeline on site.....	72
Figure 33:	Cross-section showing the section with the measurement jetty. The position of the measurements on the vertical wall is indicated.....	72
Figure 34:	Detail of force transducer for force measurements on vertical wall.....	73
Figure 35:	Velocity meter in front of dummy.....	73
Figure 36:	Velocity meter in front of pipeline.....	73
Figure 37:	Definition figure of three different crest levels taken into account.....	76
Figure 38:	Comparison between measured and predicted average overtopping rates, using van der Meer et al. (1998, left column), Owen (1980, middle column) and Besley (1999, right column) prediction formulae; for crest freeboards $R_{c1}$ (a), $R_{c2}$ (b) and $R_{c3}$ (c).....	77

- Figure 39: Measured and predicted (top (a): van der Meer et al., 1998; bottom (b): Besley (1999)) non-dimensional average overtopping rates and 95 % confidence limits as a function of the non-dimensional crest freeboard for the crest freeboard  $R_{c3}$ , using surface roughness reduction factor  $\gamma_f = 0.51$ . Also indicated are predicted overtopping rates for  $\gamma_f = 0.50$  and  $\gamma_f = 0.55$  ..... 80
- Figure 40: Velocities measured in front of the pipeline on Febr. 8<sup>th</sup> 2004..... 84
- Figure 41: Location map and layout of Rome yacht harbour at Ostia..... 86
- Figure 42: Design cross section of the west breakwater at the overtopping wave tank. ... 87
- Figure 43: Foreshore grid bathymetry at Ostia (Tiber delta) (left panel) and local wave climate from directional wave records in the period 1990-1992 at a depth of -12 m MSL (buoy location in P0). P1, P2 and P3 indicate the points at which SWAN model results were extracted..... 87
- Figure 44: Left panel: Layout of the overtopping measurement station in Rome yacht harbour. The convention for wind and wave angles is also indicated. A local frame of reference has been defined:  $\zeta$  is the normal direction to the tank,  $\eta$  is the tangent direction.  $\Delta\phi_w = \phi_w - \beta_t$  is the relative wind direction being  $\beta_t$  the normal to the tank ( $^\circ$ N) and  $\phi_w$  is the wind direction ( $^\circ$ N),  $\Delta\beta_w = \beta_0 - \beta_t$  is the relative wave direction being  $\beta_w$  the wave direction ( $^\circ$ N). Right panel: aerial photo of the overtopping measurement station (nov 2003)..... 89
- Figure 45: Cross section and photo of the wave overtopping tank operational at Ostia breakwater. .... 90
- Figure 46: Scatter plots of the most important parameters recorded during the 86 overtopping events. Here  $Q^* = \frac{q_{\Delta h}}{\sqrt{gH_{m0}^3}}$ ,  $\xi_0 = \frac{\tan \alpha}{\sqrt{\frac{2\pi H_{m0}}{gT_{m-1,0}^2}}}$ ,  $w$  is the local wind speed,  $\Delta\beta_w$  is local wave direction relative to the normal to breakwater axis.  $H_{m0}$  is the significant wave height at the toe of the structure. .... 94
- Figure 47: Correlation between the mean hourly overtopping rate  $q_{\square h}$  and the maximum overtopping volume  $V_{\max}$  measured in the corresponding hour..... 96
- Figure 48: Comparison between the measured adimensional mean overtopping discharges and those predicted using Van der Meer et al. (1998) for breaking waves using  $\gamma_f = 0.5$  (solid line thick line) together with the 95% confidence.
- $$Q^* = \frac{q_{ov}}{\sqrt{gH_{m0}^3}} \sqrt{\frac{s_0}{\tan \alpha}} \quad \text{and} \quad R^* = \frac{R_c}{H_{m0}} \frac{\sqrt{s_0}}{\tan \alpha} \frac{1}{\gamma_b \gamma_\beta \gamma_v}$$
- Error bars indicate the maximum and the minimum value of mean unit overtopping discharge obtained using the two illustrated methods. .... 97
- Figure 49: Comparison between the measured adimensional mean overtopping discharges and those predicted using Van der Meer et al. (1998) for breaking waves using  $\gamma_f = 0.5$  (solid line thick line) together with the 95% confidence limits (solid thin lines).  $Q^* = \frac{q_{ov}}{\sqrt{gH_{m0}^3}}$  and  $R^* = \frac{R_c}{H_{m0}} \frac{1}{\gamma_\beta}$ . Error bars indicate the maximum and the minimum value of mean unit overtopping discharge obtained using the two illustrated methods..... 98
- Figure 50: Comparison between the measured mean unit overtopping discharges and those predicted using Owen (1980) formula (solid line) and with crest berm correction as proposed by Besley (1999) (dashed line) during six of the seven

measured storms with overtopping  $Q^* = \frac{q_{ov}}{gH_{m0}T_{om}}$  and  $R^* = \frac{R_c}{H_{m0}} \left( \frac{s_{om}}{2\pi} \right)^{0.5}$ . Error

bars indicate the maximum and the minimum value of mean unit overtopping discharge obtained using the two illustrated methods.  $\gamma_f = 0.5$ ..... 99

Figure 51:	Aerial view of Samphire Hoe with the study area in the foreground.....	101
Figure 52:	Section of the Samphire Hoe Seawall.....	102
Figure 53:	Violent wave overtopping at Samphire Hoe (Photograph courtesy of Eurotunnel and the White Cliffs Countryside Project).....	102
Figure 54:	The three tanks in position at Samphire Hoe.....	103
Figure 55:	The predicted overtopping discharges shown varying with the water level ..	105
Figure 56:	Trapezoidal distribution of overtopping discharges.....	107
Figure 57:	Measurements and predictions of overtopping during Storm 02.....	108
Figure 58:	Measurements and predictions of overtopping during Storm 03.....	108
Figure 59:	Location of Petten field site.....	109
Figure 60:	Measuring points at Petten field site (distance and height in metres).....	110
Figure 61:	Groyne section measurements Jarkus section 20,830.....	113
Figure 62:	ASMIV results near MP 6.....	114
Figure 63:	Water level at MP3 during the December 2003 storm.....	114
Figure 64:	Wave height and wave period during the December 2003 storm.....	115
Figure 65:	Spectra (including low frequency energy) calculated for instruments 031, 171 and 066.....	117
Figure 66:	Cross section of the model set-up of the Zeebrugge breakwater in the LWI wave flume.....	120
Figure 67:	Longitudinal cross section of the UPVLC wind and wave test facilities.....	120
Figure 68:	Cross section of the Zeebrugge scale model at UPVLC.....	120
Figure 69:	Zeebrugge model test results (no wind).....	121
Figure 70:	Zeebrugge model test results (influence of wind).....	121
Figure 71:	Cross-section of the complete 2D model set-up in the wave flume (values in cm model).....	125
Figure 72:	Cross-section of the 2D breakwater in the wave flume (values in mm model; elevations in m prototype).....	125
Figure 73:	Position and orientation of the Ostia breakwater in the wave basin for the 3D tests.....	126
Figure 74:	Cross-section with the overtopping tank in the wave basin (values in m model).....	126
Figure 75:	Ostia model test results.....	127
Figure 76:	Test set-up for 2D tests.....	129
Figure 77:	Plan view of the 3D model.....	130
Figure 78:	Samphire Hoe model test results.....	131
Figure 79:	Tested cross-section (dimensions in mm).....	132
Figure 80:	Layout in basin for testing 0° and 10°.....	133
Figure 81:	Layout in basin for testing 25°.....	133
Figure 82:	Layout in basin for testing 45° and 60°.....	134
Figure 83:	Evaluation of proposed direction factor against data from AAU.....	135
Figure 84:	Standard cross section. $H_0$ is the design wave height.....	136
Figure 85:	Tested cross-sections.....	138
Figure 86:	Porous media test: Velocity vectors for the whole domain, showing fully developed flow at the outlet.....	145
Figure 87:	Samphire Hoe: Overview of the test section.....	145



Figure 88:	Samphire Hoe: Computed water surface profiles at 0.5s intervals between $t = 2.0s$ and $t = 4.0s$ .....	146
Figure 89:	Computational domain on a non-uniform Cartesian cut-cell mesh for sea dike problems. WG0 to WG5 indicate the locations of five wave gauges. $l_1=1.0$ m, $l_1 + l_2 + l_3=6.3$ m and $d=0.7$ m. ....	148
Figure 90:	Velocity fields induced by the regular (left) and irregular (right) waves over a sea dike from $t = 32.2$ to $33.4$ s. ....	150
Figure 91:	Wave reflection as function of wave frequency for a selected condition; measured at MP17 on the Petten foreshore. ....	152
Figure 92:	Comparison between measured and computed contribution of low frequency energy. ....	153
Figure 93:	Increase of mean wave overtopping discharge as function of the ratio of low-frequency energy and total energy.....	154
Figure 94:	Computational domain with step porous structure.....	156
Figure 95:	The Darcy-Weisbach friction factor $\lambda$ against Reynolds numbers. ....	157
Figure 96:	Instantaneous dimensionless jet velocities (solid breakwater).....	157
Figure 97:	Free surface configuration of the Ostia breakwater model (scale 1/20), modelled using the VOFbreak <sup>2</sup> code, and showing wave breaking in front of and wave overtopping over the porous breakwater. ....	159
Figure 98:	Simulation results calculated at time 20 s for the 1/20 scale model. ....	159
Figure 99:	Dimensionless discharge ( $Qh$ ) plotted against dimensionless freeboard ( $Rh$ ) for the physical model and the numerical model. ....	161
Figure 100:	Categorisation of overtopping hazards at Samphire Hoe, low, moderate and high .....	168
Figure 101:	Public watching / dodging overtopping at Oostende .....	168
Figure 102:	Beach, seawall and promenade at San Sebastian, Spain .....	169
Figure 103:	Artificial beach, breakwaters and resort at Lanzarote.....	169
Figure 104:	Yacht harbour of Salivoli (Tuscany) during storm in November 2001 .....	169
Figure 105:	West Harbour, Hartlepool, under 1:50 year storm, physical model.....	169
Figure 106:	Extracts from video of overtopping incident at Giant's Causeway, 16 August 2002 .....	170
Figure 107:	Suggested velocity / depth limits from Ramsbottom <i>et al.</i> (2004).....	172
Figure 108:	Wave loads on person dummies (from tests at LWI, see Appendix J) .....	173
Figure 109:	Wave loads on person dummies (from tests at LWI, see Appendix J) .....	174
Figure 110:	Decision tree for choosing valuation techniques.....	177
Figure 111:	Prototype results, 2D and 3D test results with comparison to Besley formula.....	181
Figure 112:	Relative mean overtopping rates from LWI tests plotted against the relative freeboard with comparison to Van der Meer formula and prototype results..	182
Figure 113:	Relative mean overtopping discharges from FCFH (3D) and UGent (2D) tests plotted against the relative freeboard with comparison to Van der Meer formula and prototype results.....	183
Figure 114:	Reduction of wave overtopping due to reduction of wave run-up on the seaward slope for the Zeebrugge storm data .....	186
Figure 115:	Discharge rates and the effect of the transport factor $W_s$ .....	188
Figure 116:	Scaling map for wave overtopping results over coastal structures from small-scale model tests .....	192
Figure 117:	Results of the application of the parameter map for scaling to the test case of Zeebrugge .....	193



---

Figure 118:	Results of the application of the parameter map for scaling to the test case of Ostia.....	193
Figure 119:	Observations versus NN predictions .....	204

## List of symbols

$A_c$	= height of armour in front of crest element in relation to S.W.L.	[m]
$B$	= berm width, measured horizontally	[m]
$c_i$	= inshore wave celerity	[m/s]
$C_r$	= average reflection coefficient ( $= \sqrt{m_{0,r}} / \sqrt{m_{0,i}}$ )	[%]
CF	= complexity-factor of structure section = 1, 2, 3 or 4	[-]
$h$	= water depth just before the structure (before the structure toe)	[m]
$h_{\text{deep}}$	= water depth in deep water	[m]
$h_t$	= water depth on the toe of the structure	[m]
$h_b$	= berm depth in relation to S.W.L. (negative means berm is above S.W.L.)	[m]
$D_{n50}$	= nominal diameter of rock	[m]
$D_n$	= nominal diameter of concrete armour unit	[m]
$D(f,\theta)$	= directional spreading function, defined as:	[°]
	$S(f, \theta) = S(f) \cdot D(f,\theta) \text{ met } \int_0^{2\pi} D(f,\theta)d\theta = 0$	
$f$	= frequency	[Hz]
$f_p$	= spectral peak frequency i.e. frequency at which $S_n(f)$ is a maximum	[Hz]
$f_b$	= width of a roughness element (perpendicular to dike axis)	[m]
$f_h$	= height of a roughness element	[m]
$f_L$	= centre-to-centre distance between roughness elements	[m]
$g$	= acceleration due to gravity ( $= 9,81$ )	[m/s <sup>2</sup> ]
$G_c$	= width of armour in front of crest element	[m]
$H$	= wave height	[m]
$H_{1/x}$	= average of the highest 1/x th of the wave heights derived from time series	[m]
$H_{x\%}$	= wave height exceeded by x% of all wave heights	[m]
$H_s$	= $H_{1/3}$ = significant wave height	[m]
$H_{m0}$	= estimate of significant wave height based on spectrum = $4\sqrt{m_0}$	[m]
$H_{m0,\text{deep}}$	= estimate of significant wave height at deep water	[m]
$H_{m0,\text{toe}}$	= estimate of significant wave height at the toe of the structure	[m]
$k$	= angular wave number ( $= 2\pi/L$ )	[rad/m]

$L_{\text{berm}}$	= horizontal length between two points on slope, $1.0 H_{m0}$ above and $1.0 H_{m0}$ below middle of the berm	[m]
$L_{\text{slope}}$	= horizontal length between two points on the slope, $Ru_{2\%}$ above and $1.5 H_{m0}$ below S.W.L.	[m]
$L$	= wave length measured in the direction of wave propagation	[m]
$L_{0p}$	= peak wave length in deep water = $gT_p^2/2\pi$	[m]
$L_{0m}$	= mean wave length in deep water = $gT_m^2/2\pi$	[m]
$L_0$	= deep water wave length based on $T_{m-1,0} = gT_{m-1,0}^2/2\pi$	[m]
$m_n$	= $\int_{f_1}^{f_2} f^n S(f) df = n^{\text{th}}$ moment of spectral density	[m <sup>2</sup> /s <sup>n</sup> ]
	lower integration limit = $f_1 = \min(1/3.f_p, 0.05 \text{ full scale})$	
	upper integration limit = $f_2 = 3.f_p$	
$m_{n,x}$	= $n^{\text{th}}$ moment of x spectral density	[m <sup>2</sup> /s <sup>n</sup> ]
	x may be: i for incident spectrum r for reflected spectrum	
$N_{ow}$	= number of overtopping waves	[-]
$N_w$	= number of incident waves	[-]
$P(x)$	= probability distribution function	
$p(x)$	= probability density function	
$P_V$	= $P(\underline{V} \geq V) =$ probability of the overtopping volume $\underline{V}$ being larger or equal to $V$	[-]
$P_{ow}$	= probability of overtopping per wave = $N_{ow}/N_w$	[-]
$q$	= mean overtopping discharge per meter structure width	[m <sup>3</sup> /m/s]
$R_c$	= crest freeboard in relation to S.W.L.	[m]
RF	= reliability-factor of test = 1, 2, 3 or 4	[-]
$Ru$	= run-up level, vertical measured with respect to the S.W.L.	[m]
$Ru_{2\%}$	= run-up level exceeded by 2% of the incident waves	[m]
$s$	= wave steepness = $H/L$	[-]
$s_{0p}$	= wave steepness with $L_0$ , based on $T_p = H_{m0}/L_{0p} = 2\pi H_{m0}/(gT_p^2)$	[-]
$s_{0m}$	= wave steepness with $L_0$ , based on $T_m = H_{m0}/L_{0m} = 2\pi H_{m0}/(gT_m^2)$	[-]
$s_0$	= wave steepness with $L_0$ , based on $T_{m-1,0} = H_{m0}/L_0 = 2\pi H_{m0}/(gT_{m-1,0}^2)$	[-]
$S_{\eta,i}(f)$	= incident spectral density	[m <sup>2</sup> /Hz]
$S_{\eta,r}(f)$	= reflected spectral density	[m <sup>2</sup> /Hz]
$S(f, \theta)$	= directional spectral density	[(m <sup>2</sup> /Hz)/°]

$t$	= variable of time	[s]
$T$	= wave period = $1/f$	[s]
$T_m$	= average wave period (time-domain)	[s]
$T_p$	= spectral peak wave period = $1/f_p$	[s]
$T_{H1/x}$	= average of the periods of the highest $1/x$ th of wave heights	[s]
$T_s$	= $T_{H1/3}$ = significant wave period	[s]
$T_{mi,j}$	= average period calculated from spectral moments, e.g.:	[s]
$T_{m0,1}$	= average period defined by $m_0/m_1$	[s]
$T_{m0,2}$	= average period defined by $\sqrt{m_0/m_2}$	[s]
$T_{m-1,0}$	= average period defined by $m_{-1}/m_0$	[s]
$T_R$	= record length	[s]
$v_z, v_x$	= particle velocities in direction $z$ , and $x$	[m/s]
$V$	= volume of overtopping wave per unit crest width	[m <sup>3</sup> /m]
$\alpha$	= slope angle	[°]
$\alpha_{wall}$	= angle that steep wall makes with horizontal	[°]
$\alpha_{berm}$	= angle that sloping berm makes with horizontal	[°]
$\beta$	= angle of wave attack with respect to the structure alignment (0° is perpendicular to the structure axis)	[°]
$\eta(t)$	= surface elevation with respect to S.W.L.	[m]
$\gamma_b$	= correction factor for a berm	[-]
$\gamma_f$	= correction factor for the roughness of or on the slope	[-]
$\gamma_\beta$	= correction factor for oblique wave attack	[-]
$\gamma_v$	= correction factor for a vertical wall on the slope	[-]
$\xi_0$	= breaker parameter (= $\tan\alpha/s_0^{1/2}$ )	[-]
$\mu_{(x)}$	= mean of measured parameter $x$ with normal distribution	[..]
$\sigma$	= directional spreading	[°]
$\sigma_{(x)}$	= standard deviation of measured parameter $x$ with normal distribution	[..]
$\theta$	= direction of wave propagation	[°]
$\omega$	= angular frequency = $2\pi f$	[rad/s]

## 0 Introduction

The present text is the Full Scientific and technical report of the FP 5 project CLASH: Crest Level Assessment of coastal Structures by full scale monitoring, neural network prediction and Hazard analysis on permissible wave overtopping (EVK3-CT-2001-00058). This report is the final deliverable (D46) of the project and gives an account of the detailed scientific and technical outcome of the project referring to the whole project period (January, 1<sup>st</sup>, 2002 – December, 31<sup>st</sup>, 2004). For each Workpackage (WP), this report describes the work carried out and summarises the most important results and conclusions.

More detailed information on the scientific results and a description of the methodologies on how they are achieved are provided in the WP-related deliverables to which reference is made.

The project consortium was composed as follows:

<b>Partner</b>	<b>Abbreviation</b>	<b>Country</b>
<b>Universiteit Gent</b>	<b>Ugent</b>	<b>BE</b>
<b>Flanders Community Coastal Division</b>	<b>FCCD</b>	<b>BE</b>
<b>Flanders Community Flanders Hydraulics</b>	<b>FCFH</b>	<b>BE</b>
<b>Leichtweiss Institut für Wasserbau</b>	<b>LWI</b>	<b>D</b>
<b>Aalborg University</b>	<b>AAU</b>	<b>DK</b>
<b>Universidad Politécnica de Valencia</b>	<b>UPVLC</b>	<b>E</b>
<b>Modimar</b>	<b>MOD</b>	<b>IT</b>
<b>Delft Hydraulics</b>	<b>DH</b>	<b>NL</b>
<b>Infram</b>	<b>INF</b>	<b>NL</b>
<b>Rijkswaterstaat</b>	<b>RIKZ</b>	<b>NL</b>
<b>Manchester Metropolitan University</b>	<b>MMU</b>	<b>UK</b>
<b>University of Edinburgh</b>	<b>UEDIN</b>	<b>UK</b>
<b>Hydraulic Research Wallingford</b>	<b>HRW</b>	<b>UK</b>

Prof. J. De Rouck (Universiteit Gent) was the CLASH-coordinator.

For more information :

**Prof. dr. ir. J. De Rouck**

**Department of Civil Engineering – Ghent University**

**Technologiepark 904 ; 9052 Zwijnaarde ; Belgium**

**[Julien.Derouck@Ugent.be](mailto:Julien.Derouck@Ugent.be) ; [Nathalie.Rousseau@Ugent.be](mailto:Nathalie.Rousseau@Ugent.be)**

## 0.1 Overall objectives of the project :

The project origins from **two observations** :

- The proven fact that small scale model testing under predicts wave run-up on rough slopes;
- the lacking of generally applicable prediction methods for crest height design or assessment with respect to wave overtopping.

Therefore, the first overall objective of CLASH is to validate the present design methods by full scale monitoring of wave overtopping, small scale laboratory modelling and numerical modelling, and to solve the matter of scale/model effects and possible under predictions.

In order to tackle the problem of suspected scale/model effects, CLASH will pay large attention to full scale monitoring of wave overtopping at four different full scale sites with different structures and subjected to a variety of conditions representative for European coasts (Atlantic Ocean, Mediterranean Sea and North Sea). Two sites (a rubble mound breakwater (Zeebrugge (Belgium)) and a seadike in very shallow water (Petten (the Netherlands))) are already extremely well instrumented for measuring wave characteristics and wave run-up. Extra instrumentation is needed to focus on wave overtopping. Measurements at the Petten field site were focussed on long waves on the shallow foreshore as such long waves can not be reproduced in small scale research. The site located in the United Kingdom, Samphire Hoe (a vertically walled reclamation in moderate water depth) has been equipped with a simple hazard monitoring system. Instrumentation is required to measure more quantitative results of wave heights, wave overtopping volumes and spray. The fourth location, Ostia (Italy), a rubble mound breakwater, will be overtopped every winter and is an ideal location to validate this kind of structure. Instrumentation for wave characteristics and wave overtopping measurements had to be installed.

The full scale measurements of wave overtopping are to be simulated rigorously in various laboratories on a smaller scale in order to investigate scale effects and, if possible, by numerical simulation as such simulations can be done on full scale without scale effects. Each site is modelled in two different laboratories; in order to eliminate effects of different construction, measuring and analysis systems at each laboratory. Most of these tests are done

in wave flumes (2D). However, for both Ostia and Samphire Hoe site 3D modelling in a wave tank are performed too. Parametric tests are carried out in one laboratory per site. Finally, both two and three dimensional additional ‘white spot’ tests are carried out.

Numerical modelling is a helpful tool to solve the problem of scale effects. Actual models were capable of simulating wave breaking, vertical acceleration, the formation of spray, and of calculating detailed fluid behaviour (e.g. throw velocities, volume of water in an overtopping plume, maximum height of the plume and impact pressure on the structure) at prototype scale (without scale effects). Thus, numerical flume codes can be used to help assess scaling effects present in laboratory experiments. There were, however, a number of modelling difficulties that needed to be addressed. Firstly, while most codes included a porosity model, which can be applied to rubble mound breakwaters, these models are isotropic and thus not suited to modelling the air / armour layer. Secondly, as air is entrained by the breaking wave the fluid starts to become compressible – and energy is dissipated. Finally careful calibration of the bed and wall friction coefficients was required for optimised simulation of the wave-structures interaction.

The second overall objective is to make use of the many existing (sometimes site specific) data sets on overtopping and to develop a generally applicable design method. This method is developed to recognise patterns in large data sets, a large number of parameters when there is a lack of physical understanding, or lack of description of the physics of the phenomenon : the method of a neural network. The sophisticated technique of neural network modelling, which is a technique capable of recognizing patterns in large data sets, has proven to be very effective. A general algorithm of a neural network has already been developed. Through the calibration and validation of neural networks a prediction method can be obtained where the relevant parameters are input and the wave overtopping discharge is output.

Many, site specific, investigations have provided an enormous amount of data sets with respect to (mean) wave overtopping discharges (some published as complete reports, others in possession of the partners of CLASH). More than 10000 tests in different databases and for different structures are available. The first action is to gather all this existing data on wave overtopping and to screen the data on consistency in order to get a homogeneous total data set. This comprehensive work is required as it will form the basis of the prediction method. Also “white spots” in the data set are detected and extra tests are performed to fill this gap in

knowledge. The algorithm is trained on the screened data set and will form a first prediction method. After reaching conclusions on scale effects the neural network is corrected and also the full scale measurements and small scale and numerical simulations are added. This will give the final prediction method.

The knowledge on safety limits for overtopping hazards or guidance on acceptable levels of wave overtopping, including spray, has hardly been improved during the last two decades and is very poor. Permissible levels of wave overtopping discharge  $q$  [ $\text{m}^3/\text{s}$  per meter structure]. This may be sufficient for simple flooding studies, but gives insufficient information for the estimation of safety limits for people or for structures and other socio-economic impacts of wave overtopping. At low wave overtopping discharges, the contribution of spray is increasingly important, but there are no methods available to predict spray volumes or travel distances. More guidance is required and is delivered by this project.

The work necessary to meet the overall goals of CLASH is grouped into the following specific objectives :

1. to measure / monitor wave overtopping events at three different locations and for various structure types at full scale and to measure long waves at a fourth site to study their effect on wave overtopping;
2. to gather and screen the enormous amount of data on wave overtopping which is available. The screening of the database will a.o. result in a list of “white spots”;
3. to simulate measured storms and overtopping in small scale facilities and by numerical models in order to investigate and solve the problem of suspected scale effects. Extra tests are foreseen to fill in the “white spots” of the database;
4. to train the algorithm of a neural network to this data set, and later on, include the conclusions on scale effects and the new measurements;
5. to derive / refine limits for safety of pedestrians, car users, ... and limits of overtopping for hazard to buildings and related items, also taking into account the impacts on social and economic life in densely populated areas near the coast;
6. to develop a practical guideline on crest level assessment of coastal structures;
7. to establish communication among partners, with end-users and with the coastal engineering community.



The major innovations provided by CLASH can be summarised as follows :

CLASH intends to solve the problem of suspected scale effects in small scale modelling of overtopping by :

- full scale monitoring and measuring at different sites, including different geometries and circumstances (wave conditions and water depth);
- simulation by small scale and numerical modelling, including required improvements on numerical modelling.

CLASH will develop a generic prediction method for overtopping by :

- use of the enormous amount of existing data on overtopping;
- use of full scale measurements, extra measurements (small scale and numerical);
- incorporating the conclusions on and consequences of possible scale effects in small scale model tests;
- use of a new, but proven, technique of the neural network modelling.

CLASH will perform a hazard analysis, including socio-economic impacts in order to improve guidance on permissible overtopping.

CLASH will produce a guideline on wave overtopping / crest level design by means of a generic prediction tool and guidance on consequences of overtopping and permissible levels of overtopping.

To tackle these objectives, a detailed structure and overall methodology was established. The work to be done was structured in 10 distinct but clearly interrelated workpackages. Fig. 1 shows the interconnection diagram of the project's Workpackages. Each WP is described hereafter, giving for each of them the objectives, a description of the work performed and the conclusions / achievements.

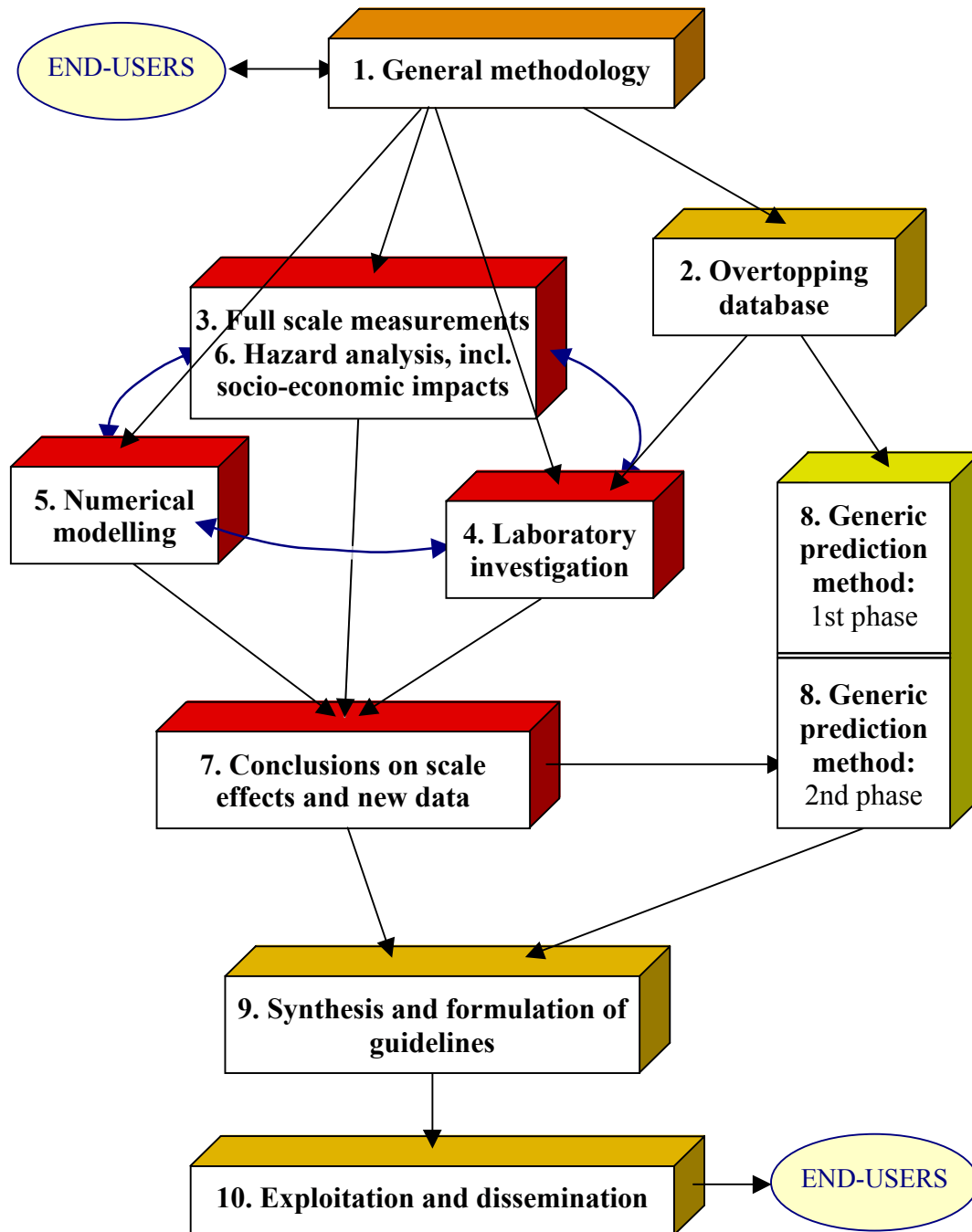


Figure 1: Interconnection diagram.

## **1 WP1 : General methodology**

### **1.1 Objectives**

The principal objectives of WP1 are to outline the overall methodology of the project and to detail the various connected tasks as follows :

- the collection of full scale data is crucial and the installation, measurements and analysis has to be established in detail for each site;
- the inventory of available overtopping data sets and detailed description of what will be required;
- detailing of similarity in the physical model tests and the numerical work.

### **1.2 Description of work performed**

All partners have contributed in setting up a general methodology, which is structured WP by WP and which details the agreements and the work to be carried out within a specific WP. Early in the project a draft report on this general methodology was written and spread amongst partners (Geeraerts & De Rouck, 2002). After one year the optimized version of this methodology report was spread (Boone et al., 2003).

### **1.3 Conclusions / achievements**

The main conclusion of this WP is the General Methodology Report, which provided guidelines to be followed during the whole project.

This workpackage delivered the following reports :

- the general methodology, draft version (D2)
- the report on general methodology (D5)

Additionally one milestone was achieved :

the general methodology for the whole project (M1).

## 2 WP2 : Overtopping database

**Important Note:** Given the very important character of this WP and the importance of the parameters defined in this WP, for good understanding of the further project, this WP is described into more detail within this final CLASH report.

### 2.1 Objectives

The final objective of this task is to create a screened homogeneous data base on wave overtopping tests at coastal structures, based on existing data bases at the possession of partners and elsewhere in Europe and worldwide. This data base is the input for the generic prediction method described in WP 8.

The final intention of the extended database on wave overtopping is dual:

- The objective of the overtopping database on its own is to give an inventory as complete as possible of reliable overtopping tests. It is estimated that more than half of the (reliable) data on overtopping existing in the world, is included in the database. Each overtopping test is included in the database by means of 31 parameters, what should give for each test a brief but complete overall view of the entire test situation with corresponding measured overtopping discharge.
- The more fundamental objective of the creation of an overtopping database is to use it for the development of a neural network method to predict mean overtopping discharges. The creation of a generic prediction method for wave overtopping, applicable for all kind of coastal structures, was a second task of the European CLASH-project (see WP 8).

### 2.2 Description of work performed

#### 2.2.1 *Origin of overtopping data*

During the last 30 years quite a lot of research has been done to overtopping at coastal structures, resulting in a lot of overtopping information available at different universities and

research institutes all over the world. The first phase of composing a database consisted therefore in collecting as much of these present data as possible. As the data were gathered within the CLASH project, a lot of data are originating from CLASH partners, but also data from non-CLASH institutes within Europe as well as from outside Europe contribute to the database. The percentage of data which was received from CLASH partners in the final database is about 80%.

Distinction could be made between publicly available data, often related to basic research and already described in literature, and confidential reports, in most cases related to overtopping tests performed for specific sites and practical situations. The publicly available data take about 75% of the data in the database, the remaining 25% concern confidential data.

During the first phase of the set-up of the database, about 6500 tests were gathered. During the second and last phase, not only about 4000 new overtopping tests were added, but also improvements were made on some parameters of the already existing database, resulting in an extended and improved final database. The 4000 extra overtopping tests added to the preliminary database contain prototype measurements gathered within CLASH (see WP 3), model tests performed within CLASH (see WP 4) and additional tests gathered from outside CLASH.

The improvements made in the final database concern mainly the values of the roughness/permeability factor  $\gamma_f$  (see section 2.2.5.3). As in the first stage of the CLASH project, little was known about the combined effect of roughness and permeability of structure slopes composed of concrete armour blocks, this effect was included in the preliminary database by means of estimated values for  $\gamma_f$ , see Verhaeghe et. al., 2003a. The white spot tests performed in this context, resulted in more precise roughness/permeability factors  $\gamma_f$  for a lot of armour types (see WP 4), replacing the estimated values of  $\gamma_f$  included in the first preliminary database.

Other improvements made on the preliminary database concern slightly adapted ideas on how to schematise special shaped structures, and new, better definitions for some parameters.

## 2.2.2 Methodology for gathering overtopping information

To obtain a complete and reliable overtopping database, detailed information on all overtopping measurements was needed. The reliability of the database was all the more important regarding its fundamental objective: to function as starting point for the development of a neural network prediction method.

From this point of view as much information as possible was gathered for all test series. Not only information about wave characteristics, test structure and corresponding discharge was gathered, but also information concerning the test facility used to perform the tests, the processing of the measurements and the precision of the work performed was looked upon.

For each overtopping test it was tried to answer following questions:

- considering the **wave characteristics**:
  - which were the wave characteristics of the measured or generated storm?
    - regular or irregular waves?
    - long-crested or short-crested waves?
    - characteristic wave heights, characteristic wave periods?
    - incident wave angle?
  
- considering the **test structure**:
  - what kind of structure was tested? (E.g. vertical wall? sloping structure?...)
  - which were the geometrical parameters of the structure?
  - which materials were used to construct the test section?
  - what was the exact foreshore?
  
- considering the measured **overtopping**:
  - what exactly was measured?
    - overtopping volume and/or percentage of waves overtopping?
  - how was overtopping volume measured?
    - by measuring increase of water level or weight of overtopping water?
  
- considering the **test facility** in which the tests were performed (not applicable for prototype tests):

- which test facility was used?
    - a wave basin or a wave flume? (3D or 2D tests?)
    - possibilities/restrictions of wave generation system?
  - was reflection compensation performed during testing?
    - active or passive wave absorption?
  - which model scale was used?
- considering the **processing** of the measurements:
    - did the researcher perform time domain analysis and/or spectral domain analysis?
    - did the researcher perform reflection analysis?
      - separation of incident and reflected waves or only determination of total waves?
    - how did the researchers measure incident waves?
      - calibration of the test facility (before construction of the structure) at the location of the structure, measurement of waves at the toe of the structure during testing or only measurement of waves at deep water?

Depending on the answers to these questions, each test could be assessed on reliability and complexity. This was taken into account in the database by defining for each test a Reliability Factor RF and a Complexity Factor CF, being a measure for reliability of the performed test and the complexity of the overtopping structure respectively. More detailed information on these two factors is given in section 2.2.6.

### 2.2.3 *Parameters in the database*

In view of using the overtopping database for the development of a neural network prediction method, each test had to be characterised by a fixed number of parameters. These parameters had to be chosen in such a way that an overall view as complete as possible of the overtopping test is achieved by these parameters. This implies inclusion of attacking wave characteristics, test structure properties, the measured overtopping result, but also the reliability of the measurements and the complexity of the structure should be represented.

At the same time it was tried to limit the number of parameters. Preference for simplicity over needless complexity can be mentioned here, given the fact that a neural network only can act well if the number of input parameters is restricted. This restriction does not depend only on

the number of tests which are available for the development of the neural network, but also the distribution of the tests within the available parameter ranges is important.

However at the moment of the set-up of the database, the precise parameters influencing the overtopping phenomenon were not known. During the development process of the neural network, the network revealed which of the parameters included in the database were significant in characterising the overtopping phenomenon. This implies that not all parameters in the overtopping database are equally relevant for the neural network prediction method.

Ultimately three groups of parameters were defined: general parameters, structural parameters and hydraulic parameters. The general parameters are related to general information about the overtopping test, the structural parameters serve to describe the test structure and the hydraulic parameters are describing the wave characteristics and the measured overtopping.

Two possible approaches can be distinguished regarding the wave characteristics describing the overtopping phenomenon. In a first approach the measured overtopping is linked to the waves measured at the toe of the structure, just before they attack the structure. The second approach considers only the deep water wave characteristics to link to the overtopping discharge. In this last case, the slope of the foreshore is an additional influencing parameter.

Both approaches appear in literature, although the most recent overtopping formulae recommend to use the wave characteristics at the toe of the structure. As one of the goals of the overtopping database is to provide detailed information on existing overtopping measurements, and to leave open the possibility to use either the wave characteristics at deep water or at the toe of the structure, the wave characteristics at both locations are included in the database. Additionally a parameter describing the slope of the foreshore is introduced.

The ultimate number of parameters included in the final database is 31. The parameters are enumerated below by group, together with a brief description. More detailed information follows in sections 2.2.4 (hydraulic parameters), 2.2.5 (structural parameters) and 2.2.6 (general parameters).



- 3 general parameters:

“Name”, “RF” and “CF”

1	Name	This parameter assigns a unique name to each test.
2	RF [-]	The ‘Reliability Factor’ gives an indication of the reliability of the test. It can adopt the values 1, 2, 3 or 4.
3	CF [-]	This parameter, called the ‘Complexity Factor’ gives an indication of the complexity of the test structure. It can adopt the values 1, 2, 3 or 4.

- 11 hydraulic parameters:

“ $H_{m0 \text{ deep}}$ ”, “ $T_p \text{ deep}$ ”, “ $T_m \text{ deep}$ ”, “ $T_{m-1,0 \text{ deep}}$ ”, “ $\beta$ ”, “ $H_{m0 \text{ toe}}$ ”, “ $T_p \text{ toe}$ ”, “ $T_m \text{ toe}$ ”, “ $T_{m-1,0 \text{ toe}}$ ”, “ $q$ ” and “ $P_{ow}$ ”

1	$H_{m0 \text{ deep}}$ [m]	Significant wave height from spectral analysis = $4\sqrt{m_0}$ , determined at deep water
2	$T_p \text{ deep}$ [s]	Peak period from spectral analysis at deep water
3	$T_m \text{ deep}$ [s]	Mean period either from spectral analysis = $m_2/m_0$ or from time domain analysis (zero-downcrossing) at deep water
4	$T_{m-1,0 \text{ deep}}$ [s]	Mean period from spectral analysis at deep water = $m_{-1}/m_0$
5	$\beta$ [°]	Angle of wave attack relative to the normal on the structure
6	$H_{m0 \text{ toe}}$ [m]	Significant wave height from spectral analysis = $4\sqrt{m_0}$ at the toe of the structure
7	$T_p \text{ toe}$ [s]	Peak period from spectral analysis at the toe of the structure
8	$T_m \text{ toe}$ [s]	Mean period either from spectral analysis = $m_2/m_0$ or from time domain analysis (zero-downcrossing) at the toe of the structure

9	$T_{m-1,0 \text{ toe}}$ [s]	Mean period from spectral analysis at the toe of the structure = $m_1/m_0$
10	$q$ [ $m^3/s.m$ ]	Overtopping discharge (volume per second) per meter width
11	$P_{ow}$ [-]	Percentage of the waves resulting in overtopping

- 17 structural parameters:

“ $h_{deep}$ “, “ $m$ “, “ $h$ “, “ $h_t$ “, “ $B_t$ “, “ $\gamma_f$ “, “ $\cot\alpha_d$ “, “ $\cot\alpha_u$ “, “ $\cot\alpha_{excl}$ “, “ $\cot\alpha_{incl}$ “, “ $R_c$ “, “ $B$ “, “ $h_b$ “, “ $\tan\alpha_B$ “, “ $B_h$ “, “ $A_c$ “ and “ $G_c$ “

1	$h_{deep}$ [m]	Water depth at deep water
2	$m$ [-]	Slope of the foreshore
3	$h$ [m]	Water depth just seaward of the toe of the structure
4	$h_t$ [m]	Water depth on the toe of the structure
5	$B_t$ [m]	Width of the toe of the structure
6	$\gamma_f$ [-]	Roughness/permeability factor for the structure
7	$\cot\alpha_d$ [-]	Cotangent of the structure slope downward of the berm
8	$\cot\alpha_u$ [-]	Cotangent of the structure slope upward of the berm
9	$\cot\alpha_{excl}$ [-]	Mean cotangent of the structure slope, without contribution of the berm
10	$\cot\alpha_{incl}$ [-]	Mean cotangent of the structure slope, with contribution of the berm
11	$R_c$ [m]	Crest freeboard of the structure
12	$B$ [m]	Width of the berm
13	$h_b$ [m]	Water depth on the berm
14	$\tan\alpha_B$ [-]	Tangent of the slope of the berm
15	$B_h$ [m]	Width of the horizontally schematised berm
16	$A_c$ [m]	Armour crest freeboard of the structure
17	$G_c$ [m]	Width of the structure crest

### 2.2.4 Determination of the hydraulic parameters

The wave characteristics and the measured overtopping are described by means of 11 hydraulic parameters, which are mentioned in the previous section.

Often several of these parameters were not available in the corresponding report of the test, simply because they were not measured or at least not written down during performing the test. In this context the following cases could be distinguished:

- only deep water wave characteristics were available, wave characteristics at the toe of the structure were missing
- only wave characteristics at the toe of the structure were available, deep water wave characteristics were missing
- only time domain analysis was performed to determine the wave characteristics
- only one or two of the three spectral wave periods at deep or shallow water were available
- the percentage of waves resulting in overtopping  $P_{ow}$  [-] was not measured

With the aim of obtaining an as complete database as possible, it was tried to find an acceptable value for these missing parameters where possible. Well-founded assumptions based on previous research and extra calculations were used to do this. Following sections describe these in detail. However, in some cases it was simply not possible to estimate missing hydraulic parameters accurately. Preference was given to leave the value of the missing parameter blank in the database in these cases. An example here concerns the value of  $P_{ow}$  [-], i.e. the percentage of waves overtopping. In most cases the percentage of waves overtopping was not measured during testing. As this parameter represents an overtopping result, additional to the mean overtopping discharge, it can not be estimated if not measured, leading to a blank value in the database if not available. Other cases leading to blank values in the database are treated in section 2.2.4.2.

The described calculations and estimations in sections 2.2.4.1 to 2.2.4.3 all led to approximate values for some of the wave characteristics. As this consequently had an influence on the reliability of the values, this fact was incorporated in the database by adapting the value of the reliability factor RF. If any calculations or estimations were needed, a minimum value of 2 was assigned to the factor RF. What exactly the value of RF stands for and how exactly the

influence of calculations and estimations was included, is explained in section 2.2.6.3 in detail.

To distinguish calculated/estimated parameters from measured parameters in the database, estimated/calculated values are marked with specific colours in the database, depending on the type of calculation/estimation. More information on this is given in section 2.2.7.

#### **2.2.4.1 Calculation of incident wave characteristics from given deep water wave characteristics and foreshore**

For a part of the gathered overtopping tests, wave characteristics were only available at deep water, wave characteristics at the toe of the structure were missing.

In these cases numerical simulations with the SWAN model were made: starting from the deep water wave characteristics and the present foreshore, the wave characteristics at the toe of the structure were calculated.

The version of SWAN which was used in this study is SWAN Cycle III version 40.11 (last revision October 19, 2000). The one-dimensional version of SWAN is used.

#### **2.2.4.2 Estimation of characteristic wave parameters in relatively deep water**

If characteristic wave parameters were missing, commonly used fixed relationships between wave parameters are used to approximate them.

As for double peaked or bi-model spectra, the value of the peak period  $T_p$  is irrelevant, corresponding overtopping tests have no value for  $T_p$ . In these cases the value of  $T_p$  is left blank in the database.

During part of the overtopping tests the wave characteristics were only measured at the toe of the structure and not in deep water. In case of relatively deep water at the toe of the structure, it was assumed that wave characteristics in deep water were the same as at the toe. When the water depth at the toe was rather shallow on the contrary, wave breaking was likely to appear, implicating that the spectral shape of the wave characteristics probably changed drastically compared to at deep water. In these cases the deep water wave characteristics ( $H_{m0 \text{ deep}}$ ,  $T_{p \text{ deep}}$ ,  $T_{m \text{ deep}}$  and  $T_{m-1,0 \text{ deep}}$ ) were also left blank in the database.

### 2.2.4.3 Determination of $H_{m0\ toe}$ from $H_{s\ toe}$ in shallow water depths

As wave height distributions in shallow water deviate from those in deep water due to the effects of the restricted depth-to-height ratio, the Rayleigh distribution is no longer valid and the known relationships between deep water wave heights can no longer be used.

In case of overtopping tests with rather shallow water depth at the toe of the structure the method of Battjes and Groenendijk (2000) can be used to determine the value of  $H_{m0\ toe}$  starting from  $H_{s\ toe}$ .

The input parameters for the point model are the given value  $H_{1/3\ toe}$ , the slope of the foreshore 1:m and the water depth  $h$  at the toe of the structure, leading to the corresponding value of  $H_{m0\ toe}$ .

This method allows us to determine a good approximation of the significant wave height at the toe of the structure in case of shallow water depths, on condition that the foreshore slope can be approximated by a uniform slope 1:m.

Table 3.7 (section 2.2.6.3) describes in detail how the value of the reliability factor RF was determined if calculations according to Battjes and Groenendijk (2000) were made.

### 2.2.5 *Determination of the structural parameters*

The starting-point for the determination of the structural parameters was the fact that as much overtopping structures as possible had to be schematised by these and only these parameters. Studying a lot of different overtopping sections, this finally led to the 17 structural parameters as described in section 2.2.3.

In this section, a detailed description is given of the methodology which was followed for determining these 17 parameters for all included overtopping tests in the database. As some values of parameters are approximations of the real situation, it is very important for the user of database to know exactly what value of which parameter stands for what structure part.

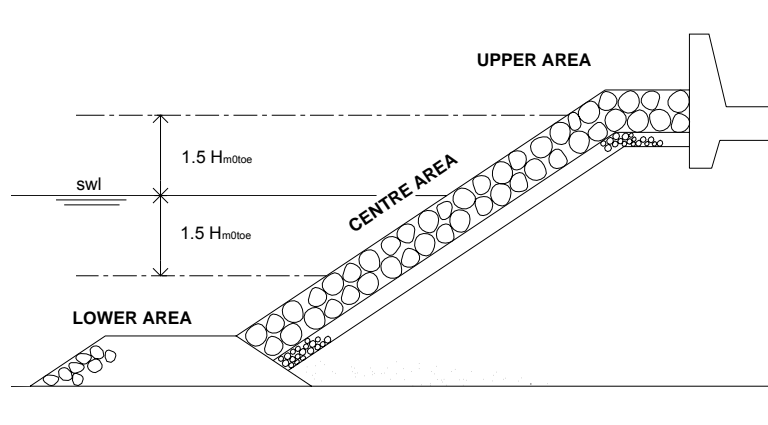
### 2.2.5.1 General schematisation of the structure in three areas

The first schematisation step of each overtopping structure consists of splitting up the structure into three main parts. The starting point here are the waves which attack the structure, as it is important to schematise the structures in the way the attacking waves ‘feel’ the structure. This implies that a geometrically identical structure can have a different schematisation depending on the water level and the attacking waves.

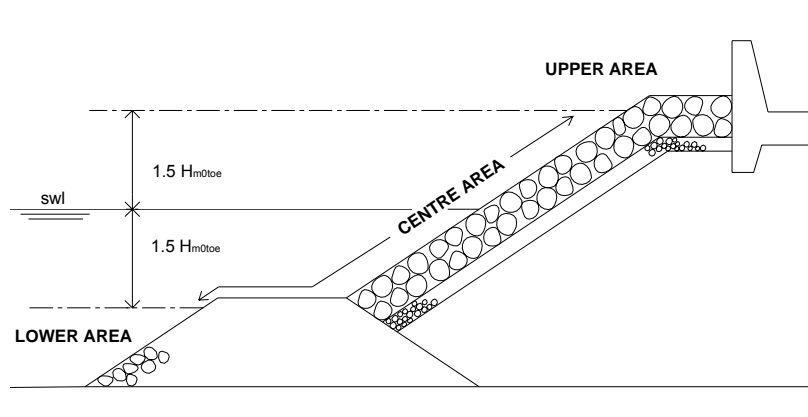
It is logical that the structure part around the swl is very important for the waves. According to the size of the waves, this area will be larger or smaller. Referring to Van der Meer et. al. (1998), the governing part of the structure where the wave action is concentrated on, is defined as the part between  $1.5H_{m0toe}$  above and  $1.5H_{m0toe}$  below the water line.

The area marked off by the value of  $1.5H_{m0toe}$  above and  $1.5H_{m0toe}$  below swl will be called the ‘**centre area**’ of the structure. The area below the centre area is called then the ‘**lower area**’ of the structure and the area above the centre area is called the ‘**upper area**’ of the structure. Depending on the wave height and the water level, the upper or lower area may be lacking.

Fig. 2 gives an example of the structure parts of a rubble mound structure. As can be seen in the example in Fig. 2, depending on the wave height and the water depth near the structure, the centre area can extend the structure slope only (a), but it can e.g. also enclose part of the toe structure (b). Logically lots of other possibilities can occur.



(a)



(b)

**Figure 2: Main structure parts of rubble mound structure**

### 2.2.5.2 Berm, toe and crest of a structure

Looking at structure sections of coastal structures in general (although in the context of this overtopping study), one can often distinguish:

- a structure body (consisting of a vertical wall, a sloping part or a combination of both), possibly containing a structure berm,
- a structure toe (meant to structurally protect the lower part of the structure), and
- a structure crest (often with a strengthening function for the upper part of the structure).

For the schematisation of a structure section, it was needed to clearly distinguish these three structure parts. In a lot of cases this distinction was quite straight forward. However in some

cases confusion could arise. This section examines in detail how the distinction between a berm, a toe and a crest was performed in the context of the set-up of the overtopping database. Fig. 3 to 6 are illustrations of this. The figures are discussed further in the text one for one.

It was defined that a structure berm is most likely situated in the centre area of the structure (= area between  $1.5H_{m0\ toe}$  above and  $1.5H_{m0\ toe}$  below swl, see previous section). If the ‘berm’ (‘berm’ refers here to the name assigned to it in the corresponding report) is situated lower, it is more likely to be felt by the waves as a toe. If the ‘berm’ is situated higher, it is more likely to be felt as a crest. In connection with the position of the berm, a toe is defined as most likely to appear in the lower area of the structure (= lower than  $1.5H_{m0\ toe}$  below swl) and a crest in the upper area of the structure (= higher than  $1.5H_{m0\ toe}$  above swl).

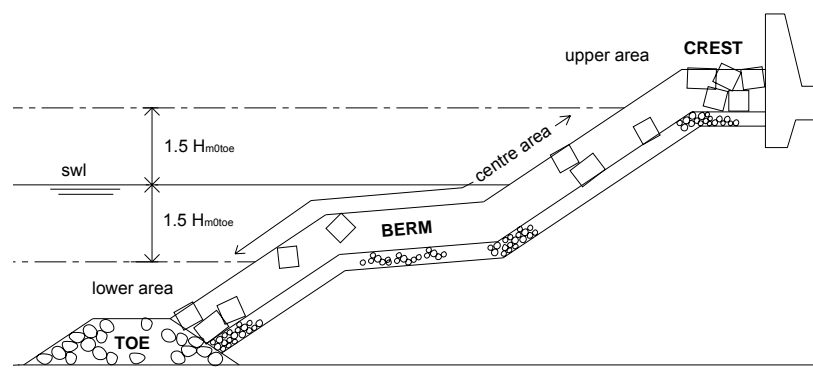
Consequently it may happen that what is called a ‘berm’ in the original report, is called a ‘toe’ or ‘crest’ for the database, although the above described levels of toe, berm and crest are not totally binding, i.e.:

- tests with very small values of  $H_{m0\ toe}$ , leading to a very restricted centre area, are often schematised with a berm which is not situated in the centre area of the structure
- structure types with quite large toes, situated in relatively shallow water, can be schematised with a toe situated in the centre area of the structure
- low crested structures of which the upper point of the structure has a level within  $1.5H_{m0\ toe}$  above swl, are schematised with a crest situated in the centre area of the structure.

Above mentioned examples can be referred to as structures which do not fulfil the most likely position of a berm.

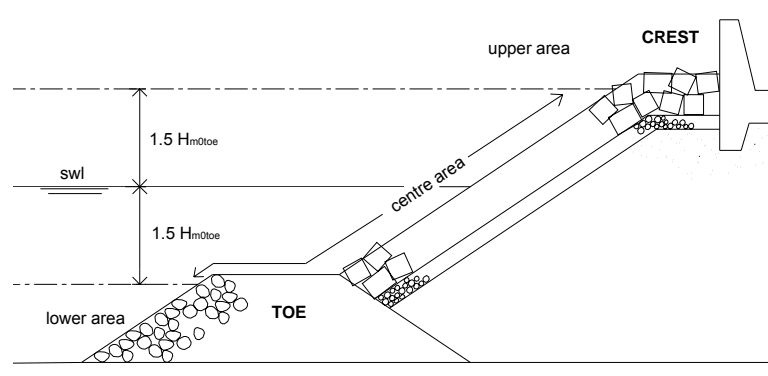
In Fig. 3 a typical rubble mound structure is shown. The centre area, defined by the value of the wave height  $H_{m0\ toe}$ , contains a slightly sloping berm. The crest is situated in the upper area, the toe is situated in the lower area. This example corresponds with the most common position of the mentioned three structure parts.





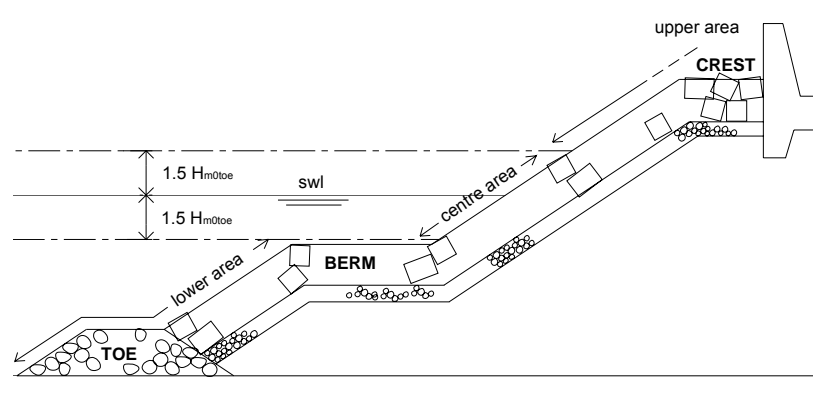
**Figure 3: Typical position of berm, crest and toe**

Fig. 4 gives an example of a structure with a high situated toe. The different structure materials contribute to the preference of schematising the lower part of the structure here as a large toe and not a berm.



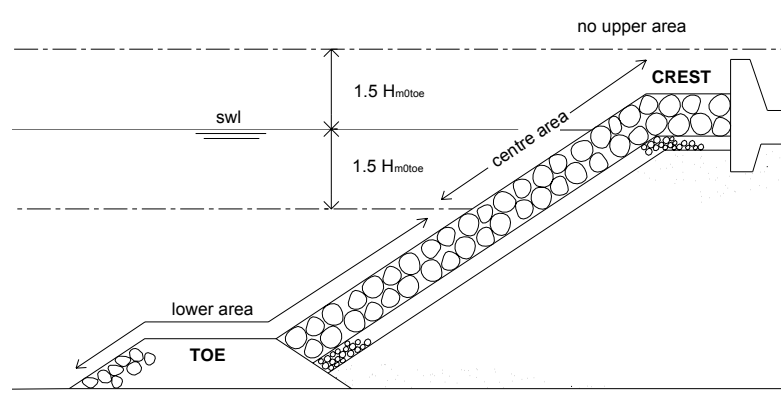
**Figure 4: Structure type with large toe**

Fig. 5 shows a structure for which the small value of  $H_{m0\text{ toe}}$ , leads to a situation in which the berm is situated in the lower part of the structure. It is quite logic in this case that it concerns a berm here and not a toe.



**Figure 5: Structure type with low situated berm**

In Fig. 6 at last an example is given of a structure with a low situated crest. Because of the high water level, the entire structure is situated lower than the  $1.5H_{m0\text{ toe}}$ -line above swl.



**Figure 6: Structure type with low situated crest**

It may be clear that it is not always straight-forward how to schematise a horizontal or slightly sloping part of a structure. In some cases more than one schematisation possibility exists.

Additional to the levels of the berm, crest and toe of a structure, some restrictions regarding the slope and the length of a berm are made in the schematisation for the database.

### 2.2.5.3 Determination of structural parameters

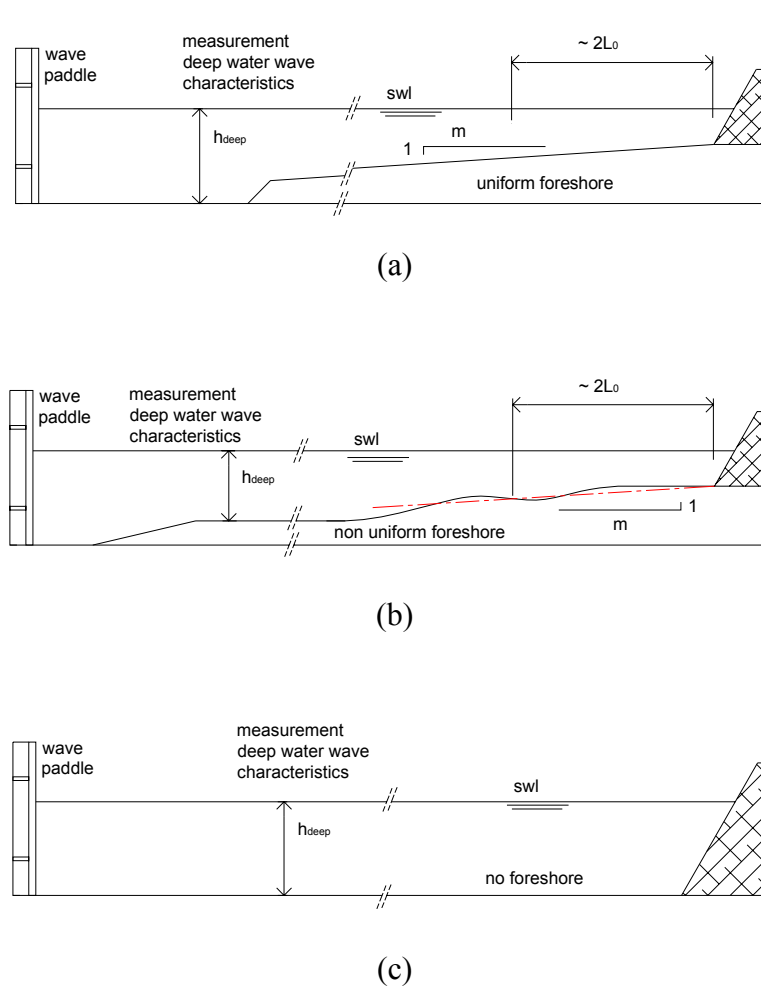
This section explains how to determine the schematisation parameters for a rather easy-to-schematise overtopping structure. In section 3.6.5 the schematisation of more complex sections is treated.

The 17 schematisation parameters are subsequently enumerated below with a detailed explanation how to determine them.

#### 2.2.5.3.1 Water depth at deep(er) water: $h_{\text{deep}}$ [m]

This is the water depth at deep(er) water. At this water depth the deep wave characteristics  $H_{m0\text{ deep}}$ ,  $T_{p\text{ deep}}$ ,  $T_{m\text{ deep}}$  and  $T_{m-1,0\text{ deep}}$  are present. This definition indicates that for laboratory tests,  $h_{\text{deep}}$  is not necessarily the deepest water depth which appears in the flume or basin. Depending on the location of the wave gauges, the value of  $h_{\text{deep}}$  is situated between the water depth at the toe of the structure and the deepest water depth in the flume. In Fig. 7 some

possibilities of measurement locations of  $h_{\text{deep}}$  are given. In the first graph (a), the deep water depth corresponds to the water depth in front of the wave paddle of the flume. In graph (b) an intermediate water depth is taken as the value for  $h_{\text{deep}}$  and finally graph (c) considers the special case in which no foreshore is present, resulting in a water depth  $h_{\text{deep}}$  equal to the water depth just in front of the structure.



**Figure 7: Determination of  $h_{\text{deep}}$  [m] and  $m$  [-]**

#### 2.2.5.3.2 Slope of the foreshore: $m$ [-]

The slope of the foreshore is described by the parameter  $m$  [-] by means of 1 (unit measured vertically) :  $m$  (units measured horizontally). If no uniform sloping foreshore exists, one has to approximate the value of  $m$ . A relevant approximation consists of the mean value of  $m$  over a horizontal distance of about 2 wave lengths  $L_{0p}$  in front of the structure. The restriction of the approximation to the foreshore just in front of the structure can be justified as this part is qualifying for the incident wave characteristics.

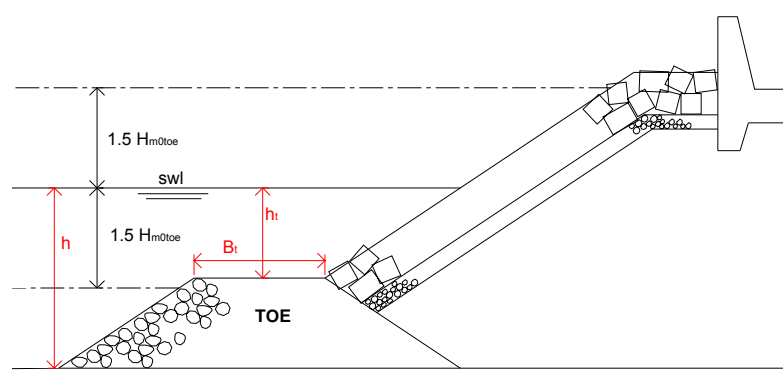
In Fig. 7 the values of  $m$  are indicated. Graph (c) is a special case with a flat bottom of the flume. Theoretically the value of  $m$  should be equal to infinite in such cases, but as a real, finite value is more workable, a value of 1000 was given to  $m$  in the database in these cases.

#### 2.2.5.3.3 Waterdepth in front of the toe: $h$ [m]

The value of  $h$  [m] refers to the water depth just seaward of the toe of the structure (Fig. 8). It is often referred to as the water depth ‘at the toe of the structure’. In case of a flat flume bottom, the value of  $h$  is equal to the value of  $h_{\text{deep}}$ .

#### 2.2.5.3.4 Toe paramers: $h_t$ [m], $B_t$ [m]

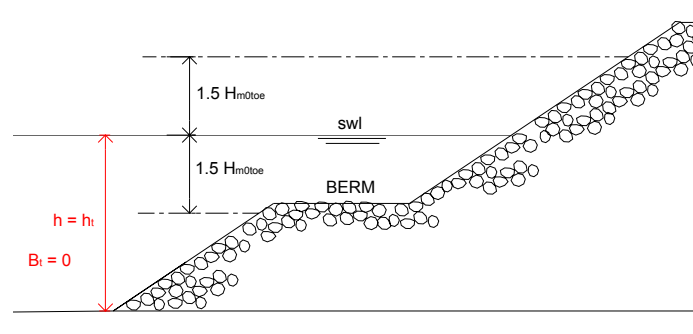
These are the water depth on the toe respectively the width of the toe. The value of  $h_t$  [m] is measured in the middle of the toe. The value of  $B_t$  [m] is measured on top of the toe. This is illustrated in Fig. 8.



**Figure 8: Determination of  $h$  [m] ,  $h_t$  [m] and  $B_t$  [m]**

It has to be mentioned that the front slope of the toe is not included in the database, because it seems a less important parameter in view of the overall low position of the toe regarding to the water level. Moreover the front slope of a structure toe is in most cases  $\approx 1:2$ . An extra restriction for the definition of a toe could therefore be that the slope should be  $\approx 1:2$ .

If the structure has no toe, the value of the water depth on the toe  $h_t$  equals the value of the water depth at the toe of the structure  $h$ . In this case the width of the toe  $B_t$  is equal to zero, e.g. Fig. 9.



**Figure 9: Determination of  $h$  [m] ,  $h_t$  [m] and  $B_t$  [m] in case of no toe**

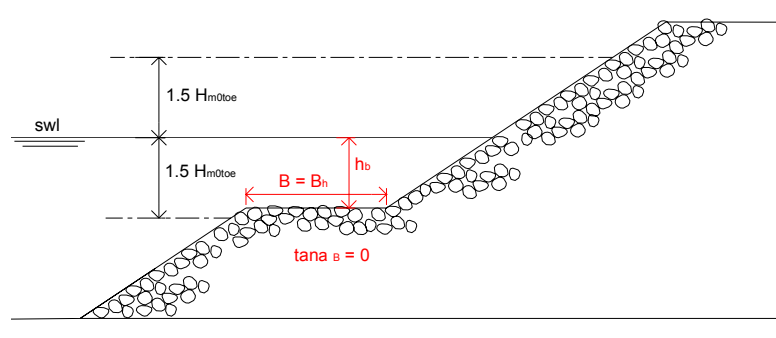
#### 2.2.5.3.5 Berm parameters $B$ [m], $h_b$ [m], $\tan\alpha_B$ [-], $B_h$ [m]

These four parameters describe the berm of an overtopping structure (Fig.10). The value of  $B$  [m] represents the berm width and is measured horizontally.  $h_b$  [m] is the water depth on the berm, measured in the middle of the berm. If the berm is situated above swl, the value of  $h_b$  is negative.

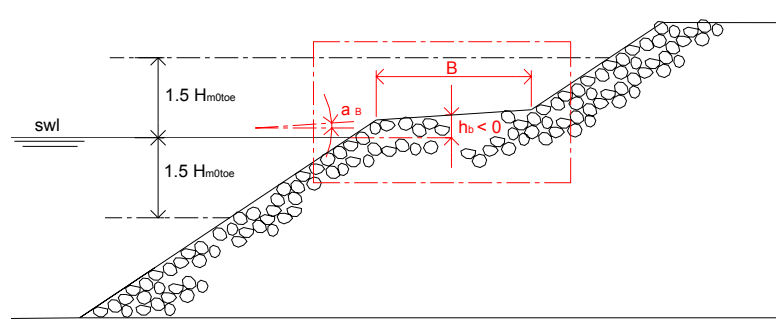
$\tan\alpha_B$  [-] is the tangent of the slope of the berm. If the berm is horizontal,  $\tan\alpha_B = 0$ .

The value of  $B_h$  [m] refers to the width of the horizontally schematised berm. In case of a horizontal berm (i.e.  $\tan\alpha_B = 0$ ) the value of  $B_h = B$ , but for a sloping berm,  $B_h < B$ . The value of  $B_h$  can be obtained by extending the upper and lower slope of the structure up to the level of the middle point of the berm. By connecting these two points, the horizontal schematisation of the berm is obtained.

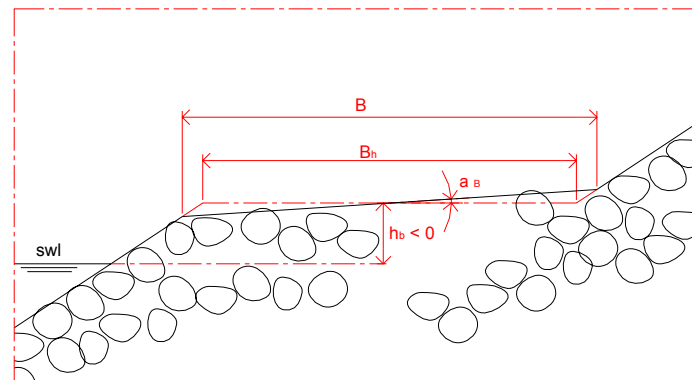
Fig. 10 (c) consists of the enlarged box of Fig. 10 (b), explaining the difference between  $B_h$  and  $B$ .



(a)



(b)



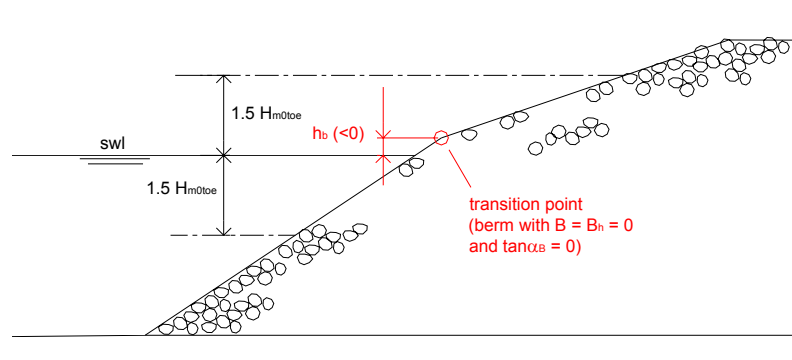
(c)

**Figure 10: Determination of  $B$  [m],  $B_h$  [m],  $\tan \alpha_B$  [-],  $h_b$  [m]**

If the structure has no berm, the values of  $B$ ,  $B_h$ ,  $\tan \alpha_B$ ,  $h_b$  are all equal to zero, except in case of a composite slope.

In case of a composite slope,  $h_b$  is defined as the transition depth between two successive slopes. Although no berm is present in this case, the value of  $h_b$  is different from zero. Defining  $h_b$  as the transition depth between two successive slopes, amounts to defining a berm

at this location with a berm width and slope equal to zero (Fig. 11). How the slopes of the composite slope are schematised is described in section 2.6.3.7.



**Figure 11: Determination of the transition depth  $h_b$  [m] in case of a composite slope**

#### 2.2.5.3.6 Crest parameters: $R_c$ [m], $A_c$ [m], $G_c$ [m]

These parameters describe the upper part of an overtopping structure (Fig. 12).

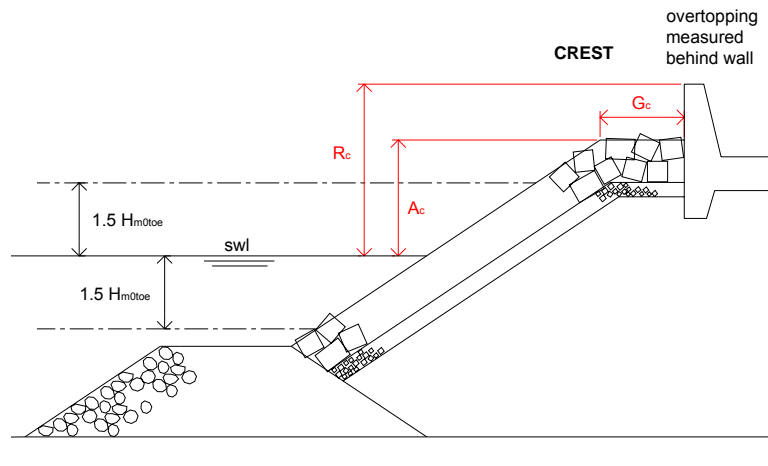
$R_c$  [m] is the crest freeboard of the structure. It is the distance, measured vertically, from swl to the point of the structure where overtopping is measured. This is not always the highest point of the structure, e.g. Fig. 12 (c).

$A_c$  [m] is called the armour crest freeboard of the structure. In case of armoured structures it is the distance, measured vertically from swl to the upper limit of the armour layer. In case of structures without armour, e.g. vertical structures or smooth slopes,  $A_c$  may be used together with  $R_c$  and  $G_c$ , to describe the crest of the structure more detailed, e.g. Fig. 12 (e).

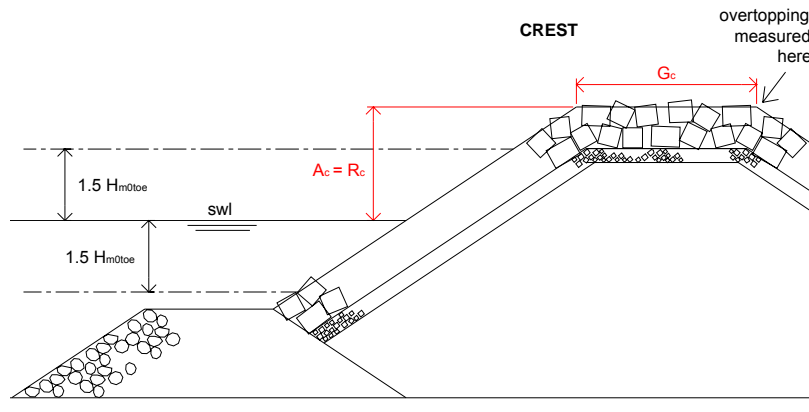
In a lot of cases,  $A_c = R_c$ .

$G_c$  [m] represents the crest width.

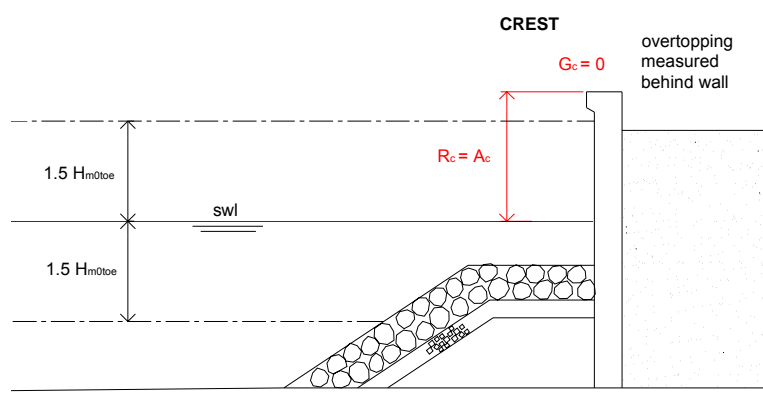
Fig. 12 gives several examples of crest structures with an indication of the corresponding parameters. As can be seen on the different figures,  $R_c$  can adopt a value larger, smaller or equal to  $A_c$ .



(a)



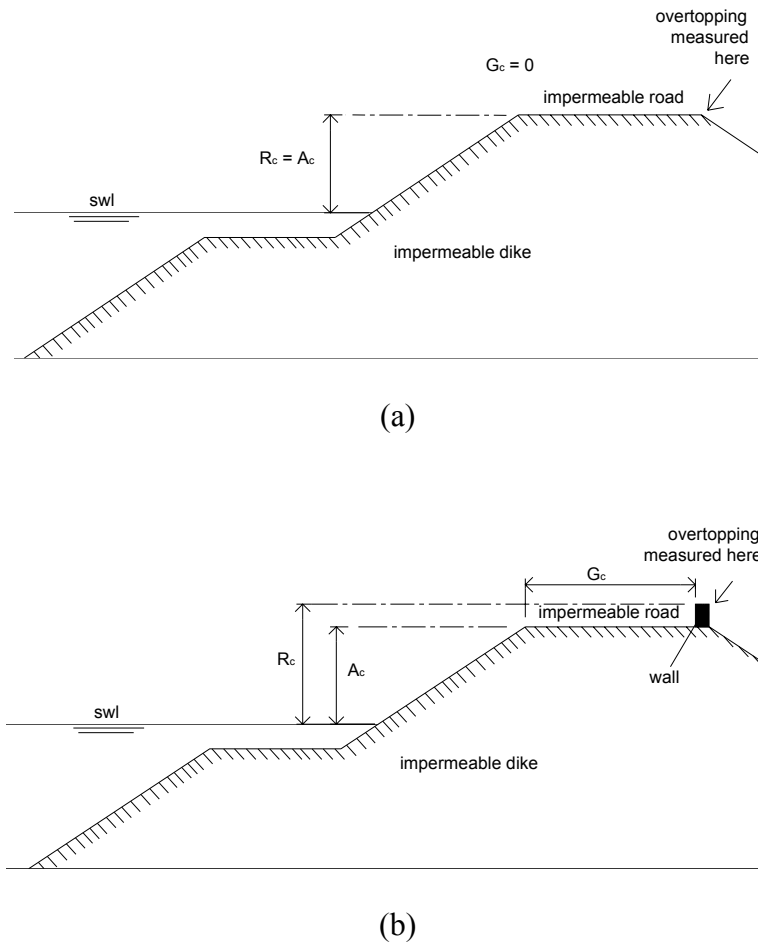
(b)



(c)







**Figure 13: Determination of  $G_c$  [m]**

#### 2.2.5.3.7 Slope parameters: $\cot\alpha_d$ [-], $\cot\alpha_u$ [-], $\cot\alpha_{\text{excl}}$ [-], $\cot\alpha_{\text{incl}}$ [-]

These parameters describe the slope(s) of the overtopping structure (figure 3.16 to 3.20). It has to be stressed that the toe and the crest of the structure are not included in these four slope parameters, as these are already described by separate parameters.

The four parameters provide three ways to describe the overtopping structure:

- with  $\cot\alpha_d$  and  $\cot\alpha_u$  or
- with  $\cot\alpha_{\text{excl}}$  or
- with  $\cot\alpha_{\text{incl}}$

The advantage of using two parameters to describe the structure slope is that in case of several sloping parts a more detailed schematisation of the structure can be made.

$\text{Cot}\alpha_d$  [-] and  $\text{cot}\alpha_u$  [-] are the cotangents of the mean slopes in the centre area of the structure below ( $\text{cot}\alpha_{\text{down}}$ ) and above ( $\text{cot}\alpha_{\text{up}}$ ) the berm respectively.

$\text{Cot}\alpha_{\text{excl}}$  [-] and  $\text{cot}\alpha_{\text{incl}}$  [-] are calculated ‘average’ slopes.  $\text{Cot}\alpha_{\text{incl}}$  is the average slope where the berm (if it is located in the centre area of the structure) is included in this average value ( $\text{cot}\alpha_{\text{inclusive berm}}$ ).  $\text{Cot}\alpha_{\text{excl}}$  is the average slope where the present berm is not taken into account ( $\text{cot}\alpha_{\text{exclusive berm}}$ ). If a structure has no berm,  $\text{cot}\alpha_{\text{incl}} = \text{cot}\alpha_{\text{excl}}$ .

It can be mentioned that the slope angles are presented here by means of their cotangent instead of their tangent (which was used for the slope of the berm). The reason for that is that the structure slopes can adopt values up to and even larger than  $90^\circ$  (see section 2.2.5.4 for this last case). A value of  $90^\circ$  results in a zero value of the cotangent of the slope (instead of an infinite value for the tangent of the slope), a value larger than  $90^\circ$  results in a negative value of the cotangent of the slope (instead of a positive value of the tangent of the slope, indistinguishable from the tangent of a slope of  $90^\circ - \alpha$ ). The other way round, the cotangent of a horizontal berm results in an infinite value, explaining the use of the tangent for the berm.

How the four slope parameters exactly are determined, is explained below (Fig. 14 and 15).

The upper slope of the structure  $\alpha_u$  is the slope upward the berm. It is determined by taking the point of the structure at a level of  $1.5H_{m0 \text{ toe}}$  above swl and connecting it with the leeside endpoint of the berm. If the crest of the structure is situated in the centre area of the structure (this implies that the crest is situated less than  $1.5H_{m0 \text{ toe}}$  above swl), then the starting point of the crest has to be used instead of the point at level  $1.5H_{m0 \text{ toe}}$  above swl to determine  $\alpha_u$ .

The lower slope of the structure  $\alpha_d$  is the slope downward the berm. It is determined by taking the point of the structure at a level of  $1.5H_{m0 \text{ toe}}$  below swl and connecting it with the seaside endpoint of the berm. If the toe of the structure is situated in the centre area of the structure (this implies that the toe is situated less than  $1.5H_{m0 \text{ toe}}$  below swl), then the starting point of the toe has to be used instead of the point at level  $1.5H_{m0 \text{ toe}}$  below swl to determine  $\alpha_d$ .

The average slope  $\alpha_{\text{incl}}$  is determined by taking the point on the upper slope at a level of  $1.5H_{m0 \text{ toe}}$  above swl and connecting it with the point on the lower slope at a level of  $1.5H_{m0 \text{ toe}}$  below swl. The subscript ‘incl’ refers to the fact that if there is a berm, it is included into the value of  $\text{cot}\alpha_{\text{incl}}$ . Also here applies that, if the toe and/or the crest of the structure are situated into the centre area, the lowest and/or the highest point which determine  $\text{cot}\alpha_{\text{incl}}$  are

determined by the nearest point of the toe (instead of by  $swl - 1.5 \cdot H_{m0\ toe}$ ) and/or the nearest point of the crest (instead of by  $swl + 1.5 \cdot H_{m0\ toe}$ ).

The average slope  $\alpha_{excl}$  is determined by subtracting the horizontal width of the berm  $B_h$  from the horizontal distance between the two points which determine  $\alpha_{incl}$  and dividing this value by the vertical distance between the two points which determine  $\alpha_{incl}$ .

In Fig. 14 the four slope angles are indicated, in graph (a) for a simple rubble mound structure without berm, in graph (b) for a rubble mound structure with a horizontal berm and in graph (c) for a rubble mound structure with a sloping berm.

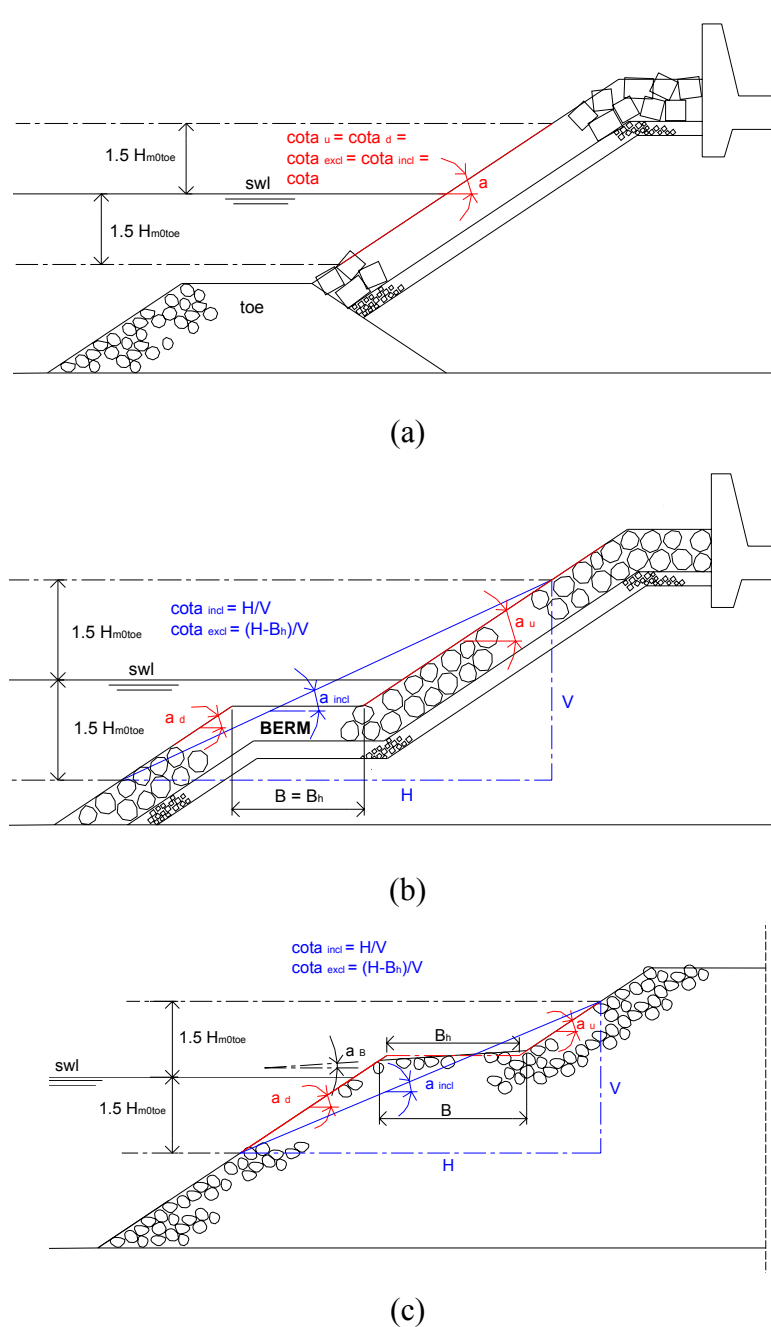
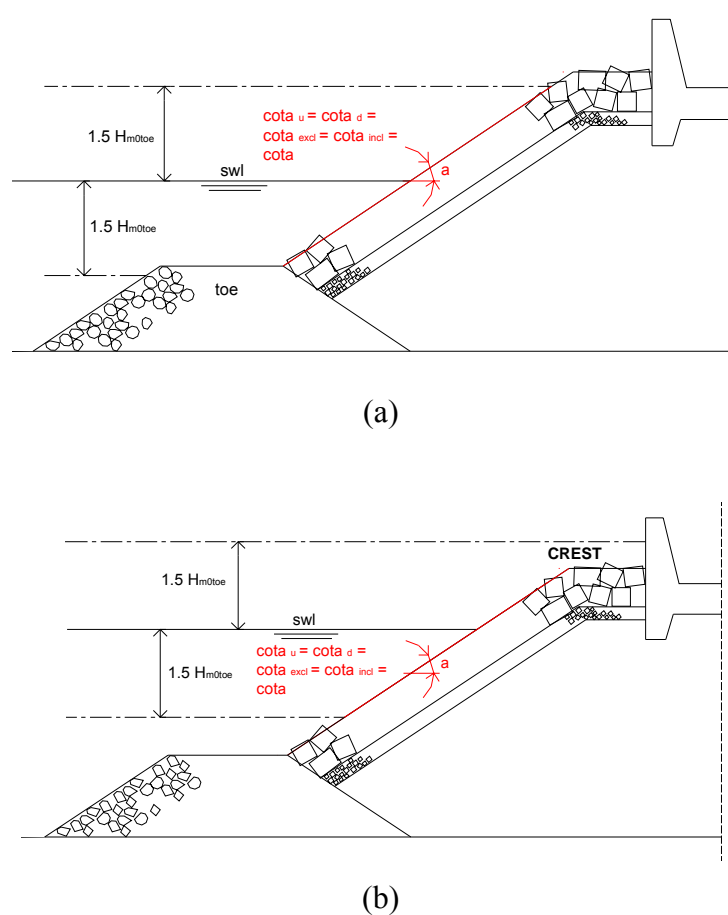


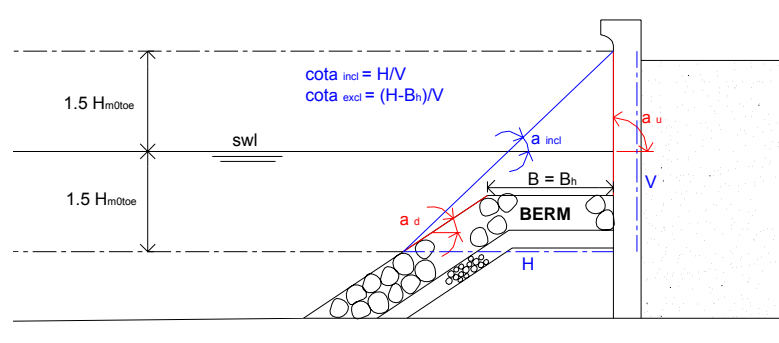
Figure 14: Determination of the structures slope parameters

In Fig. 15 two extra examples regarding the determination of the structure slope parameters are given. In graph (a) the toe is situated in the centre area of the structure. As can be seen on the figure the starting point of the toe is used to determine  $\alpha_d$  instead of the point at level  $1.5H_{m0\text{ toe}}$  below swl. In graph (b) the crest is situated in the centre area of the structure. Analogous the starting point of the crest is used to determine  $\alpha_u$  here instead of the point at level  $1.5H_{m0\text{ toe}}$  above swl.



**Figure 15: Determination of the structures slope parameters, extra examples**

As mentioned already, the use of the two parameters  $\cot\alpha_u$  and  $\cot\alpha_d$  allows a better schematisation than the use of only one of the average slope  $\cot\alpha_{excl}$  or  $\cot\alpha_{incl}$ . An example of a structure type for which the use of an average slope leads to a bad schematisation is given in Fig. 16.

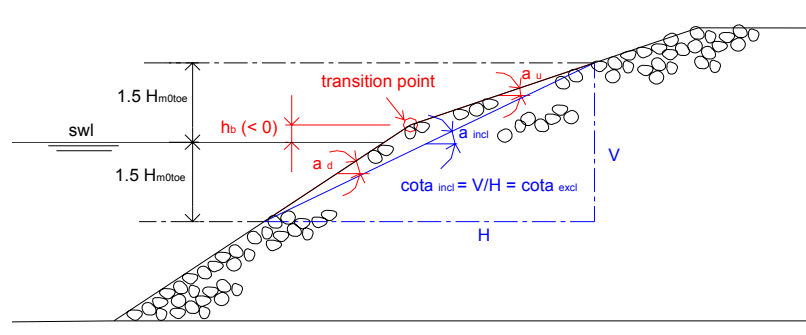


**Figure 16: Structure type for which at least two slope parameters are requested**

The use of the two slope parameters  $\cot\alpha_u$  and  $\cot\alpha_d$  also allows to schematise composite slopes (structures consisting of subsequent different slopes without a horizontal part in between) very well. As mentioned in section 2.2.5.3.5 the position of the transition point is indicated by  $h_b$ . The slope upward respectively downward the transition point is defined now by  $\cot\alpha_u$  and  $\cot\alpha_d$ .

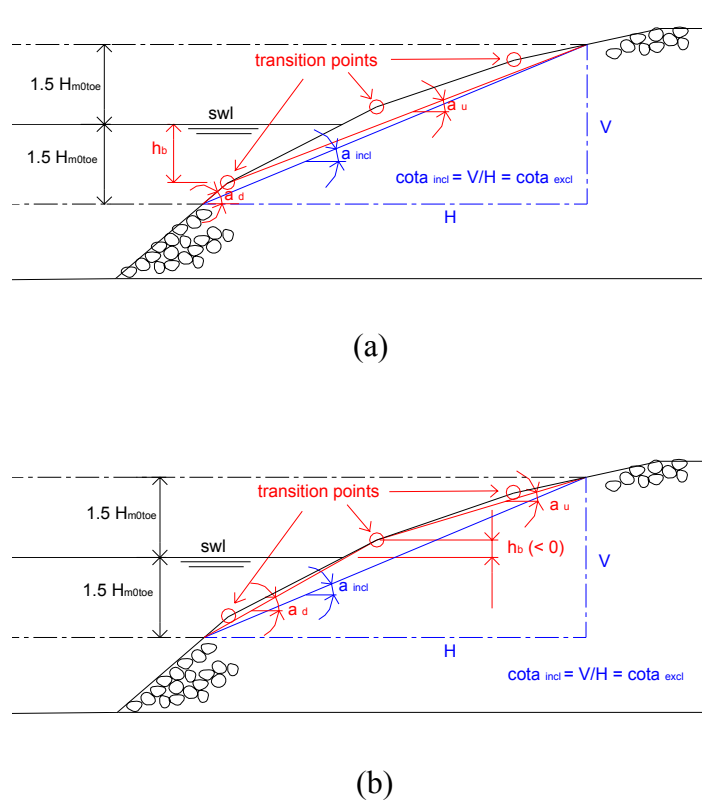
For composite slopes composed of more than two subsequent different structure slopes (and consequently more than one transition point), a rougher schematisation is needed, even with two parameters  $\cot\alpha_d$  and  $\cot\alpha_u$ .

Fig. 17 shows a composite slope with only one transition point. By using  $\cot\alpha_d$  and  $\cot\alpha_u$ , the structure is schematised very well.



**Figure 17: Schematisation of a composite slope composed of 2 subsequent slopes**

Fig. 18 shows a composite slope consisting of more than 2 subsequent slopes. Graph (a) and (b) give two possible schematisations, determined by the choice of the transition depth  $h_b$ . As can be seen on the figures, the schematisation in graph (b) fits the structure best.



**Figure 18: Schematisation of a composite slope composed of more than 2 subsequent slopes**

#### 2.2.5.3.8 Roughness factor: $\gamma_f$ [-]

The parameter  $\gamma_f$  [-] gives an indication of the roughness and the permeability of the structure. The rougher and more permeable a structure, the lower the overtopping will be as more energy is dissipated. Values for  $\gamma_f$  for several revetment types are presented by TAW (2002), resulting from new research with irregular waves, also on large scale, from 1974 up to 2002. TAW (2002) prescribes a value of 1 for  $\gamma_f$  in case of an impermeable smooth structure, and a value of 0.7 respectively 0.55 in case of a rubble mound structure with 1 respectively 2 layers of rock.

As already mentioned, extensive research was performed within the CLASH project to the roughness and permeability of different armour layers of rubble mound structures, especially with the aim of providing new information on the  $\gamma_f$  - value of these armour types for the set-up of the overtopping database (see Pearson et al., 2004b). Within this study, 426 new tests were performed on 10 types of armour layers, for each armour block starting from an identical hydrodynamic stability. Mean overtopping discharges on these structures were studied, together with the results of overtopping tests performed in 1999 (see Franco et al., 1999).

This study resulted in slightly adapted  $\gamma_f$ -values for rock slopes, and additionally, in new  $\gamma_f$ -values for several concrete armour units. Table 1 gives a summary of the obtained  $\gamma_f$ -values for the tested armour layers (see Pearson et al., 2004b).

**Table 1: New derived values for  $\gamma_f$   
(see Pearson et al., 2004b)**

<b>Type of armour layer</b>	<b><math>\gamma_f</math></b>
Smooth impermeable surface	1.00
Rock (1 layer, impermeable core)	0.60
Rock (1 layer, permeable core)	0.45
Rock (2 layers, impermeable core)	0.55
Rock (2 layers, permeable core)	0.40
Cubes (1 layer, smooth positioning, 30% porosity)	0.50
Cubes (2 layers, random positioning)	0.47
Antifers	0.47
HARO's	0.47
Accropods	0.46
X-blocks	0.45
Core-locs	0.44
Tetrapods	0.38

It can be remarked that this research resulted in a remarkably lower value of  $\gamma_f$  for a 2 layered rock slope (with permeable core): 0.40 instead of 0.55. An armour layer consisting of 2 layers of cubes or antifers performs somewhat worse than a 2 layered rock slope:  $\gamma_f = 0.47$  instead of 0.40. Tetrapods, with a  $\gamma_f$ -value of 0.38, seem to be the best armour blocks regarding roughness and permeability.

Additionally to table 1, values of  $\gamma_f$  for other types of armour layers were estimated, based on included data in the database. Table 2 gives an overall view of estimated values of  $\gamma_f$ . This



table is not supported by extensive research and has to be considered therefore as a provisional table.

**Table 2: Estimated values for  $\gamma_f$  based on included overtopping tests**

Type of armour layer	$\gamma_f$
SHEDS	0.55
Seabeas	0.50
Berm breakwater (reshaping)	0.40
Dolosse	0.43
Icelandic berm breakwater (not reshaping)	0.35

More types of armour units are present in the database than mentioned above. Some armour layers consist of very specific armour blocks which are not mentioned here, others consist of impermeable coverings with an energy-dissipating layout, e.g. stepped slopes. For these types of armour layers, a well-considered estimation of the roughness/permeability factor  $\gamma_f$  was made.

For composite structures such as vertical walls with a rubble mound protection, often kind of ‘average’ had to be determined for  $\gamma_f$ .

As the influence of the roughness/permeability of the part of the structure, which is situated below SWL, is found to be low (see TAW, 2002), the value of  $\gamma_f$  was determined only by the structure part situated above swl. This implies that in case of a vertical wall with a rubble mound protection situated entirely below SWL, a value of  $\gamma_f = 1$  was assigned to the structure. In case two different roughnesses/permeabilities appeared above SWL, a weighed average (considering the vertical distance) was taken for the  $\gamma_f$ -value over the height of  $1.5H_{m0\ toe}$  above SWL, taking into account the width of the eventually present berm (i.e. horizontal distance).

To distinguish estimated values of  $\gamma_f$  from the derived values of  $\gamma_f$  from model tests (table 1), all estimated values of  $\gamma_f$  are marked in the database in red colour, see section 2.2.7.

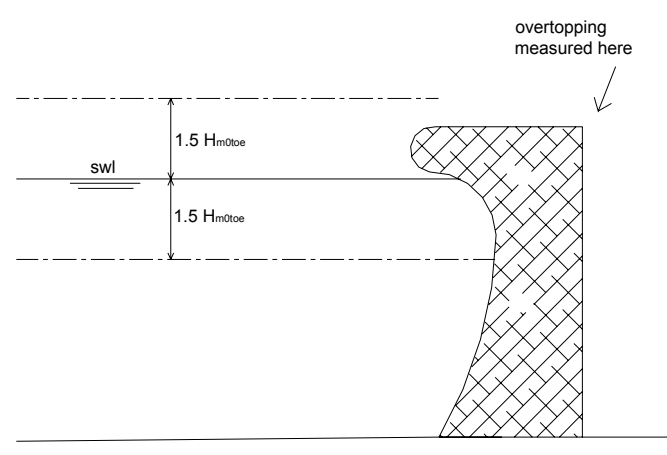
It has to be remarked here that the recent values for  $\gamma_f$  as mentioned in table 1 and 2 were only determined in the latest stage of the CLASH project. The developed neural network within CLASH (see Pozueta et al., 2004a), makes use of older values of  $\gamma_f$ , which are slightly different from the ones in table 3.4 and 3.5. The values which are used for the neural network prediction method of Pozueta et al. can be found in the corresponding report and user manual of the neural network prediction method (Pozueta et al., 2004b).

#### **2.2.5.4 Influence of a recurve wave wall**

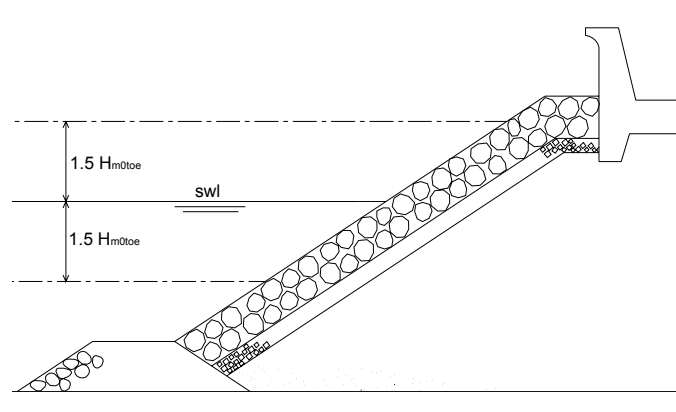
Quite a lot of coastal structures are equipped with a (small or large) recurve wave wall with the aim of reducing the phenomenon of wave overtopping. A recurve wave wall ‘turns’ the waves at the top of the structure back seawards resulting in a lower overtopping quantity to some extent, depending on the relative height and the dimensions of the recurved part of the wave wall. At the moment of writing this study (end of 2004 - beginning of 2005), studies on the influence of a recurve wave wall are ongoing (see Pearson et al., 2004a), but the exact influence of the presence of it on the overtopping quantity is not known yet. In expectation of more detailed knowledge on this subject, the influence of a recurve wave wall was assessed as described in this section.

Within the set-up of the database, distinction was made between large and small recurve wave walls, leading to a different way of schematising the corresponding tests (Fig. 19).

A large recurve wave wall is defined within this study as a recurve wave wall having a dominant effect on the structure layout. A small recurve wave wall on the other hand is defined as a minor construction part, such as an extra curve which is given to a small wall on top of a rubble mound structure.



(a)



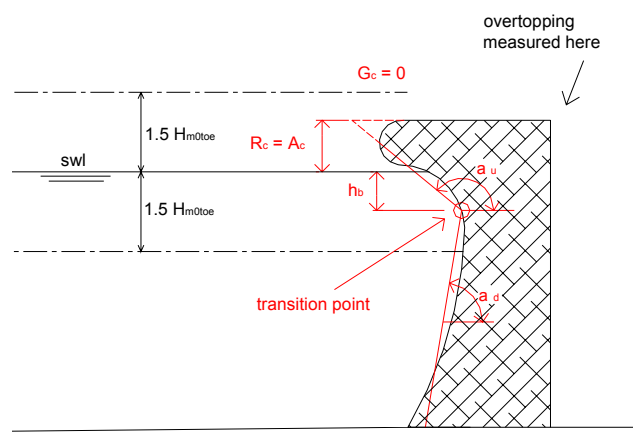
(b)

**Figure 19: Distinction between a large (a) and a small (b) recurve wave wall**

How each of these is incorporated in the schematisation of the structure for the database is explained below.

#### 2.2.5.4.1 Case (a): large recurve wave wall

As a large recurve wave wall influences the entire structure shape, it seems most adequate to include it in the main parameters describing the outlook of the structure (Fig. 19 (a)). In this way, the recurve wave wall can be considered as a composite slope consisting of two different slopes separated by a transition point at depth  $h_b$ . The upper slope leans back seaward introducing a negative value for the cotangent of it. In Fig. 20 the same recurve wave wall as in Fig. 19(a) is represented, together with a possible schematisation of it. The schematisation parameters describing the recurve wave wall are given in the figure.



**Figure 20: Schematisation of a large recurve wave wall**

The transition point is chosen rather arbitrary, providing upper and down slope with a good fitting to the structure.

#### 2.2.5.4.2 Case (b): small recurve wave wall

Compared to previous case, a small recurve wave wall is much less dominant regarding to the overall structure layout (Fig. 19(b)). It is clear that in case of a small recurve wave wall a description of it by means of the structure slope is not adequate.

The methodology for a small recurve wave wall which is used here, is based on the method proposed in TAW (2003) for vertical walls, in which the effect of a recurve wave wall is accounted for as a higher roughness of the structure felt by the waves, resulting in a lower value of  $\gamma_f$ .

Determining the final value of  $\gamma_f$  for the database is performed therefore in two steps. In a first step, the  $\gamma_f$ -value for a structure is determined according to section 2.2.5.3.8, resulting in a  $\gamma_f$ -value accounting for the roughness/permeability of the present armour layer. In a second step an eventually extra reduction for a recurve wave wall is carried out. How exactly this extra reduction is determined, based on TAW (2003), and extended for rough structure types, is described below.

Equations (1) and (2) describe the applied reduction for a small recurve wave wall. ' $\gamma_{f \text{ armour}}$ ' refers to the value of the roughness/permeability factor obtained solely due to the effect of roughness and permeability of the armour layer. This corresponds to the value of  $\gamma_f$  which is obtained by applying the methodology described in section 2.2.5.3.8 The mentioned ' $\gamma_f$ ' in

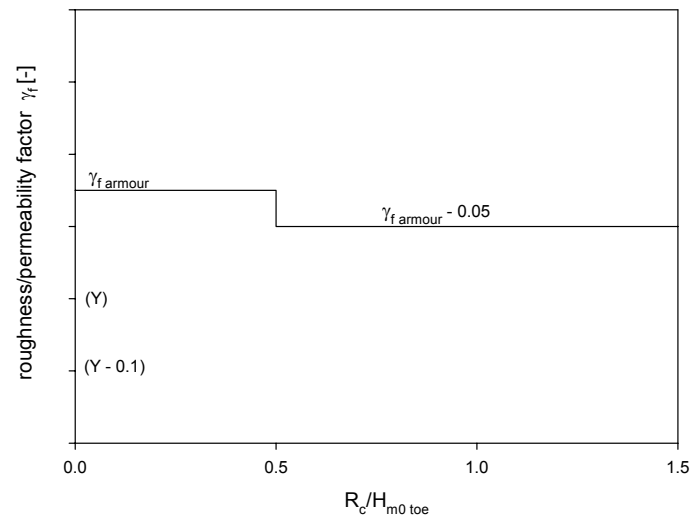
equations (1) and (2) refers to the final value of the roughness and permeability factor, including -beside the roughness/permeability of the armour layer- the effect of a small recurve wave wall. When further in this study the roughness/permeability factor ' $\gamma_f$ ' is mentioned, the effect of a small recurve wave wall is included.

In case of a <b>rough</b> structure, i.e. $\gamma_{f \text{ armour}} < 0.9$ :		(1)
for $R_c / H_{m0 \text{ toe}} \geq 0.5$	: $\gamma_f = \gamma_{f \text{ armour}} - 0.05$	
for $R_c / H_{m0 \text{ toe}} < 0.5$	: $\gamma_f = \gamma_{f \text{ armour}}$	

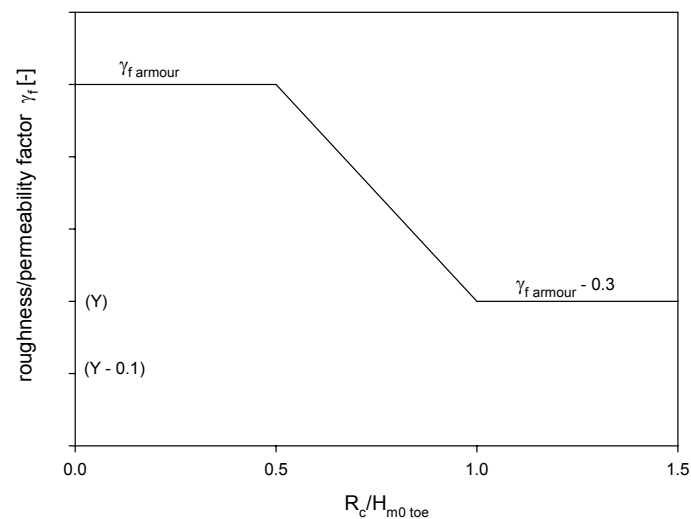
In case of a <b>smooth</b> structure, i.e. $\gamma_{f \text{ armour}} \geq 0.9$ :		(2)
for $R_c / H_{m0 \text{ toe}} > 1$	: $\gamma_f = \gamma_{f \text{ armour}} - 0.3$	
for $R_c / H_{m0 \text{ toe}} \leq 0.5$	: $\gamma_f = \gamma_{f \text{ armour}}$	
for $0.5 < R_c / H_{m0 \text{ toe}} \leq 1$	: interpolation	

As the effect of a recurve wave wall on the overtopping phenomenon is only significant for relatively high crests (for low crests the waves just pass the structure without 'feeling' the recurve wave wall), the reduction depends on the value of  $R_c / H_{m0 \text{ toe}}$ . As can be derived from equations (1) and (2), the reduction due to the presence of a small recurve wave wall is limited for rough structures. This is done to exclude unrealistic low values of  $\gamma_f$ .

In Fig. 21, equations (1) for rough structures and (2) for smooth structures are graphical represented in respectively graph (a) and graph (b).



(a)



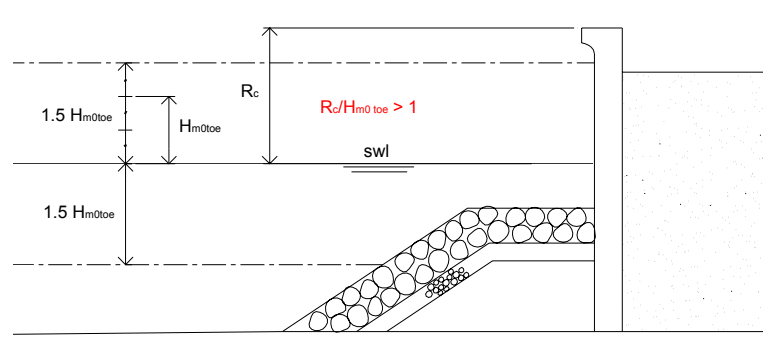
(b)

**Figure 21: Reduction factor for rough structures, graph (a) and smooth structures, graph (b)**

Although the discontinuity in the reduction factor for rough structure types at the value of  $R_c / H_{m0 toe} = 0.5$  (see graph (a) of Fig. 21), cannot appear in reality, it was utilised as approximation for practical use.

Fig. 22 shows an example of a structure with a small recurve wave wall. The value of  $\gamma_{f armour}$  is equal to 1, as the rubble mound structure is situated below the swl. Regarding the level of

the recurve wave wall ( $R_c / H_{m0\ toe} > 1$ ), equation (2) and Fig. 21, graph (b) leads to a value of  $\gamma_f$  equal to  $1 - 0.3 = 0.7$ .



**Figure 22: Influence of a small recurve wave wall on  $\gamma_f$**

As the reduction of  $\gamma_f$  to account for the presence of a small recurve wave wall concerns an estimation of  $\gamma_f$ , these reduced values are also marked in red in the database (see section 2.2.7).

## 2.2.6 Determination of the general parameters

The database contains for each overtopping test three general parameters: “Name”, “RF” and “CF”. This section explains how exactly these parameters are assigned a value.

### 2.2.6.1 Name of the test

The first parameter “Name” assigns a unique name to each test. It consists of a basic ‘test series’ number, which is the same for all the tests within the same test series, followed by a unique number for each test. The parameter “Name” always is composed of 6 characters. E.g. test 36 from test series 178 has the unique code: 178-036.

This parameter is just meant to recognise each test but has no further meaning.

### 2.2.6.2 The complexity factor CF

The complexity factor CF gives an indication of the complexity of the overtopping structure. As already mentioned in section 2.2.5.5, it is impossible to represent each structure type of the database exactly by means of the 17 structural parameters. Depending on the degree of

approximation which is obtained with the 17 structural parameters, the value of the complexity factor CF is determined.

Table 3 gives an overall view of the values the complexity factor CF can adopt. For each value a short explanation is given.

**Table 3: Values of the complexity factor CF**

<b>CF</b>	<b>Meaning</b>
1	simple section: the parameters describe the section exactly or as good as exactly
2	quite simple section: the parameters describe the section very well, although not exactly
3	quite complicated section: the parameters describe the section appropriate, but some difficulties and uncertainties appear
4	very complicated section: the section is too complicated to describe with the chosen parameters, the representation of the section by them is unreliable

The value of the complexity factor CF is only influenced by the schematisation of the test by means of the 17 structural parameters.

### 2.2.6.3 The reliability factor RF

The reliability factor RF gives an indication of the reliability of the considered overtopping test.

Table 4 gives an overall view of the values the reliability factor RF can adopt. For each value a short explanation is given.



**Table 4: Values of the reliability factor RF**

<b>RF</b>	<b>Meaning</b>
1	very reliable test: all needed information is available, measurements and analysis were performed in a reliable way
2	reliable test: some estimations/calculations had to be made and/or some uncertainties about measurements/analysis exist, but the overall test can be classified as 'reliable'
3	less reliable test: some estimations/calculations had to be made and/or some uncertainties about measurements/analysis exist, leading to a classification of the test as 'less reliable'
4	unreliable test: no acceptable estimations could be made, calculations and/or measurements/analysis include faults, leading to an unreliable test

The reliability factor RF is determined by several factors:

- the precision of the measurements/analysis of the researchers performing the overtopping tests
- the possibilities of the test facility used to perform the tests
- the estimations/calculations that had to be made because of missing values

Table 5 gives a detailed overall view of the qualifying factors of RF, and the corresponding value assigned to it, as determined for all overtopping tests included in the overtopping database.

**Table 5: Determination of the reliability factor RF**


---

- absorption system of the test facility:
 

---

  - active wave absorption is available: RF = 1
  - only passive wave absorption was available: RF = 2
  - no wave absorption system is available:
    - if low reflective structure: RF = 2
    - if high reflective structure: RF = 3

---
- wave generation system of the test facility:
 

---

  - regular waves are generated: RF = 4
  - irregular waves are generated:
    - if short-crested: RF = 1
    - if long-crested:
      - RF depending on angle of wave attack:
        - if  $\beta = 0^\circ$ : RF = 1
        - if  $0 < \beta \leq 30^\circ$ : RF = 2
        - if  $30 < \beta \leq 45^\circ$ : RF = 3
        - if  $\beta > 45^\circ$ : RF = 4

---
- wave measurements:
 

---

  - reflection analysis is performed (separation of incident from reflected waves):
    - RF = 1
  - no reflection analysis is performed (only total waves): RF = 3

---
- water depth at the toe of the structure:
 

---

  - if  $h \text{ [m]} \leq 0$  (implicating that no wave characteristics at the toe are known or possible to calculate): RF = 4
  - if  $h \text{ [m]}$  very small and no wave characteristics at the toe are available (no accurate calculations with SWAN are possible):
    - RF = 4

---

**Table 5 : Determination of the reliability factor RF (continue)**


---

- reliability of estimated wave periods at the toe of the structure if no calculations with SWAN (reliability dependent on degree of wave breaking):

---

→ if wave heights are known at deep water and at the toe of the structure:

- if  $H_{m0toe}/H_{m0deep} > 0.6$ : RF = 1  
(little breaking waves; spectral shape at the toe of the structure  $\approx$  spectral shape at deep water; reliable estimation)
- if  $H_{m0toe}/H_{m0deep} < 0.4$ : RF = 3  
(breaking waves; spectral shape at the toe of the structure  $\neq$  spectral shape at deep water; breaking = more energy for the low frequent component; no reliable estimation)
- if  $0.4 < H_{m0toe}/H_{m0deep} < 0.6$ : RF = 2  
(partially breaking waves; less reliable estimation)

→ if wave heights are only known at the toe of the structure:

- if  $H_{m0toe}/h < 0.73$ : RF = 1  
(little breaking waves)
- if  $H_{m0toe}/h > 1$ : RF = 3  
(breaking waves)
- if  $1 > H_{m0toe}/h > 0.73$ : RF = 2  
(partially breaking waves)

---

- Calculations with Battjes and Groenendijk (2000)

---

RF = 2

---

**Table 5 : Determination of the reliability factor RF (continue)**


---

 • Calculations with SWAN:
 

---

→ Reliability dependent on dimension of situation:

- if two-dimensional situation (model test in wave flume): RF = 2
- if three-dimensional situation (model test in wave basin or prototype measurement): RF=3

→ Reliability dependent on degree of wave breaking ( $T_{m-1,0}$  always estimated):

➤ if  $H_{m0toe}/H_{m0deep} > 0.6$ : RF = 2  
(little breaking waves)

➤ if  $H_{m0toe}/H_{m0deep} < 0.4$ : RF = 4  
(breaking waves)

➤ if  $0.4 < H_{m0toe}/H_{m0deep} < 0.6$ : RF = 3  
(partially breaking waves)

➤ if  $H_{m0toe}/h < 0.73$ : RF = 2  
(little breaking waves)

➤ if  $H_{m0toe}/h > 1$ : RF = 4  
(breaking waves)

➤ if  $1 > H_{m0toe}/h > 0.73$ :  
RF = 3  
(partially breaking waves)

→ Reliability dependent on foreshore steepness:

- if foreshore slope 1/30 or less steep: RF = 2
  - if foreshore slope steeper than 1:30: RF = 3
- 

It has to be stressed that the indicated RF -values in table 5 are minimum values. This means that if more than one of the mentioned influence factors appears within one test, at least the highest value of RF (lowest reliability) should be restricted and eventually even a higher value of RF should be assigned to the corresponding test.

### 2.2.6 *Layout of the overtopping database*

The final database consists of more than 10500 overtopping tests which are represented by an equal number of rows in one datasheet.

All tests were put into the database in model values. As often in corresponding reports everything is given in prototype values, it was important to take note of the model scale of the tests to recalculate the values to the original model values. The prototype tests on the contrary were included by means of their real measured values (=prototype values).

It could be important for researchers who use the overtopping database for further research to know which parameter values in the database concern real measured values, which ones concern calculated values and which ones concern estimated values. This can not be checked by the value of the reliability factor RF as this factor only gives an overall indication of the reliability of the test.

To distinguish these cases from each other it was therefore decided to use colours in the datasheet to mark the calculated and estimated values, to make distinction from the real measured values possible.

Following colours were used:

- if wave characteristics at the toe of the structure were calculated with SWAN: values marked in blue
- if wave heights at the toe of the structure were calculated from  $H_{1/3}$  from time series with the method Battjes and Groenendijk (2000): values marked in green
- if wave period parameters were estimated from other period parameters: values marked in red
- if values of the roughness/permeability factor  $\gamma_f$  are estimated, which is the case for all armour layers which are not present in table 3.4, and also if an extra reduction for a small recurve wave wall according to equations (1) and (2) was included in it: values marked in red

Additionally to the already mentioned 31 columns in the database (resulting from 3 general parameters, 11 hydraulic parameters and 17 structural parameters), 2 more columns are part of the datasheet.

The first added column (column 32) is called “Remark” and contains a remark additional to the test. This is done mainly thinking of the neural network application of the database. One of the reasons are the model and scale effects which affect small scale overtopping measurements in specific cases.

Column 32 marks the three mentioned types of tests, and advises against using for the neural network development. Additionally for the laboratory tests with wind generation the generated wind velocity is mentioned.

The total number of prototype tests is 132. A number of 223 laboratory tests is performed with wind generation. Finally 154 tests concern synthetic laboratory test sections.

By excluding these series of tests from the neural network development, a network which is able to predict overtopping in laboratory, including the model effect of wind, and including scale effects, is obtained. A correction factor accounting for scale effects and the effect of wind in accordance with the scaling map of Kortenhaus et al. (2005), leads to a prediction of the mean overtopping discharge to be expected in prototype.

A second added column to the database (column 33) concerns the state of each overtopping test, regarding the confidentiality. For public tests, column 33 contains a reference to a report or paper describing the tests. This allows interested researchers to find more information on specific tests. As mentioned in section 2.2, about 75% of all data is publicly available.

Table 6 gives an overall view of the information summarised in the overtopping database.

**Table 6: Information in the database**

<b>Column number</b>	<b>Contents</b>	<b>Nature of parameter</b>
1	Name	general
2	$H_{m0 \text{ deep}}$ [m]	hydraulic
3	$T_p \text{ deep}$ [s]	hydraulic
4	$T_m \text{ deep}$ [s]	hydraulic
5	$T_{m-1,0 \text{ deep}}$ [s]	hydraulic
6	$h_{\text{deep}}$ [m]	structural
7	$m$ [-]	structural
8	$\beta$ [°]	hydraulic
9	$h$ [m]	structural
10	$H_{m0 \text{ toe}}$ [m]	hydraulic
11	$T_p \text{ toe}$ [s]	hydraulic
12	$T_m \text{ toe}$ [s]	hydraulic
13	$T_{m-1,0 \text{ toe}}$ [s]	hydraulic
14	$h_t$ [m]	structural
15	$B_t$ [m]	structural
16	$\gamma_f$ [-]	structural
17	$\text{cota}_d$ [-]	structural
18	$\text{cota}_u$ [-]	structural
19	$\text{cota}_{\text{excl}}$ [-]	structural
20	$\text{cota}_{\text{incl}}$ [-]	structural
21	$R_c$ [m]	structural
22	$B$ [m]	structural
23	$h_b$ [m]	structural
24	$\tan\alpha_B$ [-]	structural
25	$B_h$ [m]	structural
26	$A_c$ [m]	structural
27	$G_c$ [m]	structural
28	RF	general
29	CF	general
30	$q$ [m <sup>3</sup> /s/m]	hydraulic
31	$P_{\text{ow}}$ [-]	hydraulic
32	Remark	extra information
33	Reference	extra information

### 2.3 Conclusions / achievements

A database containing 10532 tests on wave overtopping has been set-up. Each test in the database has been described by 31 carefully selected parameters including wave characteristics, geometrical characteristics of the structure, overtopping related parameters and general information.

All of these parameters and how to define their value, have been described carefully and into detail.

The screened and homogeneous database has been used to develop a neural network to predict wave overtopping at coastal structures (see WP8).

This workpackage delivered the following reports :

- the report on the overtopping database (D6)

Additionally one milestone was achieved :

The wave overtopping database which is a collection of existing data on wave overtopping (M2).



### 3 WP3 : Full scale measurements

#### 3.1 Objectives

The main objective is to collect and analyse reliable full scale data on, or related to, wave overtopping at four different prototype sites.

Other task objectives are :

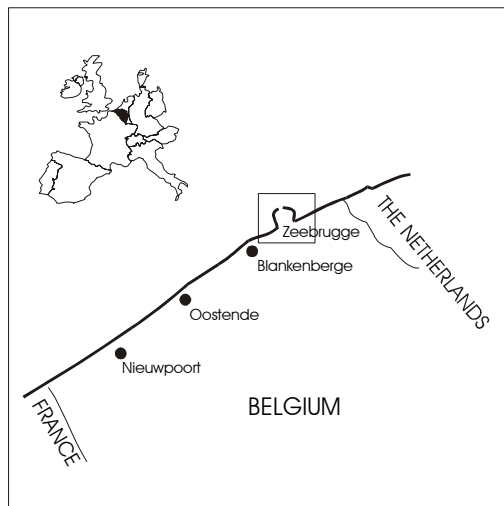
- to (supplementary) instrument the sites in such a way that the incident wave field is measured correctly;
- to (supplementary) instrument the sites, so that overtopping is measured correctly;
- to (supplementary) instrument and measure the long wave phenomenon on very shallow water and breaking waves at one site.

#### 3.2 Description of work performed

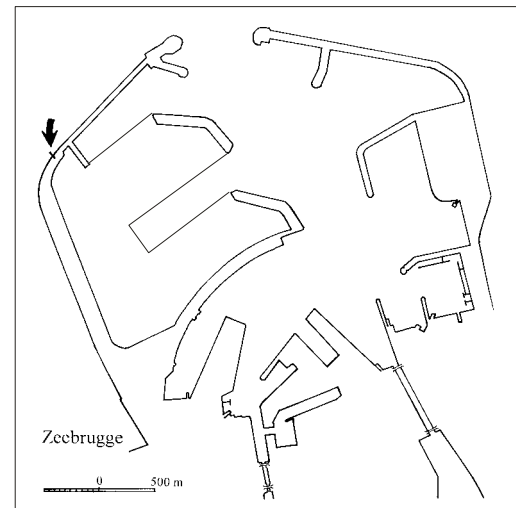
##### 3.2.1 Site 1 : Zeebrugge (Belgium)

The Zeebrugge field site is situated on the eastern part of the Belgian Coast (Fig. 23) at the outer Zeebrugge harbour (Fig.24). The outer harbour is protected by two rubble mound breakwaters. The slope of the breakwater is ca. 1:1.5 (1:1.4 where the measurements take place) and is protected by 25 tons grooved cubes which are somewhat flattened (Height/Width = 0.85). The core consists of quarry run (2-300 kg) and 1-3 ton rocks form a filter layer (Fig. 25). On the landward side, a filter construction is placed between the core and the sandfill.

The tidal range varies 4.30 m between  $Z+0.32$  and  $Z+4.62$  (mean spring tide) and  $Z+0.90$  and  $Z+3.88$  (mean neap tide) ( $Z + 0.00 = MLLWS + 0.08$ ). The design conditions are: significant wave height  $H_s = 6.20$  m, maximum peak period  $T_p = 10$  s, water level  $Z + 6.76$ . The average sea bottom level is about  $Z - 7.00$ , so the breakwater is about 20 m high, with the crest level at  $Z + 12.40$  (theoretical design level).

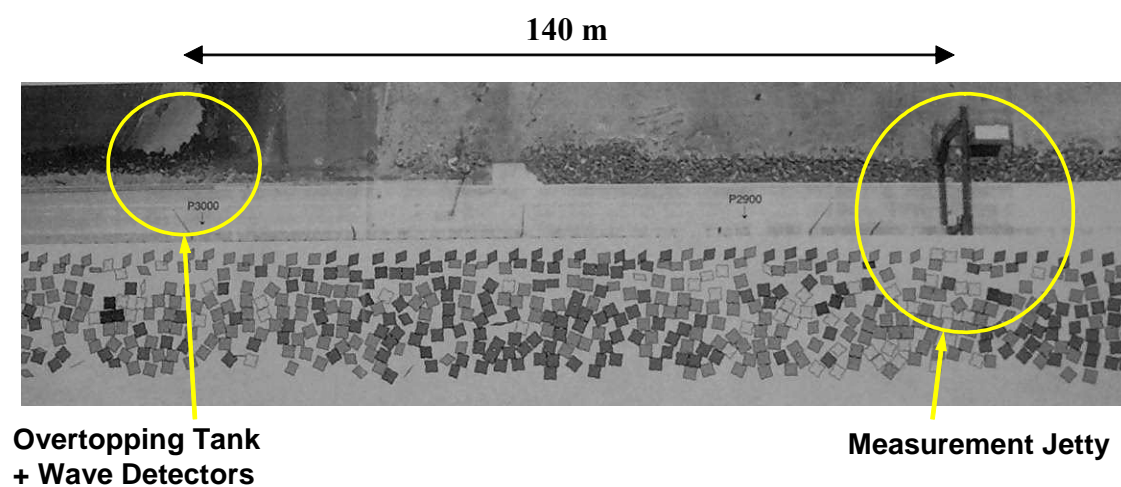


**Figure 23: Location of Zeebrugge harbour at the Belgian North Sea Coast**

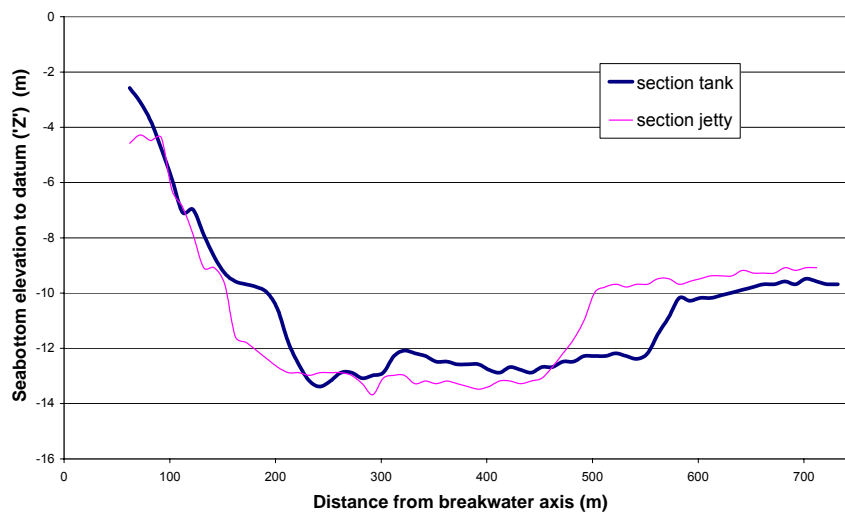


**Figure 24: Location of the field site at Zeebrugge harbour**

Full scale measurements are carried out on the northern part of the western breakwater of the outer harbour (Troch et al. (1998)). Two cross-sections (P2860 and P3000) of the breakwater, with an interspace of approximately 140 m, are instrumented. Fig. 25 shows a plan view with both instrumented cross-sections indicated. Bathymetric surveys in front of both instrumented cross-sections have been carried out in 1999. Results were confirmed during the surveys of 2002. Fig. 26 gives bathymetry for both cross-sections. Bottom elevation is referred to “Z”-level as defined above. The foreshore is characterized by an erosion pit in front of the breakwater and a flat slope more seaward.



**Figure 25: Plan view with indication of both instrumented cross-sections**



**Figure 26: Bathymetry for two instrumented cross-sections**

In the first cross-section (P2860) a measurement jetty of 60 m length is constructed on top of the breakwater. It is supported by a steel tube pile ( $\varnothing = 1.80$  m) at the breakwater toe and by concrete columns on top of the breakwater. Instruments placed in this cross-section are a directional wave rider buoy and a non-directional wave rider buoy to measure wave characteristics in front of the structure, a radar and an infrared meter to measure the water level and wave height in front of the structure and an anemometer. These are the instruments directly used within CLASH. Besides them, also run-up measurements along the breakwater's slope and pressure measurements inside the breakwater are carried out. Table 7 provides all available instruments and their position.

**Table 7: Measurement devices installed at the Zeebrugge rubble mound breakwater.**

Channel N°	Sensor	Z [m]	X [m]	Variables measured
1	Pressure sensor 3498	3.1	-6.88	hydrodynamic pressure
2	Pressure sensor 3499	0.83	-12.66	hydrodynamic pressure
3	Pressure sensor 3502	3.06	-7.26	hydrodynamic pressure
4	Pressure sensor 3504	0.74	-2.48	hydrodynamic pressure
5	Pressure sensor 3505	0.74	-8.96	hydrodynamic pressure
6	Pressure sensor 3507	0.77	-6.88	hydrodynamic pressure
7	Pressure sensor 3511	3	-2.48	hydrodynamic pressure
8	Pressure sensor 381	2.44	-2.48	hydrodynamic pressure
9	Pressure sensor 382	2.51	-6.88	hydrodynamic pressure
10	Pressure sensor 383	-0.35	-37.6	hydrodynamic pressure
11	Pressure sensor 384	2.32	8.97	hydrodynamic pressure
12	Pressure sensor 385	2.43	-10.06	hydrodynamic pressure
13	Pressure sensor 386	2.36	-7.78	hydrodynamic pressure
14	Pressure sensor 388	2.43	3.97	hydrodynamic pressure
15	Pressure sensor 137	1.09	-37.6	hydrodynamic pressure
16	Pressure sensor 138	2.9	-18.46	hydrodynamic pressure
17	Run-up gauge 1	11.96	-15.31	wave run-up
18	Run-up gauge 2	11.26	-13.51	wave run-up
19	Run-up gauge 3	10.64	-11	wave run-up
20	Run-up gauge 4	9.58	-9.12	wave run-up
21	Run-up gauge 5	7.45	-6.93	wave run-up
22	IR-Laser Waveheight meter	17.11	-30	surface elevation
23	Radar	17.11	-30	surface elevation
24	Waverider I buoy (close)	0	-150	surface elevation
25	Waverider II buoy (far)	0	-215	surface elevation
26	Stepgauge Spiderweb 1	2.75	-18.45	wave run-up & surface elevation
27	Stepgauge Spiderweb 2	4.03	-17.84	wave run-up & surface elevation
28	Stepgauge Spiderweb 3	6.39	-14.82	wave run-up & surface elevation
29	Stepgauge Spiderweb 4	7.3	-13.34	wave run-up & surface elevation
30	Stepgauge Spiderweb 5	9.5	-11.4	wave run-up & surface elevation
31	Stepgauge Spiderweb 6	10.14	-9.44	wave run-up & surface elevation
32	Stepgauge Spiderweb 7	11.12	-7.26	wave run-up & surface elevation
33	Pressure sensor 1123960	overtopping		hydrodynamic pressure
34	Pressure sensor 1123962	overtopping		hydrodynamic pressure
35	Digital wavedetector 1	overtopping		presence of seawater
36	Digital wavedetector 2	overtopping		presence of seawater
37	Digital wavedetector 3	overtopping		presence of seawater
37b	Digital wavedetector 4	overtopping		presence of seawater
37c	Digital wavedetector 5	overtopping		presence of seawater
38	Digital wavedetector 6	overtopping		presence of seawater
39	Wind speed	17.5	-32	wind speed
40	Wind direction	17.5	-30	wind direction
	Videocamera	14		video images of the run-up

## Wave overtopping measurements

Fig. 27 shows the cross section in which wave overtopping measurements are carried out. The instruments to measure the wave overtopping are: an overtopping tank and wave detectors. The wave overtopping measurements are supported by means of 2 video cameras. Measurement instruments in this cross-section are described here.

Wave overtopping (i.e. the amount of green water washed over the crest of the breakwater) is caught in a concrete tank (28 m<sup>3</sup>). The overtopping tank is placed just behind the crest of the breakwater (Fig. 28). To ensure a continuous measurement of wave overtopping, a compound weir is placed in the northern side wall of the overtopping tank. The weir controls the outflow of the water.

The water height in the tank is measured by two pressure transducers at the bottom of the overtopping tank. Signals of these transducers are sampled at  $f_s = 10$  Hz. These pressure sensors are connected to both ends of a tube. Five tubes are also connected to this tube. The other ends of these five tubes are equally distributed over the bottom of the tank. Starting from the measured water levels and the continuity equation a methodology has been developed to calculate the incoming overtopping rates (see Troch et al., 2004 and Geraerts & Boone, 2004).

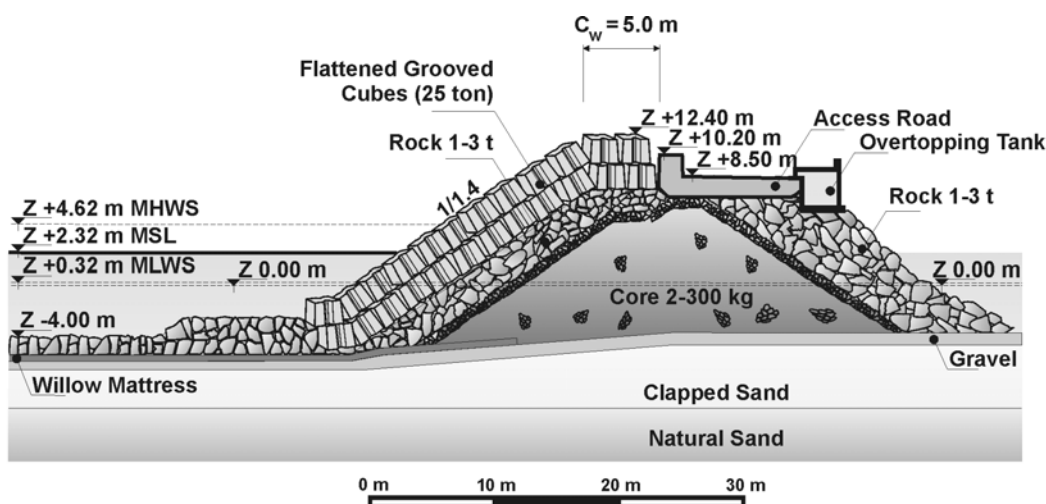


Figure 27: Cross-section of the Zeebrugge rubble mound breakwater at the location of the wave overtopping tank.



**Figure 28: View at the overtopping tank on site.**



**Figure 29: Detail of one wavedetector.**



**Figure 30: Global view showing four different wave detectors.**

On and near the crest armour units six wave detectors have been installed (Fig. 29 and Fig. 30). They measure the number of overtopping waves. By considering these measurements together one gets an idea about the extent of an overtopping event.

A wave detector consists of two electrodes which get short-circuited electrically when an overtopping wave hits the electrodes.

### **Measurements to identify hazards from wave overtopping**

Several instruments to identify and measure hazards resulting from wave overtopping have been installed at the Zeebrugge field site during CLASH. Within this framework wave forces on instrumented dummies, an instrumented pipeline and a vertical wall are measured. These impact measurements are supported by velocity measurements of overtopping water. Moreover, an investigation for the breaking of window glass is carried out. A detailed description of all measurement devices and the design is given in Geeraerts et al. (2003) and in Geeraerts & Boone (2004).



Three dummies have been installed and instrumented. Two of them are placed on the crest wall directly behind the armour units. The third (smaller) one is placed at the landward side of the access road on top of the breakwater's crest. The dummies are a rough schematization of human beings. They are instrumented to get information about the magnitude of forces exerted by overtopping waves on people walking or standing on top of a breakwater. Fig. 31 shows a general view at the three dummies as installed on site. Dimensions of the dummies' bodies are (1.70 m \* 0.50 m) for the large dummies and 1.40 m \* 0.40 m for the 'child' dummy. Forces on the dummies are measured by means of so-called S-shaped load cells (Tedeo-Huntleigh).



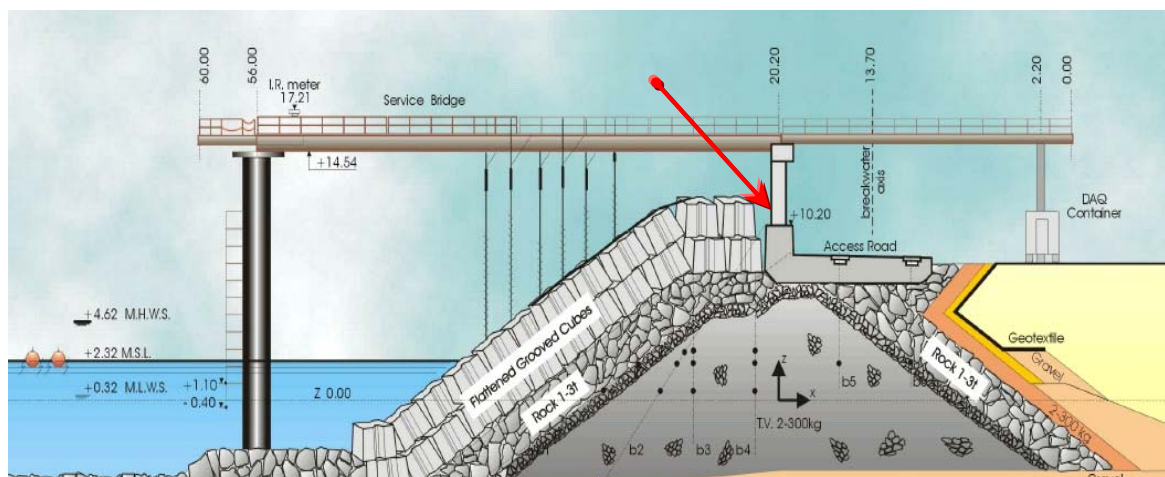
**Figure 31: Global view showing three installed instrumented dummies on site.**

In many harbours pipelines to transport oil or gas are installed on top of a breakwater. To gain information about overtopping wave forces on such pipelines, an instrumented "pipeline" (Fig. 31 and 32) has been installed. In fact it concerns a steel dredging hose with length = 6.00 m, diameter  $D = 0.65$  m and a wall thickness  $t = 0.01$  m. Horizontal and vertical force components on the pipeline are measured. Fig. 32 shows a general view of the pipeline as installed on site.



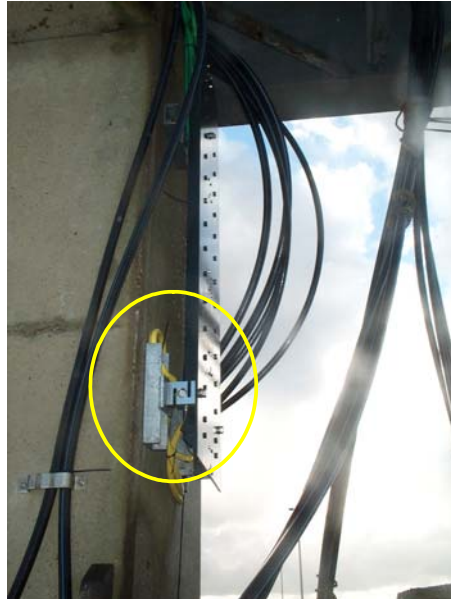
**Figure 32: Global view showing the instrumented pipeline on site.**

Force and pressure measurements on a vertical wall are carried out by measuring the force on an aluminium plate, with the same dimensions as the body plate of the dummies (1.70 m \* 0.50 m), mounted to the concrete column supporting the measurement jetty (see Fig. 33). This column serves as vertical wall. Forces are measured by three S-shaped load cells, with the same positioning and capacity as for the dummies. Fig. 34 shows a detail of the mounted body plate with indication of a mounted load cell. Moreover, pressures are measured by five flush-mounted pressure sensors positioned along a vertical line in the centre of the aluminium plate.



**Figure 33: Cross-section showing the section with the measurement jetty. The position of the measurements on the vertical wall is indicated.**





**Figure 34: Detail of force transducer for force measurements on vertical wall.**

Two velocity meters are installed at two locations between the armour units near the crest wall. One is located near the pipeline (Fig. 36); the other is situated in front of the large dummy nearest to the measurement jetty (Fig. 35). Each velocity meter consists of 2 (near pipeline) or 3 (near dummy) units that are horizontally installed on a metal frame. The one near the dummy consists of 3 units as the dummy is much higher than the pipeline. Each unit contains 3 pairs of electrodes which detect the presence of water at this location.



**Figure 35: Velocity meter in front of dummy.**



**Figure 36: Velocity meter in front of pipeline.**

## Measurement Results

Wave overtopping has been measured at the Zeebrugge breakwater during nine storms. An overview is given in Table 8.

**Table 8: Storms measured in Zeebrugge**

Storm No.	Date	Time	Duration (s)
1	6 November 1999	11h30 – 13h30	7200
2	6-7 November 1999	23h45 – 01h45	7200
3	8 November 2001	16h15 – 18h15	7200
4	26 February 2002	12h30 – 14h30	7200
5a	27 October 2002	17h00 – 18h00	3600
5b	27 October 2002	18h00 – 19h00	3600
5c	27 October 2002	19h00 – 20h15	4500
6	29 January 2003	10h00 – 12h00	7200
7	7 October 2003	12h00 – 14h00	7200
8	22 December 2003	00h00 – 02h00	7200
9	8 February 2004	14h45 – 16h45	7200

The time spans indicated are the time spans during which the *SWL* is almost constant (around the moment in time of high water  $t_{HW}$ ) and during which wave overtopping occurred.

Table 9 summarizes the wave characteristics for the different storms.

The wave overtopping data analysis results have been summarised in Table 10. The mean overtopping discharge per m structure width  $q$ , calculated according to three different methods as described in Troch et al. (2004) and Geeraerts & Boone (2004), is given there, together with the number of overtopping events.

**Table 9: Wave characteristics, surf similarity parameter and water level for the storms.**

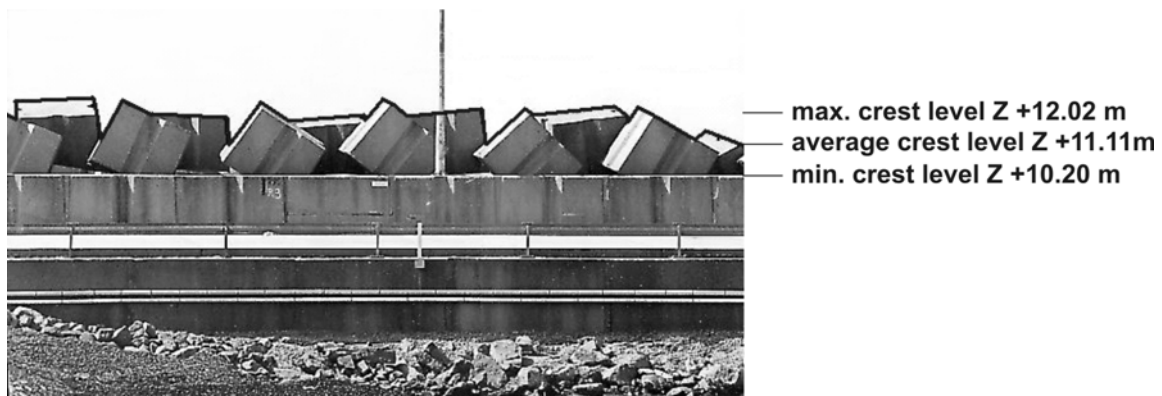
Storm No.	$H_{m0}$ (m)	$H_s$ (m)	$T_{m-1,0}$ (s)	$T_p$ (s)	$T_m$ (s)	$\xi_0$ (-)	SWL (m Z)
1	3.04	2.89	6.88	7.34	5.70	3.52	5.28
2	2.60	2.44	6.93	9.3	5.36	3.88	5.11
3	3.47	3.31	8.41	10.28	6.35	4.05	5.01
4	2.63	2.52	6.49	7.91	5.32	3.68	4.21
5a	3.74	3.61	7.50	8.57	6.21	3.46	4.40
5b	3.86	3.71	7.64	8.57	6.35	3.47	4.60
5c	3.71	3.55	7.98	8.57	6.45	3.70	4.35
6	3.16	3.03	7.28	7.91	5.94	3.66	4.71
7	3.23	3.08	7.00	7.91	5.84	3.47	4.77
8	3.03	2.88	7.33	8.57	5.85	3.76	5.26
9	3.59	3.41	7.37	8.57	6.14	3.47	5.32

**Table 10: Average overtopping rates for all storms, calculated using the 3 methods based on the continuity equation, the individual overtopping volumes and the water depth jumps, respectively with  $N_{ov}$  the number of overtopping events.**

Storm No.	$q_{ceq}$ (l/sm)	$q_{vi}$ (l/sm)	$q_{\Delta h}$ (l/sm)	$N_{ov}$ (-)	$N_{ov}/hour$ (-)
1	3.161E-02	5.709E-02	4.677E-02	10	5
2	2.299E-02	2.211E-02	1.842E-02	3	1.5
3	2.825E-01	3.310E-01	3.588E-01	29	14.5
4	3.919E-03	1.010E-02	9.031E-03	1	0.5
5a	4.037E-01	5.158E-01	4.404E-01	19	19
5b	5.919E-01	8.585E-01	5.963E-01	30	30
5c	6.296E-01	7.036E-01	6.780E-01	31	24.8
6	8.479E-02	9.620E-02	8.646E-02	9	4.5
7	6.410E-02	8.920E-02	7.280E-02	9	4.5
8	2.900E-02	6.680E-02	5.590E-02	2	1
9	2.200E-01	5.910E-01	5.630E-01	16	8

Storms 1, 2, 4, 6, 7 and 8 have  $q$ -values lower than 0.1 l/sm, showing that there has been very little wave overtopping during these storms. Storms 3, 5a, 5b, 5c and 9 have  $q$ -values ranging between 0.3 (for storm 3) and 0.9 l/sm (for storm 5b), indicating more severe wave overtopping. The storms with small overtopping rates have a smaller number of overtopping events  $N_{ov}$ , whereas the storms with larger overtopping rates have a larger  $N_{ov}$ .

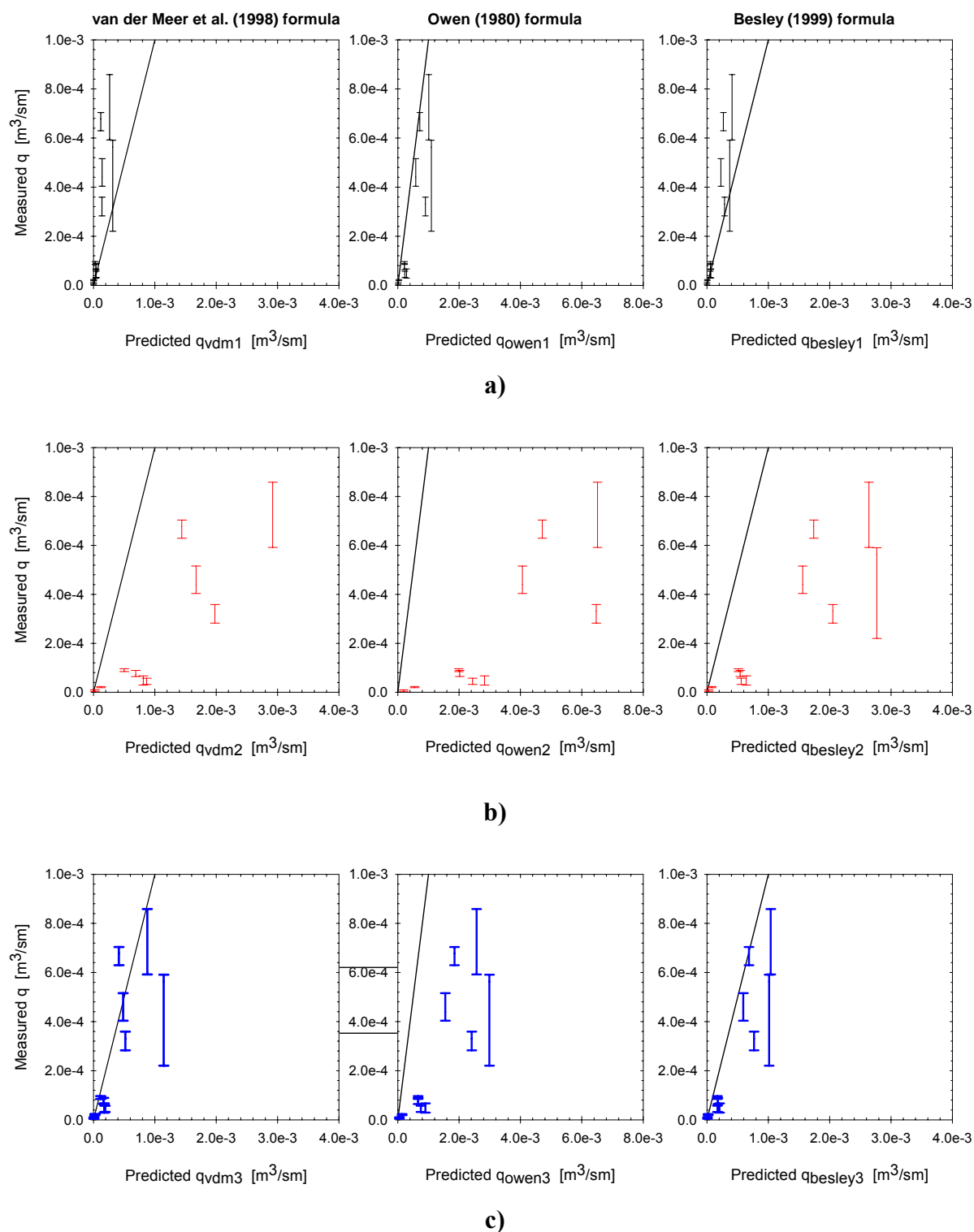
A comparison between the field data and three widely used prediction formulae has been made. The three prediction formulae used are the one according to Owen (1982); the update of the latter by Besley (1999) and the formula by van der Meer et al. (1998). In the formula by Besley (1999) the influence of a permeable crest berm is incorporated. All three formula need a value for the crest freeboard, i.e. the vertical distance between the still water level and the crest level, as input. Since this crest level is a very important parameter in the prediction, but is not clearly defined at the Zeebrugge site, three different values have been considered (Fig. 37). As minimum crest level the value corresponding to  $R_c$  as defined in WP2 was taken (i.e.  $Z+10.20$  m). As maximum crest level the value corresponding to  $A_c$  as defined in WP2 was taken. However, as can be seen in Fig. 37,  $A_c$  is not clearly defined for the Zeebrugge breakwater. For this reason the geometrical average of the bold line indicating the upper part of the armour in Fig. 37 was taken, i.e.  $Z+12.02$  m. Since water can pass in between the crest units of the armour, it was considered wise to consider also a third value for the crest level, i.e. the average value of the maximum and minimum crest level, i.e.  $Z+11.11$  m.



**Figure 37: Definition figure of three different crest levels taken into account.**

The measured average overtopping rates have been compared to the predicted average overtopping rates from van der Meer et al., Owen and Besley, in Fig. 38, for the three crest levels and associated crest freeboards. The range of the measured  $q$ -values obtained using the

three methods is indicated in Fig. 38 using a vertical bar. Linear scales have been used in the graphs.



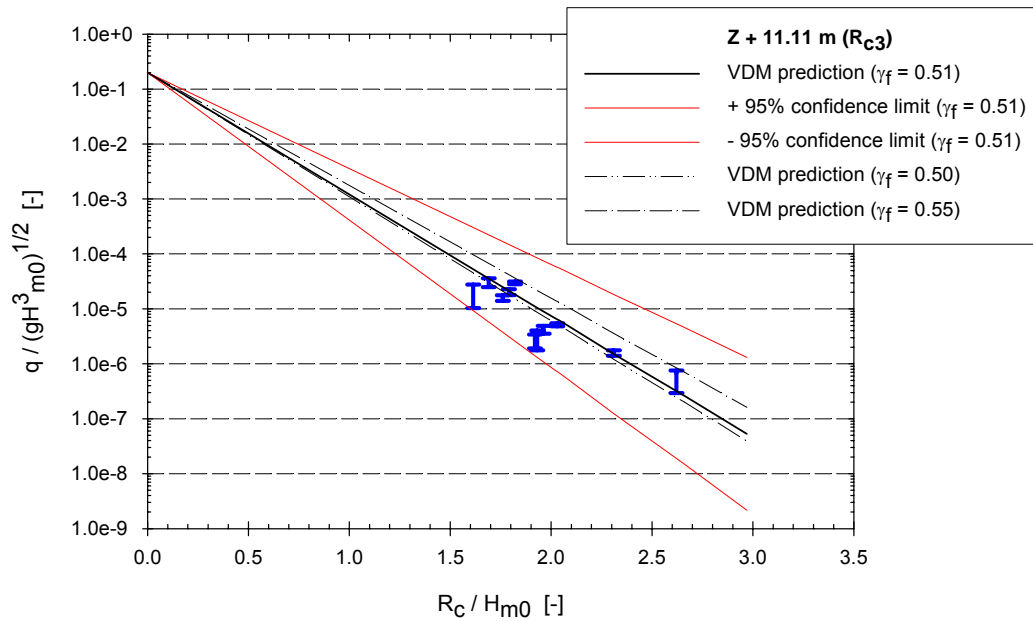
**Figure 38: Comparison between measured and predicted average overtopping rates, using van der Meer et al. (1998, left column), Owen (1980, middle column) and Besley (1999, right column) prediction formulae; for crest freeboards  $R_{c1}$  (a),  $R_{c2}$  (b) and  $R_{c3}$  (c).**

For the maximum crest level at  $Z + 12.02$  m (using  $R_{c1}$ , cf. Fig. 38(a)), the van der Meer et al. prediction underestimates the measured average overtopping rates by a factor up to about 6 (e.g. storm 5c), especially for higher  $q$ -values. Owen's prediction however slightly overestimates the measured overtopping rates, and the reduction of Besley shows good agreement for smaller  $q$ -values and underestimates larger  $q$ -values.

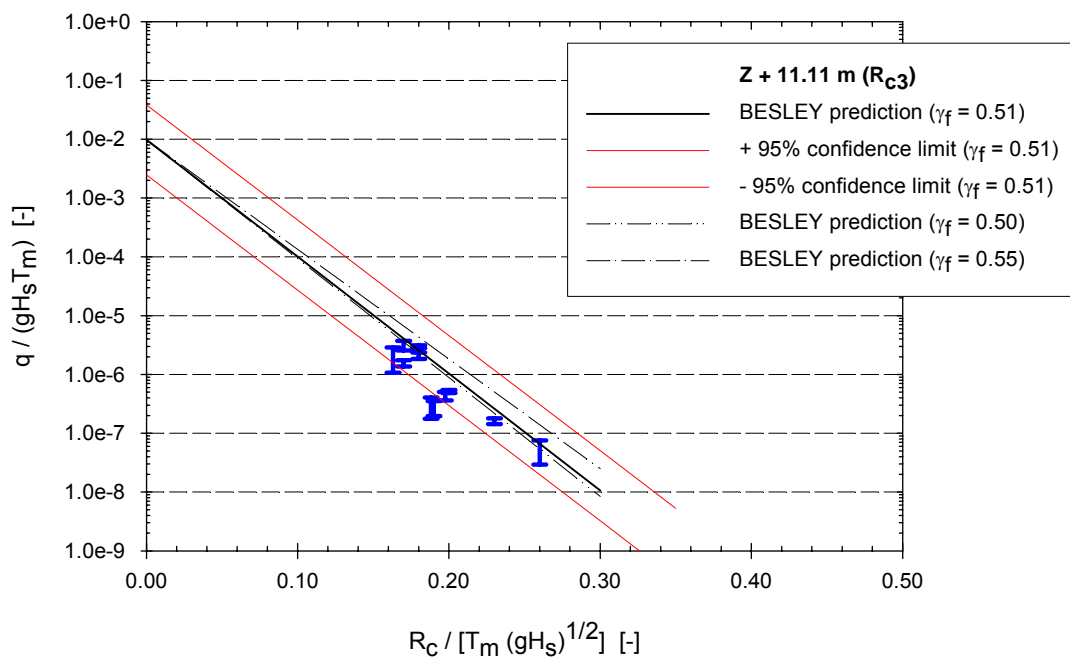
Using the minimum crest level at  $Z + 10.20$  m (using  $R_{c2}$ , cf. Fig. 38(b)), the predicted average overtopping rates from all formulae considerably overestimate the measured  $q$ -values. The van der Meer et al. and Besley predictions have the same magnitude, and the Owen prediction is about three times as large for the large overtopping rates. Finally, using the actual average crest level at  $Z + 11.11$  m (using  $R_{c3}$ , cf. Fig. 38(c)), the predicted  $q$ -values by van der Meer et al. and Besley are in relatively good agreement with the measured  $q$ -values, and the Owen prediction overestimates the measured average overtopping rates by a factor up to about 7 (for storm 3). In general best agreement between measured and predicted overtopping rates is observed using van der Meer et al.'s and Besley's prediction formulae for the actual average crest level  $Z + 11.11$  m and  $R_{c3}$ . Moreover Besley's prediction using  $R_{c3}$  is always on the safe (conservative) side.

A more traditional presentation of the prediction formulae is given in Fig. 39, where a dimensionless overtopping discharge (using a logarithmic scale) is plotted versus a dimensionless crest freeboard. The thick solid line is the prediction formula itself, the thin solid lines are the 95 % confidence intervals of the formula (based on variation coefficients provided by the author of the formula). For the prediction formula a roughness coefficient  $\gamma_f = 0.51$  was used. This factor originates from field measurements on run-up on the Zeebrugge breakwater (see Troch et al., 2004). The measured field data have been plotted in the same graph using vertical bars to indicate the scatter from using the three calculation methods. Fig. 39(a) and 39(b) show the resulting graphs for van der Meer et al. and Besley, respectively, for  $R_{c3}$  ( $Z + 11.11$  m).

The measured overtopping rates are within the 95 % confidence intervals of both prediction formulae (except one storm, for Besley's prediction, in Fig. 39(b)), and therefore good agreement is found between measured and predicted values. Also indicated in Fig. 70 are the prediction formulae using the recommended values for the surface roughness reduction factor  $\gamma_f = 0.50$  and  $\gamma_f = 0.55$  (applicable for designing a structure). For the case of the Zeebrugge breakwater, the value  $\gamma_f = 0.50$  shows best agreement with the measured overtopping rates.



a)



b)

**Figure 39: Measured and predicted (top (a): van der Meer et al., 1998; bottom (b): Besley (1999)) non-dimensional average overtopping rates and 95 % confidence limits as a function of the non-dimensional crest freeboard for the crest freeboard  $R_{c3}$ , using surface roughness reduction factor  $\gamma_f = 0.51$ . Also indicated are predicted overtopping rates for  $\gamma_f = 0.50$  and  $\gamma_f = 0.55$ .**



For average overtopping rates up to 1 l/sm very good agreement between the prototype average overtopping rates and the prediction formulae of van der Meer and Besley is achieved, taking into account the precise choice of surface roughness and crest freeboard parameters.

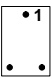
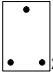
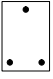
Wave impacts and overtopping velocities have been measured at the Zeebrugge breakwater since January 16<sup>th</sup>, 2003. From that moment on 3 storms have occurred: Oct. 7<sup>th</sup>, 2003, Dec. 22<sup>th</sup>, 2003 and Febr. 8<sup>th</sup>, 2004. The wave characteristics for these storms are repeated in Table 11.

**Table 11: Wave characteristics on Oct. 7<sup>th</sup>, 2003, Dec. 22<sup>th</sup>, 2003 and Febr. 8<sup>th</sup>, 2004.**

Storm No.	Date	Time	MWL (Z+ ...m)	H <sub>m0</sub> (m)	T <sub>p</sub> (s)
7	Oct. 7 <sup>th</sup> , 2003	12.00 - 14.00	4.77	3.23	7.91
8	Dec. 22 <sup>th</sup> , 2003	00.00 – 02.00	5.26	3.03	8.57
9	Febr. 8 <sup>th</sup> , 2004	14.45 – 16.45	5.32	3.59	8.57

No impacts were measured on the child dummy (dummy 1). Tables 12 and 13 present for each of these three storms the measured loads for the two most severe wave impact for the two respective dummies on the crest wall. From these tables it can be concluded that the highest impacts on the dummies - ca. 8100 N for dummy2 and ca. 8800 N for dummy3 - are measured during the storm of Febr. 8<sup>th</sup>, 2004

**Table 12: Total and individual impacts measured by load cells (LC) on dummy2 during resp. storms**

Date	LC1  (N)	LC2  (N)	LC3  (N)	Total impact (N)
Oct. 7 <sup>th</sup> , 2003	2520	120	655	3295
	610	800	590	2000
Dec. 22 <sup>th</sup> , 2003	375	405	390	1170
	315	430	155	900
Febr. 8 <sup>th</sup> , 2004	5590	1335	1185	<b><u>8110</u></b>
	2405	1790	1235	<b>5430</b>

**Table 13: Total and individual impacts measured by load cells (LC) on dummy3 during resp. storms**

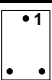

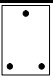
Date	LC1  (N)	LC2  (N)	LC3  (N)	Total impact (N)
Oct. 7 <sup>th</sup> , 2003	1245	1005	1375	3625
	665	995	1050	2710
Dec. 22 <sup>th</sup> , 2003	970	250	490	1710
	270	385	740	1395
Febr. 8 <sup>th</sup> , 2004	4970	1640	2225	<b><u>8835</u></b>
	1950	1015	1340	<b>4305</b>

Table 12 and 13 give measured loads for all load cells for respectively the plate on the vertical wall and the pipeline, together with the total load on both instruments during the two most heavy wave impacts.

**Table 14: Total and individual impacts measured by load cells (LC) on the vertical wall during resp. storms**

Date	LC1 (N)	LC2 (N)	LC3 (N)	Total impact (N)
Oct. 7 <sup>th</sup> , 2003	45	305	275	625
	135	55	105	295
Dec. 22 <sup>th</sup> , 2003	10	115	135	260
	205	50	-10	245
Febr. 8 <sup>th</sup> , 2004	411	630	386	<b><u>1427</u></b>
	505	115	110	<b>730</b>

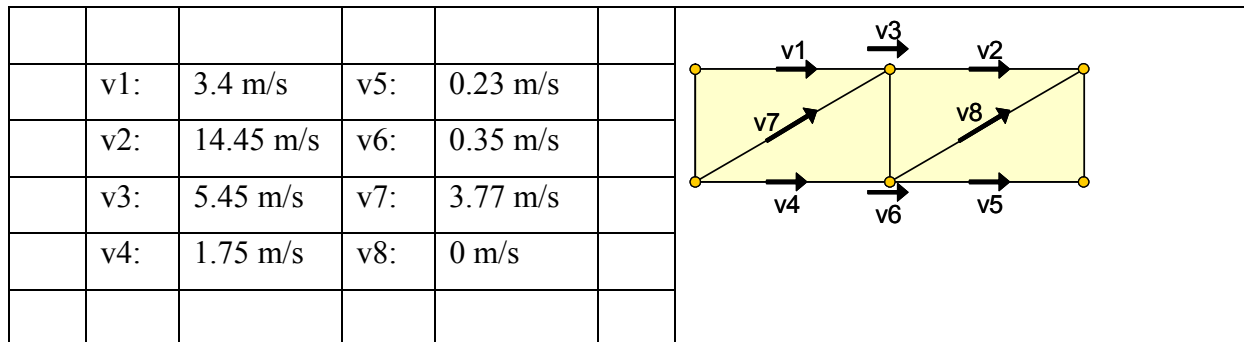
The maximum load (1425 N) on the vertical wall is measured on Febr. 8<sup>th</sup>, 2004.

**Table 15: Total and individual impacts measured by load cells (LC) on the pipeline during resp. storms**

Date	LC1 (N)	LC2 (N)	LC3 (N)	LC4 (N)	Total impact (N)	$\alpha$ (°)
Oct. 7 <sup>th</sup> , 2003	-450	-450	410	600	1350	-41.6
	465	525	285	215	1110	63.3
Dec. 22 <sup>th</sup> , 2003	805	815	645	565	2020	53.3
	725	890	645	1310	2535	39.5
Febr. 8 <sup>th</sup> , 2004	-2820	-2755	2460	2790	<b>7660</b>	-46.7

Comparable to the measurements of the dummies and the vertical wall, the highest total impact appears at Febr. 8<sup>th</sup> 2004. Impacts up to 5585 N and 7660 N are calculated over the whole length of the pipeline. These values correspond to line loads of resp. 930 N/m and 1300 N/m.

Maximum overtopping velocities have been measured during the Febr. 8<sup>th</sup> storm. At the moment of maximum impact at the pipeline (7660 N) velocities are measured in front of the pipeline. Fig. 40 gives an overview of the measured velocities at this specific moment. A maximum velocity of more than 14 m/s was measured.



**Figure 40: Velocities measured in front of the pipeline on Febr. 8<sup>th</sup> 2004.**

## Conclusions

The measurement set-up, using a waverider buoy to measure incident waves and an overtopping tank to catch the volumes of overtopping water, and equipped with an outflow weir on a short side and water depth measurements, has been used successfully to obtain reliable field data.

Eleven storm records have been used in the analysis of the field data, with duration between 1 and 2 hours, with significant wave heights ranging between 2.6 m and 3.9 m and peak periods ranging between 7 and 10 s. Although the measured storm conditions are considerably lower than the design storm conditions (with  $H_s = 6.20$  m and  $T_p = 9.0$  s), average overtopping rates close to 1 l/s.m (and  $\frac{q}{\sqrt{gH_s^3}} = O(10^{-5})$ ) have occurred.

Three methods for deriving the average overtopping rate inside the overtopping tank have been used, based on measurements of outflow discharge over the weir and instantaneous water depth inside the overtopping tank. These methods yield results that are in good agreement.

Average overtopping rates from the field data have been compared with predicted values from the widely used prediction formulae from van der Meer et al. (1998), Owen (1980) and

Besley (1999). For application of these formulae to the case of a rubble mound breakwater, the value of the reduction factor for the surface roughness of the armour layer used is 0.51. The actual value for the crest freeboard parameter  $R_c$  for the case of the Zeebrugge breakwater is not obvious, and therefore a sensitivity analysis has been carried out, varying the crest freeboard between a maximum value  $R_{c1}$  (with crest level at  $Z + 12.02$  m), and a minimum value  $R_{c2}$  (with crest level at  $Z + 10.20$  m), and the average value  $R_{c3}$  (with crest level  $Z + 11.11$  m) between maximum and minimum values. Best agreement between measured and predicted values is observed using the average crest level (with  $R_{c3}$ ) and van der Meer et al's and Besley's prediction formulae.

For average overtopping rates up to 1 l/s.m very good agreement between the prototype average overtopping rates and the prediction formulae of van der Meer and Besley is achieved, taking into account the precise choice of surface roughness and crest freeboard parameters.

The measurement system to identify hazards is operational since January 2003. Since then, three storms with overtopping have been measured at the Zeebrugge breakwater: Oct. 7th, 2003, Dec. 22th, 2003 and Febr. 8th, 2004.

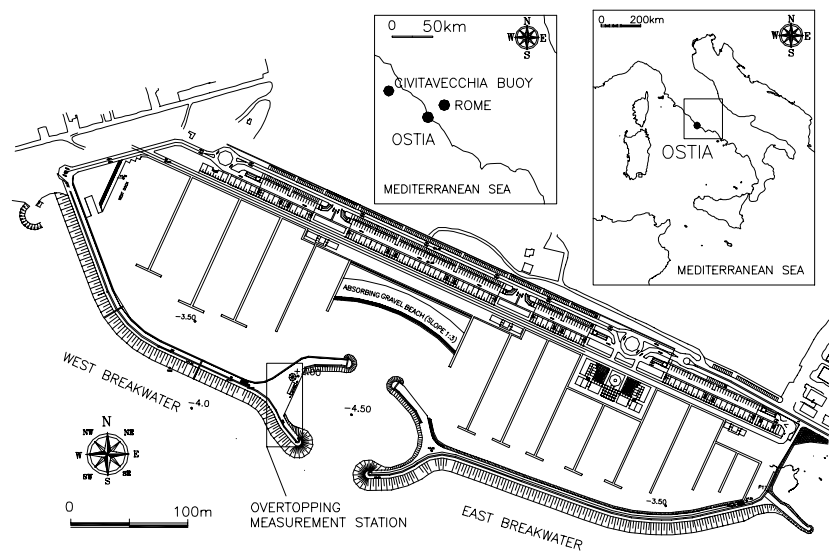
The highest impacts on the devices are measured during the storm of Febr. 8<sup>th</sup>, 2004: up to 8834 N/dummy and 7660 N/pipeline were measured. It has to be noted that these impacts were measured during a storm with only "moderate" mean wave overtopping  $q = 0.6$  l/s/m.

### 3.2.2 Site 2 : Ostia (Italy)

The measurement station is located in the new private yacht harbour of Rome, along the eroding sandy shores of Ostia, about 25 km from Rome, just South-West of the main mouth of the river Tiber, facing the Tyrrhenian Sea in central Italy (see Fig. 41). The harbour is protected by two rubble mound breakwaters (the west breakwater extending for some 600 m, the east one for 700 m), which converge to a central straight entrance to form an elliptic-shaped outer harbour with variable depths up to -5 m MSL. A gravel absorbing beach (slope 1:3) was created inside the harbour just facing the entrance in order to absorb waves penetrating into the basin.

The design cross-section of the final part of the west breakwater, which was chosen for the installation of the overtopping tank, is shown in Fig. 42. The crest level of the crown wall is set at +4.5 m MSL, also to reduce the visual impact. The rock armour seaward design slope is 1:3.5. The design armour stone gradation is 3-7 t.

The local tidal range is quite small (0.4 m), the water level at the structure toe is about -4.0 m MSL; waves at the toe of structure are depth-limited. The local wave climate can be obtained from the analysis of directional wave records available from a buoy installed at a depth of 12 m (see P0 in Fig. 43) during the period 1990-1992. As shown in Fig. 3 the highest and most frequent waves mainly come from the sector 240-250°N while there is a secondary sector between 190°N and 210°N.



**Figure 41: Location map and layout of Rome yacht harbour at Ostia.**

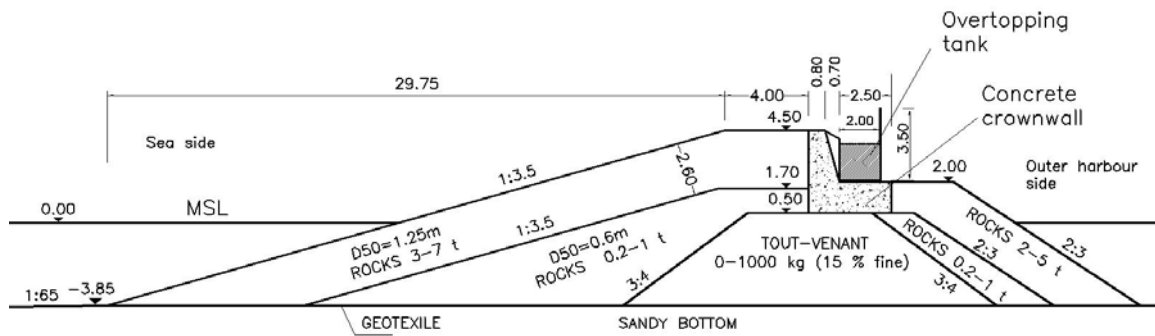


Figure 42: Design cross section of the west breakwater at the overtopping wave tank.

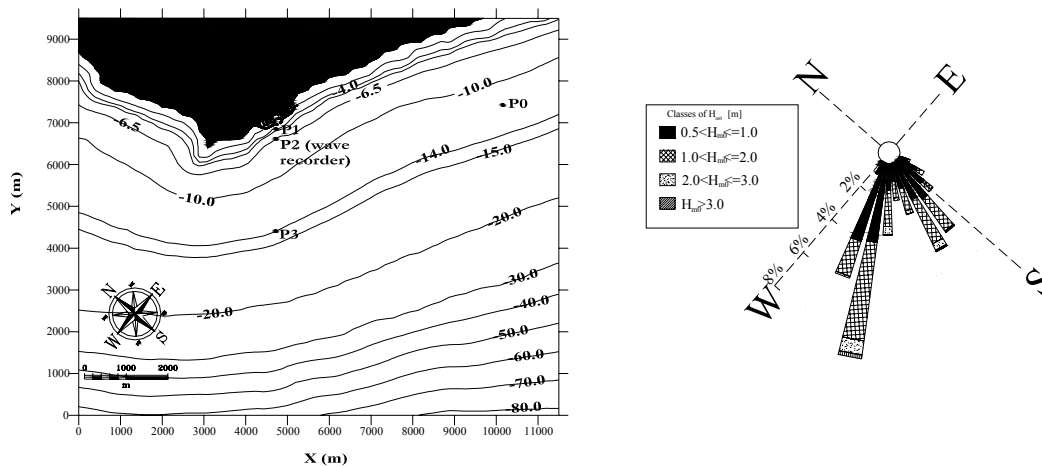


Figure 43: Foreshore grid bathymetry at Ostia (Tiber delta) (left panel) and local wave climate from directional wave records in the period 1990-1992 at a depth of -12 m MSL (buoy location in P0). P1, P2 and P3 indicate the points at which SWAN model results were extracted

The overtopping station is aimed at measuring individual volumes of waves overtopping the breakwater and the main meteorological and oceanographic conditions (waves, water levels, rain, wind, atmospheric pressure). The layout of the station with the location of all the instruments is shown in Fig. 44 together with the convention used in assessing the normal and tangential components of the wave attack and wind. The individual wave overtopping measurement technique also used with success in the companion field site of Zeebrugge

(Troch *et al.*, 2004). The method makes use of a tank collecting the overtopping waves; being the horizontal area of the tank known, the volume of each overtopping wave can be obtained by measuring the water level jumps.

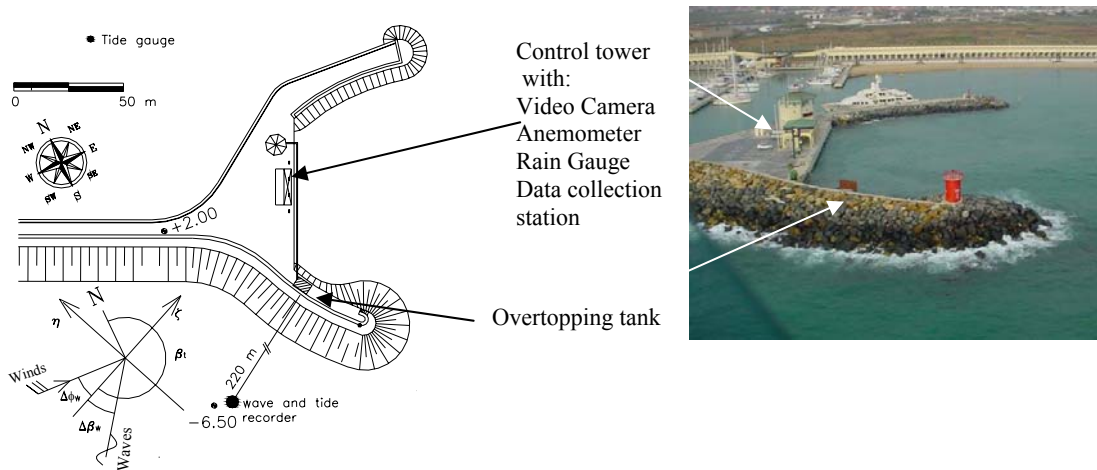
The station was installed on the crown slab near the head of the west breakwater because of experienced localized occurrence of overtopping, vicinity to port control tower (daily control activity by the harbour personnel) and lack of interference with harbour activities and vehicular traffic. A simple steel tank (4 m x 2 m x 2 m height) was built and installed behind the parapet wall in October 2002 (see Fig. 45). A 1.5 m high screen was mounted on the inner side of the tank to ensure the collection of the highest overtopping waves, whose efficiency was actually confirmed by video records.

An outflow weir prevents the tank to be completely filled up during the overtopping storms. The outflow weir is designed in order to ensure a minimum outflowing discharge when collecting small overtopping waves, that are expected to induce small water level jumps of the water level inside the tank (order of magnitude of 1 cm) and larger outflow discharge when the level increases more quickly (10-20 cm) as a consequence of larger overtopping waves. The selected shape of the weir is therefore made up of two parts. The lower part begins 0.475 m from the tank base (see Fig. 45) and is a narrow rectangular vertical opening (width of 0.01 m, height of 0.54 m). The upper part is a V-shaped weir of height 0.97 m and upper width of 0.51 m.

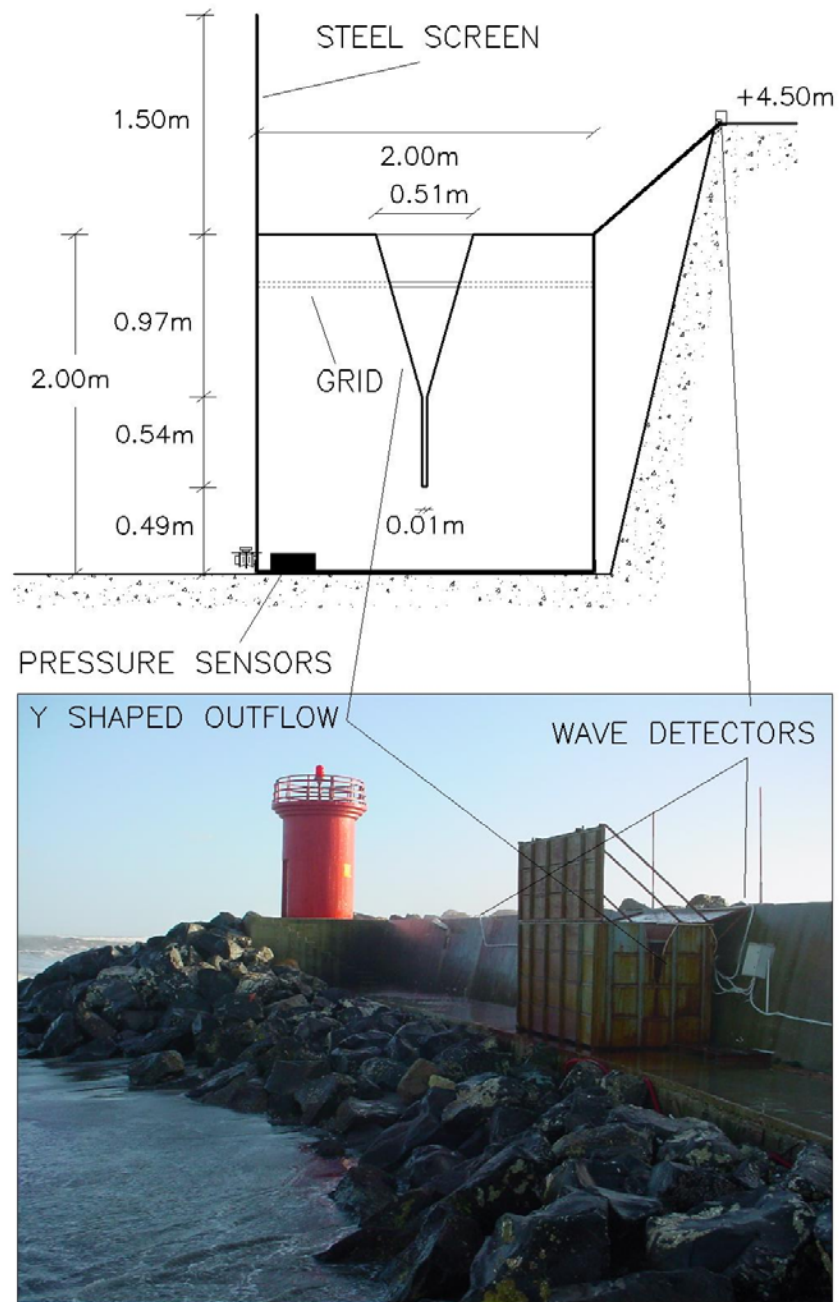
The instantaneous water level inside the tank is measured by two pressure transducers (Druck 1830 PTX) working in the range 0-3 m which are installed in a box fixed on the bottom of the tank and hydraulically connected to the four corners of the tank to reduce the sloshing effects on the measurements. In late 2002 only one pressure transducer was installed; the second transducer was installed one year later in order to have redundancy of the measurements. The transducers signals, sampled at 10 Hz, are transmitted in real time by cable to a personal computer located in the nearby control tower and stored for later analysis. The water depth multiplied by the horizontal area of the tank (8 m<sup>2</sup>) gives the instantaneous volume of water inside the tank.

The normal to the long side of the wave tank (parallel to the wall), is aligned with the offshore direction of 229° N.





**Figure 44:** Left panel: Layout of the overtopping measurement station in Rome yacht harbour. The convention for wind and wave angles is also indicated. A local frame of reference has been defined:  $\zeta$  is the normal direction to the tank,  $\eta$  is the tangent direction.  $\Delta\phi_w = \phi_w - \beta_t$  is the relative wind direction being  $\beta_t$  the normal to the tank ( $^{\circ}\text{N}$ ) and  $\phi_w$  is the wind direction ( $^{\circ}\text{N}$ ),  $\Delta\beta_w = \beta_w - \beta_t$  is the relative wave direction being  $\beta_w$  the wave direction ( $^{\circ}\text{N}$ ). Right panel: aerial photo of the overtopping measurement station (nov 2003).



**Figure 45: Cross section and photo of the wave overtopping tank operational at Ostia breakwater.**

## Measured overtopping events

During fall-winter 2003-2004 seven severe storms with overtopping were recorded for a total of 86 hours of data. Table 16 indicates the dates and the durations of the recorded overtopping events.

During the first two recorded storms some connection problems occurred due to an unexpected oxidation of the electric contacts; hence the measurements stopped after about 9 hours of overtopping for both the storms. Storms 5 and 7 may be regarded as double peaked storms: hence, though the overtopping events didn't occur for a few hours within each storm, they are classified as single storms. Also during storms 6 and 7, the cable connection between the control tower and the tank experienced some problems and some measurements are missing. It is finally worth mentioning that the starting time of the records may be different from the actual starting time of the overtopping events as the instruments were not measuring continuously and the acquisition process had to be started each time by the research team.

Wave, sea level and wind conditions showed very moderate variation over typical duration of one hour; all the data have been therefore analysed on an hourly basis.

**Table 16: Dates and duration of the recorded overtopping events at Ostia breakwater.**

Storm No.	Date Dd/mm/yyyy	Start - end time of overtopping measurement (GMT+1)	Valid inshore (P2) wave and sea level records duration [hrs]	Valid offshore wave records duration at Civitavecchia [hrs]	Valid sea level records duration in the harbour [hrs]	Valid overtopping records duration [hrs]
1	05/10/2003	10:00 – 19:00	9	9	9	9
2	08/10/2003	00:00 – 09:00	9	9	9	9
3	23/10/2003	21:00 – 00:00	-	3	3	3
4	30/10/2003	09:00 – 20:00	-	2	11	11
5	27-28/11/2003	17:00 – 19:00	-	26	26	26
6	14-15/01/2004	18:00 – 15:00	-	21	21	13
7	23-24/01/2004	09:00 – 15:00	-	15	15	15
					total	86

Deep water wave characteristics have been retrieved from a directional wave buoy located offshore Civitavecchia (50 km north of Ostia), moored on a 100m depth (see Fig. 41 for the buoy location).

The non-directional wave recorder installed within the CLASH project provided information on wave characteristics in shallow water, since it was moored on a 6.5 m depth. Unfortunately, this instrument worked properly only during the first two storms: between storms 2 and 3 fishing activities (unauthorized in that area) caused serious damages to the wave recorder that required a long repairing time. In order to overcome the lack of information on shallow water wave conditions, consistently with the procedures used within the CLASH project (Steendam *et al.*, 2004), the state-of-the art spectral model SWAN (Ris *et al.*, 1999) was applied to study wave propagation from offshore to the harbour breakwater using, as offshore boundary conditions, the wave parameters provided by the Civitavecchia buoy. The bathymetry used in the calculations is shown in Fig. 43. Table 17 summarizes the ranges in which wave parameters in Ostia at P1 and Civitavecchia as well as relative freeboards ( $R_c/H_{m0}$ ) at P1 varied during overtopping measurements for all recorded storms.

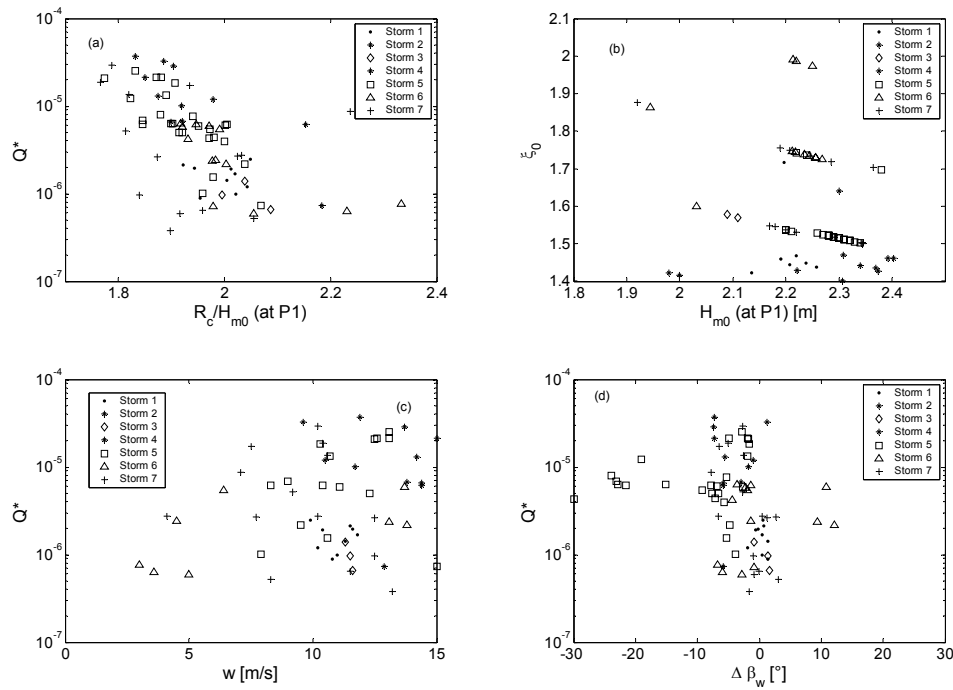
**Table 17: Ranges of variability of main wave parameters at toe (Ostia-P1) and offshore (Civitavecchia RON buoy) during the overtopping storms.**

Storm No.	Ostia at P1 (SWAN hindcasting); (in italic: measured data) (-4.0 m MSL)					Civitavecchia (-100 m MSL)		
		$H_{m0SWAN}$ [m]	$T_{pSWAN}$ [s]	Dir [°N]	$R_c/H_{m0}$	$H_{m0}$ [m]	$T_p$ [s]	Dir [°N]
1	Min	<i>2.14</i>	<i>8.39</i>	<i>230</i>	<i>2.05</i>	3.06	8.00	246
	Max	<i>2.26</i>	<i>9.56</i>	<i>229</i>	<i>1.92</i>	3.17	8.30	244
2	Min	<i>2.22</i>	<i>8.39</i>	<i>228</i>	<i>1.98</i>	3.01	8.00	242
	Max	<i>2.40</i>	<i>10.90</i>	<i>222</i>	<i>1.83</i>	3.47	10.00	234
3	Min	<i>2.09</i>	<i>8.39</i>	<i>228</i>	<i>2.09</i>	2.43	7.70	243
	Max	<i>2.11</i>	<i>8.39</i>	<i>230</i>	<i>2.00</i>	2.56	7.70	246
4	Min	<i>1.98</i>	<i>7.37</i>	<i>223</i>	<i>2.18</i>	2.34	6.90	232
	Max	<i>2.00</i>	<i>7.37</i>	<i>223</i>	<i>2.15</i>	2.27	6.90	234
5	Min	<i>2.15</i>	<i>7.37</i>	<i>199</i>	<i>2.07</i>	3.33	7.70	192
	Max	<i>2.38</i>	<i>10.89</i>	<i>227</i>	<i>1.77</i>	4.17	9.50	243
6	Min	<i>1.94</i>	<i>9.56</i>	<i>222</i>	<i>2.33</i>	1.95	8.30	236
	Max	<i>2.28</i>	<i>12.41</i>	<i>239</i>	<i>1.92</i>	4.16	9.50	292
7	Min	<i>1.74</i>	<i>9.56</i>	<i>222</i>	<i>2.57</i>	1.64	5.60	237
	Max	<i>2.37</i>	<i>10.90</i>	<i>224</i>	<i>1.77</i>	3.07	6.50	238

Wave overtopping rates have been calculated using two of the methods described in Troch et al. (2004) as explained in detail in Briganti *et al.* (2005, in review). Hence, according to the two different methods used, the overtopping rates computed using the numerical integration of the continuity equation will be referred as  $q_{ce}$ , while the value obtained applying the graphical method based on the level jumps in the overtopping signal (whose number is  $N_{jumps}$ ) will be referred as  $q_{\Delta h}$ .

In the following the number of overtopping events ( $N_{ov}$ ) will be considered equal to  $N_{jumps}$ .

In order to correlate the measured overtopping discharges with the most important related parameters, it is useful to analyse the scatter plots shown in Fig. 46.



**Figure 46: Scatter plots of the most important parameters recorded during the 86**

**overtopping events. Here  $Q^* = \frac{q_{\Delta h}}{\sqrt{gH_{m0}^3}}$ ,  $\xi_0 = \frac{\tan \alpha}{\sqrt{\frac{2\pi H_{m0}}{gT_{m-1,0}^2}}}$ ,  $w$  is the local wind speed,  $\Delta\beta_w$  is**

**local wave direction relative to the normal to breakwater axis.  $H_{m0}$  is the significant wave height at the toe of the structure.**

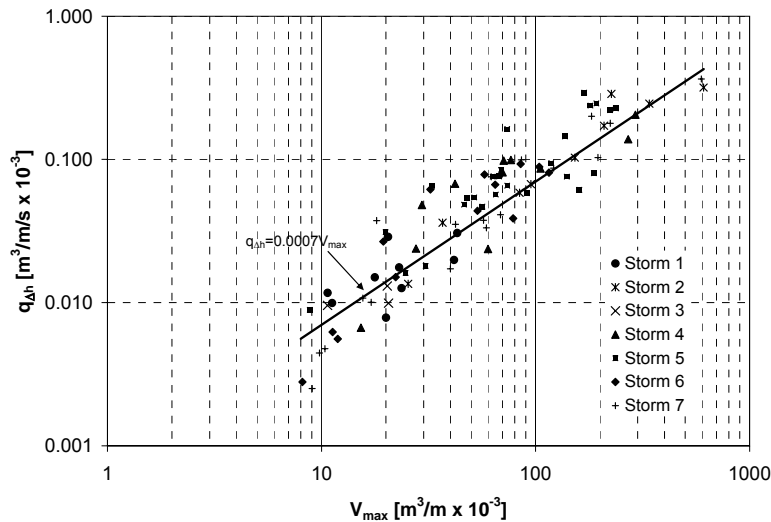
The non-dimensional wave overtopping rate  $Q^* = q_{\Delta h} / \sqrt{gH_{m0}^3}$  has been plotted against the wind speed module ( $w$ ), the relative freeboard ( $R_c/H_{m0}$ ) and the wave angle at the toe of the structure ( $\Delta\beta_w$ ). Also the surf similarity parameter ( $\xi_0$ ) has been plotted against the  $H_{m0}$  at the toe. A good inverse correlation is observed between  $Q^*$  and  $R_c/H_{m0}$ . Larger values of the dimensionless overtopping discharge ( $Q^*$ ) generally occurred with larger values of  $w$ .

Table 3 illustrates some parameters related to the peak mean unit overtopping discharges measured in all the recorded storms. It is evident that the  $H_{m0}$  at the toe of the structure spans within a very limited range, as it is depth-limited, while wave overtopping peak rates show a large variability among the storms.

**Table 18: Maxima values of measured average hourly overtopping rates during each of the 7 storms with corresponding relevant parameters.**

Storm No.	Time	$q_{\Delta h}$ [m <sup>3</sup> /m/s] x 10 <sup>-6</sup>	$q_{ce}$ [m <sup>3</sup> /m/s] x 10 <sup>-6</sup>	$H_{m0}$ [m]	$T_p$ [s]	$\Delta\beta$ [°]	$\xi$	$V_{max}$ [m <sup>3</sup> /m]	$N_{ov}$	$R_c/H_{m0}$
1	18:00	30.61	12.50	2.22	8.39	1	1.33	0.038	6	1.92
2	07:00	245.06	569.35	2.39	10.9	-7	1.46	0.340	4	1.83
3	22:00	13.07	20.44	2.09	8.39	-1	1.58	0.020	3	2.04
4	14:00	205.09	142.10					0.293	14	
5	13:00	293.06	256.95	2.34	9.56	-3	1.50	0.169	19	1.83
6	13:00	92.90	35.75	2.22	10.9	11	1.99	0.085	8	1.97
7	09:00	364.64	292.55	2.34	9.56	-3	1.50	0.595	13	1.79

Since the hazard related to wave overtopping is strictly related to the individual overtopping volumes (see Franco et al., 1995) it is also interesting to look for the correlation between the maximum individual volume per unit length recorded during each hour ( $V_{max}$ ) and the mean overtopping discharge (here  $q_{\Delta h}$  has been used as it is directly computed starting from the knowledge of individual overtopping volumes). This correlation is shown on a logarithmic scale in Fig. 47. No relevant differences appear in the correlation between these two parameters among the measured storms. Data have been plotted with a best-fitting line (regression coefficient  $R^2=0.74$ ) that reads:  $q_{\Delta h} = 0.0007V_{max}$ .



**Figure 47: Correlation between the mean hourly overtopping rate  $q_{\Delta h}$  and the maximum overtopping volume  $V_{\max}$  measured in the corresponding hour.**

### Comparison between measured overtopping rates and prediction formulae

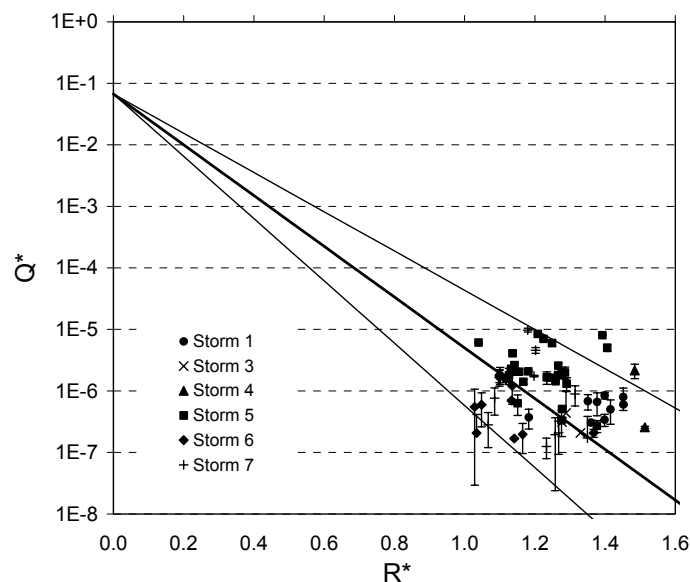
The overtopping events presented in this study are associated to oblique wave attacks and depth limited wave heights. Among the existing formulae, based on model studies, two of the most commonly used have been selected for predicting  $q_{ov}$  for the Ostia rock breakwater under investigation. The elder one is the one proposed by Owen (1980), originally developed for a straight and bermed impermeable slope subject to head-on irregular wave attacks. The use of a roughness factor extends the range of applicability of the formula to rough porous rubble mound structures. The alternative formula here considered for comparison is the van der Meer *et al.* (1998) formula, which included the effect of oblique wave attack, the formula here adopted makes use of the recommendations by TAW (2004). This latter formula, being the most widely used one for predicting overtopping rates at rubble mound breakwaters, will be presented first.

The comparison with the overtopping discharges predicted by the van der Meer *et al.* (1998) formula using the friction coefficient  $\gamma_f=0.5$  (Fig. 48 and Fig. 49) shows that almost all the prototype values fall within the confidence limits of the formula; only a few values for storm 5 and storm 7 fall out of the 95% confidence band of the parameter  $b_v$  used in the cited formula for defining the slope of the line in the  $Q^*$ - $R^*$  plane. As far as the storm 5 is concerned, the values show relatively large overtopping rates with high values of  $R_c/H_{m0}$ , as a possible consequence of an overestimation by SWAN of wave height reduction at P1 induced



by breaking. However it is worth pointing out that there is only a moderate tendency of the central value of the formula to underestimate the overtopping discharges. Furthermore it is to be considered that the used formula does not take into account the presence of the crest berm which has the effect of reducing the overtopping.

It can be concluded that prototype measurements are reasonably well predicted by the van der Meer *et al.* (1998) formula when using the suggested values of the reduction factors. However, when the effect of the crest berm (as it is present in reality) would be taken into account in this formula, the formula would underestimate the prototype results. Moreover, the roughness factor to be used for predictions is considerably smaller in this case (see also WP4), which results in an additional underprediction.

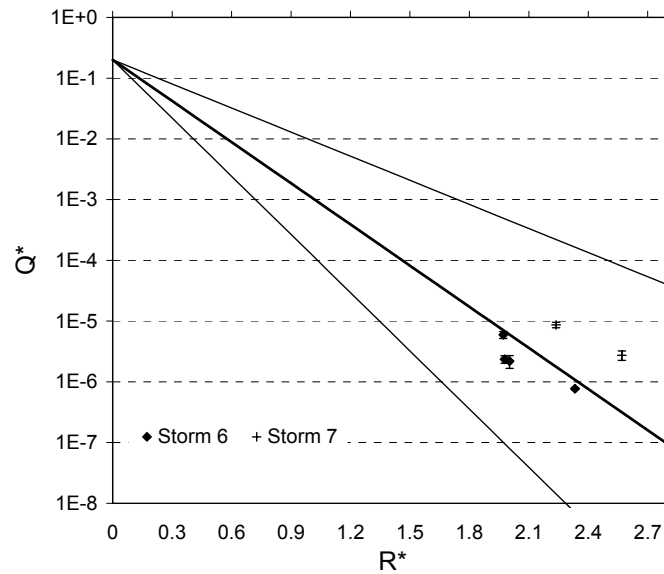


**Figure 48: Comparison between the measured adimensional mean overtopping discharges and those predicted using van der Meer *et al.* (1998) for breaking waves using  $\gamma_f = 0.5$**

(solid line thick line) together with the 95% confidence.  $Q^* = \frac{q_{ov}}{\sqrt{gH_{m0}^3}} \sqrt{\frac{s_0}{\tan \alpha}}$  and

$$R^* = \frac{R_c}{H_{m0}} \frac{\sqrt{s_0}}{\tan \alpha} \frac{1}{\gamma_b \gamma_\beta \gamma_v}. \text{ Error bars indicate the maximum and the minimum value of mean}$$

unit overtopping discharge obtained using the two illustrated methods.

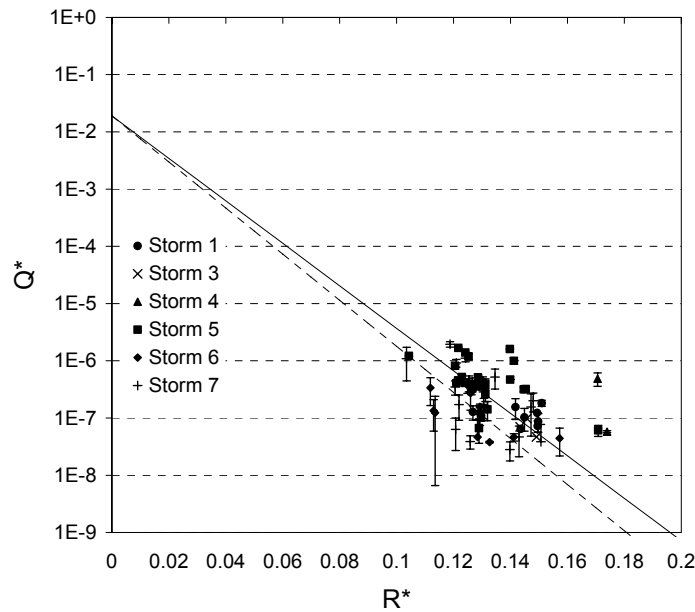


**Figure 49: Comparison between the measured adimensional mean overtopping discharges and those predicted using van der Meer et al. (1998) for breaking waves using  $\gamma_f = 0.5$  (solid line thick line) together with the 95% confidence limits (solid thin lines).**

$$Q^* = \frac{q_{ov}}{\sqrt{gH_{m0}^3}} \quad \text{and} \quad R^* = \frac{R_c}{H_{m0}} \frac{1}{\gamma_\beta}$$

**Error bars indicate the maximum and the minimum value of mean unit overtopping discharge obtained using the two illustrated methods.**

Fig. 50 illustrates the results of the comparison, being the Owen (1980) formula results represented by a solid line and Besley (1999) corection for accounting the presence of a crown berm by a dashed line. The prediction formulae, especially with the correction for the berm, has a tendency to underestimate the values of the overtopping rate.



**Figure 50: Comparison between the measured mean unit overtopping discharges and those predicted using Owen (1980) formula (solid line) and with crest berm correction as proposed by Besley (1999) (dashed line) during six of the seven measured storms with**

**overtopping  $Q^* = \frac{q_{ov}}{gH_{m0}T_{om}}$  and  $R^* = \frac{R_c}{H_{m0}} \left( \frac{s_{om}}{2\pi} \right)^{0.5}$ . Error bars indicate the maximum and the minimum value of mean unit overtopping discharge obtained using the two illustrated methods.  $\gamma_f = 0.5$ .**

## Conclusions

During the CLASH project an extensive (86 hours) and valuable field measurements of wave overtopping have been recorded at Rome-Ostia yacht harbour and analysed by MODIMAR. The setup of the prototype station is similar to the one presented in Troch *et al.* (2004) for Zeebrugge and developed during CLASH project as well. The reliability of the overtopping measurement procedure thereby introduced is then confirmed by the analyses here reported. Some relevant differences between the two sites may be highlighted. The Ostia site is characterised by a wide shallow foreshore which induces wave breaking before the structure hence, during overtopping storms, waves are always depth limited at the toe of the structure. Both wave measurements and wave model results (SWAN), validated on the recorded data of two storms, have been used to describe wave conditions across the foreshore and at the toe of the structure during overtopping storms. Furthermore, the Ostia rock breakwater has a slope

of 1:4, that is more gentle than the one of the Zeebrugge instrumented breakwater armoured with Antifer cubes (slope 1:1.4). Moreover oblique wave attacks causing overtopping have been also recorded and presented. It may be concluded that the most relevant difference between the two sites relies in the dissipation processes sustained by the waves in the propagation on the foreshore and on the structure itself.

A comparison of the measurements with two existing prediction formulae (i.e. the one proposed by van der Meer et al., 1998 and the one by Owen, 1980 with corrections by Besley, 1999) have been carried out. Both selected formulae show reasonably good estimates of the actual overtopping rates. It has to be noted that in this case prototype oblique waves and spectral characteristics which diverge from JONSWAP spectra have been taken into account for the first time.

The comparison carried out in the framework of CLASH seems however to confirm the suspected scale effects for wave overtopping at sloping rubble mound structures. The Owen (1980) formula as corrected by Besley (1999) to take into account the effect of a permeable crest berm, tends to underestimate the prototype results. The van der Meer et al. (1998) formula corresponds quite well to the prototype results. However, if the crest berm would be taken into account in the latter formula, it would also underestimate the results.

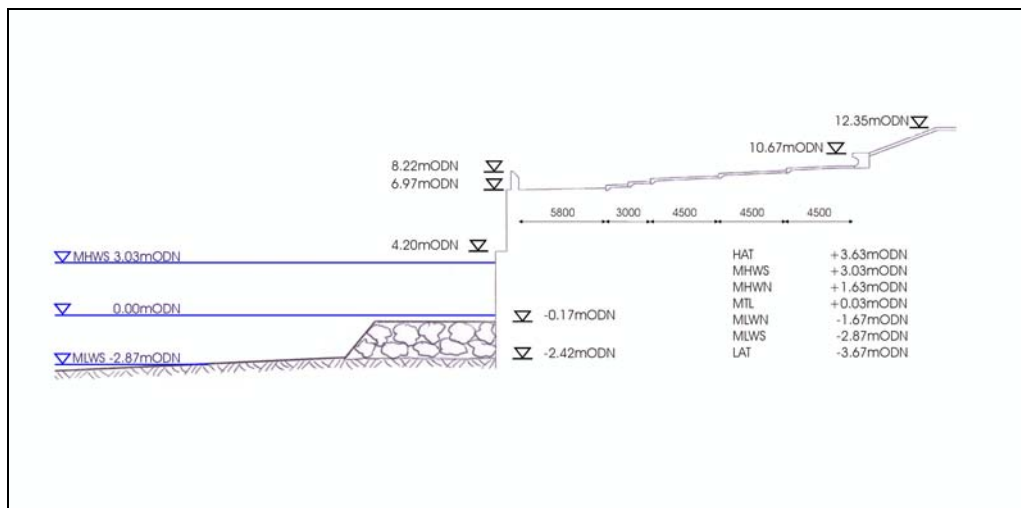
### 3.2.3 Site 3 : *Samphire Hoe (UK)*

Samphire Hoe, shown in Fig. 50 where the study area has been boxed, is located in the Southeast corner of England immediately to the west of Dover, and is an area of reclaimed land comprising  $4.9\text{Mm}^3$  of chalk marl excavated from the Channel Tunnel. The area of approximately  $300000\text{m}^2$  is enclosed by a vertical seawall with a crest level at  $+8.22(\text{mODN})$  and a toe level at  $-2.42(\text{mODN})$ . To the top of the seawall is a 1.25m parapet wall fronting a 25m stepped promenade where the field monitoring equipment is deployed (see Fig. 51). Samphire Hoe, which is owned by Eurotunnel, has been landscaped and is operated by the White Cliffs Countryside Project as a public recreational area. The reclamation is exposed to waves from the southwest and southeast, and is subject to overtopping by spray (often termed white water overtopping) on approximately 30 days per year as a result of waves breaking over the rubble toe berm and impacting on the seawall face (see Fig. 52). Whole wave overtopping (usually termed “green water overtopping”) is also observed regularly.



**Figure 51: Aerial view of Samphire Hoe with the study area in the foreground**

HRW has designed and implemented over six years an overtopping hazard warning system using tailored input data from the UK Met Office, see Gouldby *et al.* (1999). These systems use forecasts of wind speed and direction with predicted tide and surge levels, to predict potential occurrences of hazards from wave overtopping. This system does not use direct calculations of overtopping discharges, but has been steadily refined over 5 years of operation, using hourly observations of hazard from overtopping, categorised as low, medium or severe, and recorded by on-site personnel who are responsible for the safety of the public. The site is, therefore, an ideal location to set up a programme of field measurements. In particular, the existing hazard warning system facilitated the identification of potential storms prior to the deployment of the field monitoring equipment.



**Figure 52: Section of the Samphire Hoe Seawall**

The principal objective in the design of the field monitoring equipment, was to be able to capture sufficient overtopping discharges across the promenade to determine with sufficient accuracy both the total volume and the spatial distribution. As can be seen from Figure 52, the overtopping discharge is distributed over a wide area and it would clearly have been impracticable to attempt to capture all of this discharge. Moreover, certain constraints were imposed on HRW by the site owner that prevented the placement of tanks in certain areas. Also, the equipment had to be transported to the site and installed on each visit, and so it had to be handled easily, constructed quickly and be easily transportable.



**Figure 53: Violent wave overtopping at Samphire Hoe (Photograph courtesy of Eurotunnel and the White Cliffs Countryside Project)**

The main pieces of equipment for measuring the overtopping, were three volumetric tanks placed across the promenade of the seawall. The first tank was placed directly behind the

parapet wall, and the others were placed inline with the first on the first and second steps of the promenade. This arrangement, along with the control box attached to the rear of the parapet wall, can be seen in Fig. 54. Each of the three tanks are divided into two compartments, each with a nominal capacity of 240 litres, and equipped with 350mbar Druck PTX1830 pressure transducers.



**Figure 54: The three tanks in position at Samphire Hoe**

The overtopping discharges captured in the tank compartments were allowed to drain freely, and so it was necessary only to capture the instantaneous head in each compartment following each individual overtopping event. This was necessary because the compartments would fill in a very short period during extreme conditions, but more particularly, it enabled the individual wave-by-wave discharges to be determined.

Design of the tanks was based on wave overtopping predictions and spatial distribution of the overtopping as suggested by Jensen & Sorensen (1979).

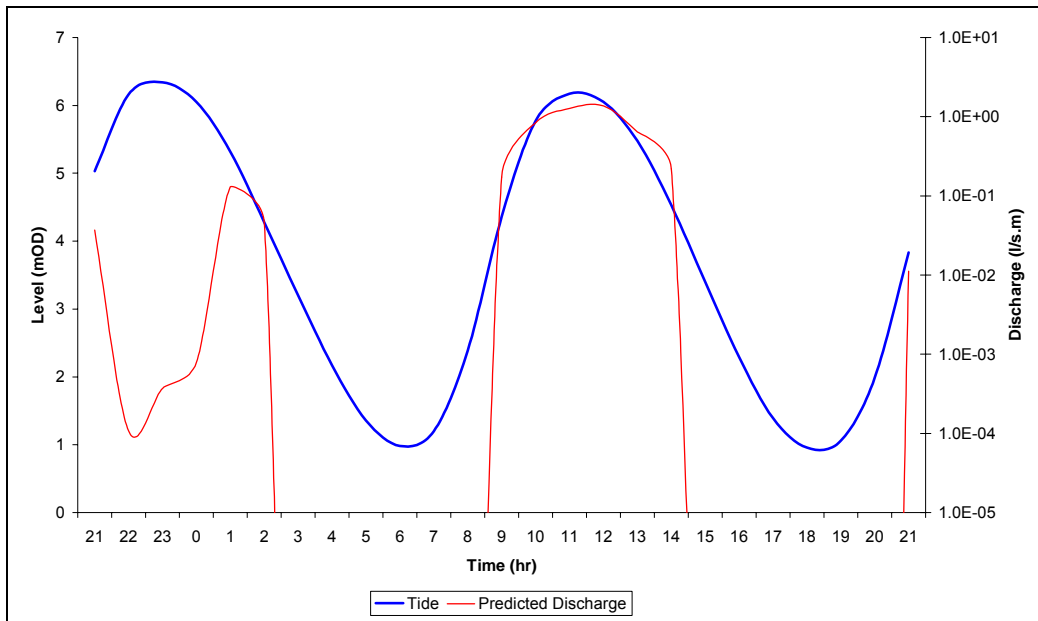
## Measurement Results

During the winter and spring of 2003 there were few storms that caused overtopping at Samphire Hoe, but weather forecasts suggested two occasions when it was useful to deploy the monitoring equipment at Samphire Hoe. The first visit was during March '03 where one storm was monitored on the 10<sup>th</sup>, and the second visit was during May '03 when storms were monitored on the 1<sup>st</sup> & 2<sup>nd</sup>. A range of conditions were encountered during these visits, and overtopping varied from light spray to high discharges from waves impacting violently on the seawall. For simplicity the three monitored storms will be referred to simply as Storm 01 (10 March), Storm 02 (1 May) & Storm 03 (2 May).

During Storm 01 overtopping water was seen to appear regularly over the top of the parapet wall, but this was in general sporadic and was spread along the length of the western splay wall. Those discharges that did pass over the top of the parapet wall were blown widely across the promenade as spray by high wind velocities, but no measurable quantities of overtopping discharge entered into the tanks. A conservative estimate of the mean overtopping discharge rate for this storm would be of the order of say 0.05 l/s.m.

Storm 02 was characterized by waves with  $H_s$  ranging from 1.5 to 2.2 m, while  $T_m$  was about 5.5 s. During the early stages of Storm 02 the wind speeds were at force 7, resulting in similar plumes of spray witnessed during the earlier storm. Predicted overtopping discharges are shown in Fig. 54 against the water level for this storm. From Fig. 54 it can be seen that a maximum overtopping discharge of approximately 1.4l/s.m was predicted at 12:00, but a peak discharge of 0.28l/s.m was recorded during the storm. This discrepancy is partially explained by the presence of the high winds, as most of the overtopping discharges were being blown across the seawall promenade and not falling into the overtopping tanks.





**Figure 55: The predicted overtopping discharges shown varying with the water level**

Storm 03 was characterized by wave heights  $H_s$  ranging between 1.3 and 2.6 m,  $T_m$  was about 6 s. For this storm there were very high winds during the early stages of the storm, and observations were made in this area when plumes of overtopping water were being blown over distances in excess of 100 m. Considerable quantities of this discharges were falling directly behind the parapet wall, where individual discharge volumes of between approximately 300 l/m and 500 l/m were estimated. If it is assumed that this represents about half the water in each overtopping event, then the remaining half was being blown across areas of the order of 3000 m<sup>2</sup>. Clearly the conditions were hazardous, and it was possible to determine a qualitative description of the hazards.

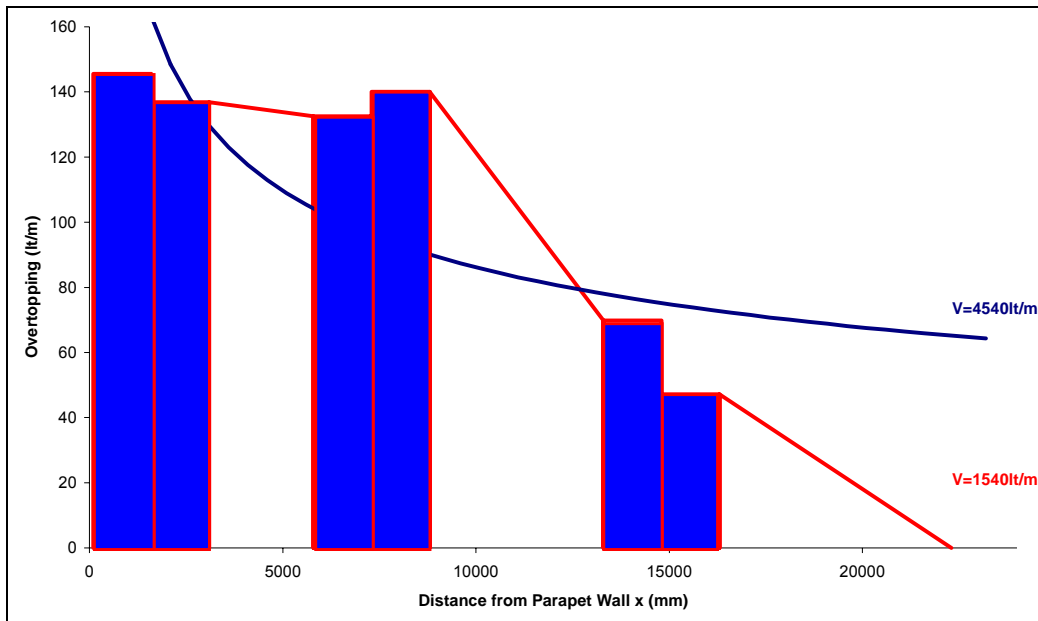
The volumes of water landing across the promenade became less severe on each tier, with the least landing on the top tier. It was decided that the only way to gain an improved scientific understanding of the potential hazards involved, was to stand directly in the path of the overtopping plume. It was agreed that standing on the top tier was equivalent to standing in a very heavy rain shower. Towards the lower tier, where it was still considered to be reasonably safe, the experience was similar to that which might be expected during a heavy hailstorm accompanied by a firm push on the back. Under these conditions, any unprepared people would be at high probability of being knocked over. Conditions directly behind the parapet wall were too hazardous to be approached closely. Later, when the water level had risen far enough to bring the overtopping to the measurement site, the wind speeds had become

insignificant. Without the winds the overtopping discharges were being directed vertically upwards and coming down in the area directly behind the parapet wall.

Each of the storms, specifically Storms 01 & 02, lasted several hours, and the water levels and wave conditions changed throughout this time. To allow for this, the measurements have been divided up into  $\frac{1}{2}$  hour periods. Each  $\frac{1}{2}$  hour period was assessed separately, and the recorded mean discharges were compared with Besley's (1999) predictions for mean overtopping discharges for a composite vertical wall. Strictly speaking, this technique is not wholly correct, as the Samphire Hoe seawall is actually slightly battered, stepping back as it does in three distinct sections. Nonetheless, they do provide an adequate means of comparing the results to known methods for these types of structures. Increased factors of 1.3 & 1.4 for walls battered to 10:1 & 5:1, respectively, are given by Bruce *et al.* (2001), and it is probable that these could be applied to composite structures, too.

Having established the individual overtopping discharges in each of the tank compartments, it was first necessary to approximate the discharges that had fallen outside of the tanks. Only then could a realistic comparison be made. The anticipated spatial distribution of the discharges might be similar to that described by Jensen & Sorensen (1979). Whilst this serves as a useful description, more often the actual behaviour was very different. For example, from the account of Storm 03 given above, it is noted that the overtopping discharges were often directed vertically upwards and came down directly behind the parapet wall, with the result that discharges were only captured in the front two tank compartments. For other events there was little difference among the volumes collected in the front four compartments.

For the analysis of the data a trapezoidal distribution of the individual volumes was assumed between the recorded data points and the back of the promenade 23.2 m from the seawall crest. The trapezoidal distribution of a large discharge is shown in Fig. 55, which shows overtopping distributed across all 6 tank compartments. Different distributions were assumed depending on how many tanks received a discharge, but each assumed this basic approach. In effect, the missing water was calculated between compartments 2 & 3, 4 & 5 and from the end of 6 to the point at 23.2 m in front of the recurve as appropriate. When the last discharge was in compartments 1, 3 or 5 then the distribution would stop at that point. The total discharge is therefore the sum of the discharges in the tanks and the interpolated discharges between the tanks. A comparison of the difference between a trapezoidal (1540 l/m) and a logarithmic discharge (4540 l/m) is also shown in Fig. 55 for the same captured volumes, and it is clear from this example that the trapezoidal distribution is a more realistic approximation.



**Figure 56: Trapezoidal distribution of overtopping discharges**

The analysed results of Storm 02 are shown in Fig. 56, and those for Storm 03 are shown in Fig. 58. These figures compare the field measurements with Besley's (1999) empirical overtopping prediction method for a composite vertical seawall. It is clear that they show that the general behaviour over the valid range is in agreement with the predictions. The most significant observation that can be made is that the data are slightly below the prediction line in Fig. 57 but more or less on the prediction line in Fig. 58. This should be expected as much of the overtopping water was being blown across the promenade during Storm 02, and so therefore the captured overtopping will be below that predicted. However, for Storm 03 the wind had little or no affect on the overtopping plumes, and so we see a good agreement with the prediction. For a more detailed discussion on these field measurements refer to Pullen *et al.* (2004a). No storms were measured at Samphire Hoe during the wintern 2003– 2004.

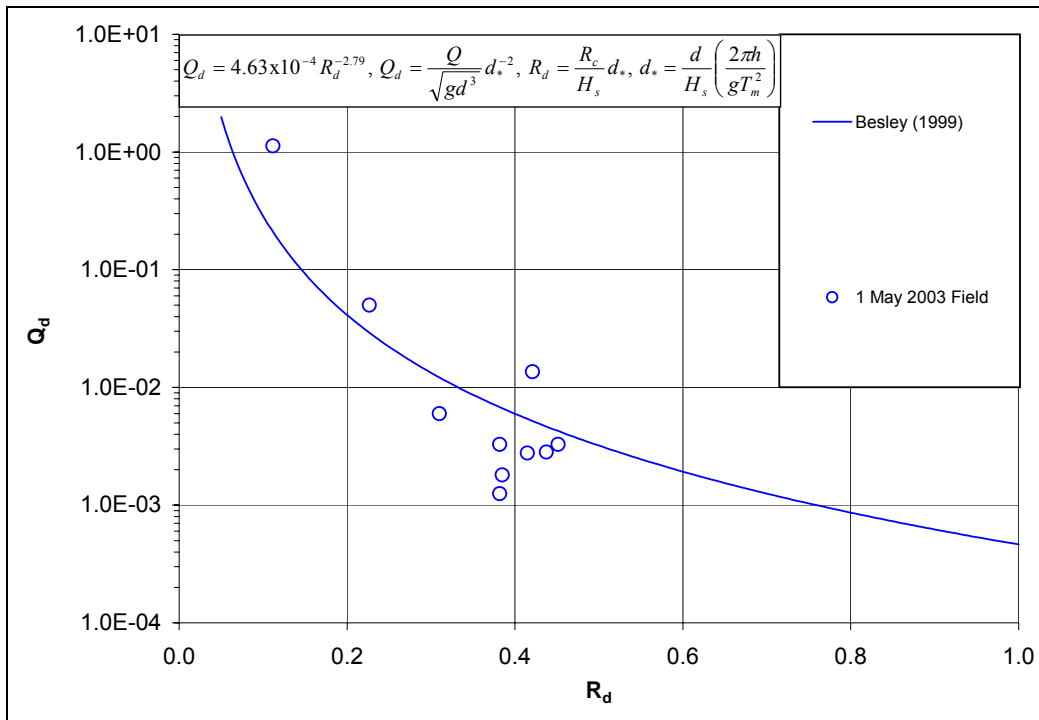


Figure 57: Measurements and predictions of overtopping during Storm 02

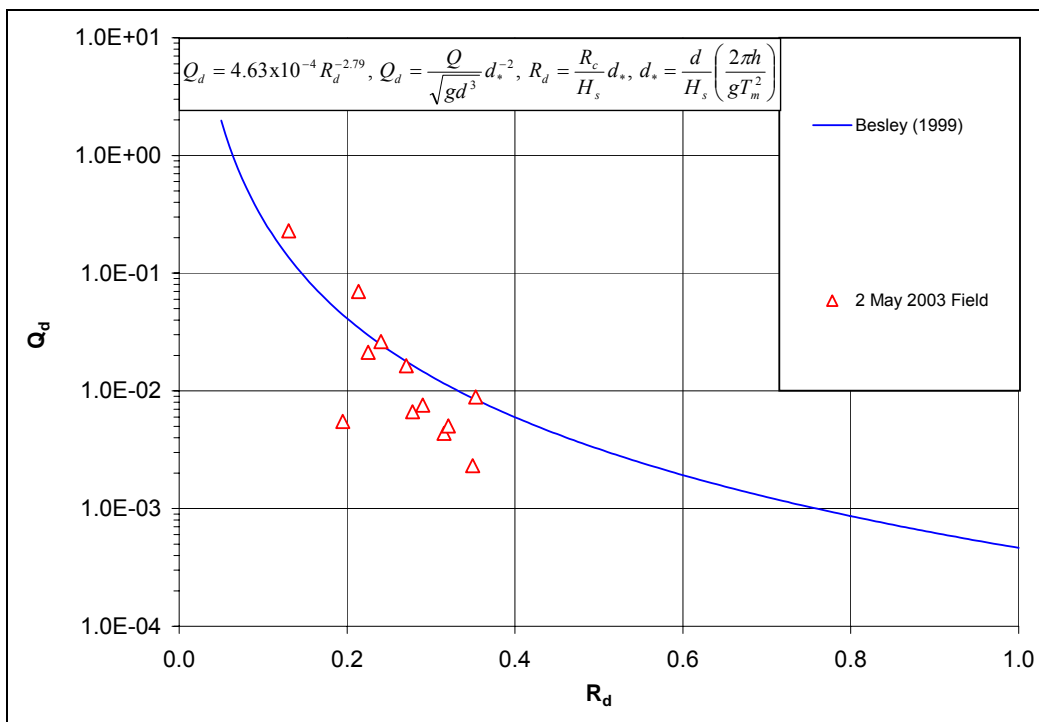


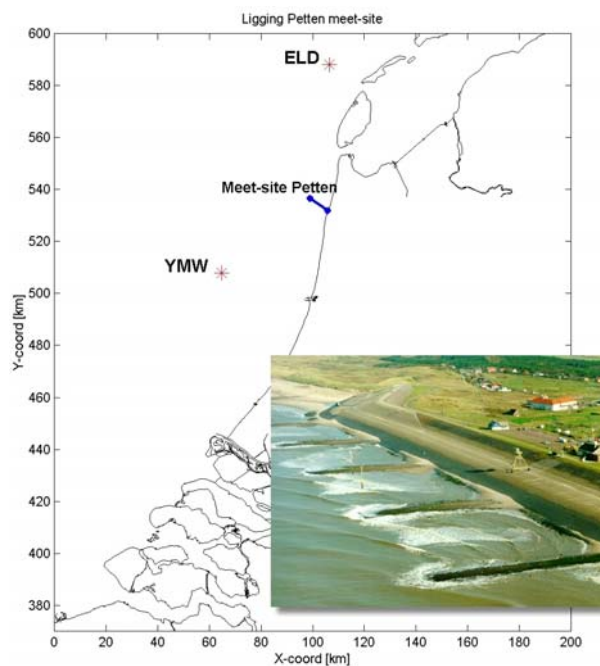
Figure 58: Measurements and predictions of overtopping during Storm 03

## Conclusions

Wave overtopping has been measured successfully at the Samphire Hoe field measurement site. The results are in agreement with the empirical prediction method for a composite vertical wall by Besley (1999). The spatial distribution of the overtopping has been established.

### 3.2.4 Site 4 : Petten (The Netherlands)

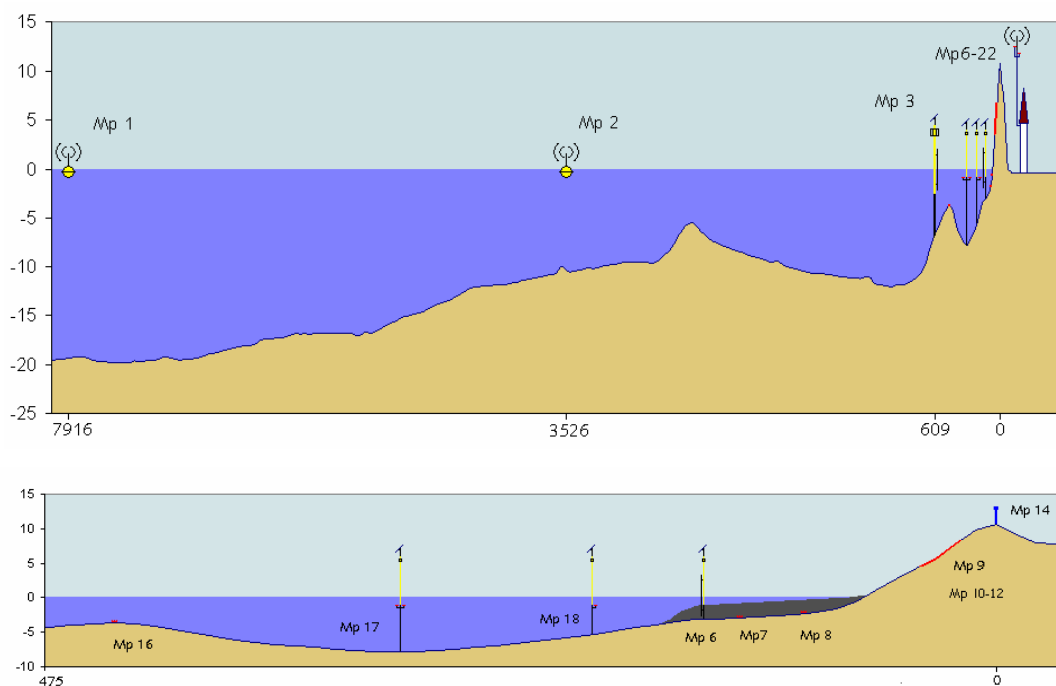
The field site is located off the coast of the province of North Holland near the town of Petten, where the Petten Sea Defence (Fig. 59) gives local shelter to the coastline. Determination of the height of the sea dike is based on a safety level with a chance of exceedence of 1/10000 per annum, and measures 12.75 metres above Dutch vertical reference level NAP. Over the years the adjacent dune areas have retreated, so that in comparison with the coastline the Petten Sea Defence extends slightly out into sea.



**Figure 59: Location of Petten field site**

To gain an understanding of wave propagation from deep water to the coastline, on-site measurements are taken at various distances from the dike at measuring points within or near section 20,830 of the Rijkswaterstaat annual coastal sounding programme. Wave run-up measurements are furthermore taken along the dike slope for use by the Road & Hydraulic Engineering Division. Fig. 59 shows the locations of all measuring points in a cross-shore profile corresponding with the measuring section. To avoid confusion, an enlarged graph of the relevant area shows the positions immediately offshore.

Some of the factors in selecting the measuring equipment are the location, the variables to be measured and the instruments available. The measuring points (MPs), the types of instrument and the locations are listed in table 19.



**Figure 60: Measuring points at Petten field site (distance and height in metres)**

### Morphological measurements

Especially during the last season some extra morphological measurements have been done to investigate the variability of the bottom profile in front of the dike.

Currents and waves cause sediment transport which in turn leads to constant changing of the cross-shore profile at the Petten Sea Defence. As the cross-shore profile has a direct effect on wave height, it is essential to monitor not only the waves but also the bottom topography changes. During storm season 2003–2004, the seabed was mapped several times by means of

soundings and groin section measurements. These random registrations do give information on the general seabed behaviour during the storm season, but not on the erosion depth during storms. To map the maximum erosion depth, which defines the maximum wave height, during storm season 2003–2004 the seabed level near MP 6 was also measured non-stop with an ASMIV seabed staff.

**Table 19: Measuring points and equipment at Petten field site**

Measuring point	Sensor/instrument	Dist. to ref. pt. <sup>1</sup> [m]	X coord RD [m]	Y coord RD [m]	Z [ <i>NAP</i> +/- m]	Location
MP 13	Anemometer (131), wind vane (132); Barometer (133)	-35	105798	531673	0.00	<i>Dijk te Kijk</i>
			105798	531673	0.00	
MP 22	Barometer (221)	-35	105798	531673	0.00	<i>Dijk te Kijk</i>
MP 14	Video camera 1 (141)	-0.2	105769	531693	17.3	Crest of dike
MP 19	Video cameras 2, 3 (191, 192)	1.1	105759	531677	16.6	Crest of dike
MP 12	Pressure sensor (121)	12.7	105749	531683	9.28	Dike's upper slope
MP 11	Pressure sensor (111)	18.2	105744	531685	7.23	Dike's upper slope
MP 9	Wave run-up staff (091)	19.4 (centre)	105743	531686	6.92 (centre)	Dike's upper slope
MP 10	Pressure sensor (101)	25.6	105738	531689	5.70	Dike's lower slope
MP 8	Pressure sensor (081)	55.7	105720	531719	0.55	Dike's lower slope
MP 7	Pressure sensor (071)	75.4	105703	531730	0.23	Groyne post
	Pressure sensor (072)	75.4	105703	531730	-0.29	Groyne post
MP 6	Capacitance wire (061)		105663	531752	-0.38	}
	Pressure sensor (062)	122.9	105663	531752	-0.92	}
	Radar level meter (063)	122.7	105663	531752	9.01	} Breaker
	Anemometer (064)	122	105663	531752	12.58	} bar post
	Wind vane (065)	122	105663	531752	12.58	}
	Water level staff (066)	122	105663	531752	-0.93	}
	ASM-IV (067)	122.7	105661	531715		}
MP 18	Pressure sensor (181)	170,5	105617	531771	-1.20	Sea bed
MP 17	Pressure sensors (171, 175)	276.7	105522	531817	-3.13	Sea bed
	Current meters (172, 173,174)	276.7	105522	531817	-3.13	Sea bed
MP 16	Pressure sensors (161,162)	436.6	105377	531886	-2.50	Sea bed
MP 3	Water level staff (031)	609	105234	531985	-3.00	Post
	Digital level meter (032)	609	105234	531985	0.00	Post
	Radar level meters (033/034)	609	105234	531985	11.32	Post
MP 2	Directional waverider (021)	3526	102896	533802		Petten <i>Polder</i>
MP 1	Directional waverider (011)	7916	99003	535832		<i>NAP</i> -20m

<sup>1</sup> The distance to the reference point is defined in relation to section 20,830 with zero coordinates

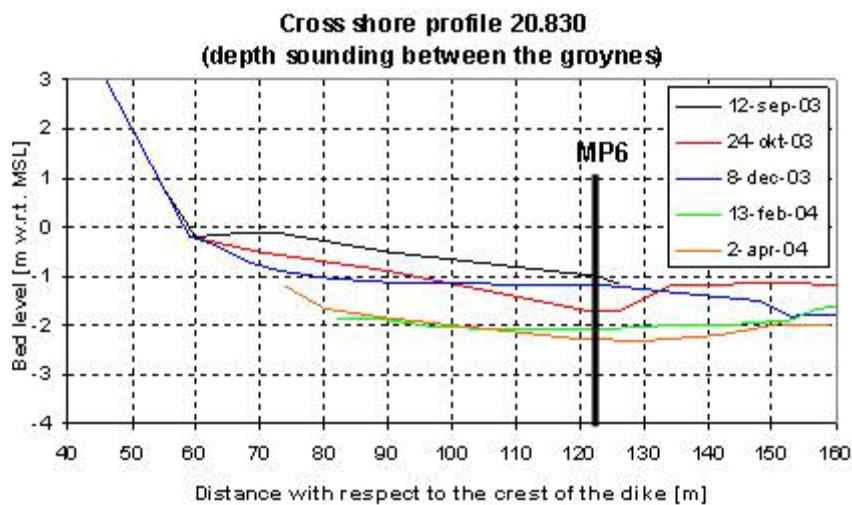
x = 105767, y = 531690 (corresponding with approx. the crest of the dike) and direction (nautical) 297,9 degrees



### *Groyne section measurements*

The groin section measurements were carried out for 7 parallel sections between the groins north and south of the measuring section. By using ‘WESP’, the seabed topography was registered to 100–150 metres seaward of the crest of the dike. The groin section measurements during storm season 2003-2004 were carried out on the following dates:

12 September 2003, 24 October 2003, 8 December 2003, 13 February 2004 and 2 April 2004



**Figure 61: Groyne section measurements Jarkus section 20,830**

Fig. 61 shows the results for the central section, i.e. section 20,830, corresponding with the measuring section. The registration on 12 September 2003 shows a typical summer profile with a large quantity of sand off the toe of the dike. It furthermore clearly shows that during the storm season there was considerable seabed erosion along the full section.

The data required for 3D processing are digitally available in ASCII format (X, Y, Z).

### *ASMIV sea bed staff*

Fig. 62 gives the levels near MP 6 as measured by the seabed staff from 17 October 2003 to 31 April 2004.

Fig. 62 shows that during the most recent storm season the bed level near MP 6 is subject to major changes. To determine the effect of erosion on the waves just off the dike, however, it does not suffice to make measurements at one single location. A more detailed analysis, where the ASMIV data are linked to spatial information, i.e. soundings and groin section measurements, is therefore strongly recommended.

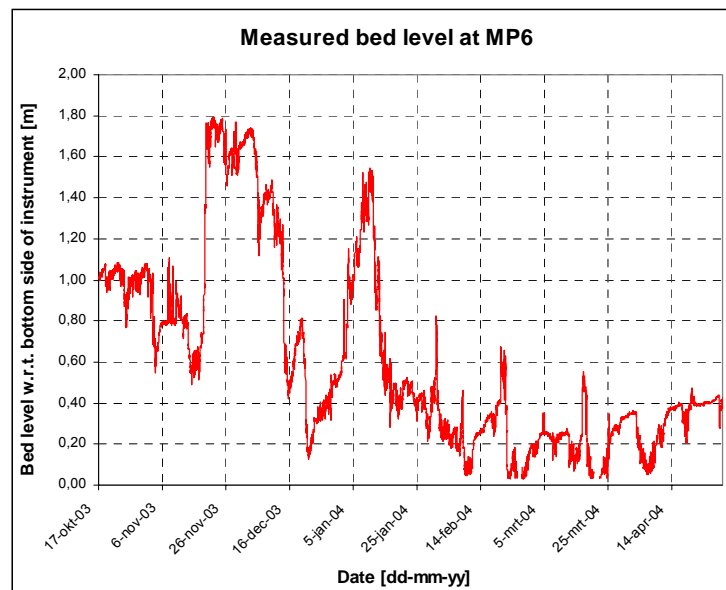


Figure 62: ASMIV results near MP 6

### Wave measurements

During the two storm seasons three interesting storm periods occurred : 25-28 October 2002, 20-22 December 2003 and 7-9 February 2004. Here the most interesting one will be described, storm period 20-22 December 2003. Figure 63 and 64 show the water levels and wave heights during this storm period.

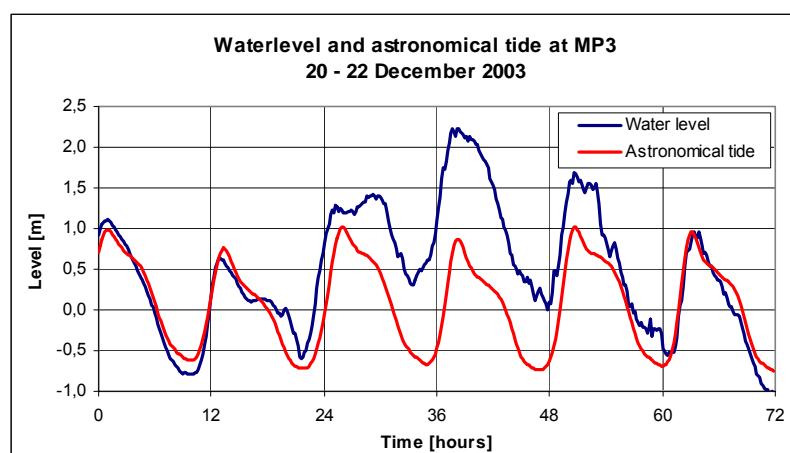


Figure 63: Water level at MP3 during the December 2003 storm.

Figure 64 clearly shows that on the first day and over a short period of time, wave height near MP 1 increases strongly to nearly 4 metres. The highest waves were measured at high tide in the early afternoon of 21 December, when wave height  $H_{m0}$  varied between 2 metres off the dike and nearly 7 metres near MP 1.

The wave period  $T_{m-1,0}$ , which is susceptible of low frequency energy, i.e. long waves, increases to a maximum of approx. 11 seconds at MP 1. Another clear illustration is that after the peak of the storm  $T_{m-1,0}$  decreases only very gradually, which can be explained by the fact that there is still an extensive amount of low frequency energy present in the area after the storm.

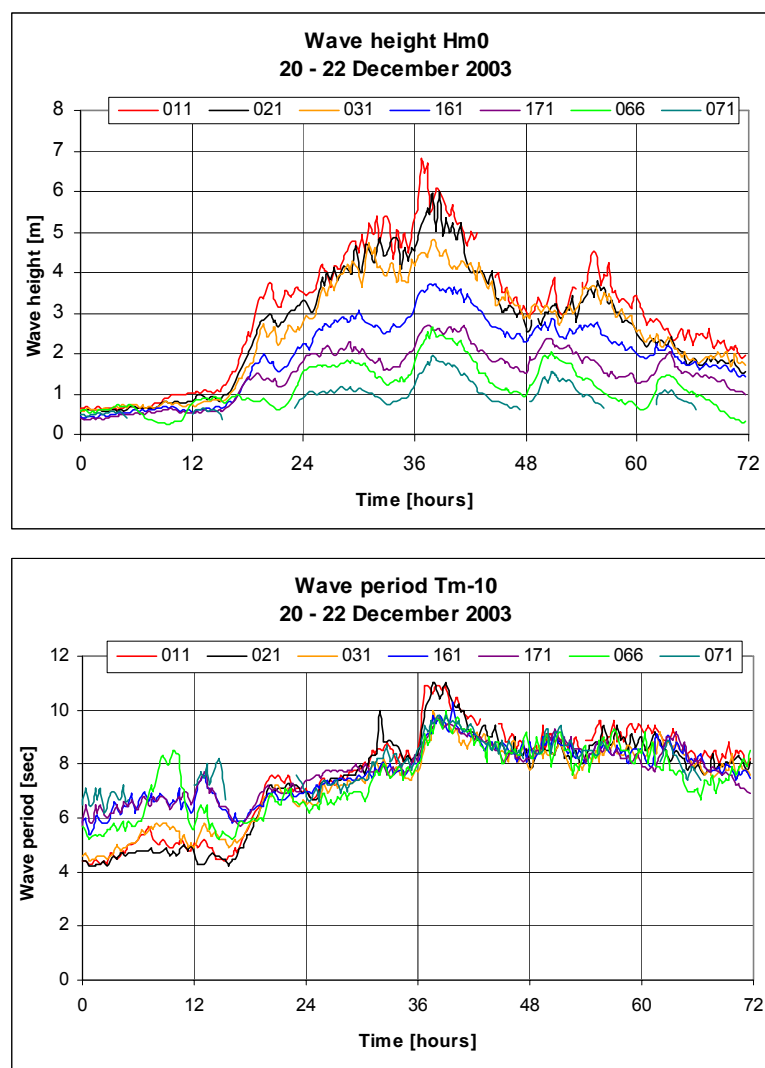


Figure 64: Wave height and wave period during the December 2003 storm.

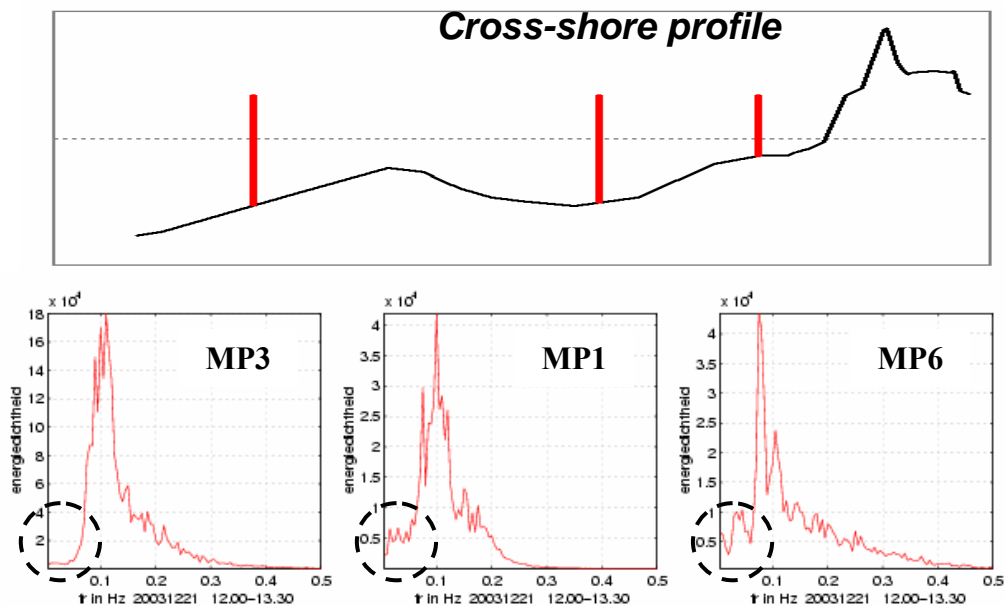
### ***Wave run-up measurements***

Run-up against the upper slope of the dike is measured by, among other instruments, a run-up staff placed in the dike revetment. The bottom end of this staff, which is 12 metres long, lies at NAP +5.70 metres. On 21 December 2003 run-up was measured between 12:45 hours and 18:00 hours, where it exceeded the levels NAP +6 metres, NAP +7 metres and NAP +8 metres during 527 seconds, 51 seconds and 12 seconds respectively. The highest run-up was NAP +8.91m.

### ***Low-frequency waves***

On the Petten field site, low frequency waves are most often measured during storm, where a distinction can be made between two types of long waves: low frequency waves originating from an earlier storm field elsewhere, also referred to as swell, and low frequency waves generated locally. This local generating is caused by the interaction between shorter waves and wave breaking in shallow water. The low frequency waves generated locally, with  $T_{m-1,0}$  exceeding 75 seconds, do not run up against the dike but cause a temporary water surface elevation, which enables shorter waves to run up higher against the dike.

To get an impression of the quantity of low frequency energy generated locally during the storm of 20–22 December, wave spectra are calculated for the peak of the storm (Fig. 65). It shows that there was some, although minimal, increase in low frequency energy between MPs 3 and 17 and between MPs 17 and 6.



**Figure 65: Spectra (including low frequency energy) calculated for instruments 031, 171 and 066.**

To gain an understanding of the relative share of the energy of low frequency waves (LFE) in the energy of the total spectrum, an analysis was made of both a storm period (27-28 October 2002) and a very calm day with (seaward) eastern wind (13 October 2002). On 13 October the  $H_{m0\_LFE}$  is no more than 0.04 metres but this is a relative share of 10% to 20% in wave height, and of 1% to 4% in the wave energy. It turns out that under storm conditions the low frequency wave height  $H_{m0\_LFE}$  increases considerably (on 27 October to approx. 0.60 metre). Local generating of long waves causes this increase. On 27 October the relative share of long waves compared to the total spectrum is approx. 10% ( $(H_{m0\_LFE}/H_{m0\_TOT})^2 = 0.30 * 0.30$ ).

## Conclusions

At the Petten field site, long waves are measured under both calm and stormy conditions. On 13 October 2002, a calm day with a seaward wind and short waves at a height of approx. 0.40 metres at MP 3, the relative share of long waves in the total spectrum's energy amounts 1% to 4%. The wave height for the filtered low frequency part of the spectrum is approx. 0.04 m.

Under storm conditions, the relative share of low frequency energy increases as a result of local generating of long waves. On 27 October, a storm day with waves up to approx. 5.5

metres at MP 3, values are measured up to approx. 0.60 metres for wave height  $H_{m0\_LFE}$ . With their long periods ( $T_{m-1,0}$  is approx. 75 sec), these long waves do not run up against the dike, but result in a temporary water surface elevation of approx. 0.30 m. The relative share of long waves in the total spectrum's energy is approx. 10%.

### 3.3 General conclusion for WP3

This WP delivered the following reports / deliverables:

a) for the Zeebrugge site:

- the report on full scale measurements, 1<sup>st</sup> full winter season (D15)
- the report on full scale measurements, 2<sup>nd</sup> full winter season (D31)

b) for the Ostia site:

- the report on full scale measurements, 1<sup>st</sup> full winter season (D16)
- the report on full scale measurements, 2<sup>nd</sup> full winter season (D32)

c) for the Samphire Hoe site:

- the report on full scale measurements, 1<sup>st</sup> full winter season (D17)
- the report on full scale measurements, 2<sup>nd</sup> full winter season (D33)

d) for the Petten site:

- the report on full scale measurements, 1<sup>st</sup> full winter season (D19)
- the report on full scale measurements, 2<sup>nd</sup> full winter season (D37)

Two milestones were achieved within this WP:

After the first full winter season (month 18 for the Zeebrugge, Ostia and Samphire Hoe site and month 19 for the Petten site), full scale measurements of all four sites are analysed and reported (M3). After the second full winter season (month 30 for the Zeebrugge, Ostia and Samphire Hoe site and month 31 for the Petten site), measurements of all sites are analysed and reported.

## 4 WP 4 : Laboratory investigation

### 4.1 Objectives

The main objective was to carry out a focused and well-directed set of scale model tests in order to provide data on overtopping for the comparison with full scale results. This comparison is performed in WP7 in order to solve the problem of suspected scale effects.

Another objective was to generate more and also missing data on overtopping to complete the homogeneous database (results of WP2). In WP2 possible missing parameters ranges were detected. These missing parameter ranges were the base for the additional tests carried out under WP4.

### 4.2 Description of work performed

Three different prototype sites were modelled in two different laboratories each. Additional tests to cover white spots in the database were carried out in three different laboratories. First the site specific tests are discussed and then the additional tests.

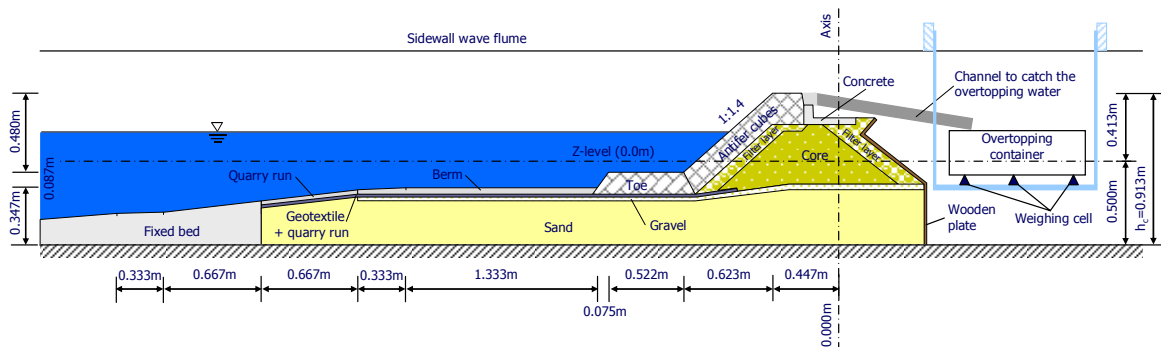
#### 4.2.1 Site 1 : Zeebrugge

CLASH focuses on investigations of wave overtopping for different structures in prototype and in laboratory. The Zeebrugge breakwater has been modelled in small-scale in the wave flume of Leichtweiß-Institute (LWI) at a scale of 1:30 and in the wind and wave test facility of the Universidad Politécnica de Valencia (UPVLC) at a 1:30 scale. The model investigations have concentrated on parametric tests on wave overtopping (LWI, UPVLC) and the analysis of measurement uncertainties and model effects (LWI, UPVLC) as well as the reproduction of storms (LWI, UPVLC), the influence of wind effects (UPVLC) and the positioning of armour elements (LWI, UPVLC).

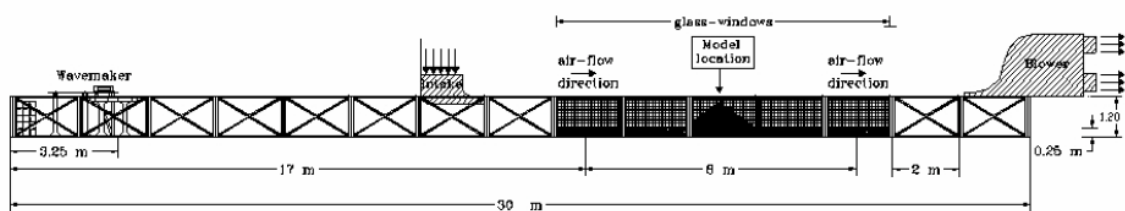
At LWI results regarding overtopping discharges for parametric tests, velocities of overtopping waves and forces on model dummies on top of the breakwaters crown wall were achieved. Altogether 226 tests have been performed; many of them were focussing on various uncertainty measurements such as repeatability, influence of position of the overtopping tray,

position of wave gauges, and various analysis methods. Furthermore, the influence of the armour layer was tested by exchanging the layer two times and performing the same tests. At UPVLC 53 parametric tests with and without wind, 17 repeatability and variability tests without wind, and 18 prototype tests with and without wind have been performed.

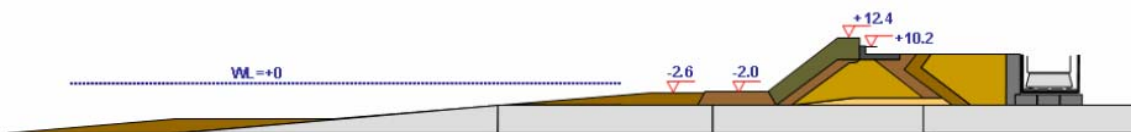
Fig. 66 gives a cross-section of the model set-up in the LWI flume. Fig. 67 and Fig. 68 give a cross-section of respectively the wind and wave facility and the Zeebrugge model at UPVLC.



**Figure 66: Cross section of the model set-up of the Zeebrugge breakwater in the LWI wave flume.**



**Figure 67: Longitudinal cross section of the UPVLC wind and wave test facilities.**



**Figure 68: Cross section of the Zeebrugge scale model at UPVLC.**

Fig. 69 and Fig. 70 show graphical representations of all model tests in a typical non-dimensional plot. Fig. 69 gives all parametric tests together with storm reproductions (all without wind), while Fig. 70 gives the influence of wind (three different wind speeds) on the measured overtopping.



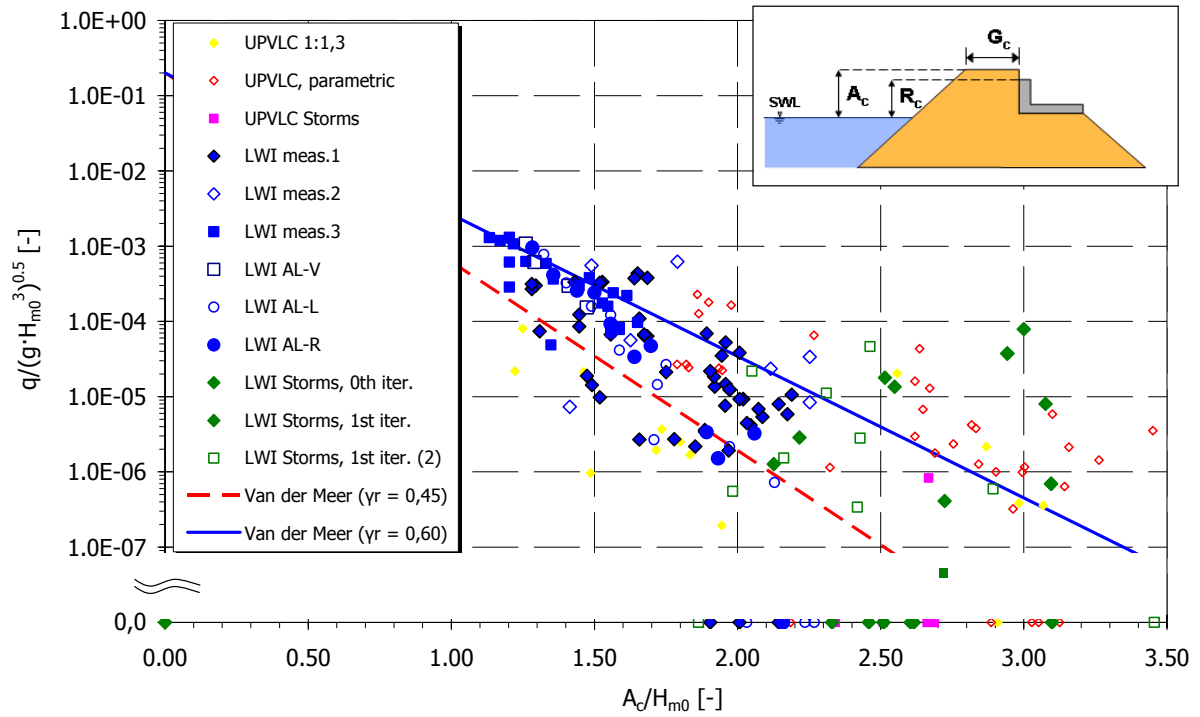


Figure 69: Zeebrugge model test results (no wind).

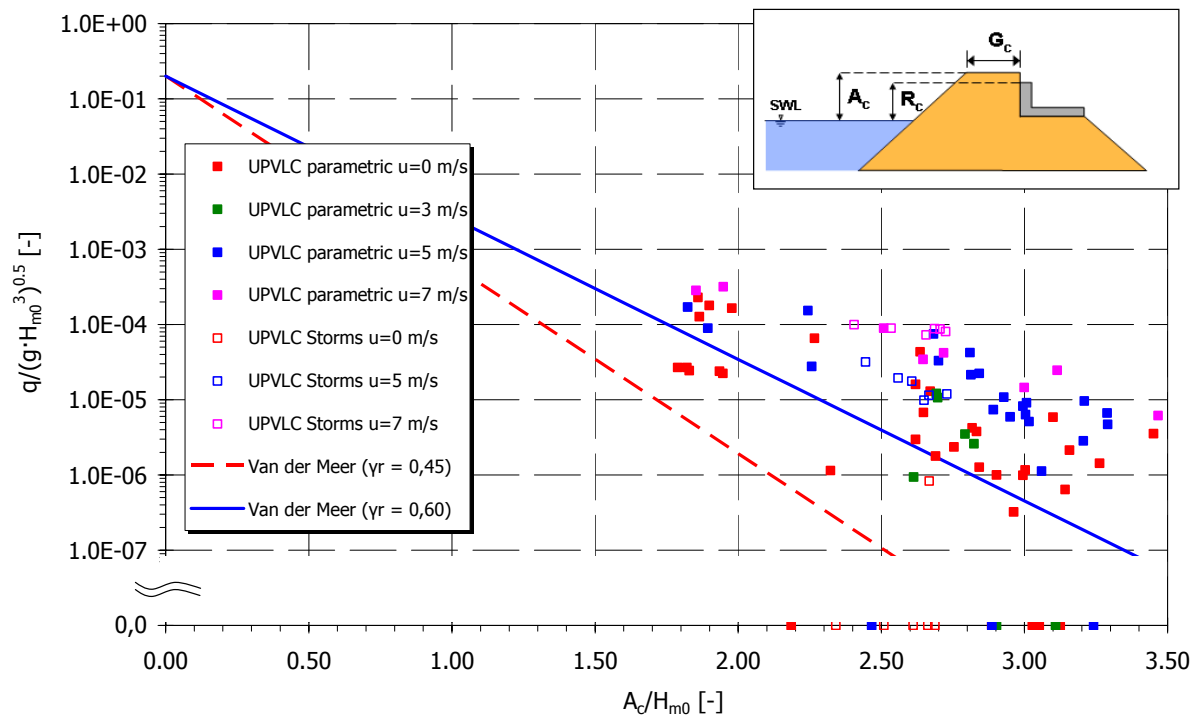


Figure 70: Zeebrugge model test results (influence of wind).

## Conclusions

The analysis of results of tests at both institutes provides the following conclusions with respect to overtopping:

### Uncertainty of measurements:

- Repeatability of tests with respect to wave parameters was found to be very good in both flumes. Regarding overtopping, mean differences were found to be slightly higher at LWI as compared to UPVLC. Both values increase when different wave generation files are used;
- Different wave analysis (different time windows) and wave generation methods (different time series from the same spectrum file) have no significant influence on the measured wave parameters;
- The number of waves generated in the flume has some effect on wave overtopping measurements, a comparison of 200 to 1000 waves has led to 20% differences in wave overtopping, although this is accompanied by using different wave generation files which has caused differences in results of the same order of magnitude;

### Model effects:

- Significant differences were found in overtopping measurements when the overtopping tray is moved as compared to prototype. This may either result from a different pattern of armour layer stones in front of the tray or the influence of the side wall of the flumes;
- Widening of the tray collecting the overtopping water has led to differences in overtopping in the same range of test repeatability. The widening was limited to a factor of 2.0 at LWI (first test phase) for which the former results (uncertainty of measurements) were obtained. For tests in the second test phase (reproduction of storms) the tray was widened up to 1.0 m in the model which seemed to have a larger influence than 10%;

- Repositioning of the armour units significantly affects the overtopping rates. Small changes in the positioning of armour elements may change the overtopping rate by a factor of 2.0 and more;
- Wind influences were investigated in detail by UPVLC and resulted in differences of up to one order of magnitude when wind speeds up to 7.0 m/s were compared with no wind in the model. It is however still unclear how wind can be scaled from prototype to the model;
- Further differences in overtopping measurements in Zeebrugge may result from the unknown placement pattern of the bottom armour layer (rectangular pattern in the models) and long waves in prototype, which have not been varied in the model.

#### **Scale effects:**

- The comparison between model and prototype results has shown some clear differences for low overtopping rates which could partly be explained by some model effects. For further conclusions on scale effects, reference is made to WP7.

More details on the model tests on the Zeebrugge breakwater are found in Kortenhaus et al. (2004).

#### **4.2.2 Site 2 : Ostia**

The Ostia breakwater has been modelled in small-scale in the wave flume of Ghent University (UGent) at a scale of 1:20 and in the wave basin at Flanders Hydraulics (FCFH) at a scale of 1:40. The model investigations have concentrated on parametric tests on wave overtopping (mainly at UGent, a limited number at FCFH) as well as the reproduction of storms (UGent, FCFH). In 2D further tests with regular waves are performed for the calibration of the numerical models (WP5). Altogether 180 2D tests have been performed at UGent on the Ostia breakwater. Many of them were focussing on various uncertainties with regard to the measurements and the model such as repeatability, influence of the spectral type, influence of the breakwater's slope, influence of a longer foreshore, influence of the packing density of the armour, influence of a permeable or impermeable core .... Also tests with a smooth structure

were performed to make an as accurate as possible comparison between a smooth and a rough structure.

AT FCFH 71 3D tests have been performed on the Ostia breakwater. These tests were mainly storm reproductions, but also some parametric tests were performed. For the storm reproductions, the influence of the angle of wave attack was investigated. Parametric tests were selected to have the same wave parameters as in 2D in order to achieve a situation as good as possible suited for direct comparison between 2D and 3D.

Fig. 71 gives a cross section of the wave flume with the Ostia model and foreshore, including the positions of the wave gauges. Fig. 72 gives a cross section of the 2D breakwater model itself. Fig. 73 and Fig. 74 show respectively a view on the position and orientation of the 3D model in the wave basin and a cross section with the overtopping tank of the model and the foreshore.

Fig. 75 gives results from both the 2D and the 3D model in a typical non-dimensional overtopping graph.

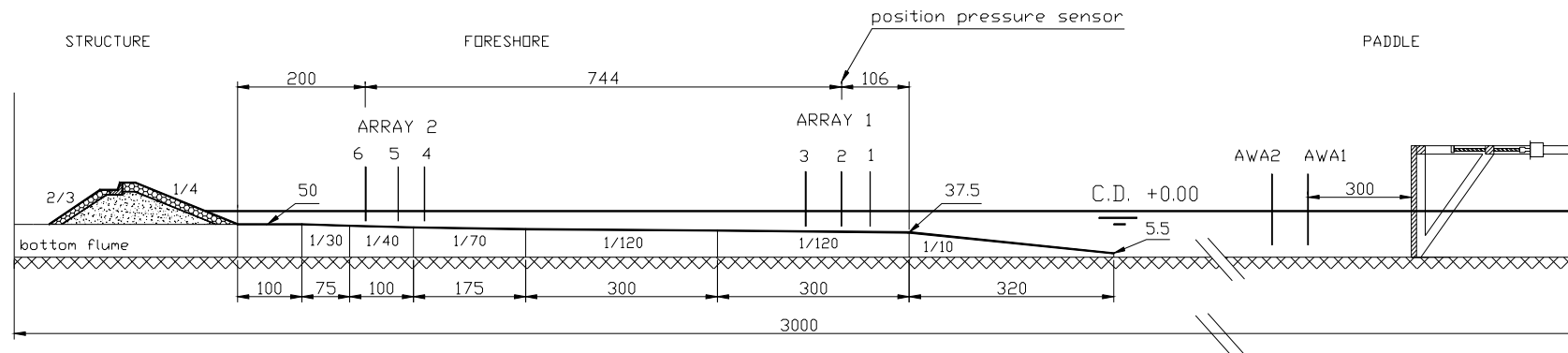


Figure 71: Cross-section of the complete 2D model set-up in the wave flume (values in cm model).

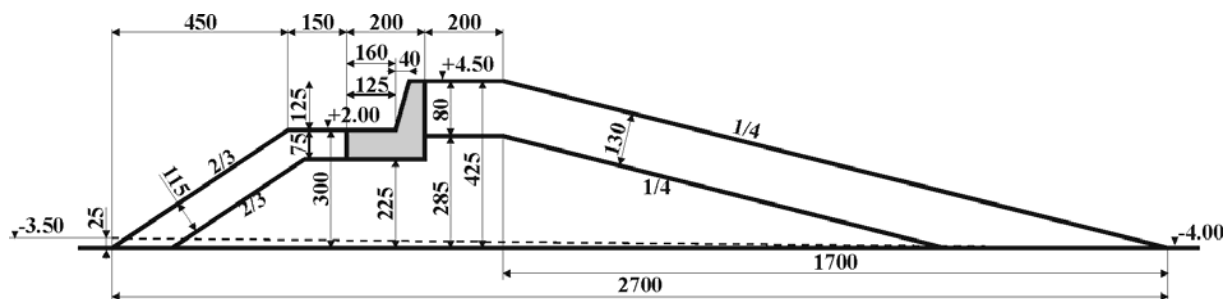


Figure 72: Cross-section of the 2D breakwater in the wave flume (values in mm model; elevations in m prototype).

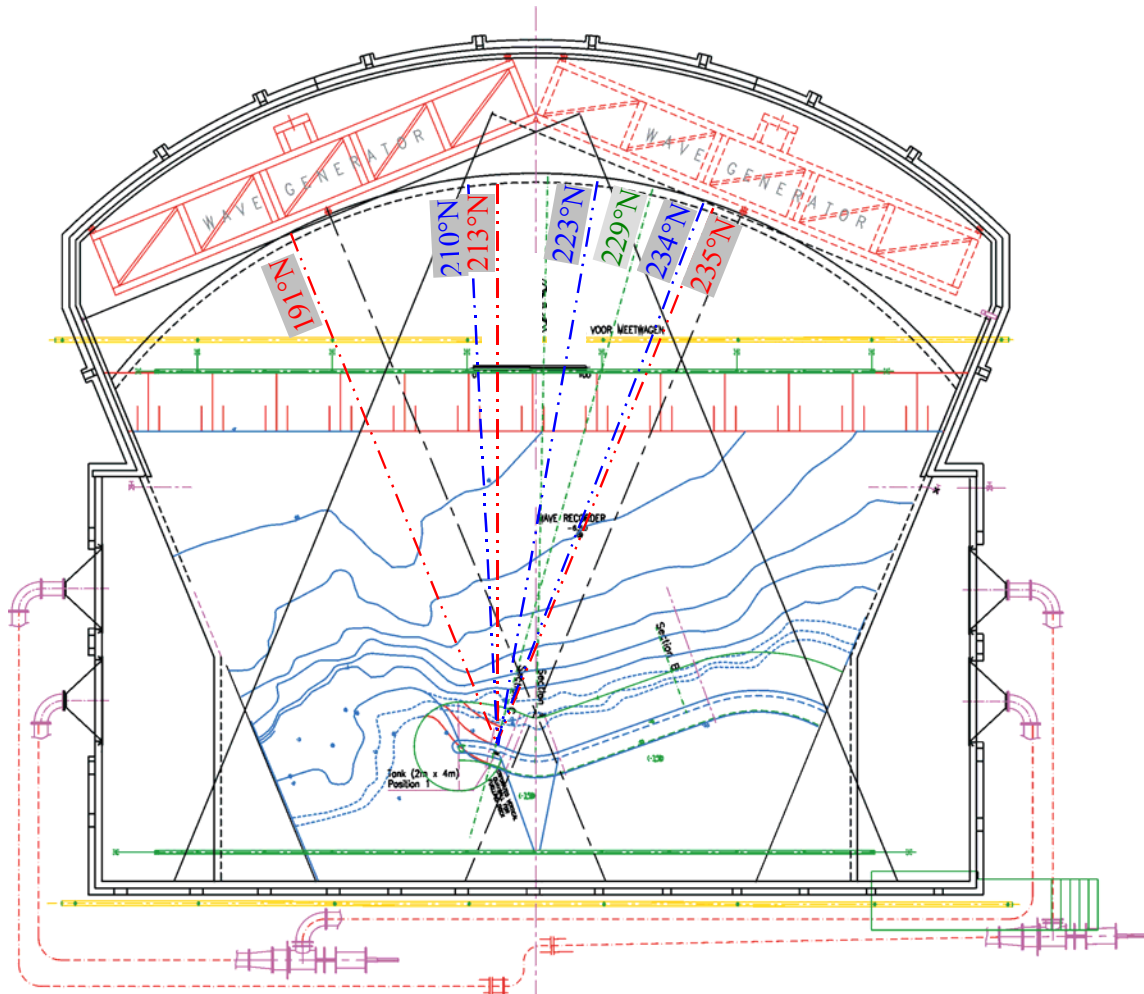


Figure 73: Position and orientation of the Ostia breakwater in the wave basin for the 3D tests.

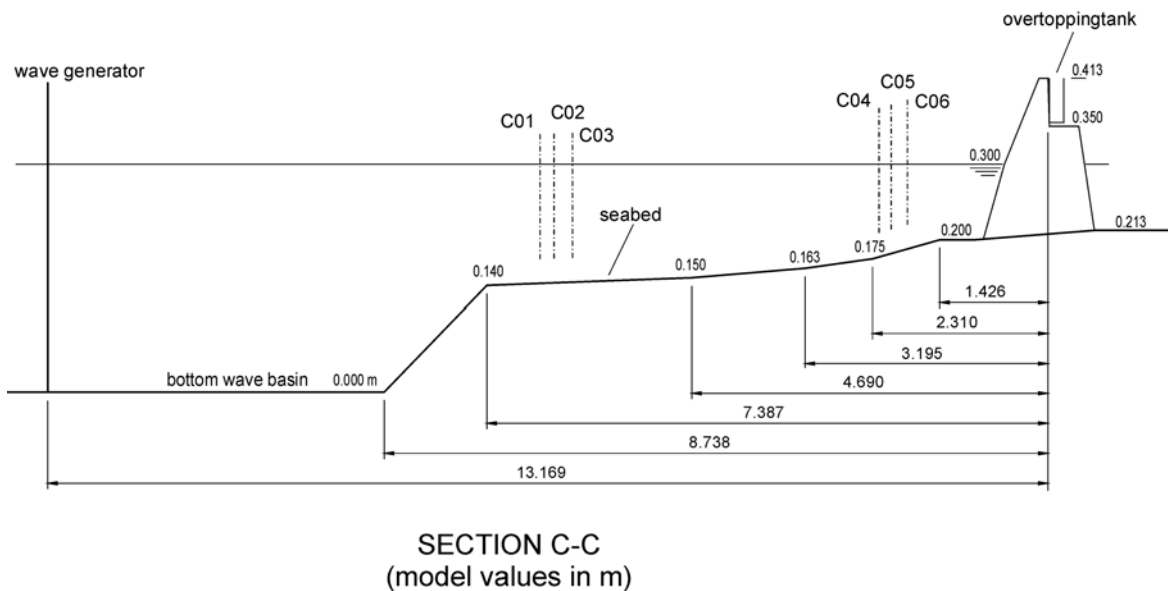


Figure 74: Cross-section with the overtopping tank in the wave basin (values in m model).

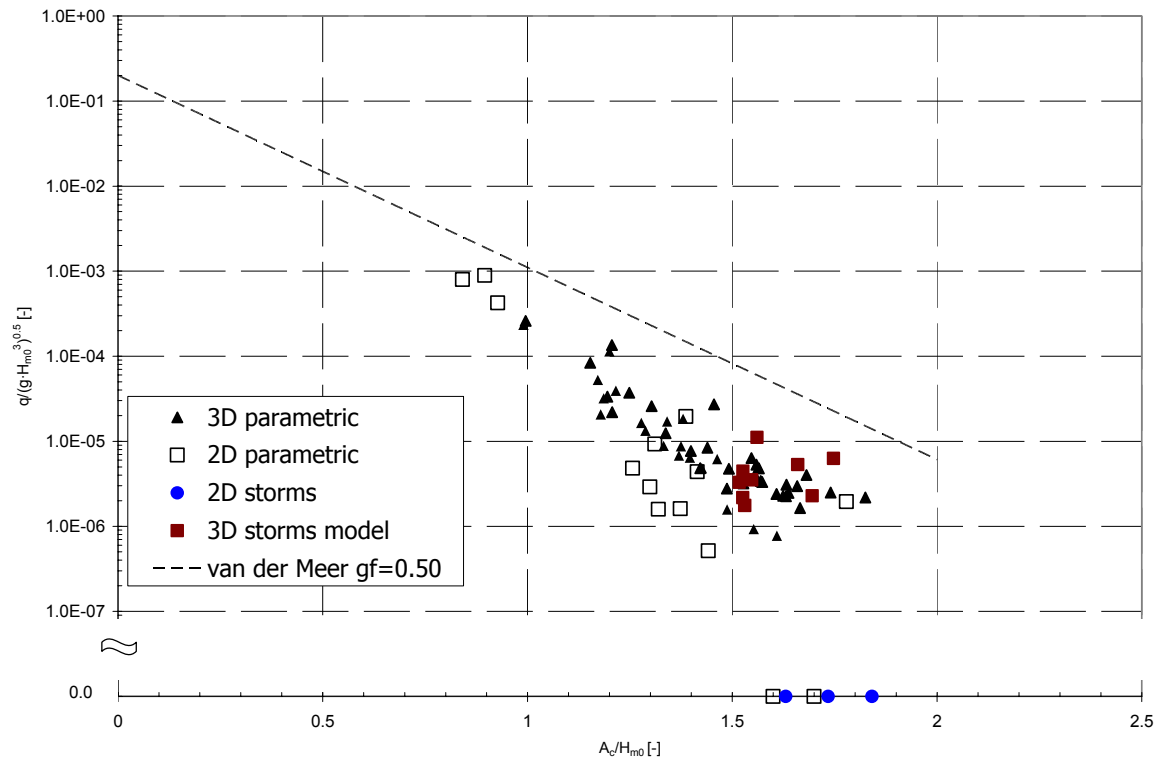


Figure 75: Ostia model test results.

## Conclusions

The analysis of results of tests at both institutes provides the following conclusions with respect to overtopping:

2D storm reproductions result in ZERO overtopping, even when applying an impermeable core and an armour with very low porosity. To obtain some overtopping in the 2D model the water level must be increased with 0.70 cm as compared to the prototype situation, which means an increase of the dimensionless crest freeboard from ca. 1.85 to 2.15. To obtain overtopping discharges comparable to the prototype, the water level increase must be 1.30 m. This means a very big change of the dimensionless crest freeboard, i.e. from 1.85 to 2.45.

3D storm reproductions do give some overtopping, but end up a factor 5 to 10 smaller than in prototype.

Comparison of 2D and 3D model results indicates the existence of a clear 3D effect, which also could be observed from prototype videos showing a very non-uniform distribution of overtopping along the breakwater.

Parametric tests in 2D only produce overtopping for water levels 0.70 m higher than in prototype. Apart from this, the 2D parametric test results are rather similar to the 3D parametric test results. However, 2D results are generally lower than 3D results.

From the parametric tests a roughness coefficient  $\gamma_r = 0.30$  has been determined for the Ostia Breakwater, based on a comparison with the smooth structure tests. To determine this coefficient, the presence of the permeable crest berm has been taken into account.

Further in WP4 additional tests to determine  $\gamma_r$  for different armour types are described. The values found there for rock are higher than what is found here for the Ostia case. However in this case the structure's slope is considerably flatter (1/4) than in case of the additional tests (1/1.5 – 1/2). It is clear that the roughness coefficient is not constant for all slopes.

More details on the tests on the Ostia breakwater are found in Geeraerts & Willems (2004). The main results are also presented in Geeraerts et al. (2004).

#### 4.2.3 Site 3 : *Samphire Hoe*

The Samphire Hoe seawall has been modelled in small-scale in the wave flume of Edinburgh University (UEDIN) at a scale of 1:40 and in the wave basin at Hydraulic Research Wallingford (HRW) at a scale of 1:20. The model investigations have concentrated on parametric tests on wave overtopping (HRW) as well as the reproduction of storms (HRW and UEDIN). Moreover, at both HRW and UEDIN the spatial distribution of the wave overtopping has been measured. At HRW the influence of wind on wave overtopping was studied too.

Fig. 76 gives the model set up together with a cross section of the model seawall for the 2D tests. Fig. 77 shows a plan view of the 3D model.

Fig. 78 gives the results of both 2D and 3D model tests compared to the prediction for these kind of structures by Besley (1999). Both 2D and 3D test results are generally in good agreement with the overtopping formula of Besley (1999) for composite vertical walls.

The spatial distribution of overtopping water behind the wall was measured both for the 2D and the 3D tests. The results confirm the exponential decay with the landward distance. From the test with wind it was observed that the wind will increase the landward distance of the splash down location of the overtopping water as expected. When the overtopping discharge is low it was observed that wind could increase the overtopping discharge by one magnitude.



For much higher discharge almost no influence of wind on the overtopping discharge was observed.

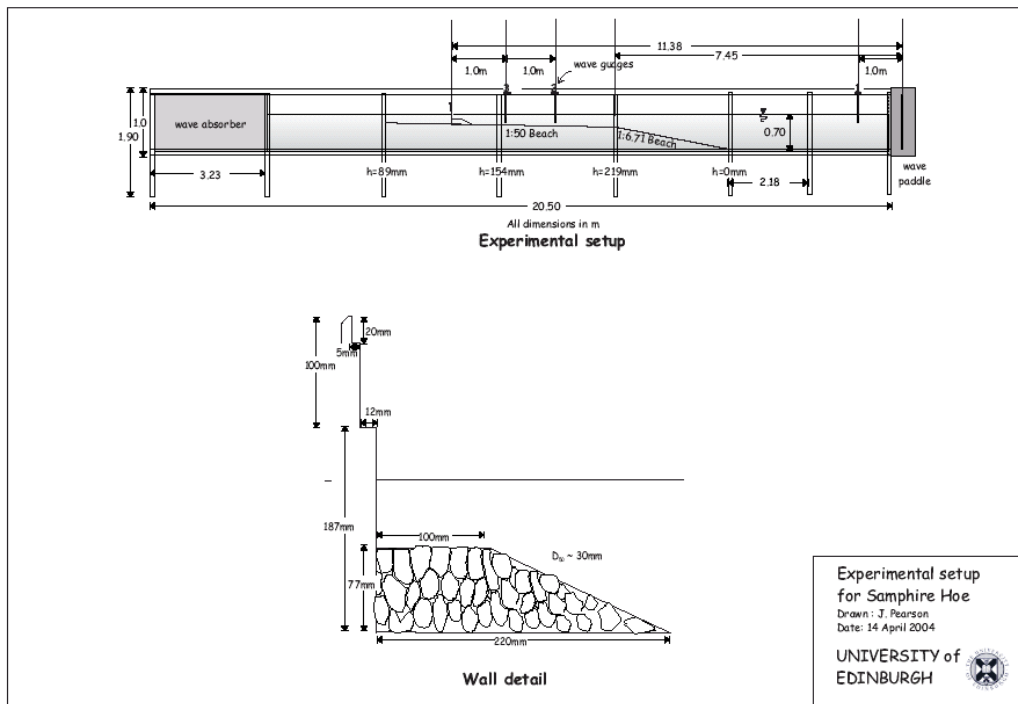


Figure 76: Test set-up for 2D tests.

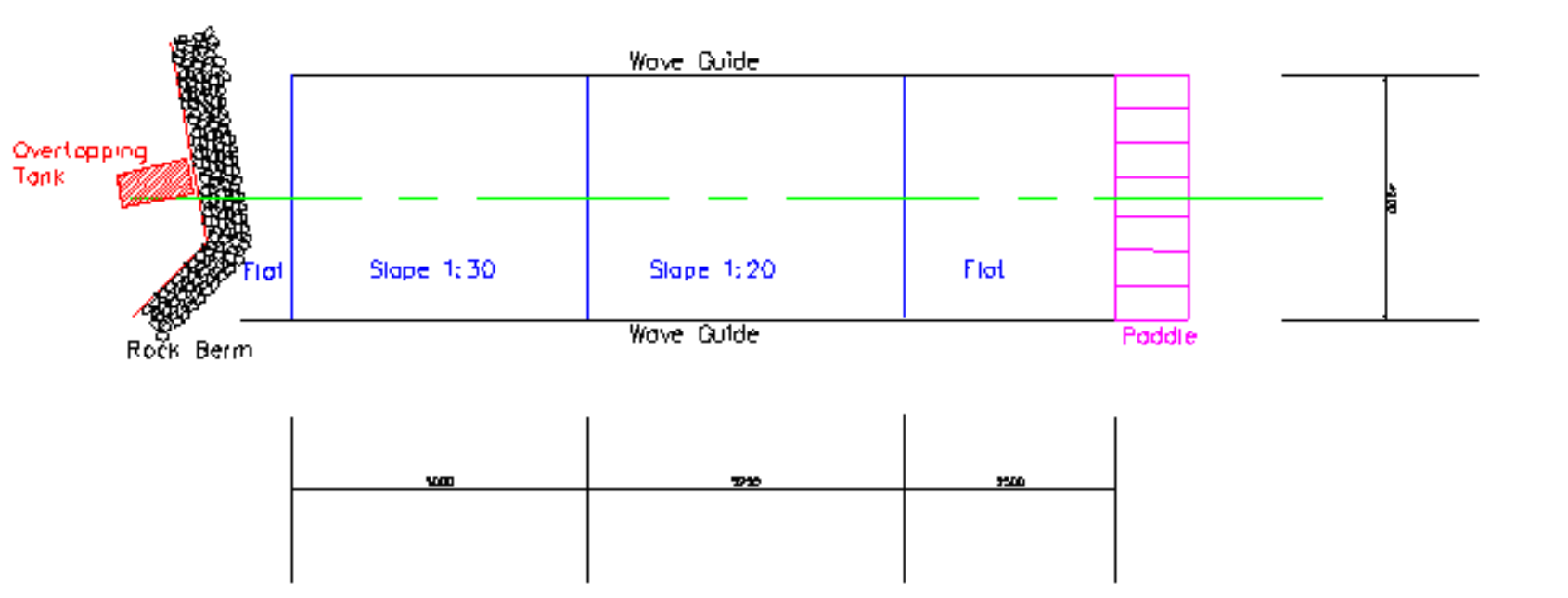


Figure 77: Plan view of the 3D model.

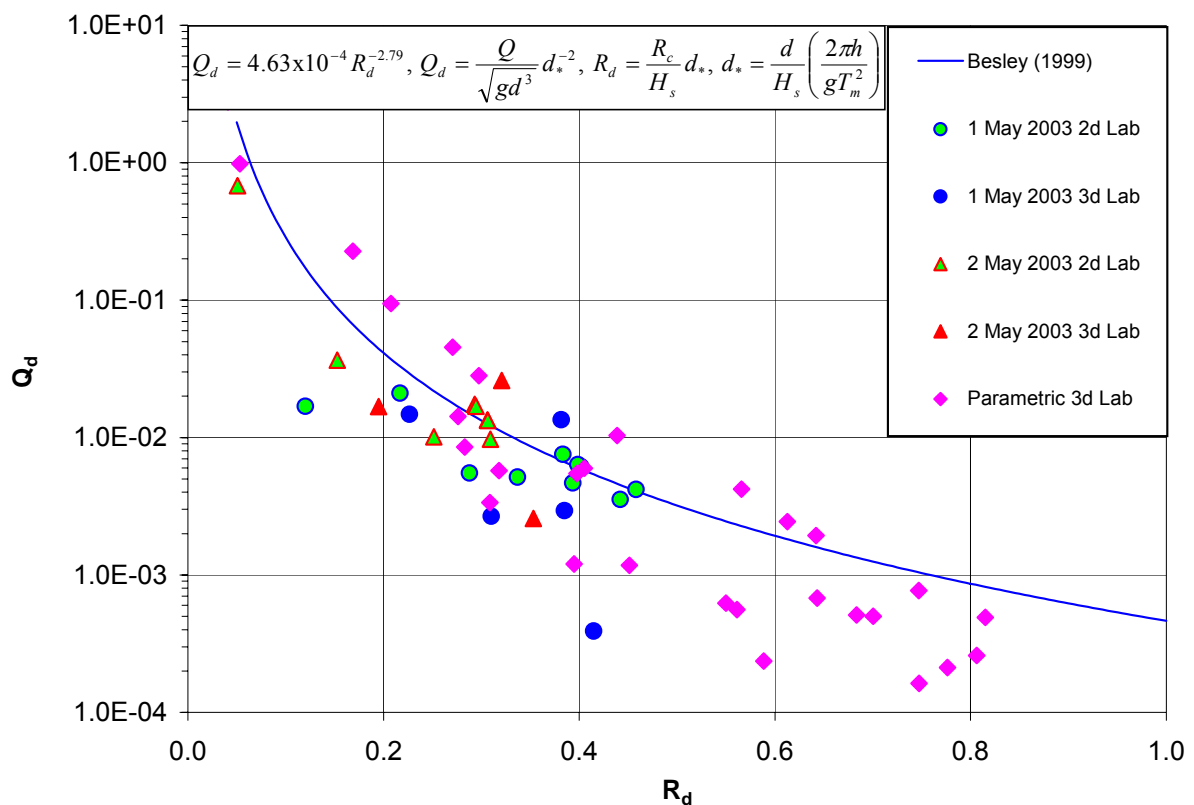


Figure 78: Samphire Hoe model test results.

## Conclusions

The results from field and 2d & 3d laboratory measurements of mean overtopping discharges have been compared. These results have also been compared with the empirical prediction method of Besley (1999) for a composite vertical wall. There are differences among the results, and these can generally be ascribed to modelling effects. These are due to differences between the overtopping tanks in the field and the laboratory, and the presence of wind. It has been shown that there are no scale effects when the field and laboratory measurements are compared, and that generally the results are in agreement with Besley (1999).

More details on the tests on Samphire Hoe seawall are found in Pullen (2004). The main results are also presented in Pullen et al. (2004).

#### 4.2.4 Additional tests

Four different white spots in the database were selected for additional tests:

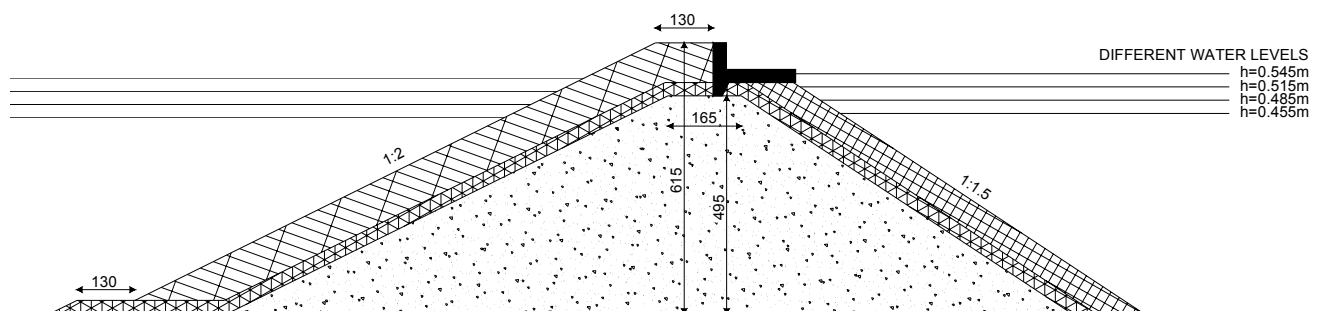
- a) Wave obliquity and spreading
- b) Structure roughness/permeability
- c) Low wave steepness ( $s_{0p} < 0.01$ )
- d) Berm breakwaters

##### *Part A : influence of wave obliquity*

Three different 3-dimensional models with different orientation were constructed and tested at Aalborg University in order to give information on the influence of wave obliqueness and wave spreading (directionality) on the overtopping of conventional rubble mound breakwaters. On each of the three models tests were performed with both rock and cubes as armour.

The number of tests performed was 736. All tests were performed with a minimum of 1500 irregular waves. Overtopping was measured in an array of trays in order to collect information on the spatial distribution. Furthermore the variation in time of the overtopping was measured.

Fig. 79 shows the cross-section which was tested. Fig. 80, 81 and 82 show the three different orientations with regard to the wavemaker of the model in the basin.



**Figure 79: Tested cross-section (dimensions in mm).**

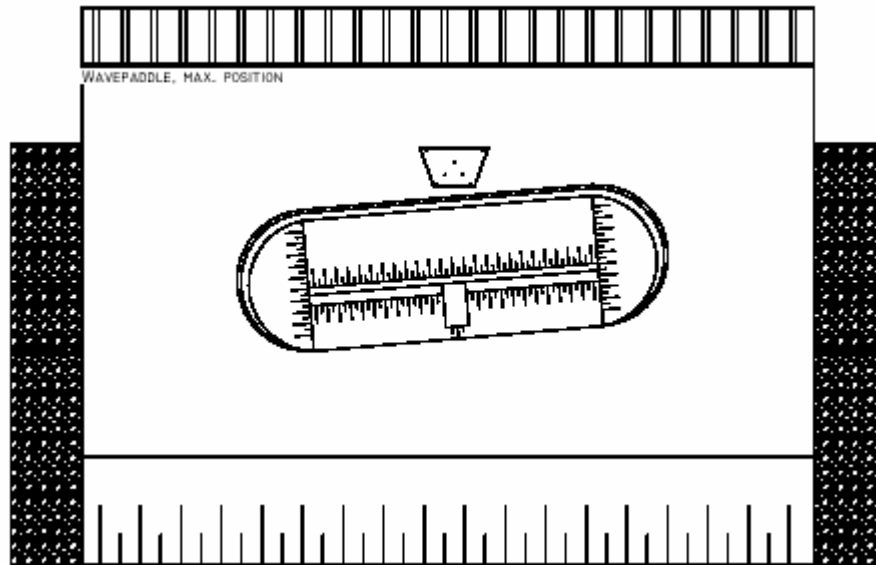


Figure 80: Layout in basin for testing  $0^\circ$  and  $10^\circ$ .

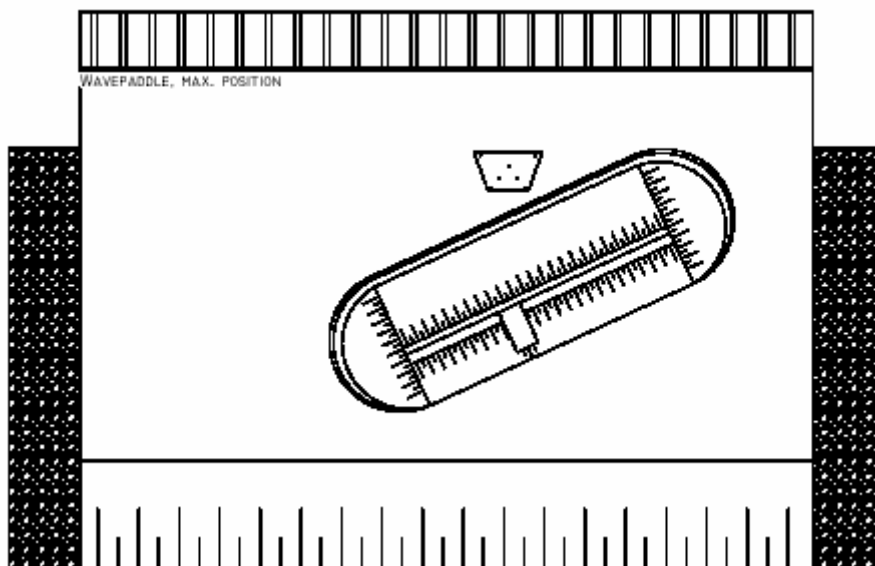


Figure 81: Layout in basin for testing  $25^\circ$ .

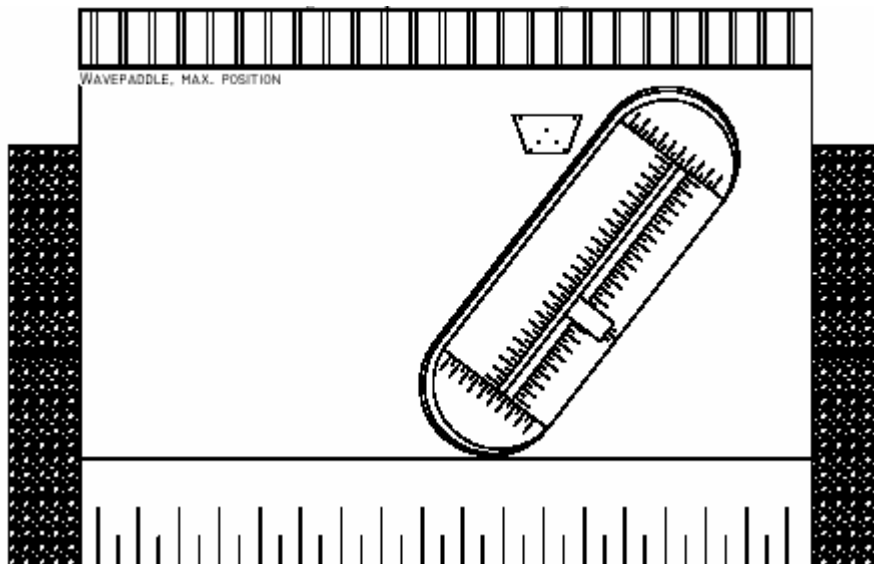
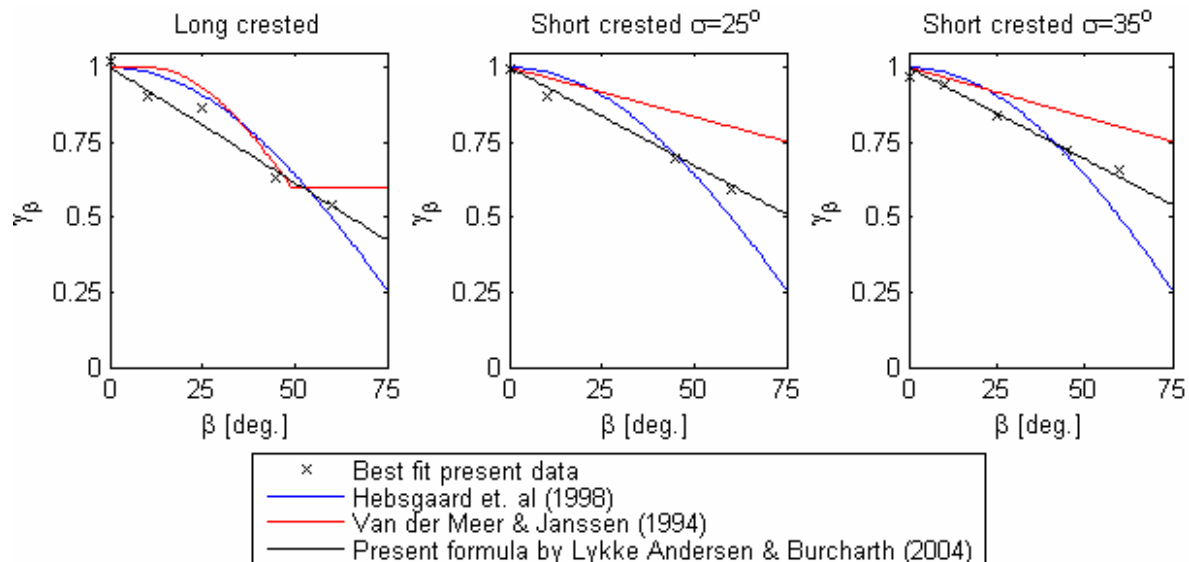


Figure 82: Layout in basin for testing 45° and 60°.

The method to predict overtopping comprised two steps. Depending on the waves (wave height, period, breaker type etc.) and type of structure (geometrical lay out, roughness, porosity etc.) a formula describing the overtopping for head-on long crested waves is first found. Effects of wave obliqueness and wave spreading are then introduced through a correction factor. The overall idea is that the correction factor can be used more or less generic improving the value of flume tests on new structures. The correction factor is given in Eq.3 and evaluated in Fig. 83 against new data from AAU model tests.  $\beta$  is the mean wave direction in degrees and  $\sigma$  is directional spreading in degrees.

$$\gamma_{\beta} = 1 - (0.0077 - 4.6 \cdot 10^{-5} \cdot \sigma) \cdot \beta \quad (3)$$



**Figure 83: Evaluation of proposed direction factor against data from AAU.**

The results obtained related to 3D white spot tests were:

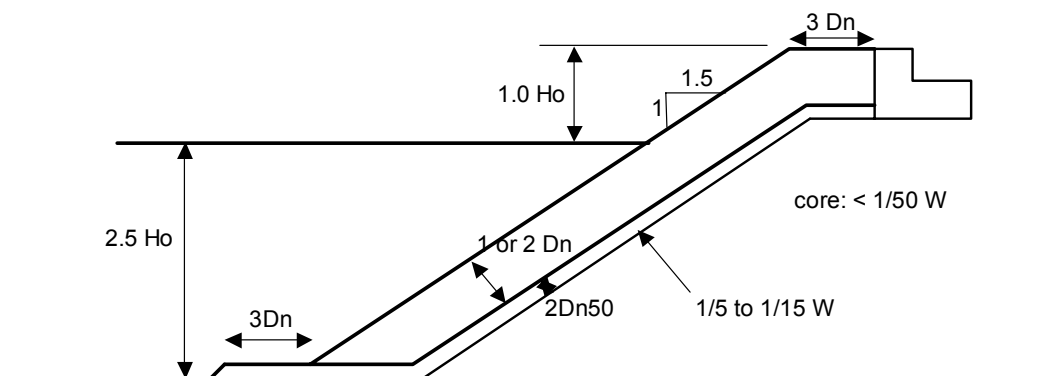
- 1) In relation to the formulae of Van der Meer & Janssen (1994), all tests performed correspond to non-breaking waves. The results from tests with head-on wave attack correspond to a roughness factor ( $\gamma_f$ ) between 0.3 and 0.45 which is a significantly lower value than suggested by Van der Meer & Janssen (1994).
- 2) Very good agreement exists between the data from the present tests and the formula of Hebsgaard et al. (1998) derived on the basis of long crested waves only. Consequently as expected the agreement to the present test results from short crested very oblique wave attack is not so good. Consequently a new/modified formula for the correction factor has been proposed by Lykke Andersen and Burcharth (2004a) to take into account the directional spreading and wave obliquity (eq. 3). The new correction factor makes it possible to predict overtopping for oblique wave attack up to 60 degrees.
- 3) The intensity of wave overtopping behind the breakwater decreased very rapidly with the horizontal distance from the breakwater crest. In Lykke Andersen and Burcharth (2004a) a diagram presenting the spatial distribution is given.

*Part B : determination of roughness factors*

14 different models with a standard cross-section, as shown in Fig. 84, were constructed at University of Edinburgh with different armour configurations. 307 tests have been performed in total covering the following armour configurations:

- 1) Smooth slope
- 2) Rock (2 different sizes)
- 3) Cubes (2 layers random placed)
- 4) Antifer cubes
- 5) Haro
- 6) Tetrapod
- 7) 1 layer of cubes
- 8) Accropod
- 9) CoreLoc®
- 10) Xbloc®

Smooth slopes and rock were tested as reference cases.



**Figure 84: Standard cross section.  $H_0$  is the design wave height.**

Dependent on the available model units (with their specific weight), the design wave height was tuned to represent a “similar stability behaviour” for all tested types of armour units.

Rock and cubes were tested both with 1:1.5 and 1:2 front slopes.

Results of the present study, together with results from previous studies (Aminti-Franco 1988, Franco-Cavani 1999) and parallel tests undertaken at AAU and UGent, were discussed amongst CLASH-partners. It was concluded that the roughness factor depends on the slope of



the structure. Finally, a deeper study of the results lead to the selection of roughness factors  $\gamma_f$  for a sloping structure with slope 1:1.5, a crest berm width of  $3D_n$ , and a permeable core / underlayer.

Table 20 presents the roughness factors which have been determined for the various tested armour layers.

**Table 20: Roughness factors for breakwaters with slope 1:1.5, with crest berm width of  $3D_n$  with a permeable core / underlayer. Values valid for breakwaters only (not for revetments).**

Type of armour	No Layers	Final $\gamma_f$
Smooth		1.00
Rock	2	0.40
Cube	2	0.47
One layer of cubes	1	0.50
Antifer	2	0.47
Haro	2	0.47
Tetrapod	2	0.38
<i>Dolosse (estimated)</i>	2	0.43
Accropode	1	0.46
Coreloc®	1	0.44
Xbloc®	1	0.45
<i>Berm Breakwater (estimated)</i>		0.40
<i>Icelandic Bermbreakwater (estimated)</i>		0.35
<i>Seabeas &amp; Sheds (estimated)</i>		0.50

### *Part C : influence of wave steepness*

Very limited data existed in the first database with wave steepness ( $s_{0p}$ ) less than 1%. Therefore white spot tests were carried out at University of Gent to study the influence of low wave steepness on three different smooth structures.

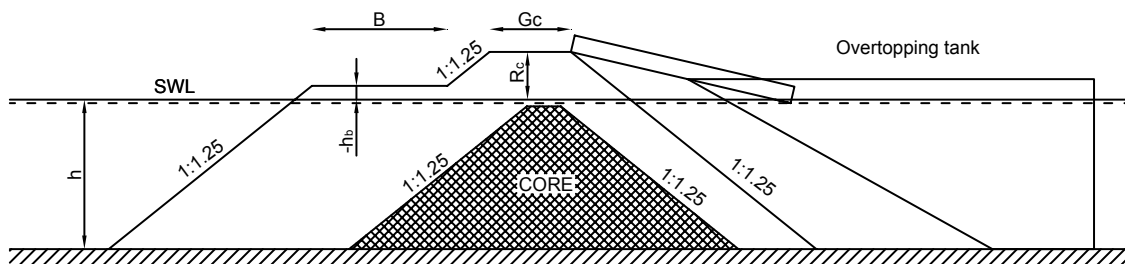
- 1) simple smooth dike
- 2) simple smooth dike with a small vertical part (same crest level as geometry 1)

- 3) simple smooth dike with a small vertical part and an impermeable sloping crest (crest level slightly higher than geometry 1 and 2)

From the test results it can be concluded that for same wave height in front of the structure waves with steepness  $s_{0p} < 0.017$  produce more overtopping on the simple smooth dike than waves with higher steepness. For the two geometries where a vertical part is present the distinction between higher steepness is not as clear as for the simple smooth dike. However, the waves with  $s_{0p} < 0.017$  generally produce more overtopping. The specific set-up of the tests allowed determination of the influence of the vertical part on top of the dike and the crest width.

*Part D : berm breakwaters*

Overtopping as well as front and rear slope stability were studied on reshaping berm breakwaters with a homogeneous berm. 82 tests have been performed at Aalborg University in order to describe the influence of sea state, crest freeboard and crest width. Fig. 85 gives the start profile of the tested geometries.



**Figure 85: Tested cross-sections.**

All of the 700 tests were performed with a minimum of 1500 irregular long crested waves, and repeated minimum once (Lykke Andersen and Burcharth (2004b)).

The conclusions fall into three categories:

- 1) A new and reliable overtopping formula was derived. In order to make design easier only non-reshaped geometrical parameters are included in the formula. The stability index  $H_0T_0$  is used as an indicative measure of the reshaping as the formula does not

contain geometrical parameters which describe the reshaping directly. For dynamically stable profiles the actual reshaping can be estimated by the method of Van der Meer (1992). Wave parameters are related to the incident waves at the toe of the structure.

$$Q_* = 4.56 \cdot 10^{-3} \cdot (H_0 T_0)^{1.31} \cdot s_{0p}^{-2.95} \cdot \exp[-13.9 \cdot R_*^{0.40} - 0.92 \cdot G_*^{1.24} - 0.76 \cdot h_{b*}^{1.32} \cdot B_*^{1.24}]$$

where

$$Q_* = \frac{q}{\sqrt{g \cdot H_{m0}^3}}$$

$$H_0 T_0 = \frac{H_{m0}}{\Delta \cdot D_{n50}} \cdot \sqrt{\frac{g}{D_{n,50}}} \cdot T_m$$

No reshaping takes place for  $H_0 T_0 < 30$ . For such cases use  $H_0 T_0 = 30$ .  $H_{m0}$  is the significant wave height at the toe of the structure (frequency domain parameter).

$$R_* = \frac{R_c}{H_{m0}} ; \quad G_* = \frac{G_c}{H_{m0}} ; \quad B_* = \frac{B}{H_{m0}}$$

$$h_{b*} = \frac{3 \cdot H_{m0} - h_b}{3 \cdot H_{m0} + R_c} \quad \text{when } h_b > 3 \cdot H_{m0} \text{ use } h_{b*} = 0$$

The new overtopping formula covers a white spot.

- 2) Front side slope stability was studied in order to describe the damage due to the waves. Good agreement between measured and calculated profiles by the method of Van der Meer (1992) was observed in all cases with dynamically stable profiles. For statically stable reshaping breakwaters the method overpredicts the amount of reshaping.
- 3) Rear side slope stability was studied in order to link the mean overtopping discharge and the rear slope erosion. Although only valid for small scale tests Lykke Andersen and Burcharth (2004b) presented diagrams relating the rear side damage to the overtopping.

### 4.3 General conclusion for WP4

This WP delivered the following reports / deliverables:

a) for the Zeebrugge model:

- the report on laboratory measurements (D18)
- the final report on laboratory measurements (D34)

b) for the Ostia model:

- the report on laboratory measurements (D20)
- the final report on laboratory measurements (D35)

c) for the Samphire Hoe model:

- the report on laboratory measurements (D21)
- the final report on laboratory measurements (D36)

d) for the additional tests:

- the report on additional tests (D24)

Two milestones were achieved within this WP:

After the first full winter season (month 18 for the Zeebrugge, Ostia and Samphire Hoe site and month 19 for the Petten site), full scale measurements of all four sites are analysed and reported (M3). After the second full winter season (month 30 for the Zeebrugge, Ostia and Samphire Hoe site and month 31 for the Petten site), measurements of all sites are analysed and reported

## 5 WP5 : Numerical modelling

### 5.1 Objectives

The main objective of this task is to use numerical simulation of wave overtopping in order to contribute to the solution of the problem of suspected scale effects.

A second objective of the workpackage is to improve existing codes in such a way that they are able to really simulate wave overtopping in a reliable way.

Another objective is to numerically model long waves on the shallow foreshore at site 4 in order to understand the phenomenon of long waves and the effect on wave overtopping.

### 5.2 Description of work performed

The main objective of this work package is to use numerical simulation software which solves an appropriate set governing equations in order to predict wave overtopping, and thus to address the problem of suspected scale effects. In order to achieve this objective it has been necessary to improve the capabilities of two existing models namely, the AMAZON-SC code developed by MMU and the VOFbreak<sup>2</sup> codes developed by UGent. Furthermore, to enable the simulation of 3D effects a numerical wave basin, called LVOF, has been developed by UGent. The MMU code, AMAZON-SC, is a numerical wave flume based on the free surface capturing approach, while the UGent codes are based on the volume of fluid approach. Both models have been made available to the commission as a confidential deliverable (D26) and the enhancements made have been described in two reports (Ingram et al; 2003 and Ingram et al; 2004).

Realistic simulations of wave overtopping require numerical methods which are able to simulate accurately the shoaling, breaking and possible overturning of waves prior to their impact on the coastal defence. It is a further requirement that the simulation continues after impact, modelling the formation of the overtopping jet and the reflection of the wave. Both the AMAZON-SC and LVOF codes solve the turbulent Navier-Stokes equations in order to provide such detailed simulations. The MMU code, AMAZON-SC, is a numerical wave flume based on the free surface capturing approach, while the UGent code, LVOF, is a numerical wave basin based on the volume of fluid approach. The codes have been applied to various

cases, discussed by Ingram et al (2004), including: a test problem involving wave overtopping of a smooth sea dike, wave overtopping at Samphire Hoe (one of the structures which has been examined both in the field as part of WP3 and experimentally as part of WP4 and an investigation of scale effects on rough impermeable structures and at Ostia breakwater. In order to perform these simulations the modelling capabilities of the codes have been improved. In the case of the MMU code the existing 2D code has been extended to include the effects of porosity and turbulence, while the team at UGent have developed a new 3D numerical model (Li et al., 2004b).

The remaining objective was to simulate long waves on the shallow foreshore at Petten in order to understand the phenomenon of long waves and their effect on overtopping. These simulations were conducted by Delft Hydraulics using ODIFLOCS and SURFBEAT and these simulations together are described by van Gent and Giarrusso (2003).

Additional modelling work has been conducted by HR Wallingford using their ANENOME-OTT to investigate the propagation of bore waves across the hinterland behind a sloping sea defence and to compare the predictions from the AMAZON-CC and ANENOME-OTT codes with experimental measurements for overtopping jet velocities (Richardson et al., 2003). MMU have also applied the AMAZON-CC code to study the applicability of shallow water models to impulsive overtopping by comparing predicted overtopping volumes with experimental results obtained under the VOWS project (Richardson et al., 2002; Shiach et al., 2004). This additional modelling has been conducted using models which are based on the shallow water equations (derived by considering the depth integrated form of the Navier-Stokes equations) which provide a computationally efficient but less sophisticated model of overtopping. Using shallow water methods typically allows 1000 waves to be simulated in less than one hour on a desktop PC, as opposed to the significant computational resources required to run the 2D and 3D numerical solvers based on full Navier-Stokes equations for only a few waves.

### 5.2.1 *Free surface capturing*

One approach which can be used to develop a 2DV numerical wave flume (or fully 3D numerical wave basin) is the free surface capturing approach (Kelecy and Pletcher, 1997). This approach forms, together with a novel Cartesian cut cell treatment (Causon et al. 2001) forms the basis of the AMAZON-SC code (Qian et al., 2003a). Specifically, in this case, the mathematical model of an immiscible two fluid system is formulated as a set of partial differential equations which govern the motion of an inviscid, incompressible, variable density fluid. These equations consist of a mass conservation (density) equation (which is mathematically equivalent to the volume fraction transport equation), momentum equation and an incompressibility constraint that are solved simultaneously using the finite volume method. The formulation is based on the artificial compressibility method (Chorin, 1967; Beddhu et al., 1994) in which the pressure, density and velocity fields are directly coupled to produce a hyperbolic system of equations. To achieve a time accurate solution for unsteady flow problems an implicit dual time iteration technique has been used (Soh and Doodrich, 1988; Rogers and Kwak, 1990) in which the solution at each real time step is obtained by solving a steady state problem in a pseudo time domain. To evaluate the inviscid fluxes, Roe's flux function is adopted locally at each cell interface assuming a 1D Riemann problem in the direction normal to the cell face. To achieve a second order accurate solution in space, a piecewise linear model for the stored cell centre variables is used in conjunction with a slope limiter to prevent overshoots or undershoots in the interpolated data at cell interfaces before the two Riemann states are computed. At the pseudotime iteration level, however, a first order upwind scheme is sufficient to calculate the inviscid fluxes and the resultant linear equations are solved using an approximate LU factorisation scheme (Pan and Lomax, 1988). At every real time step, once the flow variables including density, have been calculated, the position of the material interface can be defined as the contour with the average density value of the two fluids. A number of different boundary conditions including inlet, outlet (open boundary) and solid walls are implemented to facilitate the applications to real flow problems. Complex geometries (Causon et al., 2001) arising in real coastal engineering problems can be easily represented by cut cells which provide a fully boundary fitted mesh capability without any mesh generation in the conventional sense. A novel scheme has also been proposed for the accurate treatment of the pressure gradient term within the free surface capturing method for flows under the influence of gravity (Qian et al., 2003b). The vertical pressure gradient term

is split into hydrostatic and kinematic pressure gradient terms which are then calculated separately in order to exactly balance the gravity source term in each cell.

In order to extend the solver to deal with rubble mound structures, a porosity model must be included. In order to achieve this, the body force term of the Navier-Stokes equations is extended to include terms modelling the porosity, using the method proposed by Huang et al. (2003). In this model the frictional losses associated with the porous structure are parameterised using the three following quantities;  $K_p$  ( $m^2$ ) is the permeability coefficient of the structure,  $N_w$  is the, dimensionless, intrinsic porosity of the structure, and,  $C_f$  is a dimensionless turbulent resistance associated with the structure. In general  $N_w$  is a design parameter of the structure and is known along with a nominal diameter  $d_n$  of the rubble. The turbulent resistance may be determined using the correlation proposed by Arbabhiramar and Dinoy (1973). Whilst various correlations exist for computing  $K_p$  Huang et al. (2003) recommend using the correlation proposed by McDougall, i.e.,

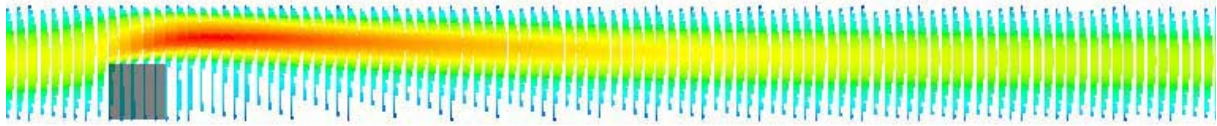
$$K_p = 1.643 \times 10^{-7} \left( \frac{d_n}{d_0} \right)^{1.57} \frac{N_w^3}{(1 - N_w)^2}$$

where  $d_0=10\text{mm}$ .

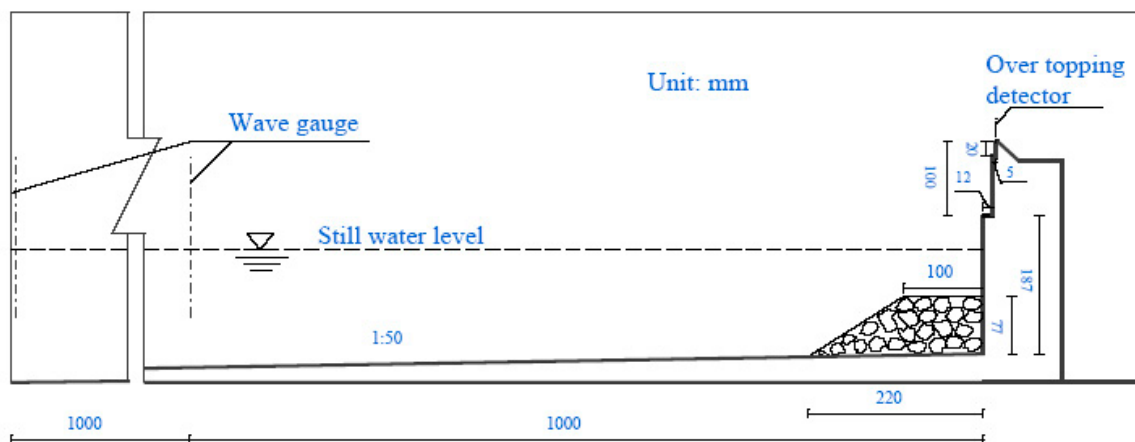
To complete the numerical solution the intrinsic permeability and porosity coefficients are stored for each grid cell in the computational domain. The additional terms in the body force vector are then computed for each porous grid cell. Rubble mound structures are thus represented by defining a region of grid cells with non-zero  $N_w$ .

In order to test the porosity model the updated solver has been applied to the steady state test case described by (Fu et al., 1996). A porous block is located in a two dimensional channel with height. The downstream part of the channel is long enough for the fully developed flow to be recovered behind the block. The inlet velocity profile is prescribed to as a parabolic distribution and the average velocity is chosen to ensure a Reynolds number of 500. Fig. 86 shows the computed velocity distribution, analysis of the velocity distributions along the edges of the block show good agreement with the results of Fu et al. (1996).





**Figure 86: Porous media test: Velocity vectors for the whole domain, showing fully developed flow at the outlet**

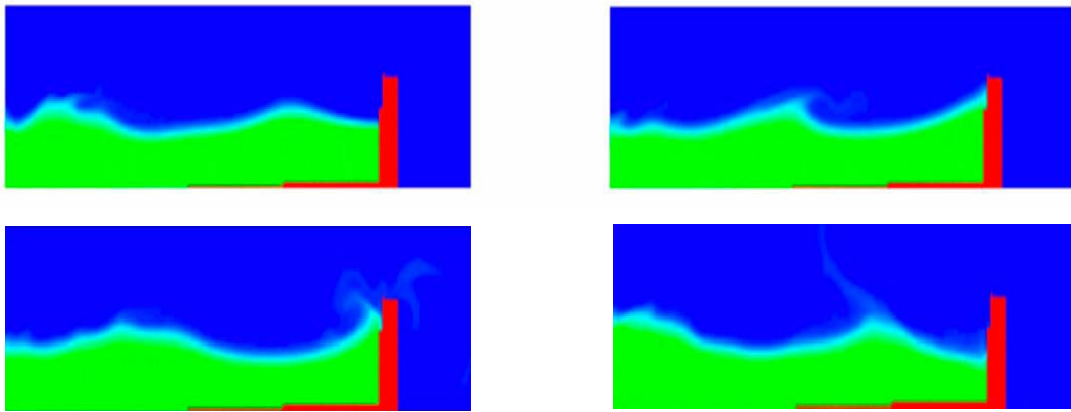


**Figure 87: Samphire Hoe: Overview of the test section**

### *Samphire Hoe*

The AMAZON-SC code has been applied to examine selected wave overtopping events at Samphire Hoe. The computational domain, geometry of the sea wall and the locations of the numerical wave gauges is shown in Fig. 87. This test section is identical to that modelled in the Edinburgh experiments (WP4). The armour at the toe of the structure consists of fairly angular, 4 ton, narrowly graded rock with a  $d_{n50}$  of around 1.5m. The porosity of the toe is estimated at approximately  $N_w = 35\%$  and that consequently, using the equation,  $K_p = 4.35 \times 10^{-5} m^2$ , while  $C_f = 0.06407$ . The simulated case uses a series of random waves at the seaward boundary generated using a JONSWAP spectrum with the same spectral parameters as those used in the laboratory experiment ( $T_p = 0.9416s$  and  $H_s = 0.1037m$ ), it should be noted that it is not possible to use the same time series as the information required for the seaward boundary condition cannot easily be reconstructed from the available wave gauge data. The resulting time series has been examined for significant event and the simulation was started at an appropriate time. Fig. 88 shows the interaction of two large waves with the

seawall over a five second period. The second wave results in an overtopping event, which occurs between 3.44 and 3.5 seconds after the start of the simulation. During this event  $0.033 \text{ m}^3$  overtops the wall, which at prototype scale equates of an instantaneous discharge of  $1.32 \text{ m}^3$ . This low overtopping discharge is composed almost entirely of spray and results from the wave breaking near the toe of the rubble mound. Repeating the simulations at a model scale of 1:20 (i.e. twice the laboratory scale) show almost identical behaviour indicating that for the tested flow conditions the turbulent effects of the rubble mound structure are negligible. This conclusion is in agreement with the results obtained by Pullen et al (2004).



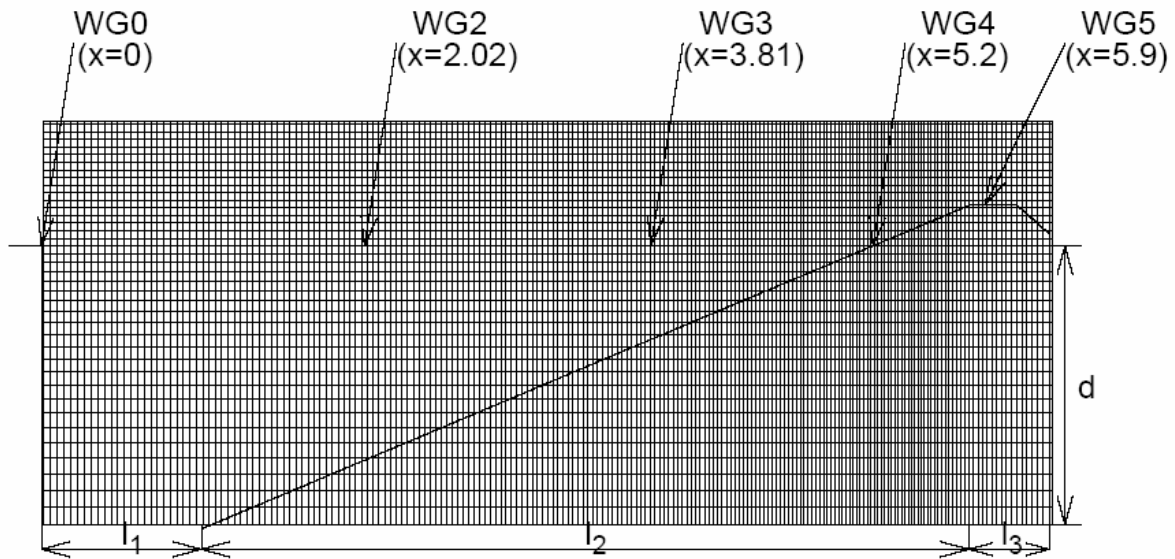
**Figure 88: Samphire Hoe: Computed water surface profiles at 0.5s intervals between  $t = 2.0\text{s}$  and  $t = 4.0\text{s}$**

### 5.2.2 Volume of Fluid methods

The VoF method is one of the most popular schemes used for free surface flows and has an established track record (Youngs, 1982; Hirt and Nichols, 1981; Lafaurie et al., 1994; Ubbink and Issa, 1999; Troch et al., 2003). It should be noted that the method is intrinsically mass conservative. Additionally, no special procedures are required to model topological changes of the free surface. The location of the free surface is computed by tracking the evolution of the volume fractions (denoted  $\alpha$ ) in all the cells. A volume fraction of 0 or 1 indicates that a cell contains only one fluid whilst a volume fraction  $0 < \alpha < 1$  indicates the cell contains a mixture, by convention  $\alpha = 0.5$  is used to represent interfaces. The initial distribution of  $\alpha$  is specified by considering the shape and location of the initial interface. A solution procedure used to update  $\alpha$  involves a two stage process: firstly, an interface reconstruction algorithm; and, secondly, an advection algorithm for  $\alpha$ .

Under the CLASH project, UGent have developed a new solver (Li et al., 2004b) for modelling of wave run-up and wave overtopping events using a VoF method. The code is capable of simulating the breaking of the periodic wave trains on the seaward slope of a sea

dike. The solver is based on a split implicit time differencing scheme, which solves the spatially filtered Navier-Stokes equations on a Cartesian cut cell mesh using a cell staggered finite volume (FV) formulation, while incompressibility is enforced through an iterative Poisson solver for the pressure. The free surface is tracked using a VoF method that is simple enough to solve practical problems but still general enough to describe the physical behaviour of the free surface. The key to this development is the use of an implicit process. In this approach, the pressure and surface tension over mixed cells are treated implicitly. Thus allowing the application of the normal dynamic free surface boundary condition to be significantly simplified. In this way, the pressure at mixed cells is incorporated directly into the corresponding field equation, while the surface tension effects are modelled as part of the body force terms. Furthermore, no explicit expression for interface reconstruction is required during tracking, this is similar to the level set method widely applied to many fields. The resulting algorithm can be easily extended to three spatial dimensions (Li et al., 2004b). UGent's work in this area has been to develop an approach which preserves both the smoothness of the interface and its sharp definition over one cell; this requires that numerical diffusion associated with the upwind advection scheme must not be excessive. To achieve this a weighted upwind advection scheme is used together with an operator split second order explicit Adams Bashforth method. When applied to test cases involving complex flows caused by waves, the results demonstrate that the proposed approach is computationally efficient. The current solver, LVOF, comprises (Li et al., 2004a,b): a large eddy simulation model of turbulence, using the dynamic form of Smagorinsky's model; a fully implicit cell staggered FV approach with a cut cell Cartesian technique; a novel VoF advection scheme; a blend of second and fourth order artificial damping; and, an absorbing generating boundary condition for a wave generator. This solver has been applied to: study the wave overtopping over coastal structures; to study the effect of current on breaking wave structure interactions; to investigate the effects of viscosity on the wave boundary layer; to estimate wave impacts; and, 3D effects.



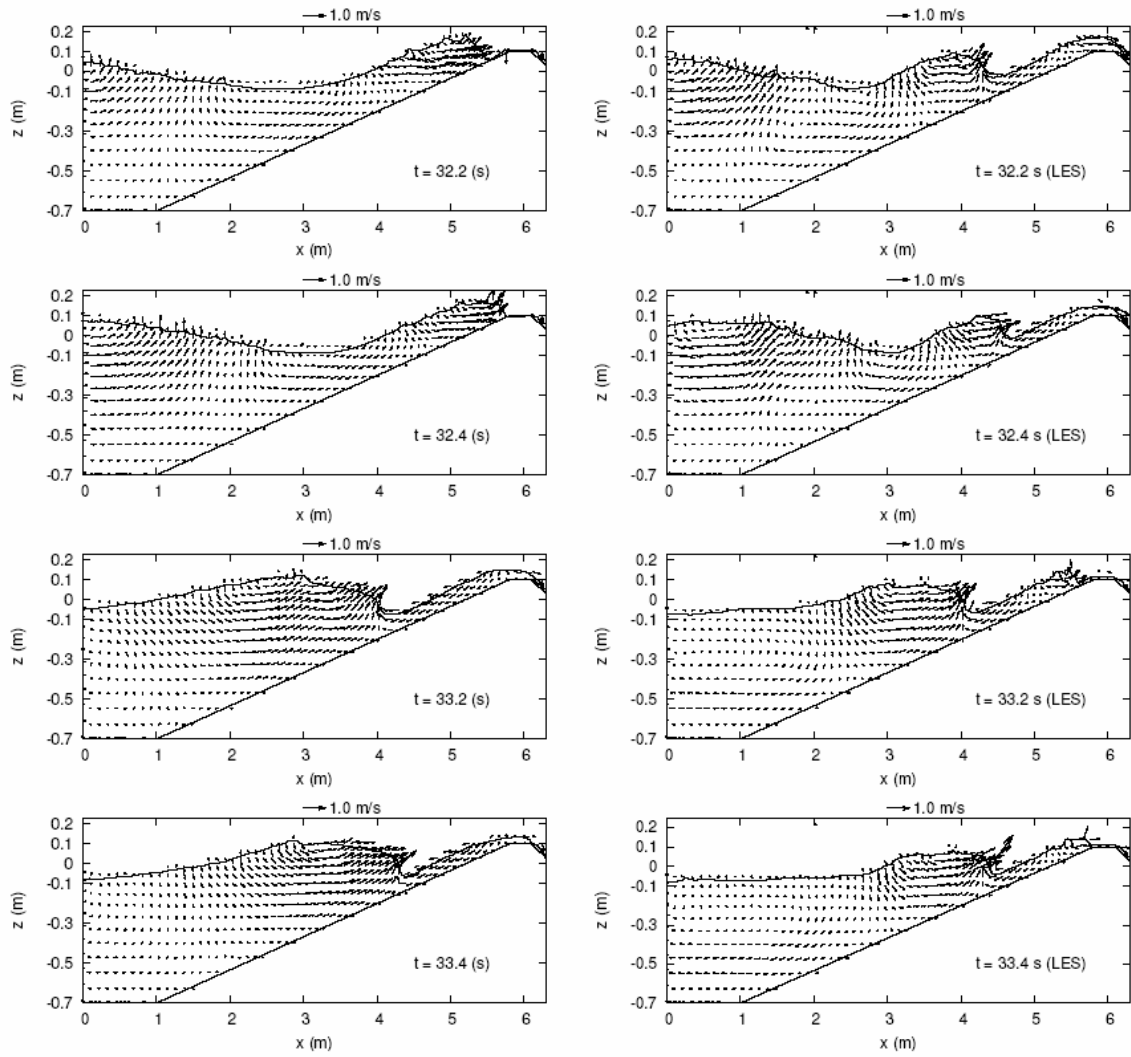
**Figure 89: Computational domain on a non-uniform Cartesian cut-cell mesh for sea dike problems. WG0 to WG5 indicate the locations of five wave gauges.  $l_1=1.0$  m,  $l_1 + l_2 + l_3=6.3$  m and  $d=0.7$  m.**

*Test Case: Wave overtopping on a smooth sea dike*

In order to validate the numerical modelling approach described previously, two well known test cases associated with overtopping of waves on a smooth sea dike have been selected. Both cases involve wave breaking on the seaward slope of the dike during overtopping. Flows are driven by a wave generator, located at the seaward boundary, for either regular or irregular waves. For the former case, monochromatic waves ( $H=0.16$  m,  $T=2$  s) are generated in 0.7 m deep water, while in the latter case the waves are created by superimposing series of regular waves drawn from an appropriate energy spectrum. Computations are conducted in the numerical flume, with the computational domain overlaying the dike has a total length of 6.3 m and a height of 1 m (see Fig. 89, the bathymetry of the foreshore and the dike embankment itself are generated by cutting the dike out of the background Cartesian mesh, using Cartesian cut cells. A number of tests have been performed on this problem to examine the convergence history, the effects of mesh refinement, dynamic and static LES models, the development of waves at the dike crest, pressure measurements on the dike slope, wave induced velocity fields, breaking wave current structure interactions and, the effect of viscosity on the wave generated boundary layer. Finally some three dimensional tests have been performed, using long crested waves and a uniform dike cross-section. Full details of these tests are detailed in

report D27 and in the literature (Li et al. 2004a,b). To illustrate the capabilities of the LVOF code, however, the development of the wave induced velocity field is considered.

Fig. 90 shows the velocity fields at times from  $t = 32.2$ s to  $33.4$ s for both regular and irregular waves. It illustrates the wave induced motions on the seaward slope of the dike during the wave attack, run-up, rundown, waves breaking to overtopping of one wave. As expected, motions caused by the irregular waves are more complex than those by the regular waves. Generally, as more waves pass over the dike crest, the flow becomes fully turbulent after an initial transient period so that the features of the flow pattern tend to be very complex, often subjected to the steepness of the free surface most likely associated with a cycle of splashing and the vortex formation created by the velocity. Waves continuously break, while the energy of waves is dissipated by turbulence and convected by vortices. At  $t = 32.2$  s, the wave height increases as it shoals on the front face. By  $32.4$  s, a violent overtopping jet will occur again. Additionally, the corresponding motions display the down wash at  $t = 33.2$  s, while the next big wave is approaching the dike. Finally, the wave breaks on the upper reach of the dike at  $t = 33.4$  s.



**Figure 90: Velocity fields induced by the regular (left) and irregular (right) waves over a sea dike from  $t = 32.2$  to  $33.4$  s.**

### 5.2.3 Long waves

The crest elevation of dikes is determined on the basis of estimates of wave overtopping discharges. For instance, dikes along parts of the Dutch coast have a crest elevation such that a maximum mean overtopping discharge of 1 l/s/m can occur. These estimates of wave overtopping discharges are based on empirical formulae that require the wave conditions at the toe of the dike. The wave conditions at the toe of the dike are different from those at deep water. Numerical models are used to compute the wave propagation over the foreshore to provide the wave conditions at the toe of the dike. Especially for shallow foreshores this wave propagation is complex, for instance due to the effects of wave breaking. Wave breaking on shallow foreshores involves not only dissipation of energy but also a transfer of wave energy to other wave frequencies, for instance from short waves to low frequency waves (i.e., 'long waves'). Nowadays, procedures to assess the wave conditions at the toe of dikes do not take into account energy in low frequency waves. This means that part of the wave energy is neglected. Therefore, it is relevant to study the possible influence of low frequency waves on wave overtopping. The purpose of this part of WP5, is to provide insight into the possible influence of low frequency waves on mean wave overtopping discharges. For this purpose, field measurements on the foreshore of the Petten Sea defence (which has been studied under WP3) and numerical model results are used.

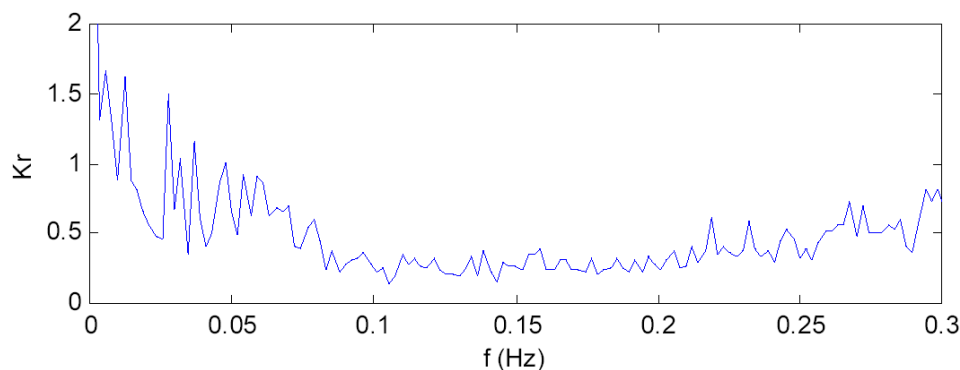
Rijkswaterstaat (RIKZ) have performed field measurements at the Petten Sea defence for some time. This site is characterised as a dike with a shallow foreshore and waves have been measured at several locations on the foreshore, and also wave run-up measurements have been performed during a number of storm events. A description of the field measurements is given in De Kruif (2000) and Hordijk (2003). All data signals from these field measurements have been provided by Rijkswaterstaat (RIKZ). Storms measured in January 1995 have been used for analysis in a number of previous studies. Analysis of these storms has included: an analysis of low frequency waves (e.g. De Haas et al. (1999)), comparisons with physical model tests (van Gent, 1999, 2001; van Gent et al., 2001), and comparisons with numerical models (van Gent and Doorn, 2001).

This part of WP5 is mainly focussed on the storm period October 25-28, 2002, although the storms of January 1995 have also been considered. During the 2002 storms more measurement equipment was operational than during 1995 events. It is important to note, however, that the sandy foreshore has not been stable over the years; fluctuations have been observed from year to year, from season to season, and also within storms. The Petten Sea defence is so high that the probability of occurrence of wave overtopping events is almost



negligible. Therefore, measured wave conditions in combination with a numerical model that can simulate wave overtopping (using an artificially lower crest level) for observed wave conditions have been considered.

The field measurements were analysed to obtain a number of test conditions with an approximately constant water level and significant wave height. These conditions were then analysed to obtain incident waves from the measured surface elevations. This analysis shows that the dike reflects low frequency waves up to 100% (on average 61%), while wave reflection coefficients based on the energy in the short waves are on average 23%. Fig. 90 shows the dependency of reflection coefficient on frequency for one of these conditions. It should be noted that the accuracy of the reflection analysis is reduced at higher frequencies.



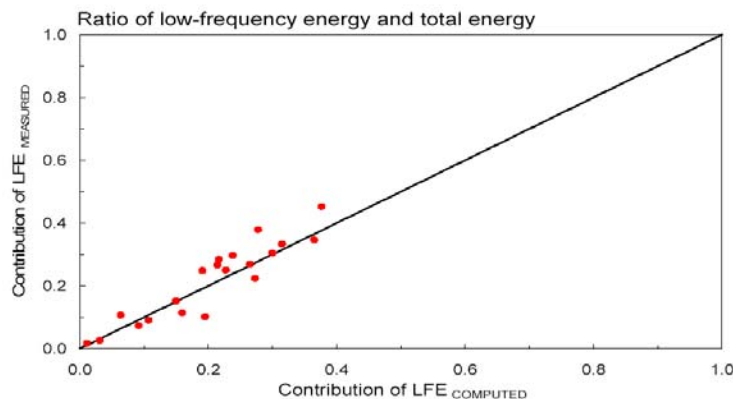
**Figure 91: Wave reflection as function of wave frequency for a selected condition; measured at MP17 on the Petten foreshore.**

Two different numerical models have been applied to examine the overtopping performance, one for wave propagation over the foreshore and one for the wave motion on the dike itself. The TRITON model was used for wave propagation over the foreshore, whilst the ODIFLOCS model has been used to simulate the wave motion and subsequent overtopping on the dike. TRITON has been used to examine whether the amount of low frequency energy can be computed accurately and it has then been applied to obtain wave conditions at the toe of the dike. Time signals from measurements and computations have been used as input for the ODIFLOCS model in order to simulate wave overtopping. Because the Petten Sea defence on site is so high that no wave overtopping occurs, in the computations the crest was artificially lowered.

The TRITON model solves the Boussinesq equations developed at Delft Hydraulics. This model is described by Borsboom et al. (2001a,b & c) and Groeneweg et al. (2003). Boussinesq type



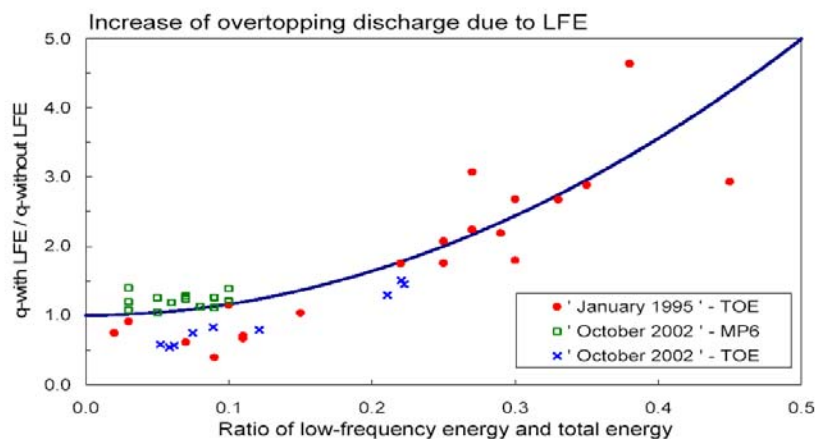
wave models are in principle suitable to model wave propagation in coastal regions and harbours. Especially for the wave propagation of short waves, where nonlinear effects, dispersion and shoaling play an important role, this type of model can be adequately applied and provide valuable information on the wave field (e.g., time series of surface elevations and velocities in shallow regions) which cannot accurately be obtained from many other types of models. In TRITON wave breaking is described using a new method by Borsboom et al. (2001c) where wave breaking is modelled as an eddy viscosity model in combination with a surface roller. Another important aspect of the model is the modelling of weakly reflecting boundaries, based on the concepts by Borsboom et al. (2001a,b & c). A validation of the model based on measured conditions on the foreshore of Petten is given in van Gent and Doorn (2001). From an analysis of the January 1995 storms it can be concluded that the model is capable of providing good estimates of the amount of low frequency waves for these 20 storm conditions. Fig. 92 illustrates the accuracy of the numerical model.



**Figure 92: Comparison between measured and computed contribution of low frequency energy.**

The ODIFLOCS numerical model is a time domain model which can simulate the wave motion on the slope of coastal structures (van Gent (1994); van Gent (1995)). The model allows for simulations of normally incident wave attack on various types of structures. Use is made of the nonlinear shallow water wave equations where steep wave fronts are represented by bores. The model is based on concepts by Hibberd and Peregrine (1979) who developed a numerical model with an explicit dissipative finite difference scheme (Lax Wendroff) for impermeable slopes without friction. Consequently, the model allows for simulations of the wave interaction with permeable coastal structures. The model is able to deal with either regular or irregular waves which attack various types of structures with arbitrary seaward slopes, smooth or rough, permeable or impermeable, overtopped or not. Since the nonlinear shallow water

wave equation overestimates the nonlinear effects, because these effects are not counteracted by frequency dispersion, inaccuracies will occur when wave the waves are propagated over long distances. Therefore, for many applications it is advisable to start the wave simulations at the toe of the structure. On the slope itself the distances are relatively small and nonlinear effects are more important than frequency dispersion. Many applications show that sufficiently accurate results can be obtained. Tests based on the conditions identified previously show that conditions with the highest percentage of low frequency energy result in the highest increase of the mean wave overtopping discharge (Fig. 93).



**Figure 93: Increase of mean wave overtopping discharge as function of the ratio of low-frequency energy and total energy.**

The results of this analysis indicate that for the studied storm conditions low frequency energy increases the mean overtopping discharge with a factor up to a maximum of 5. This increase depends on the percentage of low frequency energy. For the analysed storm period October 2002, a much lower factor was found (up to 1.4). Also for a condition considered as a super storm condition a factor of 1.4 was found. A factor of 1.4 would have a rather small effect on the required crest elevation due to the influence of low frequency energy.

#### 5.2.4 Scale Effects

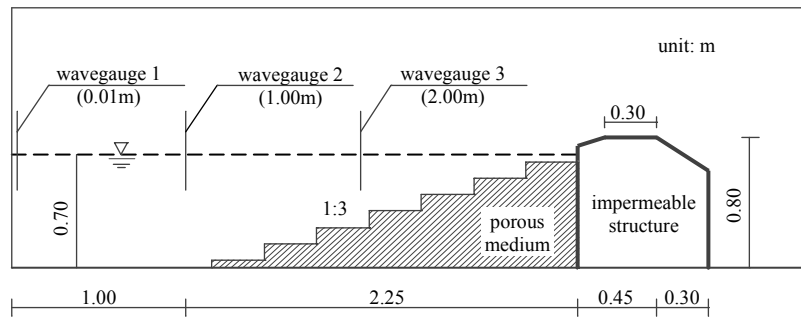
Results reported under WP4 have shown that the measured volumes in laboratory simulations of overtopping on the rough porous breakwaters at Zeebrugge and Ostia are lower than those observed in the prototype measurements. It is clear that scale or model effects are present. Experiments have been conducted at UPV to investigate the effects of wind (model effect) at

Zeebrugge, whilst the work in this part of workpackage 5 aims to support the research towards the effects of scale on overtopping.

When Froude scaling is applied to overtopping on a rough structure the relative roughness probably scales correctly as the thickness of the overtopping jet is expected to scale according to the Froude law, whilst the length scale of the armour layer is a characteristic length and will have been scaled accordingly. Unfortunately the viscosity of the fluid will not have been scaled so, even if, the characteristic velocity of the overtopping jet scales with the Froude law the Reynolds number will be different. Work on smooth and rough dikes (Schulz, 1992) has shown that provided the model and prototype structures are both in regimes with high enough Reynolds numbers the friction-factor can be considered to be constant. Schulz (1992) suggests that provided the Reynolds number is above  $10^5$  the friction factor can effectively be considered to be constant. This threshold of hydraulic independence is supported by work on an armoured sea wall by Sakakiyama & Kajima (1998); see WP7 (Chapter 8) for further details.

#### **6.2.4.1 Numerical simulation of 2D wave overtopping on a porous model structure.**

In order to provide an understanding of the physics, a simple structural configuration has been tested, under regular wave conditions, using AMAZON-SC. The model scale structure (Fig. 94), consists of a porous breakwater ( $K=0.56$ ,  $N_w=35\%$ ), 0.7m tall with 1:3 front face, consisting of ten, 10cm tall steps (to simulate an armour layer). Behind the porous face is a solid, impermeable region, 0.8m tall. The breakwater was subjected to 0.16m high regular waves with a period of 2.0s. and overtopping was measured across the crown of the structure. The numerical study allowed instantaneous measurements of both jet velocity and jet thickness to be obtained. In addition to the porous tests the structure has been tested with a completely impermeable configuration. To examine the effects of scale both configurations have been tested with Froude scalings of 1:2, 1:1, 2:1 and 4:1 and in addition the model scale test has been subjected to 2s waves of 0.08, 0.10, 0.12 and 0.16m; the complete test matrix thus comprises 14 tests.



**Figure 94: Computational domain with step porous structure**

For each case the instantaneous discharge and the overtopping jet thickness have been measured and used to compute the instantaneous jet Reynolds number, by analogy with steady state flow over rough surfaces the Darcy-Weisbach friction factor has then been computed and plotted on the Moody diagram. This analysis, following the approach taken by Schulz (1992) and which is based on a quasi-static assumption, is shown in Fig. 95. The results show that for hydraulic independence (i.e. approximately constant  $\lambda$ ) the Reynolds number,  $Re$ , should be above  $10^5$ , requiring tests to be undertaken at scales larger than 4:1 (i.e. in a 100m wave flume, with a 3.2m high wall in 2.8m of water). It should be noted however, that at smaller Reynolds numbers (e.g.  $Re \leq 10^4$ ) the difference in friction factor is fairly small and the associated dimensionless jet velocities (Fig 96) and overtopping volumes are similar. It is worth noting that the characteristic length scale associated with the tested structure is large and that the variation in  $l$  with  $Re$  is larger for smoother structures.

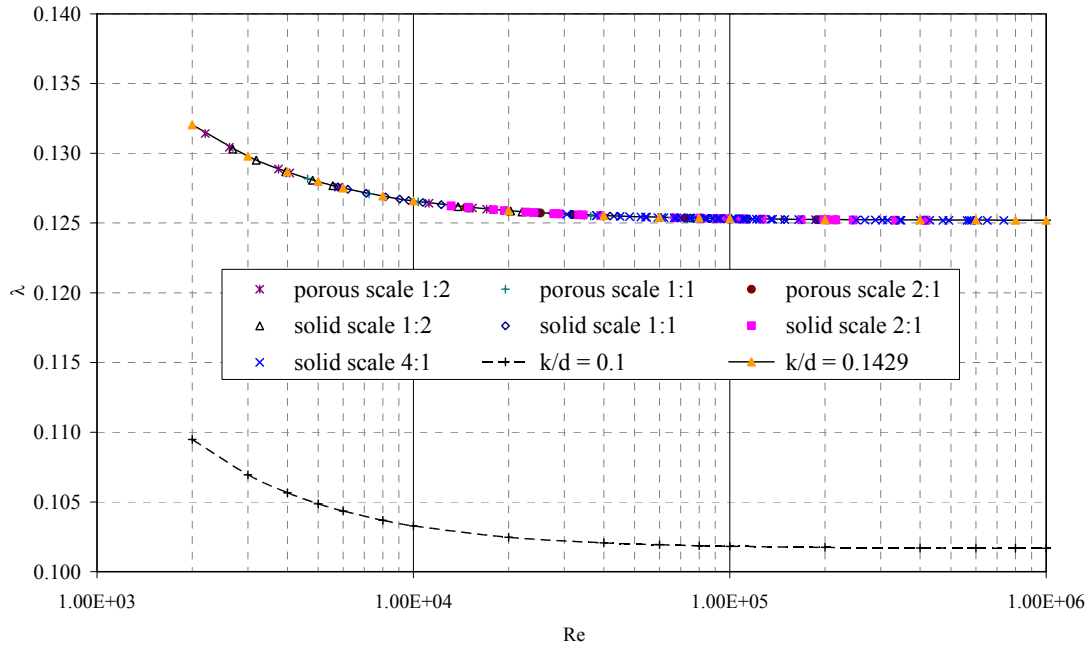


Figure 95: The Darcy-Weisbach friction factor  $\lambda$  against Reynolds numbers.

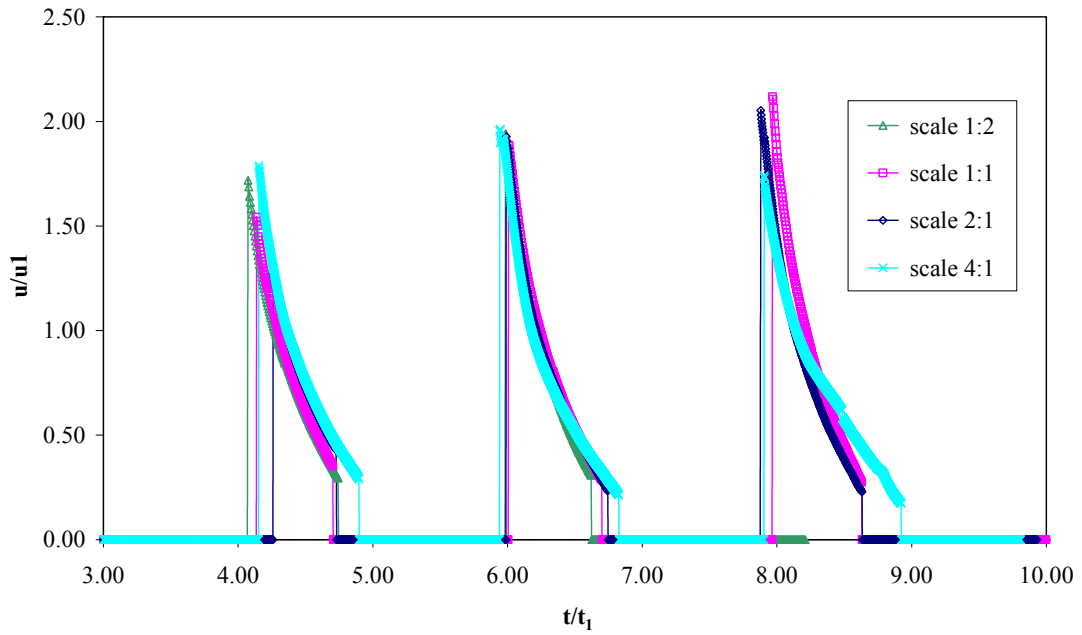


Figure 96: Instantaneous dimensionless jet velocities (solid breakwater)

### 6.2.4.2 Numerical simulation results of 2D wave overtopping at Ostia breakwater

#### Introduction

Numerical simulations of wave overtopping at the Ostia porous rubble mound breakwater have been carried out using the UGent VOFbreak<sup>2</sup> code. As a reference case, the 2D 1/20 physical scale model (tested in the UGent wave flume within WP 4) has been used. The physical scale model dimensions have been adopted in the numerical model. Regular wave conditions have been used, identical to the characteristics of the regular wave tests in the physical model. The 1/20 model is used as the reference case for simulating overtopping at the Ostia breakwater, and the numerical model has been used at scales 1/10 and 1/1 subsequently. The scaling is carried out using Froude scaling laws, keeping gravity and viscosity constant for the three different model sizes.

#### Model description

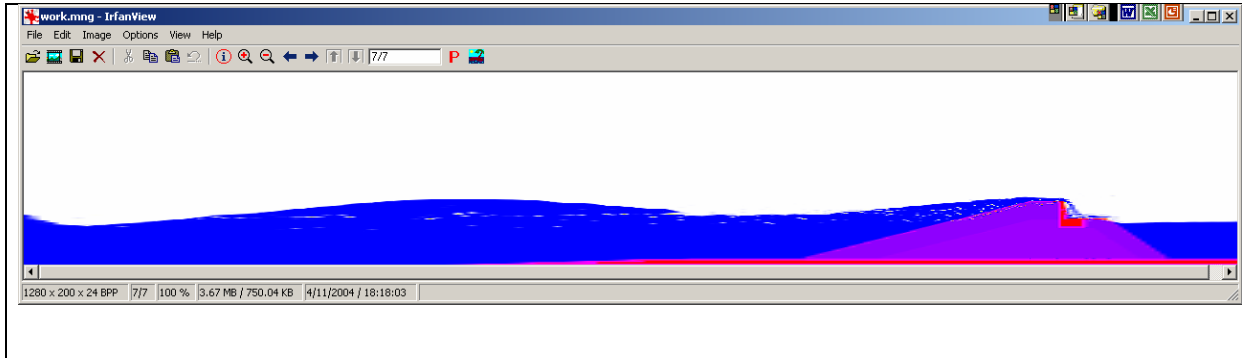
Incident wave conditions are: wave height  $H = 0.175$  m, wave period  $T = 2.24$  s in water depth (near the paddle)  $d = 0.80$  m (and 0.30 m at the toe). The porous breakwater is composed of a core and an armour layer, with material characteristics as given in Table 21.

**Table 21: Material characteristics for the 1/20 Ostia scale model**

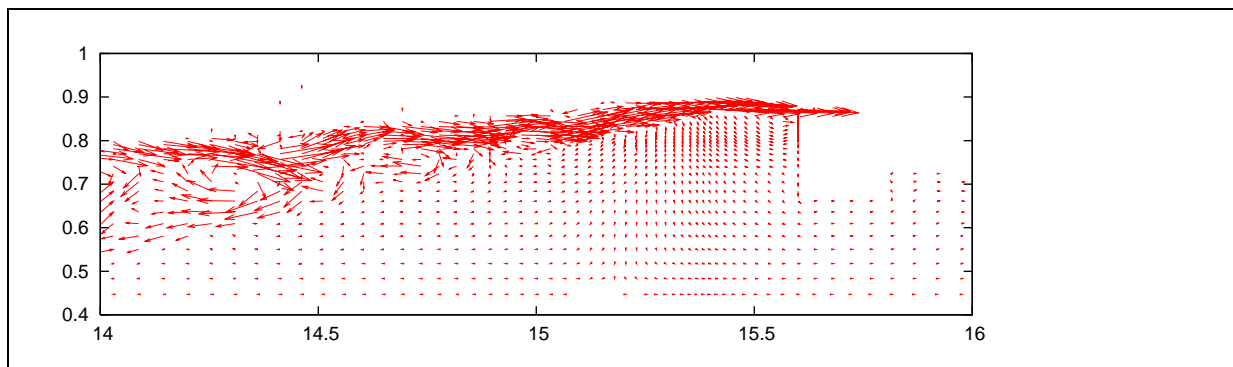
	Core	Armour layer
Porosity $n$ [-]	0.39	0.44
Stone diameter $d_{50}$ [m]	0.025	0.075
Shape factor $\alpha$ [-]	0	0
Shape factor $\beta$ [-]	2.9	2.7

## Simulation results

A typical result of the numerical simulation of the free surface configuration for the 1/20 scale model after 5 waves is shown in Fig.97. The velocity fields calculated at time 20.0 s for the 1/20 scale model is shown in Fig.98.



**Figure 97: Free surface configuration of the Ostia breakwater model (scale 1/20), modelled using the VOFbreak<sup>2</sup> code, and showing wave breaking in front of and wave overtopping over the porous breakwater.**



**Figure 98: Simulation results calculated at time 20 s for the 1/20 scale model.**

The results taken from the simulations are the averaged (during one wave period) layer thickness  $h$ , the averaged flux (or overtopping rate)  $q$  and the averaged Reynolds number  $Re$ , taken at two specific locations: on the breakwater slope (at the intersection with the SWL) and on the crest (seaward side). For scaling the 1/20 model to scales 1/10 and 1/1, two approaches have been used. In the first approach the permeability has been kept constant (stone diameter and  $\beta$  are not scaled, so  $b$  is constant), using the second approach, the permeability has been scaled (stone diameter has been scaled).

Reynolds numbers on the slope and on the crest are derived from the results: for the small scale model (1/20) we obtain  $Re = 7000$  on the slope and 1800 at the crest. For the prototype (1/1) we obtain  $Re \sim 1 \times 10^5$  at the crest and  $5 \times 10^5$  at the slope.

Since the core is completely saturated during wave overtopping, porous flow scale effects will be minimal. For flow in the lower part of the run-up wedge (i.e. on the slope), the 1/20 model yields a Reynolds number  $Re \approx 0.7 \times 10^4$  (close to the critical value  $Re_{crit} = 1 \times 10^5$  for wave overtopping), and higher  $Re$ -values for larger scales, so no scale effects are expected in this region. For flow in the upper part of the run-up wedge (i.e. on the crest), the 1/20 model yields a Reynolds number  $Re \approx 0.2 \times 10^4$  so scale effects are expected in this region.

### 5.2.5 *Shallow water models*

Violent overtopping events are difficult to model using current numerical methods. Ideally, the Navier-Stokes equations should be solved to provide a good model of the overtopping events, using some form of free surface resolving model. However, numerical solvers for these equations require extensive computational resources and, as such are impractical for design calculations by a practicing engineer on a desk top computer, thus an alternative method is required.

A depth averaged formulation of the Navier-Stokes equations exists in the shallow water equations (SWE). As the SWE are depth averaged, any vertical velocity is neglected. Thus, these equations, in theory, may not be suitable as a basis for a numerical model for violent wave overtopping where vertical velocities are a major feature. However, SWE models are easy to implement and computationally efficient. Therefore, before discarding them altogether, an analysis of the limitations of the SWE model is required.

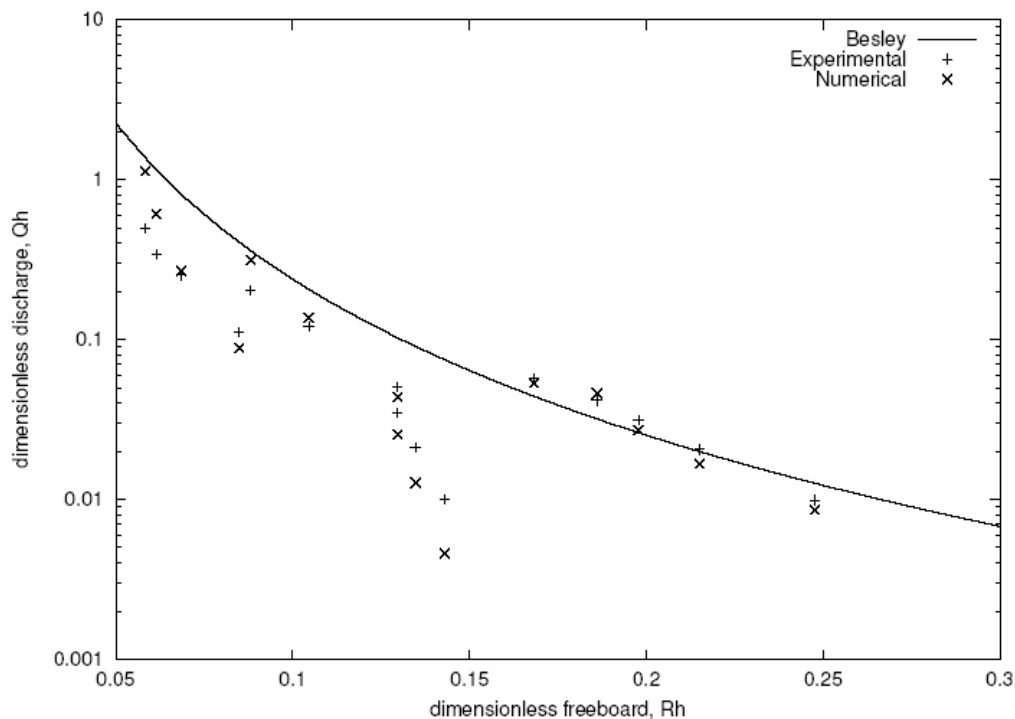
Existing models that make use of the SWE to model wave run-up and overtopping include ODIFLOCS and ANEMONE. These models have been used to give predictions of wave run-up and overtopping of sea dikes where wave conditions are less impacting and violent overtopping is less likely to occur. Shiach et al. (2004) used the AMAZON-CC code to perform detailed comparisons between the VOWS wave overtopping experiments on a 10:1 battered wall (Allsop et al., (2004)). The numerical scheme used is based on the MUSCL Hancock scheme (van Leer, 1984) which is a high resolution Godunov type scheme that uses MUSCL reconstruction to prevent spurious oscillations and incorporates the surface gradient method



(Zhou et al., 2001, 2002) was implemented to model both the seawall and the approach bathymetry.

Comparisons between water surface elevations of the physical and numerical models show that although the waves occur at the same time, the numerical surface over predicts the heights of each wave. This can be attributed to the lack of dispersion within the shallow water equations that are being used in non-shallow water. Fig. 99 shows the dimensionless discharge ( $Q_h = (Q/(gh^3)^{0.5})/h^{*2}$ ) plotted against the dimensionless freeboard ( $R_h = (R_c/H_s)h^*$ ) for the physical model and the numerical model.

Shiach et al. (2004) concluded that the shallow water equations provide a useful alternative to more computationally expensive models for violent wave overtopping provided the  $h^*$  parameter does not fall below 0.075 and that the seaward boundary condition is sufficiently close to the structure. This model provides a useful engineering design tool with 1000 wave simulations taking less than two minutes to run on a moderately fast PC.



**Figure 99: Dimensionless discharge ( $Q_h$ ) plotted against dimensionless freeboard ( $R_h$ ) for the physical model and the numerical model.**

## Conclusions

The AMAZON-SC code developed by MMU, which provides a numerical wave flume in which the flow equations are solved both in the air and the water, has been extended under the CLASH project to include both the effects viscosity and a porous flow model. The resulting flow code has been applied to examine a selected overtopping event from the experimental study of Samphire Hoe before being applied to examine the effects of scale on the overtopping of both permeable and impermeable rough structure. The results on scaling are in broad agreement with those from previous experimental work, indicating that for hydraulic independence of the friction factor the Reynolds number, associated with the overtopping jet, should be greater than  $10^5$ . The results from these scale effect test have helped to enlighten the discussion on scaling effects undertaken in WP7.

At UGent, a new solver based on a Large Eddy Simulation (LES) turbulence model has been developed for the simulation of overtopping of water waves over sloping and vertical structures in a numerical wave tank. The new solver has been validated with two test cases for both regular and irregular waves, respectively. These results demonstrate that UGent's new solver can describe most of the significant features of breaking wave-induced flows. In particular, the wave form is well captured even during a lengthy computation that agrees with measurements available under grid refinements. As a result, this solver can yield detailed information of wave-induced motions on design in coastal engineering using CFD.

Long wave simulations of the Petten site have been computed and the effect of surf-beat at this site has been assessed.

Computations by MMU and HRW have shown that under certain circumstances shallow water models may be used to provide reasonable estimates of overtopping discharge for impulsive overtopping of near vertical sea walls and for overtopping jet velocities for mildly sloping structures.

This workpackage delivered the following reports :

- the draft report on numerical modelling (D9)
- the report on simulation of long waves (D25)

- the numerical model (D26)
- the final report on numerical modelling (D27)

Additionally one milestone was achieved :

New numerical modelling techniques have been implemented (M4)

## 6 WP 6 : Hazard analysis including socio-economic impacts

### 6.1 Objectives

The overall aim of this workpackage is the derivation / refinement of guidance on various levels of hazard imposed on people by overtopping at seawalls and related sea defence structures.

Specific objectives are

- To compare measured events and hindcast events with records of observed hazard in order to derive / refine limits for safety of pedestrians of different levels of mobility, car users, etc.
- To derive / refine limits of overtopping for hazard to buildings and related items
- To evaluate the risk of economic losses

### 6.2 Description of work performed

#### 6.2.1 *Background to development on hazard assessment guidance*

This section gives some definitions and key parameters in the hazard assessment.

Based on the degrees of overtopping related to coastal structures expected hazards can be identified. Hazards from wave overtopping may arise under three general categories:

- a) Direct hazard** of injury or death to people living, working or travelling in the area defended;
- b) Damage to property, operation and / or infrastructure** in the area defended, including loss of economic (environmental or other) resource, or disruption / delay to an economic activity / process;
- c) Damage to defence structure(s)**, either short-term or longer-term.

Hazards or consequences of overtopping are both site- and event-specific, see discussion in Bouma *et al.* (2004). The hazards are driven by overtopping processes usually categorised by the direct responses:

- mean overtopping discharge,  $q$ ;

- peak overtopping volumes,  $V_i$  and  $V_{max}$ ;
- overtopping velocities, horizontally and vertically,  $v_x$  and  $v_z$ ;

Less direct responses may also be needed in assessing the effects of these processes, perhaps categorised by:

- overtopping falling distance,  $x_c$ ;
- pulsating (quasi-static) or impulsive pressures,  $P_{qs}$  or  $P_{imp}$ ;
- post-overtopping flow depths,  $h$ , and horizontal velocities,  $v_x$ .

When considering the effects of wave action, it may be convenient to start by defining degrees of overtopping under three levels of severity and two types of load application:

**Light overtopping**, no impulsive effects or direct structural damage to lightly engineered structures, minor or very local flooding, damage chiefly by inundation only;

**Moderate overtopping**, no impulsive effects and little / no direct structural damage to engineered structures, local flooding causing some inundation damage;

**Heavy overtopping** requiring significant engineering to resist direct effects without damage, overtopping flows / volumes are unlikely to cause damage to a well engineered defence structure, but local and wider flooding is possible as is flood flow damage to lighter structures;

**Overtopping flows** with no significant “slam” effect, damage caused by velocity driven drag forces;

**Impulsive overtopping** with sudden and wave “slam” forces generally caused by the leading edge of an overtopping jet or bore, may lead to direct damage to property close behind and/or damage to the defence itself.

Depending on the expected levels of overtopping, the risks of economic losses can be identified. In making funding decisions, makers of policies to decide on acceptable levels of overtopping will be confronted with assessing both the costs and benefits of controlling

overtopping. Clearly, these assessments take place within a decision-making process context that is different for each of the EU member states. The research under WP 6 provides guidance to determine the perceptions and valuation of hazards.

### 6.2.2 Existing Guidance

Previous research, taking into account different overtopping processes lead to guidance on overtopping hazards already available at the start of the project. This guidance is summarized in table 22 which indicates limits for the average overtopping rate  $q$ . The mean discharge is expressed as flow rate per metre run of seawall, typically l/s.m.

**Table 22: Initial Guidance on Tolerable Mean Overtopping Discharges (l/s.m)**

<b>Embankment Seawalls :-</b>				
No damage		$q$	<	2
Damage if crest not protected	2	<	$q$	< 20
Damage if back slope not protected	20	<	$q$	< 50
Damage even if fully protected			$q$	> 50
<b>Promenade Seawalls :-</b>				
No damage		$q$	<	50
Damage if promenade not paved	50	<	$q$	< 200
Damage even if promenade is paved		$q$	>	0.2
<b>Buildings :-</b>				
No damage		$q$	<	0.001
Minor damage to fittings etc	0.001	<	$q$	< 0.030
Structural damage		$q$	>	$3 \times 10^{-5}$
<b>Vehicles :-</b>				
Safe at moderate / higher speeds			$q$	< 0.001
Unsafe at moderate / higher speeds	0.001	<	$q$	< 0.02
Dangerous		$q$	>	0.02
<b>Pedestrians :-</b>				
Wet, but not unsafe		$q$	<	0.003
Uncomfortable, but not unsafe	0.003	<	$q$	< 0.03
Dangerous		$q$	>	0.03

It has been argued (see e.g. Besley, 1999) that use of mean overtopping discharges only in assessment of safety levels is questionable. It was regarded as probable that the maximum individual volume was of much greater significance than the average discharge to hazards. Franco *et al.* (1994) and Besley (1999) have shown that, for a given level of mean discharge, the volume of the largest overtopping event can vary significantly with wave condition and structural type. There are however two difficulties in specifying safety levels with reference to peak volumes and not to mean discharges. Firstly, methods to predict peak volumes are significantly less well-validated than for mean discharge. Secondly, the data relating individual overtopping events to hazard levels have been rare.

Within CLASH, however, other important parameters, as defined in section 6.2.1 have been taken into account to refine the guidance on overtopping hazards.

### **6.2.3 New evidence on personnel hazards**

Every year, people drown after being swept from breakwaters, seawalls and rocky coasts. Example incidents for the UK gleaned from a single source for 1999-2002 are summarised in Appendix C to the report by Allsop (2004) (Deliverable D38) and for Italy between 1983 and 2002 in Appendix D to this report. To the individual, the waves responsible for such incidents may appear to be sudden and surprising, so it is probable that the people concerned had relatively little idea of the hazard to which they exposed themselves. It is however likely that many of these events could be predicted by informed analysts using some weather / wave forecasting and the results of recent research.

An early example of a custom-built overtopping warning system is described by Gouldby *et al.* (1999) for the low-lying reclamation at Samphire Hoe near Dover. This artificial reclamation was formed by chalk spoil from the excavations of the Channel Tunnel retained by a vertical sheet pile wall. The broad promenade is widely used as a leisure resource, but is subject to wave overtopping during storms. Careful management of access was therefore important to ensure visitor safety. A warning system was therefore developed in which overtopping above agreed thresholds were predicted by output from an appropriate numerical wave model. Wave conditions were correlated with incidents of known overtopping hazard, categorised as low, moderate or high, see Fig. 100. These warning levels were then communicated by the use of warning flags, and ultimately by closing access to the seawall.

Examples of the occurrence of perceived hazards are categorised, and mean overtopping discharges were calculated for each “hazard” event. These were used by Allsop *et al.* (2003) to support the continuing use of  $q \leq 0.03$  l/s.m as a safe limit for (unaware) pedestrians when subject to impulsive jets.



**Figure 100: Categorisation of overtopping hazards at Samphire Hoe, low, moderate and high**



**Figure 101: Public watching / dodging overtopping at Oostende**

The general approach to reducing risks is however only possible where an owner / operator has the means and resources to obtain advance forecasts of hazards, and then to operate such an exclusion system. Elsewhere it is generally only possible to issue warnings.

#### **6.2.4 Perceptions of overtopping**

It is appreciated by engineers and coastal managers that seawalls reduce wave overtopping, but it requires a sophisticated understanding to be aware that seawalls do not always stop, but simply reduce overtopping. Under storm action, waves still overtop seawalls, sometimes frequently and perhaps violently. These processes may excite considerable public interest, see the example in Fig. 101 at Oostende where tourists gather during storms (situation before June 2004).



The key problem identified during the PPA project is that most messages to tell the public about the seaside and coastal activities (particularly those marketing a vision) present only the “sunny” view of coastal processes. There is no motivation for the developer / architect / advertiser to show “stormy” or winter views where hazards might be more easily perceived. This imbalance is compounded by tools that communicate messages of hazard well to engineers and scientists, but do not carry the same message to members of the public.

Examples of this problem are illustrated in Fig. 102, 103, 104 and 105. The first of these show example of coastal structures as experienced by most members of the public. The sun is shining, the waves are small. There are no obvious hazards. Contrasting views of substantially greater hazard are shown in Fig. 104 and 105 showing severe waves at two small harbours. The first photo shows waves of  $H_s = 3-3.5\text{m}$  at the Italian harbour of Salivoli (Tuscany) in November 2001. The second shows waves equivalent to  $H_s = 4\text{m}$  at the harbour of Hartlepool, UK, as modelled at a scale of about 1:40. All coastal engineers will be able to perceive equivalent levels of hazard to either situation, experienced as she / he is in scaling the process to full scale. The problem identified by the non-engineer members of the PPA project is that members of the public cannot easily make the same mental jump. To them, there is no obvious hazard from waves of 50-100 mm height! It was clear, therefore, that any graphic or photograph seeking to explain wave / coastal / overtopping processes would have to take account of this perception “blind-spot”.



**Figure 102:** Beach, seawall and promenade at San Sebastian, Spain



**Figure 103:** Artificial beach, breakwaters and resort at Lanzarote



**Figure 104:** Yacht harbour of Salivoli (Tuscany) during storm in November 2001



**Figure 105:** West Harbour, Hartlepool, under 1:50 year storm, physical model

### 6.2.5 *Changing public perceptions*

Changes to public behaviour will partially be driven by changes to direct management practices at coastal sites, but will also require improvements in awareness of potential hazards, and some understanding of the key drivers. This will require changes on a number of fronts: increasing general awareness of sea / coastal processes; greater awareness of hazards posed by wave overtopping and related processes; and use of site specific warnings.

At the most general level, work is needed by coastal engineers in general to engage with the public media to explain coastal engineering processes in general. Most such work is most obviously focussed on teaching, where each learning increment builds on previous understanding. A major danger in producing simplifying explanations are the consequences of media tendencies to sensationalise the issue, submerging reality in hyperbole. Use of the term “freak waves” for any large wave (however predictable by modelling of wave statistics or processes of wave-wave interactions) is the prime example of such distortions. The use of such “tabloid” expressions debases the public view of the probability of encountering large waves. A particular area of weakness is the widespread lack of understanding of shoaling of swell waves, likely to give inshore waves many times greater than offshore where waves of low steepness (say  $s_{op} < 0.5\%$ ) shoal up over steep slopes. Given that this is exactly the process by which surfing waves are generated, it is perhaps surprising that so few professionals and public appreciate the process which was probably the prime cause of the incident at Giant’s Causeway shown in Fig. 106.



**Figure 106:** Extracts from video of overtopping incident at Giant's Causeway, 16 August 2002

In this incident on 16 August 2002 at Giant's Causeway, 8 children and a "responsible" adult were swept into the sea by a "freak" wave. All were rescued, but this incident highlights typical misperceptions of risk in such situations, and lack of serious attention to warnings.

With climate change bringing increased storminess, there will be more locations where these hazard will increase. The public are aware of climate change, but will not make the link to overtopping hazards unless better informed. This is aggravated by media references to "freak waves" that are in truth entirely predictable by an informed person, and media concentration on tsunamis and other "televisual" hazards of very low probability.

### **6.2.6 Awareness of coastal processes**

The most immediate action of any owner or responsible authority aware of a potential hazard is to ensure that the public are made aware of the hazard. The general issue of hazards on coastal structures has been discussed by Halcrow (1997) and Heald (2002) who show examples of poor signage.

Some tools that can be used to train coastal engineers, scientists, and perhaps managers, may not be so useful in informing the public. Example cartoons developed by HRW and the PPA project for the UK Environment Agency are shown in Appendix M to the mentioned deliverable to illustrate the development of overtopping and possible damage under extreme storms.

### **6.2.7 Post overtopping velocities and loads**

#### ***Overtopping velocities***

Until recently, few data have been available on overtopping velocities. Pearson *et al* (2002) have presented measurements at small and large scales of upward velocities ( $u_z$ ) from vertical / battered walls under impulsive and pulsating conditions. They related the measured upward velocity  $u_z$  to the inshore wave celerity given by  $c_i = (gh)^{1/2}$ . Relative velocities,  $u_z/c_i$ , were plotted against the wave breaking parameter,  $h^*$ . Non-dimensional velocities were roughly

constant at  $u_z/c_i \approx 2.5$  for pulsating and slightly impulsive conditions  $h^* > 0.2$ , but overtopping velocities increase significantly for impulsive conditions when  $h^* \leq 0.2$  reaching  $u_z/c_i \approx 3 - 7$ .

For simply sloping embankments, Richardson *et al* (2002) measured crest velocities of around  $u_z/c_i \approx 2$  behind a 1:2 slope under plunging conditions. Simulations for 1:1-1:5 slopes discussed in Appendix H to deliverable D38 showed overtopping bore velocities in the range  $u = 2-5$  m/s.

Further data on overtopping velocities have been presented by Romestaing in Appendix F to D38. Analysis of video of overtopping velocities in the Samphire Hoe 3D model gave peak velocities of  $u_z = 1-9$  m/s, corresponding to  $u_z/c_i \approx 0.2 - 1.2$ , much lower than found by the VOWS tests. Analysis of video recordings from the Carlyon 3D model, gave horizontal overtopping velocities behind the recurve seawall of  $u_x = 3.5$  to 5.5 m/s.

These levels of velocity may be put into context by findings from UK studies on flood risks to people, see Ramsbottom *et al.* (2004) who present hazard classification tables based on flow depths and velocities. The suggested limits are re-represented here as Fig. 107. As these velocity / depth limits were originally derived for relatively steady flows, it would be wise to take a precautionary view of these limits in the derivation of any suggested limits. The middle threshold in Fig. 107 suggests that flow velocities above  $u_z \geq 2.5$  m/s will be difficult to resist for depths greater than  $d > 0.5$  m, and  $u_z \geq 5$  m/s will be difficult to resist for depths greater than  $d > 0.25$  m.

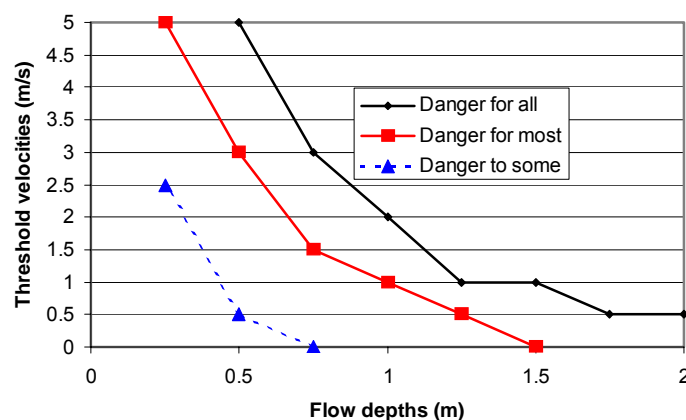


Figure 107: Suggested velocity / depth limits from Ramsbottom *et al.* (2004)

### ***Post overtopping wave loads on structures***

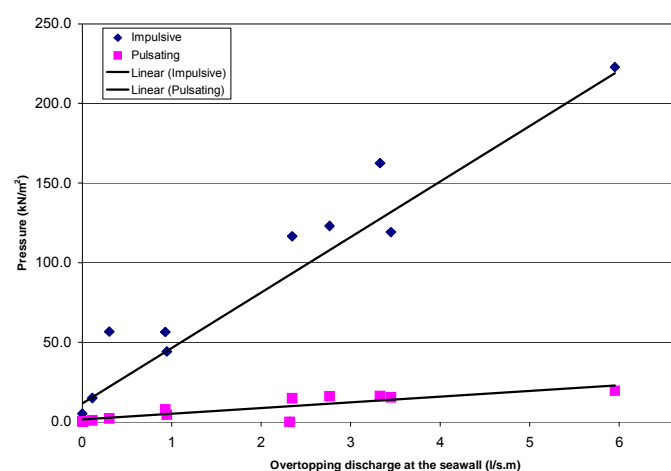
Wave loads have seldom been measured on defence structures, buildings behind sea defences, or on people. Under CLASH, post overtopping loads on person-sized dummies and a length of pipeline have been measured at full scale at Zeebrugge (Geeraerts & Boone, 2004), and at small scale at LWI (Kortenhaus et al., 2004) and HRW.

For test conditions described by Romestaing in Appendix F to D38, wave pressures measured on the 1m high secondary wall set 7m back from the primary (recurve) wall measured.

The impulsive pressures were approximately 11 x greater than the quasi-static loads. Extrapolating the trend lines in Figure 22 down to an overtopping condition of  $q = 0.03$  l/s.m suggest that the quasi-static pressures might reduce to  $p_{q-s} \approx 2$  kN/m<sup>2</sup>, but that impulsive pressures might not fall below  $p_{imp} \approx 20$  kN/m<sup>2</sup>. These may be put into context when noting that few buildings are designed for horizontal wind loads above  $p_{av} \approx 0.5$  kN/m<sup>2</sup>.

Measurements on the person dummies are also discussed in the above mentioned Appendix J, and a summary graph of results is shown here in Fig. 109.

These measurements suggest that wave loads on a person increase rapidly for increasing overtopping discharges. Advice quoted in Appendix J cites work by Endoh et al as giving force limits on individuals of up to  $F_h = 140$  kN. Given other data collected for this and related studies, this force limit appears much too high.



**Figure 108: Wave loads on person dummies (from tests at LWI, see Appendix J)**

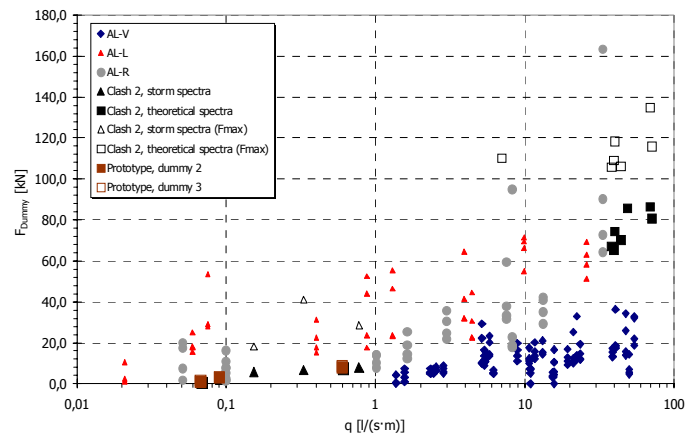


Figure 109: Wave loads on person dummies (from tests at LWI, see Appendix J)

### 6.2.8 Present Guidance

This section presents the present state of knowledge on tolerable wave overtopping. It includes guidance derived from the CLASH field and laboratory work, and builds on previous guidance, see Fukuda *et al.* (1975), Owen (1980), Besley (1999) and Allsop *et al.* (2003). A number of limits are suggested in Table 23 for mean overtopping discharge or peak overtopping volume. These limits derive from a generally precautionary principle informed by previous guidance and by the various observations and measurements made by the CLASH partners and research colleagues.

**Table 23: Suggested limits for overtopping mean discharges or peak volumes\***

<i>Hazard type / reason</i>	<i>Mean discharge, q</i>	<i>Peak volume, V<sub>max</sub></i>	<i>Comments or other limits</i>
<b><i>Pedestrians</i></b>			
Unaware pedestrian, no clear view of the sea, relatively easily upset or frightened, narrow walkway or close proximity to edge	0.03 l/s.m	2-5 l/m at high level or velocity	
Aware pedestrian, clear view of the sea, not easily upset or frightened, able to tolerate getting wet, wider walkway.	0.1 l/s.m	20-50 l/m at high level or velocity	
Trained staff, well shod and protected, expecting to get wet, overtopping flows at lower levels only, no falling jet, low danger of fall from walkway	1-10 l/s.m	500 l/m at low level,	$d \cdot u^2 < 1-5$ $m^3/s^2 \cdot m$ (see Fig. 107)
<b><i>Vehicles</i></b>			
Driving at moderate or high speed, impulsive overtopping giving falling or high velocity jets	0.01-0.05 l/s.m	5 l/m at high level or velocity	
Driving at low speed, overtopping by pulsating flows at low levels only, no falling jets	10-50 l/s.m	1 m <sup>3</sup> /m	
<b><i>Property</i></b>			
Sinking small boats set 5-10m from wall. Damage to larger yachts	q = 10 l/s.m	1 - 10 m <sup>3</sup> /m	Volumes depend on vessel position etc., form of overtopping flow and wave transmission
Significant damage or sinking of larger yachts	q = 50 l/s.m	5 - 50 m <sup>3</sup> /m	

\* Overtopping at "Low level" is overtopping flowing over or close to the promenade. Overtopping at "high level" is overtopping flying through the air.

High or low velocities depending on flow depth, see Fig. 107 for guidance.



### 6.2.9 Valuing overtopping hazards

The perception of direct hazards indicates that the risk of death is an ultimate level of hazard. If this is to be included into the economic assessment this is to be decided on by the decision makers themselves. If, the answer is yes, then Bouma et al. (2004) (Deliverable D39) provide valuation methods based on methods available in literature.

Deliverable D38 gives outline details of deaths from overtopping and related processes in Italy and UK. In many cases the context is such that this valuation will not take place in such an explicit way but will be dealt with implicitly by introducing safety norms. These norms may not necessarily define the acceptable level of overtopping (**defence standard**) but might also provide norms with respect to:

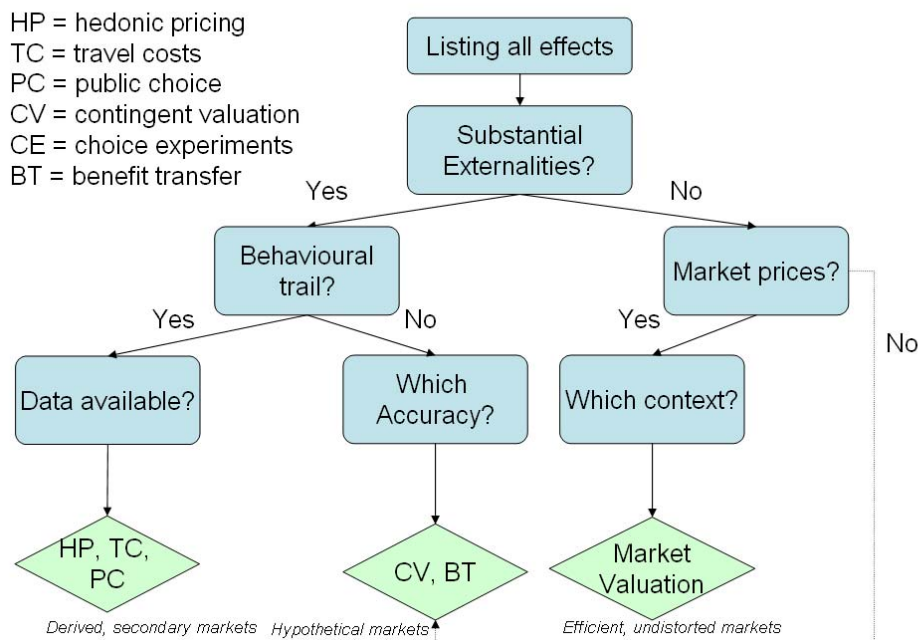
- **Acceptance of human activities** (thereby modifying the land use category and/or habitat status of the area affected by the overtopping (hazard zone))
- **Acceptance of occasional hazard** at acceptable probability (acceptable risk) by providing for temporary use and/or short-term evacuation with reliable warning and evacuation systems, and/or use of temporary / demountable defence systems;

With respect to the valuation of hazards these can be either be valued by using existing values or by applying valuation techniques. When the effects of overtopping are to be valued by using monetary provided by the valuation literature, examples are given in Bouma et al. (2004).

Hence, if policy makers want to assess effects (hazards) themselves in order to be site specific these values can be derived by applying valuation techniques. Selecting the appropriate valuation techniques is related of the type of effects that are to be valued. For example, damage to houses and furniture, can be defined by using market prices (market analysis). Whereas damage to ecosystems (defined as an externality) can be valued by using a Contingent Valuation Method (CVM). If no substantial externalities occur than the effects can be valued by using market prices related to the hazard. Fig. 110 provides a simple decision-rule to identify the appropriate valuation technique.



## Choice of Valuation Methods



**Figure 110: Decision tree for choosing valuation techniques**

Environmental economists tend to prefer pure survey based CV methods, but when market prices for direct and indirect damages can be obtained, mixed approaches can be more informative for decision making.

When evaluating flood alleviation schemes by means of Cost-Benefit Analysis, identifying and imputing a value on costs and benefits is an essential task. However, other crucial factors are the determination of the appropriate discount rate and the project life of the proposed flood alleviation scheme.

The outcome of the use of a valuation technique is often used to calculate present values in the context of Cost-Benefit Analyses. This implies that weights are attached to the effects of flooding in the future. Deliverable D39 provides details on selecting a discount rate and the use of discounting tables and annuities in Cost-Benefit Analysis. Two case studies, incorporated in the mentioned deliverable illustrate how the effects of overtopping can be valued. The first case of *De Haan* shows how the total damage of overtopping can be estimated by applying the technique of public pricing. By using this techniques the averting expenditures are determined. Since people would not normally spend more to prevent a problem than would be caused by the problem itself, averting expenditures can provide a

lower-bound estimate of the damage caused by pollution (Tietenberg, 2000). In the context of flooding, a vast amount of measures can be categorised as Averting Expenditures. Averting Expenditures on bringing back the natural retention capacity of a river can be mentioned e.g. creation, development and management of retention and flood control areas (Schuijt, 2001). Other examples are the construction of storage reservoirs, waterproofing of the lower floors of existing buildings, flood warning systems, levees or walls to prevent inundation from floods below some specific design flood flow, drainage and pumping facilities, diversion structures, channel modifications, construction of elevated boulevards (dikes), efforts to raise homes and the creation of individual dikes around properties.

The second case (Rapallo) illustrates the use of market prices to calculate the damage to property and the method Value of a Statistical Life to estimate the direct hazard.

### ***Summary of hazard assessment and valuation procedures***

When the optimum level of overtopping prevention is to be determined the procedure of a Cost Benefit Analysis is proposed. However, it must be stated that such a formal procedure will often not take place as the prevention of overtopping is often covered by meeting legal standards with respect to meeting the requirements on reducing the risks of flooding.

If a formal Cost Benefit Analysis is performed the following steps should be undertaken:

1. Define the project;
2. Determine the physical effects (including the prevention of hazards);
3. Choosing the discount rate;
4. Valuation of the physical effects and calculating the Net Present Value;
5. Performing a sensitivity analysis.

Clearly, before the costs and benefits of preventing overtopping can be assessed the project and its system boundaries need to be clearly defined. Questions need to be answered such as what is the project and the area for which the hazards and physical impacts are to be identified. While using a certain discount rate the present value of the costs and benefits can be calculated. The prevented hazards of overtopping are presented as benefits. The example of the Haan show that for the valuation of these damages estimates can be derived by looking

similar projects at other sites for which the costs spend by governments provide an indication (public pricing). However, each benefit item itself can also be valued separately for which an array of valuation techniques are available.

## **Conclusions**

Guidance on permissible wave overtopping has been refined based on new prototype measurements and laboratory modelling.

From the socio-economic point of view, methods to value hazards have been presented.

This workpackage delivered the following reports :

- the report on hazard analysis (D38)
- the report on socio-economic impacts (D39)

Additionally one milestone was achieved :

- the hazard analysis (including socio-economic impacts) workpackage is completed (M11).

## 7 WP 7 : Conclusions on scale effects and new data

### 7.1 Objectives

The main objective of WP 7 is to compare full and large scale measurements on overtopping with simulation by laboratory scale model tests and numerical modelling and to come to a conclusion on suspected scale effects. This conclusion is essential for WP8, where the database will be used to develop a generic prediction tool.

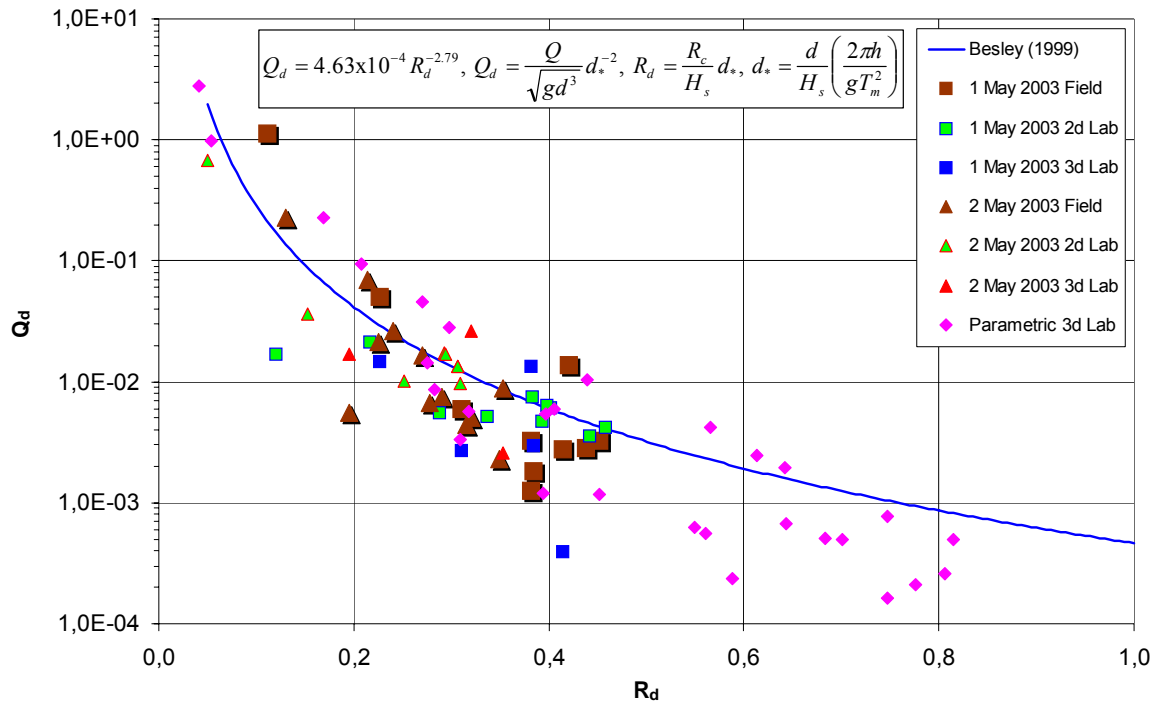
### 7.2 Description of work performed

The work in WP 7 comprises a number of steps which has finally led to a conclusion on scale effects for the structures investigated within CLASH. The background research and the aforementioned procedure is described in this section.

#### 7.2.1 *Samphire Hoe vertical wall*

Videos have been recorded from the field and the model tests which show very similar behaviour in the water mass being thrown up at the vertical wall. The significant difference seems to be the wind blowing much of the spray beyond the overtopping container.

In Fig. 111 the overtopping results from the prototype as well as the model tests at UEDIN (2D) and HRW (3D) are plotted together with the overtopping rate against the freeboard  $R_d$ . The Besley formula (1999) is also plotted. It should be noted that the 1 May storm data with strong wind effects have been multiplied by a factor of 3.0 to account for the spray blown beyond the overtopping containers.



**Figure 111: Prototype results, 2D and 3D test results with comparison to Besley formula**

The results in Fig.111 show a relative good agreement between the Besley curve, most of the data points and the prototype storms. No major differences between field and model data can be observed suggesting that there are only few model (except wind effect) and scale effects.

### 7.2.2 Zeebrugge rubble mound breakwater

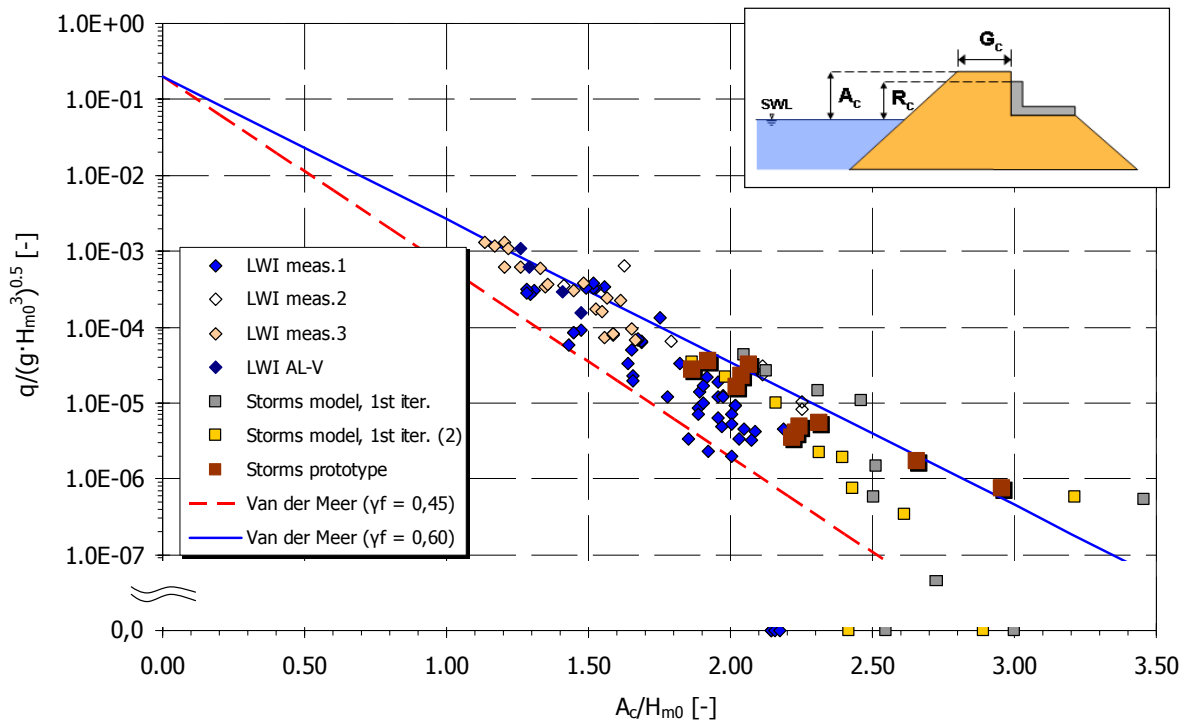
In Fig. 112 all overtopping results at LWI and the prototype results are plotted together as relative mean overtopping rate against the relative freeboard  $A_c/H_{m0}$ . The Van der Meer formula for non-breaking waves, Van der Meer (1998), for a roughness factor of  $\gamma_r = 0.60$  and  $\gamma_r = 0.45$  were also plotted.

The results in Fig. 112 show a relative good agreement between the curves, most of the data points and the prototype storms. However, there is some reasonable scatter in the data and three observations which are of particular importance:

- for higher relative crest freeboard  $A_c/H_{m0} > 1,7$  the parametric tests seem to be slightly lower than the prototype storms. This is supported by some of the data points which are even zero for  $A_c/H_{m0} > 2,0$
- storm reproductions at UPVLC have shown that only one of the three storm events could be reproduced without wind. The other two reproductions had zero overtopping.

- higher wind speeds in the flume gave considerably higher wave overtopping rates. This cannot be seen from Fig. 112 but has been reported by Kortenhaus et al. (2004b) and González-Escrivá et al. (2004)

Details of differences and reasons for the scatter of the data points are explained in Kortenhaus et al. (2004a)

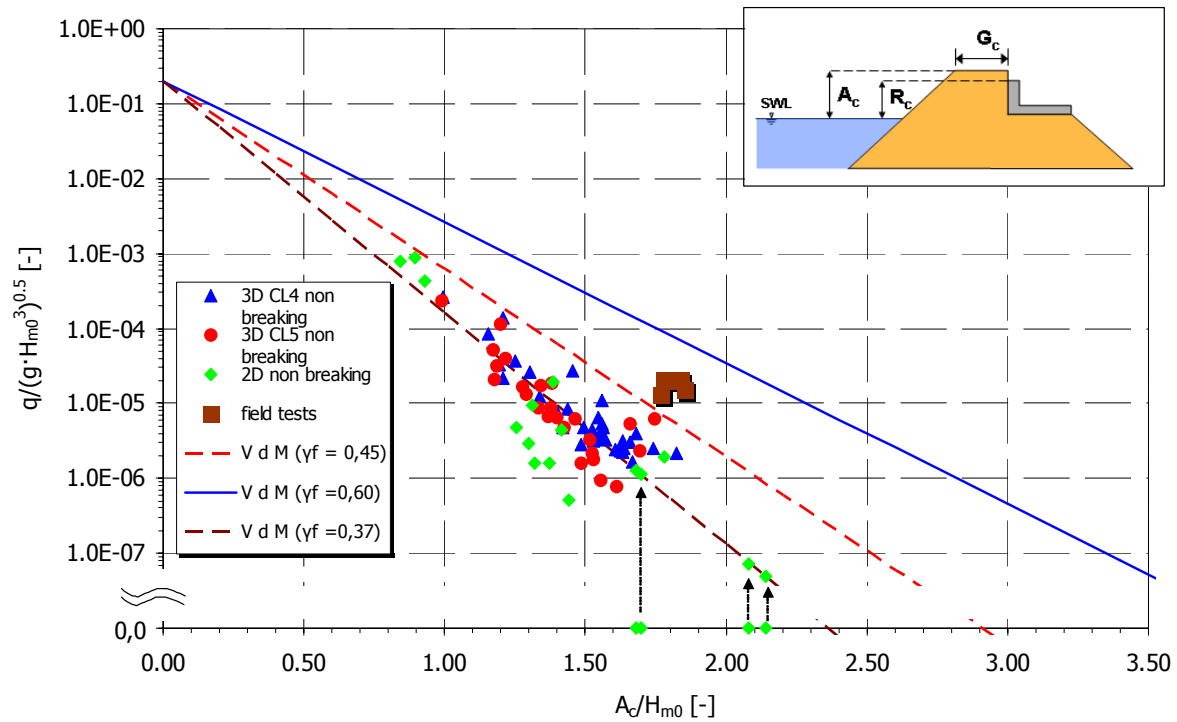


**Figure 112: Relative mean overtopping rates from LWI tests plotted against the relative freeboard with comparison to Van der Meer formula and prototype results**

### 7.2.3 Ostia rock breakwater

For the Ostia breakwater the comparison of videos from field and model is shows that more overtopping occurs in the field rather than in the model. It seems that similar waves cause different behaviour on the slope of the breakwater.

In Fig. 113 all overtopping results at FCFH (3D) and UGent (2D) as well as the prototype results are plotted together as relative mean overtopping rate against the relative freeboard  $A_c/H_{m0}$  (for the Ostia breakwater  $R_c = A_c$ ). The Van der Meer formula for non-breaking waves and a roughness factor of  $\gamma_f = 0.60$ ,  $\gamma_f = 0.45$  and  $\gamma_f = 0.37$  were also plotted.



**Figure 113: Relative mean overtopping discharges from FCFH (3D) and UGent (2D) tests plotted against the relative freeboard with comparison to Van der Meer formula and prototype results<sup>1</sup>**

All results in Fig.113 show a relative good agreement between most of the laboratory data points although some scatter can be observed due to variation of some model parameters and influence of wave period. The prototype storm results are higher than the model results (up to a factor of 10).

There are four data points in Fig.113 where the relative mean overtopping rate is zero. No overtopping occurred during the model tests for these data points. It can be assumed, that in the field overtopping could emerge for these ratios  $A_c/H_{m0}$  since the measurement accuracy in the flume is not high enough for these small overtopping volumes. In order to calculate prototype values from these data points and account for scale effects, a mean overtopping rate greater than zero has to be determined. Using the Van der Meer formula and a roughness factor of  $\gamma_f = 0.37$  (i.e. best fit through all data), all data points of the model tests can be represented as shown in Fig. 113. By means of this curve it is possible to achieve relative mean overtopping discharges for the data points with no overtopping. The arrows in Fig. 113 indicate this procedure.

<sup>1</sup> Note: almost all data points above a relative crest freeboard of  $A_c/H_{m0} > 1.6$  during the model tests were zero whereas prototype data still resulted in overtopping rates

#### 7.2.4 *Method to account for scale effects*

A number of possible reasons for differences between prototype and model scale has been listed in Kortenhaus et al. (2005) (Deliverable D40). It has been shown that all measurement uncertainties and model effects may have a considerable effect on wave overtopping so that most data points fall within the differences of one standard deviation of the result. Therefore, scale effects are very difficult to observe since differences in the resulting plots may be all due to model effects only.

##### a) Requirements for scale effects

The theoretical investigations and review of the available literature in Deliverable D40 has shown that differences in wave run-up heights for rough slopes (both permeable and impermeable) have been observed in many cases. Therefore, the wave run-up height should be included in any guidance on how to scale wave overtopping. The following requirements may be derived from the literature and observations in the model and prototype tests:

- scaling effects have only been observed for sloped structures but not for vertical ones;
- the scaling factor must be higher for lower overtopping rates; it even has to work for ‘no overtopping’ measurements in the flume, knowing that for the same conditions some overtopping is measured in prototype;
- roughness of the slope has to be included; critical Reynolds numbers can be defined;
- the core permeability needs to be included where lower permeability in the core creates more run-up on the slope and more overtopping
- wind effects should be included since wind increases wave overtopping rates considerably;

##### b) Factor resulting from scale effects on wave run-up

The second and third requirement may be fulfilled by a simple approach. Schulz (1992) and others have indicated that the increase of run-up heights from small-scale to large-scale models are in the range of 15%. If this is introduced as an additional ‘roughness’ factor (to be



treated in the same way as a traditional roughness factor) to a standard wave overtopping formula it gives:

$$\frac{q_{\text{red}}}{\sqrt{g \cdot H_{m0}^3}} = q_0 \cdot \exp\left(b \frac{R_c}{H_{m0}} \cdot \frac{1}{\gamma_f} \cdot \frac{1}{\gamma_s}\right) \quad (4)$$

where  $\gamma_s$  is the scaling reduction due to scale effects on the seaward slope ( $\gamma_s = 1,15$  here). Eq. (4) differs from the standard wave overtopping formula by a factor  $1/\gamma_s$  only so that  $q_{\text{red}}$  can be calculated as  $q_{\text{red}} = q(1/\gamma_s)$ . The relative scaling factor  $f_{s,q} = q_{\text{red}}/q$  can then be calculated as:

$$f_{s,q} = \frac{q_{\text{red}}}{q} = \frac{q^{1/\gamma_s}}{q} \quad (5)$$

where  $q_{\text{red}}$  is the theoretically reduced overtopping rate as given by Eq. (4). In Fig.114 the factor given by Eq. (5) is plotted against the wave overtopping discharge using the Zeebrugge parametric tests at LWI from the first test phase. The latter have been scaled up to prototype conditions using Froude law. Each data point is then achieved by performing the following steps:

- derive  $q$  for specified tests from measurements;
- scale  $q$  up to prototype using Froude law (if  $q$  is from model tests);
- calculate the reduced overtopping rate using Eq. (4);
- calculate  $f_{s,q}$  for each data point using Eq. (5)

Furthermore, an additional formula for a factor  $f_{\text{scale\_nowind}}$  has been plotted which shows a similar behaviour than Eq. (5) but is closer to the data. This curve can be described by the following equation:

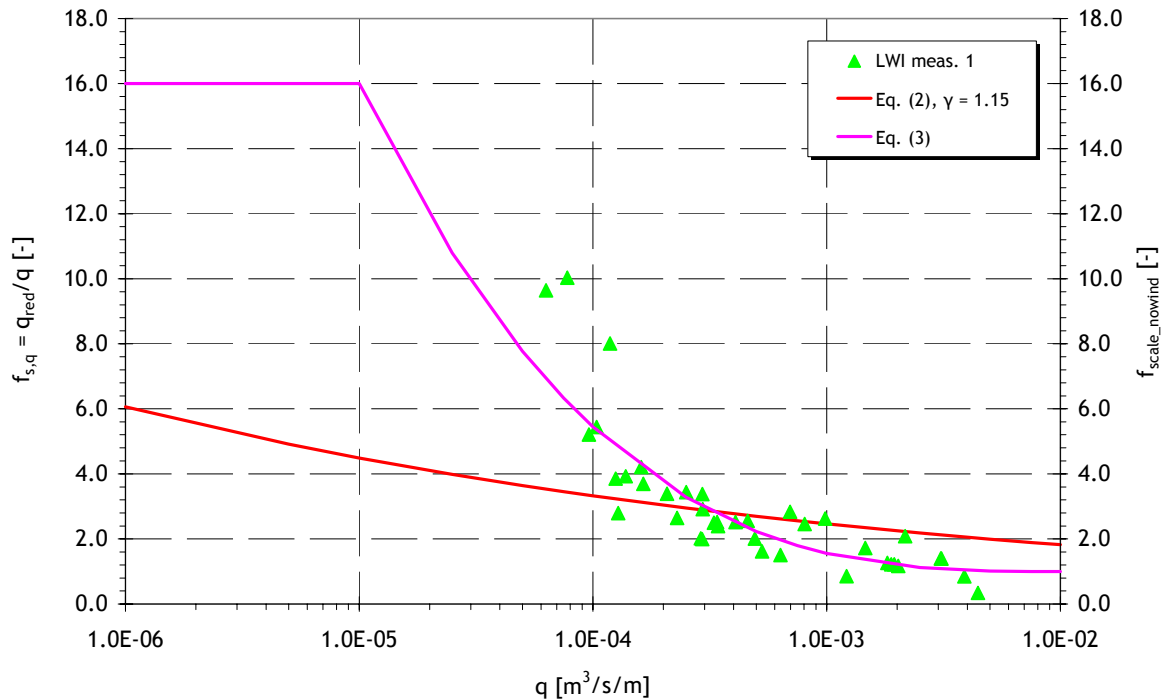
$$f_{\text{scale\_nowind}} = \begin{cases} f_{\text{scale\_nw}} & \text{for } \gamma_f \leq 0.7 \\ 5 \cdot (1 - f_{\text{scale\_nw}}) \cdot \gamma_f + (f_{\text{scale\_nw}} - 1) \cdot 4.5 + 1 & \text{for } 0.7 < \gamma_f < 0.9 \end{cases} \quad (6a)$$

where

$$f_{\text{scale\_nw}} = \begin{cases} 16.0 & \text{for } q_{\text{SS}} < 1 \cdot 10^{-5} \text{ m}^3 / \text{s} \cdot \text{m} \\ 1.0 + 15 \cdot \left( \frac{-\log q_{\text{SS}} - 2}{3} \right)^3 & \text{for } q_{\text{SS}} < 1 \cdot 10^{-2} \text{ m}^3 / \text{s} \cdot \text{m} \\ 1.0 & \text{for } q_{\text{SS}} \geq 1 \cdot 10^{-2} \text{ m}^3 / \text{s} \cdot \text{m} \end{cases} \quad (6b)$$

It should be noted that  $q_{SS}$  is a value based on small scale measurements, but already scaled up to prototype scale by means of Froude scaling law.

Eq. (6a) delivers a scaling factor for really rough structures when  $\gamma_f \leq 0.7$ . When  $\gamma_f \geq 0.9$  the structure is smooth and the scaling factor will be  $f_{scale\_nw} = 1.0$ . In between both values a linear interpolation can be assumed.



**Figure 114: Reduction of wave overtopping due to reduction of wave run-up on the seaward slope for the Zeebrugge storm data**

It can be seen from Fig.114 that factors may easily go up to one order of magnitude for lower overtopping rates whereas they are still in the same range as without run-up reduction for higher overtopping rates. Since data from comparison between small-scale and large-scale model do not support regions of overtopping ratios lower than  $1 \cdot 10^{-5} \text{ m}^3/\text{s}\cdot\text{m}$  the formula will not go up to higher values than a factor of 16.0.

Eq. (5) is determined for a scaling factor which is only valid for rough slopes and no wind effects. The latter can be assumed since comparisons between large-scale and small-scale tests are always referring to tests in either the GWK in Hannover or the Delta flume in De Voorst which both do not include any wind.

Therefore, a method needs to be found which summarises the various influences of scale and wind effects. This method will be discussed in the subsequent section. Since the magnitude of

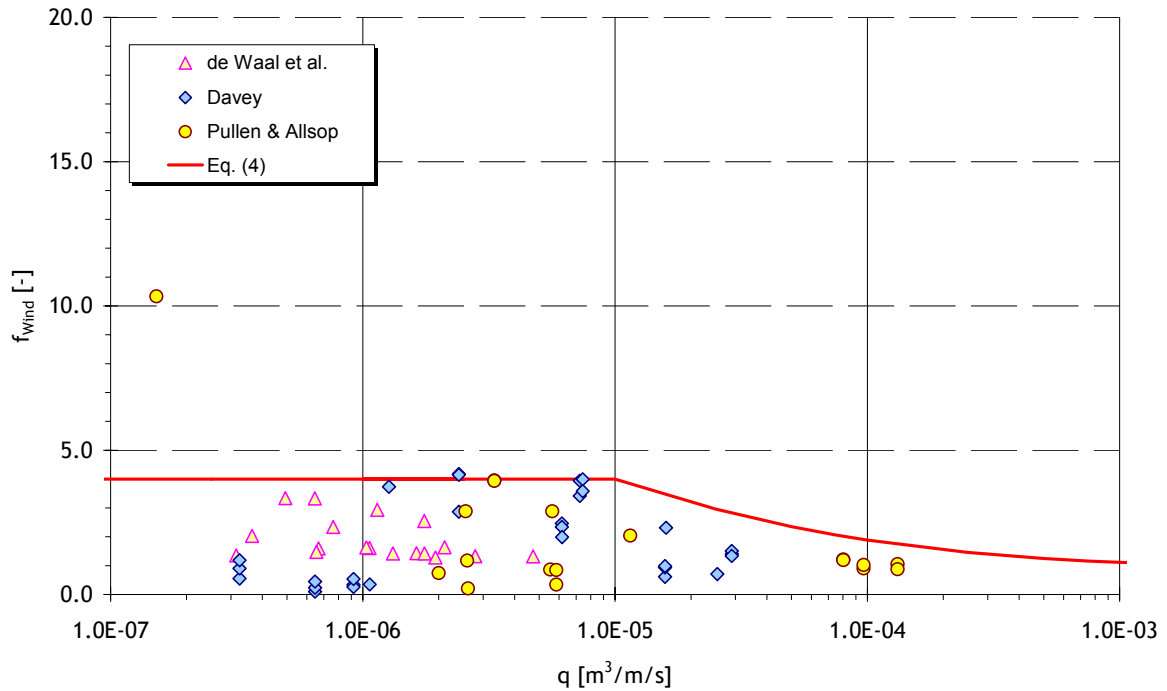
the influence of scaling the core material is not known up to date this influence will be ignored in the following.

c) Factor resulting from wind effect on vertical structures

It is possible to examine the results of de De Waal et al. (1996), Davey (2004) and Pullen & Allsop (2004) (D36), as described in D40. By examining the data it is possible to ascribe the following formula to the transport factor  $f_{\text{wind}}$  (Fig.115):

$$f_{\text{wind}} = \begin{cases} 4.0 & \text{for } q_{\text{SS}} < 1 \cdot 10^{-5} \text{ m}^3 / \text{s} \cdot \text{m} \\ 1.0 + 3 \cdot \left( \frac{-\log q_{\text{SS}} - 2}{3} \right)^3 & \text{for } q_{\text{SS}} < 1 \cdot 10^{-2} \text{ m}^3 / \text{s} \cdot \text{m} \\ 1.0 & \text{for } q_{\text{SS}} \geq 1 \cdot 10^{-2} \text{ m}^3 / \text{s} \cdot \text{m} \end{cases} \quad (7)$$

In this instance the factor 4.0 is not a scaling factor as previously described, but it can be used to make an allowance for the effects of the wind, and also has the advantage of not using a separate technique. It is especially important to make this distinction, because it has been demonstrated in D36, that there are no scaling effects for vertical and composite vertical structures. Fig.114 shows that a factor of 4.0 provides a conservative estimate of the effect of the overtopping discharge  $q$ .



**Figure 115: Discharge rates and the effect of the transport factor  $f_{wind}$ .**

d) Overall procedure

*Input*

The final CLASH-procedure to determine the overtopping discharge, taking into account scale effects starts with a mean overtopping rate predicted by small-scale model tests  $q_{SS}$

Besides the  $q_{SS}$  the following parameters are required:

- wave height  $H_{m0}$  at the toe of the structure (output scale<sup>2</sup>),
- roughness coefficient  $\gamma_f$  for the seaward side of the structure,
- width of the seaward berm  $B$  of the structure,
- water depth over the horizontal berm  $d_h$ ,
- slope of the structure below the berm  $\cot\alpha_d$ ,
- slope of the structure above the berm  $\cot\alpha_u$

For a more detailed description of these parameters see Verhaeghe et al. (2003). The wave height  $H_{m0}$  is needed to distinguish between model scale, full-scale or any other scale in between. The roughness coefficient  $\gamma_f$  is needed to distinguish between a smooth and a rough

<sup>2</sup> output scale' means that  $H_{m0}$  needs to be given in the scale where the final result with respect to wave overtopping rates are needed

structure whereas all other parameters are needed to select vertical structures or sloped structures.

### *Output*

There are three possible outputs of the procedure which are:

- mean overtopping rate with possible **wind effect**  $q_{wind}$ : wind may play a role for all vertical structures and all smooth (sloping) structures which are believed to have no scale effects
- mean overtopping rate with possible **scale and wind effects on rough structures**  $q_{scale\_wind}$ : this output will only be relevant for rough structures and includes both possible scale and wind effects.
- mean overtopping rate with **scale effects on rough structures without wind**  $q_{scale\_nowind}$ : this output will only be relevant for rough structures and includes only scale effects. The main interest of this third output is to predict wave overtopping rates for large-scale tests without wind.

The prediction method gives all these four mean overtopping discharges  $q_{SS}$ ,  $q_{wind}$ ,  $q_{scale\_wind}$  and  $q_{scale\_nowind}$ . Differences between these values may give the user a good idea what kind of effect could play a role in his given situation.

### *Step 1: vertical structure?*

Step 1 checks whether the structure is vertical or not (Fig. 116). If the structure is vertical or almost vertical continue with ‘Step 4: Procedure wind effect’. If this is not the case go to ‘Step 2: rough structure?’.

*Note:* To help distinguishing between vertical and non-vertical structures there are two configurations using the input parameters of the CLASH database which indicate a vertical structure. These are:

- if  $\cot \alpha_u < 1$  and  $\cot \alpha_d < 1$  the structure is vertical or almost vertical.
- if  $\cot \alpha_u < 1$  and  $B > 0$  and  $d_h > 0$  there is most probably a berm below swl and a vertical structure on top of the berm.

Please note that this parameter distinction cannot be used when parapets are used with the structure. Furthermore, for some complex structures the simple distinction proposed here may fail to give the correct answer.

### Step 2: rough structure?

Step 2 checks whether the structure is rough or smooth. If the structure is rough, continue with Step 3: rough sloping structure, if the structure is smooth continue with ‘Step 4: Procedure wind effect’.

*Note:* The roughness of a structure may be distinguished from the roughness coefficient  $\gamma_f$  of the CLASH database. If  $\gamma_f$  is smaller than 0.9 the structure is considered to be a rough sloping structure otherwise the structure is smooth.

### Step 3: rough sloping structure

Within this step the first decision to be made is whether to consider the influence of wind or not. If yes, the factor for scale and wind effects  $f_{\text{scale\_wind\_max}}$  can be calculated as follows:

$$f_{\text{scale\_wind\_max}} = \begin{cases} 24.0 & \text{for } q_{\text{SS}} < 1 \cdot 10^{-5} \text{ m}^3 / \text{s} \cdot \text{m} \\ 1.0 + 23 \cdot \left( \frac{-\log q_{\text{SS}} - 2}{3} \right)^3 & \text{for } q_{\text{SS}} < 1 \cdot 10^{-2} \text{ m}^3 / \text{s} \cdot \text{m} \\ 1.0 & \text{for } q_{\text{SS}} \geq 1 \cdot 10^{-2} \text{ m}^3 / \text{s} \cdot \text{m} \end{cases} \quad (8)$$

It should be noted that this factor includes both the influence of scale and wind effects, the latter being a model rather than a scale effect. Furthermore, Eq. (6) suggested a maximum factor of 16.0 for scale effects without any wind. Assuming that factors for scale and wind effects should be multiplied to achieve an overall factor, a theoretical factor for wind of 1.5 would be obtained. This is lower than indicated in Eq. (7) for vertical walls, which is believed to be due to the effect of wind for vertical structures being larger than for rough sloping structures.

Eq. (8) delivers a scaling factor for really rough structures when  $\gamma_f \leq 0.7$ . When  $\gamma_f \geq 0.9$  the structure is smooth and the scaling factor will be  $f_{\text{scale}} = 1.0$ . In between both values a linear interpolation can be assumed so that the scaling factor for rough slopes  $f_{\text{scale\_wind}}$  can be determined by:

$$f_{\text{scale\_wind}} = \begin{cases} f_{\text{scale\_wind\_max}} & \text{for } \gamma_f \leq 0.7 \\ 5 \cdot (1 - f_{\text{scale\_wind\_max}}) \cdot \gamma_f + (f_{\text{scale\_wind\_max}} - 1) \cdot 4.5 + 1 & \text{for } 0.7 < \gamma_f < 0.9 \end{cases} \quad (9)$$

If there is no wind it needs to be decided under which scale the procedure is applied. Therefore, a distinction will be made with respect to the wave height  $H_{m0}$ . For wave heights at output scale  $H_{m0} < 0.5$  m the factor for scaling is  $f_{\text{scale}} = 1.0$ . For all other cases the calculation of  $f_{\text{scale\_nowind}}$  can be performed using Eq. (6). Go to Step 5: Final calculation of mean wave overtopping rate to finalise the procedure.

#### *Step 4: Procedure wind effect*

For structures other than rough structures there might be a wind effect. First a decision has to be made whether wind effects are to be considered or not. If not, the factor for the wind-influence is set to  $f_{\text{wind}} = 1$ . If wind effects have to be considered, they can be calculated using Eq. (7).

Finally the factor for wind effects can be applied to the overtopping rate  $q_{\text{SS}}$  which is performed in “Step 5: Final calculation of mean wave overtopping rate”.

#### *Step 5: Final calculation of mean wave overtopping rate*

The final calculation of mean wave overtopping rates should include both a calculation for wind effects and smooth structures and a calculation for scale and wind effects and rough structures as follows:

$$q_{\text{wind}} = q_{\text{SS}} \cdot f_{\text{wind}} \quad (f_{\text{wind}} \text{ (eq. (7))}) \quad (10)$$

$$q_{\text{scale\_wind}} = q_{\text{SS}} \cdot f_{\text{scale\_wind}} \quad (f_{\text{scale\_wind}} \text{ (eq. 8-9)}) \quad (11)$$

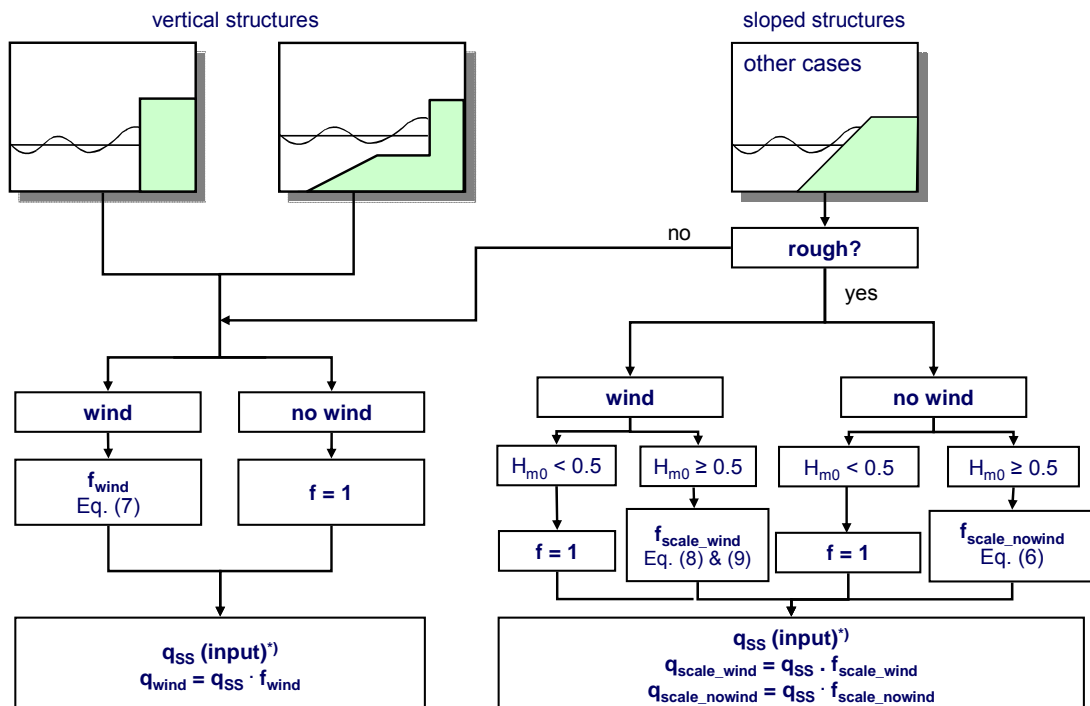
$$q_{\text{scale\_nowind}} = q_{\text{SS}} \cdot f_{\text{scale\_nowind}} \quad (f_{\text{scale\_nowind}} \text{ (eq. (6))}) \quad (12)$$

#### *Step 6: Scaling map for coastal structures*

The procedure described above is summarised in a simple scaling map for wave overtopping over coastal structures obtained from small-scale model tests (Fig.116). This map is only needed when

- wave heights  $H_{m0}$  for the structure the user is interested in are higher than 0.5 m;
- the user starts from model scale with wave heights  $H_{m0} < 0.5$  m

Furthermore, the distinction between vertical and sloped structures as given by the parameters as given in the ‘input’ to the overall procedure are only valid for structures which do not have parapets or overhanging elements.



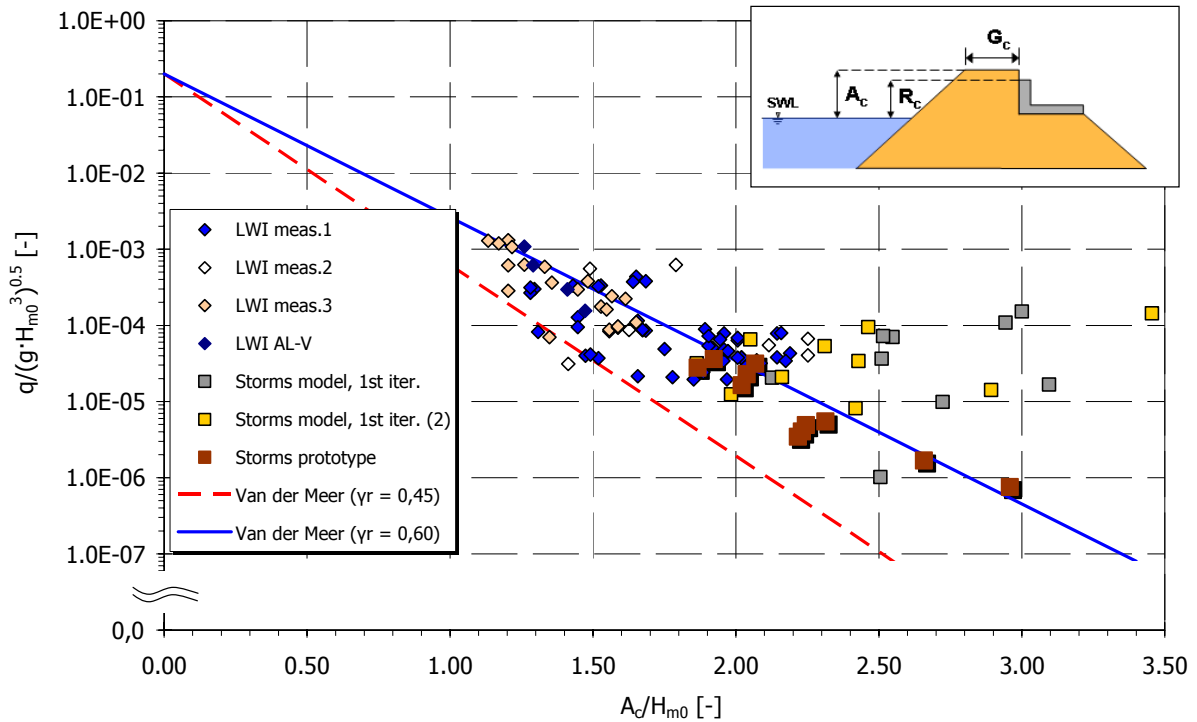
\*) zero overtopping rates from small-scale model tests can be overcome by the method as described in Fig. 113

**Figure 116: Scaling map for wave overtopping results over coastal structures from small-scale model tests**

e) Application of procedure to data from Zeebrugge and Ostia

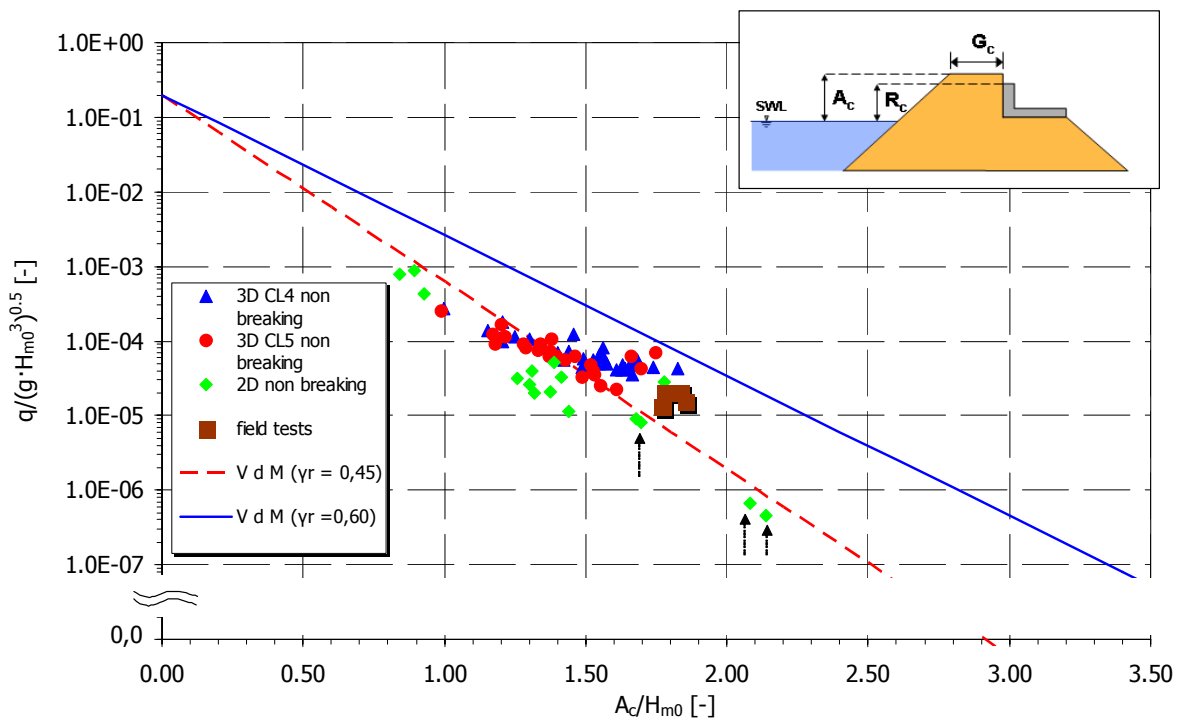
The aforementioned final procedure to account for scale effects (Fig. 116) has been applied to data from hydraulic model tests for the Zeebrugge and Ostia case. First, the Zeebrugge test case (Fig. 112) has been used. The results are shown in Fig. 117. It can be seen that compared to the results in Fig. 112 that the increase in wave overtopping rates for the parametric tests such as ‘LWI meas. 1’ and ‘LWI meas. 2’ lead to a better comparison of scale model and prototype data. In general, there is a significant increase of the mean overtopping rate mainly for relative crest freeboards  $A_c/H_{m0} \geq 1.7$  where the overtopping rates are up to 24 times higher. Especially the reproductions of storm data during the second phase of the LWI tests are now much higher than the prototype storm data. However, this second phase data have been produced with a different model construction and possibly with a different armour layer setup. This has been shown to have significant influence on the overtopping rates and it is therefore very difficult to compare the different phases of the Zeebrugge tests directly.





**Figure 117: Results of the application of the parameter map for scaling to the test case of Zeebrugge**

In a second step the method was also applied to the data of the Ostia case as shown in Fig. 113. The results of the modifications obtained are given in Fig. 118.



**Figure 118: Results of the application of the parameter map for scaling to the test case of Ostia**

The four data points indicated by the arrows in Fig. 118 correlate to the ones mentioned in before, where the zero value for the mean overtopping rates of four data points was substituted by mean overtopping rates using the Van der Meer formula. The model and prototype data show a much better agreement in Fig. 118 than in Fig. 113 before where especially for the lower overtopping rates a higher increase of all model tests was achieved. In Fig. 118, a roughness factor  $\gamma_r = 0.45$  fits well to the data, whereas before the application of the scaling procedure this was  $\gamma_r = 0.37$ . Comparing the application for Zeebrugge and Ostia it seems that the developed method gives acceptable results for the cases investigated here.

## Conclusions

Results for all field and model investigations have been plotted for the investigated sites using data from the field and two models of smaller scale. Results have shown that model tests performed for the vertical wall in Samphire Hoe do not deviate much from the prototype data points. However, for the steep Zeebrugge rubble mound breakwater and for the flatter slope in Ostia differences between prototype and model have been observed in the order of up to one order of magnitude.

A new parameter map for scaling was proposed for scaling wave overtopping rates obtained from small-scale model tests with wave heights smaller than 0.5 m. The map depends on whether or not the structure is ‘rough and sloping’ and eventually suggests a scaling predictor. The latter was then applied to the test cases of Zeebrugge and Ostia.

This workpackage delivered the following reports / deliverables:

- the completed dataset, including full scale measurements and full scale data (D28)
- a final report (D40), containing a conclusion on scale effects and how to deal with them

Additionally one milestone was achieved:

- the formulation of the conclusion on scale effects (M12)

---

## **8 WP 8 : Prediction method**

### **8.1 Objectives**

The objective of this workpackage is to develop a generic prediction method for overtopping discharges at major types of coastal structures. This prediction method is based on the final wave overtopping database. The prediction method that was developed and described is based on the technique of Neural Network modelling. Moreover, a method was developed to obtain the confidence intervals around these predictions. The latter is a new essential step since neural network modelling results in a tool that acts for users as a kind of black box. Therefore, predictions are extended with information regarding their reliability.

### **8.2 Description of work performed**

For the design, safety assessment and rehabilitation of coastal structures reliable predictions of wave overtopping are required. Several design formulae exist for dikes, rubble mound breakwaters and vertical breakwaters. Nevertheless, often no suitable prediction methods are available for structures with non-standard shapes. The overtopping highly non linear dependency of many wave and structural characteristics makes the problem difficult to solve. Within CLASH, a method is developed to provide a conceptual-design tool to estimate wave overtopping discharges for a wide range of coastal structures. Only one schematisation is used for all types of coastal structures, where not only dikes, rubble mound breakwaters or vertical breakwaters are defined, but also other non-standard structures are included. Additionally, not only is the effect of the most common parameters (i.e. wave height, wave period and crest freeboard) analysed herein, but also the effect of many other wave/structural characteristics is considered. The prediction method described is based on the technique of Neural Network modelling. For this purpose use is made of a data set obtained from a large number of physical model tests. Most of these data were provided by the partners of the CLASH project. The present investigation focuses on the development of a neural network for estimating mean overtopping discharges. Also the confidence intervals around these predictions are determined. It is important that predictions are extended with information regarding their reliability. The main activities under this workpackage are described in Deliverable D41 (Pozueta et al, 2004). Hereafter information is combined into a summary of activities in the entire workpackage.

### *Description of database*

The database used for the set up of the present neural network (hereafter “NN”), is the database created within the framework of the European project CLASH. This database includes tests collected from several laboratories and new tests performed within the CLASH project to fill in “white spots” in the parameter domain. This database is described in detail in WP2 of this report.

About 10,000 tests are included in this database. Each of these tests is described by a number of parameters that represent hydraulic information (incident wave characteristics, measured overtopping discharge) and structural information (characteristics of the test section). Moreover, each of the tests includes some general information regarding the estimated reliability of the test and the complexity of the structure. The **reliability** of each test was estimated and defined in terms of a *Reliability Factor (RF)*. The values of the *RF* ranged from  $RF = 1$ , for a ‘very reliable’ test (i.e. test for which all needed information was available, no estimations needed, reliable measurements), to  $RF = 4$ , for a ‘not-reliable’ test (i.e. test for which the estimation of some parameters was not acceptable and for which the measurements included many uncertainties). In the same way, the **complexity** of each test was established on the basis of the complexity of the structure and was defined in terms of a *Complexity Factor (CF)*. The values of the *CF* ranged from  $CF = 1$ , for a test with a ‘very simple’ structure (i.e. test for which the parameters describe the cross-section exactly), to  $CF = 4$ , for a test with a ‘very complex’ structure (i.e. test for which the cross-section cannot accurately be described by the chosen parameters).

These *Reliability* and *Complexity Factors* played an important role in the configuration of the NN. With the purpose of giving more weight to tests with high reliability in the NN configuration, the *RF* and the *CF* were combined into a kind of *Weight Factor*. This *WF* was defined as a combination of the *RF* and *CF* according to  $WF = (4-RF) \cdot (4-CF)$ . This *Weight Factor* was defined for each of the tests and was taken into account in the *training (calibration)* of the NN.

Since the quality of the NN depends highly on the quality of the database (erroneous data can severely degrade the performance of the NN), the initial database of more than 10,000 tests

was reduced by removing the data that was qualified as ‘non-reliable’ tests (e.g. tests with a ‘reliability factor’  $RF = 4$ , as defined previously) or the data for which the cross-section was considered as ‘very complex’ (e.g. tests with a ‘complexity factor’  $CF = 4$ , as defined previously). All remaining tests related to registered overtopping events were considered (i.e. all tests such that  $q \neq 0 \text{ m}^3/\text{s}/\text{m}$ ). Some data corresponding to overtopping events such that  $q > 10^{-6} \text{ m}^3/\text{s}/\text{m}$  were rather randomly checked and clear inconsistencies within the database were eliminated. The resulting database consisted of 8,372 tests.

Since most of the tests in the database originate from small-scale tests, very low overtopping discharges are likely to be less accurate due to measurement techniques/errors in these small-scale tests. Relatedly, it should be noted that for the NN configuration, all the tests with observed overtopping discharges  $q < 10^{-6} \text{ m}^3/\text{s}/\text{m}$  (i.e. 1 ml/s/m), were considered as less accurate than larger overtopping discharges, and were given a weight factor  $WF = 1$  (i.e.  $RF = CF = 3$ ).

### *Parameters involved*

Due to the large number of parameters involved in the process of wave overtopping, it is difficult to describe the influence of all of them. The technique of NN modelling allows for the analysis of wave overtopping with a larger amount of structure characteristics.

For the description of the wave field, the effects of 3 parameters were considered here: the spectral significant wave height at the toe of the structure ( $H_{m0}$ ), the mean spectral wave period at the toe of the structure ( $T_{m-1,0}$ ), and the direction of wave attack ( $\beta$ ). For the description of the geometrical shape of the structure, the effects of 12 parameters were considered: the water depth in front of the structure ( $h$ ), the water depth at the toe of the structure ( $h_t$ ), the width of the toe berm ( $B_t$ ), the roughness/permeability of the armour layer ( $\gamma_f$ ), the slope of the structure downward of the berm ( $\cot \alpha_d$ ), the slope of the structure upward of the berm ( $\cot \alpha_u$ ), the width of the berm ( $B$ ), the water depth on the berm ( $h_b$ ), the slope of the berm ( $\tan \alpha_b$ ), the crest freeboard of the structure ( $R_c$ ), the armour crest freeboard of the structure ( $A_c$ ) and the crest width of the structure ( $G_c$ ).

### *Neural network modelling*

Neural networks (NN) are data analyses or modelling techniques commonly used in artificial intelligence. NN are often used as generalised regression techniques for the modelling of cause-effect relations and have proven to be very effective in solving difficult optimization problems in a variety of technical and scientific fields. They are an alternative technique for processes in which the interrelationship of parameters is unclear while sufficient experimental data is available. This technique has been successfully used in the past. Examples of NN modelling on coastal structures are: Mase *et al.* (1995); Van Gent and Van den Boogaard (1998); Medina *et al.* (1999, 2002, 2003); and Panizzo *et al.* (2003). Here, NN are used for prediction of mean wave overtopping discharges and makes use of a much larger data set than in the other NN studies. Details regarding the NN constructed on the basis of the database are described in Pozueta *et al.* (2004).

NN are organised in the form of layers and within each layer there are one or more processing elements called 'neurons'. A standard multi-layer feed-forward NN consists of several units connected in one direction only. The first layer is called the input layer and consists of a number of neurons equal to the number of input parameters. The last layer is called the output layer and consists of a number of neurons equal to the number of output parameters to be predicted. The layers between the input and output layers are called hidden layers and consist of a number of neurons to be defined in the preparation of the NN. Each neuron in each layer receives information from the preceding layer through connectivities. A weight factor is assigned to each connectivity as a result of the training of the NN. The input of a neuron consists of a weighted sum of the outputs of the preceding layer; for the current investigation, the output of a neuron is generated using a non-linear activation function for the hidden layers and a linear activation function for the output layer (Haykin, 1994). This procedure is followed for each neuron. The output neuron generates the final prediction of the NN.

A number of NN techniques have been used during the past decade to solve a variety of hydraulic engineering problems. The most popular technique is the use of static feedforward NN models with one hidden layer and a backpropagation learning algorithm (Rumelhart & McClelland, 1986). In the present study a three-layered NN (one hidden layer) is applied as

well. The learning rule used herein is called the *standard error back-propagation rule* and it is the most common learning rule for this type of network.

Since it was the aim of the NN to be applicable both for small-scale and prototype conditions, all the input and output parameters in the database were scaled to  $H_{m0,toe} = 1$  m using Froude's similarity law. The advantage of using Froude's law, taking into account that the database was mainly based on small-scale tests, is that a better generalisation for large-scale applications can be obtained. Since physical knowledge was then incorporated in the NN, this procedure allowed for predictions at different scales. This approach required somehow a less complex configuration of the NN, since the number of input-patterns used reduced from 15 to 14 (once all input-patterns were scaled to  $H_{m0,toe} = 1$  m, this parameter,  $H_{m0}'$ , is constant and was not used anymore as a separate input pattern to the NN).

For user applications, when a prediction of the wave overtopping discharge is required for a certain input-pattern [ $H_{m0}$ ,  $T_{m-1,0}$ ,  $\beta$ ,  $h$ ,  $h_t$ ,  $B_t$ ,  $\gamma_f$ ,  $\cot \alpha_d$ ,  $\cot \alpha_u$ ,  $B$ ,  $h_b$ ,  $\tan \alpha_b$ ,  $R_c$ ,  $A_c$ ,  $G_c$ ] this input-pattern is scaled according to Froude's similarity law to an input-pattern with a wave height on which the NN was trained ( $H_{m0,toe} = 1$  m). The NN prediction ( $q'$ ) is then scaled back ( $q$ ) to the original wave height using again Froude's law.

In the NN-modelling Froude's scaling law was used to extrapolate the information from small-scale tests to prototype conditions. However, the small-scale tests may, to some extent, be affected by scale effects. However, there is no clear quantitative evidence on the magnitude of scale effects for each test condition (type of structure, wave conditions, etc). Nevertheless, in Workpackage 7 suggestions are given to estimate the (combined) magnitude of model, scale and wind effects. The NN predictions do not incorporate the influence of model, scale and wind effects but, as described later in this chapter, the NN output can be corrected by using estimates of model, scale and wind effects.

### *Training and testing of NN*

The preparation of the NN model was performed in two phases, the *training/learning* phase and the *testing/validation* phase.

The process of calibration or *training* phase of the NN involves the adjustment of its configuration (calibration of the NN's weights) based on the performance of standard operations that allows the NN to *learn* from the input-output relations for each of the parameters included in the tests selected as *training set*. The iterative adjustment of the NN's weights or *training* of the NN is performed by minimisation of some *cost function* (error function) that quantifies the differences between the predicted outputs and the desired measured/observed outputs, often called *targets*. A common form of the *cost function* is a superposition of the squared differences. For the minimisation of the *cost function*, gradient based methods turned out to be the most efficient. For the computation of the gradient of the cost function, the well known error-backpropagation rule was used. It should be noted that the training of the NN was performed considering the logarithm of the observed overtopping discharges scaled with Froude's law ( $\log q_{obs}'$ ) as the targets. The root-mean-square (RMS) error used herein is defined as follows:

$$RMS_{train} = \sqrt{\frac{1}{N_{train}} \sum_{n=1}^{N_{train}} ((\log q_{obs}')_n - (\log q_{NN}')_n)^2} \quad (13)$$

where  $N_{train}$  is the number of tests considered in the NN training.

Once trained (or during training), the correct performance of the resulting model is evaluated with a *testing set*, i.e. a set of input-output combinations not used before for training. This step is called *validation* or *testing* phase of the NN.

It should be noted, that the actual partition of the data over the training and testing sets may significantly affect the outcome of the NN. Therefore, special attention must be given to this aspect. The present strategy was to train many NN's each time with different data in the training and testing phase. *Resampling Techniques* (Van den Boogaard *et al.*, 2000) were used for the construction of such training and testing sets.

#### *Optimum number of neurons in the hidden layer*

An important step in the configuration of the NN is to find the optimal number of neurons in the hidden layer. By increasing the number of neurons in the hidden layer, the differences between the NN output and the desired (observed) output of the data used for training will decrease because more hidden neurons lead to more degrees of freedom (more adjustable



parameters in the NN model). However, after a certain number of hidden neurons, the NN starts to model *noisy fluctuations* in the dataset which is unfavourable for the accuracy of the real predictions; the performance of the NN for the training set increases (RMS error decreases), while that of the testing set decreases (RMS error increases). At that moment the NN is said to be *overtrained*. To avoid *overtraining* of the NN, an *early stopping* (Heskes, 1997) criterion is used in the NN training process. With this technique, the training process of the NN is stopped when the performance of the NN in the testing set starts to decrease. The optimal number of hidden neurons can be found by training the NN several times for a range of number of neurons in the hidden layer, and comparing each time the performance of the NN (RMS error) on the training and testing sets. The optimum number of hidden neurons was chosen as 20, since the use of more hidden neurons did not increase the accuracy of the NN while it increased the complexity of its architecture.

### *Confidence intervals*

After obtaining the optimal NN configuration, predictions of mean overtopping discharges could be made; i.e. for a set of input parameters, a set of output parameters (overtopping discharge) could be obtained. Van Gent and Van den Boogaard (1998) developed a method to add information on the reliability of NN predictions. The method to add information on the *reliability* of the NN predictions has been developed further within this investigation, and makes use of how the available data are spread over the entire domain of applications. With the double purpose of solving the matter of choosing the data to be used in the training and testing phases, and assessing the uncertainty of the NN predictions, resampling techniques were used.

Resampling techniques are generic devices used for uncertainty analysis in statistics and model calibration. The use of these techniques involves the development of a set of NNs (*resamples*) based on the original database. This implies firstly that the training and testing processes are redone many times solving the problem of representativeness of the training and testing sets; and secondly, that the set of NNs developed results in a *set of predictions* (a so called *ensemble*) of overtopping discharge, allowing the estimation of the reliability of the predictions (i.e. standard deviation or 95 % confidence intervals). As a result, the NN does not only give a prediction of the wave overtopping discharge but also a measure for the uncertainty of the prediction.

The two most commonly applied forms of resampling are *jackknifing* and *bootstrapping* (Efron, 1982). In the current investigation, the technique of *bootstrap resampling* was used.

A *bootstrap* resample is a random selection of  $N$  data out of the  $N$  original data. The  $N$  individual draws within one such resample are independent but with replacement so that every time there is a probability of  $1/N$  that a particular sample (input-output combination) of the original set is selected. At the end some samples are then selected once or more than once while other samples are absent in a resample. The samples selected in each resampling correspond to the tests that are used for the training of the NN, while the ones not selected correspond to the tests that are used in the testing/validation of the NN. The probability that an original sample is not present in a resample is  $(1-1/N)^N$  which for large  $N$  is close to  $1/e$ . Therefore, within each resample, the probability that a test was selected (used for training) was 63%, while the probability that a test was not selected (used for testing) was 37%. In this way a set of  $L$  of such resamples is generated. This  $L$  should be sufficiently large and in practice it is typically of the order of a hundred or a few hundreds, somewhat depending on the statistics to be computed. For each resample of the data set (and the corresponding division into a training and testing set) the NN is trained.

A set of about 500 NNs or resamples was performed herein. As a result, the bootstrap yielded 500 estimates of the wave overtopping discharge ( $\log q_1', \dots, \log q_{500}'$ ). The estimate of the model (NN output) is given by the mean of all these predictions,

$$1/L \cdot \sum_{i=1}^L \log q_i', \text{ where } L = 500, \text{ in this case.} \quad (14)$$

In the bootstrap resampling the weights are included as follows. If a weight  $WF$  is assigned to a particular input-output pattern,  $i$ , and within a resampling this pattern is selected  $N$  times, the total weight of the pattern is set to  $WF_i \cdot N$ . The contribution of this pattern to the cost function is then,

$$WF_i \cdot N \cdot ((\log q_{obs}')_i - (\log q_{NN}')_i)^2 \quad (15)$$

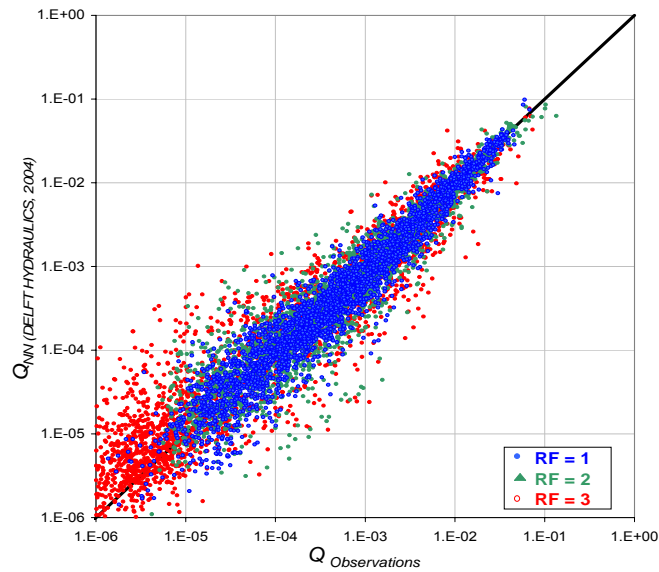
and the total cost function during training in a bootstrap resample is the superposition of such terms for all the input-output patterns that are actually selected.

The set of 500 NNs is further used to provide the uncertainty of the model with respect to the accuracy of its predictions. This uncertainty can be quantified by a standard deviation, or the variance, or a confidence interval. In this respect, the prediction method developed herein provides several statistics. Besides the mean of the predictions which is used as the model prediction ( $\mu = q_{NN}$ ), the output of the prediction method includes the standard deviation or spread,  $\sigma$ , and quantiles of several orders,  $q_{2.5\%}$ ,  $q_{5\%}$ ,  $q_{25\%}$ ,  $q_{50\%}$ ,  $q_{75\%}$ ,  $q_{95\%}$  and  $q_{97.5\%}$ . The 95% confidence interval is given by the quantiles  $q_{2.5\%}$  and  $q_{97.5\%}$ .

It should be noted that the uncertainty assessment is based on how data is spread over the entire domain of application; it still assumes that the database is correct. The uncertainty levels do not account for systematic error or inaccuracies in the database (for instance caused by model effects, scale effects or measurement equipment).

#### *Performance of Neural network*

Fig. 119 shows the observed wave overtopping discharge ( $q_{obs}$ ) versus the predicted wave overtopping discharge ( $q_{NN}$ ). As described in the previous section, the predicted overtopping discharge (model prediction) corresponds to the mean of the set of 500 NNs. It can be observed that the predictions of the NN are reasonably accurate, especially in the range of high overtopping discharges. In this respect, it should be noted that the repetition of a certain test in the laboratory often can give a factor 5 difference.



**Figure 119: Observations versus NN predictions**

The  $(Q_{obs}, Q_{NN})$  samples are plotted with the corresponding Reliability Factor ( $RF$ ) of the observed overtopping discharge. It can be observed that the majority of the relatively large differences between measured and predicted discharges corresponds to tests with low reliability ( $RF = 3$ ). These  $(Q_{obs}, Q_{NN})$  samples are non-dimensional overtopping discharges where  $Q = q / (g H_s^3)^{0.5}$ .

It should be noted that the predictions are mainly based on small-scale tests. In reality model effects, scale effects and wind may cause differences between results in small-scale tests and in reality. Scale and model effects for overtopping have been dealt within CLASH WP 7. The presented NN takes into account scale and model effects by applying an appropriate factor on the NN – output.

## Conclusions

A prediction method has been developed for the estimation of the mean wave overtopping discharge for many types of coastal structures, and the assessment of the uncertainties of these predictions.

The presented results show that Neural Networks can successfully be used to model the relationship between the input parameters involved in the process of wave overtopping and

the mean overtopping discharge at coastal structures. As for any NN, also the quality of the present NN is largely determined by the quantity and quality of the database.

Resampling techniques have been used for the estimation of the uncertainties of the NN predictions. In general, it has been shown that the agreement between the predicted overtopping discharge and the measured overtopping discharge is good; the predictions are rather accurate compared to the observed overtopping discharges.

The output of the Neural Network can be corrected to take into account influences of model effects, scale effects and wind, when predicting wave overtopping discharges for prototype conditions.

This workpackage delivered the following reports :

- a preliminary generic prediction method for wave overtopping based on a preliminary wave overtopping database (D10)
- the report on the preliminary generic prediction method (D11)
- the final generic prediction method (D41)
- the final report on generic prediction method (D42)

The following milestones were achieved :

- first version of the neural network is finished (M5)
- the generic prediction method is available (M13)

## 9 WP 9 : Synthesis and formulation of guidelines

### 9.1 Objectives

Objectives of this workpackage are :

- to synthesise all obtained results and to check to the objectives of the project and to draw final conclusion;
- to draw up a guideline on crest level design or assessment based on permissible overtopping the guideline will be short and focussed on practical application by end users.

### 9.2 Description of work performed

Based on the contributions of the different WP-leaders, a final full scientific report, which is the present report (D46), has been written. The main results and the overall conclusions of the project have been summarised. For detailed information this final report refers to the individual WP-reports and deliverables.

A guideline on crest level design and assessment has been written (D43). The generic prediction method together with the permissible overtopping as concluded from the hazard analysis in WP 6 forms the basis for this guideline. The background on how to deal with the scale / model effects is also incorporated in this guideline.

The generic CLASH overtopping prediction method is an applicable and validated procedure to design and assessment of the crest height of coastal structures with regard to overtopping hazards. The CLASH overtopping prediction methodology is published on the internet, including (1) the hazard analysis method (WP 6), (2) the scale and model effects analysis method (WP 7) and (3) the NN general prediction method (WP 8).

### 9.3 Conclusions / achievements

CLASH WP9 has produced a **guideline** on wave overtopping/crest level design by means of a generic prediction tool and guidance on consequences of overtopping and permissible levels of overtopping.

A final project report (D46) has been written at the end of the project. The guidelines (D43), including the generic prediction method (exe-file) are available through the internet as well.

This workpackage delivered the following reports / deliverables :

- the guidelines, including the generic prediction method (D43)
- the final project report (D46)

Additionally one milestone was achieved :

An overall synthesis is made and the guidelines have been formulated (M14).

---

## 10 WP 10 : Exploitation and dissemination of the results

### 10.1 Objectives

The only but very important objective of this workpackage is to exploit and to disseminate the final results of the project as wide as possible.

### 10.2 Description of work performed

Dissemination of project results has already started in an early phase of the project and was constantly updated during the course of the project. The following activities have taken place so far:

- a website has been created at the beginning of the project and is permanently updated under <http://www.clash-eu.org>;
- papers have been presented at conferences and have been submitted to international journals;
- expert seminars have been organised to disseminate the key results of CLASH obtained so far (e.g. Oceanology International in London on 18 March 2004);
- a flyer of CLASH has been designed and distributed during international conferences and amongst partners for disseminating the information to colleagues and clients;
- a Powerpoint presentation is available and can be downloaded from the web page. The presentation introduces the project and gives the key objectives together with some information on further contacts;
- a CLASH poster has been drafted and presented to an international audience at the Coastal Structures Conference 2003 in Portland/USA;
- News Letters have been set up to circulate key information inside the project to maintain a permanent high level of information at all participating institutes;

Exploitation of CLASH results will start immediately after the project is finished. However, the overall CLASH database is already available and has been used by CLASH partners to homogenise their databases of test results and to obtain comparison data sets for tests performed in their flumes. Results from hazard analyses due to overtopping have already led to proposals of design guidance on hazards in the UK.



## Conclusions

The dissemination of project results is on its way and is making good progress within and outside CLASH. All partners are contributing to these issues by submitting papers to conferences and journals, by holding national seminars or conferences and contributing to international ones. CLASH has been internationally presented at various conferences which are very relevant for the coastal engineering community such as the ICCE conference 2002 in Cardiff, UK, the Coastal Structures Conference in Portland/USA in 2003, and the ICCE 2004 conference in Lisbon/Portugal. CLASH is therefore already well known by the international coastal engineering community.

In terms of exploitation of the project the key CLASH results (e.g. database, hazard analysis, scale effects, generic prediction method) will be used by all project partners for their further research and consultancy projects. It is also expected that end-users will download these results from the website and use them within their own projects. It is therefore expected that CLASH will have a significant input to the coastal community worldwide working on the design of coastal structures related to wave overtopping.

This workpackage delivered the following reports :

- the technological implementation plan, draft version (D12)
- the technological implementation plan, final version (D44)
- the project website ([www.clash-eu.org](http://www.clash-eu.org)) (D47)

## 11 Acknowledgements

CLASH was a EU 5<sup>th</sup> framework research project, funded by EU under contract number EVK3-CT-2001-00058. The financial support of the EU is very much acknowledged. Furthermore our EC-scientific officers Mr. H. Barth and previously Mr. C. Fragakis are very much acknowledged for their understanding cooperation during the whole project duration. The authors also want to thank all CLASH-partners for the fruitful cooperation.

## 12 References

- Allsop, W. (2004). Report on hazard analysis. CLASH – WP 6 report ([www.clash-eu.org](http://www.clash-eu.org)), HR Wallingford, UK.
- Allsop, W., Bruce, T., Pearson, J., Alderson, J & Pullen, T.A. (2003). Violent overtopping at the coast, when are we safe? Int. Conf. on Coastal Management, Brighton, pp 54-69, ISBN 0 7277 3255 2, publ. Thomas Telford, London.
- Allsop, N., Bruce, T., Pearson, J., and Besley, P. (2004) “Wave overtopping at vertical and steep seawalls.” Water and Maritime Engineering Journal, page In Press.
- Aminti P., Franco L. (1988) Wave overtopping on rubble mound breakwaters, Proc. 21st International Conference on Coastal Engineering, Vol.1, ch.57, pp. 770-781, Malaga, 20-25 June 1988, Ed.Billy Edge, ASCE, NewYork, 1989.
- Arbhabhiramar, A. and Dinoy, A. (1973). Friction factor and Reynolds number in porous media flow. Journal of the Hydraulics Division, ASCE, 99(HY6):901–911.
- Battjes, J.A., Groenendijk, H.W. (2000). Wave height distributions on shallow foreshores, Coastal Engineering, 40, pp.161-182.
- Beddhu, M., Taylor, L., and Whitfield, D. (1994). A time accurate calculation procedure for flows with a free surface using a modified artificial compressibility formulation. Applied Mathematics and Computation, 65(1):33–48.
- Besley, P. (1999). Wave overtopping of seawalls: design and assessment manual. R&D Technical Report, HR Wallingford, no. W178, Wallingford, U.K., 37 pp., 5 tables (also from: <http://www.environment-agency.gov.uk/commondata/105385/w178.pdf>).
- Borsboom, M., Doorn, N., Groeneweg, J., and van Gent, M. (2001a). A boussinesq type wave model that conserves both mass and momentum. In Edge, B. (editor), “Coastal Engineering 2000,” pages 148–161. ASCE, Reston, Virginia.
- Borsboom, M., Groeneweg, J., Doorn, N., and van Gent, M. (2001b). Flexible boundary conditions for a boussinesq type wave model. In “Proceedings of Waves 2001, San Francisco,” pages 884–993. ASCE.
- Borsboom, M., Groeneweg, J., Doorn, N., and van Gent, M. (2001c). Near shore wave simulation with a boussinesq type wave model including wave breaking. In “Proceedings of Coastal Dynamics 2001”, Lund, Sweden pages 759–768. ASCE.
- Boone, C., Geeraerts, J., De Rouck, J. (2002). General Methodology Report (D5) CLASH –

- WP 1 report ([www.clash-eu.org](http://www.clash-eu.org)), Ghent University, Belgium, 127 pp.
- Bouma, J.J., Schram, A., François, D.(2004). Report on socio-economic impacts. (D39) CLASH- WP6 report ([www.clash-eu.org](http://www.clash-eu.org)), Ghent University, Belgium.
- Briganti, R., Bellotti, G., Franco, L., De Rouck, J., Geeraerts, J. (2005). Field measurements of wave overtopping at the rubble mound breakwater of Rome-Ostia yacht harbour. Manuscript submitted for publication – Coastal Engineering (Elsevier).
- Bruce, T, Allsop, N.W.H. & Pearson, J. (2001). Violent overtopping of seawalls – extended prediction methods Proc. Coastlines, Seawalls and Breakwaters 2001 ICE, publ Thomas Telford, London.
- Bruce, T. Pullen, T. Allsop, W. & Pearson, J. (2005). How far back is safe? Spatial distributions of wave overtopping. Proc. Coastlines, Seawalls and Breakwaters, ICE, Thomas Telford, London.
- Burcharth, H.F. and Lykke Andersen, T. (2003). Overtopping and rear slope stability of reshaping breakwaters. COPEDEC VI, Colombo, Sri Lanka.
- Causon, D., Ingram, D., Mingham, C., and Pearson, R. (2001). A Cartesian cut cell method for shallow water flows with moving boundaries. *Advances in Water Resources*, 24(2001):899–911.
- Chorin, A. (1967). The numerical solution of the Navier-Stokes equations for an incompressible fluid. Report NYO148082, New York University.
- Davey, T. (2004). Overtopping discharge - effect of wind. MEng project report, School of Engineering & Electronics, University of Edinburgh, Edinburgh, U.K.
- De Rouck, J., Van de Walle, B., Geeraerts, J., Troch, P., Van Damme, L., Kortenhuis, A., Medina, J, 2003. Full scale wave overtopping measurements. Proc. of Conf. Coastal Structures '03, Portland, USA, pp. 494-506.
- De Haas, P., Rijks, D., Ruessink, B., Roelvink, J., Reniers, A., and van Gent, M. (1999). Onderzoek naar lange golven bij Petten (in Dutch); Investigations on long waves at Petten. Report H3345, University Utrecht and Delft Hydraulics, Delft.
- De Waal, J.P.; Tonjes, P.; van de Meer, J.W. (1996). Wave overtopping of vertical structures including wind effects. *Proceedings 25th International Conference Coastal Engineering (ICCE)*, ASCE, Volume 2, Orlando, Florida, USA, pp. 2216-2229.
- De Kruif, A. (2000). Storm data of the Petten field site: 1995-2000. Report RIKZ/OS/2000/34X, Rijkswaterstaat (RIKZ), The Hague, The Netherlands.

- Dodd, N. (1998). A numerical model of wave run-up, overtopping and regeneration. Proc. ASCE Journal of Waterways, Port and Coastal Engineering, 124(2):73–81.
- Efron, B. (1982). The Jackknife, the Bootstrap and Other Resampling Plans, 92pp., SIAM, Philadelphia, PA.
- Endoh K & Takahashi S (1994). Numerically modelling personnel danger on promenade breakwater due to overtopping waves. Proc. 24th ICCE, Kobe, pp 1016-1029, publ. ASCE.
- Franco, L., de Gerloni, M. & van der Meer, J.W. (1994). Wave overtopping on vertical and composite breakwaters. Proc 24<sup>th</sup> Int Conf Coastal Eng., Kobe, ASCE.
- Franco, L., De Gerloni, M., Van Der Meer, J. (1995). Wave overtopping on vertical and composite breakwaters, Proc. 24<sup>th</sup> ICCE, Kobe, Japan, 23-28 October 1994. Ed. B. Edge, ASCE, NY.
- Franco L., Cavani A (1999). Overtopping Response Of Core-Locs, Tetrapods And Antifer Cubes, Coastal Structures '99, Proc. Int.Conf. CS'99- Santander (Spain) 7-10 June 1999, vol.1, pp.383-387, Edited by I.Losada, Balkema, Rotterdam 2000.
- Franco, L., Briganti, R., Bellotti, G. (2004). Report on full scale measurements, Ostia, 2<sup>nd</sup> full winter season (D32), CLASH - WP3 report ([www.clash-eu.org](http://www.clash-eu.org)), Modimar, Rome, Italy.
- Fu, W., Huang, H., and Liou, W. (1996). Thermal enhancement in laminar channel flow with a porous block. International Journal of Heat and Mass Transfer, 39(10):2165–2175.
- Fukuda N., Uno T. & Irie I (1974). Field observations of wave overtopping of wave absorbing revetment" Coastal Engineering in Japan, Vol 17, pp 117-128, Japan Society of Civil Engineers, Tokyo.
- Geeraerts, J., De Rouck, J., (2002). General Methodology Draft Report (D2). CLASH – WP 1 report ([www.clash-eu.org](http://www.clash-eu.org)), Ghent University, Belgium, 99 pp.
- Geeraerts, J., Troch, P., De Rouck, J., Van Damme, L., Pullen, T. (2003). Hazards resulting from wave overtopping – Full scale measurements. Proc. Conf. Coastal Structures, Portland, Oregon, USA, pp. 481-493.
- Geeraerts, J., Boone, C. (2004). Report on full scale measurements Zeebrugge – Second Full Winter Season. CLASH – WP 3 report ([www.clash-eu.org](http://www.clash-eu.org)), Ghent University, Belgium, 71 pp.
- Geeraerts, J., Willems, M. (2004). Final report on laboratory measurements – Ostia (D31). CLASH - WP 4 report ([www.clash-eu.org](http://www.clash-eu.org)), Ghent University, Belgium, 79 pp.
- Geeraerts, J., Troch, P., De Rouck, J., Willems, M., Franco, L., Bellotti, G., Briganti, R. (2004). Wave overtopping at Ostia yacht harbour breakwater – Comparison between

prototype and model tests in 2D and 3D. 29<sup>th</sup> International Conference on Coastal Engineering, Lisbon, Portugal.

Goda, Y. (2000). Random seas and design of maritime structures. Advanced series on Ocean Engineering, Vol. 15, . World Scientific Publishing Co, ISBN 981-02-3256-X.

Gouldby B.P., Sayers P.B. & Johnson D. (1999). Real-time hazard forecasting: Review of implementation and two years operation at Samphire Hoe, Dover. Paper to MAFF Conference on River and Coastal Engineers, Keele.

González-Escrivá, J.A.; Garrido, J.; Medina, J.R.; Geeraerts, J. (2004). Laboratory real storm reproduction using wind. *Proceedings 29th International Conference Coastal Engineering (ICCE)*, ASCE, Lisbon, Portugal, 13 pp.

Groeneweg, J., Doorn, N., Borsboom, M., and van Gent, M. (2003). Boussinesq type modelling of measured wave breaking on a circular shoal. In McKee-Smith, J. (editor), “Coastal Engineering 2002,” volume 1, pages 495–507. ASCE, World Scientific, New Jersey.

Halcrow. (1997). Public safety of access to coastal structures, Report to Environment Agency, EA report 522.

Heald, G. (2002). Design on the Rocks?, Proc. Breakwaters, coastal structures & coastlines, pp 471-481, (ICE) ISBN 0 7277 3042 8, Thomas Telford, London.

Haykin, S. (1994). Neural networks: a comprehensive foundation. Macmillan College Publishing Company, Inc.

Hebsgaard, M., Sloth, P. and Juul, J. (1998). Wave overtopping of rubble mound breakwaters. ICCE 1998, Copenhagen. Paper no. 325.

Heskes, T. (1997). Practical confidence and prediction intervals. In Mozer, Jordan and Petsche (eds.), Advances in neural information processing systems 9, Cambridge, MIT Press.

Hibberd, S. and Peregrine, D. (1979) “Surf and run-up on a beach: a uniform bore.” *Journal of Fluid Mechanics*, 95(2):323–345.

Hirt, C. and Nichols, B. (1981) “Volume of Fluid (VoF) methods for dynamics of free boundaries.” *Journal of Computational Physics*, 39:201–225.

Hordijk, D. (2003). Report on field measurements (D19); Petten sea defence; storm season 2002/2003. CLASH - WP3 report ([www.clash-eu.org](http://www.clash-eu.org)). Technical Report RIKZ/OS/2003/135X, Rijkswaterstaat (RIKZ), The Hague, The Netherlands.

Huang, C., Chang, H., and Hwung, H. (2003). Structural permeability effects on the

interaction of a solitary wave and a submerged breakwater. *Coastal Engineering*, 49(2003):1–24.

Ingram, D., Causon, D., Gao, F., Mingham, C., Troch, P., Li, T. and De Rouck, J. (2003). Improvements Made to the Numerical Wave Flumes VOFbreak<sup>2</sup> and AMAZON-SC. CLASH - WP 5 Report, Manchester Metropolitan University, UK.

Jensen, O.J. & Sorensen, T., 1979. Overspilling / overtopping of rubble mound breakwaters. Results of studies, useful in design procedures. *Coastal Engineering Vol. 3* 1979 pp. 51-65.

Kelecy, F. and Pletcher, R. (1997). The development of a free surface capturing approach for multidimensional free surface flows in closed containers. *Journal of Computational Physics*, 138:939–980.

Kortenhaus, A.; Medina, J.R.; González-Escrivá, J.A.; Garrido, J. (2004a). Laboratory measurements on the Zeebrugge breakwater (D33). CLASH – WP 4 report ([www.clash-eu.org](http://www.clash-eu.org)), Braunschweig/Valencia, 74 pp.

Kortenhaus, A.; Oumeraci, H.; Geeraerts, J.; De Rouck, J.; Medina, J.R.; González-Escrivá, J.A. (2004b). Laboratory effects and other uncertainties in wave overtopping measurements. *Proceedings 29th International Conference Coastal Engineering (ICCE)*, ASCE, Lisbon, Portugal, 13 pp.

Kortenhaus, A.; Van der Meer, J.W.; Burcharth, H.F.; Geeraerts, J.; Pullen, T.; Ingram, D.; Troch, P. (2005). Quantification of measurement errors, model and scale effects related to wave overtopping (D40). CLASH – WP 7 report., Braunschweig, Germany, 60 pp.

Lafaurie, B., Nardone, C., Scardovelli, R., Zaleski, S., and Zanetti, G. (1994). Modelling merging and fragmentation in multiphase flows with SURFER. *Journal of Computational Physics*, 113:134–147.

Li, T., Troch, P., and De Rouck, J. (2004a). Large eddy simulation of wave overtopping on non-uniform Cartesian cut cell grids. In Chung, J., Izumiyama, K., Sayed, M., and Hong, S. (editors), “Proceedings of The Fourteenth (2004) International Offshore and Polar Engineering Conference, Toulon, France,” volume 3, pages 276–284. ISOPE, Cupertino, California, USA.

Li, T., Troch, P., and De Rouck, J. (2004b). Wave overtopping over a sea dike. *Journal of Computational Physics*, 198:686–726.

Lykke Andersen, T. and Burcharth, H. F. (2004a). Report on Additional Tests (D24);

- CLASH – WP 4 report ([www.clash-eu.org](http://www.clash-eu.org)), Aalborg University, Denmark.
- Lykke Andersen, T. and Burcharth, H.F. (2004b). Overtopping and rear slope stability of reshaping and non-reshaping berm breakwaters. ICCE 2004, Lisbon, paper 290.
- Mase, H., Sakamoto, M and Sakai, T. (1995). Neural network for stability analysis of rubble-mound breakwaters. *J. of Waterway, Port, Coastal and Ocean Engrg*, ASCE, nov/dec 1995, pp. 294-299.
- Medina, J.R. (1999). Neural network modelling of runup and overtopping. *ASCE, Proc. Coastal Structures 1999*, Santander, Vol. 1, pp 421-429.
- Medina, J.R, J.A. González-Escrivá, J. Garrido and J. De Rouck (2002). Overtopping analysis using neural networks. 28<sup>th</sup> International Conference on Coastal Engineering, Cardiff, UK.
- Medina, J.R, Garrido, J., Gómez-Martín, E. and C. Vidal (2003). Armour damage analysis using neural networks. *ASCE, Proc. Coastal Structures 2003*, Portland, USA.
- Owen, M.W. (1980). Design of sea walls allowing for wave overtopping, Rep. EX924, HR Wallingford.
- Owen M.W. (1982). The hydraulic design of sea-wall profiles. *Proc. ICE Conf. on Shoreline Protection*, September 1982, pp 185-192, publ. Thomas Telford, London, UK.
- Pan, D. and Lomax, H. (1988). A new approximate LU factorisation scheme for the Navier-Stokes equations. *AIAA Journal*, 26:163–171.
- Panizzo, A., R. Briganti, J.W. van der Meer and L. Franco (2003). Analysis of wave transmission behind low-crested structures using neural networks. *ASCE, Proc. Coastal Structures 2003*, Portland.
- Pearson J., Bruce T., Allsop W. & Gironella X (2002). Violent wave overtopping – measurements at large and small scale, 28th International Conference on Coastal Engineering, Cardiff, UK.
- Pearson, J., Bruce, T., Allsop, W., Kortenhuis, A., Van der Meer, J.W. (2004a). Effectiveness of recurve wave walls in reducing wave overtopping on seawalls and breakwaters, 29th International Conference on Coastal Engineering, Lisbon, Portugal, Book of Abstracts, Paper No 319.
- Pearson, J., Bruce, T., Franco, L., Van der Meer, J. (2004b). Report on additional tests, part B, CLASH WP4 report, University of Edinburgh, Edinburgh, United Kingdom.
- Pedersen, J. W. (1996). Wave Forces and Overtopping on Crown Walls of Rubble Mound Breakwaters – An Experimental Study. Series Paper 12, *Hydraulics & Coastal Engineering*



Laboratory, Department of Civil Engineering, Aalborg University.

Pozueta, B., Van Gent, M.R.A., Van den Boogaard, H.F.P. (2004a). Neural Network prediction method, CLASH – WP8 report ([www.clash-eu.org](http://www.clash-eu.org)), Delft Hydraulics, Delft, The Netherlands.

Pozueta, B., M.R.A. Van Gent, H.F.P. Van den Boogaard, and J.R. Medina (2004b), Prediction method; Neural network modelling of wave overtopping at coastal structures (November, 2004), Delft Hydraulics report H3969.

Pullen, T.A. & Allsop, N.W.H. (2004a). Samphire Hoe field measurements. CLASH - WP 3 report ([www.clash-eu.org](http://www.clash-eu.org)), Technical Report TR133, HR Wallingford, UK.

Pullen, T.; Allsop, N.W.H. (2004b). Clash workpackage 4 - Samphire Hoe physical model studies. CLASH – WP 4 report ([www.clash-eu.org](http://www.clash-eu.org)), no. TR 147, HR Wallingford, U.K.

Pullen, T., Allsop, W., Bruce, T., Pearson, J., Geeraerts, J. (2004). Violent wave overtopping at Samphire Hoe: Field and laboratory measurements. 29<sup>th</sup> International Conference on Coastal Engineering, Lisbon, Portugal.

Qian, L., Causon, D., Ingram, D., and Mingham, C. (2003a). A Cartesian cut cell two fluid solver for hydraulic flow problems. ASCE Journal of hydraulic Engineering, 129(9):688–696.

Qian, L., Causon, D., Ingram, D., and Mingham, C. (2003b). A pressure splitting scheme for free surface capturing methods for flows with gravity effects. Journal of Computational Physics, page submitted.

Ramsbottom D, Wade S, Bain V, Floyd P, Penning-Rowell E, Wilson T & Fernandez A (2004). Flood Risks to People, *Phase 2 Interim Report 1, R & D Report FD 2321/IR1*, DEFRA Flood Management section, London.

Richardson, S., Ingram, D., Mingham, C., and Causon, D. (2002). On the Validity of the Shallow Water Equations for Violent Wave Overtopping. In Edge, B. (editor), “Ocean Wave Measurement and Analysis,” pages 1112–1125. ASCE, Reston, Virginia.

Richardson, S., Pullen, T., and Clarke, S. (2003). Jet velocities of overtopping waves on sloping structures: Measurement and computation. In Smith, J. (editor), “Proceedings of the 29th International Congress on Coastal Engineering,” volume 2, pages 2239–2250. ASCE, Reston, Virginia, World Scientific, New Jersey.

Ris, R.C., Booij, N. and Holthuijsen, L.H. (1999). A third-generation wave model for coastal regions, Part II: Verification, J. Geoph. Research, 104, C4,7667-7682.

- Rogers, S. and Kwak, D. (1990). An upwind difference scheme for the time accurate incompressible Navier-Stokes equations. *AIAA Journal*, pages 113–134.
- Rumelhart, D.E. and J.L. McClelland (1986). *Parallel distributed processing: Explorations in the microstructure of cognition*, Vol. 1, Cambridge, MIT Press.
- Sakakiyama, T. and Kajima, R. (1998). Scale effects on wave overtopping of seawall covered with armour units. In “Proceedings 26th International Conference on Coastal Engineering (ICCE).”
- Shiach, J., Mingham, C., Ingram, D., and Bruce, T. (2004). The applicability of the shallow water equations for modelling violent wave overtopping. *Coastal Engineering*, 51(1):1–15.
- Schulz, K.-P. (1992). Maßstabeffekte beim Wellenaufwurf auf glatten und rauhen Böschungen. *Mitteilungen Leichtweiß-Institut für Wasserbau der Technischen Universität Braunschweig*, Heft 120, Braunschweig, Germany, S. 135-244.
- Soh, W. and Doodrich, J. (1988). Unsteady solution of incompressible Navier-Stokes equations. *Journal of Computational Physics*, 79:113–134.
- Steendam, G.J., J.W. van der Meer, H. Verhaeghe, P. Besley, L. Franco and M.R.A. van Gent (2004). The international database on wave overtopping. *Proc. ASCE, 29th ICCE*, Lisbon, Portugal.
- TAW (2002). Technical report wave run-up and wave overtopping at dikes, Technical Advisory Committee on Flood Defence, The Netherlands.
- TAW (2003). Leidraad Kunstwerken, B2 Kerende hoogte, mei 2003 (in Dutch). Technical Advisory Committee on Water Defences, The Netherlands.
- TAW (2004). Dutch Technical Advisory Committee on Flood Defence. Technical Report on Wave Run-up and Wave overtopping at dikes. Delft, The Netherlands.
- Troch P., De Rouck J., Van Damme L. (1998). Instrumentation and prototype measurements at the Zeebrugge rubble mound breakwater, *Coastal Engineering* 35, pp. 141 – 166.
- Troch, P., Li, T., De Rouck, J., and Ingram, D. (2003). Wave interaction with a sea dike using a VOF finite volume method. In Chung, J., Prevosto, M., Mizutani, N., Kim, G., and Grilli, S. (editors), “Proceedings of the 13th International Offshore and Polar Engineering Conference,” volume 3, pages 325–332. International Society of Offshore and Polar Engineering.
- Troch, P., Geeraerts, J., Van de Walle, B., De Rouck, J., Van Damme, L., Franco, L., Allsop, W. (2004) Full scale wave overtopping measurements on the Zeebrugge rubble mound

- breakwater. Coastal Engineering, Elsevier. Vol. 51 / 7 pp. 609-628.
- Ubbink, O. and Issa, R. (1999). A method for capturing sharp fluid interfaces on arbitrary meshes. Journal of Computational Physics, 153:26–50.
- Van den Boogaard, H., Mynett, A.E. and Heskes, T. (2000). Resampling techniques for the assessment of uncertainties in parameters and predictions of calibrated models. Proc. Hydroinformatics Conference, IOWA.
- van der Meer, J. W. (1992). Stability of the seaward slope of berm breakwaters. Coastal Engineering, Vol. 16, pp 205-234.
- van der Meer, J.W. and Janssen, J.P.F.M. (1994). Wave run-up and wave overtopping at dikes. Wave forces on inclined and vertical wall structures, ASCE.
- Van der Meer, J.W. (1998). Wave run-up and overtopping. In: *Pilarczyk, K.W. (ed.): Dikes and revetments*, Rotterdam/Brookfield: A.A. Balkema, pp. 145-160.
- van der Meer, J.W., Tönjes, P., de Waal, H. (1998). A code for dike height design and examination, Proceedings International Conference on Coastlines, Structures and Breakwaters, Institution of Civil Engineers, London, Thomas Telford, London, pp. 5 - 19.
- van Gent, M. (1994). The modelling of wave action on and in coastal structures.” Coastal Engineering, 22:311–339.
- van Gent, M. (1995). Wave interaction with permeable coastal structures. Ph.D. thesis, Delft University of Technology, Delft University Press, Delft, The Netherlands.
- van Gent, M.R.A and H.F.P. Van den Boogaard (1998). Neural network modelling of forces on vertical structures, ASCE, Proc. ICCE 1998, Vol. 2, pp. 2096-2109.
- van Gent, M. (1999). Physical model investigations on coastal structures with shallow foreshores; 2d model test on the Petten sea defence. Report H3129, Delft Hydraulics, Delft.
- van Gent, M., de Kruif, A., and Murphy, J. (2001). Field measurements and laboratory investigations on wave propagation and wave run-up. In “ASCE, Proc. Waves 2001,” pages 734–743.
- van Gent, M. and Doorn, N. (2001). Wave propagation and wave run-up on dikes with shallow foreshores. In “ASCE, Proc. Coastal Dynamics 2001, Lund, Sweden.”, pages 769–778.
- van Gent, M. and Giarrusso, C. (2003). Influence of low-frequency waves on wave overtopping: A study based on field measurements at the Petten Sea-defence, CLASH – WP

---

5 report (D25), ([www.clash-eu.org](http://www.clash-eu.org)), published as Report H4297, WL| Delft Hydraulics, The Netherlands.

van Leer, B. (1984). On the Relation Between the Upwind Differencing Schemes of Godunov, Engquist, Osher and Roe. *SIAM Journal on Scientific and Statistical Computing*, 5(1):1–20.

Verhaeghe, H., J.W. van der Meer, G.-J. Steendam, P. Besley, L. Franco and M.R.A. van Gent (2003). Wave overtopping database as the starting point for a neural network prediction method, ASCE, Proc. Coastal Structures 2003, Portland.

Verhaeghe, H.; Van der Meer, J.W.; Steendam, G.J. (2003). Database on wave overtopping at coastal structures. CLASH - WP 2 report ([www.clash-eu.org](http://www.clash-eu.org)), Infram, Marknesse, The Netherlands, 34 pp.

Youngs, D. (1982). Time dependent multi-material flow with large fluid distortion. In Morton, K. and Baines, M. (editors), “Numerical Methods for fluid dynamics,” pages 237–285. Academic Press, London.

Zhou, J., Causon, D., Ingram, D., and Mingham, C. (2002). Numerical solutions of the shallow water equations with discontinuous bed topography. *International Journal for Numerical Methods in Fluids*, 38:769–788.

Zhou, J., Causon, D., Mingham, C., and Ingram, D. (2001). The surface gradient method for the treatment of source terms in the shallow water equations. *Journal of Computational Physics*, 168:1–25.